land

Climate Change and Environmental Sustainability

Volume 4

Edited by

Bao-Jie He, Ayyoob Sharifi, Chi Feng and Jun Yang

Printed Edition of the Topics Published in *Atmosphere, Buildings, Land, Remote Sensing, Sustainability*

www.mdpi.com/journal/land

MDPI

Climate Change and Environmental Sustainability-Volume 4

Climate Change and Environmental Sustainability-Volume 4

Editors

Bao-Jie He
Ayyoob Sharifi
Chi Feng
Jun Yang

MDPI • Basel • Beijing • Wuhan • Barcelona • Belgrade • Manchester • Tokyo • Cluj • Tianjin

Editors
Bao-Jie He
Chongqing University
China

Chi Feng
Chongqing University
China

Jun Yang
Northeastern University
China

Ayyoob Sharifi
Hiroshima University
Japan

Editorial Office
MDPI
St. Alban-Anlage 66
4052 Basel, Switzerland

This is a reprint of articles from the Topics published online in the open access journal *Atmosphere* (ISSN 2073-4433), *Buildings* (ISSN 2075-5309), *Land* (ISSN 2073-445X), *Remote Sensing* (ISSN 2072-4292), *Land* (ISSN 2073-445X) (available at: https://www.mdpi.com/topics/Climate_Environmental).

For citation purposes, cite each article independently as indicated on the article page online and as indicated below:

LastName, A.A.; LastName, B.B.; LastName, C.C. Article Title. *Journal Name* **Year**, *Volume Number*, Page Range.

ISBN 978-3-0365-3066-6 (Hbk)
ISBN 978-3-0365-3067-3 (PDF)

185 k words

Contents

About the Editors

Bao-Jie He is a Research Professor of Urban Climate and Built Environment at the School of Architecture and Urban Planning, Chongqing University, China. Prior to joining Chongqing University, Bao-Jie He was a PhD researcher at the Faculty of Built Environment, University of New South Wales, Australia. Bao-Jie is working on the Cool Cities and Communities and Net Zero Carbon Built Environment project. Bao-Jie has strong academic capability and has published around 80 peer-reviewed papers in high-ranking journals and given oral presentations at reputable conferences. Bao-Jie acts as the Topic Editor-in-Chief, Leading Guest Editor, Associate Editor, Editorial Board Member, Conference Chair, Sessional Chair, and Scientific Committee of a variety of international journals and conferences. Dr. He received the Green Talents Award (Germany) in 2021 and National Scholarship for Outstanding Self-Funded Foreign Students (China) in 2019. Dr. He was ranked as one of the 100,000 global scientists (both single-year and career top 2%) by the Mendeley, 2021.

Ayyoob Sharifi works at the Graduate School of Humanities and Social Sciences, Hiroshima University. He also has a cross-appointment at the Graduate School of Advanced Science and Engineering. Ayyoob's research is mainly at the interface of urbanism and climate change mitigation and adaptation. He actively contributes to global climate change research programs such as the Future Earth and is currently serving as a lead author for the Sixth Assessment Report (AR6) of the Intergovernmental Panel on Climate Change (IPCC). Before joining Hiroshima University, he was the Executive Director of the Global Carbon Project (GCP)—a Future Earth core project—leading the urban flagship activity of the project, which is focused on conducting cutting-edge research to support climate change mitigation and adaptation in cities.

Chi Feng received his joint PhD training in South China University of Technology (China) and KU Leuven (Belgium). He is now a research professor in the School of Architecture and Urban Planning, Chongqing University (China) and is leading a research group of more than 10 members. His research topics cover coupled heat and moisture transfer in porous building materials, as well as the hygrothermal performance of building envelopes and built environments. He has led eight international and national research projects, including the China–Europe round robin campaign on material property determination (nine countries participated), the National Natural Science Foundation of China, and the National Key R&D Program of China. He has published more than 60 peer-reviewed journal/conference papers at home and abroad. He is drafting two Chinese standards and participating in another nine international/national ones.

Jun Yang is working at the Urban Climate and Human Settlements Lab, Northeastern University (Shenyang China). His research expertise involves urban climate zones, urban ecology, urban human settlements, and sustainability. As PI or Co-PI, he has been involved in 50 research projects, receiving a total of 15 million RMB from EGOV.CN (e.g., NFC, MOST, and MOE) since 2002. He has authored and co-authored more than 160 papers and book chapters and published more than 50 English papers and more than 110 Chinese papers in academic journals. He is now the Associate Editor of the *Social Sciences* section of the *International Journal of Environmental Science and Technology*, sits on the Editorial Board of *PLOS One*, *PLOS Climate*, and *Frontiers in Built Environment*, is a Lead Guest Editor of *Complexity*, and a Guest Editor of *IEEE Journal of Selected Topics in Applied Earth Observations and Remote Sensing*.

Preface to "Climate Change and Environmental Sustainability-Volume 4"

The Earth's climate is changing; the global average temperature is estimated to already be about 1.1 °C above pre-industrial levels. Indeed, we are now living in conditions of a climate emergency. Climate change leads to many adverse events, such as extreme heat, flooding, bushfire, drought, and many other associated economic and social consequences. Further warming is projected to occur in the coming decades, and climate-induced impacts may exceed the capacity of society to cope and adaptive in a 1.5 °C or 2 °C world. Therefore, urgent actions should be taken to address climate change and avoid irreversible environmental damages.

Climate change is interrelated with many other challenges such as urbanisation, population increase and economic growth. For instance, cities are now the main settlements of human being and are major sources of greenhouse gas emissions that are key contributors to climate change. Moreover, rapid and unregulated urbanisation in some contexts further causes urban problems such as environmental pollution, traffic congestion, urban flooding and heat island intensification. In the absence of well-designed measures, increasing urbanisation trends in the next two–three decades are likely to further aggravate such problems. Overall, climate change and many other challenges have deteriorated the sustainable development of the world.

The United Nations proposed the Sustainable Development Goals in 2015. Goal 13, Climate Action, emphasises the need for urgent action to combat climate change and its impacts in order to enhance sustainability. To achieve this, there is a need to develop a holistic framework that considers mitigation—the decarbonisation of society—to address the challenge of climate change from the root, and adaptation—an immediate action—to increase the resilience of and protect society from climate-induced hazards. The framework prioritises the transformation of the traditional methods of environmental modifications in various fields, including transportation, industry, building, energy generation, agriculture, land use and forestry, towards sustainable ones to limit greenhouse gas emissions. The framework also highlights the significance of sustainable environmental planning and design for adaptation in order to reduce climate-induced threats and risks. Moreover, it encourages the involvement and participation of all stakeholders to accelerate climate change mitigation and adaptation progress by developing sound climate-related governance systems.

The framework also calls for the support and engagement of all societal stakeholders. To support the achievement and implementation of the framework, this book focuses on climate change and environmental sustainability by covering four key aspects, including climate change mitigation and adaptation, sustainable urban–rural planning and design, decarbonisation of the built environment in addition to climate-related governance and challenges. Climate change mitigation and adaptation covers topics of greenhouse gas emissions and measurement, climate-related disasters and reduction, risk and vulnerability assessment and visualisation, impacts of climate change on health and well-being, ecosystem services and carbon sequestration, sustainable transport and climate change mitigation and adaptation, sustainable building and construction, industry decarbonisation and economic growth, renewable and clean energy potential and implementation in addition to environmental, economic and social benefits of climate change mitigation.

Sustainable urban–rural planning and design deals with questions of climate change and regional economic development, territorial spatial planning and carbon neutrality, urban overheating mitigation and adaptation, water-sensitive urban design, smart development for urban habitats,

sustainable land use and planning, low-carbon cities and communities, wind-sensitive urban planning and design, nature-based solutions, urban morphology and environmental performance in addition to innovative technologies, models, methods and tools for spatial planning. Decarbonisation of the built environment addresses issues of climate-related impacts on the built environment, the health and well-being of occupants, demands on energy, materials and water, assessment methods, systems and tools, sustainable energy, materials and water systems, energy-efficient design technologies and appliances, smart technology and sustainable operation, the uptake and integration of clean energy, innovative materials for carbon reduction and environmental regulation, building demolition and material recycling and reusing in addition to sustainable building retrofitting and assessment. Climate-related governance and challenges concerns problems of targets, pathways and roadmaps towards carbon neutrality, pathways for climate resilience and future sustainability, challenges, opportunities and solutions for climate resilience, the development and challenges climate change governance coalitions (networks), co-benefits and synergies between adaptation and mitigation measures, conflicts and trade-offs between adaptation and mitigation measures, mapping, accounting and trading carbon emissions, governance models, policies, regulations and programs, financing urban climate change mitigation, education, policy and advocacy of climate change mitigation and adaptation in addition to the impacts and lessons of COVID-19 and similar crises.

Overall, this book aims to introduce innovative systems, ideas, pathways, solutions, strategies, technologies, pilot cases and exemplars that are relevant to measuring and assessing the impact of climate change, mitigation and adaptation strategies and techniques in addition to public participation and governance. The outcomes of this book are expected to support decision makers and stakeholders to address climate change and promote environmental sustainability. Lastly, this book aims to provide support for the implementation of the United Nations Sustainable Development Goals and carbon neutrality in efforts aimed at achieving a more resilient, liveable and sustainable future.

Anthropogenic activities are significant drivers of climate change and environmental degradation. Such activities are particularly influential in the context of the land system that is an important medium connecting earth surface, atmospheric dynamics, ecological systems, and human activities. Assessment of land use land cover changes and associated environmental, economic, and social consequences is essential to provide references for enhancing climate resilience and improving environmental sustainability. On the one hand, this book touches on various environmental topics, including soil erosion, crop yield, bioclimatic variation, carbon emission, natural vegetation dynamics, ecosystem and biodiversity degradation, and habitat quality caused by both climate change and earth surface modifications. On the other hand, it explores a series of socioeconomic facts, such as education equity, population migration, economic growth, sustainable development, and urban structure transformation, along with urbanization. The results of this book are of significance in terms of revealing the impact of land use land cover changes and generating policy recommendations for land management. More broadly, this book is important for understanding the interrelationships among life on land, good health and wellbeing, quality education, climate actions, economic growth, sustainable cities and communities, and responsible consumption and production according to the United Nations Sustainable Development Goals. We expect the book to benefit decision makers, practitioners, and researchers in different fields, such as climate governance, crop science and agricultural engineering, forest ecosystem, land management, urban planning and design, urban governance, and institutional operation.

Prof. Bao-Jie He acknowledges the Project NO. 2021CDJQY-004 supported by the Fundamental Research Funds for the Central Universities and the Project NO. 2022ZA01 supported by the State Key Laboratory of Subtropical Building Science, South China University of Technology, China. We appreciate the assistance of Mr. Lifeng Xiong, Mr. Wei Wang, Ms. Xueke Chen, and Ms. Anxian Chen at School of Architecture and Urban Planning, Chongqing University, China.

Bao-Jie He, Ayyoob Sharifi , Chi Feng, Jun Yang
Editors

land

MDPI

Article

Are Land Use Options in Viticulture and Oliviculture in Agreement with Bioclimatic Shifts in Portugal?

Cristina Andrade [1,2,*], André Fonseca [2,3] and João Andrade Santos [2,3,4]

[1] Natural Hazards Research Center (NHRC.ipt), Instituto Politécnico de Tomar, 2300-313 Tomar, Portugal
[2] Centre for the Research and Technology of Agro-Environmental and Biological Sciences (CITAB), Universidade de Trás-os-Montes e Alto Douro (UTAD), 5001-801 Vila Real, Portugal; andre.fonseca@utad.pt (A.F.); jsantos@utad.pt (J.A.S.)
[3] Institute for Innovation, Capacity Building and Sustainability of Agri-Food Production, Universidade de Trás-os-Montes e Alto Douro (UTAD), 5001-801 Vila Real, Portugal
[4] Department of Physics, School of Sciences and Technology, Universidade de Trás-os-Montes e Alto Douro (UTAD), 5001-801 Vila Real, Portugal
* Correspondence: c.andrade@ipt.pt; Tel.: +351-249-328-100

Abstract: Land and climate are strongly connected through multiple interface processes and climate change may lead to significant changes in land use. In this study, high-resolution observational gridded datasets are used to assess modifications in the Köppen–Geiger and Worldwide Bioclimatic (WBCS) Classification Systems, from 1950–1979 to 1990–2019 in Portugal. A compound bioclimatic-shift exposure index (BSEI) is also defined to identify the most exposed regions to recent climatic changes. The temporal evolution of land cover with vineyards and olive groves between 1990 and 2018, as well as correlations with areas with bioclimatic shifts, are analyzed. Results show an increase of CSa Warm Mediterranean climate with hot summer of 18.1%, followed by a decrease in CSb (warm summer) climate of −17.8%. The WBCS Temperate areas also reveal a decrease of −5.11%. Arid and semi-arid ombrotypes areas increased, conversely humid to sub-humid ombrotypes decreased. Thermotypic horizons depict a shift towards warmer classes. BSEI highlights the most significant shifts in northwestern Portugal. Vineyards have been displaced towards regions that are either the coolest/humid, in the northwest, or the warmest/driest, in the south. For oliviculture, the general trend for a relative shift towards cool/humid areas suggests an attempt of the sector to adapt, despite the cover area growth in the south. As vineyards and olive groves in southern Portugal are commonly irrigated, options for the intensification of these crops in this region may threaten the already scarce water resources and challenge the future sustainability of these sectors.

Keywords: Köppen–Geiger climate classification; Worldwide Bioclimatic Classification System (WBCS); bioclimates; thermotypes; ombrotypes; vineyards; olive groves; Portugal

Citation: Andrade, C.; Fonseca, A.; Santos, J.A. Are Land Use Options in Viticulture and Oliviculture in Agreement with Bioclimatic Shifts in Portugal?. *Land* **2021**, *10*, 869. https://doi.org/10.3390/land10080869

Academic Editor: Baojie He

Received: 20 July 2021
Accepted: 17 August 2021
Published: 19 August 2021

1. Introduction

Land provides the main basis not only for human livelihoods but also for well-being. It endows means for agriculture practices thus contributing to the food supply, also providing freshwater, and fostering biodiversity in the several intricate ecosystems [1]. Land use also plays a relevant role in the climatic system, being closely intertwined [2]. As such, climate change, as well as climate and weather extremes, are important stress factors to land ecosystems and biodiversity, which are thus becoming increasingly vulnerable [3,4]. Global population growth has implications for global food consumption, raw materials, and energy. An expansion of areas under agricultural and forestry systems [5,6] is, therefore, required to warrant food security. However, land-use intensification can decisively contribute to land/soil degradation and, henceforth, potentiates desertification [7,8].

Climate change has already deeply impacted biodiversity, ecosystems, and agro-forestry systems [9–11]. Global warming and changes in the precipitation patterns are

fostering an increase in arid/dry regions, and ultimately the expansion of desertic areas. Climate change has increased the frequency, intensity, and duration of extreme events, such as droughts and heatwaves, namely in the Mediterranean region [12–15]. Changes in precipitation spatial patterns and temporal regimes not only affect the water content in reservoirs but also soil water availability [16,17]. These modifications in the regional climatic features are reflected on different time scales, from the annual-mean conditions to seasonality, daily cycle, and variability [18], which in turn affect crop-relevant bioclimatic conditions, such as growing season length, thermal forcing, chill accumulation or water availability for irrigation [19–21].

Changes in temperature and precipitation patterns are key factors triggering shifts in the climate of a region. These variables are fundamental to classify climates in different categories, such as in the Köppen–Geiger climate classifications system [22], but also for the Worldwide Bioclimatic Classification System (WBCS) [23,24]. Recent studies projected changes for the Iberian Peninsula (IP) not only for the Köppen–Geiger climatic classification [25] but also for the major divisions of the WBCS, mainly for the IP southernmost regions [11]. Since 1986, the IP has experienced an acceleration of land use for agriculture and forestry, promoted by the integration of these countries into the European Union [26]. The European Union's reform of the agriculture policies, under the Common Agricultural Policy, CAP, was a key factor for the observed changes, also observed in agricultural practices and cultivated species. Overall, these factors (climate and policies) jointly exacerbated land degradation, which is already particularly apparent in coastal areas, drylands, river deltas, riverine estuaries, permafrost, amongst others. Therefore, sustainable land management [27] is urgent to balance these projected changes, while maintaining crop yields, animal growth rates, water management, soil health, and land conditions [28].

The Portuguese viticultural sector is of major socioeconomic relevance, owing to the relatively high generated economic income and the important share of national exports [29], currently being Portugal the 10th wine exporter and the 11th wine producer [30]. Mainland Portugal has a total of 12 wine regions (WR), with a fluctuation of vineyard land cover from 271,507 ha in 1989 to 189,668 ha on 31/07/2020 [31] (Supplementary Materials Figure S1; Table S3). With an opposite trend, wine production increased from about 5.8 Mhl in 2009/10 to about 6.5 Mhl in 2019/20 [32] (Figure S2). Different denominations of origin (DO) can also be found within each WR (Figure S1).

On the other hand, the production of olive oil is also highly relevant to the Portuguese economy. Although Spain is the world's leading producer, Portugal, with a production of about 100,000 tons, currently holds the seventh position in the world production ranking, along with Turkey (183,000 tons), Tunisia (120,000 tons), and Morocco (200,000 tons) [33]. These rankings in both viticulture and oliviculture are particularly noteworthy taking into account the relatively small size of the country and are thereby key factors for its socio-economic development.

The main goal of this research aims to answer the question: 'Are land use options in viticulture and oliviculture in agreement with ongoing bioclimatic shifts in Portugal?'. This is a highly relevant question since, water management in viticulture and oliviculture demands adaptation strategies of these industries to climate change, while minimizing environmental impacts. This is particularly important not only for Portugal but for the Mediterranean regions increasingly exposed to extreme climate events [1,11,12]. Therefore, this assessment is of utmost relevance.

To answer the aforementioned question, the Köppen–Geiger climatic classification and the WBCS were applied in the first step, while a comparison between two 30-year periods, namely 1950–1979 and 1990–2019, was carried out to relate recent past climatic shifts with land-use changes. From the WBCS, which encompasses the bioclimates, the thermotypes, and ombrotypes, a compound bioclimatic-shift exposure index (BSEI) was computed to identify the most exposed regions in Portugal to bioclimatic shifts. In a second phase, the spatial patterns for the extension of vineyards and olive groves for 1990, 2018,

and between 1990–2018 are presented. Subsequently, correlations between ombrotypes and thermotypes were calculated for 1990, 1995, 2007, 2010, 2015, and 2018.

2. Materials and Methods

2.1. Data and Study Area

In this study, four high-resolution gridded observational datasets were used between 1950 and 2019. The methodology for the development of this dataset is described by Fonseca and Santos [34]. A two-step approach was carried out: (1) monthly baseline (1971–2000) patterns were estimated at 1-km grid resolution resorting to multivariate linear regressions (exploratory variables: elevation, latitude, and distance to the coastline). Kriging of residuals from baseline normals of a network of weather stations was applied for bias corrections; (2) further, bilinearly interpolated daily temperature anomalies were then added to the daily baseline patterns to obtain the final datasets regarding temperature.

The daily precipitation totals (P, in mm), maximum (TX, in °C), mean (TG, in °C), and minimum (TN, in °C) temperatures, are defined on a 0.01° regular grid. Two 30-year periods were analyzed, i.e., 1950–1979 and 1990–2019, aiming at finding climatic shifts already in progress in mainland Portugal.

The study area is within the geographical sector: 36.95° N–42.16° N and 9.48° W–6.17° W (Figure 1). However, all figures presented herein will be clipped excluding the grid boxes over the Atlantic Ocean. Figure 1a shows a hypsometric chart, with a spatial resolution of 3 arc-second, and was compiled from mosaics retrieved from STRMGL3S Nasa Shuttle radar topography second sub-sampled V003 distributed by (MEaSUREs) SRTM [35]. The area of interest also includes 18 districts in mainland Portugal (Figure 1b). All maps are projected onto the GCS ETRS 1989 Geographical Coordinate System.

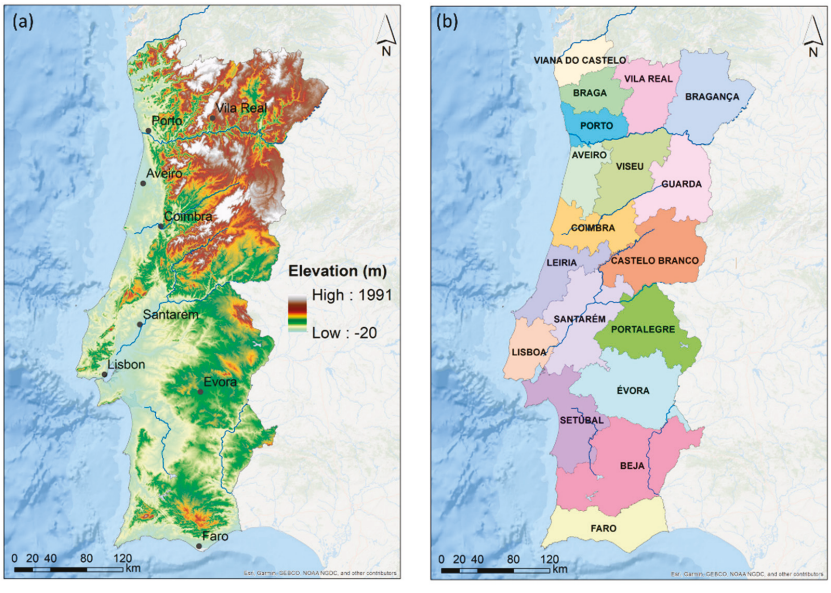

Figure 1. Mainland Portugal (**a**) elevation (in m) and (**b**) the related 18 districts.

The land use and occupation maps were retrieved from https://snig.dgterritorio.gov.pt/ accessed on 30 June 2021 [36], for the years 1990, 1995, 2007, 2010, 2015, and 2018. This satellite-based land cover open access dataset known has the Official Administrative Chart of Portugal (CAOP 2020) is available throughout the country on an annual timescale. For this study, only the spatial representation of monocultures was taken into consideration (vineyards or olive groves separately). The level that presents both vineyards and olive

groves land use was disregarded to avoid misleading conclusions. However, the total area evolution for both cultures and the related total amount of production are subsequently presented in tables and graphics between 1989 and 2020 (when available).

2.2. Köppen's Climate Classification

Köppen's climate classification is based on a subdivision of major climate types, which are represented by five capital letters, from A to E (considered the main group), followed by two others. In our study, C is used for temperate climates in the mid-latitudes. The second letter identifies the seasonal precipitation type: S for steppe, W desert, while f indicates no dry season. The last letter specifies the level of heat, with a for hot summer, b for warm summer, c for cold summer, d for very cold winter, and h and k are associated with hot and cold climates, respectively. The whole calculation follows the methodology described by Kottek et al. [37] in Tables S1 and S2, whereas the nomenclature (Table S1) and color scheme follow Andrade and Contente [25]. In this study, the concept of high-altitude type (H climates) was not applied. Further details on this methodology can be found in Andrade and Contente [25].

2.3. Worldwide Bioclimatic Classification System (WBCS)

The WBCS includes four major divisions, according to Rivas-Martínez et al. [23,24]. The first division corresponds to the macrobioclimate, which is subsequently split into the other three: bioclimates (Table 1), ombrotypes (Table 2), and thermotypes (Table 3). The major bioclimatic divisions comprise the computation of three additional indices: the continentality index (CI), the annual ombrothermic index (OI), and the thermicity index (TI). However, four additional ombrothermic indices are also computed: the ombrothermic index of the hottest month of the summer quarter (Ios_1), the ombrothermic index of the hottest two months of the summer quarter (Ios_2), the ombrothermic index of the summer quarter (Ios_3) and the ombrothermic index of the 4 months resulting from adding the summer quarter and the month immediately preceding it (Ios_4). Further details can be found in Rivas-Martínez et al. [23,24], while a summary of the main equations can be found in Andrade and Contente [11].

Table 1. Bioclimatic classification for Mediterranean and temperate macrobioclimates, according to Rivas-Martínez et al. [23] (Adapted with permission from Andrade and Contente [11]).

Bioclimates	Abbr.	CI [1]	OI [1]
1. Mediterranean pluviseasonal oceanic	Mepo	≤21	>2.0
2. Mediterranean pluviseasonal continental	Mepc	>21	>2.0
3. Mediterranean xeric oceanic	Mexo	≤21	1.0–2.0
4. Mediterranean xeric continental	Mexc	>21	1.0–2.0
5. Mediterranean desertic oceanic	Medo	≤21	0.2–1.0
6. Mediterranean desertic continental	Medc	>21	0.2–1.0
7. Mediterranean hyperdesertic oceanic	Meho	≤21	<0.2
8. Mediterranean hyperdesertic continental	Mehc	>21	<0.2
9. Temperate hyperoceanic	Teho	≤11	>3.6
10. Temperate oceanic	Teoc	11–21	>3.6
11. Temperate continental	Teco	>21	>3.6
12. Temperate xeric	Texe	≥4	≤3.6

[1] In this Table, CI is the continentality index and OI is the ombrothermic index.

2.4. The Bioclimatic-Shift Exposure Index (BSEI)

The compound bioclimatic-shift exposure index (BSEI) is computed by adding the statistically significant differences between the bioclimates, ombrotypes, and thermotypes between 1990–2019, and 1950–1979, respectively. For each difference, two values are attributed, 0 when there is no change, 1 when a change in the climatic type occurs between the two 30-year periods. The three types are equally weighted in the final value of BSEI. This is performed for each grid point within the study area, separately. Therefore, BSEI will

vary from 0, indicating regions not exposed to bioclimatic shifts, to 3, signalling regions highly exposed to bioclimatic shifts (changes in the three classifications simultaneously: bioclimatic, ombrotype, and thermotype) (Table 4). Despite its very simple definition, BSEI is a useful tool to assess the degree of change in climatic conditions at a given location/region, i.e., the degree of exposure to climate change.

Table 2. Ombrothermic horizons, according to Rivas-Martínez et al. [23] Adapted with permission from Andrade and Contente [11]).

Ombrothermic Horizons	Abbr.	OI [1]
1. Lower ultrahyperarid	Uhai	0.0–0.1
2. Upper ultrahyperarid	Uhas	0.1–0.2
3. Lower hyperarid	Hai	0.2–0.3
4. Upper hyperarid	Has	0.3–0.4
5. Lower arid	Ari	0.4–0.7
6. Upper arid	Ars	0.7–1.0
7. Lower semiarid	Sai	1.0–1.5
8. Upper semiarid	Sas	1.5–2.0
9. Lower dry	Sei	2.0–2.8
10. Upper dry	Ses	2.8–3.6
11. Lower subhumid	Sui	3.6–4.8
12. Upper subhumid	Sus	4.8–6.0
13. Lower humid	Hui	6.0–9.0
14. Upper humid	Hus	9.0–12.0
15. Lower hyperhumid	Hhi	12.0–18.0
16. Upper hyperhumid	Hhs	18.0–24.0
17. Ultrahyperhumid	Uhu	>24.0

[1] In this Table, OI is the ombrothermic index.

Table 3. Thermotypic horizons, to Mediterranean and temperate macrobioclimates. Tp is only used if CI $\geq$ 21, or TI, TIc < 120, according to Rivas-Martínez et al. [23] (Adapted with permission from Andrade and Contente [11]).

Thermotypic Horizons	Abbr.	TI [1], Tic [1]	Tp [1]
1. Lower inframediterranean	Imei	515–580	>2600
2. Upper inframediterranean	Imes	450–515	2400–2600
3. Lower thermomediterranean	Tmei	400–450	2250–2400
4. Upper thermomediterranean	Tmes	350–400	2100–2250
5. Lower mesomediterranean	Mmei	285–350	1800–2100
6. Upper mesomediterranean	Mmes	220–285	1500–1800
7. Lower supramediterranean	Smei	150–220	1200–1500
8. Upper supramediterranean	Smes	120–150	900–1200
9. Lower oromediterranean	Omei	–	675–900
10. Upper oromediterranean	Omes	–	450–675
11. Lower crioromediterranean	Cmei	–	100–450
12. Upper crioromediterranean	Cmes	–	1–100
13. Pergelid	Gme	–	0
14. Infratemperate	Ite	>410	>2351
15. Lower thermotemperate	Ttei	350–410	2176–2350
16. Upper thermotemperate	Ttes	290–350	2000–2175
17. Lower mesotemperate	Mtei	240–290	1700–2000
18. Upper mesotemperate	Mtes	190–240	1400–1700
19. Lower supratemperate	Stei	120–190	1100–1400
20. Upper supratemperate	Stes	–	800–1100
21. Lower orotemperate	Otei	–	590–800
22. Upper orotemperate	Otes	–	380–590
23. Lower criorotemperate	Ctei	–	100–380
24. Upper criorotemperate	Ctes	–	1–100
25. Pergelid	Gme	–	0

[1] In this Table, CI is the continentality index, TI is the thermicity index and TIc is the compensated thermicity index, Tp is the annual positive temperature (tenths of °C), when the mean monthly temperature is higher than 0 °C.

Table 4. Bioclimatic-shift expose index (BSEI) interpretation.

BSEI	Degree of Exposure
0	Not exposed
1	Weakly exposed
2	Moderately exposed
3	Highly exposed

2.5. Statistical Analysis

For the bioclimates, ombrotypes, and thermotypes, a comparison between a recent past period 1990–2019, and preceding past conditions 1950–1979 (baseline climate) was undertaken. Anomalies (percentage of change) were computed as the differences between the most recent period and the baseline climate. The statistically significant anomalies (S.S.) were assessed by the Mann–Whitney–Wilcoxon test (MWW), at a 5% significance level [38,39], using the 30-year mean values for each period and location of the study area. This nonparametric test assumes equal medians under the null hypothesis (H_o), against the alternative hypothesis (H_a) of different medians.

For each land use and occupation map, the areas of vineyards and olive groves were extracted to assess their spatial-temporal development. Further, the data was compared with the bioclimates, ombrotypes, and thermotypes of the recent period to analyze the shift of land use in both cultivars. The overall methodological schematics of this study can be depicted in Figure 2.

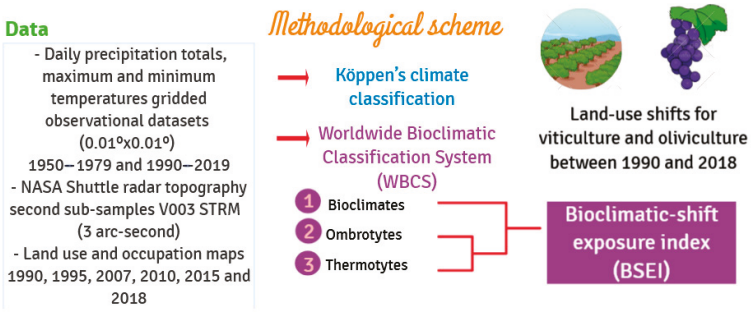

Figure 2. Methodological schematics of this study.

3. Results

3.1. Köppen–Geiger Climate Classification and WBCS

The spatial representation of the Köppen–Geiger climate classification in mainland Portugal for the period 1950–1979 reveals three climate types (Figure 3a). Two within the CS 'warm temperate/Mediterranean with dry summer' and one Cf 'warm temperate/Mediterranean fully humid' (Table S1). The prominent climate was CSa (warm temperate/Mediterranean with hot summer) in 53.9% of the territory, CSb (warm temperate/Mediterranean with warm summer) in 45.8%, and only 0.03% for Cfb (warm temperate/Mediterranean fully humid with hot summer) (Table 5, Tables S1 and S2). Besides a small area in the very southwest (Faro district, Figure 1b), the CSb type is mostly found in the northern half of the country, northwards of the Tagus River basin. Conversely, the CSa type is predominant in the southern half, and a small region between the Vila Real and Bragança districts (Figures 1a and 3a). The small area of Cfb climate is located in a mountainous region in the northwest (Figures 1b and 3a).

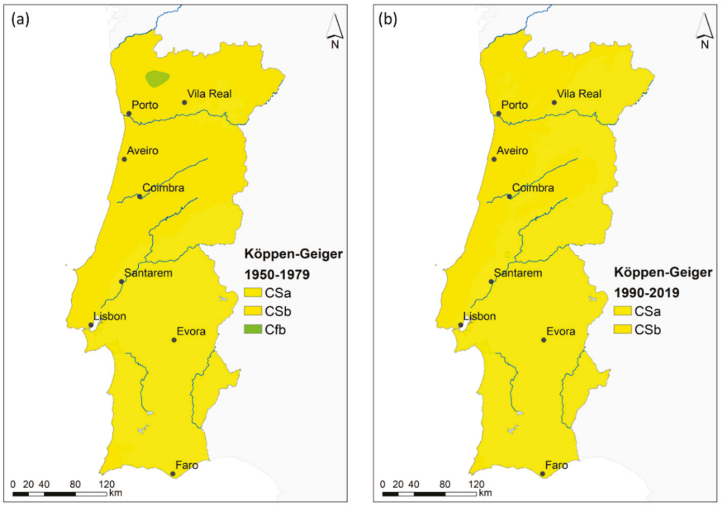

Figure 3. Köppen–Geiger climate classification for (**a**) 1950–1979 and (**b**) 1990–2019.

Table 5. Percentage of the territory (in %) for each Köppen–Geiger climate classification for mainland Portugal for 1950–1979 and 1990–2019.

Köppen–Geiger Climate Classification	1950–1979	1990–2019	% Change
CSa	53.90	72.00	↑ 18.10
CSb	45.80	28.00	↓ 17.80
Cfb	0.03	0.00	↓ 0.03

For 1990–2019, only two types are found (CSa and CSb), with an increase of +18.1% in CSa type (hot summer) and a resulting decrease of −17.8% in CSb (warm summer), a milder climate (Table 5). This later climate type is now depicted along the north-central western coast and in mountainous areas in the northern half of the country.

The changes depicted in the Köppen–Geiger climatic system are also translated for the WBCS classification in which only two macroclimates were found for the two time periods, the Mediterranean and the temperate, which decreased from 1950–1979 to 1990–2019. This can be inferred by observing Figure 4a,d, where the bioclimates are derived from the macroclimates identified by the prefix M for the Mediterranean and T for temperate.

The results also show a transition from three bioclimates in 1950–1979 to four in 1990–2019, though Teho only underwent an increase of +0.03% (Table 6). Nevertheless, the most striking difference is related to the loss of temperate regions (−5.14%) of Teoc, with an increase of Mepo of +4.78%. These changes have occurred mainly in northwestern Portugal (Figure 4a,d).

Climate change has also affected the ombrotypes. They changed from seven to eight types (Figure 4b,e), with the emergence of a new ombrotype, Sas, within the semi-arid ombrothermic horizons, and corresponding to 0.74% of the territory in 1990–2019 (Table 6). The most relevant changes have occurred for Sei, within the arid ombrothermic horizons with an increase of +24.07%, followed by an overall decrease in almost all humid horizons. The exception was for Sus (upper subhumid), though with a marginal increase of only 1.02% in 1990–2019. Although the Ses (upper dry) ombroclimate area has decreased −13.66%, it is still worth noting the decrease in the percentage of the territory of humid and hyper-humid regions (Sui, Hui, Hus, and Hhi), with an overall total decrease of −12.17% in

1990–2019. These changes have occurred mainly in central (in the vicinity of Serra da Estrela mountainous region) and northwestern Portugal (Figure 4b,e).

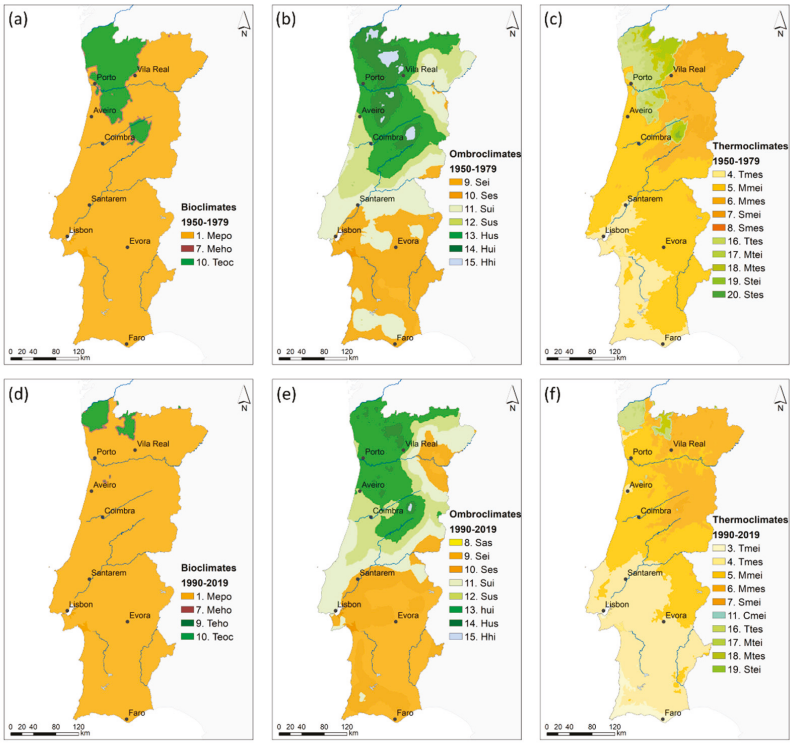

Figure 4. Classification for (**a**) bioclimates; (**b**) ombrotypes; and (**c**) thermotypes between 1950–1979 and (**d**–**f**) the same as for (**a**–**c**) but between 1990–2019.

Table 6. Percentage of the territory (in %) for each bioclimate, ombrotype, and thermotype classification for mainland Portugal, for the periods 1950–1979 and 1990–2019.

	Classification	1950–1979	1990–2019	% Change
Bioclimates	1. Mepo	91.40	96.18	↑ 4.78
	7. Meho	0.80	1.13	↑ 0.33
	9. Teho	0.00	0.03	↑ 0.03
	10. Teoc	7.80	2.66	↓ 5.14
Ombrotypes	8. Sas	0.00	0.74	↑ 0.74
	9. Sei	3.63	27.70	↑ 24.07
	10. Ses	38.13	24.47	↓ 13.66
	11. Sui	23.98	18.54	↓ 5.44
	12. Sus	10.96	11.98	↑ 1.02
	13. Hui	15.23	15.16	↓ 0.07
	14. Hus	7.07	1.37	↓ 5.70
	15. Hhi	1.00	0.04	↓ 0.96

Table 6. *Cont.*

	Classification	1950–1979	1990–2019	% Change
Thermotypes	3. Tmei	0.00	10.74	↑ 10.74
	4. Tmes	20.73	28.89	↑ 8.16
	5. Mmei	45.35	37.25	↓ 8.10
	6. Mmes	14.32	19.06	↑ 4.74
	7. Smei	9.53	0.91	↓ 8.62
	8. Smes	0.28	0.00	↓ 0.28
	11. Cmei	0.00	0.48	↑ 0.48
	16. Ttes	2.21	1.30	↓ 0.91
	17. Mtei	3.17	0.40	↓ 2.77
	18. Mtes	1.95	0.80	↓ 1.15
	19. Stei	2.31	0.17	↓ 2.14
	20. Stes	0.15	0.00	↓ 0.15

Regarding the thermotypes, the findings are consistent with the previous WBCS types. A loss of the territory with temperate thermotypic horizons is verified, e.g., within the thermotemperate (Ttes, −0.91%), mesotemperate (Mtei and Mtes, −2.77 and −1.15%, respectively), and supratemperate (Stei −2.14% and Stes non-existent in 1990–2019) (Table 6). Nonetheless, within the Mediterranean thermotypic horizons, changes were also found. There was a major increase in the thermomediterranean horizons (Tmei and Tmes, +10.74 and +8.16%, respectively), followed by mixed results for the mesomediterranean horizons, with a decrease of −8.10% for Mmei and an increase of +4.74% for Mmes. Lastly, a decrease in the supramediterranean thermotypic horizons are found (Smei and Smes, −8.62 and −0.28%, respectively), as well as the arising of a small region of Cmei (+0.48%) in 1990–2019. The gain of Tmei and Tmes areas (associated with more arid/dry conditions) have occurred mainly in the southern half of the country (Figure 4c,f), whilst the loss of temperate thermotypic horizons was registered in the northwesternmost regions.

3.2. The Bioclimatic-Shift Expose Index (BSEI)

The BSEI captures the accumulated changes that have occurred between 1990–2019 and 1950–1979 between bioclimates, ombrotypes, and thermotypes. Thus, it captures the most exposed regions to the bioclimatic shifts analyzed in the previous sub-section. Regions with no changes have a zero score, while regions with changes in the three WBCS indicators have a score of three. Figure 5a depicts the highest exposures (BSEI = 3, highly exposed) in Viana do Castelo, Braga, Porto, Aveiro, Viseu, and Guarda districts. These outcomes are consistent with both the loss of temperate regions and the increase of more arid/dry bioclimatic types in the former regions (Figure 4). Large areas with BSEI = 2 (moderately exposed) can still be found in the aforementioned districts, as well as in the northeast (Bragança). On the other hand, in the southern half of the country, BSEI = 2 can be found in the Santarém, Portalegre, Évora, Beja, and Faro districts (Figure 5a). In these latter regions, however, changes are mostly due to shifts in the ombrotypes and thermotypes (Figure 4b,c,e,f).

For a better understanding of the extent of exposure to the bioclimatic shifts, the areal mean values for each district were computed. The Braga district is the most exposed (BSEI = 3), followed by Viana do Castelo, Vila Real, Porto, Viseu, Guarda, and Évora districts, all of them with BSEI = 2 (Figure 5b). All the remaining districts have BSEI = 1 (weakly exposed).

3.3. Land-Use Changes for Viticulture and Oliviculture from 1990 to 2018

The vineyard cover area in Portugal has decreased from 1990 to 2018 (only land use levels for monocultures were considered). The decrease is approximately 6% (126 km^2) (Figure 6a), mainly in the Lisboa district. New vineyard cover areas are, however, observed in Alentejo (mostly Évora district) and in northwestern Portugal, which are in both cases

areas with higher BSEI values. For the olive groves, the area has significantly increased by approximately 62% (1717 km^2) (Figure 6b), mainly in Faro, Beja, Vila Real, and Bragança districts, among which only Vila Real shows a higher BSEI (2, moderate exposure).

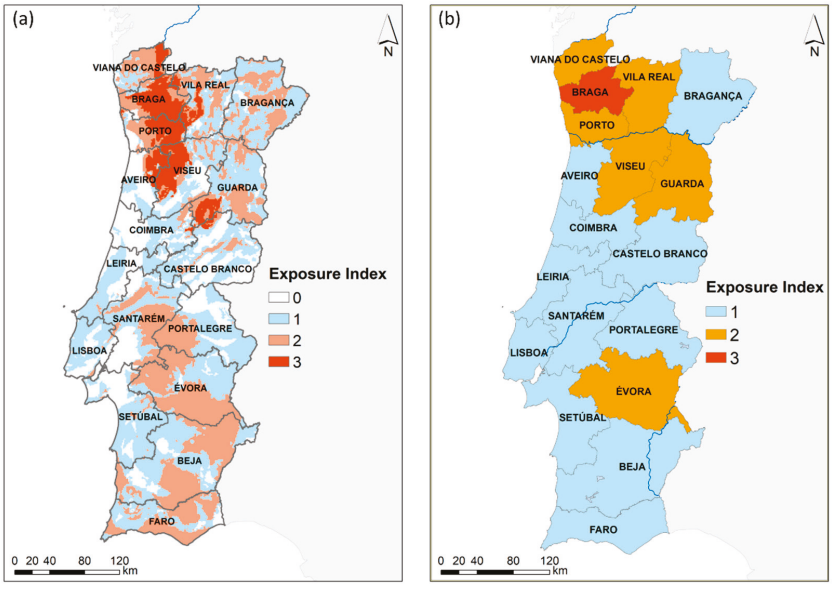

Figure 5. (**a**) Bioclimatic-shift exposure index (BSEI) for mainland Portugal and (**b**) related areal mean values for each district (note: BSEI attained between 1990–2019 and 1950–1979).

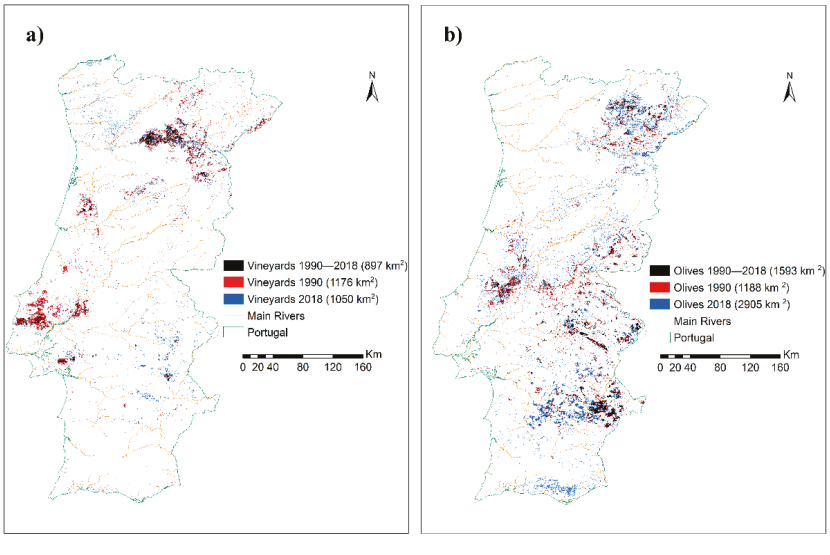

Figure 6. Spatial representation and related area (in km^2) of (**a**) vineyards and (**b**) olive groves in Portugal for the period between 1990 and 2018. Areas maintained throughout the period in black (persistent areas), only for 1990 in red (discontinued areas), and 2018 in blue (emerging areas).

Concerning the evolution of the growing bioclimatic conditions in the vineyard cover area from 1990 to 2018 (Figure 7a), there is a shift towards new regions that are both humid (Hui), in northwestern Portugal (Vinho Verde WR), and dry (Sei), in southern Portugal (Alentejo WR) (Figure S1). Conversely, a decrease in the areas classified as subhumid (Sus and Sui) is also apparent. Hence, vineyards are gradually occupying more extremes conditions in terms of climate humidity. The change in thermotype conditions of vineyards areas is not statistically significant (Figure 7c).

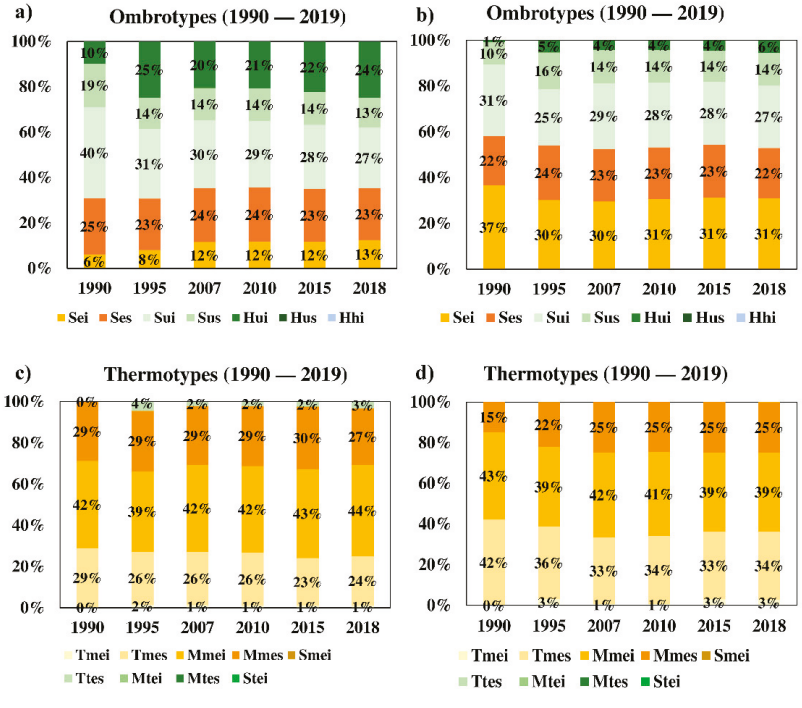

Figure 7. Percentage area regarding each land use and occupation map for vineyards (**a**,**c**) and olive groves (**b**,**d**) according to each specific climatic classification: (**a**,**b**) ombrotype and (**c**,**d**) thermotype for the recent past period (1990–2019).

For the temporal evolution in land use for olive groves, there is a general trend for a shift towards more humid (an increase of cover area in classes Hui and Hus) and cooler areas (increase in Mmes and decreases in the warmer classes of Mmei and Tmes).

4. Discussion

The present climatic characterization aimed at identifying the regions in mainland Portugal that have endured the most significant bioclimatic shifts from 1950–1979 to 1990–2019. Most of the areas or districts that experienced more accentuated alterations in the bioclimatic classes from one period to the other are located in northwestern Portugal. For the second period (1990–2019), satellite-based land cover data are available throughout the country on an annual timescale. Therefore, the evolution of vineyard and olive grove areas was analyzed to assess to what extent have these crops been expanded to more susceptible zones to bioclimatic shifts. To our knowledge, there are no related studies regarding oliviculture and viticulture that use the Köppen–Geiger climatic classification, the WBCS, as well as the compound BSEI to evaluate the bioclimatic shifts. Therefore, it

was not possible to compare the methodology used in this study since there are no similar cases for comparison.

The evolution in the vineyard cover area from 1990 to 2018 (Figure 7a) shows a bidirectional displacement, towards the regions with more extreme bioclimates in the territory. The vineyard area has been increasing in the relatively cool and humid regions of northwestern Portugal (Vinho Verde WR), as well as in the warm and dry regions of southern Portugal (Alentejo WR) (Figure S1). In effect, from 2018 to 2020, vineyard areas have increased in the north, e.g., in Minho 2267 ha, in Douro/Porto 3212 ha, but also southern Portugal, in Alentejo VR 513 ha (Table S3). These regions are, nevertheless, located in areas for which the BSEI indicates stronger bioclimatic shifts during the last decades (Minho WR, Douro/Porto WR, and Alentejo WR). Even though the increase in the vineyard area in regions with cooler and more humid climates can be considered a climate-smart adaptation strategy, thus enhancing the climate resilience of the sector, the pronounced bioclimatic shifts observed in these regions may considerably affect the regional terroirs and, as a result, the wine typicity and style [40]. In addition, the emergence of vast areas with irrigated vineyards under the typically warm and dry conditions of southern Portugal will threaten the already limited water resources [41], thereby requiring more efficient water management and water-saving agricultural practices. The lack of water availability may indeed challenge the future sustainability of the sector in this region. This will be particularly relevant under the projected future warmer and drier climates, which will exacerbate the current warm and dry conditions, becoming irrigation even more vital [20].

As for viticulture, the olive grove land cover in Portugal has been changing between 1990 and 2018 (Figure S3). These fluctuations have also impacted olive yield, which was approximately 700,000 t in 2019 (Figure S4). The recent area expansion occurred mainly in the Faro, Beja, Vila Real, and Bragança districts, the last two showing relatively high BSEI (Figure 6b). Regions in the north are indeed gradually experiencing climatic conditions that were more typical of southern Portugal a few decades ago and are, thereby, becoming more suitable for oliviculture. Although the area of olive groves has undergone a significant increase in southern Portugal, most of them irrigated, the progressively higher relative coverage in cooler climates, still predominantly rainfed orchards, may already suggest higher awareness and a more or less conscious attempt of the sector to adapt to the ongoing climate change. It is worth mention that the construction of the Alqueva dam in the Guadiana River, which has created one of the biggest artificial lakes in Europe had a huge impact in the inner southern region of mainland Portugal. The increase in the regional water resources, allowed the implementation of a wide water distribution and irrigation systems. This fact influenced the expansion of vineyards and olive groves, among other cultures in this region during the timeframe analyzed in this study.

5. Conclusions

The present study assessed the climate change trends that have already influenced the Köppen–Geiger climate classification and the WBCS between 1950 and 2019 in mainland Portugal. For this purpose, a comparison between two 30-year periods, i.e., 1950–1979 and 1990–2019, was undertaken for these two climate classifications. It is worth mentioning that these calculations were carried out using high-resolution gridded datasets, with approximately 1 km grid resolution, thus providing accurate and detailed information throughout the country. To our knowledge, this is the first study analyzing these climate classifications in Portugal at such a high resolution.

The spatial representation of the Köppen–Geiger climate classification revealed three climate types (Figure 3a) in 1950–1979. The leading climate type was CSa, in 53.9% of the territory, CSb in 45.8%, and a very small percentage of 0.03% for Cfb. The CSa type was predominant in the southern half of Portugal and a narrow region in the south of the Vila Real and Bragança districts (Figures 1a and 3a). The CSb was dominant throughout most of the northern half of Portugal, mostly northwards of the Tagus River basin. However, a clear bioclimatic shift in 1990–2019 was detected, with an increase of +18.1% in CSa type,

associated with hot summers, and a corresponding decrease of −17.8% in CSb, associated with warm summers, and therefore, a milder climate (Table 5). These findings are in general agreement with Andrade and Contente [25].

The results also hint at shifts in the WBCS four major divisions from 1950–1979 to 1990–2019, related to a decrease of −5.11% in the temperate macroclimate in the northwest, followed by an increase in the Mediterranean macroclimate. This change impacted the bioclimates since a transition from three bioclimates in 1950–1979 to four bioclimates in 1990–2019 was identified, with the decrease of −5.14% for Teoc, counterbalanced by an increase of +4.78% for Mepo. As previously, these changes have occurred mainly in the northwestern regions of Portugal (Figure 4a,d). The ombrotypes changed from seven to eight types (Figure 4b,e), with a new ombrotype, Sas, within the semi-arid ombrothermic horizons, corresponding to +0.74% of the territory in 1990–2019 (Table 6). The overall decrease of −12.17% in the percentage of the territory of humid and hyper-humid regions (Sui, Hui, Hus and Hhi), in detriment of an increase of +24.81% of semi-arid and arid for 1990–2019, is particularly noteworthy.

For the thermotypes, a loss of 7.12% in the percentage of the territory associated with all temperate thermotypic horizons was found (Table 6). Within the Mediterranean thermotypic horizons, changes were also found. There was a major increase in the thermomediterranean horizons of +18.9%. For the mesomediterranean horizons, a decrease of −8.10% for Mmei, an increase of +4.74% for Mmes, followed by a loss of −8.9% in supramediterranean thermotypic horizons were identified in 1990–2019. Overall, in the southern half of the country (Figure 4c,f), a gain of thermomediterranean horizons, associated with more arid/dry conditions, was observed. On the other hand, the loss of both Mediterranean and temperate thermotypic horizons, with milder conditions, was registered in the northwesternmost regions. Climate shifts were observed in the major divisions of the WBCS classification are in clear accordance with the study of Andrade and Contente [11] for the IP. The changes in WBCS have direct implications in the regional exposure to bioclimatic shifts, measured by BSEI. At the district level, the Braga district (in the northwest) is the most exposed (BSEI = 3), followed by Viana do Castelo, Vila Real, Porto, also in the north, Viseu and Guarda in the center; and Évora in the south (BSEI = 2).

For both grapevines and olive trees, which are major crops in Portugal, the results highlight the growth in their land cover areas in southern regions that are becoming dryer. Furthermore, the vineyard area is increasing in the northwest, in regions that present higher values of BSEI, hence more exposed to recent past bioclimatic shifts. This may significantly affect the regional terroirs, grape berry attributes, and wine typicity and style. Conversely, the relative share of southern Portugal to the total olive grove area has been decreasing, which may already suggest an adaptation strategy of the sector, by progressively relocating olive orchards in northern regions that are currently experiencing similar conditions to those found in southern regions a few decades ago.

Both viticulture and oliviculture may be particularly challenged under future climate change scenarios, as suggested by Fraga et al. [20] for viticulture in Portugal, or by Fraga et al. [42] and Fraga et al. [43] for olive yields in Portugal and the Mediterranean region, respectively. As a result, better planning of the distribution of these key crops in Portugal should be envisioned, avoiding the increasing dependence on irrigation, which will eventually disrupt local and regional surface and underground water resources [44]. New agricultural practices and options are urging to enhance the water use efficiency of crops [45]. New water-saving and go-green policies and strategies will be particularly relevant under the projected future warmer and drier climates in Portugal [40,46]. On the other hand, warranting the future environmental and socio-economic sustainability of these sectors is of foremost relevance for the national economy and food security, thereby deserving further research. As similar problems can be found in many other regions with Mediterranean-type climates, the main outcomes from this study can be easily extrapolated to other countries worldwide.

Supplementary Materials: The following are available online at https://www.mdpi.com/article/10.3390/land10080869/s1, Table S1: Criteria to calculate the Köppen-Geiger classification for the main climates and subsequent precipitation conditions for the first two letters. For the polar climates (E) no precipitation differentiations are given, only temperature conditions are defined, consequently, the polar climates (E) must be determined first, followed by the arid climates (B) and subsequent differentiation into the equatorial climates (A) and the warm temperate and snow climates (C) and (D), respectively; Table S2: Criteria for the third letter temperature classification (h and k) for dry climates (B) and (a to d) for the warm temperate (C) and continental (D) climates following the Köppen's climate classification; Table S3: Vineyard land cover evolution (in ha) over mainland Portugal, by Wine Region; Figure S1: Viticulture regions (IGP or VR) in mainland Portugal with the associated Control origin denomination (DOC); Figure S2: Evolution of the total wine production (in hl) by viticulture region and subtotal for mainland Portugal for 2009, 2018/19, 2019/20, and 2020/21; Figure S3: Evolution of the total olive grove areas (in ha) for mainland Portugal between 1990 and 2018; Figure S4: Evolution of the total olive production (in ton) for mainland Portugal between 2000 and 2020.

Author Contributions: For this research, the author's contributions were: conceptualization, C.A. and J.A.S.; methodology, C.A. and J.A.S.; software, C.A. and A.F.; validation, C.A. and J.A.S.; formal analysis, C.A., A.F., J.A.S.; investigation, C.A., A.F., J.A.S.; resources, C.A. and A.F.; data curation, C.A. and A.F.; writing—C.A.; writing—C.A. and J.A.S.; visualization, C.A. and A.F.; supervision, C.A. and J.A.S.; project administration, J.A.S.; funding acquisition, J.A.S. All authors have read and agreed to the published version of the manuscript.

Funding: This study was funded by the European Commission-funded project "Climate Change Impact Mitigation for European Viticulture: Knowledge Transfer for an Integrated Approach—Clim4Vitis" [grant 810176]. This research was also supported by National Funds from FCT—Portuguese Foundation for Science and Technology, under the project UIDB/04033/2020.

Institutional Review Board Statement: Not applicable.

Informed Consent Statement: Not applicable.

Data Availability Statement: Not applicable.

Conflicts of Interest: The authors declare no conflict of interest.

References

1. Climate Change and Land, An IPCC Special Report on Climate Change, Desertification, Land Degradation, Sustainable Land Management, Food Security, and Greenhouse gas fluxes in Terrestrial Ecosystems, Summary for policymakers. 2019. Available online: https://www.ipcc.ch/srccl/ (accessed on 9 July 2021).
2. Tasser, E.; Leitinger, G.; Tappeiner, U. Climate Change versus Land-Use Change—What Affects the Mountain Landscapes More? *Land Use Policy* **2017**, *60*, 60–72. [CrossRef]
3. Ellis, E.C. Sustaining biodiversity and people in the world's anthropogenic biomes. *Environ. Sustain.* **2013**, *5*, 368–372. [CrossRef]
4. Martins, I.S.; Proença, V.; Pereira, H.M. The unusual suspect: Land use is a key predictor of biodiversity patterns in the Iberian Peninsula. *Acta Oecol.* **2014**, *61*, 41–50. [CrossRef]
5. Haberl, H.; Erb, K.H.; Krausmann, F.; Gaube, V.; Bondeau, A.; Plutzar, C.; Gingrich, S.; Lucht, W.; Fischer-Kowalski, M. Quantifying and mapping the human appropriation of net primary production in earth's terrestrial ecosystems. *Proc. Natl. Acad. Sci. USA* **2007**, *104*, 12942–12947. [CrossRef] [PubMed]
6. Fernández-Nogueira, D.; Corbelle-Rico, E. Land Use Changes in Iberian Peninsula 1990–2012. *Land* **2018**, *7*, 99. [CrossRef]
7. Van Vliet, J.; de Groot, H.L.F.; Rietveld, P.; Verburg, P.H. Manifestations and Underlying Drivers of Agricultural Land Use Change in Europe. Landsc. *Urban Plan.* **2015**, *133*, 24–36. [CrossRef]
8. Levers, C.; Butsic, V.; Verburg, P.H.; Müller, D.; Kuemmerle, T. Drivers of Changes in Agricultural Intensity in Europe. *Land Use Policy* **2016**, *58*, 380–393. [CrossRef]
9. De Chazal, J.; Rounsevell, M.D.A. Land-Use and Climate Change within Assessments of Biodiversity Change: *A Review*. *Glob. Environ. Chang.* **2009**, *19*, 306–315. [CrossRef]
10. Lindner, M.; Maroschek, M.; Netherer, S.; Kremer, A.; Barbati, A.; Garcia-Gonzalo, J.; Seidl, R.; Delzon, S.; Corona, P.; Kolström, M.; et al. Climate Change Impacts, Adaptive Capacity, and Vulnerability of European Forest Ecosystems. *For. Ecol. Manag.* **2010**, *259*, 698–709. [CrossRef]
11. Andrade, C.; Contente, J. Climate change projections for the Worldwide Bioclimatic Classification System in the Iberian Peninsula until 2070. *Int. J. Climatol.* **2020**, *40*, 5863–5886. [CrossRef]

12. Diffenbaugh, N.S.; Pal, J.S.; Giorgi, F.; Gao, X. Heat Stress Intensification in the Mediterranean Climate Change Hotspot. *Geophys. Res. Lett.* **2007**, 34. [CrossRef]
13. Diffenbaugh, N.S.; Giorgi, F. Climate Change Hotspots in the CMIP5 Global Climate Model Ensemble. *Clim. Chang.* **2012**, *114*, 813–822. [CrossRef]
14. Andrade, C.; Leite, S.M.; Santos, J.A. Temperature Extremes in Europe: Overview of Their Driving Atmospheric Patterns. *Nat. Hazards Earth Syst. Sci.* **2012**, *12*, 1671–1691. [CrossRef]
15. Andrade, C.; Contente, J.; Santos, J.A. Climate Change Projections of Dry and Wet Events in Iberia Based on the WASP-Index. *Climate* **2021**, *9*, 94. [CrossRef]
16. Santos, J.A.; Belo-Pereira, M.; Fraga, H.; Pinto, J.G. Understanding Climate Change Projections for Precipitation over Western Europe with a Weather Typing Approach. *J. Geophys. Res. Atmos.* **2016**, *121*, 1170–1189. [CrossRef]
17. Santos, M.; Fonseca, A.; Fragoso, M.; Santos, J.A. Recent and Future Changes of Precipitation Extremes in Mainland Portugal. *Theor. Appl. Climatol.* **2019**, *137*, 1305–1319. [CrossRef]
18. Scoccimarro, E.; Villarini, G.; Vichi, M.; Zampieri, M.; Fogli, P.G.; Bellucci, A.; Gualdi, S. Projected Changes in Intense Precipitation over Europe at the Daily and Subdaily Time Scales. *J. Clim.* **2015**, *28*, 6193–6203. [CrossRef]
19. Vidal-Macua, J.J.; Ninyerola, M.; Zabala, A.; Domingo-Marimon, C.; Gonzalez-Guerrero, O.; Pons, X. Environmental and socioeconomic factors of abandonment of rainfed and irrigated crops in northeast Spain. *Appl. Geogr.* **2018**, *90*, 155–174. [CrossRef]
20. Fraga, H.; de Cortázar Atauri, I.G.; Santos, J.A. Viticultural Irrigation Demands under Climate Change Scenarios in Portugal. *Agric. Water Manag.* **2018**, *196*, 66–74. [CrossRef]
21. Fraga, H.; Santos, J.A. Assessment of Climate Change Impacts on Chilling and forcing for the Main Fresh Fruit Regions in Portugal. *Front. Plant. Sci.* **2021**. [CrossRef]
22. Köppen, W.; Geiger, R. *Handbuch der Klimatologie*; Gebrüder Bornträger: Berlin, Germany, 1930; Volume 6.
23. Rivas-Martínez, S.; Sáenz, S.R.; Penas, A. Worldwide bioclimatic classification system. *Glob. Geobot.* **2011**, *1*, 1–634. [CrossRef]
24. Rivas-Martínez, S.; Penas, A.; del Río, S.; González, T.; Rivas-Sáenz, S. Bioclimatology of the Iberian Peninsula and the Balearic Islands. In *The Vegetation of the Iberian Peninsula.Plant and Vegetation*; Loidi, J., Ed.; Springer: Cham, Switzerland, 2017; Volume 12. [CrossRef]
25. Andrade, C.; Contente, J. Köppen's climate classification projections for the Iberian Peninsula. *Clim. Res.* **2020**, *81*, 71–89. [CrossRef]
26. Fernández-Nogueira, D.; Corbelle-Rico, E. Determinants of Land Use/Cover Change in the Iberian Peninsula (1990-2012) at Municipal Level. *Land* **2019**, *9*, 5. [CrossRef]
27. Turpin, N.; Berge, H.T.; Grignani, C.; Guzmán, G.; Vanderlinden, K.; Steinmann, H.H.; Siebielec, G.; Spiegel, H.; Perret, E.; Ruysschaert, G.; et al. An Assessment of Policies Affecting Sustainable Soil Management in Europe and Selected Member States. *Land Use Policy* **2017**, *66*, 241–249. [CrossRef]
28. Jones, N.; de Graaff, J.; Rodrigo, I.; Duarte, F. Historical Review of Land Use Changes in Portugal (before and after EU Integration in 1986) and Their Implications for Land Degradation and Conservation, with a Focus on Centro and Alentejo Regions. *Appl. Geogr.* **2011**, *31*, 1036–1048. [CrossRef]
29. Available online: https://www.ivv.gov.pt/np4/499/ (accessed on 30 June 2021).
30. Available online: https://www.oiv.int/public/medias/7909/oiv-state-of-the-world-vitivinicultural-sector-in-2020.pdf (accessed on 9 July 2021).
31. Available online: https://www.ivv.gov.pt/np4/7179.html (accessed on 9 July 2021).
32. Available online: https://www.ivv.gov.pt/np4/163.html (accessed on 9 July 2021).
33. Available online: https://www.gpp.pt/images/PEPAC/Anexo_NDICE_ANLISE_SETORIAL___AZEITE.pdf (accessed on 30 June 2021).
34. Fonseca, A.R.; Santos, J.A. High-resolution temperature datasets in Portugal from a geostatistical approach: Variability and extremes. *J. Appl. Meteorol. Climatol.* **2018**, *57*, 627–644. [CrossRef]
35. NASA. NASA Shuttle Radar Topography Mission Global 3 Arc Second Subsampled [Data Set]. Available online: https://lpdaac.usgs.gov/products/srtmgl3v003/ (accessed on 17 August 2021).
36. Available online: https://snig.dgterritorio.gov.pt/ (accessed on 30 June 2021).
37. Kottek, M.J.; Grieser, C.; Beck, B.; Rudolf, R. World map of the Köppen–Geiger climate classification updated. *Meteorol. Z.* **2006**, *15*, 259–263. [CrossRef]
38. Wilcoxon, F. Individual comparisons by ranking methods. *Biom. Bull.* **1945**, *1*, 80–83. [CrossRef]
39. Mann, H.B. Non-parametric tests against trend. *Econometrica* **1945**, *13*, 245–259. [CrossRef]
40. Santos, J.A.; Fraga, H.; Malheiro, A.C.; Moutinho-Pereira, J.; Dinis, L.-T.; Correia, C.; Moriondo, M.; Leolini, L.; Dibari, C.; Costafreda-Aumedes, S.; et al. A review of the Potential Climate Change Impacts and Adaptation options for European Viticulture. *Appl. Sci.* **2020**, *10*, 3092. [CrossRef]
41. Costa, J.M.; Oliveira, M.; Egipto, R.J.; Cid, R.J.; Fragoso, R.A.; Lopes, C.M.; Duarte, E.N. Water and Wastewater management for sustainable viticulture and oenology in south Portugal–A review. *Ciência Téc. Vitiv.* **2020**, *35*, 1–15. [CrossRef]
42. Fraga, H.; Pinto, J.G.; Viola, F.; Santos, J.A. Climate Change Projections for Olive Yields in the Mediterranean Basin. *Int. J. Climatol.* **2020**, *40*, 769–781. [CrossRef]

43. Fraga, H.; Moriondo, M.; Leolini, L.; Santos, J.A. Mediterranean Olive Orchards under Climate Change: A Review of Future Impacts and Adaptation Strategies. *Agronomy* **2021**, *11*, 56. [CrossRef]
44. Oliveira, M.; Costa, J.M.; Fragoso, R.; Duarte, E. Challenges for modern wine production in dry areas: Dedicated indicators to preview wastewater flows. *Water Supply* **2019**, *19*, 653–661. [CrossRef]
45. Martins, A.A.; Araújo, A.R.; Graça, A.; Caetano, N.S.; Mata, T.M. Towards sustainable wine: Comparison of two Portuguese wines. *J. Clean Prod.* **2018**, *183*, 662–676. [CrossRef]
46. Fraga, H.; Malheiro, A.C.; Moutinho-Pereira, J.; Santos, J.A. Future scenarios for viticulture zoning in Europe: Ensemble projections and uncertainties. *Int. J. Biometeorol.* **2013**, *57*, 909–925. [CrossRef]

land

MDPI

Article

Linking Morphological Spatial Pattern Analysis and Circuit Theory to Identify Ecological Security Pattern in the Loess Plateau: Taking Shuozhou City as an Example

Ronglei Yang [1], Zhongke Bai [1,2,*] and Zeyu Shi [1]

[1] School of Land Science and Technology, China University of Geosciences, Beijing 100083, China; 3012160004@cugb.edu.cn (R.Y.); 3012200007@cugb.edu.cn (Z.S.)
[2] Key Laboratory of Land Consolidation and Rehabilitation, The Ministry of Land and Resources, Beijing 100035, China
* Correspondence: baizk@cugb.edu.cn

Abstract: Located in an ecologically fragile area in China's eastern part of the Loess Plateau, Shuozhou City has faced environmental challenges imposed by frequent urban expansion and mining activities in recent years. As ecological security patterns (ESP) identification and optimization are significant to regional biodiversity and ecosystem services, this study combined morphological spatial pattern analysis (MSPA) and circuit theory to construct and optimize regional ESP. Results show the number and area of ecological sources in the study area decreased from 21 to 20 between 2010 and 2017. The total area of ecological sources fell from 1923.35 km^2 to 1869.37 km^2, with their proportion in the study area dropped from 18.14% to 17.64%. From 2010 to 2017, the number of obstacles increases from 63 to 80, mainly consisting of farmland, unused land, transportation land, and construction land. The area of obstacles reached 10.17 km^2 in 2017. A framework of "one protection area, two regulation areas, and three restoration areas" is proposed to optimize the ESP of the study zone. This study explored a combination of ESP analysis tools and focused on improving regional ecosystem service and biodiversity. It will support local urban planning and provide a reference for similar studies in resource-based cities.

Keywords: ecological security pattern; loess plateau; Shuozhou city; circuit theory; MSPA

Citation: Yang, R.; Bai, Z.; Shi, Z. Linking Morphological Spatial Pattern Analysis and Circuit Theory to Identify Ecological Security Pattern in the Loess Plateau: Taking Shuozhou City as an Example. *Land* **2021**, *10*, 907. https://doi.org/10.3390/land10090907

Academic Editor: Baojie He

Received: 1 August 2021
Accepted: 25 August 2021
Published: 28 August 2021

1. Introduction

With the development of science and technology and population growth, large-scale urbanization has occurred worldwide in the past few decades, which has also exacerbated many environmental problems such as global warming, vegetation destruction, the sharp decline in biodiversity, and disorder of biogeochemical cycles [1–3]. According to United Nations projections, more than 66% of the world's population will live in cities, posing a challenge to a stable and sustainable human society-natural coupling ecological security [4]. The rapid increase in urban population and area of artificially disturbed land has led to the damage of regional environment and the degradation of ecosystem services and the loss of the original stable and sustainable landscape pattern [4,5]. It is necessary to address the threat to the ecological environment brought by urban expansion and other human activities such as coal mining, and ensure landscape connectivity and ecological security [2,5,6].

Regarded as an efficient tool to guarantee regional ecosystem security, the concept of ecological security pattern (ESP) refers to the landscape's elements essential to the health and sustainability of ecological processes [1,6–8]. ESP mainly consists of ecological sources, corridors, and important ecological components that characterize regional ecosystem integrity and health [6,9]. In a narrow sense, ESP is a visual objective of ecosystem-based management [7]. Generally, ESP has vital ecological significance for ecosystem services and biodiversity by focusing on ecological processes and functions [10,11]. Some countries, such as

China, have incorporated the ESP concept into their policy-making process [7]. Furthermore, the construction and optimization of ESPs can balance economic development and regional protection, promote ecosystem services, and maintain regional biodiversity [2,9,11].

As integrated use of ecological analysis tools proved to be effective in contributing planning process, the integrative method of MSPA and circuit theory is an innovative path in ESP research [1,8,12]. The "source-corridor" combination method to identify and construct the ESP constitutes the preliminary mainstream construction paradigm of the ESP [1,13]. While some researchers directly choose forest patches or conservation areas as ecological sources, a growing number of studies applied landscape metrics and graph theory into their research to reduce subjective interferences and improve functional connectivity [1,5,14]. Among these connectivity models are the minimum cumulative resistance (MCR) model, morphological spatial pattern analysis (MSPA), circuit theory, matrix theory, and agent or individual-based modeling [1,5,15]. Ecological sources identification is a crucial starting part of ESP analysis. Although many ecological sources identification studies applied evaluation based on ecosystem services, MSPA has been increasingly involved in this field [16]. MSPA approach is designed to use binary graphs when processing recognition. It only relies on land-use data to identify core ecological patches and emphasizes the structural connection [1]. Except for being used to assess ecological connectivity of green infrastructure, MSPA can also map the ecological land patches while has no limitation on scale or type of image based on geometric concepts [16,17]. Ecological corridors assessment can be conducted by different models. Although the MCR model based on graph theory has been widely used to identify ecological corridors in an ESP, it has obvious disadvantages in revealing the differences in the ecological potential of different ecological sources. It ignores the random walking characteristics of species [2,8]. Instead, ecological corridors can be identified in circuit theory by assigning physical quantities new ecological connotations such as current, conductivity, and voltage [1,2,18]. Circuit theory considers ecological resistance value as the impedance value, and ecological flow represents random walk current [19,20]. In brief, the MSPA mainly focuses on landscape structural analysis, while the circuit theory primarily focuses on functional connectively. However, not many studies in ESP have applied the MSPA approach or circuit theory despite their advantages above. ESP identification should consider both structural and functional connectivity and might be helpful to promote the practical utility of ecology methods for urban spatial planning [1,5]. Specifically, small steppingstones (ecological obstacles) identified in circuit theory significantly impact on promoting landscape connectivity [1].

Regarding ESP optimization, scholars mainly focus on goals such as increasing landscape connectivity, increasing ecological source functions (ecosystem services), protecting and restoring steppingstones (obstacles) and maintaining biodiversity [1,7,8]. The protection of narrow ecological corridors and steppingstones is proposed to keep the ecosystem healthy [1,21]. Meanwhile, planners are suggested to balance the expansion of urban and the protection of habitats to maintain biodiversity [5]. In coal mining cities, regulation zones are proposed to facilitate natural protection and resource exploitation as areas of high ecological resistance coefficient are primarily located near coal mines [8]. As splitting green urban zones into different classes would be helpful to distinguish different supplies of different ecosystem service better, proper urban spatial optimization based on ESP analysis is essential to ensure the ecological processes continuity and ecosystem services flow [5,8]. ESP optimization focusing on the reconfiguration of land-use/land cover (LUCC) to maximize urban ecosystem services while long-term planning can adopt model reveal the optimal solutions and nature-based solutions addressing sustainability challenges. Studies have shown LUCC caused mass ecosystem service value (ESV) loss, especially during urban expansion, which is highly related to ecological problems [22–24]. In China, with rapid urbanization expansion, improving ESV and maintaining biodiversity based on LUCC is the core content and the primary significance of ESP optimization in this study [25]. Optimization of land-use structure has been proved to be worth considering by land managers and city planners, while well-regarded ecosystem assessment standards usually lack spatial details [25,26].

For decades, mining activity and urban expansion have been causing severe ecological problems in China's resource-based cities [8]. Located in eastern Loess Plateau, Shuozhou City is one of China's most important coal mining bases, the same as Ordos City and Yulin City [27]. The quality of the local ecosystem is considered to have an essential impact on the ecological environment of the surrounding area. Hence, it is vital to stabilize the local ecological environment and promote sustainable urban development. Carrying out an analysis of the ESP for Shuozhou City will help improve the safety and stability of the local ecosystem services and provide a robust ecological barrier for the soil conservation area of the Loess Plateau and the water conservation area in the north of Beijing-Tianjin-Hebei. Therefore, this study combined the MSPA approach and circuit theory to conduct an ESP analysis of Suzhou City. Questions explored are as below: (1) How to quantitatively analyze and determine the ecological source/areas of Shuozhou City in different years from the perspective of structure and process, (2) how to combine MSPA model and circuit theory to construct ESP in the study area, and (3) how to optimize the ESP in the study area based on ecological sources, corridors, and obstacles. This study will helps to improve the landscape connectivity and ESV of the study area and provide reference for ESP analysis in similar areas.

2. Materials and Methods

2.1. Study Area

Located in the northwestern part of Shanxi Province and east of China's Loess Plateau, Shuozhou City covers an area of 10,600 km^2, accounting for 6.8% of the land area of Shanxi Province (Figure 1). It consists of one county-level city, two districts, and three counties. The annual average rainfall is 420 mm, and the evaporation is large and unevenly distributed; the yearly average temperature is 5.5 °C. The landform of Shuozhou City is divided into mountains, hills, and plains, mainly composed of three ecosystems: farmland, shrubland, and grassland. The mountain area is 2678 km^2, the hill area is 3682 km^2, and the plain area is 4204 km^2, accounting for 25.35%, 34.85%, and 39.80% of the city's area, respectively.

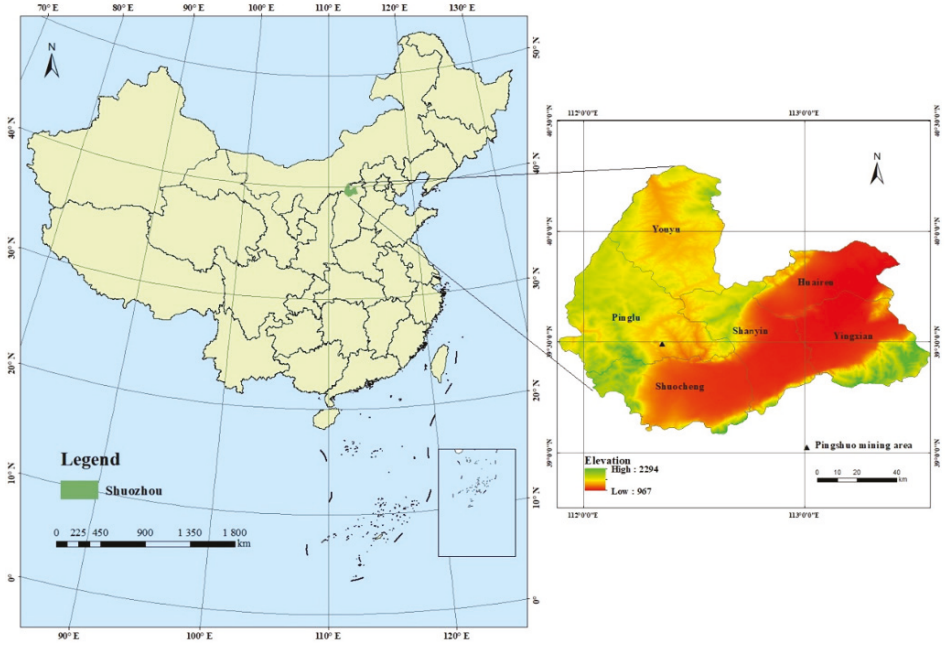

Figure 1. The spatial location of the study area.

Shuozhou City represents a batch of emerging coal mining towns in central and northern China [28]. Among the six counties and districts in the city, only Ying county has no mining conditions. In comparison the other five counties and districts are large coal producing counties, among which Shuocheng District, Pinglu District, Shanyin County, and Huairen City are national key coal-producing bases. Opencast mining is the foremost coal mining approach in Shuozhou City, with the Pingshuo mine (one of the largest opencast coal mines in China) located in the southwest of the city [28]. Ecological restoration in the Pingshuo mine's adjacent area was initiated in 1988, and most reclaimed land is used for forest and farmland [29]. Overall, this study area is a specific ecologically fragile area on the Loess Plateau in northern China. According to the Ministry of Environmental Protection of the PRC, Shuozhou City mainly consists of three ecosystems: farmland, shrubland, and grassland. The importance of environmental protection in this area is ranked as extremely high [30]. It is adjacent to the soil conservation area of the Loess Plateau and the water conservation area in the north of Beijing-Tianjin-Hebei, an important ecological function area in China [31]. The agricultural land in Shuozhou City is mainly medium and low-yield land, with a large proportion of low-yield land. There are also problems of soil desertification and salinization. The soil fertility of farmland is low, and the nutrient content is lower than other places of the Shanxi province. Regional ecological problems are mainly as bellows: soil desertification and soil erosion caused by natural and human activities, soil salinization concentrated in the Sanggan River Basin, and low utilization efficiency of natural reserves such as saline-alkali land.

2.2. Data Sources

The research data mainly includes land-use data for the three phases of 2010, 2015, and 2017 and digital elevation model (DEM) data has a resolution of 30 m (Table 1). Use ENVI 5.2 software to preprocess the fourth-phase remote sensing images such as radiation calibration, atmospheric correction, and splicing, and extract the normalized vegetation index, temperature vegetation drought index, and impervious surface coefficient. With land-use data collected from Shuozhou City government and online remote sensing data, the land-use data was classified into forest land, wetland, grassland, orchard, farmland, unused land, transportation land, construction land (including urban land, rural residential area) and mining land. With the help of a Google image map, live images of ecological obstacles on the map are captured and displayed.

Table 1. Data sources and description.

Data Type	Data Time	Data Accuracy	Data Sources
Landsat 5 TM remote sensing image	2010/8, 2015/7, 2017/8	30 m, cloud cover is less than 5%	USGS (United States Geological Survey, https://earthexplorer.usgs.gov/, accessed on 1 June 2021)
Google Earth map	2020/9	Level 12	Google Earth
Land-use data	2010, 2015, 2017	Vector data	Resource and Environmental Science Data Center of Chinese Academy of Sciences (http://www.resdc.cn, accessed on 1 June 2021), Shuozhou City Government
Digital elevation model	2010	30 m	Geo-spatial data cloud (http://www.gscloud.cn/, accessed on 1 June 2021)
Study area boundary data	1989	Vector data	National Basic Geographic Information Center, Shuozhou City Government

2.3. Identify ESP

The paradigm of constructing an ecological security pattern is to develop a vital stereotype of a comprehensive network including ecological sources, corridors, and key nodes. The model consists of three steps. First of all, identify ecological sources based on

land-use data and the MSPA approach. Subsequently, constitute a resistance surface by setting different land-use types as essential resistance factors. The third step is to extract ecological corridors and obstacles based on circuit theory and multiple software modules. Lastly, ESP of the study area is identified, and optimization suggestions is proposed. Figure 2 shows the framework of the ESP identification process in this study.

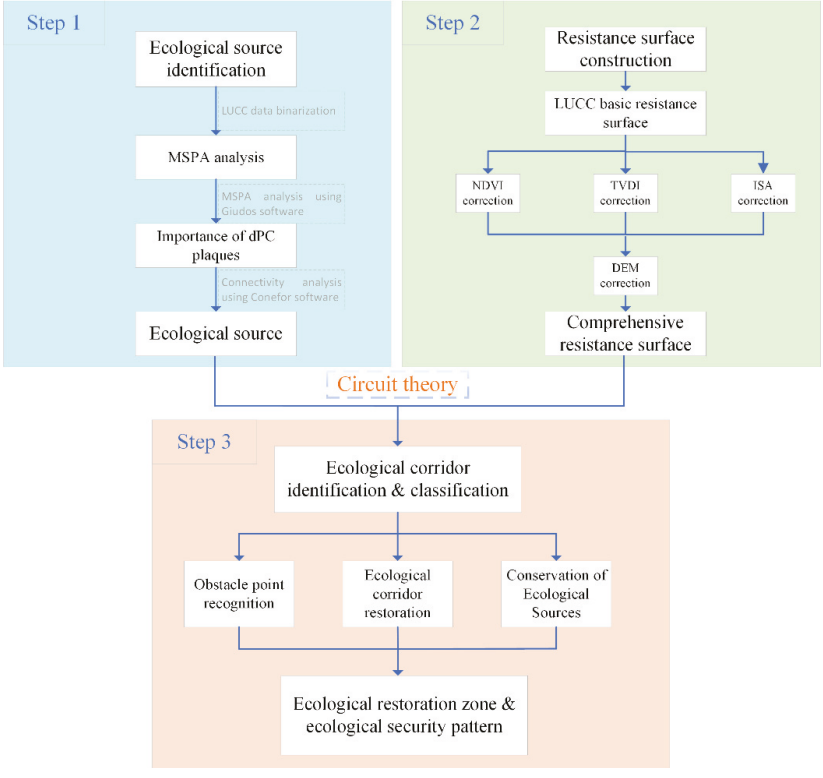

Figure 2. Framework for identifying ESP.

2.3.1. MSPA Pattern Analysis

The MSPA method can extract seven pattern classes at the pixel level, each of which has its own ecological meaning (Table 2). Using the MSPA method, the raster data of the current land-use needs to be binarized first, and the new layer generated only includes foreground data and background data. Through GUIDOS (Graphic User Interface for the Description of image Objects and their Shapes) software, geometric analysis is conducted on the spatial form of the foreground data [1]. Depending on the land-use type data collected, this study set forest land, grassland, orchard, wetland, and water area as the foreground data and other land-use types as the background data for MSPA [2]. As edge width represents the size of the edge effect produced by the patch and will decide cell numbers identified as core patch, the edge width is set to the default value of 90 m during the pre-process of MSPA [16]. Considering the study area is relatively large, a cell scale of 90 m $\times$ 90 m is defined as the main ecological element in the study area. After data accuracy requirements are satisfied, MSPA patterns analysis is conducted with the help of GUIDOS software [1].

Table 2. MSPA pattern classes definition [1,16].

Pattern Class	Ecological Meaning
Core Islet	Large habitat patches can serve as source areas while also provide habitats or migration places for wildlife.
Perforation	Small patches weakly connected, providing places for species to spread and communicate and promoting matter and energy flow.
Edge	A transition area between the core patch and the non-green landscape area: the edge of the internal patch having edge effects.
Bridge	A transition zone between the core patch and the non-green landscape area; has an edge effect protecting the ecological process of the core area.
Loop	Connects corridors inside the same core area to provide access to species diffusion and energy exchange within the core patch.
Branch	Only one side is connected to an edge, bridge, loop, or perforation.

2.3.2. dPC Analysis Using Conefor 2.6

The probability of connectivity (PC) and the important values of the patches (dPCs) are vital to analysis in identifying ecological sources [8,10]. As landscape connectivity affects the degree of migration and movement of organisms between different patches, landscape connectivity is of great significance to ecological processes, biodiversity protection, and the balance of ecosystems [32,33]. Landscape connectivity can be divided into structural connectivity and functional connectivity [1,8]. Structural connectivity represents the physical landscape connectivity, which reflects the continuity of the landscape on a spatial scale. Regional connectivity of ecological processes is characterized by functional connectivity. Meaning the migration ability of different organisms to different landscapes, functional connectivity is more complicated to evaluate and is usually extended.

Conefor 2.6 is mainly a landscape connectivity recognition software developed by Santiago Saura and Josep Torne [34,35]. The software can calculate the degree of patch connectivity and identify core patches vital to ecological connectivity. The commonly used indicators are the overall connectivity index (IIC), the possible connectivity index (PC), and the patch importance index (dPC). This paper mainly selects the patch importance index (dPC) to evaluate the importance of the core area and determines the ecological source of study area by sorting the size of the patch importance index. The specific formula is shown in Formula (1).

$$\mathrm{dPC} = \frac{\mathrm{PC} - \mathrm{PC}_{\mathrm{remove}}}{\mathrm{PC}} \times 100\% \quad (1)$$

dPC demonstrates the importance of plaques, and the possible connectivity index of a particular patch is demonstrated by PC. The PC value is greater than or equal to 0 and less than or equal to 1. When the PC value grows, the connectivity of the patch is also improved. PC removal represents the possible connectivity index after removing the patch.

2.3.3. Resistive Surface Construction and Ecological Corridor Identification

In-circuit theory, the landscape is abstracted into units with different resistance values, reflecting the degree of a hindrance to the movement of species or energy in various landscape patches. Land-use types are widely applied in ecological resistance surfaces construction. Different land-use types can directly reflect the types of ecosystems and are the essential resistance factors of ecological resistance surfaces [36]. Concerning the research of Peng Jian et al. [37], the resistance value of each land-use type in the study area is set to 1~300: forest land is 1, the wetland is 5, grassland is 10, the orchard is 20, farmland is 50, unused land is 100, transportation land is 150, construction land is 200, and mining land is 300. Due to the difference in biophysical characteristics of the same land-use, the degree of obstacles formed is different, according to the normalized difference vegetation index (NDVI), temperature vegetation dryness index (TVDI), and waterproof surface coefficient. Impervious surface area (ISA) and DEM elevation data are used to

correct the resistance value. First, the study area's construction land and non-construction land (including forest land, grassland, orchard, wetland, farmland, water area, and other land types) are revised separately. Considering the impact of elevation differences on species movement and gene exchanges, DEM data was used for both construction land and non-construction land for correction. The normalized vegetation index reflects the vegetation coverage status and the quality of the habitat [38]; the temperature vegetation drought index can indicate the surface water content; the higher the value, the lower the surface water content [39,40]. The average annual evaporation of the study area is much greater than the precipitation. The surface water content is the main limiting factor for vegetation growth. Therefore, TVDI and NDVI are selected to correct the resistance value of non-construction land. The impervious surface index ISA is the proportion of waterproof materials in the pixel that reflects human activities intensity [41]. Use an impervious index to correct construction land resistance value. This paper constructs the resistance value formulas of different land types:

$$R = Cf \times R_i \quad (2)$$

In Formula (2): R_i represents the resistance value of ground category i; Cf is the correction coefficient, which is composed of TVDI, NDVI, ISA, and DEM. The calculation formula is as follows:

$$Cf = 1/2f + 1/2DEM \quad (3)$$

Use the Linkage Mapper tool on the ArcGIS 10.2 platform to extract the corridors with the least resistance to connecting ecological sources. The calculation steps are: create a weighted cost distance surface by calculating the cost weighted distance (CWD) from each pixel on the resistance surface to the nearest source; calculate the least cost path (LCP) in the direction of the ecological corridor; finally, set the cutoff Distance (this article put the cutoff distance to 5000) to generate galleries.

2.3.4. Obstacles Identification and Ecological Zoning

This indicates the area where the resistance to the movement of the species is more excellent between the source areas. The key point of restoration in this paper is the obstacle point located in the ecological corridor in 2017. After the restoration, the connectivity between the source areas can be greatly improved. By setting the search radius of the moving window, use the Barrier Mapper tool to identify obstacles. The experiment of adjusting the search radius shows that when the radius is less than 200 m, some obstacles are not recognized; the position of obstacles greater than 200 m remains unchanged, so this paper sets the search radius to 200 m. The ratio of the difference ΔLCD to the search radius D before and after the pixel resistance value is changed (ΔLCD/D, that is, the improvement per meter) is used to characterize connectivity improvement after the obstacle is removed. When the ratio increases, the degree of connectivity between the source areas also increases. After the obstacles are identified, they are superimposed with the current land-use map to analyze their current uses and formulate restoration strategies based on their spatial distribution. The systematic restoration of industrial and mining land should be continuously promoted from part to the whole, from meeting the necessary needs of ecological safety to improving conditions, forming a distribution of point, line, and surface restoration projects. Therefore, taking the urgency, completeness, and integrity of the system restoration as the goal, the key restoration points are set as the first-level restoration area. Except for the critical issues in 2017, the ecological corridors are selected as the second-level restoration area. The corridors that disappeared in 2000–2017 is designated as a three-level repair area.

3. Results

To fully demonstrate characteristics of ecological structure and function in the study area, this section consists of three parts. Land-use patterns, MSPA patterns, ecological

sources, ecological corridors, and obstacles are established in sequence. ESP identification and optimization are explored, focusing on obstacles restoration and environmental zoning.

3.1. Ecological Distribution Characteristics

Figures 3 and 4 show the spatial distribution and area changes of land-use types from 2010 to 2017. During this period, grassland, woodland, farmland, orchard, wetland, industrial and mining land, and unused land decreased. The decreasing rate was orchard (−5.39%) and unused land (−3.02%), industrial and mining land (−1.9%), grassland (−0.92%), woodland (−0.68%), wetland (−0.49%), and farmland (−0.19%). At the same time, from 2010 to 2017, the residential areas and transportation land area increased, with the area of residential areas increasing by 10.19% and the area of transportation land increasing by 8.54%. The growth of residential areas and transportation land is the most stable and significant. The expansion edge is mainly located in the residential area of Shuocheng District in the southwest. The expansion area of traffic land is mainly located between the residential areas of the counties, urban areas, and other areas—the traffic arteries of the city.

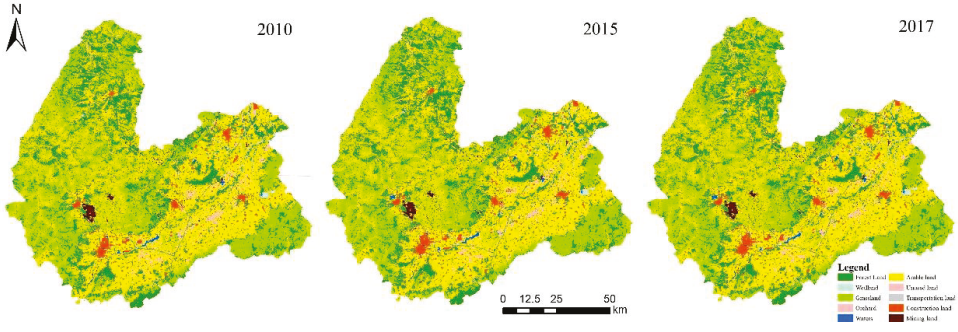

Figure 3. Land-use type distribution from 2010 to 2017.

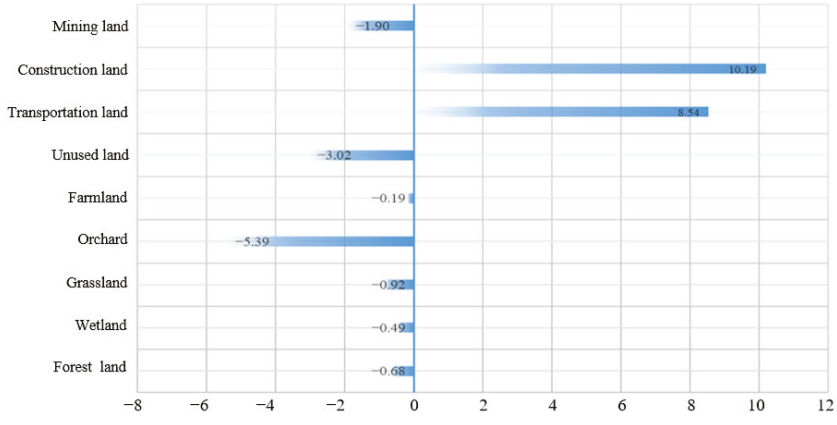

Figure 4. Percentage change of land-use type area from 2010 to 2017.

MSPA patterns distribution of study area from 2010 to 2017 is shown in Figure 5. As listed above, this study regards forest land, grassland, orchard, wetland, and water as the prospect analysis land categories of MSPA. The core area accounts for 52.93% of the foreground area. As structural corridors in the landscape, bridges account for about 8.36% of the total area of the foreground data. Both edges and perforations are affected

by edge effects; these regions account for 20.05% and 2.40% of the foreground data area, respectively. The branch is the interruption of the corridor connection, accounting for 8.90% of the foreground data area. Islets are isolated patches, accounting for approximately 5.19% of the foreground data area. Loop is conducive to species migration in the same patch, accounting for 2.17% of the prospect data area [1].

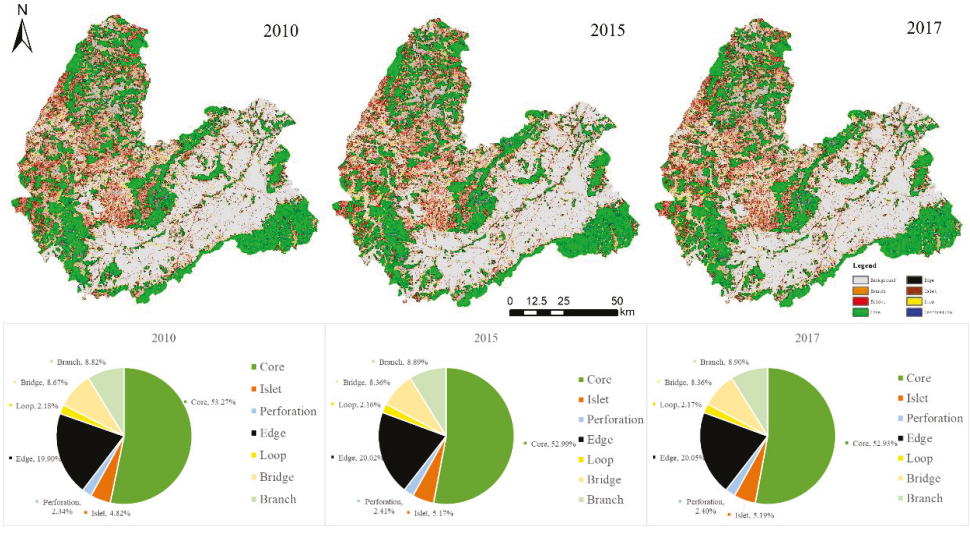

Figure 5. Distribution and proportion of pattern classes based on MSPA.

From 2010 to 2017, the number and area of Shuozhou City's ecological sources declined, and the ecological sources within the city were unevenly distributed. Figure 6 shows the ecological sources and resistance surface in 2010, 2015, and 2017. Results show that Shuozhou City had 21 ecological sources in 2010, 20 ecological sources in 2015, and 20 ecological sources in 2017. Among them, the ecological sources with dPC > 5 were 6, 5, and 5 in 2010, 2015, and 2017, respectively. These ecological sources with dPC > 5 are large-scale ecological patches. Nanshan Nature Reserve in Yingxian County in the southeast, Zijin Mountain Nature Reserve in Shuozhou City in the southwest, Sanggan River Reserve the north-central and northwest. These ecological sources are distributed in blocks or strips in the study area's outer suburbs and central area, such as the southeast, southwest, north-central, northwestern areas, and central-western and central-eastern parts of the hinterland of the study area. The ecological source is scarce in the other regions, and space is scattered, which significantly affects the local ecological connectivity. The total area of the three phases of ecological source areas are 1923.35 km^2, 1873.93 km^2, and 1869.37 km^2, respectively, accounting for 18.14%, 17.68%, and 17.64% of the total area. Focusing on 2017, the ecological sources marked by the red numbers 1 and 2 and 5 have remained stable. Still, the ecological source 3 increased significantly from 83.20 km^2 in 2010 to 176.12 km^2 with an increase of 111.68%. On the other hand, ecological source 4 decreased significantly with its area changing from 255.99 km^2 to 157.63 km^2 in 2017, dropping 38.42% in 7 years.

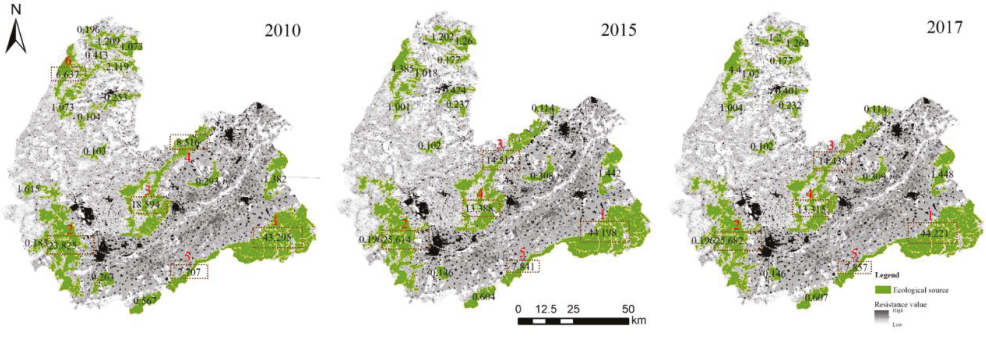

Figure 6. Ecological sources and resistance surface from 2010 to 2017. Black numbers as their dPC values represent the core patches' importance, while the red number represents the dPC rank, and the dPC value is greater than 5.

3.2. Ecological Corridors and Obstacles Identification

From 2010 to 2017, the number of ecological corridors in Shuozhou City decreased slightly, and the total length of the least costly path and the area of ecological corridors increased (Figure 7). The number of ecological corridors in 2010 was 34, and the number of ecological corridors in 2015 was 33. The total length of the minimum cost path increased from 555.95 km to 605.62 km, increasing 8.93%. It shows that the ecological source area of the study area saw a decline in landscape connectivity from 2010 to 2017, and the area with a significant decrease in connectivity was mainly located in Youyu County in the northern part of the study area. The scope of ecological source area decreased, and the length of ecological corridors increased. The area of potential ecological corridor restoration has increased. From 2010 to 2017, the areas of ecological corridors (corridor currents) in Shuozhou City were 567.63 km^2, 697.22 km^2, and 700.61 km^2, respectively, accounting for 5.36%, 6.58%, and 6.61% of the total area of Shuozhou City. From 2010 to 2017, the area of ecological corridors in Shuozhou City increased by 23.43%. It is found that the land-use types in the potential ecological corridor area in Shuozhou City in 2017 are mainly: woodland (65.45%), grassland (18.98%), farmland (9.03%), wetland (4.77%), the proportions of unused land, construction land, mining land, and transportation land are all less than 1%.

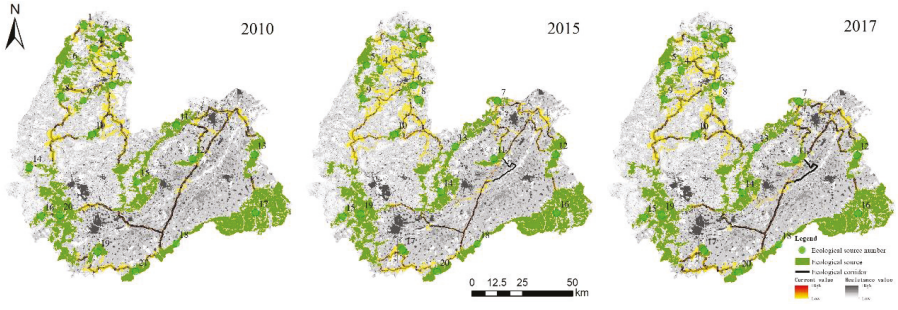

Figure 7. Ecological corridors and current distribution in corridors from 2010 to 2017. The black number is the ecological source number.

From 2010 to 2017, the number of obstacles in the study area increased, mainly distributed around residential areas, industrial and mining land, and transportation. The Barrier Mapper tool identified obstacles in the three phases of study areas as 63 in 2010, 69 in 2015, and 80 in 2017. The total area of obstacles in 2010–2017 was 7.88 km^2, 8.48 km^2, and 10.17 km^2. Among them, the obstacles on the corridor are 44 in 2010, 46 in 2015, and 54 in 2017. The total area of the obstacles on the corridor is 4.31 km^2, 5.01 km^2, and

6.10 km^2, respectively; most of them are located in the middle south area of Shuozhou City. Results show that land-use types in the obstacles are mainly farmland, unused land, transportation land, and construction land. In 2010, the proportion of farmland in the obstacles of Shuozhou City reached 72.84%, and the proportion of unused land reached 11.29%. In 2017, the proportion of farmland in the obstacles of Shuozhou City further increased to 80.88%, the proportion of unused land was 6.85%, and that of transportation land. The ratio is 4.27%, and construction land accounts for 4.15%. These blocks of human activity destroys local habitats' quality, and contiguous areas of unused land, transportation land, and construction land have separated the habitat.

3.3. ESP Identification and Optimization

Obstacle point analysis provides a visual representation of key elements that impact ecological connectivity and provides key information for ESP optimization [1]. Through the Barrier Mapper tool, 80 obstacles were identified in 2017, with an area of 10.17 km^2, of which 54 obstacles were located on the corridor, with an area of 6.1 km^2 (Figure 8). The land-use types of obstacles are mainly farmland, unused land, transportation land, and construction land. Obstacles in 2017 are distributed primarily on the eastern suburbs, the mining area in the north-central area, and the residential and mining areas in the south. These areas also have a certain amount of ecological corridors, but they are usually narrow. Therefore, repairing obstacles and even obstacles on ecological corridors is of great value to the overall landscape connectivity [1,8]. Obstacles with high ecological resistance coefficients are mainly distributed in farmland, residential areas, or around these areas [8]. As mentioned above, between 2010 and 2017, the residential regions in Shuozhou City increased by 10.19%, and the area of transportation land increased by 8.54%. Figure 8e,f show real-life photos of residential areas at obstacles. Such areas have a negative effect on the ESP. Therefore, the key to protecting and repairing such obstacles is to scientifically plan residential area expansion activities [2]. Timely ecological restoration of abandoned land in residential areas while strengthening vegetation restoration ensures connectivity between source areas. At the same time, transportation land increasing is highly related to the process of urban development. The negative effect of transportation land on the connectivity of the landscape pattern is worthy of attention, and their live pictures are shown as in Figure 8b–d.

Based on ESP identified above, it is suggested to establish a framework of "one protection area, two regulation areas, and three restorations area" to optimize the ESP of the study area (Figure 9) [8]. The ecological sources are unevenly distributed in the study area, the ecological corridors are tight and narrow, and the intensity of human construction disturbance is relatively high. First of all, setting a protection area of the ecological sources area is vital. According to the research results, the study area has 20 ecological sources in 2017, with an area of 1869.37 km^2, accounting for 17.64% of Shuozhou City. It is an important part of the ESP locally. Secondly, it regulates and supervises construction areas dominated by residential areas and transportation land and mining areas dominated by coal mines. The area is 549.79 km^2 and contains 53 mines. Regulation on construction land and mines can reduce the conflict and promote the long-term stability of the ESP. Additionally, limiting the uncontrolled growth of construction land will maximize urban ecosystem services [42]. Finally, delimit the three-level ecological restoration areas of Shuozhou City. It is suggested to set the obstacles as the first-level ecological protection and restoration area with an area of 10.17 km^2. The potential ecological corridor area in 2017 is proposed to be the secondary ecological protection and restoration area, which includes 33 ecological corridors and an area of 700.61 km^2. The ecological corridor area of 159.40 km^2 that disappeared from 2010 to 2017 is advised to be set as a tertiary ecological protection and restoration area because it has an excellent ecological endowment before being destroyed and can improve landscape connectivity. Land-use types in different restoration areas are shown in Table 3. In summary, the role and significance of zoning an optimized ESP are to ensure the ecosystem services of ecological sources, limit the

disruption of ecological connectivity by urban expansion and resource exploitation, and the decline and loss of ecosystem services [5,8,24]. Through the comprehensive optimization of points, lines, and planes (such as restoration of obstacles and ecological corridors, and protection of ecological sources), optimized ESP will improve ecological connectivity of the study area, promote regional ecosystem services, and maintain biodiversity by facilitating species migration across the whole area [1,9,42].

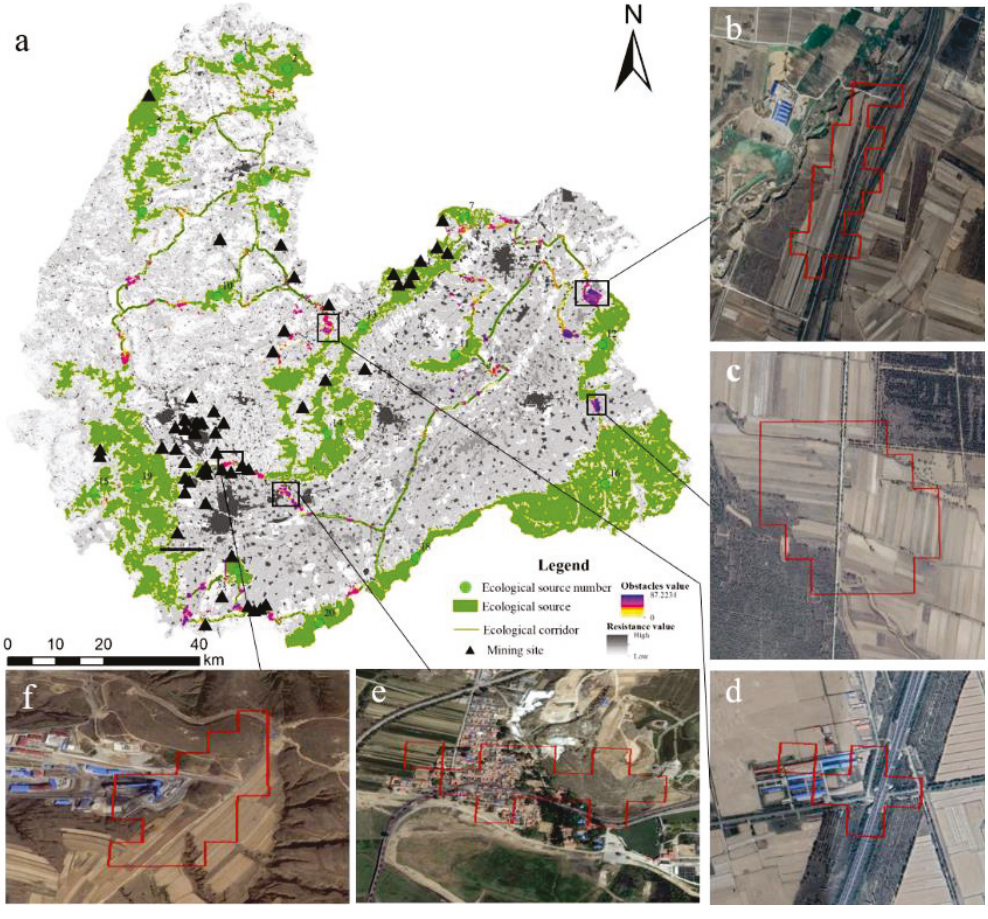

Figure 8. (**a**) Partial details of corridors and obstacles. Subfigures (**b**–**f**) are subfigures showing a real view of the obstacles.

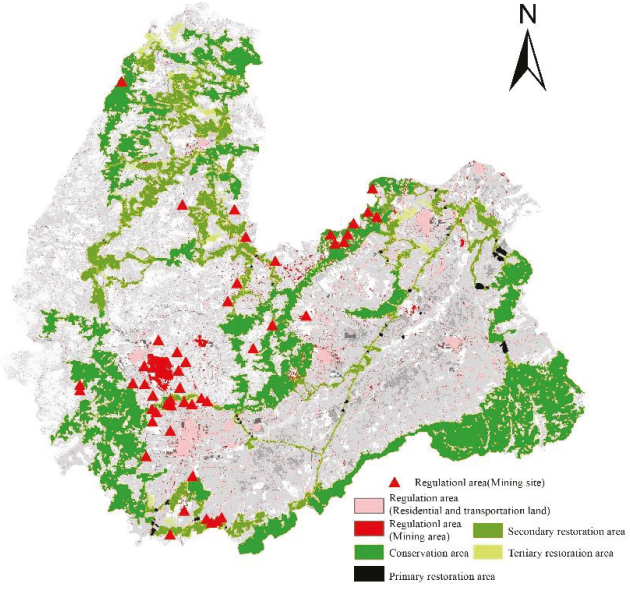

Figure 9. Ecological protection and restoration zoning.

Table 3. Proportion of land-use type area in tertiary ecological restoration zones in 2010 and 2017.

Land Type	2010			2017		
	Primary Restoration Area (%)	Secondary Restoration Area (%)	Tertiary Restoration Area (%)	Primary Restoration Area (%)	Secondary Restoration Area (%)	Tertiary Restoration Area (%)
Forest Land	3.68	66.49	51.66	1.90	65.45	50.42
Wetland	1.27	4.02	4.27	0.90	4.77	4.02
Grassland	0.89	18.77	0.09	0.97	18.98	20.84
Orchard	0.00	0.05	21.26	0.00	0.03	0.09
Farmland	72.84	9.03	19.09	80.88	9.03	19.32
Unused land	11.29	0.37	0.85	6.85	0.38	1.16
Transportation land	5.84	0.70	1.02	4.27	0.74	2.15
Construction land	4.19	0.43	0.35	4.15	0.48	1.65
Mining land	0.00	0.14	1.40	0.08	0.14	0.35

4. Discussion

4.1. Distribution Characteristics of Ecological Sources

Ecological sources are the cornerstone of the ESP and core patches that provide ecosystem service [1–3]. Expansion of construction land and long-term mining activities has a major impact on the disturbance of natural ecosystems, primarily distributed in the ecological source area. Landscape characteristics also have a significant impact. For example, ecosystems in Shuohzou City have to face the harsh challenges of high cold and drought. The factors above have caused Shuozhou City's ecosystem vulnerability. Therefore, identifying key ecological sources to protect is of great significance in protecting different ecosystems. The Sanggan River Basin, Nanshan Provincial Nature Reserve, and Zijinshan Provincial Nature Reserve are essential ecological barriers and oases in the study area. Long-term protection of these areas requires scientific planning by local government to active ecological conservation and restoration measures. Source 1 contains Yingxian Nanshan Provincial Nature Reserve and Yingxian Town Ziliang Provincial wetland parks, the former is a provincial forest ecological reserve in Shanxi, providing essential places

for wildlife and water conservation, and the latter, as wetland parks, provide habitats for migrating waterfowl and play an essential role in maintaining ecological security. Source 2 is the Zijinshan Provincial Nature Reserve in Shuozhou City, which plays a vital role as an ecological barrier to the severe land disturbances caused by mining and urban expansion in the east of the mining area, and to guarantee the sustainability of the ecosystem and optimize the ecology at the edge of urban growth. The environment provides essential value. Sources 3 and 4 are the Sanggan River Provincial Reserve in Shanxi. It is a nature reserve that mainly protects poplars, Pinus sylvestris, Pinus tabulaeformis plantations, and wild animals, migrating waterfowl, and their habitats. It is a wetland in Shanxi Province. The largest nature reserve in the area retains various ecological systems, which have the unique value of protecting the natural background, storing species, maintaining the value of natural aesthetics, and cultivating natural aesthetics. Source 5 as mainly consists of forest is located on the southern outskirts of the study area, which plays a vital role in constructing the "Southwestern Baili Ecological Corridor" in Shuozhou City. It is worth noting that the importance of ecological source patches in Youyu County, the northernmost part of Shuozhou City, declined between 2010 and 2017. The increase in the distance has served as a warning to the ESP of the region and the study area as a whole [1].

4.2. Multi-Year ESP Characteristics of Shuozhou City

The evaluation results show hidden dangers in the overall ESP, and the spatial distribution of ecological sources is unbalanced. While ecosystems and ecosystem services are pretty vulnerable to human activities, land-use change (mostly related to infrastructural development in the urban expansion process) is regarded as having a tremendous impact on ecosystem services [26,43]. For example, study shows that the global loss of ESV caused by land-use changes from 1997 to 2011 was 4.3–20.2 trillion USD per year [44]. Back to this research, the overall regional connectivity is poor, and the east–west faults are serious, increasing the resistance to the migration of biological species. The interference of the infrastructural development in urban expansion and coal mining aggravates the loss of ESV in the whole city area. The increase of construction land and the development of agricultural lands, such as farmland, also makes the habitat in the study area more fragmented and the connectivity further decreased, as shown in Table 3. The analysis of obstacles and ecological corridors shows that from 2010 to 2017, the fragmentation of ecological sources in Youyu County in the north of Shuozhou City has increased, and the weighted cost path has increased. However, the ecological corridors in the north are still dense and can be targeted. In this area, measures such as afforestation and water and soil conservation will be increased to control and reduce the frequency and intensity of human activities (such as urban expansion, transportation construction, and mining development, etc.). Shanyin County in the central part of Shuozhou City and Ying County in the east and central part of Shuozhou City have scarce ecological sources and a small number of ecological corridors. Identifying obstacles in the area and prioritizing ecological protection and restoration zoning will play a key role in improving the landscape connectivity of the area. At the same time, Yingxian County in the southeast of Shuozhou City, Shuocheng District in the southwest, the central and northern Shanyin County, and the northwestern part of Huairen City has a large number of ecological source areas. It is imperative. Based on the Chinese government's ecological restoration strategy, an integrated management model of mountains, water, forests, fields, lakes, and grasses can be constructed, and the coupling between ecological processes can be analyzed in-depth, which will help optimize the local ESP and promote the sustainable development of both urban and environment [45].

4.3. Strategy of ESP Optimization in Shuozhou City

Characterized by vast amounts of coal resources and a fragile arid environment, Shuozhou City faces twin ecological challenges of urban expansion and coal mining [8]. As described earlier, it is proposed to establish a framework of regional ecological protection, regulation, and restoration areas, i.e., one protected area (ecological sources), two key regu-

lation areas (construction area and mining area), and three key restoration areas (obstacles, ecological corridors, and disappearing ecological corridors) to optimize the ESP in the study area. Considering the arid and cold climate conditions and previous experience, forest and grassland ecosystems are the priority options for ecological conservation and restoration in Shuozhou City. Monitoring and protecting of water and lake ecosystems are essential, as they undertake important water conservation and biodiversity maintenance functions. Considering the small proportion of water area in the identified ecological corridors and obstacles, their restoration level is relatively low. Unused land is the prominent place where soil erosion occurs. The protection and restoration of unused land need to be planned and implemented scientifically based on ecological studies.

Specifically, it is suggested putting efforts on farmland protection, grassland conservation, woodland nurturing, and wetland protection in the first-level restoration area. In the secondary restoration area, the protection and preservation of ecological land are still strengthened. The landscape connectivity between the unused farmland, forest land, and grassland, the restoration of damaged land, and the water and soil conservation are also emphasized. The tertiary protection and restoration area reflect the invasion and destruction of ecological corridors by land-used for transportation and residential areas. The proportion of traffic land in the tertiary restoration area increased from 1.02% to 2.15% from 2010 to 2017. The increase was 110.78%; the ratio of residential areas increased from 0.35% to 1.65%, increasing 371.43%. Meanwhile, although the area of industrial and mining land in the ecological protection and restoration area is small, from spatial distribution, the amount of obstacles around industrial and mining land and ecological restoration areas is relatively large. Restoration measures such as mine wasteland restoration and vegetation restoration on both sides of the road based on strengthening the habitat management and protection are vital to reinforce ecological restoration conservation and landscape connectivity [46]. Furthermore, the protection and optimization of environment based on different ecological restoration projects can enhance the regional ecological security and maximize ESV as it is well-known resource-based cities' mining and ecological restoration are simultaneous [8,24].

5. Conclusions

Habitats close to urban sprawl edge and human activity areas are facing the challenge of fragmentation, shrinkage and functional degradation, while habitats near ecological sources normally have a more stable situation and healthy ecosystem service function. Based on ESP identification and optimization, this study focus on improving ecological connectivity and structure function of the study area. It is suggested to prioritize the protection and restoration of ecological sources, ecological corridors, and obstacles. Specifically, this study proposes different levels of restoration strategies [37,47], and the research conclusions are as follows: From 2010 to 2017, ecological sources dropped from 21 to 20, and the total area dropped from 1923.35 km^2 to 1869.37 km^2 in 2017. Additionally, the number of ecological corridors has decreased from 34 to 33 in almost one decade. Obstacles of the study area also increased from 63 to 80 since 2010. This paper proposed an optimized ESP by zoning "one protection area, two regulation areas, and three restorations areas." Firstly, prioritize protecting 20 ecological source areas, with a total area of 1869.37 km^2, accounting for 17.64% of the whole city. Secondly, construction land is suggested to be under supervision and management with an area of 549.79 km^2 and contains 53 mines. Finally, the primary restoration area is the obstacles according to the priority of protection and restoration. It counts for an area of 10.17 km^2. The secondary restoration area is the 2017 ecological corridor with an area of 700.61 km^2. The tertiary restoration area is the disappearance of the 2000–2017 potential ecological corridor with an area of 159.40 km^2. This study on identifying and optimizing the ESP of resource-based cities based on the MSPA method and circuit theory can be a valuable reference for urban planners and similar resource-based cities such as Ordos City and Yulin City [1,2,27].

This study aims to explore the landscape connectivity and ecological function of the study area by combining MSPA and circuit theory [1]. Nevertheless, there is still room for adjustment in different application scenarios of the MSPA approach despite it provides a new method for landscape analysis. The establishment of a comprehensive ecological source identification system will also make up for the limitations of MSPA in in situ identification [18]. Circuit theory may ignore some details of the actual movement characteristics such as biological migration may be affected by human buildings such as houses and roads. Furthermore, this study did not conduct mainstream ecosystem service analysis and quantitative evaluation of optimized ESP's ecosystem service value. This will be the focus of subsequent research to complete this study and better support local ecological conservation decisions.

Author Contributions: Formal analysis, R.Y. and Z.B.; investigation, R.Y.; methodology, R.Y. and Z.S.; writing—original draft, R.Y.; writing—review and editing, R.Y. and Z.B. All authors have read and agreed to the published version of the manuscript.

Funding: This research was funded supported by National Science Foundation of China (41571508).

Institutional Review Board Statement: Not applicable.

Informed Consent Statement: Not applicable.

Data Availability Statement: Data is available for use upon request.

Acknowledgments: We appreciate Jiyuan Cheng and Huihui Wang, for their skillful assistance in laboratory and field work, and Mingjie Qian for the support in the field work.

Conflicts of Interest: The authors declare no conflict of interest.

References

1. An, Y.; Liu, S.; Sun, Y.; Shi, F.; Beazley, R. Construction and optimization of an ecological network based on morphological spatial pattern analysis and circuit theory. *Landsc. Ecol.* **2021**, *36*, 2059–2076. [CrossRef]
2. Peng, J.; Yang, Y.; Liu, Y.; Hu, Y.; Du, Y.; Meersmans, J.; Qiu, S. Linking ecosystem services and circuit theory to identify ecological security patterns. *Sci. Total. Environ.* **2018**, *644*, 781–790. [CrossRef]
3. Wang, C.; Yu, C.; Chen, T.; Feng, Z.; Hu, Y.; Wu, K. Can the establishment of ecological security patterns improve ecological protection? An example of Nanchang, China. *Sci. Total. Environ.* **2020**, *740*, 140051. [CrossRef]
4. Nathwani, J.; Lu, X.; Wu, C.; Fu, G.; Qin, X. Quantifying security and resilience of Chinese coastal urban ecosystems. *Sci. Total. Environ.* **2019**, *672*, 51–60. [CrossRef]
5. Almenar, J.B.; Bolowich, A.; Elliot, T.; Geneletti, D.; Sonnemann, G.; Rugani, B. Assessing habitat loss, fragmentation and ecological connectivity in Luxembourg to support spatial planning. *Landsc. Urban Plan.* **2019**, *189*, 335–351. [CrossRef]
6. Su, Y.; Chen, X.; Liao, J.; Zhang, H.; Wang, C.; Ye, Y.; Wang, Y. Modeling the optimal ecological security pattern for guiding the urban constructed land expansions. *Urban For. Urban Green.* **2016**, *19*, 35–46. [CrossRef]
7. Peng, J.; Pan, Y.; Liu, Y.; Zhao, H.; Wang, Y. Linking ecological degradation risk to identify ecological security patterns in a rapidly urbanizing landscape. *Habitat Int.* **2018**, *71*, 110–124. [CrossRef]
8. Li, S.; Xiao, W.; Zhao, Y.; Lv, X. Incorporating ecological risk index in the multi-process MCRE model to optimize the ecological security pattern in a semi-arid area with intensive coal mining: A case study in northern China. *J. Clean. Prod.* **2020**, *247*, 119143. [CrossRef]
9. Yu, K. Security patterns and surface model in landscape ecological planning. *Landsc. Urban Plan.* **1996**, *36*, 1–17. [CrossRef]
10. Estrada-Carmona, N.; Martínez-Salinas, A.; De Clerck, F.A.J.; Vílchez-Mendoza, S.; Garbach, K. Managing the farmscape for connectivity increases conservation value for tropical bird species with different forest-dependencies. *J. Environ. Manag.* **2019**, *250*, 109504. [CrossRef] [PubMed]
11. Kattel, G.R.; Elkadi, H.; Meikle, H. Developing a complementary framework for urban ecology. *Urban For. Urban Green.* **2013**, *12*, 498–508. [CrossRef]
12. Almenar, J.B.; Elliot, T.; Rugani, B.; Philippe, B.; Gutiérrez, T.N.; Sonnemann, G.; Geneletti, D. Nexus between nature-based solutions, ecosystem services and urban challenges. *Land Use Policy* **2021**, *100*, 104898. [CrossRef]
13. Aminzadeh, B.; Khansefid, M. A case study of urban ecological networks and a sustainable city: Tehran's metropolitan area. *Urban Ecosyst.* **2010**, *13*, 23–36. [CrossRef]
14. Epps, C.W.; Mutayoba, B.M.; Gwin, L.; Brashares, J.S. An empirical evaluation of the African elephant as a focal species for connectivity planning in East Africa. *Divers. Distrib.* **2011**, *17*, 603–612. [CrossRef]
15. Kool, J.T.; Moilanen, A.; Treml, E. Population connectivity: Recent advances and new perspectives. *Landsc. Ecol.* **2013**, *28*, 165–185. [CrossRef]

16. Soille, P.; Vogt, P. Morphological segmentation of binary patterns. *Pattern Recognit. Lett.* **2009**, *30*, 456–459. [CrossRef]
17. Wickham, J.D.; Riitters, K.H.; Wade, T.G.; Vogt, P. A national assessment of green infrastructure and change for the conterminous United States using morphological image processing. *Landsc. Urban Plan.* **2010**, *94*, 186–195. [CrossRef]
18. Li, J.; Xu, J.; Chu, J. The Construction of a Regional Ecological Security Pattern Based on Circuit Theory. *Sustainability* **2019**, *11*, 6343. [CrossRef]
19. Carroll, C.; Roberts, D.R.; Michalak, J.; Lawler, J.J.; Nielsen, S.E.; Stralberg, D.; Hamann, A.; McRae, B.H.; Wang, T. Scale-dependent complementarity of climatic velocity and environmental diversity for identifying priority areas for conservation under climate change. *Glob. Chang. Biol.* **2017**, *23*, 4508–4520. [CrossRef]
20. Proctor, M.F.; Nielsen, S.E.; Kasworm, W.F.; Servheen, C.; Radandt, T.G.; MacHutchon, A.G.; Boyce, M.S. Grizzly bear connectivity mapping in the Canada-United States trans-border region. *J. Wildl. Manag.* **2015**, *79*, 544–558. [CrossRef]
21. Pittiglio, C.; Skidmore, A.K.; Van Gils, H.A.M.J.; McCall, M.; Prins, H.H.T. Smallholder Farms as Stepping Stone Corridors for Crop-Raiding Elephant in Northern Tanzania: Integration of Bayesian Expert System and Network Simulator. *Ambio* **2013**, *43*, 149–161. [CrossRef]
22. Kreuter, U.P.; Harris, H.G.; Matlock, M.D.; Lacey, R. Change in ecosystem service values in the San Antonio area, Texas. *Ecol. Econ.* **2001**, *39*, 333–346. [CrossRef]
23. Matteucci, S.D.; Morello, J. Environmental consequences of exurban expansion in an agricultural area: The case of the Argentinian Pampas ecoregion. *Urban Ecosyst.* **2009**, *12*, 287–310. [CrossRef]
24. Wang, W.; Guo, H.; Chuai, X.; Dai, C.; Lai, L.; Zhang, M. The impact of land use change on the temporospatial variations of ecosystems services value in China and an optimized land use solution. *Environ. Sci. Policy* **2014**, *44*, 62–72. [CrossRef]
25. Elliot, T.; Almenar, J.B.; Rugani, B. Modelling the relationships between urban land cover change and local climate regulation to estimate urban heat island effect. *Urban For. Urban Green.* **2020**, *50*, 126650. [CrossRef]
26. Xue, M.; Ma, S. Optimized Land-Use Scheme Based on Ecosystem Service Value: Case Study of Taiyuan, China. *J. Urban Plan. Dev.* **2018**, *144*, 04018016. [CrossRef]
27. Woodworth, M.D. Ordos Municipality: A market-era resource boomtown. *Cities* **2015**, *43*, 115–132. [CrossRef]
28. Yuan, Y.; Zhao, Z.; Niu, S.; Li, X.; Wang, Y.; Bai, Z. Reclamation promotes the succession of the soil and vegetation in opencast coal mine: A case study from Robinia pseudoacacia reclaimed forests, Pingshuo mine, China. *Catena* **2018**, *165*, 72–79. [CrossRef]
29. Yuan, Y.; Zhao, Z.; Zhang, P.; Chen, L.; Hu, T.; Niu, S.; Bai, Z. Soil organic carbon and nitrogen pools in reclaimed mine soils under forest and cropland ecosystems in the Loess Plateau, China. *Ecol. Eng.* **2017**, *102*, 137–144. [CrossRef]
30. China, M.O.E.A. National Ecological Function Regionalization (Revised Version). 2015. Available online: http://www.mee.gov.cn/gkml/hbb/bgg/201511/t20151126_317777.htm (accessed on 25 June 2021).
31. Feng, Y.; Wang, J.; Bai, Z.; Reading, L. Effects of surface coal mining and land reclamation on soil properties: A review. *Earth-Sci. Rev.* **2019**, *191*, 12–25. [CrossRef]
32. Shaikh, F.; Ji, Q.; Fan, Y. An ecological network analysis of the structure, development and sustainability of China's natural gas supply system security. *Ecol. Indic.* **2017**, *73*, 235–246. [CrossRef]
33. Gao, J.; Du, F.; Zuo, L.; Jiang, Y. Integrating ecosystem services and rocky desertification into identification of karst ecological security pattern. *Landsc. Ecol.* **2021**, *36*, 2113–2133. [CrossRef]
34. Baranyi, G.; Saura, S.; Podani, J.; Jordán, F. Contribution of habitat patches to network connectivity: Redundancy and uniqueness of topological indices. *Ecol. Indic.* **2011**, *11*, 1301–1310. [CrossRef]
35. Rubio, L.; Saura, S. Assessing the importance of individual habitat patches as irreplaceable connecting elements: An analysis of simulated and real landscape data. *Ecol. Complex.* **2012**, *11*, 28–37. [CrossRef]
36. Ye, Y.; Su, Y.; Zhang, H.-O.; Liu, K.; Wu, Q. Construction of an ecological resistance surface model and its application in urban expansion simulations. *J. Geogr. Sci.* **2015**, *25*, 211–224. [CrossRef]
37. Peng, J.; Jia, J.L.; Hu, Y.N.; Tian, L.; Li, H.L. Construction of ESP in the agro-pastoral ecotone based on surface humid index: A case study of Hangjin Banner, Inner Mongolia Autonomous Region, China. *Chin. J. Appl. Ecol.* **2018**, *29*, 1990–1998. (In Chinese)
38. Zhao, L.; Dai, A.; Dong, B. Changes in global vegetation activity and its driving factors during 1982–2013. *Agric. For. Meteorol.* **2018**, *249*, 198–209. [CrossRef]
39. Chen, B.; Zhang, X.; Hua, K.; Xu, K. Application study of temperature vegetation drought index (TVDI) in grassland drought monitoring. *Arid. Land Geogr.* **2013**, *36*, 930–937.
40. Sandholt, I.; Rasmussen, K.; Andersen, J. A simple interpretation of the surface temperature/vegetation index space for assessment of surface moisture status. *Remote. Sens. Environ.* **2002**, *79*, 213–224. [CrossRef]
41. Liu, Z.H.; Wang, Y.L.; Peng, J.; Xie, M.M.; Li, Y. Using ISA to analyze the spatial pattern of urban land cover change: A case study in Shenzhen. *Acta Geogr. Sin.* **2011**, *66*, 961–971.
42. Elliot, T.; Bertrand, A.; Almenar, J.B.; Petucco, C.; Proença, V.; Rugani, B. Spatial optimisation of urban ecosystem services through integrated participatory and multi-objective integer linear programming. *Ecol. Model.* **2019**, *409*, 108774. [CrossRef]
43. Delphin, S.; Escobedo, F.; Abd-Elrahman, A.; Cropper, W. Urbanization as a land use change driver of forest ecosystem services. *Land Use Policy* **2016**, *54*, 188–199. [CrossRef]
44. Costanza, R.; De Groot, R.; Sutton, P.; Van Der Ploeg, S.; Anderson, S.J.; Kubiszewski, I.; Farber, S.; Turner, R.K. Changes in the global value of ecosystem services. *Glob. Environ. Chang.* **2014**, *26*, 152–158. [CrossRef]

45. Fan, F.; Liu, Y.; Chen, J.; Dong, J. Scenario-based ecological security patterns to indicate landscape sustainability: A case study on the Qinghai-Tibet Plateau. *Landsc. Ecol.* **2021**, *36*, 2175–2188. [CrossRef]
46. Kang, J.; Zhang, X.; Zhu, X.; Zhang, B. Ecological security pattern: A new idea for balancing regional development and ecological protection. A case study of the Jiaodong Peninsula, China. *Glob. Ecol. Conserv.* **2021**, *26*, e01472. [CrossRef]
47. Fu, Y.; Shi, X.; He, J.; Yuan, Y.; Qu, L. Identification and optimization strategy of county ecological security pattern: A case study in the Loess Plateau, China. *Ecol. Indic.* **2020**, *112*, 106030. [CrossRef]

land

MDPI

Article

Decoupling the Relationships between Carbon Footprint and Economic Growth within an Urban Agglomeration—A Case Study of the Yangtze River Delta in China

Fengsong Pei *, Rui Zhong, Li-An Liu and Yingjuan Qiao

School of Geography, Geomatics and Planning, Jiangsu Normal University, Xuzhou 221116, China; zhongrui@jsnu.edu.cn (R.Z.); 2020190065@jsnu.edu.cn (L.-A.L.); 3020191444@jsnu.edu.cn (Y.Q.)
* Correspondence: peifs@jsnu.edu.cn

Abstract: Carbon footprint is emerging as an effective tool for carbon emission management, especially that from fossil energy consumption. In addition, decoupling analysis is important to keep a high pace of economic growth while reducing carbon emission and its carbon footprint. Taking the Yangtze River Delta (YRD) urban agglomeration in China as a case, this paper examined the changes in carbon footprint and carbon footprint pressure by incorporating land resource limits. On this basis, we further analyzed the decoupling relationships between carbon footprint, carbon footprint pressure and economic growth. The GeoDetector was also employed to detect the spatial heterogeneity of the carbon footprint pressure. The results showed that despite the decrease of carbon emissions from 2011 to 2019 in the YRD, carbon footprint pressure still revealed an increased trend in this period. As to the decoupling relationships between carbon footprint, carbon footprint pressure and economic growth, they were improved in most of the cities in the YRD, changing from expansive coupling to weak decoupling to strong decoupling. However, the descending trend of decoupling elasticity coefficient for carbon footprint pressure is smaller than that of the carbon footprint. This result could be explained by the fact that not only carbon emission but also carbon sequestration (by productive lands including forests and grasslands) pose large impacts on carbon footprint pressure. The findings indicate the necessity not only to reduce carbon emission, but also to protect productive lands to realize low carbon economy.

Keywords: decoupling; fossil energy consumption; carbon footprint; urban agglomeration; Yangtze River Delta

Citation: Pei, F.; Zhong, R.; Liu, L.-A.; Qiao, Y. Decoupling the Relationships between Carbon Footprint and Economic Growth within an Urban Agglomeration—A Case Study of the Yangtze River Delta in China. *Land* **2021**, *10*, 923. https://doi.org/10.3390/land10090923

Received: 31 July 2021
Accepted: 30 August 2021
Published: 1 September 2021

1. Introduction

The global land surface temperature increased rapidly, at a rate of 1.59 °C between 1850 and 1900 and between 2011 and 2020 [1]. The warming is likely mainly due to a continuous increase in fossil energy consumption and thus its carbon emission [2,3]. The carbon emission from fossil energy consumption is of wide concern by scientific communities in recent years. For instance, Luderer et al. (2018) explored the residual carbon dioxide (CO_2) emissions from fossil fuels to hold global warming well below 2 °C while pursuing efforts to limit it below 1.5 °C to reach the goals of the Paris Agreement [4]. Christophe and Paul (2015) analyzed the emission limit from fossil fuel to limit global warming to 2 °C in different regions [5]. Taking the U.S. as an example, Deutch (2017) argued that it is misleading to avoid the risks of climate change by only reducing energy consumption and carbon intensity [6].

In recent years, carbon footprint became one of the widely recognized methods to evaluate the impact of carbon emission on environment pressure. For instance, Simion et al. (2013) proposed an ecological footprint indicator by integrating land occupation, CO_2 emissions from fossil energy and nuclear energy use to perform environmental sustainability assessment in European countries [7]. Zhao et al. (2014) estimated the urban

carbon footprint to assess the impact of human activities on urban environment pressure in Nanjing City, China during 2000–2009 [8]. Wiśniewski and Kistowski (2017) assessed the role and importance of carbon footprint as a tool in local planning of a low carbon economy at local levels in Poland [9]. Ma et al. (2018) analyzed the carbon footprint in passenger transport in China over the period 2006–2015 [10]. Carbon footprint (CF) frequently reflects the measure of carbon dioxide emissions directly or indirectly caused by an activity or accumulated over the life stages of a product [11,12]. There are many ways to measure carbon emission: CO_2 physical emissions, CO_2 equivalents (CO_2eq), or by translating them into biologically productive areas indirectly [13–15]. In comparison with direct carbon emission, indirect carbon footprint measurement tracks energy or resource throughput of economy development and translates it into biologically productive areas necessary to produce these flows [13,16,17]. In this paper, carbon footprint refers to the carbon emission measurement using productive lands indirectly. Concretely, the carbon footprint represents the productive land area to absorb the carbon emission from fossil energy consumption. Thus, as for different cities, natural resource endowments such as productive lands have different effects on carbon footprint [17].

To promote sustainability development, many studies explored the changes in carbon emission and their decoupling relationships with economic growth. For instance, Mikayilov et al. (2018) analyzed the decoupling relationships between CO_2 emissions and Gross Domestic Product (GDP) for a group of European economies [18]. Karakaya et al. (2019) analyzed the CO_2 emission trends and the decoupling performance between CO2 emissions and economic growth in Turkey [19]. Engo (2021) explored the decoupling indicators for carbon emissions in Egypt, Morocco, Algeria and Tunisia [20]. However, few works addressed carbon footprint, carbon footprint pressure and their decoupling relationships with economic growth by incorporating natural resource limits (e.g., productive lands) [15,21].

The Yangtze River Delta (YRD) is one of the most developed and densely populated regions in China. It is also one of the largest urban agglomerations worldwide. Taking the YRD as an example, this paper examined spatiotemporal changes in the carbon footprint and their carbon footprint pressure from fossil energy consumption. The decoupling effects between carbon footprint pressure and economic growth were analyzed at both urban and regional scales. Geodetector has many advantages for measuring spatial stratified heterogeneity and exploring their determinants [22,23]. In this study, the drivers of the change of carbon footprint pressure were analyzed using the Geodetector. The objectives of this study were to understand the decoupling relationships among economic growth, carbon footprint and carbon footprint pressure by accounting for land resource limits to realize low carbon development.

2. Study Area and Data Preprocessing

2.1. Study Area

In this paper, the study area is located in the Yangtze River Delta (YRD), China (Figure 1). The YRD lies between 118–123° E and 28–34° N, with an area of 104.985 km^2. Furthermore, it encompasses the entire Shanghai City, the southern part of Jiangsu Province (i.e., Suzhou, Wuxi, Changzhou, Nanjing, Zhenjiang, Nantong, Taizhou, Yangzhou) and the northern part of Zhejiang Province (i.e., Hangzhou, Ningbo, Shaoxing, Jiaxing, Huzhou, Taizhou and Zhoushan). The major vegetation type includes subtropical evergreen broadleaf forest, cropland, urban land, grasslands, and so on. Since economic reform in China in 1978, the YRD has witnessed fast industrialization and unprecedented urbanization. The gross domestic product (GDP) in the YRD reached US $1.74 trillion in 2016 (approximately 16.2% of the total GDP in China). The overall pattern of energy consumption in the YRD was dominated by raw coal and electricity, occupying about 40–45% and 22–33% of the total energy consumption, respectively [24].

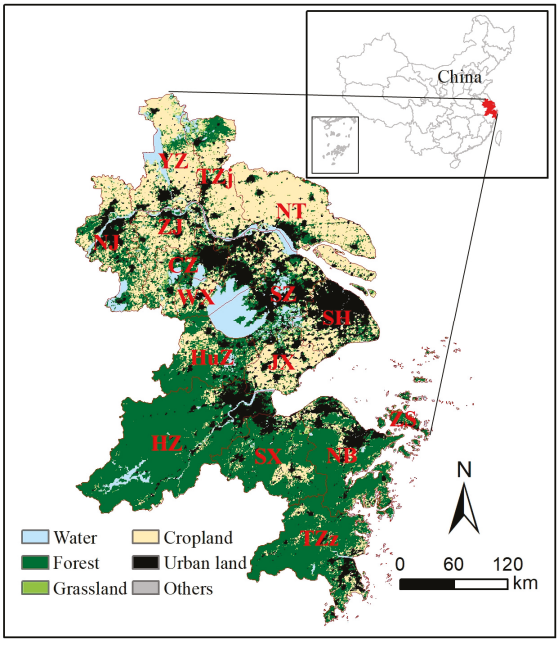

Figure 1. Location of the Yangtze River Delta (SH: Shanghai; SZ: Suzhou; WX: Wuxi; CZ: Changzhou; NJ: Nanjing; ZJ: Zhenjiang; NT: Nantong; TZj: Taizhou in Jiangsu Province; YZ: Yangzhou; HZ: Hangzhou; NB: Ningbo; SX: Shaoxing; JX: Jiaxing; HuZ: Huzhou; TZz: Taizhou in Zhejiang Province; and ZS: Zhoushan).

2.2. Data Sources and Preprocessing

The data in this study includes the dataset on fossil energy consumption by cities, a land use/cover dataset, a terrestrial net primary productivity dataset (NPP) and statistical datasets (Table 1). The fossil energy consumption dataset, which spans 2001–2019, was collected from statistical yearbooks for the 16 cities separately (e.g., Shanghai statistical yearbook, Suzhou statistical yearbook, Nanjing statistical yearbook, Hangzhou statistical yearbook, and so on). In addition, other statistical datasets, including the proportion of urban population, permanent population, urban population, GDP and built-up area, were collected by cities from several statistical yearbooks, including the Shanghai statistical yearbook, the Jiangsu statistical yearbook and the Zhejiang statistical yearbook (Table 1). Regarding the land use/cover data and the NPP data, the Moderate Resolution Imaging Spectroradiometer (MODIS) products (i.e., MCD 12Q1 and MOD17A3) were downloaded from NASA's Land Processes Distributed Active Archive Center (LP DAAC). The original data were obtained from their original sinusoidal projection to geographic grid cells using the MODIS Reprojection Tool (MRT).

Table 1. Data sources in this study.

	Data Category	Spatio-Temporal Resolution	Sources
1	Land use dataset	500 m, 2001–2019	NASA's LP DAAC
2	NPP dataset	500 m, 2019	NASA's LP DAAC
3	Fossil energy consumption (raw coal, gasoline and diesel)	By cities, 2001–2019	Statistical yearbooks of the 16 cities in the YRD
4	Proportion of urban population	By cities, 2001–2019	-
5	Permanent population	By cities, 2000, 2005–2019	Shanghai statistical yearbooks [25]
6	Urban population	By cities, 2000, 2005–2019	Jiangsu statistical yearbooks [26]
7	GDP	By cities, 2001–2019	Zhejiang statistical yearbooks [27]
8	Built-up area	By cities, 2001–2019	

3. Methods

3.1. IPCC Carbon Inventory Method to Estimate Carbon Emission from Fossil Energy Consumption

By using the data on fossil energy consumption from statistical yearbooks, this paper estimated the carbon emission from 2001 to 2019 in the YRD. The fossil energy consumption in the YRD was mainly raw coal, gasoline/gasoline products, coke, and so on [24]. For assuring the temporal continuity and consistency of the energy data for the 16 cities, raw coal, gasoline and diesel were selected for analyzing the carbon emission from fossil energy consumption. There are many ways to estimate carbon emissions, including life cycle assessment (LCA), the input output method (IO), the Kaya carbon emission identity method and the IPCC carbon inventory method [28–31]. In this paper, carbon emission from fossil energy consumption was estimated using the carbon inventory method recommended by IPCC. For the *i*-th energy, its carbon emission (E_i, ton) is calculated as:

$$E_i = M_i \times F_i \quad (1)$$

where M_i is the total amount of *i*-th type of energy consumption (10^4 ton of standard coal equivalent, tce); and F_i is the carbon emission coefficient of the *i*-th energy (t C tce-1). Table 2 shows the standard coal coefficient and carbon emission coefficient of raw coal, gasoline and diesel.

Table 2. Carbon emission factor for different types of fossil energy.

Types	Standard Coal Coefficient	Carbon Emission Coefficient
Raw coal	0.7143 (kgce/kg)	0.7559 (104 t/104 tce)
Gasoline	1.4714 (kgce/kg)	0.5538 (104 t/104 tce)
Diesel	1.4571 (kgce/kg)	0.5921 (104 t/104 tce)

3.2. Estimate the Carbon Footprint of Fossil Energy Consumption and Carbon Footprint Pressure

The terrestrial vegetation in the YRD is mainly forest, croplands, urban lands, grasslands, and so on. In particular, the carbon that is absorbed into crops is frequently released back into the atmosphere through food consumption. This implies that croplands do not contribute to a net carbon sequestration [32–34]. On the contrary, forests and grasslands show a mainly carbon sequestration effect while affecting carbon footprint changes. In this paper, a carbon footprint model was employed by incorporating the changes in natural

resource endowment such as productive lands to address the spatial changes of land use/cover. The carbon footprint of fossil energy consumption was calculated as follows:

$$CF = \sum_{i}^{3} \frac{C_i \times F_i \times P_{erf}}{EP_f} + \frac{C_i \times F_i \times P_{erg}}{EP_g} \quad (2)$$

where CF is the total carbon footprint of fossil energy consumption (hm^2) of the *i*-th region; C_i is fossil energy consumption (1×10^4 tce) of the *i*-th energy type: raw coal, gasoline or diesel; F_i is the carbon emission coefficient of the *i*-th energy type (tC tce^{-1}); EP_f and EP_g are the net ecosystem production (NEP) of the forest and grasslands, respectively. In this study, EP_f and EP_g were determined as the global average NEP of the corresponding vegetation type (i.e., 3.809592 t C per hm^2 for forest and 0.948229 t C per hm^2 for grasslands) [35,36]; P_{erf} and P_{erg} are the carbon absorption ratios of forest and grasslands in the YRD respectively. The ratios of forest and grasslands were calculated to estimate the productive land as follows:

$$P_{erf} = \frac{A_f \times EP_f}{A_f \times EP_f + A_g \times EP_g} \quad (3)$$

$$P_{erg} = \frac{A_g \times EP_g}{A_f \times EP_f + A_g \times EP_g} \quad (4)$$

where P_{erf} and P_{erg} are the forest and grasslands carbon absorption ratios, respectively, A_f and A_g are the total area of the forest and grasslands, respectively. The carbon footprint pressure index (CFP) was calculated based on estimated carbon footprint (CF) and existing productive lands as follows:

$$CFP = \frac{CF}{A_f \times EF_f + A_f \times EF_g} \quad (5)$$

where EF_f and EF_g are the equilibrium factors for forest and grasslands, respectively. The global equilibrium factor is used to facilitate the addition of the actual area of the forest and the grasslands. Concretely, the equilibrium factors of the forest (EF_f) and the grasslands (EF_g) are set to 1.34 and 0.49, respectively.

3.3. Tapio Decoupling Model to Analyze the Coupling or Decoupling Effects between Carbon Footprint, Carbon Footprint Pressure and Economic Growth

To decouple environmental pressure from economic growth, the Organisation for Economic Cooperation and Development (OECD) defined the term "decoupling" as breaking the link between "environmental bads" and "economic goods" [37]. That is, the decoupling effects of carbon emission with economic growth were assessed using the Tapio decoupling model [38,39]. Concretely, the elasticity coefficient (ε) is defined as the ratio of the change rate of carbon emission (ΔCO_2) to the change rate of GDP (ΔGDP) as follows:

$$\varepsilon = \frac{\%\Delta CO_2}{\%\Delta GDP} \quad (6)$$

$$\%\Delta CO_2 = \frac{CO_{2t+1} - CO_{2t}}{CO_{2t}} \quad (7)$$

$$\%\Delta GDP = \frac{GDP_{t+1} - GDP_t}{GDP_t} \quad (8)$$

In this paper, environmental pressure (i.e., CO_2 emissions) (ΔCO_2) was reflected by the carbon footprint and carbon footprint pressure. In addition, economic growth was represented by using per Capita GDP (ΔGDP) as an indicator. In order not to over interpret slight changes as significant, Tapio (2005) put forward the Tapio decoupling model, which gives an improvement that $\pm$20% variation of the elasticity values around

1.0 are regarded as coupling [40]. On this basis, decoupling states in the Tapio model can be further divided into three subcategories: negative decoupling, decoupling and coupling (Table 3). Concretely, decoupling occurred when the growth rate of environmental pressure is less than that of economic driver over a specific period. In particular, decoupling is strong when economic growth increases and environmental stress decreases (elasticity <0). On the contrary, decoupling is weak when both economic growth and environmental stress increase, but the growth rate of environmental stress is less than that of economic growth (0 < elasticity < 0.8). In addition, it is recessive when both economic growth and environmental stress decrease, but the decrease rate of environmental stress is bigger than that of economic growth (elasticity >1.2). Expansive negative decoupling occurs when both economic growth and environmental stress increase, but the increase rate of environmental stress is bigger than that of economic growth (elasticity >1.2). In strong negative decoupling, economic growth decreases while environmental stress increases (elasticity <0). When both economic growth and environmental stress decrease (0 < elasticity < 0.8) and the decreased rate of environmental stress is smaller than that of economic growth, there is weak negative decoupling [38].

Table 3. The degrees of coupling and decoupling.

	ΔCO_2	**ΔDGP**	ε	**Decoupling State**
Negative decoupling	>0	>0	>1.2	Expansive negative decoupling (END)
	>0	<0	<0	Strong negative decoupling (SND)
	<0	<0	0–0.8	Weak negative decoupling (WND)
Decoupling	>0	>0	0–0.8	Weak decoupling (WD)
	<0	>0	<0	Strong decoupling (SD)
	<0	<0	>1.2	Recessive decoupling (RD)
Coupling	>0	>0	0.8–1.2	Expansive coupling (EC)
	<0	<0	0.8–1.2	Recessive coupling (RC)

3.4. Driving Forces of Carbon Footprint Pressure Based on the GeoDetector Method

Many methodologies were frequently employed to explore the drivers of carbon emission, including Kaya identity, structural decomposition analysis (SDA) and logarithmic mean Divisia index (LMDI) decompose model [41–44]. The GeoDetector is a statistical method to detect spatial stratified heterogeneity and elucidate the driving factors behind it. The method has many advantages: (1) it works without the assumption of linearity of the association; and (2) it has a straight physical meaning [22,23]. Four detectors, including risk detector, factor detector, ecological detector and interaction detector, are defined in the GeoDetector [22]. The risk detector compares the difference of average values between sub-regions. The factor detector compares the accumulated dispersion variance of each sub-region with the dispersion variance of the entire study region. The smaller the ratio, the stronger the contribution of the stratum. The ecological detector compares the variance calculated from each sub-region divided according to one determinant with that divided according to another determinant. The interaction detector compares the sum of the contribution of two individual attributes vs. the contribution of the two attributes when taken together.

The spatial stratified heterogeneity is adopted by the q-statistic in the GeoDetector. Assuming that a study area is composed of N units and is stratified into $h = 1, 2, \ldots, L$ stratum. It is composed of N_h units in the stratum h. The q-statistic is defined as:

$$q = 1 - \frac{\sum_{h=1}^{L} N_h \sigma_h^2}{N\sigma^2} \quad (9)$$

where σ_h^2 and σ^2 are the stratum variance of effect Y or determinant D for the layer h and the whole region, respectively. The value range of q is $[0, 1]$. When applying different driving forces of carbon footprint pressure, the explanatory power of the determinant is stronger when the q value is larger. In this paper, five drivers were examined, including

the rate of gross domestic product (X_1), the rate of built-up area (X_2), the urbanization rate (X_3), the rate of energy consumption per unit of GDP (X_4) and the terrestrial NPP (X_5), were examined to analyze the driver forces of carbon footprint pressure from the perspective of economic development, social development, technological progress and terrestrial productivity, respectively.

In addition, interaction detection is also used to evaluate whether the interaction of different drivers can enhance or weaken their explanatory power to carbon footprint pressure. Concretely, the GeoDetector firstly calculates the q value of two judgemental factors X_1 and X_2, and marks them as $q(X_1)$ and $q(X_2)$. The combined q-statistic of the two factors are then calculated and marked as $q(X_1 \cap X_2)$. The relationship between the two factors is shown in Table 4. The details of the GeoDetector can be found in the studies by Wang et al. (2010) and Wang et al. (2016) [22,23].

Table 4. The interactive relationships in the GeoDetector.

Description	Interaction
$q(X_1 \cap X_2) < \mathrm{Min}(q(X_1), q(X_2))$	Weakened, nonlinear
$\mathrm{Min}(q(X_1), q(X_2)) < q(X_1 \cap X_2) < \mathrm{Max}(q(X_1), q(X_2))$	Weakened, single factor nonlinear
$q(X_1 \cap X_2) > \mathrm{Max}(q(X_1), q(X_2))$	Enhanced, double factors
$q(X_1 \cap X_2) = q(X_1) + q(X_2)$	Independent
$q(X_1 \cap X_2) > q(X_1) + q(X_2)$	Enhanced, nonlinear

4. Results

4.1. Changes of Productive Lands and Carbon Footprint in the YRD

4.1.1. Temporal Changes of Productive Lands, Carbon Emission and Carbon Footprint Pressure in the YRD

According to our results, total productive lands showed an increase in the YRD since the year of 2001. It peaked at 7.32×10^6 hm^2 in 2009, then gradually fell, and shrank to 6.70×10^6 hm^2 in 2019 (Figure 2a). In addition, there existed a large amount of carbon emissions owing to fossil energy consumption, with an average of 1.56×10^8 t C over the period 2001–2019. An overall increasing trend of carbon emission was found in this period in the YRD, at a rate of 5.85×10^6 t C a^{-1} ($p = 0.000$) (Figure 2a). Furthermore, the average carbon footprint was 4.24×10^7 hm^2 in the YRD between 2001 and 2019, which was about six times the amount of the average productive lands there. This indicates the severe environmental stress in the YRD in the past decades. Furthermore, a similar increasing trend was found in the past 19 years between the carbon footprint from fossil energy consumption (not shown in this paper) and the corresponding carbon footprint pressure (Figure 2b). Concretely, both total carbon footprint and carbon footprint pressure in the YRD revealed increasing trends before 2011 and then peaked in 2013. That is, the carbon footprint reached 5.25×10^7 hm^2 in 2013, which is 2.46 times that in the year 2001. Thus, despite the decreased carbon emission in the YRD from 2011 to 2019, both carbon footprint and carbon footprint pressure were still enhanced simultaneously. The phenomena could be associated with the decreased productive lands over the period of 2011–2019 in the YRD (Figure 2a).

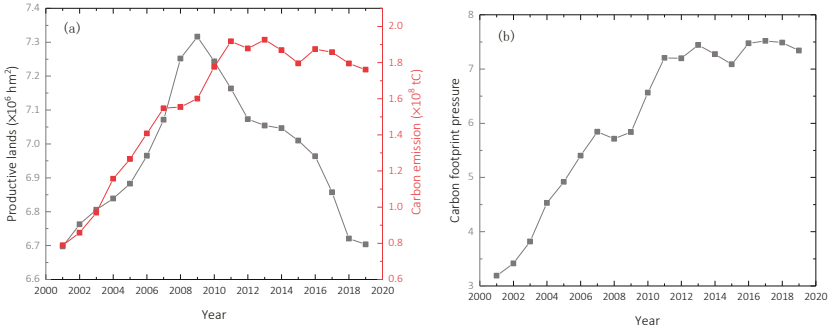

Figure 2. Changes in (**a**) productive lands and carbon emission, and (**b**) carbon footprint pressure in the YRD from 2001 to 2019.

4.1.2. Changes of Productive Lands, Carbon Emission and Carbon Footprint Pressure at City Scale

To further elucidate the change of carbon footprint pressure, spatial heterogeneities of productive lands, carbon emission from fossil energy consumption and its carbon footprint pressure were analyzed by cities, respectively. As shown in Figure 3a, total productive lands show large differences in different cities in the YRD. For example, there is a large amount of productive lands (mainly forests) in the southern YRD (e.g., northern Zhejiang Province). This is especially the case in Hangzhou, Ningbo, Shaoxing and Taizhou cities. In contrary, it has a small amount of productive lands in the northern YRD (e.g., southern Jiangsu Province). The phenomenon can be associated with the wide distribution of forest lands in the northern Zhejiang Province and croplands in the southern Jiangsu Province (Figure 1). Regarding the average carbon emission from fossil energy consumption during 2001–2019, it is obviously large in several cities including Shanghai, Suzhou and Ningbo (Figure 3b). For average carbon footprint pressure, it is relatively small in the northern Zhejiang Province in the southern YRD (Figure 3c). The result could be associated with the wide distribution of forest lands there. In comparison, carbon footprint pressure is more severe in the northern YRD. This is especially the case in Shanghai City. We found that both the averages and the slopes of the carbon footprint pressure in Shanghai City are particularly bigger due to its excessively high carbon emissions in past decades. In addition, although the average carbon footprint pressure in Suzhou and Wuxi is not very large as in Shanghai City, the slope of the corresponding carbon footprint pressure reveals a growing trend over the two cities in comparison to most other cities over the period of 2001–2019 (Figure 3d). This phenomenon could be mainly caused by the sharp decrease of productive lands in the two cities. That is, productive lands witnessed a decrease, at rates of 4153 and 4040 hm^2a^{-1} from 2001 to 2019 in Wuxi and Suzhou, respectively. The cumulative decreases in the past 19 years accounted for 33.64% and 26.86% of the total productive lands in the two cities in 2001. This result indicates the necessity to protect productive lands (e.g., forests and grasslands) to realize low carbon economy.

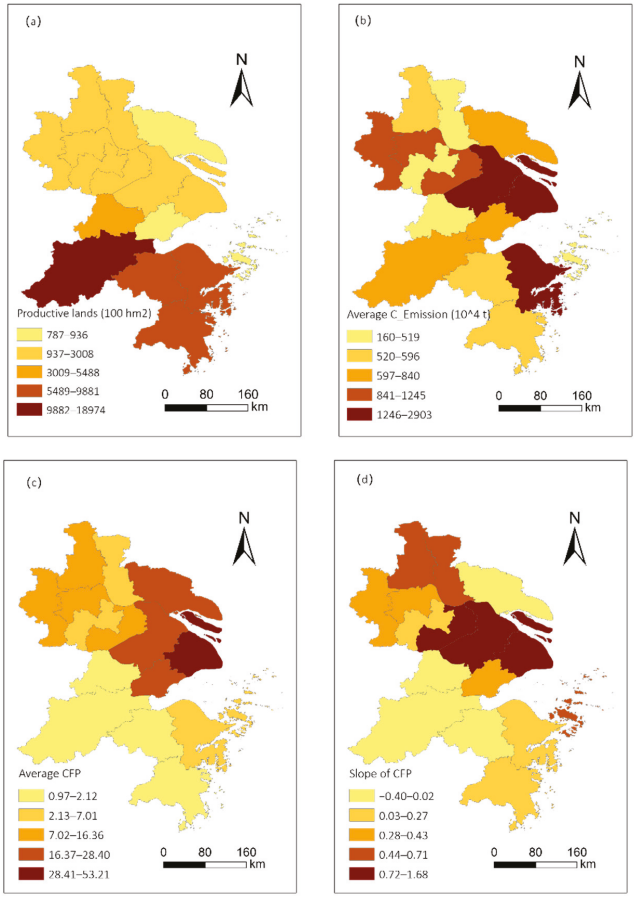

Figure 3. Spatial distribution of (**a**) average productive lands, (**b**) average carbon emission, (**c**) average carbon footprint pressure (CFP), and (**d**) the slope of CFP from 2001 to 2019.

4.2. Decoupling Analysis on Carbon Footprint, Carbon Footprint Pressure and Economic Growth

4.2.1. Decoupling analysis on the Relationships between Carbon Footprint, Carbon Footprint Pressure and Economic Growth

The decoupling relationships between carbon footprint and economic growth were analyzed by comparing their relative changes as well as the elasticity change of the carbon footprint and the carbon footprint pressure in the YRD from 2001 to 2018. As shown in Figure 4, the change rate of GDP in the YRD was all positive from 2001 to 2018. This indicates the continuous economic growth in the past 19 years. In addition, both the carbon footprint and the carbon footprint pressure revealed growing trends over the period of 2001–2019. The elasticity coefficients were therefore decreasing from 2001 to 2019. Consequently, the decoupling relationships between the carbon footprint and economic growth mainly changed from expansive coupling to weak decoupling to strong decoupling. Similar changes were also found for the carbon footprint pressure. Despite it, the elasticity coefficient of the carbon footprint pressure is bigger than that of the carbon footprint before 2009. However, the relationship was reversed after 2009. That is, the descending trend of the carbon footprint pressure is smaller than that of the carbon footprint. This difference could be associated with the changes in productive lands in the YRD.

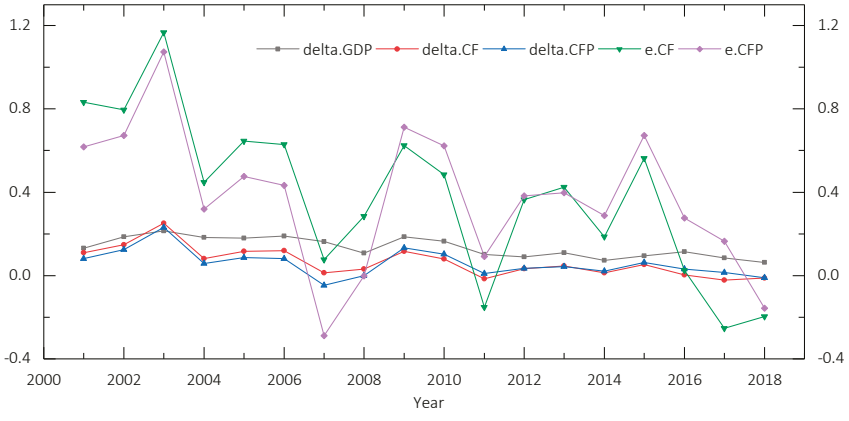

Figure 4. The change rate of GDP and CO_2, as well as the elasticity change of the carbon footprint and carbon footprint pressure of fossil energy consumption.

4.2.2. City-Based Decoupling Analysis on Carbon Footprint Pressure and Economic Growth

We further analyzed the decoupling relationships between carbon footprint pressure and economic growth in the YRD by cities. It is observed that the decoupling relationships were improved in most of the cities in the YRD in the past 19 years. For instance, Figure 5a shows the decoupling characteristics according to the average elasticity coefficient from 2001 to 2009 for different cities. We found that 12 of 16 cities were in a weak decoupling stage over this period. Meanwhile, 4 cities, including Taizhou in Jiangsu Province, Suzhou, Jiaxing and Taizhou in Zhejiang Province, were in an expansive coupling stage. However, the decoupling relationships were then improved in most of the cities over the period of 2010–2018 (Figure 5b) as: (1) from expansive coupling to weak decoupling stage (e.g., in Taizhou in Jiangsu Province, Suzhou, Jiaxing and Taizhou in Zhejiang Province); (2) from weak coupling to strong decoupling stage (e.g., in Shanghai, Wuxi, Changzhou, Yangzhou, Hangzhou, Shaoxing and Ningbo). Despite these improvements, the decoupling relationships could also be degraded in the YRD. For instance, the decoupling relationship in Zhoushan experienced a conversion from the weak decoupling stage to the expansive coupling stage.

4.3. Driving Factors of Carbon Footprint Pressure Changes

In this paper, we also examined the impacts of natural, environmental and socioeconomic factors on the changes of carbon footprint pressure in the YRD. According to the results of the factor detector in the GeoDectector, these factors were ranked according to their effects on the carbon footprint pressure in the following order: the rate of built-up area (0.290) > terrestrial NPP (0.241) > urbanization rate (0.135) > energy consumption per GDP (0.134) > GDP rate (0.133) (Table 5).

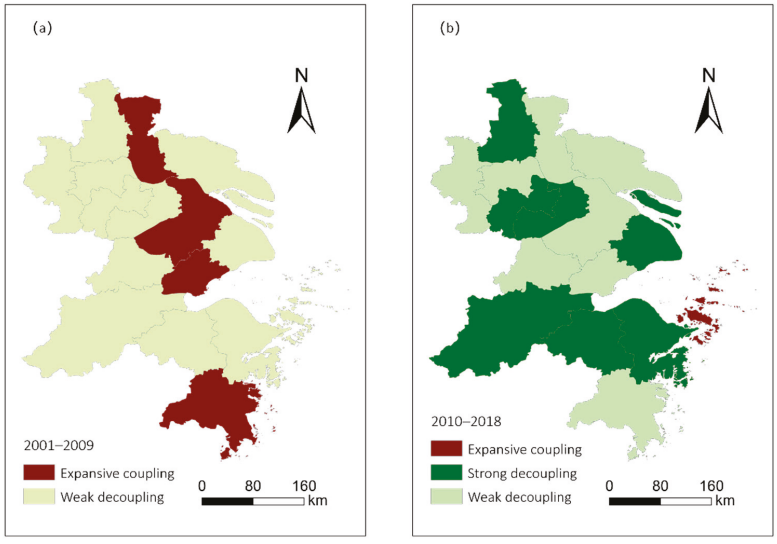

Figure 5. The decoupling characteristics of the carbon footprint pressure and economic growth for the period of 2001 to 2009 (**a**) and 2010 to 2018 (**b**).

Table 5. The *q* values of different covariates under interaction detector.

	NPP	Urbanization Rate	Energy Consumption per GDP	GDP Rate	Built-Up Area Rate
NPP	0.241				
Urbanization rate	0.477	0.135			
Energy consumption per GDP	0.483	0.971	0.134		
GDP rate	0.482	0.933	0.344	0.133	
Rate of built-up area	0.546	0.975	0.516	0.339	0.290

Table 5 also shows the response of the carbon footprint pressure to the interaction between two of the driving factors according to the interaction detector in the GeoDetector. According to the interactive detection analysis, all the interactive *q* values appeared to be higher than any *q* value of a sole factor. It is obvious that the interaction based on the urbanization rate is bigger than any other factors. In particular, the combined *q* value of the rate of built-up area and urbanization rate was 0.975, that of energy consumption per GDP and urbanization rate was 0.971, that of GDP rate and urbanization rate was 0.933, and that of terrestrial NPP and urbanization rate was 0.477. The combinations of the above-mentioned factors can better explain spatial variability of the changes in the carbon footprint pressure than most of the others. The results indicate that the urbanization rate played critical roles on the carbon footprint pressure in the YRD. In addition, the interactions between terrestrial NPP and other drivers are relatively strong. For instance, the q value of the rate of built-up area and terrestrial NPP was 0.546, that of energy consumption per GDP and the urbanization rate was 0.483, and that of the GDP rate and the urbanization rate was 0.482. This indicates that, besides the urbanization rate, carbon absorption that related to natural resource endowment (e.g., productive lands) can also be important to ease the carbon footprint pressure.

5. Discussions

In general, absolute decoupling means that economic growth coincides with absolute reduction in emission or resource use. On the contrary, relative decoupling denotes that resource use or emission increase less so than does the GDP. Actually, relative decoupling is frequent for most of the cases [45]. Regarding the carbon footprint and carbon footprint

pressure, the decoupling relationships were also obvious for the cities in the YRD. We found that the elasticity values revealed decreased trends in all the cities in the YRD. However, the carbon footprint pressure revealed increased positive trends in most of the cities in the YRD from 2001 to 2019, except for Hangzhou and Nantong. Thus, it mainly revealed a relative decoupling for most of the cities in the YRD. This is consistent with the results of Haberl et al. (2020) [45]. Regarding Hangzhou City and Nantong City, carbon footprint pressure showed a continuously decreased trend after 2007 and 2010, respectively. Despite a little fluctuation, absolute decoupling existed in the past decade. This could be associated with the increased productive lands in the two cities. Thus, not only by reducing carbon emission, it is also critical to increase productive lands and thus the uptake of CO_2 by the terrestrial biosphere to ease the environmental pressure [6].

The decoupling state is also found to be associated with the stages of economic growth in different cities. Pilatowska and Wlodarczyk (2018) analyzed the decoupling relationships between economic growth and CO_2 emissions in the European Union (EU) countries [46]. The EKC hypothesis, which assumes that environmental degradation increases with per capita income during the early stages of economic growth, and then declines with per capita income after passing beyond an income turning point [47], was tested by dividing the EU countries into three groups depending on the level of knowledge-based economy. They found that the EKC hypothesis is valid for the most high-level and some middle level knowledge-based economies [46]. Moreover, these countries are characterized by either a decreasing trend in energy intensity or the diversified energy consumption mix with a significant share of nuclear and renewable energy and also a smaller share of solid fuels. This phenomenon is consistent with the results of this study on carbon footprint pressure. For example, four cities in the early stages of rapid economic growth or low-level development, including Taizhou in Jiangsu Province, and Suzhou, Jiaxing and Taizhou in Zhejiang Province, were in an expansive coupling stage from 2001 to 2009. In addition, other cities were in a weak decoupling stage over this period. However, the decoupling relationships between carbon footprint pressure and economic growth were then dramatically improved, especially in the cities with rapid economic growth and increased productive lands (e.g., Shanghai, Wuxi, Hangzhou, Ningbo, and so on). This indicates the necessity not only to reduce carbon emission, but also to protect productive lands to realize low carbon economy.

In addition, Li et al. (2021) classified the cities in the Yangtze River Economic Belt according to the differences in the decoupling stage; they identified three categories: pre-decoupling, post-decoupling, and unstable decoupling [48]. They inferred that pre-decoupling cities are mainly dominated by high-tech industries or service industries, such as Shanghai City. Our findings partly agree with the results from Li et al. (2021). For instance, most of the cities in the YRD were in a weak decoupling stage between carbon footprint pressure and economic growth over the period 2001–2009. After 2009, Shanghai, Wuxi, Yangzhou, Hangzhou, Shaoxing and Ningbo experienced a strong decoupling stage. The phenomena could be associated with decreased carbon emission, as well as the increase of productive lands (especially in the northern Zhejiang Province) in these cities. By comparison, post-decoupling cities are characterized by resources and geographical advantages, and some cities have accelerated the decoupling by eliminating high-emission industries, extending industrial chains, and nurturing new pillar industries (e.g., the coal chemical industry) [48]. In the study area, similar results were found as well. For example, several cities, including Taizhou in Jiangsu Province, Suzhou, Jiaxing and Taizhou in Zhejiang Province, changed from expansive decoupling during 2001–2009 to weak decoupling over the period 2010–2018. In addition, unstable decoupling cities were in a critical period of industrialization with high-emissions and low-value-added industries [48]. This was especially the case for Zhoushan City in the YRD. We found that the carbon emission in this city did not change from 2001 to 2010. However, its total carbon emission in 2019 reached 4.2 times that in 2010.

Decoupling relationships between economic growth and carbon emission were frequently attributed to per capita GDP, urbanization rate, industrial structure, energy intensity, etc. [49]. In this study, we found that the built-up area rate and terrestrial NPP explained large amounts of the changes in the carbon footprint pressure. In addition, the joint explanatory power mostly reached more than 93% based on the interaction analysis between the urbanization rate and other drivers. The phenomena indicated that not only carbon emission, but also carbon sequestration, posed large impacts on the carbon footprint, as well as carbon footprint pressure. Further concerns should be addressed about the drivers of carbon sequestration such as changes in productive lands.

6. Conclusions

In past studies, few works addressed the decoupling relationship between the carbon footprint and economic growth by incorporating natural resource limits. This paper found that the decoupling relationships in the YRD were improved when incorporating the changes in productive lands in the past decades. However, the descending trend of decoupling the elasticity coefficient for carbon footprint pressure was smaller than that of the carbon footprint. In addition, not only carbon emission, but also carbon sequestration, posed large impacts on carbon footprint pressure. The findings appealed for a differential strategy to coordinate economic development and environment protection according to each city's characteristic to realize a low carbon economy. Considering the electricity transmission from one place to another, this study used only statistical data on fossil energy consumption. However, it was subject to data limitations on fossil energy consumption at the city scale. That is, for assuring the temporal continuity and consistency of the energy data at different cities, we selected only raw coal, gasoline and diesel to reflect the changes in carbon emission. More cases should be conducted using complete and comparable fossil energy data on multiple energy types. Furthermore, the Tapio model only provides the decoupling state from an elastic perspective in a certain period. However, the relationships between economic growth and carbon footprint are variable and reflects different patterns of economic development. An in-depth analysis (e.g., wavelet transform), is essential to be conducted in the time-frequency domain for richer results [50]. This paper mainly focused on the relationships between economic development and environmental factors (i.e., carbon emission and carbon footprint); it is essential to pay more attention to the role and importance of the indirect carbon footprint (e.g., biologically productive area as an indicator) as a tool in spatial planning of a low carbon economy in future studies [9].

Author Contributions: F.P. contributed to research design, data analysis, interpretation of results, and draft manuscript preparation; R.Z. and L.-A.L. contributed to the data collection; Y.Q., R.Z. and L.-A.L. performed experiments and computational analysis; F.P. and L.-A.L. drafted the paper, and all authors contributed to the final draft of the manuscript. All authors have read and agreed to the published version of the manuscript.

Funding: This research was funded by the Qinglan Project of Jiangsu Province in China, the Project of Philosophy and Social Science Research in Colleges and Universities in Jiangsu Province (Grant No. 2019SJA0915), the National Students' Project for Innovation Training Program of China (Grant Nos. 201710320027Z and 201810320020Z), and the Priority Academic Program Development of Jiangsu Higher Education Institutions.

Institutional Review Board Statement: Not applicable.

Informed Consent Statement: Not applicable.

Data Availability Statement: The datasets in this study are available within this article. The data which were derived from the original datasets but not aforementioned are available upon requests.

Acknowledgments: Special thanks are given to the three anonymous reviewers for their insightful comments and suggestions.

Conflicts of Interest: The authors declare no conflict of interest.

References

1. IPCC. Climate Change 2021: The Physical Science Basis. In *Contribution of Working Group I to the Sixth Assessment Report of the Intergovernmental Panel on Climate Change*; Masson-Delmotte, V., Zhai, P., Pirani, A., Connors, S.L., Péan, C., Berger, S., Caud, N., Chen, Y., Goldfarb, L., Gomis, M.I., et al., Eds.; Cambridge University Press: Cambridge, UK; New York, NY, USA, 2021; in press.
2. Oreskes, N. Beyond the ivory tower. The scientific consensus on climate change. *Science* **2004**, *306*, 1686. [CrossRef]
3. Scafetta, N. On the reliability of computer-based climate models. *Ital. J. Eng. Geol. Environ.* **2019**, *1*, 49–70.
4. Luderer, G.; Vrontisi, Z.; Bertram, C.; Edelenbosch, O.Y.; Pietzcker, R.C.; Rogelj, J.; De Boer, H.S.; Drouet, L.; Emmerling, J.; Fricko, O.; et al. Residual fossil CO2 emissions in 1.5–2 °C pathways. *Nat. Clim. Chang.* **2018**, *8*, 626–633. [CrossRef]
5. Christophe, M.; Paul, E. The geographical distribution of fossil fuels unused when limiting global warming to 2 °C. *Nature* **2015**, *517*, 187–190.
6. Deutch, J. Decoupling Economic Growth and Carbon Emissions. *Joule* **2017**, *1*, 3–5. [CrossRef]
7. Simion, I.M.; Ghinea, C.; Maxineasa, S.G.; Taranu, N.; Bonoli, A.; Gavrilescu, M. Ecological footprint applied in the assessment of construction and demolition waste integrated management. *Environ. Eng. Manag. J.* **2013**, *12*, 779–788.
8. Zhao, R.; Huang, X.; Ying, Z.; Ding, M.; Chuai, X. Urban carbon footprint and carbon cycle pressure: The case study of Nanjing. *J. Geogr. Sci.* **2014**, *24*, 159–176. [CrossRef]
9. Winiewski, P.; Kistowski, M. Carbon Footprint as a Tool for Local Planning of Low Carbon Economy in Poland. *Rocz. Ochr. Sr.* **2017**, *19*, 335–354.
10. Ma, F.; Wang, W.; Sun, Q.; Liu, F.; Li, X. Ecological pressure of carbon footprint in passenger transport: Spatio-temporal changes and regional disparities. *Sustainability* **2018**, *10*, 317. [CrossRef]
11. Wiedmann, T.; Minx, J. A Definition of 'Carbon Footprint'. In *Ecological Economics Research Trends*; Pertsova, C.C., Ed.; Nova Science Publishers: Hauppauge, NY, USA, 2008; Chapter 1; pp. 1–11.
12. Gao, T.; Liu, Q.; Wang, J. A comparative study of carbon footprint and assessment standards. *Int. J. Low-Carbon Technol.* **2014**, *9*, 237–243. [CrossRef]
13. Wackernagel, M.; Onisto, L.; Bello, P.; Linares, A.C.; Ina, L.S.F.; García, J.M.; Guerrero, A.I.S.; Guerrero, M.G.S. National natural capital accounting with the ecological footprint concept. *Ecol. Econ.* **1999**, *29*, 375–390. [CrossRef]
14. Pandey, D.; Agrawal, M.; Pandey, J.S. Carbon footprint: Current methods of estimation. *Environ. Monit. Assess.* **2011**, *178*, 135–160. [CrossRef] [PubMed]
15. Yang, Y.; Meng, G. The decoupling effect and driving factors of carbon footprint in megacities: The case study of Xi'an in western China. *Sustain. Cities Soc.* **2019**, *44*, 783–792. [CrossRef]
16. Inch, J. Our Ecological Footprint: Reducing Human Impact on the Earth. *Popul. Environ.* **1995**, *1*, 171–174.
17. Fang, K.; Heijungs, R.; Snoo, G.R.D. Theoretical exploration for the combination of the ecological, energy, carbon, and water footprints: Overview of a footprint family. *Ecol. Indic.* **2014**, *36*, 508–518. [CrossRef]
18. Mikayilov, J.I.; Hasanov, F.J.; Galeotti, M. Decoupling of co 2 emissions and gdp: A time-varying cointegration approach. *Ecol. Indic.* **2018**, *95*, 615–628. [CrossRef]
19. Karakaya, E.; Bostan, A.; Za, M. Decomposition and decoupling analysis of energy-related carbon emissions in turkey. *Enviro. Sci. Pollut. Res.* **2019**, *26*, 32080–32091. [CrossRef]
20. Engo, J. Driving forces and decoupling indicators for carbon emissions from the industrial sector in Egypt, Morocco, Algeria, and Tunisia. *Environ. Sci. Pollut. Res.* **2021**, *28*, 14329–14342. [CrossRef] [PubMed]
21. Huang, Y.; Yu, Q.; Wang, R. Driving factors and decoupling effect of carbon footprint pressure in China: Based on net primary production. *Technol. Forecast. Soc. Chang.* **2021**, *167*, 120722. [CrossRef]
22. Wang, J.F.; Li, X.H.; Christakos, G.; Liao, Y.L.; Zhang, T.; Gu, X.; Zheng, X.Y. Geographical detectors-based health risk assessment and its application in the neural tube defects study of the Heshun region, China. *Int. J. Geogr. Inf. Sci.* **2010**, *24*, 107–127. [CrossRef]
23. Wang, J.F.; Zhang, T.L.; Fu, B.J. A measure of spatial stratified heterogeneity. *Ecol. Indic.* **2016**, *67*, 250–256. [CrossRef]
24. Xu, X.; Yang, G.; Tan, Y.; Zhuang, Q.; Tang, X.; Zhao, K.; Wang, S. Factors influencing industrial carbon emissions and strategies for carbon mitigation in the Yangtze River Delta of China. *J. Clean. Prod.* **2017**, *142*, 3607–3616. [CrossRef]
25. Statistics Bureau of Shanghai Municipality. *Shanghai Statistical Yearbook 2020*; China Statistical Press: Beijing, China, 2020.
26. Statistics Bureau of Jiangsu Province. *Jiangsu Statistical Yearbook 2020*; China Statistical Press: Beijing, China, 2020.
27. Statistics Bureau of Zhejiang Province. *Zhejiang Statistical Yearbook 2020*; China Statistical Press: Beijing, China, 2020.
28. IPCC (Intergovernmental Panel on Climate Change). *Guidelines for National Greenhouse Gas Inventories*; IPCC: London, UK, 1996.
29. Mahony, T.O. Decomposition of Ireland's carbon emissions from 1990 to 2010: An extended Kaya identity. *Energy Policy* **2013**, *59*, 573–581. [CrossRef]
30. Jing, W.; Kai, H.; Yang, S.; Yan, L.; Hu, T.; Yue, Z. Driving forces analysis of energy-related carbon dioxide (CO_2) emissions in Beijing: An input–output structural decomposition analysis. *J. Clean. Prod.* **2017**, *163*, 58–68.
31. Jiang, R.; Li, R. Decomposition and Decoupling Analysis of Life-Cycle Carbon Emission in China's Building Sector. *Sustainability* **2017**, *9*, 793. [CrossRef]
32. Fang, J.; Guo, Z.; Piao, S.; Chen, A. Terrestrial vegetation carbon sinks in China, 1981–2000. *Sci. China Ser. D. Earth Sci.* **2007**, *50*, 1341–1350. [CrossRef]
33. Piao, S.; Fang, J.; Ciais, P.; Peylin, P.; Huang, Y.; Sitch, S.; Wang, T. The carbon balance of terrestrial ecosystems in China. *Nature* **2009**, *458*, 1009–1013. [CrossRef]

34. Pei, F.; Wu, C.; Liu, X.; Xia, L.; Yang, K.; Yi, Z.; Wang, K.; Li, X.; Xia, G. Monitoring the vegetation activity in China using vegetation health indices. *Agric. For. Meteorol.* **2018**, *248*, 215–227. [CrossRef]
35. Xie, H.; Chen, X.; Lin, K. The ecological footprint analysis of fossil energy and electricity. *Acta Ecolog. Sin.* **2008**, *28*, 1729–1735.
36. Chen, H.; Li, C.; Wang, L. Research on the regional sustainable development based on the ecological footprint theory: A case of Henan Province. *Appl. Mech. Mater.* **2013**, *361*, 199–203.
37. Organization for Economic Cooperation and Development (OECD). Indicators to Measure Decoupling of Environmental pressure from Economic Grow. 2002. Available online: http://www.oecd.org/environment/indicators-modelling-outlooks/1933638.pdf (accessed on 1 September 2021).
38. Tapio, P. Towards a theory of decoupling: Degrees of decoupling in the EU and the case of road traffic in Finland between 1970 and 2001. *Transp. Policy* **2005**, *12*, 137–151. [CrossRef]
39. Kong, Y.; He, W.; Yuan, L.; Zhang, Z.; Gao, X.; Zhao, Y.; Degefu, D.M. Decoupling economic growth from water consumption in the Yangtze River Economic Belt, China. *Ecol. Indic.* **2021**, *123*, 107344. [CrossRef]
40. Vehmas, J.; Kaivo-oja, J.; Luukkanen, J. *Global Trends of Linking Environmental Stress and Economic Growth*; Turku School of Economics and Business Administration: Turku, Finland, 2003.
41. Wen, L.; Zhang, Z. Probing the affecting factors and decoupling analysis of energy industrial carbon emissions in Liaoning, China. *Environ. Sci. Pollut. Res.* **2019**, *26*, 14616–14626. [CrossRef]
42. Cai, H.; Qu, S.; Wang, M. Changes in China's carbon footprint and driving factors based on newly constructed time series input–output tables from 2009 to 2016. *Sci. Total Environ.* **2020**, *711*, 134555. [CrossRef]
43. Apeaning, A.W. Technological constraints to energy-related carbon emissions and economic growth decoupling: A retrospective and prospective analysis. *J. Clean. Prod.* **2021**, *291*, 125706. [CrossRef]
44. Ozturk, I.; Majeed MTKhan, S. Decoupling and decomposition analysis of environmental impact from economic growth: A comparative analysis of Pakistan, India, and China. *Environ. Ecol. Stat.* **2021**, 1–28. [CrossRef]
45. Haberl, H.; Wiedenhofer, D.; Virág, D.; Kalt, G.; Plank, B.; Brockway, P.; Fishman, T.; Hausknost, D.; Krausmann, F.P.; Leon-Gruchalski, B.; et al. A systematic review of the evidence on decoupling of gdp, resource use and ghg emissions, part ii: Synthesizing the insights. *Environ. Res. Lett.* **2020**, *15*, 065003. [CrossRef]
46. Piłatowska, M.; Włodarczyk, A. Decoupling Economic Growth from Carbon Dioxide Emissions in the EU Countries. *Montenegrin J. Econ.* **2018**, *14*, 7–26. [CrossRef]
47. Stern, D. The Rise and Fall of the Environmental Kuznets Curve. *World Dev.* **2004**, *32*, 1419–1439. [CrossRef]
48. Li, K.; Zhou, Y.; Xiao, H.; Li, Z.; Shan, Y. Decoupling of economic growth from CO2 emissions in cities from the Yangtze River Economic Belt. *Sci. Total Environ.* **2021**, *775*, 145927. [CrossRef]
49. Tang, D.; Zhang, Y.; Bethel, B.J. An Analysis of Disparities and Driving Factors of Carbon Emissions in the Yangtze River Economic Belt. *Sustainability* **2019**, *11*, 2362. [CrossRef]
50. Xiang, L.; Chen, X.; Su, S.; Yin, Z. Time-Varying Impact of Economic Growth on Carbon Emission in BRICS Countries: New Evidence from Wavelet Analysis. *Front. Environ. Sci.* **2021**, *9*, 280. [CrossRef]

land

MDPI

Article

Comprehensive Evaluation of the Importance of Ecological Land in Arid Hilly Cities in Northwest China: A Case Study of the Core Urban Area of Lanzhou

Yiping Liu [1], Chengpeng Lu [1,2,*], Jinhuang Mao [1,2], Jiaxing Pang [3], Zhiliang Liu [1,2] and Muchen Hou [1,2]

[1] Institute of County Economic Development & Rural Revitalization Strategy, Lanzhou University, Lanzhou 730000, China; liuyiping@lzu.edu.cn (Y.L.); maojh@lzu.edu.cn (J.M.); zhlliu19@lzu.edu.cn (Z.L.); houmch20@lzu.edu.cn (M.H.)
[2] School of Economics, Lanzhou University, Lanzhou 730000, China
[3] College of Earth and Environment Sciences, Lanzhou University, Lanzhou 730000, China; pangjx@lzu.edu.cn
* Correspondence: lcp@lzu.edu.cn

Abstract: Cities in hilly arid areas of northwest China have generally experienced a low level of economic development; they also have unique natural characteristics such as climate, soil, terrain, environment, and surface cover. High quality ecological lands are those that provide humans and the environment with relatively high levels of ecological services including soil, water, and air purification, adsorbing pollutants, or providing water or nutrients needed by plants. In this study, ecological lands were classified as woodland, grassland, water area, and bare land. The present study constructed an ecological land model designed to evaluate the importance of such land from the perspective of ecological service function and ecological demand intensity. Results revealed that: (1) This model can help researchers to better analyze the structure and spatial characteristics of ecological land in cities and also meet the needs of ecological protection and urban management in highly urbanized areas. (2) In terms of ecological service function and ecological demand intensity, the most important ecological land is mostly distributed in densely populated and urbanized areas, and the spread of urbanization is conducive to the improvement of land ecological value for the arid hilly area of northwest China. (3) Among all types of ecological land, the water area had the highest ecological value in the study area, while the grassland had the most potential for improvement, as careful planning and use can allow grassland to function as an ecological barrier while providing good, aesthetically pleasing space for leisure activities for the general public. (4) Qilihe and Xigu districts have more generally important graded areas of forest, grassland, and bare land, although the current ecological value of these lands is limited, though they have great potential for ecological improvement.

Keywords: ecological land; ecological function; ecological demand; comprehensive evaluation; northwest China; Lanzhou city

Citation: Liu, Y.; Lu, C.; Mao, J.; Pang, J.; Liu, Z.; Hou, M. Comprehensive Evaluation of the Importance of Ecological Land in Arid Hilly Cities in Northwest China: A Case Study of the Core Urban Area of Lanzhou. *Land* **2021**, *10*, 942. https://doi.org/10.3390/land10090942

Received: 14 August 2021
Accepted: 4 September 2021
Published: 7 September 2021

1. Introduction

With the development of China's economy, society expects businesses and governments to maintain a high-quality environment. People's demand for a clean and ecologically stable living environment is growing [1]. The protection of important ecological land is an urgent task in support of the sustainable development of urban and rural areas in China, while identification and evaluation can effectively identify and screen ecological land by giving it a value, which is an important starting point for the construction of an ecologically sound civilization. Ecological land can be defined as land that provides humans, plants, and animals with environmental services including soil, water, and air purification or the mitigation of pollution, as well as providing natural land for grazing, recreation, or other needs [2]. For example, as ecological land, natural wetlands and grasslands can

provide greater amounts of ecological services for humans than urbanized lands with little green space.

The identification of an ecological source is not only related to the formulation of a land use strategy and a choice of urban development path, but is also the basis for the establishment of an urban and rural ecological security pattern. It is of great significance to the play of regional ecological benefits and the coordination of the relationship between regional ecological protection and economic development. Originally, identification of ecological land was relatively coarse; for example, nature reserves or habitats of key species were often directly selected as the source of an ecological security pattern in scientific research and practice [3,4]. However, the designation of nature reserves ignores the specific conditions and characteristics of the environment, while the habitats of key species are limited by the availability and accuracy of species observation data. To avoid these shortcomings, scholars began to try to establish an index system from multiple perspectives that could be used to evaluate the importance of ecological patches, and regard the natural ecological attributes of these patches as the core of ecological land designation. The attributes of ecological patches, such as land cover type, patch area and shape, biodiversity maintenance, ecological sensitivity, and soil and water conservation, have become common indicators for the construction of systems designed to evaluate the importance of ecological land [5,6], and some studies have also included the structural importance of ecological patches in the evaluation framework [7]. These studies have greatly improved the scientific basis of ecological source identification. However, the importance of ecological land with the same natural attributes still varies by location [8]. With the acceleration of the process of urbanization in China, a large amount of ecological land in cities has been replaced by urbanized land, which has led to a scarcity [9]. The ecological land located in an urbanized area can beautify the environment, improve the local microclimate, shield residents from noise, provide convenient and comfortable resting places for human beings, help urban residents free themselves from the shackles of a reinforced concrete jungle, and help people relax in a natural environment [10–12]. This has an important value that ecological land on the periphery of a city cannot replace. Relatively intensive activities of residents occur in areas with ecological land, which has a relatively high service efficiency and visit rate [13]. In view of this, in recent years the evaluation of the importance of ecological land has been developing continuously. In addition to the natural service function provided by ecological patches, some studies have also included the need of human society for ecological service in its evaluation systems. The goal is to comprehensively delineate the ecological land that plays an important role in urban development from the dual perspectives of nature and society [14–16]. Doing so improves the methods of identifying important ecological sources in cities and strengthens the systematic process involved in the evaluation system. However, few such studies have been conducted in China, and this small number of studies is mainly oriented to the cities of eastern China [15,16], ignoring the adaptability of arid inland cities in northwest China. The climate and soil conditions, land cover, ecological status, level of economic development, and urban spatial layout of arid hilly areas in northwest China have unique characteristics. Therefore, it is necessary to adjust the index selection, weight distribution, and calculation method according to local conditions in the process of evaluating the importance of ecological land. At the same time, China has put forward the strategy of providing for ecological protection and producing high-quality development in the Yellow River Basin [17,18]. It is of practical significance to evaluate and study the importance of ecological land use for the arid inland cities along the upper reaches of the Yellow River in support of the ecologically sound management and economic development of the whole basin. In this context, this paper hopes to establish an improved evaluation model, which will help to identify and evaluate the importance of ecological land in arid and hilly areas in northwest China, and fill the gap in related fields of study. Moreover, this paper chooses Lanzhou as a case study considering that Lanzhou is the only provincial capital city in China where the Yellow River runs through the city and also serves as an important

node of the Yellow River Basin and "one Belt and Road" initiative. For a long time, due to the dual influence of natural conditions and human activities, the ecological land in Lanzhou has been occupied and many habitats have been divided, which has greatly affected the urban environmental quality [19]. This paper expects to lay a foundation for ecological protection and high-quality development in Lanzhou through the identification of important ecological sources in its core urban area.

In light of the above discussion, this paper uses an improved model to evaluate the importance of ecological land in the core urban area of Lanzhou with specific attention to natural ecology and human needs. The purpose of this research is mainly twofold: (1) to construct a significant evaluation system for ecological land in the northwest arid hilly area, via the study's methodology; (2) to explore the structure and spatial distribution characteristics of ecological land in the core area of Lanzhou in a practical sense, to reveal the development characteristics of urban ecological land in the arid hilly region of northwest China, and to provide some guidance for the long-term development of Lanzhou.

2. Materials and Methods

2.1. Overview of the Study Area and Data Sources

Lanzhou, located at the geometric center of China, is an important central city, industrial base, transportation hub, and core node city of the Silk Road Economic Belt in northwest China. Lanzhou has jurisdiction over three counties (Yongdeng, Yuzhong, and Gaolan), five districts (Chengguan, Qilihe, Anning, Xigu, and Honggu), and three national development zones, with a total area of about 13,090 km^2. In the fourth edition of the master plan for urban Lanzhou, the urban spatial structure was described as "one river, two banks, three centers and seven groups", in which the "three centers" were composed of the Chengguan, Anning-Qilihe, and Xigu central areas, used here as the study area, covering about 1046 km^2 (Figure 1).

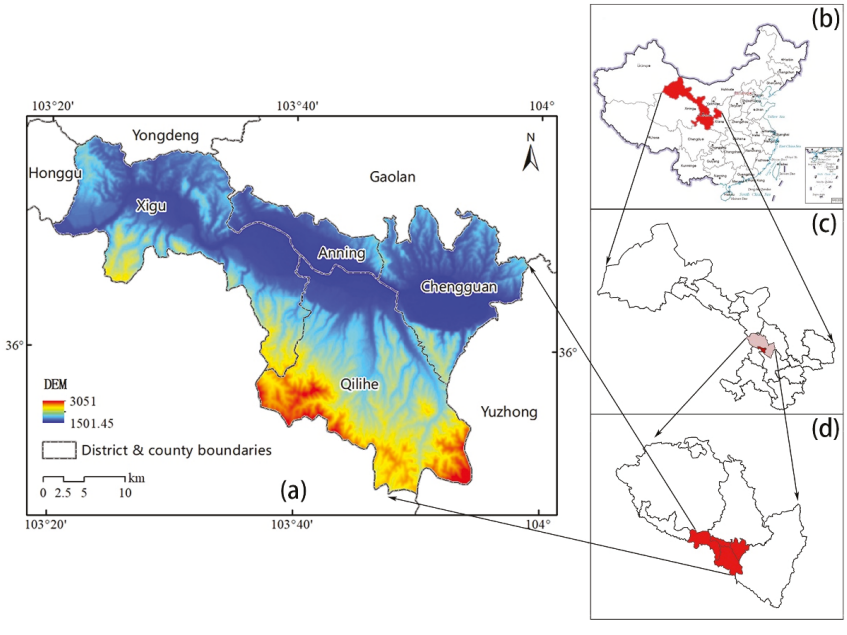

Figure 1. (**a**) Geographic location of the study area showing the elevations of Chengguan, Anning-Qilihe, and Xigu central areas. Inset maps show (**b**) the location of Gansu Province within China; (**c**) the location of Lanzhou within Gansu Province; (**d**) the locations of these central areas within Lanzhou.

The data used in this study included Landsat 8 operational land imager thermal infrared sensor remote sensing images with a resolution of 30 m acquired in 2020 as land use source data (strip number 131; line number 35), and ENVI software was used to interpret the images. Based on the current land use classification (GB/T 21010–2017), the interpretation results were divided into six land use types: cultivated land, woodland, grassland, water area, construction land, and bare land. In this study, woodland, grassland, water area, and bare land were selected as four types of ecological land in the city according to the definition of ecological land in previous studies [2,20]. Finally, the spatial distribution data of ecological land in the core urban area of Lanzhou were obtained by delineating this in the ArcGIS software (EGIS, Redlands, CA, USA). Digital elevation model data came from BIGEMAP downloader with a resolution of 15 m × 15 m. The normalized difference vegetation index (NDVI) data were extracted from ENVI software based on remote sensing images; then fractional vegetation cover was calculated by the significant linear relationship between NDVI and vegetation cover [21,22]. The remote sensing images were acquired on 26 July 2020, during which the vegetation coverage was relatively good and could reflect the vegetation situation of Lanzhou in an ideal way. Nighttime light data was based on the 2020 global nighttime light data set obtained from the National Polar-orbiting partnership-visible infrared imaging radiometer suite satellite from the official website of the U.S. National Oceanic and Atmospheric Administration, which has higher precision than previous U.S. Defense Meteorological Satellite Program Operational Linescan System light data; soil erosion data were obtained from the Harmonized World Soil Database.

2.2. Methodology Framework

Previous studies have shown that the important ecological land in a city not only should help to maintain the normal operation of the natural ecosystem but should also provide green space for the leisure and entertainment activities of human society [15,16]. Therefore, this study evaluated the importance of ecological land in the core area of urban Lanzhou from the two aspects of ecological service function and ecological demand. When evaluating the ecological function, indicators should be selected according to regional characteristics. For Lanzhou, drought and water shortage, sparse vegetation and rugged terrain are its main natural characteristics [23]. Therefore, maintenance of biodiversity, soil conservation, and water conservation have become important factors affecting the ecological development level of Lanzhou. This paper also constructs the ecological function evaluation system based on these three aspects. In terms of social demand, the intensity of the demand of urban residents for ecological land is often related to the spatial location of this ecological land, the number of services covered, and other factors; therefore, the spatial differences of human activity factors were mainly considered. In conclusion, the importance index (*EI*) of normalized ecological function and normalized ecological demand index (*DI*) were mainly introduced to characterize the comprehensive importance index (*PI*) of ecological land:

$$PI_i = EI_i + DI_i, \quad (1)$$

where PI_i is the comprehensive importance index of ecological land, EI_i is the normalized value of the importance index of ecological function, and DI_i is the normalized value of the ecological demand index. After calculating all the importance indicators, the natural breakpoint classification method was used to divide the final evaluation results into five levels: *most important*, *very important*, *important*, *generally important*, and *unimportant*. Note that an *italics font* is used for these five levels of importance throughout the paper to help the reader realize which specific category is being discussed at any point.

The specific analytical methods used to find the ecological function importance index and ecological demand index follow.

2.3. Ecological Function Importance Assessment

2.3.1. Biodiversity Maintenance Function

Different land use types have different functions in maintaining biodiversity. According to the biodiversity service equivalent formulated by Xie et al. [5] and referring to relevant research on the correction of a service value coefficient per unit area [24], the basic biodiversity service equivalent of farmland, woodland, grassland, water area, and bare land was determined to be 2.09, 9.59, 3.21, 7.32, and 1, respectively. In addition, previous studies have shown that variations in vegetation coverage will cause significant changes in the value of ecological services within a certain land use type [16,25–27]. Therefore, this paper also used the normalized vegetation index (NDVI) as a correction factor to correct the basic equivalent value; NDVI reflects the biodiversity maintenance function of ecological land:

$$EV = \frac{NDVI_i}{NDVI_t} \times EV_t, \quad (2)$$

where EV is the modified biodiversity service equivalent corresponding to grid i, EV_t is the basic biodiversity service equivalent of land use type t, $NDVI_i$ is the normalized difference vegetation indices corresponding to grid i, and $NDVI_t$ is the average $NDVI$ of ecological land type t.

2.3.2. Soil Conservation Function

The revised universal soil loss equation (RUSLE) has been widely used in the quantitative evaluation of the soil conservation function [28–33]. In this paper, the RUSLE was used to calculate the difference between potential and actual soil erosion to determine the soil conservation capacity of each land type. According to RUSLE, potential soil loss (A_0) and actual soil erosion (A) are mainly controlled by a rainfall erosion factor (R), soil Erosivity Factor (K), slope length and slope factor (LS), vegetation coverage factor (C), and engineering measures factor (P). The calculation formula of soil conservation (A_1) is as follows:

$$A_1 = A_0 - A = R \times K \times LS - R \times K \times LS \times C \times P = R \times K \times LS \times (1 - C \times P), \quad (3)$$

where R, K, LS, and C can be calculated by the RUSLE and the grid calculator function of ArcGIS [26–29]. In addition, combined with previous studies, different p-values were given to the various ecological land types in the core urban area of Lanzhou: 1 for woodland, grassland, and bare land, 0 for water area.

2.3.3. Water Conservation Function

The water conservation function was evaluated from three dimensions: distance from water area, slope, and fractional vegetation cover. Generally speaking, the closer to a water source, the higher the vegetation coverage, and the smoother the slopes, the stronger the water conservation function [15,16,34], and zones with suitable human settlements are also primarily distributed in regions with a moderate relief degree of the land surface, adequate vegetation cover and abundant water resources [35]. At the same time, due to the differences in the role of these three dimensions in water conservation in the core urban area of Lanzhou, the weights of distance to water, slope, and vegetation coverage were determined through a combination of expert scoring and the Analytic Hierarchy Process (AHP). The specific data and importance grades are shown in Table 1. The classification and weight of these indicators are only for ecological land, not including non-ecological land such as construction land. In fact, the evaluation parameters of construction land will be different from ecological land, such as slower slope and lower requirements for vegetation coverage. Moreover, the related factors used in the evaluation of the water conservation function were mainly determined according to the climatic conditions, geomorphic types, land cover, and ecological status of Lanzhou, which can represent the characteristics of cities in arid hilly areas of northwest China to a certain extent.

Table 1. Evaluation system for the function of water conservation.

Evaluation Factors	Distance from Water Area (km)	Slope (%)	FVC (%)	Importance	Value
Weight	**0.35**	**0.18**	**0.47**		
Classification	0–0.5	<5	0.5–1	*Most important*	5
	0.5–1	5–10	0.4–0.5	*Very important*	4
	1–1.5	10–15	0.3–0.4	*Important*	3
	1.5–2	15–20	0.2–0.3	*Generally important*	2
	>2	>20	0–0.2	*Unimportant*	1

Note: FVC, Fractional Vegetation Cover.

2.4. Assessment of Ecological Demand

Previous studies have shown that evaluation of the importance of ecological land not only needs to involve analysis of the land's own natural ecological functions but also needs to consider the degree of demand in a city [8,9,24]. In general, the closer ecological land is to a residential area and the more people it serves, the higher the degree of demand will exist for that land. Therefore, the intensity of the demand of urban residents for ecological land is often related to the spatial location of that land, the number of people covered by its services, and other factors [15]. Nighttime light intensity has been proven to be a good reflection of the level of human activity such as regional population density and resource consumption, and provides a visual representation of the intensity of human activity that can be represented in a geographical spatial distribution [36,37]. In view of this, the present study used the nighttime light intensity to characterize the population density of different areas in the core urban area of Lanzhou. Then, combined with the traffic conditions and the specific travel situation for residents in Lanzhou, the different demand radii of ecological land for urban residents on working days and holidays were set based on the standard of 3 km and 10 km, respectively. Finally, the kernel density estimation of ArcGIS was used to obtain the social demand intensity of ecological land under different demand radii. In addition, previous studies have pointed out that ecological land and water areas with good vegetation cover are often more attractive than other areas [13,15], so the normalized difference vegetation index (NDVI) and normalized difference water index (NDWI) should also be included in the calculation of ecological demand. In conclusion, based on the nighttime light intensity and the characteristics of ecological land, this paper constructed an ecological demand index, *NI*, of ecological land in the core urban area of Lanzhou

$$NI = \frac{0.5PD_i^1 + 0.5PD_i^2}{ED_i} \times (NDVI_i + NDWI_i), \quad (4)$$

where NI is the ecological demand index of grid i; PD_i^1 and PD_i^2 are the social demand intensities of working days and holidays corresponding to grid i, respectively, i.e., the kernel density values of nighttime light intensity under different demand radii; ED_i is the spatial distance between grid i and a densely populated area, and $NDVI_i$ and $NDWI_i$ are the normalized difference vegetation and water indices corresponding to grid i.

3. Results and Discussion

3.1. Impact of Ecological Service Function and the Intensity of Ecological Demand on the Importance of Ecological Land

The spatial distribution of important ecological land in the core urban area of Lanzhou is shown in Figure 2. This figure shows that, without considering the intensity of demand for ecological land, the spatial extent of *important* ecological land in the study area is gradually increasing from the center to the periphery and forming a continuous circular distribution. These important ecological lands are mainly composed of large areas of woodland, grassland, and bare land on the periphery of the study area. In particular, the natural barrier formed by the Qilian Mountains on the southern boundary of the city is the most concentrated and largest area of important ecological land in Lanzhou. However, even

from the perspective of ecological service capacity, many other *very important* ecological lands still exist in the urbanized area, such as the scattered urban green space along both banks of the Yellow River, and the wasteland with a low degree of development in the western part of the city. Although these ecological lands that are distributed in urbanized and densely populated areas tend to be relatively small, they still have a high ecological service value; they are irreplaceable in terms of biodiversity maintenance, soil maintenance, and water conservation. Previous studies have shown that the peripheral area of the city is often surrounded by a large area of ecological land; the ecological service capacity of this land will be significantly larger than that of the green space inside the city [38–40]. However, in the core urban area of Lanzhou, the importance of small areas of ecological land such as rivers, lakes, parks, and green spaces inside the urbanized area has not been lessened in the ecological function evaluation. The ecological function of this land should not be ignored.

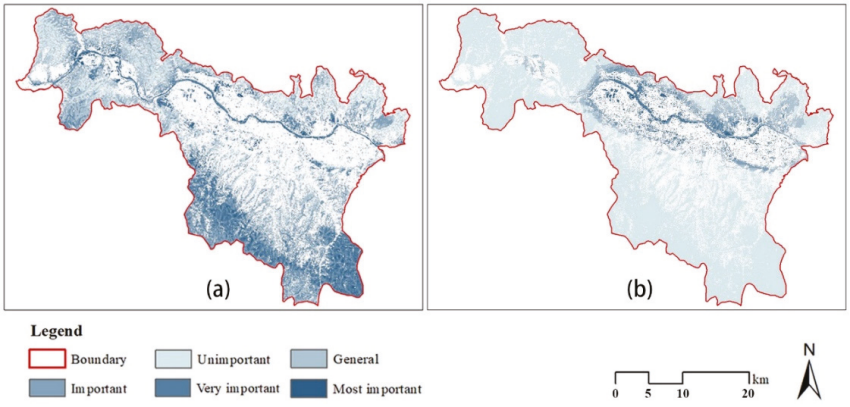

Figure 2. Maps of results of (**a**) ecological function evaluation and (**b**) ecological demand intensity evaluation in the study area.

The spatial distribution of ecological land in high demand and in the core urban area of Lanzhou is shown in Figure 2b. This figure shows that, contrary to the distribution of ecological land based on an evaluation of ecological function, the spatial distribution of ecological land based on an evaluation of ecological demand is characterized by gradually increasing importance from the periphery to the city center. The land with the highest ecological demand is concentrated in the urbanized area and surrounding areas, because this land is close to residential areas. Therefore, it can provide urgently needed ecological services for the dense population within an area of construction land. The layout of Lanzhou is affected by the topography of mountain ranges to the north and south. As a result, the construction land of Lanzhou has been expanding in the form of a strip, which also makes the land that is in high demand for ecological needs around the construction land show characteristics of being distributed in long and narrow strips in an east–west direction. Compared with a consideration only of ecological function, an evaluation based on ecological demand intensity highlights the ecological benefits and values of urban park green space and public green space in densely populated areas, such as Lanshan Scenic Resort, Baita Mountain Park, Xujiashan National Forest Park, Wuyishan Ecological Scenic Spot, Yintan Wetland Park, Lanzhou Botanical Garden, and Anning Peach Garden. In addition, in the evaluation of ecological function, the entire section of the Yellow River passing through the city provides some *very important* ecological land (Figure 2a). However, in the evaluation of the intensity of ecological demand (Figure 2b), the river section from Chaijiatai in Xigu District to Qingbaishi in Chengguan District was obviously relatively important ecological land, while most of the river sections flowing through Xigu District

were less important. This is also true because the former has more intense ecological demand and can provide ecosystem services for larger numbers of urban residents. Therefore, more attention should be paid to the ecological benefits of the river and its banks than to the development and potential use of the reach of the Yellow River in this area of high population density.

In brief, after adding the analysis of the intensity of ecological demand, the results were more in line with the actual situation of ecological protection and high-quality development in highly populated and urbanized areas. Figure 3 shows the results of this type of analysis, which includes ecosystem services and ecological demand. However, it is worth considering that, even without an analysis of the intensity of ecological demand, the ecological land within the urbanized area itself has a high ecosystem service value. This seems to be a major feature of cities in the arid areas of northwest China, unlike cities in the coastal areas of southeast China. Generally speaking, the combination of ecological protection and urban development often involves contradictory trade-offs. Urban sprawl will disturb natural ecosystems, turning a large area of green space into hard impervious surfaces, and destroy the circulation of natural material and energy [41–45]. However, it seems that the relationship between development and environmental protection needs to be reexamined in the arid hilly areas of northwest China. The cold climate and limited rainfall result in natural low biodiversity with limited green space in the arid hilly areas of northwest China. The ravines and deep valleys greatly weaken the ecological value of the non-urbanized areas. Some urban parks and public green spaces in the urbanized areas are adequately funded and maintained, which has significantly improved the ecological benefits they provide; they may even provide the most important natural services and ecological support for some cities. Therefore, urban sprawl may not necessarily be the cause of ecological damage for cities in arid hilly areas of northwest China; in contrast, urbanization may provide opportunities for ecological restoration and improvement. Of course, the premise requires land managers to pay attention to the planning for and management of existing ecological land [46], as well as managing the integrity of the overall ecological spatial pattern of the city.

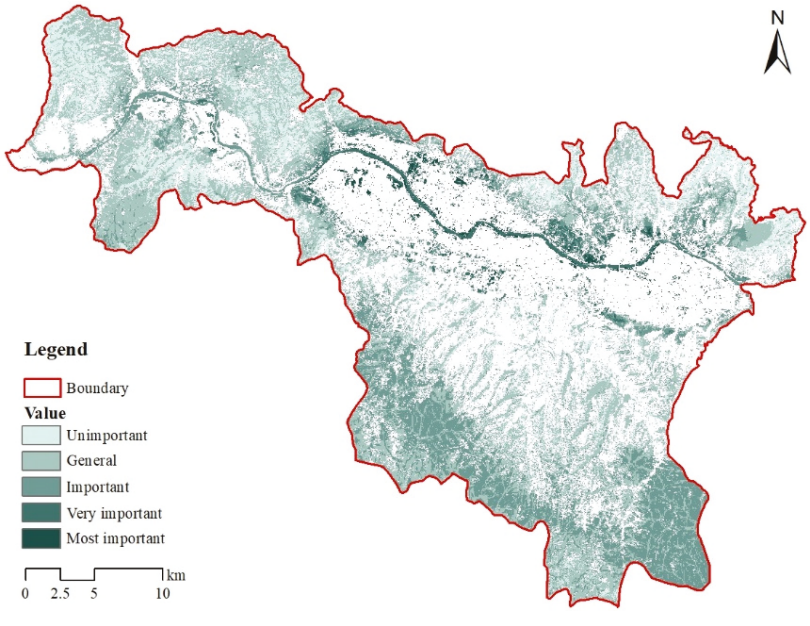

Figure 3. Comprehensive evaluation results for ecological land importance in the study area.

3.2. Analysis of the Overall Characteristics of Ecological Land Structure

The results are shown in Table 2. The *most important* ecological patches covered 12.70 km^2 (1.50% of the total ecological land, and 1.21% of the entire study area). The *very important* ecological patches covered 36.82 km^2 (4.36% and 3.52%, respectively, as described above). The *important* ecological patches covered 154.7 km^2 (18.31% and 14.80%, respectively). The *generally important* ecological patches covered 401.7 km^2 (47.52% and 38.40%, respectively). The *unimportant* ecological patches covered 239.3 km^2 (28.31% and 22.88%, respectively). Among them, the *generally important* ecological patches occupied the largest proportion, followed by the *unimportant* ecological patches, while the *important* ecological patches were the third largest area. Meanwhile, the *most important* and *very important* ecological patches covered the smallest areas of both total ecological land and the entire study area. That is, high value ecological land in the core urban area of Lanzhou is still very scarce; almost all the *most important* and *very important* ecological patches were in urbanized areas (Figure 4). Meanwhile, the large amount of ecological land outside the urbanized area was of relatively low value. This finding shows that the ecological land within an urbanized setting provides many much-needed ecological benefits. In addition, away from urbanized areas the ecological land has a low amount of green space, with rather poor-quality land; here, the ecological services of maintaining biodiversity and conserving soil and water are still weak. It is not possible to provide the higher quality ecological land typical of the urbanized area in nearby rural areas without major changes. The above problems are not only caused by the limitations of climate, terrain, and other natural conditions. Slow urban expansion has included positive steps toward environmental transformation and improvement in Lanzhou in recent years; nevertheless, these positive effects in the city itself have failed to radiate and drive the optimization of environmental conditions in the peripheral areas of the city.

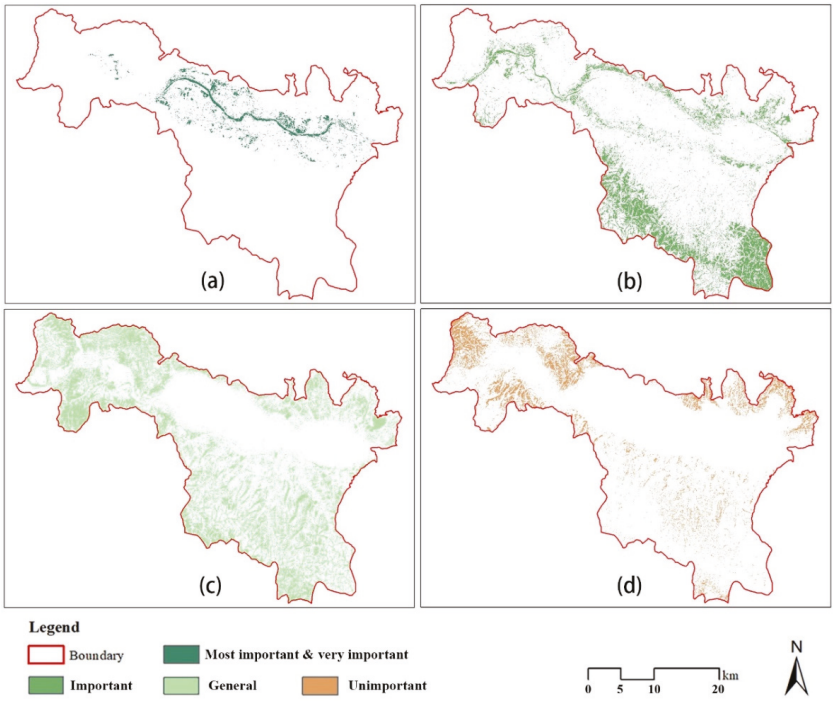

Figure 4. Distribution of: (**a**) the *most important* and *very important*, (**b**) *important*, (**c**) *generally important*, and (**d**) *unimportant* ecological land.

Table 2. Area and proportion of ecological land at different importance levels.

Importance Level of Ecological Patches	Coverage Area (km^2)	Proportion in All Ecological Land (%)	Proportion in the Study Area (%)
The *most important* ecological patches	12.70	1.5	1.21
The *very important* ecological patches	36.82	4.36	3.52
The *important* ecological patches	154.7	18.31	14.8
The *generally important* ecological patches	401.7	47.52	38.4
The *unimportant* ecological patches	239.3	28.31	22.88

Note: The proportion of non-ecological land in the study area is 19.19%.

Although the *most* and *very important* ecological patches in the urbanized area cover small, fragmented areas, this rare core urban area of Lanzhou can provide high-quality ecosystem services for urban residents. These areas should be treasured, and construction should be strictly prohibited. Land management in these areas should emphasize their ecological importance. These lands can not only beautify the living environment but also meet the daily outdoor leisure needs of urban residents. Therefore, future urban planning and land management should focus on promoting the improvement and positive environmental development of the large areas of ecological land surround the urbanized areas of this region; in addition, attention should also be paid to the protection of the core ecological space inside the city.

3.3. Analysis of Ecological Land Structure Characteristics at the Land Use Level

Figure 5 shows the distribution of the five types of ecological land in the study area. Most woodlands serve as *important* ecological land with *important* ecological patches accounting for 68.72% of the total area of woodland, while the *unimportant* and *most important* ecological patches only accounted for 0.57% and 0.45% of the total area of woodland, respectively. Woodlands in the study area typically have a high level of vegetation coverage, with a strong capacity to provide ecological services. However, most of the woodlands occur in hilly areas with deep valleys, high mountains, and frequent gullies outside the urbanized area. As a result, the relatively barren soil and steep slopes also affect the ability of humans to terraform the landscape and improve the ecological value of woodlands, to a certain extent. Nevertheless, woodland is still a land type with high ecological value in the core area of urban Lanzhou. Woodlands can serve as wind breaks and help fix blowing sand, conserve water, and help to maintain biodiversity, making them irreplaceable and in need of protection. The ecological importance of grassland and bare land is at the *generally important* level, with *generally important* ecological patches making up 56.64% and 54.30%, respectively, of their respective overall landscapes. The proportion of *important* ecological patches was 22.23% and 17.19% for these respective land types. Obviously, a considerable amount of room is available for the improvement of grassland and bare land in terms of ecological value. In the process of urbanization and land management, gradually increasing the vegetation cover in grassland and bare land will undoubtedly greatly enhance the ecological service capacity of these areas allowing them to serve complex functions. Large areas of wasteland and bare land with *generally important* ecological value can be transformed into urban green public space with high ecological value.

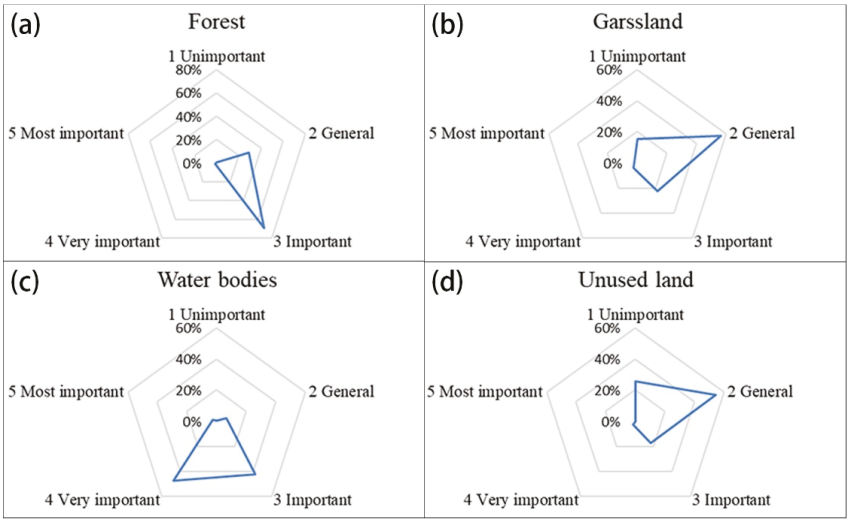

Figure 5. Distribution of ecological land by classification (*unimportant* to *most important*) and land type: (**a**) forest; (**b**) grassland; (**c**) water body; (**d**) unused land.

Water area has the highest average ecological value of ecological land types in the core urban area of Lanzhou. The *very important* and *important* ecological patches of water accounted for 47.56% and 42.38%, of the total water area, respectively. The Yellow River not only provides important ecosystem services for Lanzhou but also serves as a cultural symbol of the city. Therefore, city managers should prioritize the ecological protection of the Yellow River and its surrounding space. Therefore, the ecological transformation and improvement of the Yellow River flood discharge channels in the core urban area of Lanzhou should be strengthened, which is conducive to the formation of a beautiful urban water network system that provides ecological and recreational benefits for city residents.

Figure 6, which illustrates the proportions of various importance levels of the five ecological land types, shows that more than 40% of the grassland was classified as *unimportant*, *generally important*, *important*, and *very important* ecological land. In contrast, the proportion of grassland in the *most important* category is as high as 88.23%. Obviously, grassland makes up the highest proportion in all five types of ecological land. Therefore, from another perspective, grassland has most ecological potential in the core urban area of Lanzhou. In fact, Gansu Province, as one of the six major pastoral areas in China, has a total grassland area of about 14.17 million ha. The structural proportions of various ecological land types in the core urban area of Lanzhou reflect in miniature the distribution of land resources in Gansu Province, where grassland undoubtedly plays an important ecological barrier function across the landscapes of the province. In addition to ecological functions, the open and rolling grassland has a unique northwest-China charm in visual perception and provides excellent aesthetic value; many landscape perception studies have also pointed out that sparse forest and grassland, also known as savannahs, is the most popular landscape type among humans [47,48]. In addition, small ecological patches of grassland can effectively enhance the biodiversity of grass and other flowering plants [49], while large areas of grass and flowering plants can also form an effective ecological interface and provide sparse landscape nodes in a city, which is of great significance for wind and sand fixation, along with improving the urban landscape. However, the grassland in the core urban area of Lanzhou has not been fully given adequate attention. This is especially true for the wasteland areas outside urbanized Lanzhou, which suffer from a lack of planning and management meaning they face the risk of further ecological deterioration at any time. Therefore, city managers should strengthen the use and reestablishment of

urban grassland, and bring into full play the ecological, social, and economic benefits of grassland during the development of urban land.

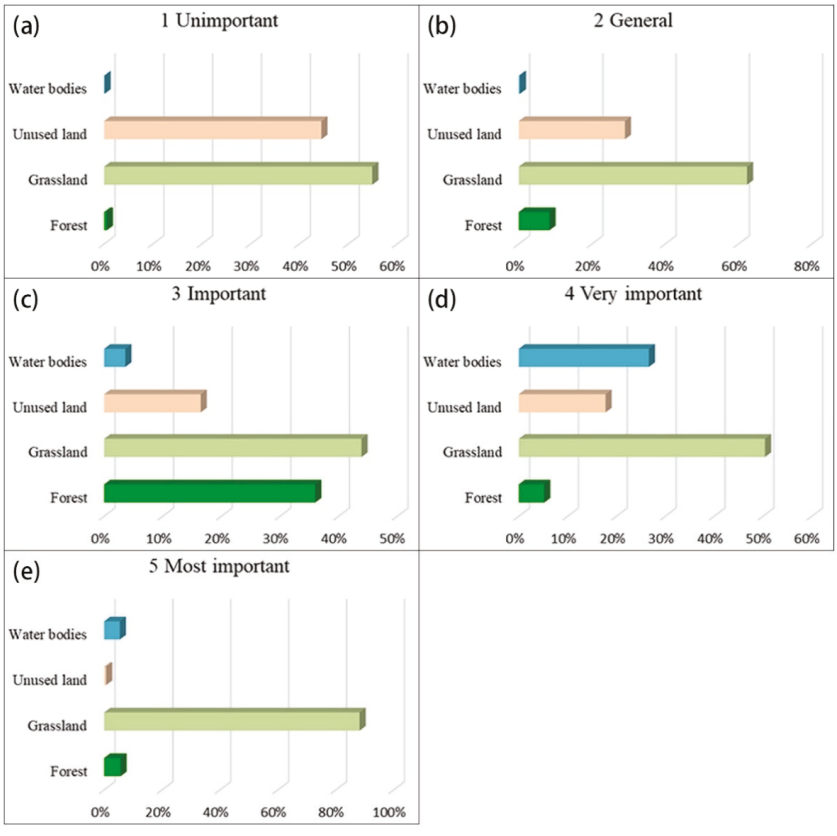

Figure 6. Percentages of the five types of ecological land as a proportion of all ecological land types within each level: (**a**) *unimportant*; (**b**) *generally important*; (**c**) *important*; (**d**) *very important*; (**e**) *most important*.

3.4. Analysis of the Structural Characteristics of Ecological Land at the Level of Spatial Distribution

Figure 7 shows the spatial distribution of the five importance levels of ecological land in Lanzhou. From the perspective of distribution and orientation (Figure 7a), ecological land of different importance levels presents significant anisotropic distribution characteristics. Among them, the districts of Chengguan and Anning had the smallest amount of ecological land, while Qilihe and Xigu districts had the most. The *most important* and *very important* ecological lands are mainly concentrated in the central and northern part of the study area, which are along the banks of the Yellow River and in the densely populated areas of Chengguan, Qilihe, and Anning. Most of the *important* ecological land is concentrated in the southern and southeastern parts of the study area, namely in the southern mountainous area of Qilihe. This area of the Qilian Mountains includes protected natural areas such as Xinglongshan and Shifogou national forest parks that lie in the continuous mountainous areas that have relatively rich plant resources. Good vegetation combined with natural topography forms a unique mountain ecological barrier. *Generally important* ecological lands are mainly distributed in the northwestern and southeastern parts of the research area, from the point of view of administrative divisions. Similarly, Qilihe and Xigu have

a large number of *generally important* ecological lands, while Chengguan and Anning districts have a relatively small number of these lands. This has occurred because the administrative areas of Qilihe and Xigu districts are larger than those of Chengguan and Anning. However, due to the relatively high proportion of urbanized land in Chengguan and Anning, the proportion of ecological land has been reduced to some extent. As a result, these districts have only a small number of *generally important* ecological land units. When reviewing the structural characteristics analysis of land types in each administrative region (Figure 7b), one can see that the *generally important* grade of ecological land in Qilihe District mainly consisted of the forest and grassland with relative steep slopes, while the *generally important* ecological land in Xigu District was mainly composed of barren grassland and undeveloped bare land. Therefore, from the perspective of land use types, the *generally important* ecological land in Qilihe District is more suitable for further ecological restoration; that is, based on maintaining the existing forest structure and function, the existing forest and grassland with poor terrain and soil quality could be transformed into high-quality forest land by means of ecological conservation and restoration with the goal of maintaining and improving the regional environment. The *generally important* grade ecological land in Xigu District, namely the grassland and bare land located in relatively flat areas, is more suitable for transformation into public green space during urbanization, so as to provide convenient recreational opportunities for urban residents in an aesthetically pleasing landscape. In recent years, Lanzhou has adopted the development strategy of "expanding east, west and north while promoting the south", with the goal of addressing the restrictions of geographical conditions to make more land readily accessible. Among these aims, the "promoting the south" and "expanding west" involve Qilihe and Xigu, respectively, especially for the *important* and *generally important* ecological land in the region. That is, management of a large number of grassland and bare land areas needs to be addressed and planned so as to protect these areas during the process of urban expansion, so as to form a more perfect green infrastructure space system during the new round of urbanization.

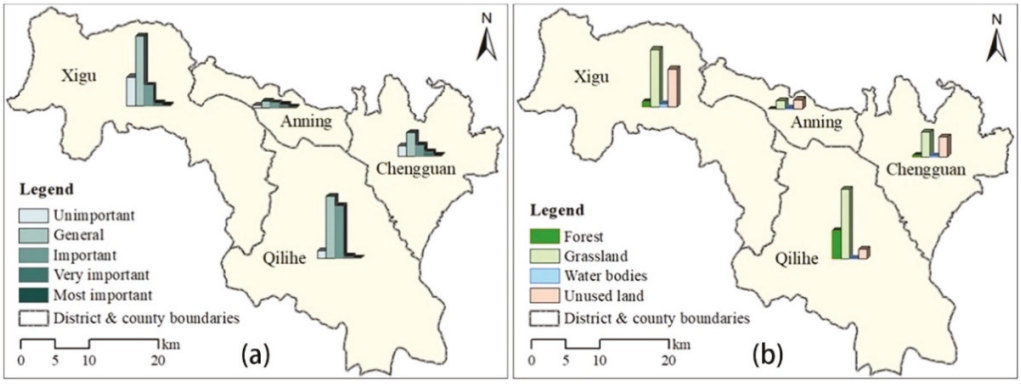

Figure 7. Distribution of various types of ecological land in different regions: (**a**,**b**) show the proportions of ecological land with different importance levels and various land types, respectively, in the core urban districts of Lanzhou.

3.5. Significance and Application

The importance evaluation of ecological land from the two aspects of ecological function and ecological demand can provide a new perspective for the identification of ecological sources and the construction of ecological patterns [16], especially in high-density urban areas. However, the existing research focuses mainly on the natural value of ecological land [50–52], and less on the importance of ecological land from the perspective of humanistic care. For the arid hilly areas in northwest China, such research is lacking.

The ecological environment in the arid hilly areas in northwest China is poor, the land is tight, and the contradiction between construction and protection is more acute. Therefore, it is particularly urgent to evaluate the importance of ecological land. Taking this as the starting point, this study makes a corresponding attempt. On the basis of comprehensively considering ecological function and ecological demand, this study mainly has two innovations in its methods: first, according to the regional characteristics of arid hilly areas in northwest China, appropriate ecological function evaluation dimensions and relevant parameters of ecological demand model are selected. Second, the classification and weight of specific indicators are refined through expert scoring and analytic hierarchy process, so as to make the evaluation method more targeted. In addition, this study takes Lanzhou as a case, which can provide reference for ecological restoration and urban design of cities in arid hilly areas in northwest China, and also has a certain practical significance. It should be noted that, although the evaluation system proposed in this study is universal for the evaluation of ecological land in arid hilly areas of northwest China, in specific operation the parameter details in the model can be adjusted appropriately according to the regional characteristics in order to produce more accurate results.

3.6. Limitations

This study mainly evaluated the importance of the core urban ecological land in Lanzhou. This was done by coupling the service function of ecological land use and the intensity of ecological demand using a simple evaluation method. The study used scientific method to systematically evaluate the sources of ecological services from different types of land use, emphasizing areas described as ecological land as opposed to urbanized or other land use types. In general, this method mainly involved the investigation of the vertical ecological process of ecological patches, i.e., the vertical superposition effect of various properties inside a certain ecological source. The study lacks a consideration of the overall horizontal ecological processes in the region. In follow-up research, it will be necessary to expand the evaluation dimension of the importance of ecological land, and include the material and information flow capacity between ecological patches into the evaluation system. In addition, Morphological Spatial Pattern Analysis (MSPA) could be used to guide the identification of habitat sources based on spatial-morphological attributes such as patch area and spatial-topological relationships. The application of MSPA in the identification of ecological sources and the construction of a regional ecological security network is becoming mature [53–56]. How to effectively integrate the concepts and methods of MSPA in the evaluation of the importance of ecological land will be the content of future in-depth exploration of this topic.

4. Conclusions

This study aims to establish an importance evaluation system for ecological land use, reveal the distribution and development characteristics of urban ecological land in the arid hilly region of northwest China represented by Lanzhou, and provide reference for ecological restoration and urban planning in Lanzhou and other arid inland cities along the upper reaches of the Yellow River. The main conclusions follow.

(1) The model used to evaluate the importance of ecological land was based on the dual perspectives of the function of providing ecosystem services and the intensity of ecological demand. This model is more suitable to evaluate for the need for ecological protection in arid and hilly areas of northwest China and highly urbanized areas. Compared with only considering the ecosystem service function of ecological land, the research results can consider the demands and needs of urban residents and can effectively identify the types of ecological land that have a high degree of ecological demand within the city, which has practical significance for the protection of ecological resources in the core of the city.

(2) For the core urban area of Lanzhou, even from a single perspective of ecological function, urban parks and public green space in densely populated areas of urbanized area

also have *very important* ecological values. After adding an evaluation of the intensity of ecological demand, the ecological importance of parks and other green space in urbanized area was further strengthened. Most of the *most important* ecological land was distributed in densely populated areas. Obviously, for cities in the arid and hilly areas of northwest China represented by the core urban area of Lanzhou, the spread of urbanized areas will not mean that the surrounding natural landscape will inevitably be destroyed. On the contrary, the development of cities may provide opportunities for the ecological restoration and renovation of surrounding barren and bare land.

(3) The *most important* and *very important* ecological land in the core area of Lanzhou only accounted for 5.86% of the total area of all ecological land within the city, indicating that high-value ecological land in the core area of Lanzhou is still very scarce. Among these important areas, the water area (mainly the Yellow River and its waterfront space) is the ecological land with the highest average ecological value in Lanzhou, followed by forest land. In addition, one can see that the land type with the highest spatial proportion among all levels of ecological land is grassland. Grassland can be said to be the ecological land with the most potential in the core urban area of Lanzhou; its ecological function will be continuously lost over time if it is not properly managed and protected. Careful planning and use can allow grassland to serve as an indispensable ecological barrier in Lanzhou, which can not only play an ecological function but can also provide good aesthetic space and recreational opportunities for the general public.

(4) From the perspective of spatial distribution, the urbanized areas of Chengguan and Anning districts accounted for a large proportion; these areas have a limited amount of ecological land, but the *most important* ecological land is also mostly distributed here. Qilihe and Xigu districts have more *generally important* graded areas of forest, grassland, and bare land, although the current ecological value of these lands is limited; nevertheless, these lands have great potential for ecological improvement, which should be considered in the future. With the accelerating development of Lanzhou in recent years, a large number of underused ecological lands in Qilihe and Xigu undoubtedly include valuable properties in the core urban area of Lanzhou. These areas will need to be continuously improved to reach their peak ecological service capacity in light of urban sprawl and urban function transfer. Appropriate land management should be carried out to further improve the level of connectivity through the construction of ecological corridors, so as to form a scientific and reasonable regional ecological security pattern and lay a healthy and sustainable material foundation for a new round of urban development.

Author Contributions: Conceptualization, Y.L. and C.L.; methodology, Y.L. and C.L.; formal analysis, Y.L., J.M., J.P., Z.L. and M.H.; investigation, Y.L., C.L., J.M., J.P., Z.L. and M.H.; writing—original draft preparation, Y.L.; writing—review and editing, C.L. All authors have read and agreed to the published version of the manuscript.

Funding: This research was funded by Fundamental Research Funds for the Central Universities (21lzujbkydx010, 2020jbkyjc002).

Institutional Review Board Statement: Not applicable.

Informed Consent Statement: Not applicable.

Data Availability Statement: The data used to support the findings of this study are available from the corresponding author upon reasonable request.

Acknowledgments: We thank LetPub (www.letpub.com (accessed on 16 August 2021)) for its linguistic assistance during the preparation of this manuscript.

Conflicts of Interest: The authors declare no conflict of interest.

References

1. Liu, Y.Q.; Wang, R.Y.; Lu, Y.; Li, Z.G.; Chen, H.S.; Cao, M.Q.; Zhang, Y.R.; Song, Y.M. Natural outdoor environment, neighbourhood social cohesion and mental health: Using multilevel structural equation modelling, streetscape and remote-sensing metrics. *Urban For. Urban Green.* **2020**, *48*, 126576. [CrossRef]
2. Yu, F.; Li, X.B.; Zhang, L.J.; Xu, W.H.; Fu, R.; Wang, H. Study of ecological land in China: Conception, classification, and spatial-temporal pattern. *Acta Ecol. Sin.* **2015**, *35*, 4931–4943.
3. Aminzadeh, B.; Khansefid, M. A case study of urban ecological networks and a sustainable city: Tehran's metropolitan area. *Urban Ecosyst.* **2010**, *13*, 23–36. [CrossRef]
4. Vergnes, A.; Kerbiriou, C.; Clergeau, P. Ecological corridors also operate in an urban matrix: A test case with garden shrews. *Urban Ecosyst.* **2013**, *16*, 511–525. [CrossRef]
5. Xie, H.; Yao, G.; Liu, G. Spatial evaluation of the ecological importance based on GIS for environmental management: A case study in Xingguo county of China. *Ecol. Indic.* **2015**, *51*, 3–12. [CrossRef]
6. Peng, J.; Zong, M.L.; Hu, Y.N.; Liu, Y.X.; Wu, J.S. Assessing landscape ecological risk in a mining city: A case study in Liaoyuan city, China. *Sustainability* **2015**, *7*, 8312–8334. [CrossRef]
7. Wu, J.S.; Zhang, L.Q.; Peng, J.; Feng, Z.; Liu, H.M.; He, S.B. The integrated recognition of the source area of the urban ecological security pattern in Shenzhen. *Acta Ecol. Sin.* **2013**, *33*, 4125–4133.
8. Peng, J.; Wang, A.; Liu, Z.X.; Ma, J.; Wu, J.S. Research progress and prospect on measuring urban ecological land demand. *Acta Georaphica Sin.* **2015**, *70*, 333–346.
9. Zhou, Z.; Meng, J.J.; Qi, Y.; Peng, F.L. Importance of ecological lands and their pattern optimization in China: A review. *Chin. J. Ecol.* **2016**, *35*, 218–225.
10. Orban, E.; Sutcliffe, R.; Dragano, N.; Jöckel, K.H.; Moebus, S. Residential surrounding greenness, self-rated health and interrelations with aspects of neighborhood environment and social relations. *J. Urban Health* **2017**, *94*, 158–169. [CrossRef]
11. Van Renterghem, T.; Botteldooren, D. View on outdoor vegetation reduces noise annoyance for dwellers near busy roads. *Landsc. Urban Plan.* **2016**, *148*, 203–215. [CrossRef]
12. Enssle, F.; Kabisch, N. Urban green spaces for the social interaction, health and well-being of older people: An integrated view of urban ecosystem services and socio-environmental justice. *Environ. Sci. Policy* **2020**, *109*, 36–44. [CrossRef]
13. Baró, F.; Palomo, I.; Zulian, G.; Vizcaino, P.; Haase, D.; Gómez-Baggethun, E. Mapping ecosystem service capacity, flow and demand for landscape and urban planning: A case study in the Barcelona metropolitan region. *Land Use Policy* **2016**, *57*, 405–417. [CrossRef]
14. Wolff, S.; Schulp, C.J.E.; Verburg, P.H. Mapping ecosystem services demand: A review of current research and future perspectives. *Ecol. Indic.* **2015**, *55*, 159–171. [CrossRef]
15. Zhang, Y.N.; Chen, Z.J.; Zhang, Y.Q.; Mei, M.Y. Urban ecological importance assessment based on ecological function and ecological demand: A case study of Changsha. *Resour. Environ. Yangtze Basin* **2018**, *27*, 2358–2367.
16. Zhang, L.Q.; Peng, J.; Liu, Y.X.; Wu, J.S. Coupling ecosystem services supply and human ecological demand to identify landscape ecological security pattern: A case study in Beijing-Tianjin-Hebei region, China. *Urban Ecosyst.* **2017**, *20*, 701–714. [CrossRef]
17. Zhang, X.C.; Liang, X.C.; Song, X.; Liu, J.S. Spatial pattern of the mismatch degrees of the high-quality development of tourism industry in the Yellow River basin. *J. Arid Land Resour. Environ.* **2020**, *34*, 201–208.
18. Wang, S.P.; Qiao, H.F.; Feng, J.; Xie, S.Y. The spatio-temporal evolution of tourism eco-efficiency in the Yellow River basin and its interactive response with tourism economy development level. *Econ. Geogr.* **2020**, *40*, 81–89.
19. Ma, L. Debate and thinking about the ecological impact of "bulldoze mountains to build new city": A case study of Lanzhou new city. *Mod. Urban Res.* **2016**, *6*, 85–90.
20. Gao, J.X.; Xu, D.L.; Qiao, Q.; Zou, C.X.; Wang, Y.; Tian, M.R.; Wang, Y. Pattern construction of natural ecological space and planning theory exploration. *Acta Ecol. Sin.* **2020**, *40*, 749–755.
21. Gozdowski, D.; Stępień, M.; Panek, E.; Varghese, J.; Bodecka, E.; Rozbicki, J.; Samborski, S. Comparison of winter wheat NDVI data derived from Landsat 8 and active optical sensor at field scale. *Remote Sens. Appl.* **2020**, *20*, 100409. [CrossRef]
22. Cao, H.Y.; Han, L.; Liu, Z.H.; Li, L.Z. Monitoring and driving force analysis of spatial and temporal change of water area of Hongjiannao Lake from 1973 to 2019. *Ecol. Inform.* **2021**, *61*, 101230. [CrossRef]
23. Song, N.Y.; Wei, L. Study on urban greening in Lanzhou from 1941 to 1949. *J. Arid Land Resour. Environ.* **2019**, *33*, 184–189.
24. Ma, C.; Li, S.; Liu, J.; Gao, Y.; Wang, Y. Regionalization of ecosystem Services of Beijing-Tianjin-Hebei Area based on SOFM neural network. *Prog. Geogr.* **2013**, *32*, 1383–1393.
25. Meng, J.J.; Wang, Y.; Wang, X.D.; Zhou, Z.; Sun, N. Construction of landscape ecological security pattern in Guiyang based on mcr model. *Resour. Environ. Yangtze Basin* **2016**, *25*, 1052–1061.
26. Bi, X.L.; Ge, J.P. Evaluating ecosystem service valuation in China based on the IGBP land cover datasets. *J. Mt. Sci.* **2004**, *2*, 48–53.
27. Zurlini, G.; Petrosillo, I.; Aretano, R.; Castorini, I.; Zaccarelli, N. Key fundamental aspects for mapping and assessing ecosystem services: Predictability of ecosystem service providers at scales from local to global. *Ann. Bot.* **2014**, *4*, 53–63.
28. Jahun, B.G.; Ibrahim, R.; Dlamini, N.S.; Musa, S.M. Review of soil erosion assessment using RUSLE model and GIS. *J. Biol. Agric. Healthc.* **2015**, *5*, 36–47.
29. Van Oost, K.; Govers, G.; Desmet, P. Evaluating the effects of changes in landscape structure on soil erosion by water and tillage. *Landsc. Ecol.* **2000**, *15*, 577–589. [CrossRef]

30. Liu, B.Y.; Nearing, M.A.; Risse, L.M. Slope gradient effects on soil lossfor steep slopes. *Trans. ASAE* **1994**, *37*, 1835–1840. [CrossRef]
31. Wischmeier, W.H.; Smith, D.D. Predicting rainfall erosion losses: Aguide to conservation planning with the universal soil loss equation. In *Agricultural Handbook No. 537*; United States Department of Agriculture: Springfield, IL, USA, 1978.
32. Wischmeier, W.H.; Smith, D.D. Rainfall energy and its relationship tosoil loss. *Trans. Am. Geophys. Union* **1958**, *39*, 285–291. [CrossRef]
33. Hu, G.; Song, H.; Shi, X.J.; Zhang, M.L.; Liu, X.J.; Zhang, X.L. Soil erosion characteristics based on RUSLE in the Wohushan reservoir watershed. *Sci. Geogr. Sin.* **2018**, *38*, 610–617.
34. Gong, S.H.; Xiao, Y.; Zheng, H.; Xiao, Y.; Ouyang, Z.Y. Spatial patterns of ecosystem water conservation in China and its impact factors analysis. *Acta Ecol. Sin.* **2017**, *37*, 2455–2462.
35. Luo, X.; Yang, J.; Sun, W.; He, B.J. Suitability of human settlements in mountainous areas from the perspective of ventilation: A case study of the main urban area of Chongqing. *J. Clean. Prod.* **2021**, *310*, 127467. [CrossRef]
36. Chen, S.L.; Chen, H.H.; Li, X. The ability of nighttime imagery in monitoring economic activity in different scales. *Sci. Geogr. Sin.* **2020**, *40*, 1476–1483.
37. Lv, Q.; Liu, H.B. Multiscale spatio-temporal characteristics of carbon emission of energy consumption in Yellow River basin based on the nighttime light datasets. *Econ. Geogr.* **2020**, *40*, 12–21.
38. Terrado, M.; Sabater, S.; Chaplin-Kramer, B.; Mandle, L.; Ziv, G.; Acuña, V. Model development for the assessment of terrestrial and aquatic habitat quality in conservation planning. *Sci. Total Environ.* **2015**, *540*, 63–70. [CrossRef]
39. Wang, L.R.; Feng, X.L.; Chang, Q.; Liu, H.; Wang, J. Pattern construction of habitat network for urban green space based on the compound model of InVEST and MCR. *Chin. Landsc. Archit.* **2020**, *36*, 113–118.
40. Han, Y.W.; Li, Y.N.; Li, F.Z. Effects of Landscape Patterns of Urban Green Spaces on "Core Habitat" Quality. *Landsc. Archit.* **2020**, *27*, 83–87.
41. Fan, H.Y.; Yu, Z.W.; Yang, G.Y.; Liu, T.Y.; Hung, C.H.; Vejre, H. How to cool hot-humid (Asian) cities with urban trees? An optimal landscape size perspective. *Agric. For. Meteorol.* **2019**, *265*, 338–348. [CrossRef]
42. Yang, G.Y.; Yu, Z.W.; Jørgensen, G.; Vejre, H. How can urban blue-green space be planned for climate adaption in high-latitude cities? A seasonal perspective. *Sustain. Cities Soc.* **2020**, *53*, 101932. [CrossRef]
43. Yang, J.; Wang, Y.C.; Xue, B.; Li, Y.F.; Xiao, X.M.; Xia, J.H.; He, B.J. Contribution of urban ventilation to the thermal environment and urban energy demand: Different climate background perspectives. *Sci. Total Environ.* **2021**, *795*, 148791. [CrossRef]
44. Sun, R.; Wang, Y.; Chen, L. A distributed model for quantifying temporal-spatial patterns of anthropogenic heat based on energy consumption. *J. Clean. Prod.* **2018**, *170*, 601–609. [CrossRef]
45. Ebrahimi, A.; Motamedvaziri, B.; Nazemosadat, S.M.J.; Ahmadi, H. Investigating the land surface temperature reaction to the land cover patterns during three decades using landsat data. *Int. J. Environ. Sci. Technol.* **2021**. [CrossRef]
46. Yang, J.; Yang, R.X.; Chen, M.H.; Su, C.H.; Zhi, Y.; Xi, J.C. Effects of rural revitalization on rural tourism. *J. Hosp. Tour. Manag.* **2021**, *47*, 35–45. [CrossRef]
47. Lis, A.; Iwankowski, P. Why is dense vegetation in city parks unpopular? The mediative role of sense of privacy and safety. *Urban For. Urban Green.* **2021**, *59*, 126988. [CrossRef]
48. Wartmann, F.M.; Frick, J.; Kienast, F.; Hunziker, M. Factors influencing visual landscape quality perceived by the public: Results from a national survey. *Landsc. Urban Plan.* **2021**, *208*, 104024. [CrossRef]
49. Vega, K.A.; Kueffer, C. Promoting wildflower biodiversity in dense and green cities: The important role of small vegetation patches. *Urban For. Urban Green.* **2021**, *62*, 127165. [CrossRef]
50. He, J.H.; Huang, J.L.; Li, C. The evaluation for the impact of land use change on habitat quality: A joint contribution of cellular automata scenario simulation and habitat quality assessment model. *Ecol. Model.* **2017**, *366*, 58–67. [CrossRef]
51. Zhang, M.D.; Zhang, F.; Li, X. Evaluation of Habitat Quality Based on InVEST Model: A Case Study of Tongzhou District of Beijing, China. *Landsc. Archit.* **2020**, *27*, 95–99.
52. Wu, M.Q.; Hu, M.M.; Wang, T.; Fan, C.; Xia, B.C. Recognition of urban ecological source area based on ecological security pattern and multi-scale landscape connectivity. *Acta Ecol. Sin.* **2019**, *39*, 4720–4731.
53. Wang, Y.; Lin, Q. The Transformation of planning ideas and the exploration of planning methods of urban green space ecological network based on MSPA. *Chin. Landsc. Archit.* **2017**, *33*, 68–73.
54. Xie, Y.S.; Wang, Q.N.; Luo, Y.Y. City-level urban green infrastructure evaluation index system based on MSPA: A case study of major cities in Sichuan province. *Chin. Landsc. Archit.* **2020**, *36*, 87–92.
55. Chen, H.Y.; Li, X. Optimization of green space habitat network of central Beijing based on MSPA-InVEST model. *Landsc. Archit.* **2021**, *28*, 16–21.
56. Chen, W.Q.; Tao, Y.; Wu, W.; Ou, W.X. Priority evaluation of ecological protect areas based on MSPA, landscape connectivity, and spatial syntax methods in the Su-Xi-Chang Region. *Acta Ecol. Sin.* **2020**, *40*, 289–298.

land

MDPI

Article

Response of NDVI of Natural Vegetation to Climate Changes and Drought in China

Huaijun Wang [1,2,*], Zhi Li [3], Lei Cao [1,2], Ru Feng [1,2] and Yingping Pan [4]

[1] School of Urban and Environmental Sciences, Huaiyin Normal University, Huai'an 223300, China; cao777050@163.com (L.C.); fengru12@mails.ucas.edu.cn (R.F.)
[2] Research Institute of Huai River Eco-Economic Belt, Key Research Base of Philosophy and Social Sciences of Colleges & Universities in Jiangsu Province, Huai'an 223300, China
[3] State Key Laboratory of Desert and Oasis Ecology, Xinjiang Institute of Ecology and Geography, Chinese Academy of Sciences, Urumchi 830011, China; liz@ms.xjb.ac.cn
[4] State Key Laboratory of Earth Surface Processes and Resource Ecology, Beijing Normal University, Beijing 100875, China; panyingping12@mails.ucas.ac.cn
* Correspondence: wanghj@ms.xjb.ac.cn; Tel.: +86-0517-8352-5126

Abstract: Temporal and spatial changes in vegetation and their influencing factors are of great significance for the assessment of climate change and sustainable development of ecosystems. This study applied the Asymmetric Gaussians (AG) fitting method, Mann-Kendall test, and correlation analysis to the Global Inventory Monitoring and Modeling System (GIMMS) third-generation Normalized Difference Vegetation Index and gridded climate and drought data for 1982–2015. The temporal and spatial changes to NDVI for natural grassland and forest during the growing season were analyzed. Relationships among NDVI, climate change, and droughts were also analyzed to reveal the influence of vegetation change. The results showed that: (1) Land use/cover change (LUCC) in China was mainly represented by increases in agricultural land (Agrl) and urban and rural land (Uril), and decreases in unutilized land (Bald), grassland, forest, and permanent glacier and snow (Snga). The increase in agricultural land was mainly distributed in the western northwest arid area (WNW) and northern North China (NNC), whereas regions with severe human activities such as southern South China (SNC), western South China (WSC), and eastern South China (ESC) showed significant decreases in agricultural land due to conversion to urban and rural land. (2) The start of the growing season (SOS) was advanced in WNW, SNC, WSC, and ESC, and the end of growing season (EOS) was delayed in WNW, NNC, and SNC. The growing season length (GSL) of natural vegetation in China has been extended by eight days over the last 34 years. However, the phenology of the Qinghai-Tibet Plateau (TP) was opposite to that of the other regions and the GSL showed an insignificant decreasing trend. (3) The NDVI increased significantly, particularly in the SNC, WSC, ESC, and the grassland of the WNW. Precipitation was found to mainly control the growth of vegetation in the arid and semi-arid regions of northwest China (WNW and ENW), and precipitation had a much greater impact on grassland than on forests. Temperature had an impact on the growth of vegetation throughout China, particularly in SNC, ESC, and WSC. (4) The Standardized Precipitation Evapotranspiration Index (SPEI) showed a downward trend, indicating an aridification trend in China, particularly in ENW, NNC, and WNW. Similar to precipitation, the main areas affected by drought were WNW and ENW and grassland was found to be more sensitive to drought than forest. The results of this study are of great significance for predicting the response of ecosystem productivity to climate change under future climate change scenarios.

Keywords: natural vegetation; NDVI; growing season; China

Citation: Wang, H.; Li, Z.; Cao, L.; Feng, R.; Pan, Y. Response of NDVI of Natural Vegetation to Climate Changes and Drought in China. *Land* **2021**, *10*, 966. https://doi.org/10.3390/land10090966

Academic Editor: Baojie He

Received: 9 August 2021
Accepted: 10 September 2021
Published: 13 September 2021

1. Introduction

As an important component of the terrestrial ecosystem, vegetation is a natural link connecting soil, atmosphere, and water. Vegetation plays a pivotal role in the ecosystem

and can act as an "indicator" within the study of global change. The growth status of vegetation is closely related to environmental factors, such as climate, water quality, and topography [1]. Climate change has altered the growth environment of plants, thereby affecting the growth of vegetation. Global changes have had a significant impact on the structure and function of terrestrial ecosystems [2–4]. Understanding the inherent relationship between vegetation and climate can illuminate the role of climate in changes to the terrestrial ecosystem.

The Normalized Difference Vegetation Index (NDVI) is the preferred indicator for analyzing vegetation changes and is widely used in the study of vegetation changes and the responses of vegetation to climate change [5,6]. Song et al. [7] found an increase and decrease in global forest vegetation cover and bare land, respectively, primarily due to human activities, with natural factors, including climate change, playing a secondary role. Chen et al. [8] found a global increase in vegetation of ~518 M ha over the past 20 years, equivalent to the area of the Amazon rainforest. Of this increase, around 33% is due to afforestation projects in China and intensive agricultural management in India. Changes to global vegetation cover from 1982 to 2011 also indicate an increasing trend in vegetation over the past 30 years, with annual changes to vegetation coverage showing an obvious seasonality [9]. Changes to vegetation in Eurasia changed from an increasing to decreasing trend around 1997, with the abrupt change in the NDVI varying from region to region [10]. There have been significant increasing trends in both the NDVI and leaf area index (LAI) in China. However, there have been downward trends in these two indices in the eastern development areas such as the Beijing-Tianjin-Hebei region and the Yangtze River Delta due accelerated urbanization. In addition, afforestation programs implemented in China over the past few decades have played an important role in promoting the greening of vegetation throughout the country [11].

Temperature and precipitation are key climate factors affecting plant growth and development. Previous studies have shown that drought resulting from rising temperatures in the Northern Hemisphere was an important driver of the decline in vegetation cover in some high-latitude regions in the 1980s [12]. Lamchin et al. [13] analyzed the correlation between the seasonal changes to the NDVI and factors such as temperature, precipitation, and evapotranspiration, thereby illustrating that temperature is the most important factor responsible for changes to the NDVI in Asia during 1982–2014. Climate warming over the past 30 years has promoted the restoration of vegetation in the central and southeast regions of the Loess Plateau, whereas it has had an inhibitory effect on the restoration of vegetation in the northwestern region [14]. Around 80% of the area in northeast China is experiencing an increase in the NDVI during the plant growing season, with temperature identified as the primary factor affecting vegetation coverage [15]. Climate factors have been identified as the primary drivers of changes in the NDVI in 46.2% of the area [16]. The NDVI in the Loess Plateau is negatively correlated with atmospheric pressure, whereas it is positively correlated with precipitation, humidity, air temperature, and sunshine hours [17]. Pang et al. [18] found that temperature over different seasons and months is positively correlated with the NDVI. In contrast, no consistent effect of rainfall on the NDVI in the Qinghai-Tibet Plateau from 1982 to 2012 has been identified.

Drought is a natural phenomenon resulting in an imbalance between water supply and water demand due to abnormally little or no precipitation over a long period of time. Drought is a common natural disaster and can occur over a wide spatial range and a long duration. Global warming has been linked with an increasing frequency and degree of drought. Therefore, studying the relationship between drought and vegetation can provide an effective theoretical basis for the management of vegetation as a climate change mitigation measure. Drought is generally quantified using drought indices such as the Palmer Drought Severity Index (PDSI), the Standardized Precipitation Index (SPI), and the Standardized Precipitation Evapotranspiration Index (SPEI) [19]. Among the many drought indices developed, the SPEI not only considers the impact of precipitation on drought, but also combines the sensitivity of the PDSI to potential evapotranspiration changes with

the multiple time scales of the SPI. Consequently, the SPEI is widely used to analyze the response of vegetation to drought [20]. Different vegetation types also respond differently to drought, and the SPEI value is not necessarily positively correlated to vegetation growth. For example, the drought in southwest China from 2009 to 2010 resulted in a significant decline in vegetation productivity in this area, and the period of vegetation restoration in some areas exceeded six months [21]. Northern China, and particularly central Inner Mongolia, has been shown to have undergone vegetation decline of between 28.1–68.8% greater than that in the mainland given drought conditions (quantified as SPEI ≤ -1) [22]. Differences in ecosystem resilience to water stress have been attributed to diversities in drought survival traits and strategies, with forests found to have the highest drought resilience, followed by croplands, grasslands, and deserts [23]. Vicente-Serrano et al. [24] found that although semiarid and sub-humid biomes respond to drought at long timescales due to the ability of plants to withstand water deficits, they lack the rapid response of arid biomes to drought.

Climate change in China is characterized by considerable spatial heterogeneity. Although there has been a significant increase in regional average temperature, there has been no significant change in precipitation [25]. The spatial differences in water and heat conditions and vegetation types have resulted in large spatial differences in vegetation changes and the responses of vegetation to climate change [26]. In addition, human activities have had a great impact on vegetation. In particular, changes in land use have increased uncertainty in the assessment of the impact of climate change. Most previous studies have not distinguished between the effects of human activities and climate change on vegetation, and few studies have explored the contribution of climate independent of meso-scale and large-scale landcover changes [27]. Human disturbance or the heterogeneity of the landscape environment has resulted in differences in the composition of vegetation types among different spatial scales. These different vegetation types show diverse species composition, community structure, and root distribution, resulting in differences in responses to changes in the external environment [28]. Therefore, understanding the differences in the response of the NDVI of different natural vegetation types to climate change is of great significance for the correct understanding of the relationship between regional vegetation cover and climate change. The current study used grid temperature, precipitation, drought, and the GIMMS NDVI3g data from 1982 to 2015 to explore the spatiotemporal changes in growth season of the NDVI for different natural vegetation types in China. The current study also analyzed the correlation between the NDVI and temperature, precipitation, and drought during the vegetation growing season to reveal the response of the NDVI to changes in climate and drought. The result of the current study can provide a theoretical basis for the construction and protection of the terrestrial ecological environment in China.

2. Study Area, Data, and Method

2.1. Study Area and Data

China can be divided into three major geographic regions based on geographic location, natural geography, and human geography: (1) the eastern monsoon region; (2) the northwest arid and semi-arid region, and; (3) the Qinghai-Tibet alpine region (TP). The 400 mm iso-precipitation line constitutes the boundary between the eastern monsoon region and the arid and semi-arid region of northwest China. The 3000-m contour line acts as the boundary between the eastern monsoon region and the Qinghai-Tibet alpine region. The northwest arid and semi-arid region and the Qinghai-Tibet alpine region are separated by Kunlun-Altun-Qilian mountains. The eastern monsoon region is roughly divided into north China and south China by the Qinling-Huaihe line, which roughly coincides with the 0 °C isotherm in January and the 800 mm annual precipitation line. On this basis, the northwest arid and semi-arid regions are divided into the western arid and semi-arid region (WNW) and eastern arid and semi-arid region (ENW). North China is divided into northern north China (NNC) and southern north China (SNC). South China is divided into western south China (WSC) and eastern south China (ESC).

The NDVI dataset used in the current study originated from the Global Inventory Monitoring and Modeling System (GIMMS) third generation NDVI (NDVI3g) (https://ecocast.arc.nasa.gov/data/pub/gimms/, accessed on 20 May 2020) released by the Global Monitoring and Simulation Research Group of the United States National Aeronautics and Space Administration (NASA). The GIMMS NDVI3g data extended from 1982 to 2015 with a spatial resolution of 8 km. This dataset eliminates the effects of volcanic eruptions, angles of solar altitude, and changes to sensor sensitivity over time, and has been widely used in the detection of global vegetation changes. The land use/land cover (LUCC) dataset originated from the Resource and Environment Science and Data Center (https://www.resdc.cn/Default.aspx, accessed on 5 April 2020) and included the years 1980, 1990, 1995, 2000, 2005, 2010, 2015, and 2020. The LUCC dataset was produced based on the Landsat Thematic Mapper/Enhanced Thematic Mapper (TM/ETM) remote sensing image of each phase as the main data source and was generated through manual visual interpretation. The spatial resolution of the LUCC dataset was 1 km, and was resampled to 8 km. Land use types included seven primary types: (1) agricultural land (Agrl); (2) forest land; (3) grassland; (4) water (Watr); (5) urban and rural land (Uril); (6) unutilized land (Bald); and (7) permanent glacier and snow (Snga). These seven primary land use types were further divided into 25 secondary types. The current study mainly focused on natural forest and grassland. Forest land was divided into forested land (Forestl), shrubland (Shrubl), and sparse forest land (Sparsel). Grassland included high-coverage grassland (Hgra), medium-coverage grassland (Mgra), and low-coverage grassland (Lgra). The focus of the current study was on the impact of climate and drought on natural vegetation. The impacts of land use change were excluded by only analyzing vegetation with unchanged forest and grassland types from 1980 to 2015. Under this approach, natural vegetation was identified as vegetation types (Forestl, Shrubl, Sparsel, Hgra, Mgra, and Lgra) that experienced no change in 1980 and 2015 (Figure 1). Figure 1 shows the monthly changes to temperature, precipitation, and the NDVI of natural vegetation in various regions.

Precipitation and temperature data used in the current study originated from a 1-km monthly mean temperature and precipitation dataset for China (https://data.tpdc.ac.cn/zh-hans/, accessed on 22 June 2020). The data are monthly average temperature and precipitation with a spatial resolution of 0.0083333° (~1 km) and a period of January 1901 to December 2017. This dataset is based on the global 0.5° climate dataset released by the Climate Research Unit (CRU) and the global high-resolution climate dataset released by WorldClim. The dataset was downscaled in China through the Delta spatial downscaling scheme and evaluated using observations collected in 1951–2016 by 496 weather stations across China. Compared with the evaluations of the CRU dataset, the mean absolute error of this dataset decreased by 35.4–48.7% for temperature and by 25.7% for precipitation. The root-mean-square error decreased by 32.4–44.9% for temperature and by 25.8% for precipitation. The Nash–Sutcliffe efficiency coefficients increased by 9.6–13.8% for temperature and by 31.6% for precipitation, and correlation coefficients increased by 0.2–0.4% for temperature and by 5.0% for precipitation. The new dataset was reliable, as the downscaling procedure further improved the quality and spatial resolution of the CRU dataset and was concluded to be useful for investigations related to climate change across China. More detailed information about this dataset can be found in [29]. The SPEI grid drought dataset with a spatial resolution of 0.5° and a monthly time resolution originated from the Global SPEI database (https://spei.csic.es/database.html, accessed on 18 May 2020). The SPEI dataset was based on monthly precipitation and potential evapotranspiration from the CRU. The present study used version 4.03 of the CRU timeseries (TS) dataset. We used the precipitation, temperature, and SPEI data reprojected and resampled, using bilinear interpolation, into the GIMMS NDVI projection and resampled to an 8 km resolution. Although this approach created a large number of replicate pixels for the SPEI, with no gain in the dataset spatial resolution, it enabled their comparison by retaining the NDVI resolution. Since the current study focused on the effects of drought on vegetation during the growing season, the SPEI data at a 6-month time scale (SPEI6) was used for analysis.

Since the vegetation growing season in China extends roughly from April to September, SPEI6 data for September indicated a drought during the growing season, whereas the data for March indicated a drought during the non-growing season.

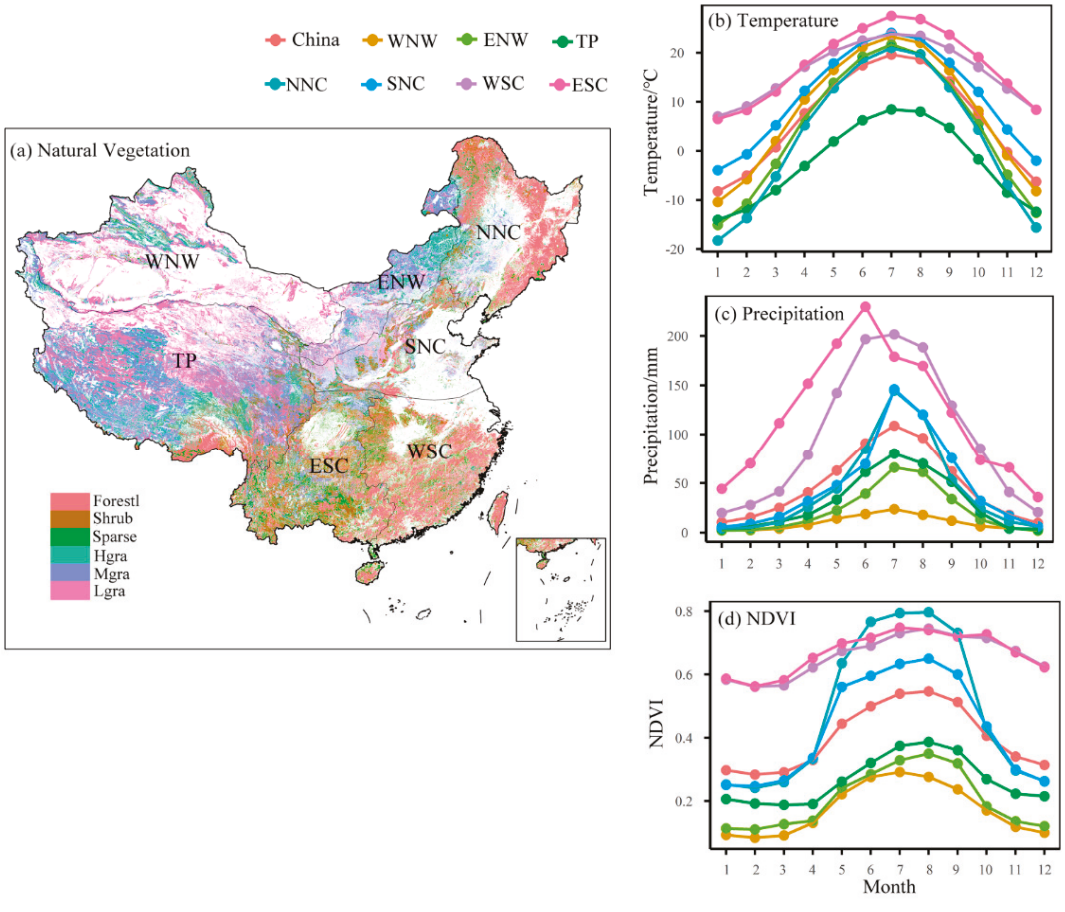

Figure 1. The distributions of natural vegetation (**a**), monthly temperature (**b**), precipitation (**c**), and Normalized Difference Vegetation Index (NDVI) (**d**) across China. Abbreviations: TP—Qinghai-Tibet alpine region; WNW—Western arid and semi-arid region; ENW—Eastern arid and semi-arid region; SNC—Southern North China; WSC—Western South China; ESC—Eastern South China; NNC—Northern North China; NDVI—Normalized Difference Vegetation Index.

2.2. Method

The present study adopted the change in area, rate of change in area, and transfer matrix to analyze the changes among different land uses in different regions of China. The asymmetric Gaussian function fitting method (AG) within the Timesat software was used to reconstruct the NDVI time series and to extract the vegetation phenology index [30]. The three extracted phenological parameters were the start of the growing season (SOS), the end of growing season (EOS), and the growing season length (GSL). The relative importance of SOS and EOS to GSL was analyzed using the Hierarchical Partitioning (HP) algorithm [31]. HP reduces multicollinearity by determining the independent contribution of each explanatory variable to the response variable, thereby allowing the relative importance values of covariates to be ranked when interpreting response variables. In this way, the contribution rates of SOS and EOS to GSL can be obtained. The trend magnitudes

of temperature, precipitation, NDVI, and drought during the growing and non-growing seasons were analyzed by Sen's slope [32] and significance was determined by the Mann-Kendall (M-K) method [33].

The test statistic S of Mann-Kendall test, is calculated by Equation (1):

$$S = \sum_{i=1}^{n-1} \sum_{k=i+1}^{n} \mathrm{sgn}(x_k - x_i) \tag{1}$$

where x_k and x_i are the sequential data values, and

$$\mathrm{sgn}(\theta) = \begin{cases} 1, \theta > 0 \\ 0, \theta = 0 \\ -1, \theta < 0 \end{cases} \tag{2}$$

The variance in S is computed by Equation (3):

$$\mathrm{var}(S) = [n(n-1)(2n+5) - \sum_{t} t(t-1)(2t+5)]/18 \tag{3}$$

where t is the extent of any given time, and n is the number of values.

Then, the test statistic Z is as follows:

$$Z = \begin{cases} \frac{S-1}{\sqrt{Var(S)}}, S > 0 \\ 0, S = 0 \\ \frac{S+1}{\sqrt{Var(S)}}, S < 0 \end{cases} \tag{4}$$

If $Z > 1.96$ ($Z < -1.96$), it means that the significant upward (downward) trend is significant at the 0.05 level.

The Sen's method was used to estimate the trend:

$$\beta = Median(\frac{x_i - x_j}{i - j}), \forall j < i \tag{5}$$

where $1 < j < \mathrm{i} < n$. Since the results of the M-K are heavily affected by time series correlation, the Yue and Pilon method [34], derived from R package "ZYP" [35], was used to remove lag-1 autocorrelation. In addition, the impact of climate change and drought on vegetation was mainly characterized by Pearson correlation analysis [36]:

$$R = \frac{\sum_{i=1}^{n} (x_i - \overline{x})(y_i - \overline{y})}{\sqrt{\sum_{i=1}^{n} (x_i - \overline{x})^2 \sum_{i=1}^{n} (y_i - \overline{y})^2}} \tag{6}$$

where R is correlation coefficient, n is the time series, x_i is the NDVI for each grid cell/regional study area, y_i is the climate variable (temperature, precipitation, SPEI) for each grid cell/regional study area, x is the average NDVI and y is the average of climate variables. The correlations calculated were tested for statistical validity at 0.05 significance level.

3. Results

3.1. Changes to LUCC from 1980 to 2015

The area of urban and rural land increased by 49% from 1980 to 2015, with the majority due to conversion of other land to farmland (51,085 km^2). There were significantly increasing trends in the areas of urban and rural land (Uril.) in all regions of China, with the smallest and largest rates of increase of 17% and 104% in NNC and TP, respectively (Figure 2, Table 1). Agricultural land (Agrl) and water increased by 33% and 20% in

WNW, respectively, mainly due to the conversion of unutilized land (Bald) and grassland. This also led to a sharp decline in unutilized land and grassland. There were significant reductions in unutilized land and grassland in ENW, while forested land (Forestl) and sparse forest land (Sparsel) increased by 20% and 17%, respectively. The area of glaciers and permanent snow (Snga) dropped sharply in TP, with most of the decline attributed to conversion to unutilized land (14,222 km^2) (Table S1). The major change in land use in NNC was due to an increase of agriculture land through the conversion of unutilized land, forest, and grassland. The area of unutilized land in SNC was reduced by 16,031 km^2, with most of this area converted to urban and rural land. Both WSC and ESC showed sharp decreases in agriculture land, with most of this area transformed into urban and rural land.

Figure 2. Gross change, net gain, and net loss of different land use/land cover (LUCC) in China from 1980 to 2015. (**a**) Throughout China; (**b**) WNW—Western arid and semi-arid region; (**c**) ENW—Eastern arid and semi-arid region; (**d**) TP—Qinghai-Tibet alpine region; (**e**) NNC—Northern North China; (**f**) SNC—Southern North China; (**g**) WSC—Western South China; (**h**) ESC—Eastern South China.

Table 1. The areas and relative changes to different land use/land cover (LUCC) in China from 1980 to 2015.

		Agrl	Watr	Uril	Bald	Forestl	Shrubl	Sparsel	Hgra	Mgra	Lgra	Snga
China	1980	1,762,034	202,729	148,945	1,996,499	1,372,015	486,377	398,411	1,020,430	1,096,193	931,243	84,952
	2015	1,786,003	211,092	221,863	1,984,536	1,353,990	486,920	399,242	995,106	1,081,483	913,987	69,009
	%	1.36	4.13	48.96	−0.60	−1.31	0.11	0.21	−2.48	−1.34	−1.85	−18.77
WNW	1980	69,257	9819	4396	1,167,635	22,248	11,125	8445	103,707	99,511	239,765	17,319
	2015	92,118	11,761	8317	1,159,588	21,521	11,119	8608	101,949	95,808	225,118	17,316
	%	33.01	19.78	89.20	−0.69	−3.27	−0.05	1.93	−1.70	−3.72	−6.11	−0.02
ENW	1980	78,574	12,321	7202	90,230	4728	6558	3527	147,240	176,404	97,131	0
	2015	78,412	11,693	11,657	88,793	5661	6485	4118	143,826	174,026	99,243	0
	%	−0.21	−5.10	61.86	−1.59	19.73	−1.11	16.76	−2.32	−1.35	2.17	0.00
TP	1980	18,628	58,517	1132	653,283	154,991	95,677	24,977	422,809	562,793	522,590	67,206
	2015	18,852	60,565	2312	665,480	154,325	95,403	25,278	424,553	563,509	521,025	51,299
	%	1.20	3.50	104.24	1.87	−0.43	−0.29	1.21	0.41	0.13	−0.30	−23.67
NNC	1980	320,340	27,992	26,100	74,683	420,310	44,057	52,876	141,428	53,231	11,944	0
	2015	373,669	26,676	30,545	62,293	405,574	45,927	46,562	119,515	50,927	11,311	2
	%	16.65	−4.70	17.03	−16.59	−3.51	4.25	−11.94	−15.49	−4.33	−5.30	0
SNC	1980	490,439	22,417	62,113	5289	75,574	54,972	26,604	58,500	85,793	48,876	9
	2015	474,408	21,555	81,278	3871	74,977	55,060	28,250	59,222	84,222	47,755	9
	%	−3.27	−3.85	30.86	−26.81	−0.79	0.16	6.19	1.23	−1.83	−2.29	0
WSC	1980	345,232	9956	8874	679	235,450	206,443	143,865	97,473	99,798	6830	9
	2015	337,742	11,509	16,723	821	233,329	206,197	145,435	98,442	98,068	6375	12
	%	−2.17	15.60	88.45	20.91	−0.90	−0.12	1.09	0.99	−1.73	−6.66	33.33
ESC	1980	436,067	51,663	37,979	2846	456,253	66,864	137,180	47,601	18,111	3695	0
	2015	407,203	56,981	66,766	2257	456,116	66,051	140,091	45,806	14,351	2733	0
	%	−6.62	10.29	75.80	−20.70	−0.03	−1.22	2.12	−3.77	−20.76	−26.04	0

Abbreviations: Agrl—Agricultural land; Watr—Water bodies; Uril—Urban and rural land; Bald—Unutilized land; Forestl—Forest land; Shrubl—Shrubland; Sparsel—Sparse forest land; Hgra—High coverage grassland; Mgra—Medium coverage grassland; Lgra—Low coverage grassland; Snga—Permanent snow and glacier; WNW—Western arid and semi-arid region; ENW—Eastern arid and semi-arid region; TP—Qinghai-Tibet alpine region; NNC—Northern North China; SNC—Southern North China; WSC—Western South China; ESC—Eastern South China.

In China, Forestl decreased by −1.31%, whereas Shrubl and Sparsel increased by 0.11% and 0.21%, respectively. The area of grassland showed a decreasing trend, with grassland area in Hgra, Mgra, and Lgra decreasing by −2.48%, −1.34%, and −1.85%, respectively. An analysis of the grids in which vegetation type did not change from 1980 to 2015 (Figure 3) showed that WNW, ENW, and TP were dominated by grassland, with the three grassland types displaying a wide distribution. Forest accounted for 74% of total natural vegetation in NNC, with forested land the most widely distributed, reaching 62%. Grassland and forest were distributed over large areas in SNC, accounting for 45% and 55% of the total area, respectively. Natural vegetation in WSC and ESC consisted mainly of forest, although the former also contained a large area of grassland.

3.2. Spatial and Temporal Distribution of Growing Season Indices

The growing season in China starts in April (day of year (DOY) 114) and ends in September (DOY 263) (Figure 4, Table 2). Therefore, throughout China, the approximate growing season (GS) period is April to September. The SOS of forest arrives earlier than that of grassland, whereas the EOS of forest extends later than that of grassland. As a result, the GSL of forest exceeded 159 days, whereas that of grassland was less than 140 days. The SOS of forest showed a significantly advancing trend, and the SOSs of Foredl, Shrubl, and Sparsel advanced by 6 d, 10 d, and 14 d over the past 34 years, respectively. In contrast, the EOS of forest showed a trend of delay, leading to extensions of the GSL of Foredl, Shrubl, and Sparsel by 12 d, 7 d, and 13 d, respectively. Although the phenological trend of grassland was consistent with that of forest, only Hgra realized a significant change.

The EOS of forest had a relatively large influence on the GSL, whereas the SOS was relatively important for the GSL of grassland (Table 2).

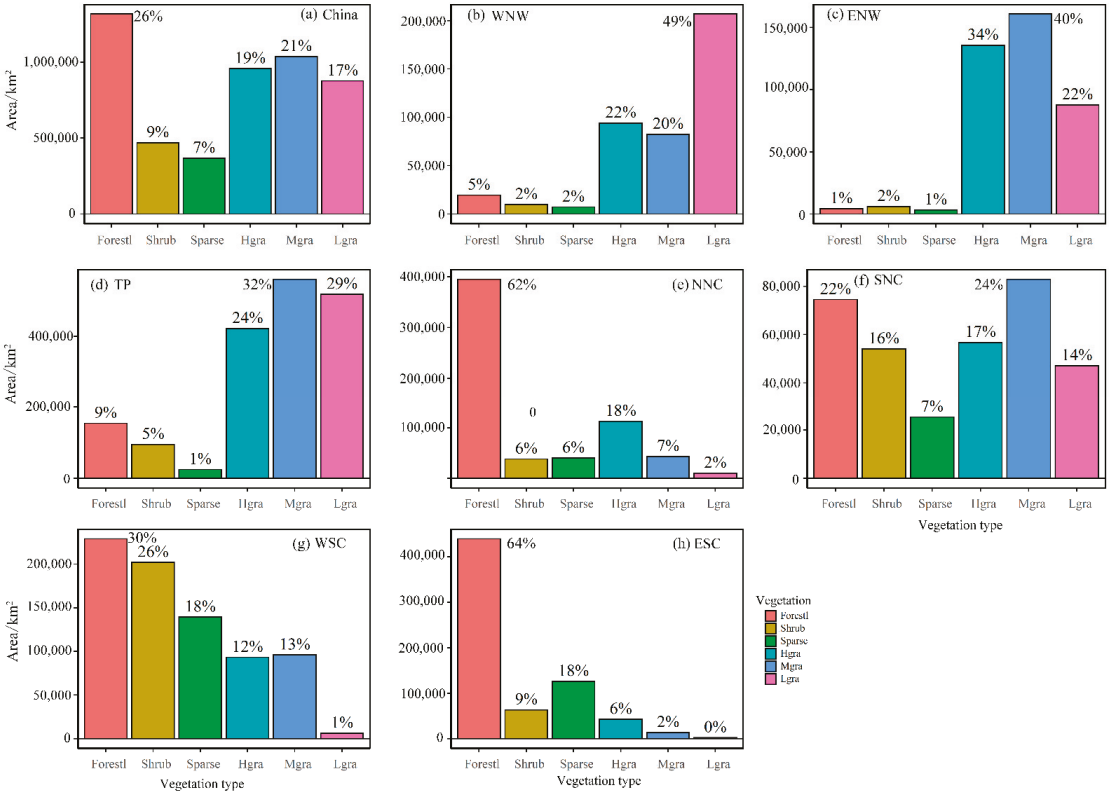

Figure 3. Areas and proportions of different types of natural forest and grassland in China from 1980 to 2015. (**a**) China; (**b**) WNW—Western arid and semi-arid region; (**c**) ENW—Eastern arid and semi-arid region: (**d**) TP—Qinghai-Tibet alpine region; (**e**) NNC—Northern North China; (**f**) SNC—Southern North China; (**g**) WSC—Western South China; (**h**) ESC—Eastern South China.

SOS and EOS decreased and increased significantly, in WNW, respectively, leading to a significant extension of the GLS (Figure 4, Table 2). The GSLs of forest and grassland were both extended by more than 15 d, and the advancement of the SOS and the delay of the EOS were equally important to the extension of the GLS. The significant delay in the EOS of forest led to a significant increase in GSL, whereas 96% of regions showed no significant changes in SOS, EOS, and GSL of grassland. This result could be attributed to spatial and regional differences. Taking SOS as an example, the eastern part of ENW showed a decreasing trend in SOS, whereas many grids in the west showed increasing trends (Figure 4d). SOS was particularly important for GLS in ENW, with its contribution rate exceeding 80% in all vegetation types.

The phonological change that occurred in TP was unique, with SOS and EOS delayed and advanced, respectively, although not significantly. The same changes were also evident at the grid scale (Figure 5). The proportion of SOS showing a significant delay (21%) far exceeded that showing a significant advance (10%), particularly for grassland. The EOS of grassland advanced, although this change was not significant. Regional GLS similarly showed no significant changes. The proportion of forest that showed a significant increase in GLS exceeded that showing a significant decrease at the grid scale. However, since

grassland accounted for 85% of all natural vegetation, the proportion of the grid with a significant decrease in GLS far exceeded that showing an increase in GLS. Zhang et al. [37] similarly showed delayed, advancing, and shortening trends in SOS, EOS, and GSL for alpine grassland, respectively. The EOS had the greatest influence on the length of forest GLS (60%), whereas the SOS was relatively important for the length of GSL of grassland.

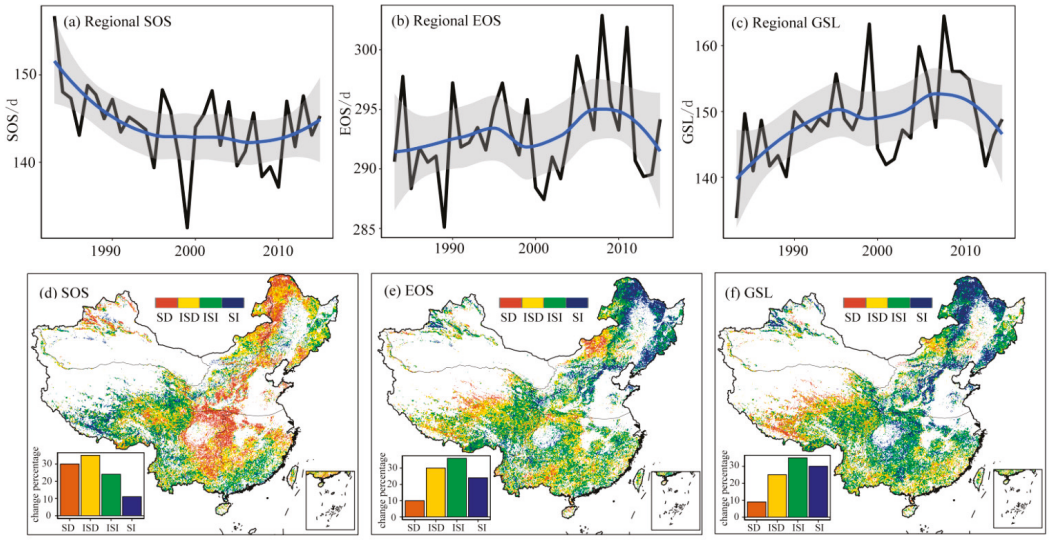

Figure 4. The temporal and spatial changes to the start of the growing season (SOS; (**a**,**d**)), end of the growing season (EOS; (**b**,**e**)), and growing season length (GSL; (**c**,**f**)) in China (SD—Significant decrease trend; ISD—Insignificant decrease trend; ISI—Insignificant increase trend; SI—Significant increase trend).

Table 2. The mean and trends in the start of growing season (SOS), end of growing season (EOS), and growing season length (GSL) in China (significant trends at 0.05 significance level are indicated in bold).

		Growing Season (Day of Year)			Trend (Days/34 Years)			Contribution Rate for GSL (%)	
		SOS	**EOS**	**GSL**	**SOS**	**EOS**	**GSL**	**SOS**	**EOS**
China	Naturalv	114	263	149	**−5**	2	8	53	46.8
	Forestl	108	267	159	**−6**	5	**12**	45	55.1
	Shrubl	112	274	162	**−10**	0	7	48	51.7
	Sparsel	107	281	173	**−14**	−1	13	40	60.2
	Hgra	119	257	139	**−5**	3	**6**	55	44.9
	Mgra	122	258	136	−4	2	7	60	40.5
	Lgra	126	256	130	−1	1	2	55	45.2
WNW	Naturalv	108	255	147	**−12**	**9**	**21**	51	48.9
	Forestl	109	254	145	**−12**	**11**	**23**	51	49.1
	Shrubl	105	258	152	**−12**	**10**	**23**	51	49.1
	Sparsel	109	254	145	**−5**	**11**	**15**	46	54.1
	Hgra	112	253	141	**−12**	**9**	**21**	56	44.5
	Mgra	105	255	150	**−12**	**9**	**19**	50	49.8
	Lgra	105	255	150	**−12**	**9**	**19**	50	49.8
ENW	Naturalv	120	255	135	−8	1	**10**	94	6.3
	Forestl	119	252	133	−4	**5**	**10**	64	36.3
	Shrubl	119	254	136	−5	**3**	**10**	88	11.8
	Sparsel	119	253	134	**−7**	**5**	**12**	64	36
	Hgra	121	254	133	−9	0	10	93	7.5
	Mgra	120	255	135	−7	2	9	84	16.3
	Lgra	120	255	136	0	3	4	89	11.5

Table 2. *Cont.*

		Growing Season (Day of Year)			Trend (Days/34 Years)			Contribution Rate for GSL (%)	
		SOS	**EOS**	**GSL**	**SOS**	**EOS**	**GSL**	**SOS**	**EOS**
TP	Naturalv	135	260	125	2	−4	−9	61	39.2
	Forestl	132	352	219	17	5	−12	34	66.3
	Shrubl	131	266	135	2	−5	−7	55	45.5
	Sparsel	131	301	170	7	8	3	35	64.6
	Hgra	133	259	127	2	−3	−6	62	38.3
	Mgra	133	257	123	1	−1	−2	67	33.3
	Lgra	136	254	117	1	−2	−4	65	34.6
NNC	Naturalv	111	253	142	−1	**6**	**8**	71	29
	Forestl	109	254	145	−2	**7**	**9**	68	32.1
	Shrubl	112	252	141	−1	**6**	**8**	67	32.9
	Sparsel	111	253	142	−3	**7**	**11**	63	37.2
	Hgra	115	250	135	−3	**4**	**7**	73	27
	Mgra	121	252	131	0	**3**	1	80	19.7
	Lgra	126	251	126	2	1	−3	88	11.6
SNC	Naturalv	102	263	161	**−9**	**8**	**16**	54	45.6
	Forestl	99	265	166	**−10**	**8**	**18**	54	45.9
	Shrubl	103	262	159	**−9**	**7**	**16**	55	44.8
	Sparsel	101	263	162	**−10**	**9**	**19**	56	44.2
	Hgra	103	261	159	**−9**	**8**	**18**	57	43
	Mgra	103	262	159	**−7**	**8**	**15**	54	45.6
	Lgra	108	260	152	**−7**	**9**	**18**	53	47.3
WSC	Naturalv	111	311	200	**−23**	−3	16	56	43.6
	Forestl	109	326	218	**−23**	−5	16	63	37.4
	Shrubl	112	310	197	**−22**	−7	16	57	42.9
	Sparsel	112	307	195	**−23**	−2	21	56	44.4
	Hgra	123	319	196	−18	−1	11	64	35.8
	Mgra	103	287	184	**−26**	9	**37**	52	47.8
	Lgra	115	283	168	**−23**	5	**28**	54	46.4
ESC	Naturalv	95	312	216	**−26**	3	24	45	54.9
	Forestl	96	318	221	**−20**	7	21	50	50.2
	Shrubl	88	298	210	**−23**	1	27	32	67.6
	Sparsel	95	303	207	**−25**	4	28	36	63.6
	Hgra	94	306	213	**−24**	4	**25**	34	65.8
	Mgra	97	304	207	**−31**	3	**37**	46	54.1
	Lgra	107	338	231	**−18**	−4	15	38	62.3

Abbreviations: Agrl—Agricultural land; Watr—Water bodies; Uril—Urban and rural land; Bald—Unutilized land; Forestl—Forest land; Shrubl—Shrubland; Sparsel—Sparse forest land; Hgra—High coverage grassland; Mgra—Medium coverage grassland; Lgra—Low coverage grassland; Snga—Permanent snow and glacier; WNW—Western arid and semi-arid region; ENW—Eastern arid and semi-arid region; TP—Qinghai-Tibet alpine region; NNC—Northern North China; SNC—Southern North China; WSC—Western South China; ESC—Eastern South China.

The NNC mainly contained forests and grasslands and showed advances and delays in regional SOS and regional EOS, respectively (Figure 4, Table 2). The same trend was observed at the grid scale, with 35% and 61% the grids showing significantly advanced SOS and significantly delayed EOS, respectively, which resulted in a significant increase in GSL of 60% (Figure 4). Although the EOS was significantly extended for forests and high-coverage grasslands, the start date of the EOS had a greater impact on the GLS (63%).

The phonological parameters of SNC show significant changes, regardless of the region or the grid scale (Table 2, Figure 5). SOS was significantly advanced in the SNC, with 55% of the grids showing a significant advancing trend. EOS and GLS were significantly increased in 37% and 54% of the grids, respectively. The regional EOS values of WSC and ESC showed significant advancing trends, whereas regional EOS did not change significantly. This trend was mirrored at the grid scale. SOS showed a significantly advancing trend in over 30% of the grids, while EOS was delayed in only 10% of the grids. Both SOS and

EOS were important to GLS in SNC, WSC, and ESC, with their contributions both between 40–60%.

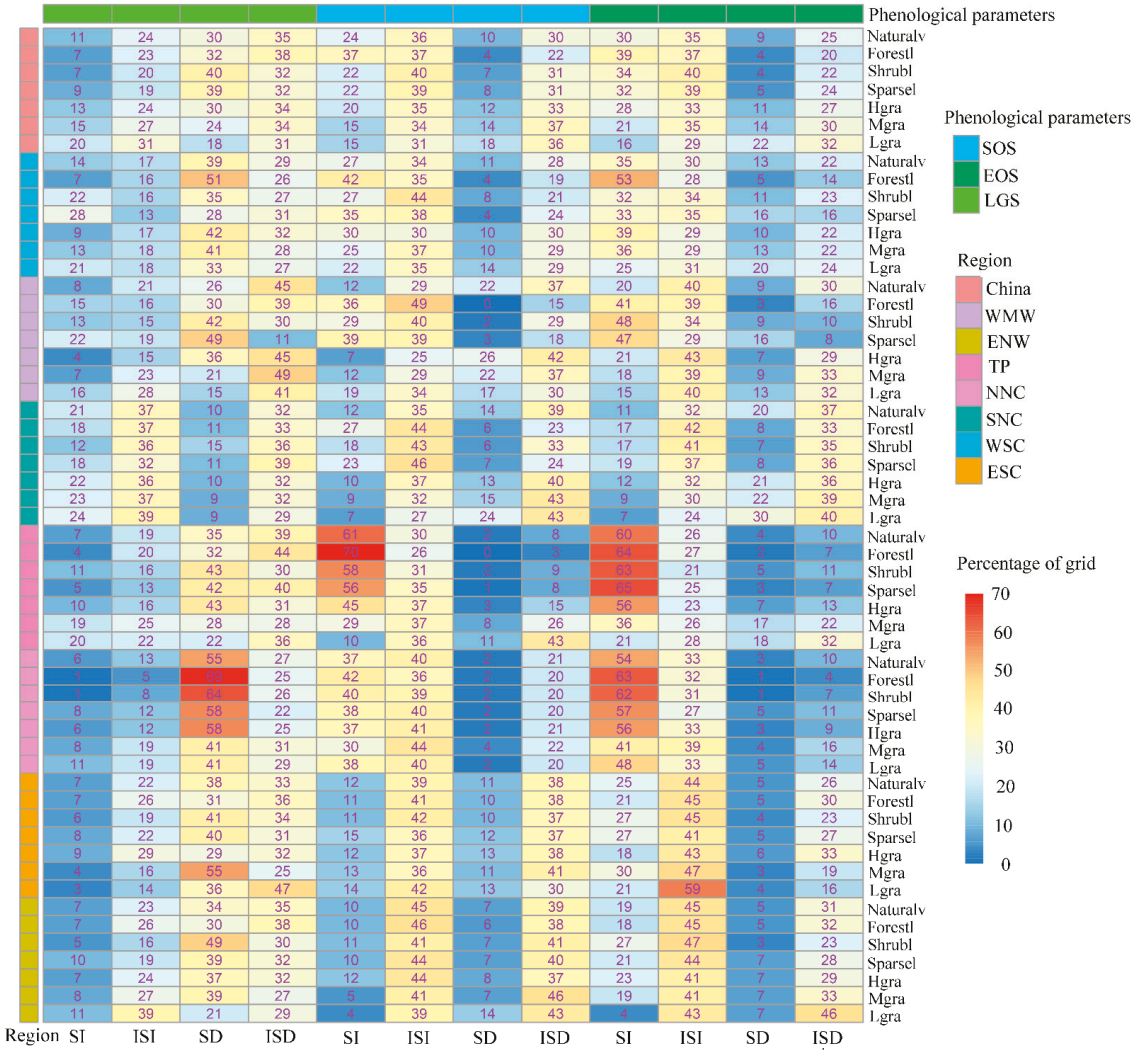

Figure 5. Percentage of grids with trends for phenological parameters (SD—significant decrease trend; ISD—insignificant decrease trend; ISI—insignificant increase trend; SI—significant increase trend. Abbreviations: Agrl—Agricultural land; Watr—Water bodies; Uril—Urban and rural land; Bald—Unutilized land; Forestl—Forest land; Shrubl—Shrubland; Sparsel—Sparse forest land; Hgra—High coverage grassland; Mgra—Medium coverage grassland; Lgra—Low coverage grassland; Snga—Permanent snow and glacier; WNW—Western arid and semi-arid region; ENW—Eastern arid and semi-arid region; TP—Qinghai-Tibet alpine region; NNC—Northern North China; SNC—Southern North China; WSC—Western South China; ESC—Eastern South China).

3.3. Climate Change and Its Relationship with the NDVI

Average precipitation, temperature, and NDVI decreased from southeast to northwest. Precipitation showed no significant change (Table 3). The grids with significant increases in precipitation were mainly located in TP. Among all the grids, 25% showed significant

increasing trends in precipitation and mainly contained grassland. The areas with significant decreases in precipitation were mainly located in eastern ENW and NNC. Among the grids in ENW and NNC, 28% and 38% showed significant decreasing trends in precipitation, respectively (Figure 6). Most areas showed significant increasing temperatures, with insignificant changes mostly found in eastern WSC and western ESC. Although there was a significant increasing trend in the NDVI, there were clear regional differences. The grids in ESC and WSC showed significant increases of 70% and 63% in the NDVI, respectively, whereas only 30% of grids in both TP and NNC showed a significant increase. Approximately 10% of the grids in each of TP, NNC, and WNW showed significant decreases in the NDVI, with this area mainly located in the alpine region.

Table 3. Regional changes to the Normalized Difference Vegetation Index (NDVI) in China and the correlations between the NDVI and precipitation and between the NDVI and temperature during the growing season (significant trends and correlations at the 0.05 significant level are indicated in bold).

Region	Vegetation	Trend			Correlation Coefficients		
		Temperature (°C/a)	Precipitation (mm/a)	NDVI	P	T	SPEI
China	Naturalv	**0.030**	0.187	**0.001**	0.12	**0.65**	−0.24
	Forestl	**0.023**	0.329	**0.001**	−0.07	**0.42**	−0.19
	Shrubl	**0.022**	0.275	**0.001**	−0.04	**0.58**	−0.23
	Sparsel	**0.022**	0.587	**0.001**	−0.05	**0.61**	−0.23
	Hgra	**0.030**	−0.060	**0.000**	**0.40**	**0.49**	0.21
	Mgra	**0.031**	0.078	**0.001**	0.29	**0.60**	−0.03
	Lgra	**0.035**	**0.418**	**0.001**	**0.34**	**0.62**	−0.13
WNW	Naturalv	**0.042**	0.184	**0.000**	**0.47**	**0.57**	−0.09
	Forestl	**0.039**	0.422	0.000	**0.35**	**0.56**	0.04
	Shrubl	**0.040**	0.383	0.000	**0.45**	0.26	0.11
	Sparsel	**0.038**	0.378	**0.001**	**0.36**	**0.62**	−0.15
	Hgra	**0.040**	0.355	**0.000**	**0.43**	**0.53**	0.13
	Mgra	**0.039**	0.429	**0.001**	**0.61**	**0.37**	0.22
	Lgra	**0.042**	0.171	**0.000**	**0.43**	**0.48**	−0.05
ENW	Naturalv	**0.047**	−0.438	0.000	**0.66**	0.09	0.46
	Forestl	**0.043**	−0.114	0.001	**0.58**	0.12	0.42
	Shrubl	**0.047**	−0.273	0.000	**0.58**	0.05	0.45
	Sparsel	**0.041**	−0.020	0.001	**0.48**	0.23	0.33
	Hgra	**0.047**	−0.830	0.000	**0.71**	−0.07	0.59
	Mgra	**0.047**	−0.452	**0.001**	**0.62**	0.14	0.40
	Lgra	**0.046**	−0.011	**0.001**	0.54	**0.25**	0.28
TP	Naturalv	**0.025**	0.365	0.000	0.06	**0.48**	−0.17
	Forestl	**0.016**	−0.164	0.000	0.04	0.01	0.00
	Shrubl	**0.019**	0.130	0.000	0.02	0.28	−0.10
	Sparsel	**0.018**	0.175	0.000	0.04	0.12	−0.08
	Hgra	**0.022**	0.425	0.000	0.22	0.32	0.19
	Mgra	**0.024**	0.439	0.000	0.06	**0.45**	−0.04
	Lgra	**0.027**	**0.668**	**0.000**	0.12	**0.55**	−0.09
NNC	Naturalv	**0.031**	−1.420	0.000	−0.18	0.23	−0.16
	Forestl	**0.030**	−1.229	0.000	**−0.33**	0.28	−0.33
	Shrubl	**0.032**	−1.128	0.000	−0.04	0.14	−0.02
	Sparsel	**0.033**	−0.970	0.001	−0.13	0.32	−0.16
	Hgra	**0.036**	−1.340	0.000	0.20	0.06	0.20
	Mgra	**0.033**	−1.224	0.001	0.32	0.05	0.32
	Lgra	**0.034**	−1.010	0.001	**0.39**	0.04	**0.35**
SNC	Naturalv	**0.032**	0.657	**0.002**	0.22	**0.39**	0.06
	Forestl	**0.034**	0.067	**0.002**	0.06	**0.43**	−0.09
	Shrubl	**0.034**	0.223	**0.002**	0.18	**0.36**	0.01
	Sparsel	**0.033**	0.592	**0.002**	0.18	**0.44**	−0.01
	Hgra	**0.033**	0.081	**0.002**	0.17	**0.40**	0.00
	Mgra	**0.036**	0.578	**0.002**	0.23	**0.40**	0.05
	Lgra	**0.036**	0.776	**0.003**	0.29	**0.37**	0.09

Table 3. *Cont.*

Region	Vegetation	Trend			Correlation Coefficients		
		Temperature (°C/a)	Precipitation (mm/a)	NDVI	P	T	SPEI
WSC	Naturalv	**0.013**	0.493	**0.001**	−0.06	**0.48**	−0.17
	Forestl	**0.011**	0.626	**0.001**	−0.04	**0.38**	−0.13
	Shrubl	**0.012**	0.568	**0.001**	−0.05	**0.42**	−0.14
	Sparsel	**0.012**	0.454	**0.001**	−0.03	**0.49**	−0.13
	Hgra	**0.014**	0.143	**0.001**	0.02	**0.41**	−0.08
	Mgra	**0.017**	−0.773	**0.001**	−0.11	**0.60**	−0.25
	Lgra	**0.014**	−0.161	**0.001**	−0.03	**0.46**	−0.16
WSC	Naturalv	**0.021**	1.303	**0.001**	−0.14	**0.59**	−0.27
	Forestl	**0.020**	1.649	**0.001**	−0.18	**0.56**	−0.29
	Shrubl	**0.022**	0.914	**0.002**	−0.12	**0.64**	−0.27
	Sparsel	**0.019**	0.893	**0.002**	−0.06	**0.59**	−0.18
	Hgra	**0.022**	1.200	**0.002**	−0.10	**0.56**	−0.23
	Mgra	**0.023**	1.424	**0.002**	−0.02	**0.62**	−0.16
	Lgra	**0.020**	3.553	**0.001**	−0.15	**0.55**	−0.22

Abbreviations: Agrl—Agricultural land; Watr—Water bodies; Uril—Urban and rural land; Bald—Unutilized land; Forestl—Forest land; Shrubl—Shrubland; Sparsel—Sparse forest land; Hgra—High coverage grassland; Mgra—Medium coverage grassland; Lgra—Low coverage grassland; Snga—Permanent snow and glacier; WNW—Western arid and semi-arid region; ENW—Eastern arid and semi-arid region; TP—Qinghai-Tibet alpine region; NNC—Northern North China; SNC—Southern North China; WSC—Western South China; ESC—Eastern South China.

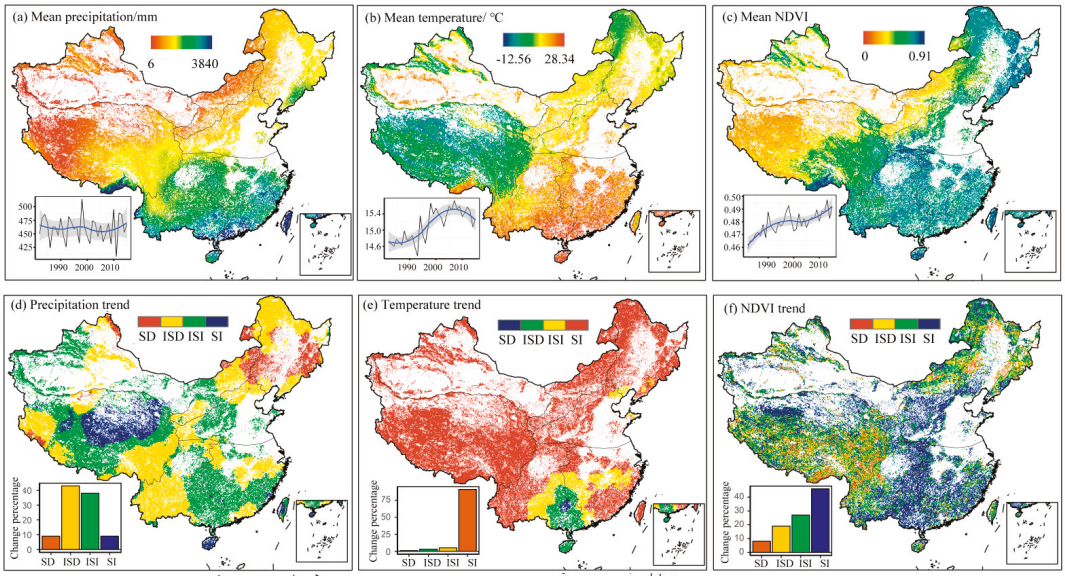

Figure 6. The mean and trends of precipitation (**a**,**d**), temperature (**b**,**e**), and the Normalized Difference Vegetation Index (NDVI; (**c**,**f**)) during the growing season in China (SD—Significant decrease trend; ISD—Insignificant decrease trend; ISI—Insignificant increase trend; SI—Significant increase trend)).

Approximately 17% of gridded NDVI showed a significant positive correlation with precipitation (Figure 7, Table S2), mainly in areas with insufficient precipitation (WNW and ENW). It should be noted that the correlation between the NDVI and forest was much smaller than that between the NDVI and grassland (Table 3). Approximately 28%, 27%, and 23% of grids for high-coverage grasslands, medium-coverage grasslands, and low-coverage grasslands were significantly correlated with rainfall, respectively, whereas 3%,

9%, and 5% of forests, shrub, and sparse forests were significantly correlated with rainfall (Table S2).

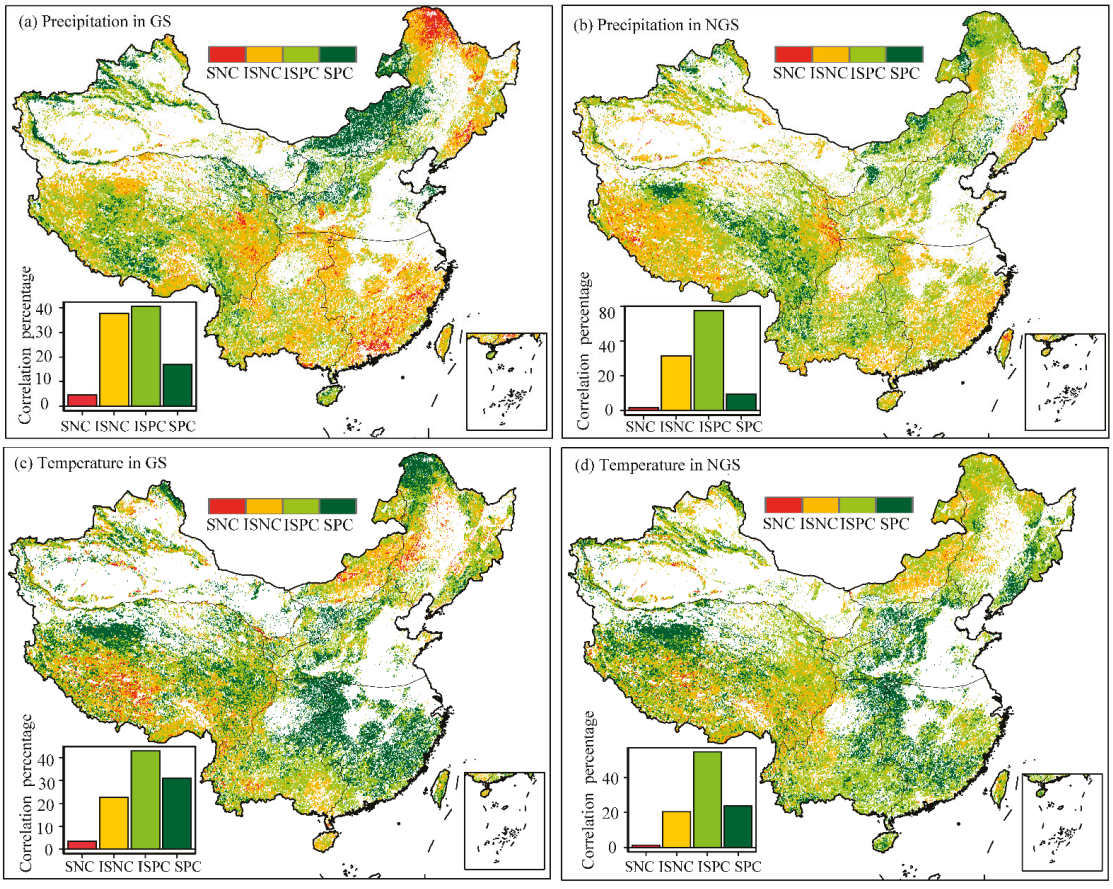

Figure 7. The correlation coefficients between the Normalized Difference Vegetation Index (NDVI) and climate variables in China. (**a**,**c**): Correlation between the growing season (GS) and the NDVI; (**b**,**d**): correlation between the GS NDVI and the previous non-growing season (NGS); SNC—Significant negative correlation; ISNC—Insignificant negative correlation; ISPC—Insignificant positive correlation; SPC—Significant positive correlation.

The grids in WNW and ENW showed significant positive correlations of 32% and 75% between the NDVI and precipitation, respectively (Figure 7, Table S2). Similarly, the proportion of grassland showing a significant positive correlation between the NDVI and grassland far exceeded that of forest. This result could be attributed to the fact that forests grow in areas with relatively abundant water resources in arid and semi-arid regions. Precipitation during the non-growing season can also have an impact on the NDVI during the growing season. A total of 11% and 17% of grids showed significant positive correlations between precipitation and NDVI in WNW and ENW, respectively. This area falls within an arid and semi-arid zone characterized by low precipitation with an uneven spatiotemporal distribution. Therefore, precipitation remains a control factor that restricts vegetation growth, thereby illustrating that vegetation growth is sensitive to changes in precipitation [24,38]. A total of 31% and 14% of grids showed significant positive correlations between temperature and the NDVI, respectively in WNW and ENW. The increase in temperature was conducive to increasing the NDVI during the growing

season. The positive correlation between regional temperature and the NDVI in WNW showed a correlation coefficient of 0.56, mainly since these regions are located in the mid-high latitudes of the Northern Hemisphere and since temperature is a primary factor limiting photosynthesis. At the same time, 18% of the grids in WNW showed significant correlations between temperature of the previous non-growing season and the NDVI. Grassland was the primary natural vegetation type in ENW. The increase in temperature promoted the growth of vegetation and resulted in a water deficit in vegetation to a certain extent, thereby generating an insignificant correlation between regional temperature and the NDVI [39].

A total of 11% of the grids in TP showed a positive correlation between the NDVI and precipitation, whereas 27% of the grids showed a significantly positively correlated between the NDVI and temperature (Figure 7, Table S2). This result indicated that temperature is a key factor controlling the growth of vegetation in TP rather than precipitation. The increase in temperature resulted in plants entering the growth period earlier, thereby extending the growth window. At the same time, the accelerated melting of seasonal snow provided water needed for early growth of plants. The precipitation and temperature of the previous non-growing season also affected the growth of the NDVI. Approximately 12% and 23% of grids showed significantly positive correlations between the NDVI and precipitation and between the NDVI and temperature, respectively. In addition, temperature and precipitation had a greater impact on the growth of the NDVI in grasslands compared to that for forest.

A total of 11% of the grids in NNC showed a significant positive correlation between the NDVI and precipitation, with most of the grids containing grassland (Figure 7, Table S2). Approximately 18% of forested land (accounting for 62% of natural vegetation) showed a significant negative correlation between the NDVI and precipitation, indicating that precipitation is not the main factor controlling forested land. Approximately 24% of grids showed significant positive correlations with temperature, with this proportion in forest far exceeding that in grassland. Precipitation during the previous non-growing season mainly affected medium- and low-coverage grasslands, whereas temperature mainly affected forests. Both precipitation and temperature in the SNC affected vegetation growth, with significant positive correlation ratios of 25% and 34%, respectively. The regional correlation coefficient showed that temperature had a great influence on vegetation in SNC, and all vegetation types showed a significant positive correlation. Precipitation during the non-growing season had little effect on vegetation growth, whereas temperature had a very large impact, with a positive correlation ratio exceeding 49%.

The response of the NDVI to temperature and precipitation was relatively consistent across WSC and ESC (Figure 7, Table S2). The impact of precipitation on the NDVI was minimal, whereas regional temperature was significantly correlated with the NDVI. The study area of the present study is mainly located in the monsoon climate area, with abundant precipitation. A total of 27% and 63% of grids in WSC and ESC showed a significant correlation between the NDVI and temperature, respectively. The temperature of the previous non-growing season also impacted the NDVI, with significant correlations in WSC and EWC evident in 25% and 37% of grids, respectively.

3.4. Effects of Drought on NDVI

There was a significant downward trend in the SPEI, evident in over 20% of the grids (Figure 8, Table 4 and S3). There was a significant downward trend in the SPEI in WNW (especially Mgrs and Lgra), evident in 36% of grids, whereas the significant declining trend fell to 76% in ENW, indicating trends of aridity in the northwest arid and semi-arid regions. There was no significant change in the SPEI in TP, although 14% of the grids (mainly in grassland) showed significant increases, indicating that humidity is increasing in some areas of TP. There was a significant downward trend in the SPEI in NNC, evident in 44% of the grids. There were no significant changes in SNC, WSC, and ESC at the regional scale and the grid scale.

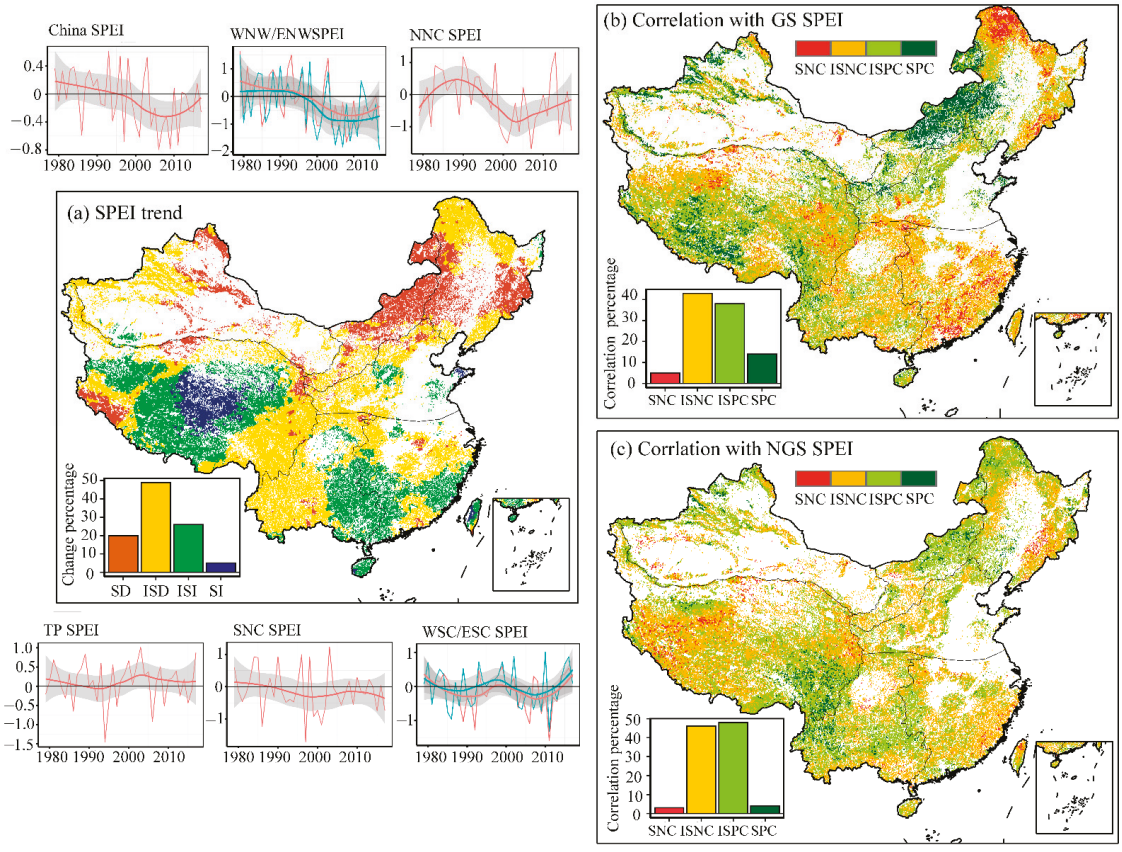

Figure 8. The changes to the Standardized Precipitation Evapotranspiration Index (SPEI) (**a**) and correlations between the SPEI and the Normalized Difference Vegetation Index (NDVI) in China (**b**): during the growing season (GS); (**c**): between the NDVI of the current GS and the SPEI of the previous non growing season (NGS).

Table 4. Regional trends in the Standardized Precipitation Evapotranspiration Index (SPEI) during the growing season in China (significant trends at the 0.05 significant level are indicated in bold).

Vegetation	China	WNW	ENW	TP	NNC	SNC	WSC	ESC
Naturalv	**−0.01585**	**−0.0304**	**−0.03668**	−0.0016	**−0.03574**	−0.00572	−0.00714	−0.00314
Forestl	**−0.01563**	−0.02704	**−0.02631**	−0.01151	**−0.03644**	−0.02102	−0.00164	0.000203
Shrubl	−0.00944	−0.0249	**−0.03157**	−0.01286	**−0.03624**	−0.01717	−0.00451	−0.0048
Sparsel	−0.00883	−0.02735	**−0.02394**	−0.00891	**−0.03733**	−0.01235	−0.00467	−0.00383
Hgra	**−0.01499**	−0.02528	**−0.04876**	0.007516	**−0.04078**	−0.01909	−0.01033	−0.00099
Mgra	**−0.01219**	**−0.0248**	**−0.04127**	0.001576	**−0.04229**	−0.01201	−0.01124	−0.00301
Lgra	−0.00978	**−0.02977**	**−0.03182**	0.003461	**−0.04378**	−0.00959	−0.0105	0.009922

Abbreviations: Agrl—Agricultural land; Watr—Water bodies; Uril—Urban and rural land; Bald—Unutilized land; Forestl—Forest land; Shrubl—Shrubland; Sparsel—Sparse forest land; Hgra—High coverage grassland; Mgra—Medium coverage grassland; Lgra—Low coverage grassland; Snga—Permanent snow and glacier; WNW—Western arid and semi-arid region; ENW—Eastern arid and semi-arid region; TP—Qinghai-Tibet alpine region; NNC—Northern North China; SNC—Southern North China; WSC—Western South China; ESC—Eastern South China.

A total of 13% of grids across entire China showed a significant positive correlation between the NDVI and the SPEI, with most of these grids containing grassland (Figure 8, Table 5). The areas showing the most sensitive the SPEI responses were WNW and ENW,

with 21% and 56% of grids in these areas showing a significantly positive correlation between the NDVI and the SPEI, respectively. At the same time, the proportion of grids showing a significant positive correlation between the NDVI and the SPEI was higher for grids containing grassland than for grids containing forest, particularly for Mgra in ENW in which 71% of grids showed a positive correlation with the SPEI. Approximately 9% of grids in TP showed a significant positive correlation between the NDVI and the SPEI, mainly distributed in grassland. This significantly positive correlation was evident in 13%, 9%, and 8% of grids containing Hgra, Mgra, and Lgra, respectively. A total of 12% and 11% of grids showed this significantly positive correlation in NNC and SNC, respectively. Similarly, a higher proportion of grids in grassland showed this correlation compared to grids containing forest. Drought had a high impact on vegetation growth of grassland, which could be attributed to the shallow root system of grassland. In contrast, the impact of drought on forest was relatively stable [40]. Xu et al. [41] similarly showed that increasing aridity resulting from drought induced more rapid and significant declines in vegetation photosynthesis. WSC and ESC showed very weak responses to drought, with the proportions of grids showing a significant positive correlation between the NDVI and the SPEI both less than 3% (Table S4). It should be noted that 16% and 14% of grids in NNC and ESC (particularly for forests) showed a significant negative correlation between the NDVI and the SPEI, indicating that drought is not a limiting factor in these areas. This result can mainly be attributed to the roots of forest trees extending to deep soil as a drought mechanism [42]. Therefore, water deficits are less restrictive on the growth of vegetation in this area, with temperature becoming the main factor affecting forest growth [43]. There was a lower number of grids in which the NDVI was significantly correlated with the SPEI during the previous non-growing season (Figure 8, Table S4), which indicates that vegetation responds relatively weakly to droughts on a scale of approximately six months. Zhou et al. [44] similarly showed an absence of a lag effect induced by agriculture on vegetation drought on a monthly scale in most parts of China; they found a significant lag in forests, whereas there tended to be no lag or a lag of less than a month in grassland and agriculture. Zhao et al. [45] highlighted the importance of the role of atmospheric aridity to vegetation activities in grasslands, and the drought scale of six months used in the present study also increased uncertainty in the results.

Table 5. Percentage of different correlation types between the Normalized Difference Vegetation Index (NDVI) and the Standardized Precipitation Evapotranspiration Index (SPEI) during the growing season (GS) in China (SNC—Significant negative correlation; ISNC—Insignificant negative correlation; ISPC—Insignificant positive correlation; SPC—Significant positive correlation).

	China				WNW				ENW				NNC			
	SPC	**ISPC**	**SNC**	**ISNC**	**SPC**	**ISPC**	**SNC**	**ISNC**	**SPC**	**ISPC**	**SNC**	**ISNC**	**SPC**	**ISPC**	**SNC**	**ISNC**
Naturalv	0.13	0.38	0.06	0.43	0.21	0.41	0.05	0.33	0.56	0.37	0.00	0.07	0.11	0.26	0.16	0.47
Forestl	0.02	0.24	0.13	0.61	0.18	0.45	0.04	0.33	0.34	0.47	0.00	0.19	0.02	0.21	0.19	0.58
Shrubl	0.06	0.39	0.05	0.50	0.24	0.33	0.03	0.40	0.41	0.50	0.00	0.09	0.20	0.23	0.21	0.36
Sparsel	0.03	0.34	0.06	0.56	0.09	0.43	0.06	0.42	0.44	0.44	0.00	0.12	0.08	0.35	0.15	0.42
Hgra	0.24	0.42	0.04	0.31	0.22	0.45	0.02	0.31	0.71	0.27	0.00	0.02	0.29	0.31	0.11	0.28
Mgra	0.19	0.47	0.02	0.32	0.30	0.43	0.02	0.24	0.54	0.39	0.00	0.07	0.31	0.45	0.04	0.21
Lgra	0.14	0.46	0.04	0.35	0.18	0.38	0.07	0.38	0.39	0.47	0.00	0.14	0.32	0.52	0.01	0.14

Abbreviations: Agrl—Agricultural land; Watr—Water bodies; Uril—Urban and rural land; Bald—Unutilized land; Forestl—Forest land; Shrubl—Shrubland; Sparsel—Sparse forest land; Hgra—High coverage grassland; Mgra—Medium coverage grassland; Lgra—Low coverage grassland; Snga—Permanent snow and glacier; WNW—Western arid and semi-arid region; ENW—Eastern arid and semi-arid region; TP—Qinghai-Tibet alpine region; NNC—Northern North China; SNC—Southern North China; WSC—Western South China; ESC—Eastern South China.

4. Discussion

The results of the present study showed that the spring phenology of China was significantly advanced by five days during 1982–2015 and the growing season was extended by eight days, basically consistent with the results of previous studies [46]. Past studies

have shown that the seasonal spatial distribution of vegetation on a global scale is mainly affected by latitudinal climate, vegetation types, and topographical elements. The mid- and high-latitude regions of the Northern Hemisphere are more strongly affected by heat and light [47]. The length of the vegetation growth season has been increasing in recent years in China, with the phenology of spring and autumn showing an advance and delayed trend, respectively [48]. The increase in temperature during spring will increase the temperature of vegetation germination and leaf expansion, which will advance the vegetation SOS [49]. A rise in temperature will increase the rate of decomposition of soil organic matter. This will more easily mineralize nutrients in the soil, thereby promoting the growth of vegetation [50]. At the same time, the water demand of vegetation will decrease during autumn, and the increase in temperature will increase and decrease the activity of photosynthetic enzymes and the degradation of chlorophyll, respectively, thereby delaying the growing season [51]. The phenology of the Qinghai-Tibet Plateau is affected by its unique environment, and phenological changes show spatial differences to those in other regions. In addition to the effects of temperature and precipitation on the Qinghai-Tibet Plateau, snow affects the phenological changes of alpine grasslands. Snowmelt can result in changes in moisture and temperature, thereby affecting the phenological period of plant species and the dynamics of plant populations. A deep and thick snow cover will delay plant growth and shorten the growth period [52]. The increase in winter temperature can lead to a sub-optimal reduced temperature of plant dormancy, the degradation of grassland, the melting of frozen soil, and an increase in aerosol concentration in the atmosphere, thereby delaying the rejuvenation period [53,54]. After correcting for adverse factors such as spring snow and ice, Zhang et al. [55] found no significant change in the SOS, consistent with the conclusion of the present study.

Vegetation coverage in China has shown a fluctuating upward trend, indicating increasing vegetation activities. The eastern part of China is affected by a monsoon climate and sufficient water and heat conditions for vegetation growth, where the northwestern region of China lacks sufficient water and heat. Therefore, the spatial coverage of vegetation in China is generally high in the southeast and low in the northwest. At the same time, areas with high vegetation coverage are mostly distributed along mountain ranges, with most of these areas containing forest vegetation. Under natural conditions, the physiological processes of plants are affected by changes in temperature. Zhang et al. [56] showed that temperature is the dominant factor affecting vegetation growth in humid temperate and cold temperate regions. The results of the present study showed general upward trends in temperature and vegetation in SNC, WSC, ESC, TP, and WNW. These results indicate that the increase in temperature in these mid-high latitudes is an important factor promoting the increase in vegetation. The results of the present study also showed that rainfall is the dominant driver of changes in vegetation in the arid and semi-arid regions of northwest China (WNW, ENW), consistent with the results of Spano et al. [57]. Although the present study did not consider the impact of human activities, it is undeniable that anthropogenic measures such as ecological engineering are important for promoting improvement in vegetation. Statistical records for China show that 42% and 32% of improved vegetated area is due to afforestation and agriculture, respectively [8]. Climate change not only directly affects the growth rate of vegetation, but also changes the physical and chemical properties of the soil (such as moisture, nutrient element content, etc.), thereby affecting the growth of vegetation. The results of the present study showed that temperature and precipitation during the non-growing season will also have an impact on the vegetation during the growing season.

The impacts of climate change can be observed by the correlation between the NDVI and the SPEI. The areas showing the highest vegetation response to drought were concentrated in WNW and ENW. This result confirms that vegetation growth in these areas is mainly affected by drought and that water is the main factor regulating vegetation growth. The correlation between the SPEI and vegetation was weak in ESC and WSC, characterized by abundant rainfall, and vegetation growth in these areas was weakly affected by drought.

Water was found to not be the main factor affecting vegetation growth. Rather, vegetation growth was found to be mainly affected by temperature and sunshine hours. Different vegetation types have different responses to drought. In general, grassland is more sensitive to drought than forest due to the shallow root system of grassland. There is a delay in replenishment of soil moisture after drought, which affects the growth of vegetation. However, the present study did not observe a lagged response of vegetation growth to drought. This discrepancy could possibly be attributed to the current study only analyzing average drought events. In addition, the spatial resolution of the SPEI dataset used in the present study was relatively coarse, and some uncertainty in the results may have been introduced by resampling the SPEI to the same resolution as the NDVI.

In regions of abundant precipitation, such as the monsoon region of China, the relationship between the NDVI and precipitation was alien with that of the NDVI and the SPEI. Regardless of regional or grid scale, the relationship was insignificant, indicating that water deficit is not an environmental factor that restrict vegetation growth in these areas. In areas with abundant precipitation, the results of the SPI calculated on the basis of precipitation, and the SPEI calculated on the basis of precipitation and potential evapotranspiration show that the changes were consistent, which demonstrated that precipitation was the major limiting factor trigger changes in drought index [25]. In the northwestern region (SNC and NNC) where precipitation was scarce, precipitation was significantly correlated with the NDVI both at the regional and grid scale, indicating that precipitation was the main factor limit vegetation growth. The correlation with the SPEI displayed that the basic correlation pattern did not changed compare with precipitation, but the proportion of grids with significant positive correlation decreased significantly. For example, in WNW, the proportion of significant positive correlation with precipitation was 32%, while the SPEI was reduced to 21%; in WNW, the proportion of significant positive correlation between precipitation and the NDVI was 75%, and the proportion of significant positive correlation with the SPEI was 56%. In the WNW and ENW regions, the temperature showed a significant increase trend. The increase in temperature led to increase in potential evapotranspiration and aggravated drought in the region, which would limit the growth of vegetation. With the temperature rising, the melting of accumulated snow and frozen soil contributed to high water availability and slow drought responses. However, the SPEI reflects meteorological drought, and hydrological drought does not respond well. In the arid area of the northwest, the vegetation on the whole shows an increasing trend, which leads to a decrease in the significant correlation ratio compared with precipitation. When used across multiple time scales, the SPEI is an effective drought index that contains information on evapotranspiration in drought monitoring, thereby making it possible to reflect the changes in water demands in arid and semiarid regions, especially under the background of global warming [58,59]. The study focuses on calculations using precipitation and potential evapotranspiration, which reflect the average state of drought, but climate model predictions show that the vegetation impact caused by severe drought is greater [60]. For example, extreme drought decreased the forest biomass by 1.2–1.6 Pg in the Amazon region [61]. The drought that occurred in southwest China from 2009 to 2010 resulted in a significant decline in vegetation productivity, and the restoration period of vegetation in some areas exceeded half a year [21].

It should be noted that the present study only analyzed the impacts of temperature, precipitation, and drought on vegetation, whereas other environmental changes, such as solar radiation [62], soil nutrients [63], topographical factors [64], land use [65], and human activity [66] were not discussed. Future research should consider the impacts of these additional environmental factors.

5. Conclusions

The present study analyzed the spatiotemporal characteristics of temperature, precipitation, drought, and the NDVI during the growing and non-growing seasons of natural vegetation in China as well as the response of the NDVI to temperature, precipitation,

and drought during the growing season. The main conclusions of the present study were as follows:

(1) The area of urban and rural land in China increased by 49% from 1980 to 2015, with most of this increase attributed to conversion from agriculture land. Agriculture land and water increased by 33% and 20% in WNW, respectively, mainly through conversion from unutilized land and grassland. The increase in urban and rural land in ENW was mainly manifested as a massive reduction in unutilized land and grassland. Much of the decrease in glaciers and permanent snow on the Qinghai-Tibet Plateau could be attributed to conversion to unutilized land. The conversion of unutilized land, forests, and grasslands to farmland in NNC resulted in a significant increase in agriculture land. There were large reductions in agricultural land in SNC, WSC, and WSC due to conversion to urban and rural land.

(2) SOS and EOS of natural vegetation in China showed trends of advancing and delay, respectively, during 1982–2015, resulting in GSL being prolonged by approximately eight days. SOS was advanced and EOS was delayed in WNW and ENW, leading to a 21 d and 10 d prolongation of GLS, respectively. Particularly in WNW, there were significant changes in the regional trends of the EOS and SOS. SOS was particularly important to GLS in ENW, with its contribution rate exceeding 80% in almost all vegetation types. Since NNC was dominated by forests and high-coverage grasslands, SOS and EOS were significantly advanced and delayed, respectively. The SOS had a greater impact on GLS than the EOS, with a contribution rate exceeding 71%. SOS was significantly advanced in SNC at both the regional and grid scales, whereas EOS and GLS also showed significant increasing trends. SOS showed a significant advancing trend in WSC and ESC, whereas EOS did not change significantly. TP showed a unique phenological change that was opposite to that in other regions. Although the phenological change in TP was not significant, SOS was delayed and EOS was advanced, resulting in a shortened GSL.

(3) Temperature in China showed a significant increasing trend, whereas there was no significant change in precipitation. Although the NDVI showed a significant increasing trend, there were clear regional differences. The NDVI was positively correlated with precipitation in WNW and ENW, and the proportion of grids showing this correlation was higher for grassland than for forest. Rising air temperature was conducive to increasing the NDVI in WNW. Temperature was shown to be the key factor to controlling the growth of vegetation in TP rather than precipitation. In addition, the NDVI was affected by the temperature of the previous non-growing season. Precipitation is not the main factor affecting forested land in NNC. Rather, temperature had the greatest effect on vegetation, particularly in forests. Precipitation and temperature were both important for vegetation growth in SNC. However, temperature had a greater impact on vegetation in SNC. Temperature was the main environmental factor affecting vegetation dynamics in WSC and ESC, whereas the impact of precipitation was minimal.

(4) In general, the SPEI showed a significant downward trend, particularly in WNW, ENW, and NNC. Drought had the greatest impact on the NDVI in WNW and ENW, with 21% and 56% of grids in this area showing a significantly positive correlation between the NDVI and the SPEI, with a higher proportion of grids showing this relationship for grassland than for forest. Approximately 10% of grids in TP, NNC, and SNC showed this significantly positive correlation, with this positive correlation much higher in grassland than in forest. The correlation between the NDVI and drought was weak in WSC and ESC, indicating that drought is not the main factor limiting vegetation growth.

Supplementary Materials: The following are available online at https://www.mdpi.com/article/10.3390/land10090966/s1, Table S1: Land Use Transfer matrix between different land use/cover change in different regions of China. Table S2: Percentage of the correlation coefficients between NDVI and climate variables (SNC—Significant negative correlation; ISNC—Insignificant negative correlation; ISPC—Insignificant positive correlation; SPC—Significant positive correlation). Table S3: Percentage of grid with trends for SPEI (SD—Significant decrease trend; ISD—Insignificant decrease trend; ISI—Insignificant increase trend; SI—Significant increase trend). Table S4: Percentage of the correlation coefficients between NDVI and SPEI (SNC—Significant negative correlation; ISNC—Insignificant negative correlation; ISPC—Insignificant positive correlation; SPC—Significant positive correlation).

Author Contributions: H.W. and L.C. contributed to the conception of the study. H.W. and Z.L. performed the data analyses. R.F. and Y.P. wrote the manuscript. All authors have read and agreed to the published version of the manuscript.

Funding: This research was supported by the National Key Research and Development Program of China (2019YFA0606902) and National Natural Science Foundation of China (41830863, 51879162, and 41701034).

Data Availability Statement: The data that support the findings of this study are available from the corresponding author upon reasonable request.

Acknowledgments: The authors thank the National Climate Center, China Meteorological Administration, for providing the meteorological data for this study. The authors would like to thank all the reviewers who participated in the review.

Conflicts of Interest: The authors declare no conflict of interest.

References

1. Jia, L.; Li, Z.B.; Xu, G.C.; Ren, Z.P.; Li, P.; Cheng, Y.T.; Zhang, Y.X.; Wang, B.; Zhang, J.-X.; Yu, S. Dynamic change of vegetation and its response to climate and topographic factors in the Xijiang River basin, China. *Environ. Sci. Pollut. R* **2020**, *27*, 11637–11648. [CrossRef]
2. Thomas, C.D.; Cameron, A.; Green, R.E.; Bakkenes, M.; Beaumont, L.J.; Collingham, Y.C.; Erasmus, B.F.; Siqueira, M.D.; Grainger, A.; Hannah, L. Extinction risk from climate change. *Nature* **2004**, *427*, 145. [CrossRef]
3. Maclean, I.M.; Wilson, R.J. Recent ecological responses to climate change support predictions of high extinction risk. *Proc. Natl. Acad. Sci. USA* **2011**, *108*, 12337–12342. [CrossRef]
4. Zheng, H.; Shen, G.; He, X.; Yu, X.; Ren, Z.; Zhang, D. Spatial assessment of vegetation vulnerability to accumulated drought in Northeast China. *Reg. Environ. Chang.* **2015**, *15*, 1639–1650. [CrossRef]
5. Kasoro, F.R.; Yan, L.; Zhang, W.; Asante-Badu, B. Spatial and temporal changes of vegetation cover in china based on modis ndvi. *Appl. Ecol. Environ. Res.* **2021**, *19*, 1371–1390. [CrossRef]
6. Luo, N.; Mao, D.; Wen, B.; Liu, X. Climate Change Affected Vegetation Dynamics in the Northern Xinjiang of China: Evaluation by SPEI and NDVI. *Land* **2020**, *9*, 90. [CrossRef]
7. Song, X.-P.; Hansen, M.C.; Stehman, S.V.; Potapov, P.V.; Tyukavina, A.; Vermote, E.F.; Townshend, J.R. Global land change from 1982 to 2016. *Nature* **2018**, *560*, 639–643. [CrossRef] [PubMed]
8. Chen, C.; Park, T.; Wang, X.; Piao, S.; Xu, B.; Chaturvedi, R.K.; Fuchs, R.; Brovkin, V.; Ciais, P.; Fensholt, R. China and India lead in greening of the world through land-use management. *Nat. Sustain.* **2019**, *2*, 122–129. [CrossRef]
9. Wu, D.; Wu, H.; Zhao, X.; Zhou, T.; Tang, B.; Zhao, W.; Jia, K. Evaluation of spatiotemporal variations of global fractional vegetation cover based on GIMMS NDVI data from 1982 to 2011. *Remote Sens.* **2014**, *6*, 4217–4239. [CrossRef]
10. Piao, S.; Wang, X.; Ciais, P.; Zhu, B.; Wang, T.; Liu, J. Changes in satellite-derived vegetation growth trend in temperate and boreal Eurasia from 1982 to 2006. *Global. Chang. Biol.* **2011**, *17*, 3228–3239. [CrossRef]
11. Zheng, K.; Tan, L.; Sun, Y.; Wu, Y.; Duan, Z.; Xu, Y.; Gao, C. Impacts of climate change and anthropogenic activities on vegetation change: Evidence from typical areas in China. *Ecol. Indic.* **2021**, *126*, 107648. [CrossRef]
12. Zhou, L.; Tucker, C.J.; Kaufmann, R.K.; Slayback, D.; Shabanov, N.V.; Myneni, R.B. Variations in northern vegetation activity inferred from satellite data of vegetation index during 1981 to 1999. *J. Geophys. Res.-Atmos.* **2001**, *106*, 20069–20083. [CrossRef]
13. Lamchin, M.; Lee, W.-K.; Jeon, S.W.; Wang, S.W.; Lim, C.H.; Song, C.; Sung, M. Long-term trend and correlation between vegetation greenness and climate variables in Asia based on satellite data. *Sci. Total Environ.* **2018**, *618*, 1089–1095. [CrossRef] [PubMed]
14. Sun, W.; Song, X.; Mu, X.; Gao, P.; Wang, F.; Zhao, G. Spatiotemporal vegetation cover variations associated with climate change and ecological restoration in the Loess Plateau. *Agric. Forest Meteorol.* **2015**, *209*, 87–99. [CrossRef]
15. Guo, J.; Hu, Y.; Xiong, Z.; Yan, X.; Ren, B.; Bu, R. Spatiotemporal Variations of Growing-Season NDVI Associated with Climate Change in Northeastern China's Permafrost Zone. *Pol. J. Environ. Stud.* **2017**, *26*, 1521–1530. [CrossRef]

16. Lin, X.; Niu, J.; Berndtsson, R.; Yu, X.; Zhang, L.; Chen, X. NDVI dynamics and its response to climate change and reforestation in Northern China. *Remote Sens.* **2020**, *12*, 4138. [CrossRef]
17. Li, P.; Wang, J.; Liu, M.; Xue, Z.; Bagherzadeh, A.; Liu, M. Spatio-temporal variation characteristics of NDVI and its response to climate on the Loess Plateau from 1985 to 2015. *Catena* **2021**, *203*, 105331. [CrossRef]
18. Pang, G.; Wang, X.; Yang, M. Using the NDVI to identify variations in, and responses of, vegetation to climate change on the Tibetan Plateau from 1982 to 2012. *Quat. Int.* **2017**, *444*, 87–96. [CrossRef]
19. Wang, H.; Pan, Y.; Chen, Y. Comparison of three drought indices and their evolutionary characteristics in the arid region of northwestern China. *Atmos. Sci. Lett.* **2017**, *18*, 132–139. [CrossRef]
20. Beguería, S.; Vicente-Serrano, S.M.; Reig, F.; Latorre, B. Standardized precipitation evapotranspiration index (SPEI) revisited: Parameter fitting, evapotranspiration models, tools, datasets and drought monitoring. *Int. J. Climatol.* **2014**, *34*, 3001–3023. [CrossRef]
21. Li, X.; Li, Y.; Chen, A.; Gao, M.; Slette, I.J.; Piao, S. The impact of the 2009/2010 drought on vegetation growth and terrestrial carbon balance in Southwest China. *Agric. Forest Meteorol.* **2019**, *269*, 239–248. [CrossRef]
22. Fang, W.; Huang, S.; Huang, Q.; Huang, G.; Wang, H.; Leng, G.; Wang, L.; Li, P.; Ma, L. Bivariate probabilistic quantification of drought impacts on terrestrial vegetation dynamics in mainland China. *J. Hydrol.* **2019**, *577*, 123980. [CrossRef]
23. Xu, H.J.; Wang, X.P.; Zhao, C.Y.; Zhang, X.X. Responses of ecosystem water use efficiency to meteorological drought under different biomes and drought magnitudes in northern China. *Agric. Forest Meteorol.* **2019**, *278*, 107660. [CrossRef]
24. Vicente-Serrano, S.M.; Gouveia, C.; Camarero, J.J.; Beguería, S.; Trigo, R.; López-Moreno, J.I.; Azorín-Molina, C.; Pasho, E.; Lorenzo-Lacruz, J.; Revuelto, J. Response of vegetation to drought time-scales across global land biomes. *Proc. Natl. Acad. Sci. USA* **2013**, *110*, 52–57. [CrossRef] [PubMed]
25. Wang, H.; Chen, Y.; Pan, Y.; Chen, Z.; Ren, Z. Assessment of candidate distributions for SPI/SPEI and sensitivity of drought to climatic variables in China. *Int. J. Climatol.* **2019**, *39*, 4392–4412. [CrossRef]
26. Wang, H.; Liu, X.; Zhang, X.; Wang, P.; Lin, H.; Yu, L. Spatiotemporal crop NDVI responses to climatic factors in mainland China. *Int. J. Remote Sens.* **2019**, *40*, 89–103. [CrossRef]
27. Zhou, Y.; Fu, D.; Lu, C.; Xu, X.; Tang, Q. Positive effects of ecological restoration policies on the vegetation dynamics in a typical ecologically vulnerable area of China. *Ecol. Eng.* **2021**, *159*, 106087. [CrossRef]
28. Yu, M.; Gao, Q. Increasing Summer Rainfall and Asymmetrical Diurnal and Seasonal Warming Enhanced Vegetation Greenness in Temperate Deciduous Forests and Grasslands of Northern China. *Remote Sens.* **2020**, *12*, 2569. [CrossRef]
29. Peng, S.Z.; Ding, Y.X.; Liu, W.Z.; Li, Z. 1 km monthly temperature and precipitation dataset for China from 1901 to 2017. *Earth Syst. Sci. Data* **2019**, *11*, 1931–1946. [CrossRef]
30. Eklundh, L.; Jönsson, P. TIMESAT for processing time-series data from satellite sensors for land surface monitoring. In *Multitemporal Remote Sensing*; Ban, Y., Ed.; Springer International Publishing: Berlin/Heidelberg, Germany, 2016; pp. 177–194.
31. Nally, R.M. Hierarchical partitioning as an interpretative tool in multivariate inference. *Aust. J. Ecol.* **1996**, *21*, 224–228. [CrossRef]
32. Sen, P.K. Estimates of the regression coefficient based on Kendall's Tau. *J. Am. Stat. Assoc.* **1968**, *63*, 1379–1389. [CrossRef]
33. Kendall, M.G. *Rank-Correlation Measures*; Charles Griffin: London, UK, 1975.
34. Yue, S.; Pilon, P.; Cavadias, G. Power of the Mann–Kendall and Spearman's rho tests for detecting monotonic trends in hydrological series. *J. Hydrol.* **2002**, *259*, 254–271. [CrossRef]
35. Bronaugh, D.; Werner, A. Zyp: Zhang + Yue-Pilon Trends Package. R Package Version 0.10-1. 2013. Available online: https://CRAN.Rproject.org/package=zyp (accessed on 5 October 2018).
36. Zhao, A.; Zhang, A.; Liu, J.; Feng, L.; Zhao, Y. Assessing the effects of drought and "Grain for Green" Program on vegetation dynamics in China's Loess Plateau from 2000 to 2014. *Catena* **2019**, *175*, 446–455. [CrossRef]
37. Zhang, X.; Du, X.; Hong, J.; Du, Z.; Lu, X.; Wang, X. Effects of climate change on the growing season of alpine grassland in Northern Tibet, China. *Glob. Ecol. Conserv.* **2020**, *23*, e01126. [CrossRef]
38. Zhang, Q.; Kong, D.; Singh, V.P.; Shi, P. Response of vegetation to different time-scales drought across China: Spatiotemporal patterns, causes and implications. *Glob. Planet. Chang.* **2017**, *152*, 1–11. [CrossRef]
39. Xu, W.; Liu, H.; Zhang, Q.; Liu, P. Response of vegetation ecosystem to climate change based on remote sensing and information entropy: A case study in the arid inland river basin of China. *Environ. Earth Sci.* **2021**, *80*, 1–14. [CrossRef]
40. Yu, Y.; Shen, Y.; Wang, J.; Wei, Y.; Nong, L.; Deng, H. Assessing the response of vegetation change to drought during 2009-2018 in Yunnan Province, China. *Environ. Sci. Pollut. R* **2021**, 1–17. [CrossRef]
41. Xu, H.J.; Wang, X.P.; Zhao, C.Y.; Yang, X.M. Assessing the response of vegetation photosynthesis to meteorological drought across northern China. *Land Degrad. Dev.* **2021**, *32*, 20–34. [CrossRef]
42. Davidson, E.A.; Verchot, L.V.; Cattânio, J.H.; Ackerman, I.L.; Carvalho, J. Effects of soil water content on soil respiration in forests and cattle pastures of eastern Amazonia. *Biogeochemistry* **2000**, *48*, 53–69. [CrossRef]
43. Thavorntam, W.; Tantemsapya, N. Vegetation greenness modeling in response to climate change for Northeast Thailand. *J. Geogr. Sci.* **2013**, *23*, 1052–1068. [CrossRef]
44. Zhou, K.; Li, J.; Zhang, T.; Kang, A. The use of combined soil moisture data to characterize agricultural drought conditions and the relationship among different drought types in China. *Agric. Water Manag.* **2021**, *243*, 106479. [CrossRef]
45. Zhao, W.; Hu, Z.; Guo, Q.; Wu, G.; Chen, R.; Li, S. Contributions of Climatic Factors to Interannual Variability of the Vegetation Index in Northern China Grasslands. *J. Clim.* **2020**, *33*, 175–183. [CrossRef]

46. Xia, J.; Yan, Z.; Jia, G.; Zeng, H.; Jones, P.D.; Zhou, W.; Zhang, A. Projections of the advance in the start of the growing season during the 21st century based on CMIP5 simulations. *Adv. Atmos. Sci.* **2015**, *32*, 831–838. [CrossRef]
47. Garonna, I.; De Jong, R.; De Wit, A.J.; Mücher, C.A.; Schmid, B.; Schaepman, M.E. Strong contribution of autumn phenology to changes in satellite-derived growing season length estimates across Europe (1982–2011). *Glob. Chang. Biol.* **2014**, *20*, 3457–3470. [CrossRef]
48. Piao, S.; Fang, J.; Zhou, L.; Ciais, P.; Zhu, B. Variations in satellite-derived phenology in China's temperate vegetation. *Glob. Chang. Biol.* **2006**, *12*, 672–685. [CrossRef]
49. He, Z.; Du, J.; Chen, L.; Zhu, X.; Lin, P.; Zhao, M.; Fang, S. Impacts of recent climate extremes on spring phenology in arid-mountain ecosystems in China. *Agric. Forest Meteorol.* **2018**, *260*, 31–40. [CrossRef]
50. Toledo, M.; Poorter, L.; Pea-Claros, M.; Alarcón, A.; Bongers, F. Climate is a stronger driver of tree and forest growth rates than soil and disturbance. *J. Ecol.* **2011**, *99*, 254–264. [CrossRef]
51. Temperature, precipitation, and insolation effects on autumn vegetation phenology in temperate China. *Glob. Chang. Biol.* **2016**, *22*, 644–655. [CrossRef]
52. Wang, X.; Wu, C.; Peng, D.; Gonsamo, A.; Liu, Z. Snow cover phenology affects alpine vegetation growth dynamics on the Tibetan Plateau: Satellite observed evidence, impacts of different biomes, and climate drivers. *Agric. Forest Meteorol.* **2018**, *256*, 61–74. [CrossRef]
53. Chen, H.; Zhu, Q.; Wu, N.; Wang, Y.; Peng, C. Delayed spring phenology on the Tibetan Plateau may also be attributable to other factors than winter and spring warming. *Proc. Natl. Acad. Sci. USA* **2011**, *108*, E93. [CrossRef] [PubMed]
54. Yi, S.; Zhou, Z. Increasing contamination might have delayed spring phenology on the Tibetan Plateau. *Proc. Natl. Acad. Sci. USA* **2011**, *108*, E94. [CrossRef]
55. Zhang, G.; Zhang, Y.; Dong, J.; Xiao, X. Green-up dates in the Tibetan Plateau have continuously advanced from 1982 to 2011. *Proc. Natl. Acad. Sci. USA* **2013**, *110*, 4309–4314. [CrossRef] [PubMed]
56. Zhang, X.; Friedl, M.A.; Schaaf, C.B.; Strahler, A.H. Climate controls on vegetation phenological patterns in northern mid-and high latitudes inferred from MODIS data. *Glob. Chang. Biol.* **2004**, *10*, 1133–1145. [CrossRef]
57. Spano, D.; Cesaraccio, C.; Duce, P.; Snyder, R.L. Phenological stages of natural species and their use as climate indicators. *Int. J. Biometeorol.* **1999**, *42*, 124–133. [CrossRef]
58. Potop, V.; Možný, M.; Soukup, J. Drought evolution at various time scales in the lowland regions and their impact on vegetable crops in the Czech Republic. *Agric. For. Meteorol.* **2012**, *156*, 121–133. [CrossRef]
59. Liu, Z.P.; Wang, Y.Q.; Shao, M.G.; Jia, X.X.; Li, X.L. Spatiotemporal analysis of multiscalar drought characteristics across the Loess Plateau of China. *J. Hydrol.* **2016**, *534*, 281–299. [CrossRef]
60. Knapp, A.K.; Carroll, C.J.; Denton, E.M.; La Pierre, K.J.; Collins, S.L.; Smith, M.D. Differential sensitivity to regional-scale drought in six central US grasslands. *Oecologia* **2015**, *177*, 949–957. [CrossRef] [PubMed]
61. Phillips, O.L.; Aragão, L.E.O.C.; Lewis, S.L. Drought sensitivity of the Amazon rainfores. *Science* **2009**, *323*, 1344–1347. [CrossRef]
62. Yan, M.; Xue, M.; Zhang, L.; Tian, X.; Chen, B.; Dong, Y. A Decade's Change in Vegetation Productivity and Its Response to Climate Change over Northeast China. *Plants-Basel* **2021**, *10*, 821. [CrossRef]
63. Wang, M.; Gong, Y.; Lafleur, P.; Wu, Y. Patterns and drivers of carbon, nitrogen and phosphorus stoichiometry in Southern China's grasslands. *Sci. Total Environ.* **2021**, *785*, 147201. [CrossRef]
64. Wang, H.; Yan, S.; Liang, Z.; Jiao, K.; Li, D.; Wei, F.; Li, S. Strength of association between vegetation greenness and its drivers across China between 1982 and 2015: Regional differences and temporal variations. *Ecol. Indic.* **2021**, *128*, 107831. [CrossRef]
65. Jiang, S.; Chen, X.; Smettem, K.; Wang, T. Climate and land use influences on changing spatiotemporal patterns of mountain vegetation cover in southwest China. *Ecol. Indic.* **2021**, *121*, 107193. [CrossRef]
66. Peng, J.; Jiang, H.; Liu, Q.; Green, S.M.; Quine, T.A.; Liu, H.; Qiu, S.; Liu, Y.; Meersmans, J. Human activity vs. climate change: Distinguishing dominant drivers on LAI dynamics in karst region of southwest China. *Sci. Total Environ.* **2021**, *769*, 144297. [CrossRef] [PubMed]

land

MDPI

Article

Spatiotemporal Evolution and Driving Forces of Sustainable Development of Urban Human Settlements in China for SDGs

Xueping Cong [1,2,*], Xueming Li [1,2] and Yilu Gong [3]

[1] School of Geography, Liaoning Normal University, Dalian 116029, China; lixueming999@163.com
[2] Human Settlements Research Center, Liaoning Normal University, Dalian 116029, China
[3] Art and Design School, Dalian Polytechnic University, Dalian 116034, China; gongyl@dlpu.edu.cn
* Correspondence: congxueping97@lnnu.edu.cn

Abstract: As the world's largest developing country, China has actively implemented the UN Sustainable Development Goals (SDGs). Sustainable development of urban human settlements is the result of localization and the deepening of sustainable development theory in China. This study combines SDGs to construct an evaluation index system for the sustainable development of urban human settlements in China, using optimization methods, such as natural breaks (Jenks), exploratory spatial data analysis, and GeoDetector, to conduct systematic research on the spatiotemporal evolution of the current sustainable development level and analyze the core driving forces of urban human settlements in 285 prefecture-level cities in China from 2000 to 2019. Our study revealed that: (1) The overall sustainable development level of urban human settlements and their subsystems in China has improved steadily, but the levels of subsystems are quite different; (2) the sustainable development level of the urban human settlements in China can be expressed as a spatial pattern of "high in the east and low in the west, high in the south and low in the north" and has relatively significant spatial correlation characteristics; notably, the development level of each subsystem has different spatial characteristics; (3) the sustainable development level of urban human settlements is mainly based on medium sustainability, and the main development model is to progress from a medium-low development level to a medium-high development level; (4) the sustainable development level of urban human settlements is mainly driven by the per capita gross domestic product (GDP), housing price-to-income ratio, investment in education and scientific research, Internet penetration, and $PM_{2.5}$.

Keywords: urban human settlements; sustainable development; temporal and spatial differentiation; driving force; prefecture-level cities in China

Citation: Cong, X.; Li, X.; Gong, Y. Spatiotemporal Evolution and Driving Forces of Sustainable Development of Urban Human Settlements in China for SDGs. *Land* **2021**, *10*, 993. https://doi.org/10.3390/land10090993

Academic Editor: Ayyoob Sharifi

Received: 10 August 2021
Accepted: 18 September 2021
Published: 21 September 2021

1. Introduction

Since the reform and opening up, China's economy has developed rapidly; the urbanization rate has increased, and the scale of urban space has expanded [1]. At the same time, human settlements are also being threatened [2], especially with the outbreak of the COVID 19 epidemic, and the global problems of human settlements, such as pollution, education interruption, economic loss, and medical resource imbalance that are becoming more prominent [3]. The United Nations convened the Human Environment Conference in Stockholm in 1972 and issued the United Nations Declaration of the Human Environment, which was the first meeting where the international community discussed the severe contradiction between the environment and development [4]. In 1987, the concept of sustainable development was clearly stated for the first time in Our Common Future [5]. Ever since, managing and developing human settlements and realizing sustainable development have become the focus of attention for all global economies. In September 2015, the United Nations General Assembly officially adopted the 2030 Agenda for Sustainable Development, which further clarified the sustainable development goals (SDGs) and the corresponding implementation methods [6]; the agenda also promoted continuous deepening of the concept of sustainable development and improvement of the world's living environment (at

a broader level and scope). As the world's largest developing country, China has always believed that peace and development are crucial for the times we live in, and globalization and multilateralism are the signs of world development [7]. Therefore, in the process of global sustainable development, starting from the global responsibility of building a community with a shared future for mankind, the country has actively responded and made important strategic deployments in the corresponding directions. Human settlements are the basis of human survival and activities, and a prerequisite for the stable development of society. The scientific concept behind them aims to find a high degree of compatibility between material and non-material environments, an ideal relationship between humans and the environment, and conformity to the objective laws regarding the development of human settlements [8]. The effective combination of urban human settlements and sustainable development can ensure the efficient operation of various systems of human settlements, while securing high-quality human settlement resources for future generations. Notably, the sustainable development of human settlements is the result of localization and deepening of sustainable development theory in China, and it is also a crucial practice and national model for adhering to the UN sustainable development goals [9].

The construction of urban human settlements has yielded relatively fruitful results. According to the different research propositions, studies on foreign urban human settlements are divided into the urban planning school, Chicago school, ekistics school, and ecological school [8,10]. Human settlements have been through a dynamic process of change, and notably, there are certain differences between cities or countries. The assessment and comparative analysis of urban human settlements are not only the basis for measuring urban planning, construction, and management, but also an effective way to highlight the gaps in urban development and identify urban problems. Therefore, the temporal and spatial dynamic evolution of urban human settlements has been the focus of research. Many scholars have considered the system coordination [11], vulnerability [12], suitability [13], wellbeing [14], satisfaction [15,16], pseudo-environment [17], and the reorganization by COVID 19 [18] of urban human settlements based on different dimensions and perspectives. Owing to the newfound focus on earth, studies on human settlements from the perspective of sustainable development have become a new research hotspot [19,20]. An increasing number of scholars believe that it is necessary to firmly build the evaluation standard of urban human settlements based on people and optimize the sustainable development route of urban human settlements [21,22]. Regarding the relevant research on the sustainable development of urban human settlements, Mele (2018) proposed that whether it is an old, industrialized country or an emerging country, if the sustainable development of human settlements is to be achieved, it is necessary to rethink the economy and development model [23]. Dahiya (2019) explained that the urban human settlements in the Asia-Pacific region still have problems, such as urban poverty, inequality, and insufficient urban public service resources, and emphasized that the New Urban Agenda can effectively resolve the current global sustainability and inclusiveness issues [24]. Corbane (2020) conducted an analysis of changes in the greenness of human settlements in 10,323 urban centers around the world, believed that the greening degree of most urban centers is lower than that outside built-up areas, and explained that the difference in human settlements between cities may also be caused by social and political factors [25]. Plata (2019) proposed that green infrastructure planning should not be limited to ecology; it should be integrated with the social environment to improve the capacity of sustainable development of urban human settlements [26]. Additionally, Rozhenkova (2019) emphasized that to achieve sustainable development of urban human settlements, a city policy database should be established for comparison [27]. Wang (2020) proposed that only when the built environment and the natural ecological environment reach a balance point can the sustainable development of human settlements be realized [28]. Wang (2020) also postulated that the sustainable development of human settlements can further improve the ecological well-being of residents [29]. With respect to research methods, Osman (2021) developed the Voluntary Local Review framework to evaluate and monitor the progress of urban human settlements in

Saudi Arabia to achieve SDGs [30]. Gonçalves (2020) believed that the Casa Azul Label and SBTool Urban Dahiya can be suitable for assessing the sustainability potential of human settlements in small towns of developing countries [31]. Xu (2019) applied the full permutation polygon synthetic indicator to evaluate the sustainability of China's urban agglomerations, and believed that the development of urban human settlements should still focus on coordination [32]. Botequilha-Leito (2020) used the strengths, weaknesses, opportunities, and threats (SWOT) method to analyze the role of performance-based planning in solving the sustainable problems of urban human settlements in Queensland [33].

In addition to different theoretical studies, different countries have different construction priorities and methods for the sustainable development of human settlements. For example, in addition to the importance of resources and the environment, the United Kingdom's evaluation criteria for human settlements involve social justice and public participation. In practice, with the city of London as the center, eight satellite cities that can not only meet the needs of life but also provide employment have been created in a concentric circle pattern; this not only helps to achieve self-sufficiency in the region, but also ensures good human settlements [34]. Germany's focus on the construction of human settlements has changed from its initial emphasis on increasing the number of residences to improving the quality of human settlements and promoting urban development based on a sustainable natural ecological environment [35]. The Netherlands has implemented reasonable plans for land use and transportation to avoid environmental pressure caused by high density, while paying attention to the construction of urban green spaces [36]. The United States of America aims at livability, health (including social, psychological, and well-being), and sustainability (including environmental problems, the disorderly spread of land, and resource consumption), to guide the sustainable development of human settlements [37]. The Chinese human settlements science considers the global, regional, city, community (village and town), and architecture at different levels, outlines natural, humanity, social, residential, and support systems as the five crucial parts of human settlements, and puts forward a sustainable development plan for human settlements [8]. Singapore adheres to the "people-oriented" principle, starting from the perspective of residents' lives, such as air quality, traffic accessibility, urban greening, and infrastructure, and attaches importance to the construction of ecological environments to build a garden city [38].

Although there have been fruitful theoretical and practical results on the improvement and development of urban human settlements, the related studies that combine urban human settlements with sustainable development are mostly theoretical discussions. These studies seldom used quantitative indicators for systematic research. Therefore, to understand the overall, continuous, and dynamic evolution of the sustainable development of urban human settlements in all prefecture-level cities in China, our study addressed the following problems: What kind of development law is implemented at the national level for the sustainable development of urban human settlements? What is the level of sustainable development of the urban human settlements of each city in China, and what are its spatiotemporal evolution characteristics? What causes the difference in the level of sustainable development across urban human settlements? The answers to these questions cannot only enrich the quantitative research on the sustainable development of urban human settlements, but also provide experience and reference to improve the quality of urban human settlements, guide the accurate positioning of various cities, and formulate urban development strategies rationally. This study considers the theory of sustainable development as the cornerstone for the construction of urban human settlements, and develops evaluation indicators and models for the sustainable development of urban human settlements under the guidance of the 2030 SDGs. Additionally, this study conducts a quantitative test of the sustainable development process of urban human settlements in various Chinese cities from 2000 to 2019. The objectives of this study are to explore the external manifestations and internal driving forces of the spatiotemporal evolution of sustainable development in urban human settlements in China over the past 20 years,

improve the sustainable development capacity of urban human settlements, and finally, realize the Chinese practice of global sustainable development.

2. Data and Methods

2.1. Overview of Study Area

China is located in eastern Asia and the west coast of the Pacific Ocean, bordered by North Korea to the east, Mongolia to the north, Afghanistan, Pakistan, and India to the west, and Myanmar, Laos, and Vietnam to the south. China starts from the heart of the Heilongjiang River in the north, to the Lydi Shoal in the south, and from the Pamirs in the west, to the intersection of the Heilongjiang and Wusuli rivers in the east. The total land area of China is about 9.6 million square kilometers, ranking third in the world. The terrain of China is high in the west and low in the east, and the climate types are diverse. The resources are abundant, but the per capita resources are relatively small; the regional distribution is uneven. China is the most populous developing country in the world. According to official data released in May 2021, the total population of the country is 1411.78 million, with a sex ratio of 105.07%. The population living in urban areas accounts for 63.89%, and the population aged 65 and above accounts for 13.50%. Notably, China is the second largest economy in the world, and the country's GDP in 2020 was 101,598.6 billion yuan, reflecting an increase of 2.3% over 2019, of which the secondary and tertiary industries accounted for 37.8% and 54.5%, respectively.

As of 2020, China has 34 provincial-level administrative divisions and 333 prefecture-level administrative divisions (including 293 prefecture-level cities). Notably, we have considered 2000–2019 as the research period. To facilitate research, the administrative divisions of the country in 2020 have been considered, and Chaohu, Bijie, Tongren, Sansha, Haidong, Danzhou, Xigaze, Qamdo, Nyingchi, Turpan, Shannan, Hami, Nagqu, and Laiwu, whose data cannot be matched due to the adjustment of administrative divisions, are eliminated. A total of 285 prefecture-level cities, with relatively stable administrative divisions since 2000, are retained as the study subjects.

2.2. Data Source

The spatial vector data were obtained from the standard map service system (http://bzdt.ch.mnr.gov.cn, accessed on 1 January 2021). The statistical indicator data were derived from the China City Statistical Yearbook, China Urban Construction Statistical Yearbook, China Environmental Statistics Yearbook, provincial and municipal statistical yearbooks, official websites of statistical bureaus, and government bulletins from 2000 to 2020. The meteorological data were obtained from publicly released information from the Institute of Geographical Sciences and Natural Resources Research, Chinese Academy of Sciences, and Resources and Environmental Sciences and Data Center (http://www.resdc.cn/data.aspx?DATAID=230, accessed on 3 February 2021). The average $PM_{2.5}$ emission concentration was obtained from the world $PM_{2.5}$ concentration map jointly released by Columbia University and the U.S. Atmospheric Composition Group (http://beta.sedac.ciesin.columbia.edu/, accessed on 19 February 2021). The average annual $PM_{2.5}$ emission concentration of prefecture-level cities in China was obtained using ArcGIS. House price data were obtained from the CEIC database (https://www.ceicdata.com/en, accessed on 4 January 2021). The energy consumption data were derived from the night light data obtained by the integrated processing of DMSP/OLS data and NPP-VIIRS data; the energy consumption was simulated and calculated [39]. Part of the data referred to the result of arithmetic processing, such as the temperature and humidity index [40], wind efficiency index [41], foreign trade dependence, and road network density.

2.3. Construction of Indicator System for Sustainable Development of Urban Human Settlements Based on SDGs

The concept of human settlements was formed in the theory of ekistics proposed by the Greek scholar Dausatias in the 1950s. Because urban human settlements are complex giant

systems, it is difficult to use a single index for its quantitative analysis, and therefore, it is mostly studied by constructing an index system [42,43]. Wu (2001) combined China's social reality and emphasized that human settlements include five major systems, namely, natural, humanity, social, residential, and support subsystems [8]. Urban human settlements and sustainable development promote each other, and the natural environment is the basis for humans to develop settlement behaviors and achieve sustainable development. As individual inhabitants, the material needs and psycho-physiological behaviors of human beings are the driving forces for a sustainable living environment. Appropriate housing for everyone is a prerequisite for a sustainable living environment. Society is a system of human interaction, and its economic development, social security, and stability are the basic requirements for a sustainable living environment. Furthermore, the infrastructure of human settlements and the fairness and efficiency of the public service system are strong supports for a sustainable living environment. Only when the five major systems are organically combined to ensure a virtuous circle and coordinated development within and among systems is achieved, can the human settlements be in a state of sustainable evolution.

To achieve steady progress in the quality and efficiency of the global ecological environment, economic structure, and social system, the UN SDGs identified by the United Nations Development Summit cover 17 goals and 169 specific targets, which were fully launched on 1 January 2016. This study considers the SDGs global indicator framework as an important basis for assessing the sustainable development of urban human settlements, while recognizing the China National Plan for implementing the 2030 Agenda for sustainable development as a supplement. In addition, this study refers to the China Human Settlements Award Evaluation Index System and relevant standards in domestic and foreign research results and closely integrates the indicators selected by the localization of SDGs, with the connotation of various systems of human settlements. Each indicator is matched to the five system layers of urban human settlements one by one, so that each indicator belongs to a certain system of human settlements and has a corresponding sustainable development goal to ensure the comprehensiveness of the selection of indicators.

The natural system includes geographic location, climatic conditions, animals and plants, and utilization of water and land resources. The ten indicators selected in this study from the three aspects of natural conditions, environmental protection, and resource utilization mainly corresponded to SDGs 6, 11, 12, and 15. The humanity system includes population development trends, population quality assurance, and improvement of quality capabilities. The nine indicators selected in this study from three aspects of population trends, cultural education, and scientific research and innovation mainly correspond to SDGs 1, 4, 5, 9, and 11. The residential system includes housing price, area, house type, parking space, water, electricity, and gas coverage. The five indicators of housing conditions and housing facilities selected in this study mainly correspond to SDGs 6, 7, and 11. A social system is a group formed by the interrelation of residents in the process of interacting with each other. This group is an organism that promotes social stability and harmony and is combined according to a certain normative system and economic relationship. The social system consists of nine indicators in three aspects, namely, economic level, living conditions, and urban safety, which mainly correspond to SDGs 2, 8, 10, 12, 14, and 16. The support system connects the artificial and natural systems. This is the result of man-made designs and construction. It is a guarantee system that provides support for human production and life. A total of seven indicators were selected in this study from three aspects of public services, communication facilities, and transportation that mainly correspond to SDGs 3, 9, and 11. Among them, SDG 13 focuses on national and global climate action strategies and plans. Considering the availability and comparability of its indicators, it was temporarily not included in the indicator system for the sustainable development of urban human settlements. As a result, constructing a multi-level urban human settlements sustainability evaluation index system (Table 1) that adapted to China's national and spatiotemporal conditions can not only improve the persuasiveness of the evaluation results but also enrich the hierarchy of the index system. This can explain China's substantive efforts for

sustainable development strategies and construction of human settlements, along with the experience and lessons in the development process.

Table 1. Index system and weight of sustainable development of urban human settlements in China.

System Layer	Index Layer	Corresponding to SDGs	Entropy Method Weight	AHP Weight	Comprehensive Weight
Natural system	Temperature and humidity index (X_1)	SDG 11.6	0.0129	0.0671	0.0325
	Wind efficiency index (X_2)	SDG 11.6	0.0144	0.0283	0.0223
	$PM_{2.5}$ concentration (X_3)	SDG 11.6	0.0292	0.0379	0.0368
	Green coverage rate in built-up area (X_4)	SDG 15.2	0.0178	0.0528	0.0339
	Park green area per capita (X_5)	SDG 11.7	0.0209	0.0196	0.0224
	Sewage treatment rate (X_6)	SDG 6.3	0.0153	0.0528	0.0314
	Harmless treatment rate of domestic garbage (X_7)	SDG 11.6	0.0145	0.0240	0.0206
	Water consumption per unit GDP (X_8)	SDG 6.4	0.0468	0.0501	0.0535
	Energy consumption per unit of GDP (X_9)	SDG 12.2	0.0130	0.0125	0.0141
	Comprehensive utilization rate of industrial solid waste (X_{10})	SDG 12.5	0.0133	0.0691	0.0335
Humanity system	The population density (X_{11})	SDG 11.3	0.0125	0.0333	0.0225
	Natural growth rate (X_{12})	SDG 11.3	0.0113	0.0178	0.0157
	Sex ratio (X_{13})	SDG 5.1	0.0111	0.0096	0.0114
	Aging rate (X_{14})	SDG 11.3	0.0151	0.0178	0.0181
	Number of college students per 10,000 (X_{15})	SDG 4.3	0.0199	0.0140	0.0185
	Compulsory education teacher-student ratio (X_{16})	SDG 4.1	0.0135	0.0124	0.0143
	Percentage of education expenditure (X_{17})	SDG 1.a	0.0360	0.0095	0.0204
	R&D investment intensity (X_{18})	SDG 9.5	0.0491	0.0295	0.0420
	Number of patents granted per 10,000 people (X_{19})	SDG 9.5	0.0139	0.0098	0.0129
Residential system	Housing area per capita (X_{20})	SDG 11.1	0.0414	0.1014	0.0716
	House price to income ratio (X_{21})	SDG 11.1	0.0275	0.0338	0.0337
	Per capita residential investment (X_{22})	SDG 11.1	0.0340	0.0338	0.0374
	Water supply penetration rate (X_{23})	SDG 6.1	0.0137	0.0338	0.0238
	Gas penetration rate (X_{24})	SDG 7.1	0.0191	0.0113	0.0162
Social system	GDP per capita (X_{25})	SDG 8.1	0.0572	0.0236	0.0406
	The proportion of tertiary industry in GDP (X_{26})	SDG 8.2	0.0279	0.0137	0.0216
	Public fiscal revenue as a proportion of GDP (X_{27})	SDG 8.1	0.0287	0.0087	0.0175
	Export dependence (X_{28})	SDG 17.11	0.0261	0.0047	0.0122
	Urban registered unemployment rate (X_{29})	SDG 10.2	0.0223	0.0158	0.0207
	Per capita disposable income growth rate (X_{30})	SDG 8.1	0.0229	0.0240	0.0259
	Per capita food production (X_{31})	SDG 2.1	0.0223	0.0129	0.0187
	Per capita aquatic product output (X_{32})	SDG 14.4	0.0283	0.0042	0.0120
	Number of criminal cases per 10,000 people (X_{33})	SDG 16.1	0.0221	0.0284	0.0277
Support system	Number of physicians per 10,000 people (X_{34})	SDG 3.8	0.0317	0.0249	0.0310
	Number of stadiums owned by 10,000 people (X_{35})	SDG 9.1	0.0300	0.0031	0.0107
	Number of cultural centers owned by 10,000 people (X_{36})	SDG 11.4	0.0256	0.0031	0.0098
	Mobile phone penetration rate (X_{37})	SDG 9.c	0.0422	0.0132	0.0261
	Internet penetration rate (X_{38})	SDG 9.c	0.0473	0.0132	0.0276
	Road network density (X_{39})	SDG 11.2	0.0125	0.0068	0.0102
	Number of buses owned by 10,000 people (X_{40})	SDG 11.2	0.0368	0.0178	0.0283

2.4. Research Methods

1. Coefficient of variation

The coefficient of variation is statistically used to characterize the degree of dispersion of the data. In this study, the coefficient of variation is used to calculate the relative difference between all the values of a certain indicator of the sustainable development of human settlements in China. The calculation formula is as follows:

$$CV = \frac{\sigma}{\mu} \quad (1)$$

where σ is the standard deviation, μ is the average value, and CV is the coefficient of variation. The larger the CV value, the larger the relative gap in the data.

2. Standardization of evaluation indicators

Because of the different attributes of evaluation indicators related to the sustainable development of urban human settlements in China, to eliminate the impact of different indicators on the same measurement unit, it is necessary to standardize the indicator data of different units and attributes, and convert them into data that have the same measurement and are directly operable. Notably, the larger the positive index value, the better the performance. The calculation formula is as follows:

$$X_{ij} = \frac{x_{ij} - \min\{x_{ij}\}}{\max\{x_{ij}\} - \min\{x_{ij}\}} \tag{2}$$

Conversely, the smaller the value of the reverse index, the better the performance. The calculation formula is as follows:

$$X_{ij} = \frac{\max\{x_{ij}\} - x_{ij}}{\max\{x_{ij}\} - \min\{x_{ij}\}} \tag{3}$$

where X_{ij} represents the standard value of the evaluation index i of the evaluation object j, x_{ij} represents the original value, and $\max\{x_{ij}\}$ and $\min\{x_{ij}\}$ represent the maximum and minimum values of the original values, respectively.

3. Combination weight determination

The subjective and objective combination method uses the objective weighting method, which is based on the entropy and subjective weighting methods of the analytic hierarchy process, to determine the indicator weights of the evaluation system for the sustainable development of urban human settlements. After calculating the weights of the entropy method and the analytic hierarchy process separately, the two are combined to form a new weight, using the Lagrangian multiplier method. This method can effectively avoid the shortcomings of the objective weighting method, namely, poor participation by decision makers and limited scope of use, and reduces the error caused by the subjective weighting method when there are too many indicators. At the same time, the advantages of the objective weighting method with high accuracy and the subjective weighting method with strong systematics can be maximized to improve the accuracy of the weight calculation results. The calculation formula is given by [44]:

$$W_j = \frac{(w_{1j}w_{2j})^{0.5}}{\sum_{j=1}^{n}(w_{1j}w_{2j})^{0.5}} \tag{4}$$

where W_j is the combined weight of the j-th index, and w_{1j} and w_{2j} are the objective and subjective weights of the jth index, respectively.

4. Measurement model of sustainable development of urban human settlements

The recently proposed sustainable development index research framework by the University of Texas at Arlington [45] improved the ability to measure the sustainable development level of human settlements of different cities in different years. First, the sustainable development level of the natural, humanity, residential, social, and support systems in urban human settlements were calculated. Then, the comprehensive sustainable development level was calculated. The higher the value, the higher the sustainable development level of the city's human settlements. The calculation formula is as follows:

$$s_i = \sum_{j=1}^{n}(w_j \times X_{ij}) \tag{5}$$

$$S = \sum_{i=1}^{m}(W_i \times s_i) \tag{6}$$

where s_i is the sustainable development level of each subsystem of urban human settlements, w_j is the weighted value of each index, X_{ij} is the standardized index value, S is the sustainable development level of urban human settlements, and W_i is the weighted value for each system layer.

5. Exploratory spatial data analysis method

Spatial autocorrelation is a common method of exploratory spatial data analysis that refers to the association of eigenvalues between a spatial unit and its neighboring units. The evaluation methods for spatial autocorrelation are divided into two categories: Global spatial autocorrelation and local spatial autocorrelation. Global spatial autocorrelation mainly describes the overall distribution of a certain feature in space and whether there is an aggregation feature. If this exists, we further analyze the model data related to the local space. This study uses spatial autocorrelation to reflect the spatial correlation pattern of the sustainable development level of urban human settlements. The global spatial autocorrelation evaluation method uses the Moran global spatial autocorrelation coefficient, and local spatial autocorrelation uses local indicator of spatial association (LISA) indicators.

6. GeoDetector

The GeoDetector method is an attribution method developed in the field of medical geography. Because the dependent variable and its related important factors have similar spatial or temporal distributions, this method has been widely used in economics, nature, society, and other fields in recent years, for spatial differentiation and mechanism research. Notably, compared with traditional measurement models, geographic detectors do not need to meet multiple assumptions, and the results are more accurate [46]. Our study uses the factor detection of the GeoDetector model to explore the spatial differentiation driving force of the sustainable development of urban human settlements. The calculation formula is as follows:

$$q = 1 - \frac{\sum_{h=1}^{L} N_h \sigma_h^2}{N\sigma^2} \quad (7)$$

where N is the number of samples in the study area, N_h is the number of samples in the area (category) h of the detection factor X, σ^2 is the total variance of Y in the study area (category), σ_h^2 is the variance of Y in the area (category) h of the detection factor X, and L is the number of regions (categories) of the detection factor X. The larger the value of q, the more significant the interpretation of X to Y, and vice versa.

3. Temporal and Spatial Differentiation of Sustainable Development of Urban Human Settlements in China

3.1. Development Trend

As seen in Figure 1, from 2000 to 2019, the overall level of sustainable development of urban human settlements in China steadily improved, portraying a continuous improvement trend. In 2000, the average level of sustainable development in urban human settlements was 0.25. By 2019, the score was 0.31, with a total growth rate of 23.61% and an average annual growth rate of 1.12%. The level of sustainable development of urban human settlements in China was specifically expressed as a gentle upward trend from 2000 to 2004, a short-term backward trend in 2005, and a significant increase in the growth rate of the development level from 2005 to 2010. In 2011, it experienced a short-term decline again and continued to rise from 2012–2016. The level of sustainable development continued to decline slightly in 2017–2018, and improved in 2019.

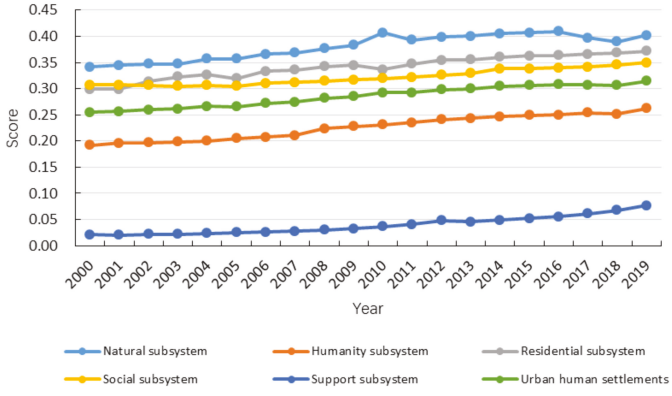

Figure 1. Trend chart of inter-annual sustainable development level of urban human settlements and subsystems in China.

3.2. Temporal and Spatial Pattern

The temporal and spatial evolution characteristics of the sustainable development level of urban human settlements include two aspects: The spatial distribution pattern and spatial correlation characteristics of the sustainable development of urban human settlements. In this study, we extracted data at five temporal points in 2000, 2005, 2010, 2015, and 2019, and used ArcGIS Jenks Natural Breaks to classify the sustainable development level of human settlements and subsystems of 285 prefecture-level cities into five levels: Low level of development, low to medium level of development, medium level of development, medium to high level of development, and high level of development. Using spatial autocorrelation, the spatial pattern characteristics and significance of the agglomeration space of the sustainable development level of urban human settlements in China were verified and visualized. The spatial distribution and LISA maps of the sustainable development level of urban human settlements in China were obtained.

3.2.1. Spatial Pattern of Sustainable Development Level of Urban Human Settlements Subsystems

1. Natural system

As seen in Figure 2, from 2000 to 2019, the spatial difference in the development level of the natural system of urban human settlements in China is relatively obvious. It shows that the overall spatial distribution characteristic is "high in the south and low in the north." The development level of the natural system in coastal cities is generally higher than that in inland cities. Overall, the areas with a relatively high level of development of the natural system of urban human settlements are concentrated in East China and Central South, and over time, high-value areas continue to gather in clusters to the southeast. From 2000 to 2019, the natural system scores of Shenzhen, Shanghai, Sanya, Hangzhou, and Xiamen were among the best. Shenzhen is at the forefront of the reform and opening up. Due to the high population and industrial density in the Pearl River Delta, the government attaches great importance to environmental governance and protection measures, and continuously strengthens investments in pollution control and governance. Air quality, anti-pollution ability, and resource conservation and utilization all have strong advantages. Per capita park green area and green coverage rate in Shanghai are both at the forefront of the country. Sanya and Xiamen have strong advantages in terms of air quality and the water environment. In recent years, under the guidance of the Double-Eight Strategy, Hangzhou has persisted in realizing the whole area of scenic spots and made every effort so that the construction of ecological civilization is in a leading position.

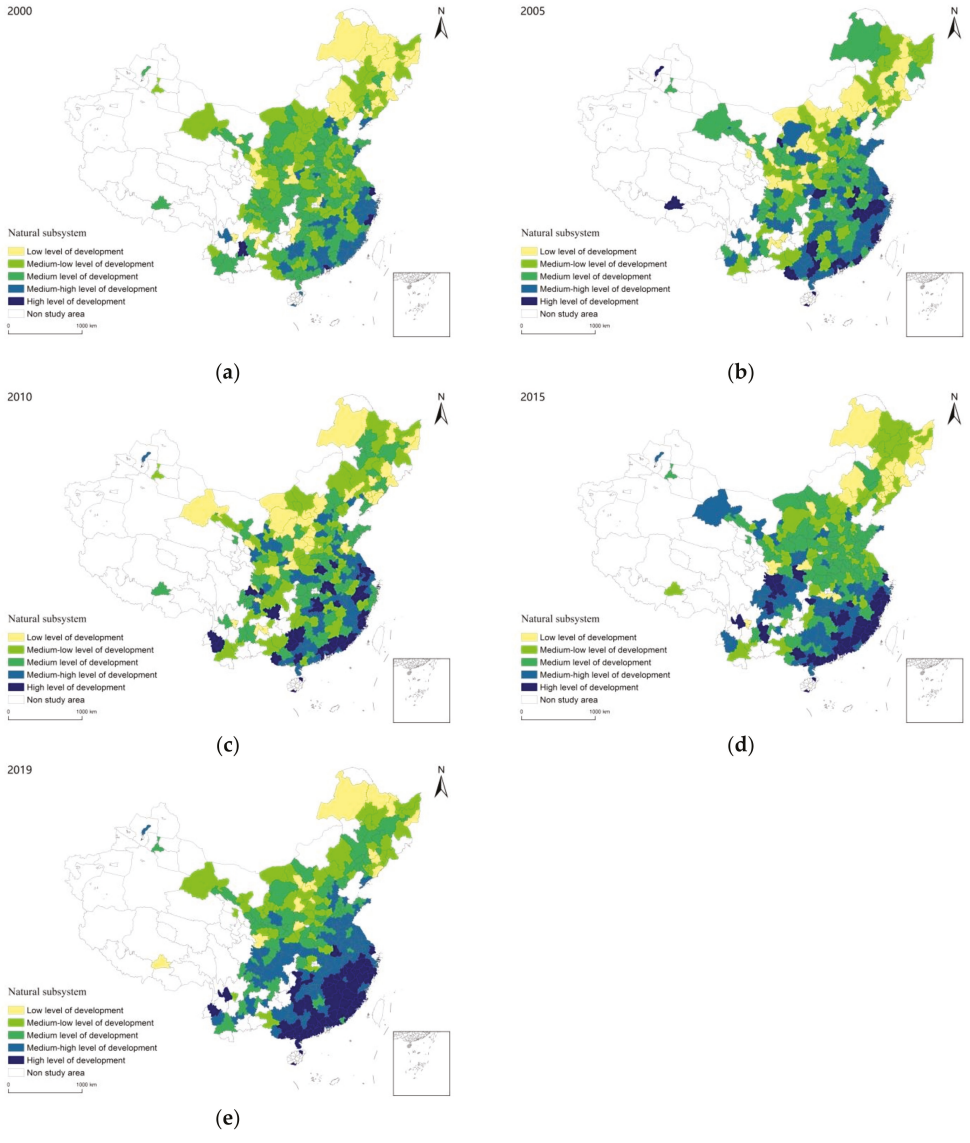

Figure 2. Spatial distribution map of the sustainable development level of the natural system of urban human settlements in China. (**a**) 2000; (**b**) 2005; (**c**) 2010; (**d**) 2015; and (**e**) 2019.

The prefecture-level cities with a low level of development of the natural system of urban human settlements were found to be concentrated in the Heilongjiang Province in the Northeast, the Shanxi Province, and the Inner Mongolia Autonomous Region in North China; areas with low development levels continue to gather in the northeast. The low level of development of the natural system of urban human settlements in Jixi, Heihe, Hulunbuir, Baishan, Tianshui, and Baiyin is mainly due to serious soil erosion, low greening, fragile ecological environment, relatively backward development, and unawareness of environmental protection.

2. Humanity system

As seen in Figure 3, between 2000 and 2019, the spatial difference in the development level of the humanity system of urban human settlements in China is relatively obvious, and the overall spatial pattern of "multi-level core-periphery" radial circle growth is prominent. From 2000 to 2019, Beijing, Hangzhou, Guangzhou, Changsha, and Wuhan were ranked high. Beijing is the capital of China, with a relatively balanced population structure. It is one of the regions with the richest educational resources. It has the largest number of well-known universities in the country, and the country's largest scientific research and academic base, with strong scientific research and innovation capabilities. Educational resources in Hangzhou have continued to expand, and the strength of online education has increased in recent years. At the same time, Hangzhou is committed to building a "Binjiang Paradise Silicon Valley." High-tech industries led by information, new medicines, environmental protection, and the application of new materials have strong momentum of development, and they have strong advantages in improving population quality. Wuhan ranks among the top in the country in terms of investment in scientific research funds and the number of patent authorizations. The developed high-tech industry has attracted a large number of young people. With a low degree of aging and a moderate population density, the population structure and quality show a positive development trend.

Notably, the prefecture-level cities with a low level of humanity system development in urban human settlements are concentrated in the Heilongjiang Province in the northeast and western regions, such as Yichun, Hegang, Shuangyashan, and Jixi in the Heilongjiang Province, Jinchang in the Gansu Province, Liaoyuan and Baishan in the Jilin Province, Wuhai in the Inner Mongolia Autonomous Region, Tongchuan in the Shaanxi Province, and Suining and Bazhong in the Sichuan Province. The main reason is that the development of these areas is relatively low; the population is constantly decreasing, education resources are scarce, and the ability of scientific research and innovation is also poor, which poses great difficulties in the overall improvement of population quality in the region.

3. Residential system

As seen in Figure 4, the development level of the residential system of urban human settlements in China presents a spatial pattern of expansion and growth from east to west, and the overall level gradually develops from a low-medium level to a medium-high level. In 2000, the high-value areas of residential system development were scattered in Kunming in the Yunnan Province, Langfang in the Hebei Province, and Zhuhai, Huizhou, and Foshan in the Guangdong Province. In 2005, a large number of areas with a high level of development in the residential system increased; this is especially true in the case of areas that developed into the Liaoning Province in East and Northeast China. During this period, the development level of the residential system in Sanya and Dalian improved significantly, mainly because these two coastal cities have good development with complete residential supporting facilities, relatively stable land prices and housing prices, and a moderate housing-price-to-income ratio. In 2009, the state carried out large-scale regulations and control of the real estate market. The real estate market tended to maintain stable and healthy development momentum. Housing security policies and supporting conditions have continuously improved. Therefore, during the period 2010–2019, the number of cities with high levels of development in the residential system continued to increase and were concentrated in the Beijing–Tianjin–Hebei urban agglomeration, the Jiangsu–Zhejiang–Shanghai area, the central part of the central and southern regions, and the southern part of the northeastern region.

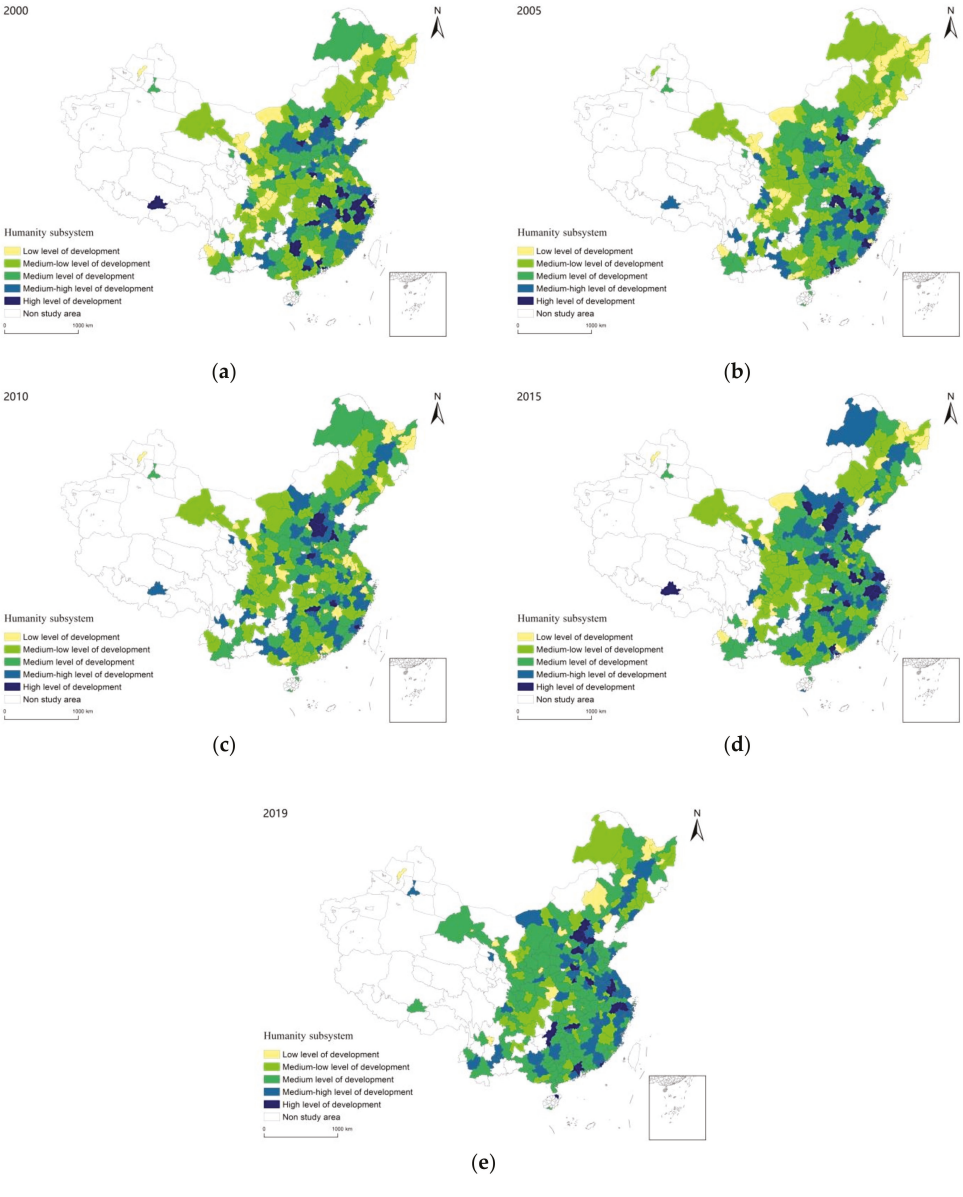

Figure 3. Spatial distribution map of the sustainable development level of the humanity system of urban human settlements in China. (**a**) 2000; (**b**) 2005; (**c**) 2010; (**d**) 2015; and (**e**) 2019.

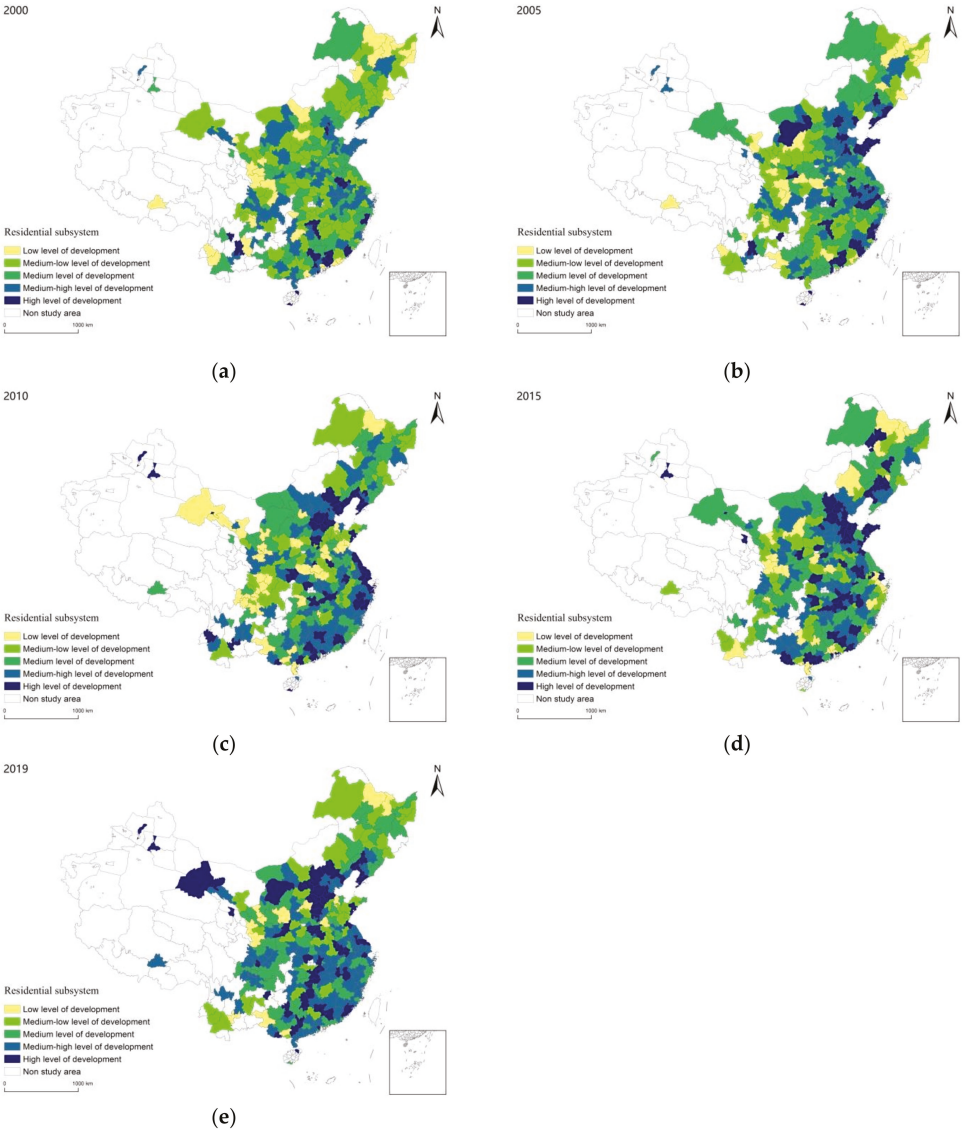

Figure 4. Spatial distribution map of the sustainable development level of the residential system of urban human settlements in China. (**a**) 2000; (**b**) 2005; (**c**) 2010; (**d**) 2015; and (**e**) 2019.

Notably, the prefecture-level cities with a low level of development of the urban human settlements residential system are concentrated in the Heilongjiang Province, the Gansu Province, and the Ningxia Hui Autonomous Region. Hegang, Heihe, and Qitaihe in the Heilongjiang Province, Tianshui, Jinchang, and Longnan in Gansu, and Guyuan and Zhongwei in the Ningxia Hui Autonomous Region have relatively low development, the per capita investment in real estate housing is relatively small, and the housing supporting infrastructure is not complete, resulting in a low level of development of the residential system.

4. Social system

As shown in Figure 5, from 2000 to 2019, the development level of the social system of urban human settlements in China shows a distribution characteristic of "high in the east and low in the west." Specifically, in 2000, cities with high levels of social systems were mainly concentrated in Heilongjiang and Liaoning in the Northeast and Jiangsu and Fujian in East China. Since the founding of New China, the Northeast, as a hotspot of China's industrialization, has made great contributions to China's economic development. Cities such as Dalian, Shenyang, and Harbin took the lead in focusing on import and export trade and strengthened the development of international cities, and together with the abundant material resources, they have a relatively high level of social development. From 2005 to 2019, the number of cities with middle–high and high development levels in the social system increased significantly. The Beijing–Tianjin–Hebei urban agglomeration, East China, and central and southern regions continue to affect the surrounding areas, and high-value areas radiate to the surrounding area. In particular, Shanghai, Shenzhen, Guangzhou, Hangzhou, and Suzhou in the eastern coastal areas, Changsha in the Hunan Province, and Ordos and Hulunbuir in the Inner Mongolia Autonomous Region have made significant progress, while the level of social system development in the Northeast has been declining. The reason is that the Northeast is deeply influenced by the concept of the planned economic system, and the ideological concepts are rigid, which has resulted in the industrial structure of the Northeast being unable to keep up with the pace of development in the country. At the same time, the aging population and loss of talent in the Northeast have led to a continuous decline in the development of the northeastern social system. The advantages of coastal cities, such as Shenzhen, Guangzhou, Shanghai, Suzhou, and Hangzhou are becoming increasingly obvious. The gross domestic product (GDP) and residents' income have grown steadily, the regional industrial structure is reasonable, the foreign economy is active, material resources such as grain and aquatic products are abundant, and the level of social system development is constantly improving.

Cities with a low level of social system development are concentrated in the southern part of the Sichuan Province and most areas of the Gansu Province. For example, Dazhou, Suining, Zhangye, and Wuwei are far from China's core economic areas. Inconvenient transportation in these regions has caused difficulties in foreign exchange. In this region, the industries are relatively poor, the structure is irrational, and the ability to integrate resources is weak. All of these have caused the city's economic aggregate, per capita level, and economic development rate to remain at the middle–low level.

5. Support system

As seen in Figure 6, from 2000 to 2019, the spatial differentiation of the development level of China's urban human settlement support system is not obvious. The overall spatial pattern shows uneven growth, with high-value areas scattered in the Beijing–Tianjin–Hebei urban agglomeration, East China, and Central South regions. From 2000 to 2010, the number of cities with a high level of development in China's urban human settlement support system was relatively small, mainly concentrated in the Beijing–Tianjin–Hebei urban agglomeration and the Guangdong Province in the central and southern regions. From 2015 to 2019, the number of cities with a high level of development in China's urban human settlement support system gradually increased, and the high-value areas radiated outward. In particular, Hubei and Zhejiang provinces have made significant progress. Specifically, Beijing, as the capital of China, focuses on the leading role of infrastructure in the process of urban construction. Infrastructure, such as medical resources, public transportation, and Internet communications, has great advantages, and the per capita public service resources are also abundant. Therefore, the level of development of the support system is relatively high, which has also driven the surrounding cities of Hengshui, Baoding, and Xingtai. Furthermore, infrastructure investment in Jiaxing, Jinhua, Wenzhou, Shenzhen, Dongguan, and other cities has increased rapidly, and the communication infrastructure is in the leading position in the country. In recent years, efforts have been made to implement

digital infrastructure operations and create a very modern infrastructure system, which has led to the development of a support system. Provincial capitals, such as Hefei, Wuhan, and Changsha, have a complete infrastructure and abundant per capita public service resources, which causes the system to develop evenly with significant progress.

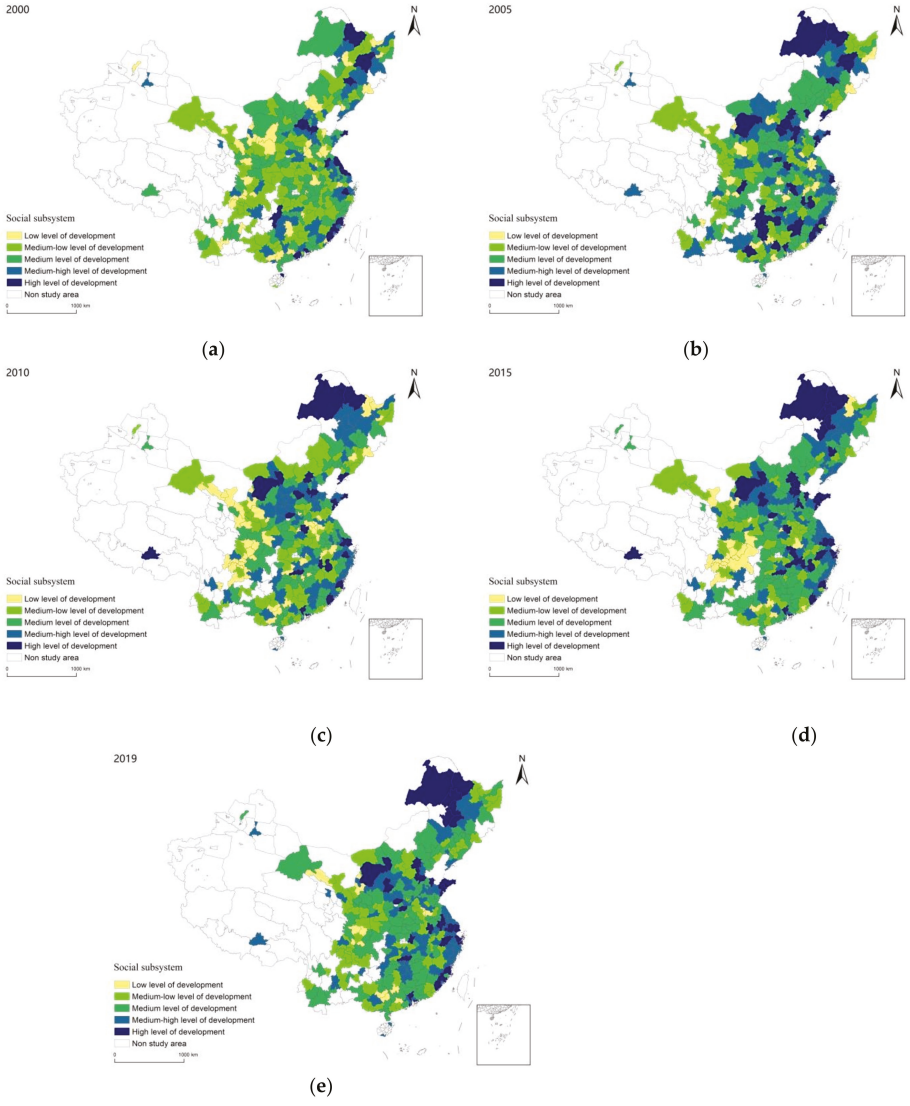

Figure 5. Spatial distribution map of the sustainable development level of the social system of urban human settlements in China. (**a**) 2000; (**b**) 2005; (**c**) 2010; (**d**) 2015; (**e**) 2019.

Notably, cities with a low level of urban human settlements support systems are concentrated in the eastern parts of the Henan, Guangxi, and Gansu provinces and the northeastern part of the Sichuan Province. Some regions, such as Guigang, Hezhou, Suining, Ziyang, Shangqiu, Xinyang, and Longnan, have underdeveloped transporta-

tion, relatively backward medical resources, low quantity and quality of public services, and poor communication infrastructure, which is far from the national average.

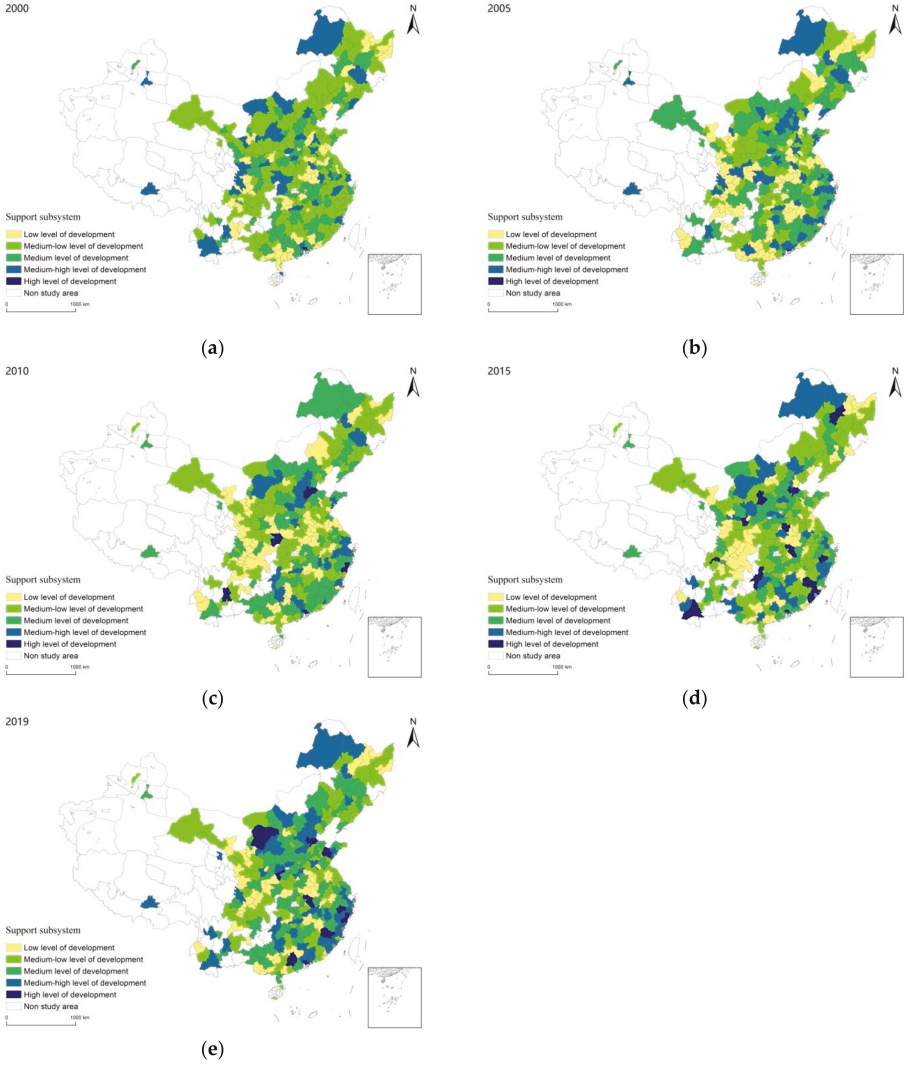

Figure 6. Spatial distribution map of the sustainable development level of the support system of urban human settlements in China. (**a**) 2000; (**b**) 2005; (**c**) 2010; (**d**) 2015; and (**e**) 2019.

3.2.2. Spatial Pattern of Sustainable Development Level of Urban Human Settlements

As seen in Figure 7 and Tables 2 and 3, between 2000 and 2019, the spatial difference in the level of sustainable development of urban human settlements in China is relatively obvious. The overall performance is spreading and growing from east to west, portraying the spatial distribution characteristics of "high in the east and low in the west; high in the south, and low in the north." On the whole, prefecture-level cities with a high level of sustainable development of urban human settlements are concentrated in the coastal areas

of East China and Central and Southern China regions, as well as the Beijing–Tianjin–Hebei urban agglomeration in North China. High-value areas continue to gather to the southeast, and prefecture-level cities with a low level of sustainable development are concentrated in the northeastern and inland cities in Northwest and North China.

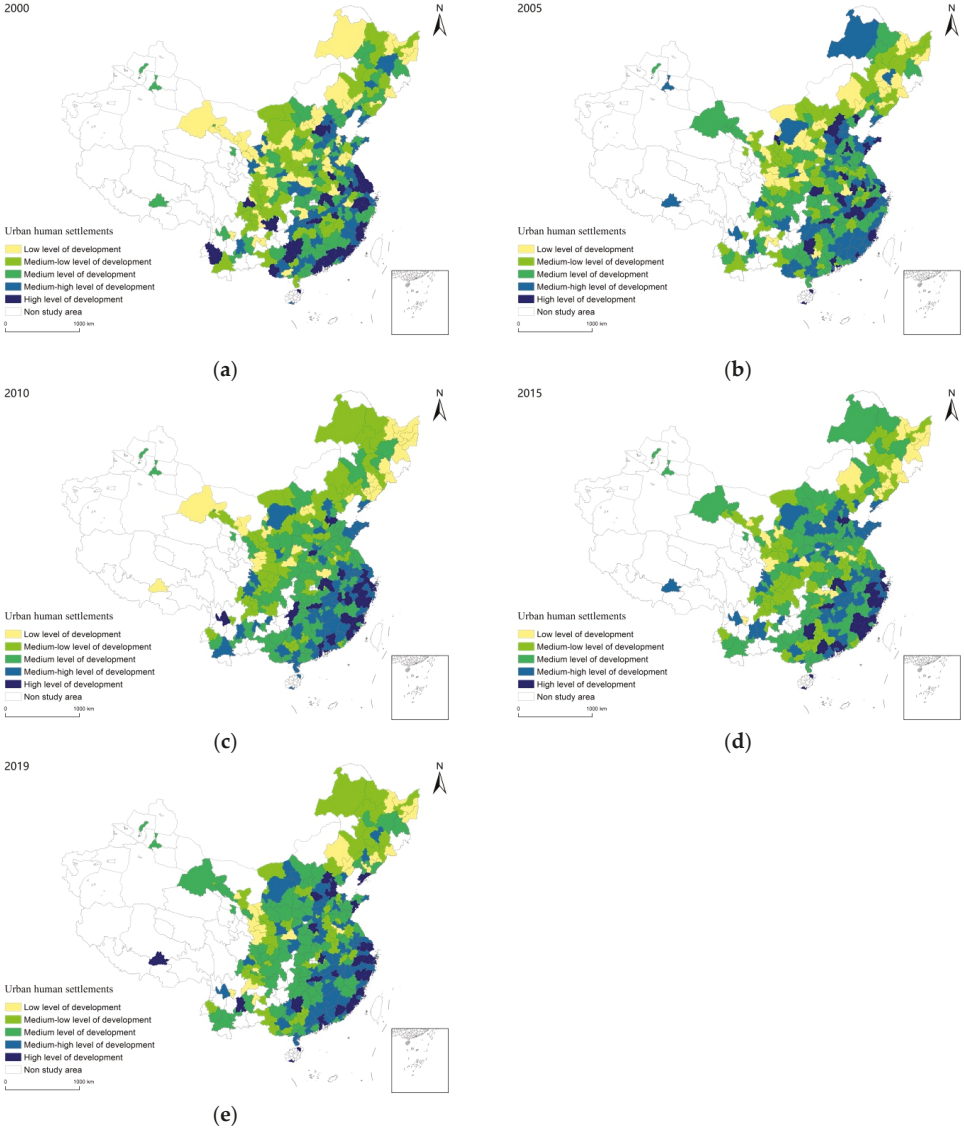

Figure 7. Spatial distribution map of the sustainable development level of urban human settlements in China. (**a**) 2000; (**b**) 2005; (**c**) 2010; (**d**) 2015; and (**e**) 2019.

Table 2. The top ten cities in China's urban human settlements development level and their scores.

Ranking	2000		2005		2010		2015		2019	
	Cities	**Scores**	**Cities**	**Scores**	**Cities**	**Scores**	**Cities**	**Scores**	**Cities**	**Scores**
1	Shenzhen	0.330	Shenzhen	0.310	Shenzhen	0.387	Shenzhen	0.361	Shenzhen	0.382
2	Guangzhou	0.313	Hangzhou	0.305	Hangzhou	0.372	Guangzhou	0.354	Shanghai	0.380
3	Hangzhou	0.306	Changsha	0.304	Guangzhou	0.370	Shanghai	0.354	Beijing	0.378
4	Shanghai	0.303	Shanghai	0.303	Suzhou	0.370	Hangzhou	0.353	Hangzhou	0.376
5	Changsha	0.300	Beijing	0.301	Changsha	0.355	Changsha	0.346	Guangzhou	0.371
6	Suzhou	0.300	Guangzhou	0.300	Wuhan	0.342	Wuhan	0.346	Changsha	0.369
7	Nanjing	0.300	Hefei	0.299	Hefei	0.340	Fuzhou	0.345	Kunming	0.368
8	Fuzhou	0.298	Nanjing	0.298	Zhuhai	0.340	Sanya	0.345	Suzhou	0.366
9	Xiamen	0.297	Sanya	0.298	Fuzhou	0.339	Guilin	0.345	Qingdao	0.363
10	Wuhan	0.295	Fuzhou	0.297	Zhengzhou	0.336	Xiamen	0.343	Sanya	0.363

Table 3. The bottom ten cities in China's urban human settlements development level and their scores.

Ranking	2000		2005		2010		2015		2019	
	Cities	**Scores**	**Cities**	**Scores**	**Cities**	**Scores**	**Cities**	**Scores**	**Cities**	**Scores**
1	Yichun	0.196	Baishan	0.220	Yichun	0.235	Baishan	0.253	Yichun	0.247
2	Baishan	0.197	Yichun	0.220	Jixi	0.243	Yichun	0.259	Baiyin	0.253
3	Hegang	0.210	Hegang	0.224	Fushun	0.243	Qitaihe	0.260	Qitaihe	0.259
4	Qitaihe	0.211	Longnan	0.225	Hegang	0.247	Jixi	0.261	Baishan	0.261
5	Shuozhou	0.213	Shuozhou	0.227	Longnan	0.247	Hegang	0.265	Hegang	0.262
6	Jixi	0.213	Baiyin	0.230	Baishan	0.251	Longnan	0.265	Jixi	0.267
7	Bazhong	0.214	Liaoyuan	0.230	Tianshui	0.252	Fushun	0.265	Dingxi	0.268
8	Tianshui	0.214	Jixi	0.232	Shuozhou	0.253	Liaoyuan	0.267	Zhongwei	0.268
9	Liupanshui	0.215	Tianshui	0.233	Qitaihe	0.253	Baiyin	0.269	Longnan	0.270
10	Tongchuan	0.215	Chaoyang	0.237	Wuwei	0.254	Wuzhong	0.270	Tianshui	0.273

Specifically, Shenzhen ranked first in the level of sustainable development of urban human settlements in China from 2000 to 2019, and Hangzhou, Changsha, Guangzhou, and Shanghai have repeatedly ranked among the top five. Shenzhen is located in the southern coastal area of Guangdong Province. It was fully urbanized in 2004 and became China's first city without a rural area. From a small fishing village to an innovative, inclusive, and dynamic modern international city, Shenzhen has developed rapidly and solidly: A good living environment and high level of greening, high level of education and strong scientific research ability, a developed transportation and road network, complete infrastructure per capita, and a high level of public services are observed, and the level of industrialization closely follows the level of urbanization. While the economy is developing rapidly, it also provides employment opportunities and social security for a large number of people who have moved into Shenzhen; therefore, the urban human settlements develop in a comprehensive, balanced, and stable manner. Hangzhou is the economic, cultural, scientific, and educational center of Zhejiang Province. It is also a well-known tourist city in the country, and its ecological civilization construction is in a leading position in China; high-tech industries dominated by new pharmaceuticals and environmental protection are also advantages of Hangzhou; owing to the rapid development of private enterprises, abundant resources, and high living quality of residents, Hangzhou's comprehensive strength of urban human settlements is good. Changsha is located in the eastern part of Hunan Province. It is an important central city in the middle reaches of the Yangtze River in China and is an important transportation hub of the country. In this city, the climate is mild, and the air quality has improved significantly; owing to the automobile, culture, and equipment manufacturing being its key industries, the city has made a great contribution to the development of the country's economy. Notably, high-tech industries, such as super hybrid rice and Beidou satellite, have brought together talent, and the sustainable development of urban human settlements has strong momentum. Guangzhou is located

in the south-central part of Guangdong Province; it has a superior geographical location and is regarded as the southern gate of China to the world. It has a long cultural history, strong political and cultural education and medical resources as advantages, high quality of the urban garden landscape, and good ecological environment. Additionally, the region has a strong economic foundation and a vigorously developing industrial sector, and the development of import and export trade, along with the modern service industry, has also contributed to the sustainable development level of urban human settlements in this region.

During the research period, among the bottom ten prefecture-level cities in terms of the sustainable development level of urban human settlements, Yichun, Hegang, Qitaihe, Jixi, Baishan, and Tianshui have shown improvements in their human settlements; however, compared to other cities, they are still in a backward position. Yichun City is located in the northeast of the Heilongjiang Province. It is a typical forestry resource-based city, and the development of its urban human settlements is very slow. This is because forestry is the main industry in Yichun, and its economic development structure is relatively simple. Due to environmental problems, such as desertification and soil erosion caused by excessive deforestation, residents' productivity and life have become severely challenged, and greater employment pressure, weak social security capabilities, and underdeveloped infrastructure have caused the population to continue to move out of these regions. All these factors have led to a low level of sustainable development of urban human settlements in Yichun and a slower rate of improvement. Hegang, Jixi, and Qitaihe are located in the northeast of Heilongjiang Province. They are important industrial and resource-based cities dominated by coal mines. The gradual depletion of energy has caused the urban economy to stagnate, the ecological environment is extremely problematic, and population loss is accelerating, resulting in Hegang becoming an empty city. Baishan is located on the west side of Changbai Mountain in Jilin Province. It is rich in natural resources, such as minerals and forestry. It has good water quality and high forest coverage, but its economic development is relatively backward, the quality of urban infrastructure and public services is low, and the overall level of urban human settlements is poor. In recent years, through economic transformation, the vigorous development of the tourism industry, and adherence to the method of green ecological development, the level of sustainable development of urban human settlements in this region has improved. Tianshui is located in the southeastern part of Gansu Province. Because it has been stuck in the traditional economic development model, its total economic volume, per capita economic level, and economic growth rate are all in a backward position. Correspondingly, the construction of urban supporting facilities has stagnated, and population loss has been serious, which has resulted in a low sustainable development level of urban human settlements.

3.2.3. Spatial Correlation Pattern of Sustainable Development Level of Urban Human Settlements

This study uses spatial autocorrelation to verify the spatial pattern characteristics and significance of the agglomeration space of the sustainable development level of urban human settlements in China. Table 4 shows that the Moran's I index of sustainable development of urban human settlements in China indicated a fluctuating decline, and the p-values were all 0 in the five frames of 2000, 2005, 2010, 2015, and 2019. This shows that the sustainable development level of urban human settlements in China's 285 prefecture-level cities presents a relatively significant and stable distribution of high and low spatial agglomeration, and the spatial agglomeration tends to weaken during the study period.

Table 4. Moran's I of the sustainable development level of urban human settlements in China.

Year	2000	2005	2010	2015	2019
Moran's I	0.2092	0.1595	0.2778	0.1819	0.1740
Z score	27.0187	20.6973	35.7311	23.5517	22.5954
P value	0.0000	0.0000	0.0000	0.0000	0.0000

As seen in Figure 8, the HH agglomeration areas for sustainable development of urban human settlements are mainly concentrated in East China and Central South, especially in the eastern coastal cities; the LL agglomeration areas are mainly distributed in the northeast area and underdeveloped cities in the west, and the scope of the LL agglomeration area in the west is significantly reduced. Specifically, the HH agglomeration areas for the sustainable development of urban human settlements in 2000 were mainly distributed in Shanghai, Nanjing, and Wuxi in the Jiangsu Province, Hangzhou and Ningbo in the Zhejiang Province, Hefei, Wuhu, and Ma'anshan in the Anhui Province, Putian and Xiamen in the Fujian Province, Nanchang and Jingdezhen in the Jiangxi Province, Wuhan and Huanggang in the Hubei Province, Changsha and Xiangtan in the Hunan Province, Guangzhou and Shaoguan in the Guangdong Province, Liuzhou and Guilin in the Guangxi Zhuang Autonomous Region, and Haikou and Sanya in the Hainan Province. The LL gathering area is mainly concentrated in the northern LL gathering area composed of Zhangjiakou in the Hebei Province, Datong and Yangquan in the Shanxi Province, Baotou and Wuhai in the Inner Mongolia Autonomous Region, Benxi in the Liaoning Province, Jilin and Baishan in the Jilin Province, and Jixi and Hegang in the Heilongjiang Province. The LL gathering area is composed of Sanmenxia in the Henan Province, Chongqing City, Panzhihua, and Luzhou in the Sichuan Province, Zhaotong in the Yunnan Province, Tongchuan and Weinan in the Shanxi Province, Lanzhou and Jinchang in the Gansu Province, and Shizuishan and Wuzhong in the Ningxia Hui Autonomous Region. In 2005, the HH cluster area decreased. Cangzhou and Hengshui in the Hebei Province, as well as Jinan, Qingdao, and other cities in the Shandong Province improved the sustainable development level of human settlements and developed into new HH agglomeration areas. The center of gravity of the LL cluster in the north shifted eastward; the LL cluster in the northeast expanded, while the LL cluster in the west shrunk, which was mainly reflected in the narrowing of the scope of the LL cluster in the Sichuan Province. In 2010, the HH agglomeration areas in eastern China, such as Zhejiang and Jiangxi, increased and showed a continuous clustering distribution, reflecting the positive promotion effect of East China. The scope of LL clusters in North China and Northeast China expanded and showed a clustered distribution pattern. In 2015, the agglomeration pattern of the HH agglomeration area in the east became clearer. The spatial scope of LL agglomeration areas has currently shrunk, mainly because the LL agglomeration areas in North China have almost disappeared. At the same time, the LL agglomeration areas in the Shaanxi Province also decreased. In 2019, the spatial distribution of HH agglomeration areas changed slightly. While the urban human settlements are developing steadily, the radiation and driving role of the eastern coastal cities should be strengthened; the northern LL area extends north again, and the western LL area extends south again. We observed that the weak interaction between Northeast China and Western China is still strong, and the sustainable development level of urban human settlements needs to be further improved in these regions.

3.3. Development Model

Based on the above detailed analysis of the sustainable development level of urban human settlements in 285 prefecture-level cities in China, the changes in the development level of each year were summarized and classified into four categories and ten sub-categories (Figure 9). The first consisted of the human settlements with strong sustainability, including two sub-categories "H" and "M"; the second consisted of human settlements with medium sustainability, including four sub-categories "H-M/L-H," "M-H/L-M," "M-H", and "L-H/M." The third consisted of human settlements with weak sustainability, including two sub-categories "H-M/L" and "M-L"; the fourth consisted of unsustainable human settlements, including two subcategories "L" and "L-H/M-L." Note that H represents the high and medium-high level of sustainable development of urban human settlements, M represents the medium development level, and L represents the low and medium-low development levels.

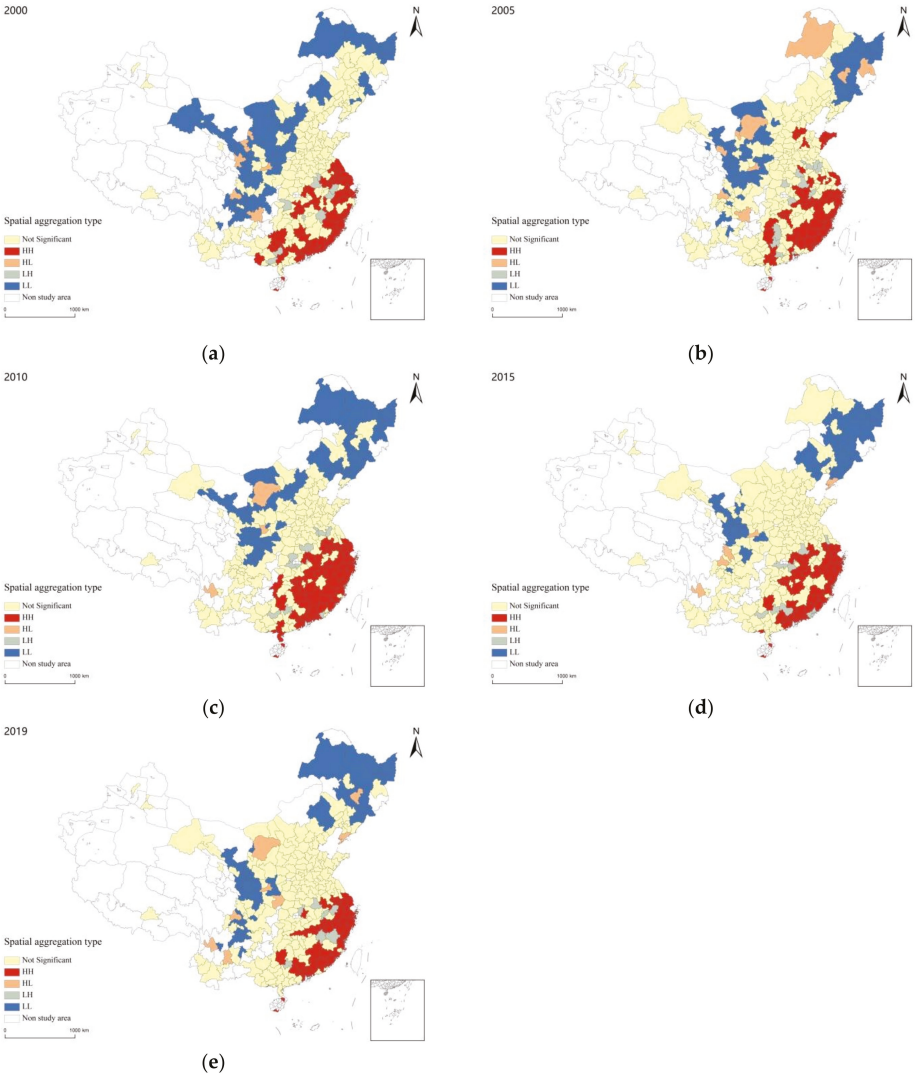

Figure 8. Spatial distribution map of the local indicator of spatial association (LISA) of the sustainable development level of urban human settlements in China. (**a**) 2000; (**b**) 2005; (**c**) 2010; (**d**) 2015; and (**e**) 2019.

From the perspective of the sustainable development model of urban human settlements, the "H" and "M" types are the optimal development models. These two types of cities have a relatively high and stable level of development in human settlements and have strong sustainable development capabilities. A total of 47 cities belong to these two types, accounting for 16% of the study area. Most of them are southeast coastal cities and provincial capitals, mainly distributed in East China and Central South, such as Shanghai, Nanjing, Hangzhou, Qingdao, Zhengzhou, Changsha, Guangzhou, Nanning, and Sanya; the living environment of cities, such as Beijing, Dalian, Chengdu, Kunming, and Karamay also have a high level of development, with outstanding advantages in sustainable development. The "H-M/L-H" and "M-H/L-M" types of development models indicate the fluctuation

phenomenon of falling or rising during the development of urban human settlements. The unstable development situation of these two types includes 31 and 26 cities, respectively, accounting for 20% of the total. The distribution is relatively scattered, mainly in the third and fourth-tier cities, such as Langfang, Jinzhou, Nantong, Wuhu, and Urumqi. These two types of cities should explore a path suitable for their own development as soon as possible to avoid weakening the sustainability of the development of urban human settlements in the process of repeated adjustments. The development level of human settlements in "M-H" and "L-H/M" cities is obviously improving from low and medium development level to medium and high. There are 28 and 47 cities in these two types, respectively, with the highest proportion reaching 26%. This shows that the sustainable development level of urban human settlements in China is constantly improving. Most of them are inland cities with a wide range of distribution, such as Shijiazhuang, Taiyuan, Hohhot, Shenyang, Kaifeng, Chongqing, and Yan'an. The Shanxi Province, Jiangxi Province, Henan Province, and Sichuan Province also performed prominently. Notably, the development level of "H-M/L" and "M-L" types of urban human settlements has declined, including a total of 42 cities, mainly distributed in the central parts of the Northeast region and East China, along with the central and southern China region, including Harbin, Fushun, Ma'anshan, Xiaogan, Yiyang, and Hezhou. This development model indicates that bottlenecks have been encountered in the development of urban human settlements, and timely and effective regulation has not been carried out, resulting in a lack of coordination within the system and restricted orderly development. Therefore, key issues should be understood to deepen reforms as soon as possible and restore good development momentum. The "L" and "L-H/M-L" types of development models are the worst, including 64 cities, accounting for 22% of the research subjects. The cities of these types are mainly inland, distributed in the western part of North China, northeastern China, and the eastern part of the western region, such as Yangquan, Hulunbuir, Chaoyang, Shuangyashan, Shangqiu, Bazhong, Tongchuan, Longnan, and Guyuan. The quality of human settlements in these cities has been in a poor state of development for a long time. Even if there was progress during the research period, it still has a low level of development, and basically, does not have the capacity for sustainable development. Thus, in these regions, urban human settlements can be effectively managed and sustainable development can be gradually realized only by deep learning from failures, drawing on the mature development model of the obvious improvement of urban human settlements, and implementing a targeted and reasonable development path.

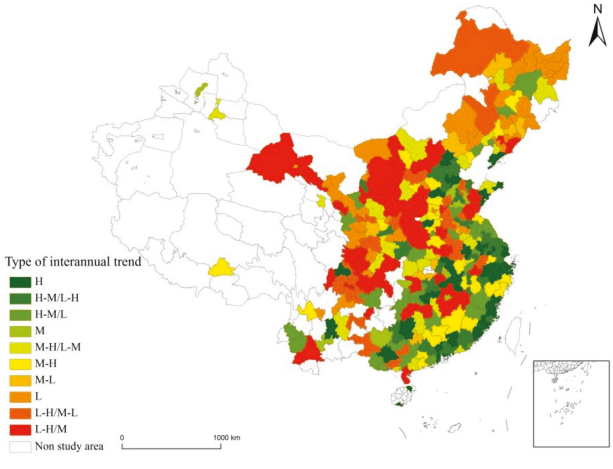

Figure 9. Spatial distribution map of the sustainable development model of urban human settlements in China.

4. Driving Forces for Sustainable Development of Urban Human Settlements in China

In this section, GeoDetector is used to detect the main factors and decisive forces that affect the spatial differentiation of the sustainable development level of urban human settlements in different periods. To improve the accuracy of the results, the top 20 indicators with a large coefficient of variation were selected as the main detection factors. SPSS was used to discretize the panel data of the selected indicators, and the indicators were converted into different types. The strength values (q values) of each indicator force were obtained using GeoDetector, and their significance was tested (Table 5).

Table 5. The determining power of driving factors of the sustainable development level of urban human settlements in China.

	2000		2005		2010		2015		2019	
	Q-Value	**Ranking**	**Q-Value**	**Ranking**	**Q-Value**	**Ranking**	**Q-Value**	**Ranking**	**Q-Value**	**Ranking**
X3	0.352 ***	1	0.271 ***	5	0.365 ***	4	0.194 ***	13	0.315 ***	9
X5	0.290 ***	4	0.168 ***	10	0.100 ***	15	0.114 ***	15	0.227 ***	12
X8	0.149 ***	12	0.122 ***	13	0.052 **	17	0.041 *	20	0.059 **	18
X15	0.262 ***	6	0.240 ***	7	0.295 ***	7	0.317 ***	4	0.322 ***	8
X17	0.256 ***	7	0.246 ***	6	0.200 ***	11	0.413 ***	3	0.428 ***	4
X18	0.024 *	20	0.070 *	17	0.434 ***	3	0.294 ***	6	0.517 ***	2
X20	0.092 **	16	0.073 **	16	0.064 ***	16	0.067 **	16	0.084 ***	17
X21	0.228 ***	8	0.371 ***	1	0.534 ***	2	0.458 ***	1	0.433 ***	3
X22	0.214 ***	10	0.160 ***	11	0.180 ***	12	0.201 ***	10	0.151 ***	13
X25	0.338 ***	2	0.329 ***	2	0.583 ***	1	0.438 ***	2	0.572 ***	1
X26	0.326 ***	3	0.280 ***	4	0.332 ***	5	0.196 ***	12	0.292 ***	10
X28	0.055 *	18	0.031	20	0.043 *	19	0.057 *	19	0.039 **	20
X30	0.143 ***	13	0.172 ***	9	0.304 ***	6	0.228 ***	9	0.387 ***	6
X31	0.073 **	17	0.063 *	18	0.048 *	18	0.067 *	17	0.090 ***	16
X33	0.226 ***	9	0.231 ***	8	0.136 ***	14	0.128 ***	14	0.125 ***	14
X34	0.136 ***	14	0.079 **	15	0.229 ***	9	0.291 ***	7	0.254 ***	11
X35	0.043 *	19	0.051 *	19	0.015	20	0.061 *	18	0.044 *	19
X37	0.117 ***	15	0.114 ***	14	0.222 ***	10	0.197 ***	11	0.114 ***	15
X38	0.266 ***	5	0.319 ***	3	0.263 ***	8	0.306 ***	5	0.362 ***	7
X40	0.154 ***	11	0.149 ***	12	0.157 ***	13	0.278 ***	8	0.409 ***	5

Note that ***, **, and * represent the significance of the factor at 1%, 5%, and 10%, respectively.

From the perspective of time series, the dominant driving factors of the sustainable development of urban human settlements in China have only experienced minimal changes, and there are certain differences in their decisive power. The driving factors with the strongest explanatory power for the sustainable development of the urban human settlements in China in 2000 were $PM_{2.5}$ concentration, per capita GDP, proportion of tertiary industry in GDP, per capita park green area, and Internet penetration rate. The core driving factors in 2005 were the ratio of house price to income, GDP per capita, Internet penetration rate, proportion of tertiary industry in GDP, and $PM_{2.5}$ concentration. In 2010, the core driving factors were per capita GDP, housing-price-to-income ratio, R&D investment intensity, $PM_{2.5}$ concentration, and proportion of tertiary industry in GDP. In 2015, the core driving factors were the ratio of housing prices to income, GDP per capita, share of education expenditure, number of college students per 10,000 people, and Internet penetration rate. In 2019, the core driving factors were per capita GDP, R&D investment intensity, housing-price-to-income ratio, education expenditure ratio, and number of buses owned by 10,000 people. As shown in Table 5, the per capita GDP, housing-price-to-income ratio, Internet penetration rate, education expenditure ratio, R&D investment intensity, and $PM_{2.5}$ concentration are the leading factors affecting the sustainable development of urban human settlements, and they have different effects in different aspects.

1. Gross domestic product (GDP) per capita

GDP per capita reflects the economic level of urban social development. Economic development is the basic requirement for promoting the sound and steady development of urban human settlements, and it is also an important indicator for measuring the living standards of urban residents. From 2000 to 2019, the per capita GDP factor had a relatively stable impact on the sustainable development of urban human settlements. Its decisive power (q) fluctuated from 0.338 in 2000 to 0.572 in 2019. In February 2021, China achieved complete poverty alleviation, but economic development remained unbalanced. The economic development of the eastern coastal cities was better than that of the western inland cities. This difference in economic levels between cities does not only affect the differences in urban construction, thereby affecting the improvement of the ecological environment, living conditions, and public services, but also the differences in residents' income levels, which in turn, affects the urban residents' well-being. Therefore, there is a strong correlation between the per capita GDP and the spatial pattern of the sustainable development level of urban human settlements.

2. Housing-price-to-income ratio

Housing provides the foundation for urban residents to settle, and the housing-price-to-income ratio is the ratio of housing prices to annual household income. It reflects not only the level of urban economic development but also the cost of living of urban residents. With rapid urbanization, housing prices are also rising, especially in first- and second-tier cities that have higher levels of urban development and increasing housing prices. As a result, the impact of real estate on urban human settlements is also increasing. The decisive power of the house price-to-income ratio factor increased from 0.228 in 2000 to 0.433 in 2019, reaching its peak in 2010. In 2010, the state began to implement strong controls on the real estate market, which reduced the differences in the development between cities to a certain extent and weakened its decisive power. An excessively low housing-price-to-income ratio is not conducive to economic transformation and upgradation. An excessively high housing-price-to-income ratio will hinder the healthy development of the economy; it will also cause residents to bear huge pressure to purchase houses and reduce the quality of life of residents. Therefore, the house-price-to-income ratio factor has become a core factor affecting the sustainable development of urban human settlements.

3. Investment in education and scientific research

Education is the endogenous driving force for national progress, and science and technology are the primary productive forces. Thus, promoting science and education can improve the life quality of people. The more high-quality talents, the stronger the promotion of the civilization of the urban population, thus, the stronger the driving force for the development of urban human settlements, and the stronger the national scientific and technological strength. At present, urban residents' pursuit of human settlements has gradually shifted from the material level to cultural improvement. High-quality sustainable development of urban human settlements is impossible without science and technology, which facilitate scientific research, technological capabilities, and increase innovation levels. In recent years, the Chinese government has continuously increased its support for education and scientific research. Public education and research and development expenditures accounted for a major proportion of the GDP; these have also become an important criterion for measuring the level of sustainable development of urban human settlements. Therefore, the government's investment in science and education has accelerated the spatial differentiation of the sustainable development level of urban human settlements, thus increasing their decisive power.

4. Internet penetration rate

The Internet penetration rate refers to the proportion of the total population that uses the Internet. Modern communication infrastructure, represented by the Internet penetration rate, reflects the degree of development of the city. Prefecture-level cities with a

higher level of modernization have a strong economic foundation and complete supporting facilities, and the quality of urban human settlements is relatively high. In 2000, China's network development was low. During 2005–2015, the Internet developed rapidly, and the coverage and development speed of the Internet were different because of the different degrees of development of cities. Therefore, the Internet penetration rate greatly affects the sustainable development patterns of urban human settlements. As of December 2019, China's Internet penetration rate reached 67%. In recent years, the steady development of the Internet has narrowed the digital divide between cities. In particular, during the COVID-19 period, the Internet industry has been extremely dynamic and resilient. Services, such as online education, online medical care, remote office, and online shopping have become a solid force for China to respond to new challenges and build a digital economy.

5. $PM_{2.5}$ concentration

$PM_{2.5}$ concentration is an important indicator of the degree of air pollution. The higher the concentration, the greater the threat to the urban natural ecological environment. It is also a key factor in global non-communicable diseases. At the same time, it will indirectly increase the pressure on medical resources and hinder social and economic development. For the sustainable development of urban human settlements, health must be a priority. Improving the health of urban residents is the basis for the development of people's livelihood, and the improvement of people's livelihood is the foundation for the sustainable development of urban human settlements. Due to different urban climate conditions, different degrees of industrialization, and uneven anti-pollution capabilities, the degree of urban air pollution is also different. Therefore, the $PM_{2.5}$ factor is an important negative driving force for the spatial distribution of the sustainable development of urban human settlements. In the past 10 years, China has attached great importance to the prevention and control of air pollution and has formed a strict scientific monitoring system; additionally, environmental protection awareness in urban residents has gradually increased, and urban air quality has been comprehensively and effectively improved. As a result, the determining power of the $PM_{2.5}$ factor was significantly weakened.

5. Discussion

Overall, the sustainable development of urban human settlements in China shows a continuous improvement trend; in particular, the growth rate of development from 2005 to 2010 is obvious. The improvement shows an east to west trend, presenting a spatial pattern of a "high in the east and low in the west; high in the south and low in the north" trend, which is consistent with the research results of Xu (2020) and Meng (2019) [47,48]. In addition, the sustainable development of urban human settlements has significant spatial correlation characteristics. Cities with a high level of sustainable development of urban human settlements are concentrated in the coastal areas of the southeast and the Beijing–Tianjin–Hebei urban agglomeration in North China. Among them, the sustainable development level of urban human settlements in Shenzhen, Hangzhou, Changsha, Guangzhou, and Shanghai has always been at the forefront. To a certain extent, this distribution law is consistent with the findings of Guo (2020) [49]. Urban human settlements in these cities are developing in a comprehensive, balanced, and stable manner, and the overall strength is relatively good. Prefecture-level cities with low levels of sustainable development are concentrated in northeastern and inland cities in the northern region. Similar to the research results of Jia (2017) [50], the development of human settlements in Yichun, Hegang, Qitaihe, and Jixi (among other cities) has always been in a backward position, related to the slow economic development of cities, prominent ecological problems, and serious population loss.

The level of development of the natural system of urban human settlements in China has continued to improve. Consistent with the results of Luo (2020) [51], the natural environment of southern cities in China is better than that of northern cities, and the development level of natural systems in coastal cities is generally higher than that in inland cities. The natural system scores of Shenzhen, Shanghai, Sanya, Hangzhou, and Xiamen

were among the best. These cities have strong advantages in terms of air quality, greening level, and resource conservation and utilization. Our study revealed that among the natural environmental factors, $PM_{2.5}$ has a great impact on the sustainable development of urban human settlements. Zhang (2020) proposed that air pollution affects the harmonious relationship between humans and land [52]. Saleem (2019) predicted that $PM_{2.5}$ will affect human health, by indirectly increasing the pressure on medical resources and hindering social and economic development [53]. Therefore, prioritizing the development of the ecological environment is crucial for our sustenance. Especially in cities with fragile ecological environments and low environmental awareness, such as Yichun, Heihe, Baishan, and Tianshui, it is necessary to improve ventilation and resource utilization efficiency [54], encourage the application of green environmental protection technologies, promote the use of clean energy, and encourage urban residents to cultivate the values of green life.

The development of the humanity system in urban human settlements in China has improved significantly, and the overall spatial pattern of "multi-level core-periphery" radial growth is indicated prominently, which to a certain extent, is consistent with the research conclusions of Liu (2019) [55]; notably, Beijing, Hangzhou, Guangzhou, Changsha, and Wuhan were ranked high with respect to development in this system. Our study revealed that unbalanced investment in education and scientific research is the main humanity environmental factor that accelerates the spatial differentiation of the sustainable development of urban human settlements, which is in agreement with the findings of Liu (2019) and Li (2019). More studies have stated that high education levels and innovative capabilities can promote high-quality urban development [55,56]. At the same time, Liu (2019) and Cao (2020) found that China's urban innovation capacity is declining from the coastal to inland areas, which coincides with the results of this study [55,57]. Therefore, it is necessary to continue and increase investment in public education and scientific research, especially in cities such as Jixi, Jinchang, Tongchuan, and Baishan, where education resources are scarce and emigration is high. At the same time, it is necessary to improve talent treatment mechanisms, maximize the stability of local talent, absorb outstanding foreign talent, and promote the improvement of local residents' cultural literacy.

The overall development of the residential system of urban human settlements presents a spatial pattern of expansion and growth from east to west, and the overall development gradually develops from a low-medium level to a medium-high level. Our study revealed that the housing-price-to-income ratio in the housing system is the main factor affecting the sustainable development of urban human settlements. This conclusion is consistent with that of Koetter (2021), Chen (2021), and Yin (2019), who believed that housing is one of the most important needs of urban residents [58], and the housing-price-to-income ratio will affect the process of urbanization [59] and the realization of urban spatial justice [60], which is of great significance to the sustainable development of urban human settlements. Therefore, it is necessary to conduct quantitative, dynamic, and refined analyses with respect to the housing-price-to-income ratio, new houses, and stock houses, and adhere to city-specific policies, especially in cities that have a low level of development in residential systems, such as Hegang, Heihe, Qitaihe, Longnan, and Zhongwei. Furthermore, it is necessary to improve the affordable rental housing system and income distribution mechanism and increase the supervision of land transactions and real estate sales.

The development of the social system of urban human settlements is slowly increasing, and the overall distribution is characterized by the "high in the east and low in the west" trend. Our study revealed that in 2000, cities with a high level of social system development were mainly concentrated in the Heilongjiang, Liaoning, Jiangsu, and Fujian provinces. After 2005, northeastern China was affected by the concept of a planned economic system, and the economic development continued to lag behind, which is consistent with the research of Han (2019) [61]. At the same time, consistent with Zhou (2019) [62], the social system development levels of Beijing, Shenzhen, Guangzhou, Shanghai, Suzhou, and Hangzhou were at the forefront. Barkhatov (2021) and Chen (2021) found that the quality

of urban life interacts with the level of economic development, and the stability of economic development greatly affects the level of sustainable development in the region; they also observed that the GDP per capita was an important indicator for measuring the level of economic development [63,64]. This point of view is consistent with the results of our study, which also revealed that there is a strong correlation between the per capita GDP and the spatial pattern of the sustainable development level of urban human settlements. Therefore, in view of the problems of poor and weak industries and irrational industrial structures in the northeastern and western regions, it is necessary to effectively change the idea of development [65] and use big data to simulate and predict the development mode of urban industrial structure, promote the optimization and upgrading of the industrial structure and diversified development, establish a modern corporate governance model, and adhere to the development of a circular and low-carbon economy to achieve a "win-win" situation of social economic development and ecological environment protection.

The development of a support system for urban human settlements has shown a significant upward trend and an overall spatial pattern of unbalanced growth. High-value areas are scattered in the Beijing–Tianjin–Hebei urban agglomeration, East China, and Central and South China. To some extent, this result is consistent with the findings of Du (2020) [66]. Among the many elements of the support system, the Internet penetration rate greatly affects the sustainable development pattern of urban human settlements, which is consistent with the results of Cioaca (2020) and Asongu (2019), who proposed that the high penetration rate and high-quality development of the Internet can strengthen the development of digital technology, which can, in turn, transform into economic and social benefits [67,68]. This can improve the sustainable development of urban human settlements. Therefore, cities with poor communication infrastructure, such as Guigang, Hezhou, Suining, and Longnan, should pay attention to the construction of modern infrastructure service facilities, increase the Internet penetration rate, and improve the level of information communication, while strengthening the construction of intelligent transportation systems, medical systems, and education systems, and accelerate the construction of new smart cities.

6. Conclusions

Over the past 20 years, the overall level of sustainable development of urban human settlements in China has steadily improved. Notably, the development of cities in the southeast was significantly higher than that in the northwest. The main development model considers the transformation from a medium-low development level to a medium-high development level. The per capita GDP, housing-price-to-income ratio, investment in education and scientific research, Internet penetration, and $PM_{2.5}$ concentration have a great impact on the spatial differentiation of the sustainable development of urban human settlements. To achieve the SDGs quickly and effectively, our study proposes high-quality green development orientation to improve the balance and coordination of the development of subsystems of urban human settlements. The research scale of this study is macroscopic, and the time span is large. To ensure the accuracy of the results, it is necessary to fully consider the availability and continuity of the data, so that some indicators cannot be adopted. At the same time, there is a lack of understanding of the psychological needs and behavioral characteristics of urban residents. Therefore, future studies should combine questionnaires, interview data, and more time-sensitive and accurate geographic information data.

Author Contributions: Methodology, software, and data curation, X.C.; formal analysis and writing—original draft preparation, X.C.; writing—review and editing, all authors; funding acquisition, X.L. and Y.G.; supervision, all authors. All authors have read and agreed to the published version of the manuscript.

Funding: This research was funded by the Ministry of Education Humanities and Social Sciences Research Program (Grant no. 18YJCZH035), the Liaoning Education Department Scientific Research

Project (Grant no. J2020060), and the Dalian Science and Technology Innovation Fund Project (Grant no. 2020JJ26GX039).

Data Availability Statement: The data presented in this study are available upon request from the corresponding author.

Conflicts of Interest: The authors declare no conflict of interest.

References

1. Chen, R.; Zhao, Z.; Xu, D.; Chen, Y. Progress of research on sustainable development index for cities and urban agglomerations. *Prog. Geogr.* **2021**, *40*, 61–72. [CrossRef]
2. Yang, J.; Wang, Y.; Xiu, C.; Xiao, X.; Xia, J.; Jin, C. Optimizing local climate zones to mitigate urban heat island effect in human settlements. *J. Clean. Prod.* **2020**, *275*, 123767. [CrossRef]
3. Guo, H.D.; Liang, D.; Chen, F.; Sun, Y.C.; Liu, J. Big earth data facilitates sustainable development goals. *Bull. Chin. Acad. Sci.* **2021**, *36*, 874–884. [CrossRef]
4. Mao, Q. Theory and practice of the science of human settlements in China. *Urban Plan. Int.* **2019**, *34*, 54–63. [CrossRef]
5. Brundtland, G.H. Report of the World Commission on Environment and Development: Our Common Future. Available online: https://sustainabledevelopment.un.org/content/documents/5987our-common-future.pdf (accessed on 8 September 2021).
6. United Nations Transforming Our World: The 2030 Agenda for Sustainable Development. Available online: https://www.un.org/ga/search/view_doc.asp?symbol=A/RES/70/1&Lang=E (accessed on 8 September 2021).
7. China's Progress Report on Implementation of the 2030 Agenda for Sustainable Development 2019. Available online: https://www.fmprc.gov.cn/web/ziliao_674904/zt_674979/dnzt_674981/qtzt/2030kcxfzyc_686343/P020190924779471821881.pdf (accessed on 8 September 2021).
8. Wu, L.Y. *Introduction to Sciences of Human Settlements*; China Architecture & Building Press: Beijing, China, 2001; ISBN 978-7-112-04506-8.
9. Gao, F.; Zhao, X.Y.; Song, X.Y.; Wang, B.; Wang, P.L.; Niu, Y.B.; Wang, W.J.; Huang, C.L. Connotation and evaluation index system of beautiful China for SDGs. *Adv. Earth Sci.* **2019**, *34*, 295–305. [CrossRef]
10. Howard, E. *Garden Cities of Tomorrow*; Jin, J.Y., Ed.; The Commercial Press: Beijing, China, 2017; ISBN 978-7-100-13386-9.
11. Li, X.M.; Guo, Y.J.; Tian, S.Z.; Bai, Z.Z.; Liu, H. The Spatio-temporal pattern evolution and driving force of the coupling coordination degree of urban human settlements system in Liaoning province. *Sci. Geogr. Sin.* **2019**, *39*, 1208–1218. [CrossRef]
12. Feng, Y.W.; Zhen, J.H.; Tian, Y.T.; Cao, Y.; Zhang, L.; Zhang, S.; Zhang, Y.F. Change in vulnerability of human settlement environment and its mechanism in Hohhot. *Econ. Geogr.* **2020**, *40*, 91–99. [CrossRef]
13. Luo, X.; Yang, J.; Sun, W.; He, B. Suitability of human settlements in mountainous areas from the perspective of ventilation: A case study of the main urban area of Chongqing. *J. Clean. Prod.* **2021**, *310*, 127467. [CrossRef]
14. Shekhar, H.; Schmidt, A.J.; Wehling, H.-W. Exploring wellbeing in human settlements—A spatial planning perspective. *Habitat Int.* **2019**, *87*, 66–74. [CrossRef]
15. Bao, J.; Zhang, Y.; Li, X.; Guo, Q. From survival to self-actualization: Quantitative evaluation of human settlement envi-ronment from the perspective of hierarchy of needs theory: A case study of Anhui province. *Urban Stud.* **2020**, *27*, 88–95. [CrossRef]
16. Ziółkowska-Weiss, K. Satisfaction with selected indicators of the quality of urban space by Polonia in the greater Toronto area. *Land* **2021**, *10*, 778. [CrossRef]
17. Tian, S.Z.; Li, X.M.; Yang, J.; Zhang, W.; Guo, J.K. Spatio-temporal coupling coordination and driving mechanism of urban pseudo and reality human settlements in the three provinces of Northeast China. *Acta Geogr. Sin.* **2021**, *76*, 781–798. [CrossRef]
18. Pierantoni, I.; Pierantozzi, M.; Sargolini, M. COVID 19—A qualitative review for the reorganization of human living environments. *Appl. Sci.* **2020**, *10*, 5576. [CrossRef]
19. Sodiq, A.; Baloch, A.A.B.; Khan, S.A.; Sezer, N.; Mahmoud, S.; Jama, M.; Abdelaal, A. Towards modern sustainable cities: Review of sustainability principles and trends. *J. Clean. Prod.* **2019**, *227*, 972–1001. [CrossRef]
20. Song, R.; Hu, Y.; Li, M. Chinese Pattern of Urban Development Quality Assessment: A Perspective Based on National Territory Spatial Planning Initiatives. *Land* **2021**, *10*, 773. [CrossRef]
21. Yang, J.; You, H.; Zhang, Y.; Jin, C. Research progress on human settlements: From traditional data to big data+. *Prog. Geogr.* **2020**, *39*, 166–176. [CrossRef]
22. Zhang, W.Z.; Xu, J.X.; Ma, R.F.; Ma, S.P. Basic connotation, current situation, and development orientation of high-quality development of Chinese cities: Based on the survey of residents. *City. Plan. Rev.* **2019**, *43*, 13–19. [CrossRef]
23. Mele, C. Human settlements and sustainability: A crucial and open issue. In Proceedings of the E3S Web of Conferences, EDP Science and the Future 2 "Contradictions and Challenges", Torino, Italy, 12–16 November 2018.
24. Dahiya, B.; Das, A. New urban agenda in Asia-Pacific: Governance for sustainable and inclusive cities. In *New U-Democrban Agenda in Asia-Pacy for Smart Ciftic*; Dahiya, B., Daes, A., Eds.; Springer Science and Businegss Media: Berlin, Germany, 2019; pp. 3–36.
25. Corbane, C.; Martino, P.; Panagiotis, P.; Aneta, F.J.; Michele, M.; Sergio, F.; Marcello, S.; Daniele, E.; Gustavo, N.; Thomas, K. The grey-green divide: Multi-temporal analysis of greenness across 10,000 urban centres derived from the Global Human Settlement Layer (GHSL). *Int. J. Digit. Earth* **2018**, *13*, 101–118. [CrossRef]

26. Reyes Plata, J.A.R.; Elías Orozco, M.E.; Villaseñor, I.Z.J. Green infrastructure and social welfare. lessons for sustainable urban development in the metropolitan zone of Leon, Mexico. In *Universitie the World Sustainable Community Series: Meeting the Goals of the Agenda 2030*; Leal Filho, W., Tortato, U., Frankenberger, F., Eds.; Springer: Cham, Switzerland, 2019; pp. 71–88.
27. Rozhenkova, V.; Allmang, S.; Ly, S.; Franken, D.; Heymann, J. The role of comparative city policy data in assessing progress toward the urban SDG targets. *Cities* **2019**, *95*, 102357. [CrossRef]
28. Wang, F.; An, L.Z.; Dang, A.R.; Han, J.Y.; Miao, C.H.; Wang, J.; Zhang, G.H.; Zhao, Y. Human-land coupling and sustainable human settlements in the Yellow river basin. *Geogr. Res.* **2020**, *39*, 1707–1724. [CrossRef]
29. Wang, J.C.; Wu, X.C.; Liu, J.; Zhang, Y.P.; Yu, Q.Y.; Wang, S.; Wang, Q.H. Sustainable innovation and practice based on rural ecological livable construction. *Chin. Agric. Sci. Bull.* **2020**, *36*, 159–164. [CrossRef]
30. Osman, T.; Kenawy, E.; Abdrabo, K.I.; Shaw, D.; Alshamndy, A.; Elsharif, M.; Salem, M.; Alwetaishi, M.; Aly, R.M.; Elboshy, B. Voluntary Local Review Framework to Monitor and Evaluate the Progress towards Achieving Sustainable Development Goals at a City Level: Buraidah City, KSA and SDG11 as A Case Study. *Sustainability* **2021**, *13*, 9555. [CrossRef]
31. Gonçalves, D.K.O.; Masiero, É.; Bragança, L.; Kakuda, F.M. Qualitative and quantitative assessment of urban sustainability in social housing using the Casa Azul label and SBTool urban in Brazil. *Appl. Sci.* **2020**, *10*, 6246. [CrossRef]
32. Xu, X.; Gao, J.; Zhang, Z.; Fu, J. An assessment of Chinese pathways to implement the UN sustainable development goal-11 (SDG-11)—A case study of the Yangtze river delta urban agglomeration. *Int. J. Environ. Res. Public Health* **2019**, *16*, 2288. [CrossRef]
33. Botequilha-Leitão, A.; Díaz-Varela, E.R. Performance based planning of complex urban social-ecological systems: The quest for sustainability through the promotion of resilience. *Sustain. Cities Soc.* **2020**, *56*, 102089. [CrossRef]
34. Qi, X.H.; Chen, Y.; Chen, L.; Chen, J. Review of literatures on human settlements. *World Reg. Stud.* **2007**, *16*, 17–24. [CrossRef]
35. Wüstemann, H.; Kalisch, D.; Kolbe, J. Access to urban green space and environmental inequalities in Germany. *Landsc. Urban Plan.* **2017**, *164*, 124–131. [CrossRef]
36. Aalbers, C.; Kamphorst, D.; Langers, F. Fourteen local governance initiatives in greenspace in urban areas in the Netherlands. Discourses, success and failure factors, and the perspectives of local authorities. *Urban For. Urban Green* **2019**, *42*, 82–99. [CrossRef]
37. Portney, K.E. *Taking Sustainable Cities Seriously: Economic Development, The Environment, and Quality of Life in American Cities*; MIT Press: Cambridge, MA, USA, 2013; ISBN 978-0-262-51827-7.
38. Zhan, D.; Zhang, X. Study on construction experiences of world livable cities and its inspiration to Beijing. *Urban Plan. Int.* **2016**, *31*, 7–13. [CrossRef]
39. Li, F.; Zhang, X.B.; Liao, B.S.; Qian, A. Capability assessment of DMSP-OLS and NPP-VIIRS nighttime light data estimating statistical indicators:a case of county-level GDP, population and energy consumption in Beijing-Tianjin-Hebei region. *Bull. Surv. Map.* **2020**, *9*, 89–93. [CrossRef]
40. Ciobotaru, A.-M.; Andronache, I.; Dey, N.; Petralli, M.; Daneshvar, M.R.M.; Wang, Q.; Radulovic, M.; Pintilii, R.-D. Temperature-humidity index described by fractal higuchi dimension affects tourism activity in the urban environment of focşani city (Romania). *Theor. Appl. Clim.* **2019**, *136*, 1009–1019. [CrossRef]
41. Kong, F. Multi-temporal scale assessment of climate comfort of habitat environment and spatial differences in China. *J. Arid Land Resour. Environ.* **2020**, *34*, 102–111. [CrossRef]
42. Fradkin, A. Early human settlement and natural formation of the Florida Everglades, USA: The Ichthyoarchaeological evidence. *J. Archaeol. Sci. Rep.* **2016**, *8*, 463–469. [CrossRef]
43. Setioko, B.; Pandelaki, E.E.; Murtini, T.W. Towards Sustainable Urban Growth: The Unaffected Fisherman Settlement Setting (with Case Study Semarang Coastal Area). *Procedia Environ. Sci.* **2013**, *17*, 401–407. [CrossRef]
44. Cong, X.; Li, X.; Li, S.; Gong, Y. Research on sustainable development ability and spatial-temporal differentiation of urban human settlements in China and Japan based on SDGs, taking Dalian and Kobe as examples. *Complexity* **2021**, 1–22. [CrossRef]
45. Das, J.T. Assessment of Sustainability and Resilience in Transportation Infrastructure Geotechnics. Ph.D. Thesis, The University of Texas at Arlington, Arlington, TX, USA, 2018.
46. Wang, J.F.; Xu, C.D. Geodetector: Principle and prospective. *Acta Geogr. Sin.* **2017**, *72*, 116–134. [CrossRef]
47. Xu, Z.; Chau, S.N.; Chen, X.; Zhang, J.; Li, Y.; Dietz, T.; Wang, J.; Winkler, J.A.; Fan, F.; Huang, B.; et al. Assessing progress towards sustainable development over space and time. *Nat. Cell Biol.* **2020**, *577*, 74–78. [CrossRef] [PubMed]
48. Meng, W.Q.; Mo, X.Q.; Li, H.Y.; Hu, B.B.; He, M.X. Spatial difference in the sustainable development level based on extended exergy analysis: Based on the data resources of Chinese 31 provinces and cities. *Acta Ecol. Sin.* **2019**, *39*, 1701–1714. [CrossRef]
49. Guo, Z.; Yao, S.M.; Chen, S.; Wu, W.; Liu, W.C. Spatial-temporal evolution of the livability levels in the Yangtze river delta urban agglomerations and its influencing factors. *Econ. Geogr.* **2020**, *40*, 79–88. [CrossRef]
50. Jia, Z.H.; Gu, G.F. Urban livability and influencing factors in Northeast China: An empirical study based on panel data, 2007–2014. *Prog. Geogr.* **2017**, *36*, 832–842. [CrossRef]
51. Luo, Z.F.; Zhang, J.; Liu, Y.T.; Zhu, L.X. Spatiotemporal evolution of urban greening in China and the affecting factors between 2000 and 2017. *Arid Land Geogr.* **2020**, *43*, 481–490. [CrossRef]
52. Zhang, X.M.; Luo, S.; Li, X.M.; Li, Z.F.; Fan, Y.; Sun, J.W. Spatio-temporal variation features of air quality in China. *Sci. Geogr. Sin.* **2020**, *40*, 190–199. [CrossRef]

53. Saleem, H.; Jiandong, W.; Aldakhil, A.M.; Nassani, A.A.; Abro, M.M.Q.; Zaman, K.; Khan, A.; Bin Hassan, Z.; Rameli, M.R.M. Socio-economic and environmental factors influenced the United Nations healthcare sustainable agenda: Evidence from a panel of selected Asian and African countries. *Environ. Sci. Pollut. Res.* **2019**, *26*, 14435–14460. [CrossRef]
54. Yang, J.; Wang, Y.; Xue, B.; Li, Y.; Xiao, X.; Xia, J.C.; He, B. Contribution of urban ventilation to the thermal environment and urban energy demand: Different climate background perspectives. *Sci. Total Environ.* **2021**, *795*, 148791. [CrossRef] [PubMed]
55. Liu, K.W.; Li, Q.C.; Wang, L.; Xiao, C. Coupling and coordination study of livable city and innovative city development in the Yangtze river delta. *Geogr. Geoinf. Sci.* **2019**, *35*, 120–126. [CrossRef]
56. Li, C. Education for Sustainable Development: Global progress and China's experience. *Chin. J. Urban Environ. Stud.* **2019**, *7*, 1–19. [CrossRef]
57. Cao, Q.F.; Ni, P.F.; Ma, H.F. A Study on the impacts of scientific and technological innovations on the coordinated devel-opment of urban clusters—An analysis based on the urban sustainable competitiveness. *J. Beijing Univ. Technol. (Soc. Sci. Ed.)* **2020**, *20*, 51–58. [CrossRef]
58. Koetter, T.; Sikder, S.K.; Weiss, D. The cooperative urban land development model in Germany—An effective instrument to support affordable housing. *Land Use Policy* **2021**, *107*, 105481. [CrossRef]
59. Chen, Y.; Chen, X.M. Impact of house price and house price-to-income ratio on urbanization of china:empirical analysis based on spatial econometric model. *Econ. Geogr.* **2021**, *41*, 57–65. [CrossRef]
60. Yin, S.; Ma, Z.; Song, W.; Liu, C. Spatial justice of a Chinese metropolis: A perspective on housing price-to-income ratios in Nanjing, China. *Sustainability* **2019**, *11*, 1808. [CrossRef]
61. Han, Z.L.; Zhao, Q.H.; Zhao, D.X.; Guan, D.Y. Population and economic coupling coordinated evolution and spatial differ-ences at county level in Northeast China during 2000–2015: Taking Liaoning province as an example. *Geogr. Res.* **2019**, *38*, 3025–3037. [CrossRef]
62. Zhou, L.; Che, L.; Sun, D.Q. The coupling coordination development between urbanization and economic growth and its influencing factors in China. *Econ. Geogr.* **2019**, *39*, 97–107. [CrossRef]
63. Barkhatov, V. Instability of socio-economic and sustainable development of Ural regions. In Proceedings of the E3S Web of Conferences, Ural Environmental Science Forum "Sustainable Development of Industrial Region" (UESF-2021), Chelyabinsk, Russia, 17–19 February 2021.
64. Chen, W.; Zhu, K.; Wu, Q.; Cai, Y.; Lu, Y.; Wei, J. Adaptability evaluation of human settlements in Chengdu based on 3S technology. *Environ. Sci. Pollut. Res.* **2021**, 1–12. [CrossRef]
65. Ren, W.; Xue, B.; Yang, J.; Lu, C. Effects of the Northeast China revitalization strategy on regional economic growth and social development. *Chin. Geogr. Sci.* **2020**, *30*, 791–809. [CrossRef]
66. Du, D.L.; Huang, J.; Wang, J.E. Assessment of smart city development status in China based on multi-source data. *J. Geoinf. Sci.* **2020**, *22*, 1294–1306. [CrossRef]
67. Cioacă, S.-I.; Cristache, S.-E.; Vuță, M.; Marin, E.; Vuță, M. Assessing the impact of ICT sector on sustainable development in the European Union: An empirical analysis using panel data. *Sustainability* **2020**, *12*, 592. [CrossRef]
68. Asongu, S.A.; Odhiambo, N.M. How enhancing information and communication technology has affected inequality in Africa for sustainable development: An empirical investigation. *Sustain. Dev.* **2019**, *27*, 647–656. [CrossRef]

land

MDPI

Article

Spatiotemporal Differentiation of the School-Age Migrant Population in Liaoning Province, China, and Its Driving Factors

Wenwen Xu [1,2], Chunrui Song [3,*], Dongqi Sun [4] and Baochu Yu [5]

[1] School of Education, Liaoning Normal University, Dalian 116029, China; xww2021@lnnu.edu.cn
[2] Department of Security, Liaoning Police College, Dalian 116036, China
[3] Human Settlements Research Center, Liaoning Normal University, Dalian 116029, China
[4] Key Laboratory of Regional Sustainable Development Modeling, Institute of Geographic Sciences and Natural Resources Research, CAS, Beijing 100101, China; sundq@igsnrr.ac.cn
[5] School of Ocean and Civil Engineering, Dalian Ocean University, Dalian 116029, China; baochuyu@dlou.edu.cn
* Correspondence: ln_scr@163.com

Abstract: This study analyzed the spatiotemporal distribution and driving factors of the floating school-age population in Liaoning Province, China from 2008 to 2020 using county-level statistical education data combined with spatial autocorrelation and the multiscale geographically weighted regression model. The major findings are as follows. From 2008 to 2020, the distribution of the school-age migrant population exhibited obvious spatial imbalance characteristics both in terms of the number and proportion of school-age migrants. Specifically, the school-age migrant population was concentrated in the municipal districts of large and medium-sized cities and continued to increase over time in the suburbs of large and medium-sized cities. Over the past 12 years, the distribution of the school-age migrant population in Liaoning Province exhibited significant spatial autocorrelation. From the number of school-age migrants, the cold and hot spot area expanded. Conversely, from the proportion of school-age migrants, the cold and hot spot area decreased gradually, whereas the cold spot area became more diffuse. Regarding the driving factors, the quantity and quality of teaching staff, the quality of teaching equipment and conditions, and the quality of the education environment played a role in promoting or restraining the differentiation of the school-age migrant population in Liaoning Province. Moreover, the degree of influence of the driving factors exhibited substantial spatial differences.

Keywords: school-age migrant population; spatial pattern; MGWR; Liaoning Province

Citation: Xu, W.; Song, C.; Sun, D.; Yu, B. Spatiotemporal Differentiation of the School-Age Migrant Population in Liaoning Province, China, and Its Driving Factors. *Land* **2021**, *10*, 1036. https://doi.org/10.3390/land10101036

Academic Editors: Baojie He, Ayyoob Sharifi, Chi Feng and Jun Yang

Received: 6 September 2021
Accepted: 30 September 2021
Published: 2 October 2021

1. Introduction

China has a large, diverse, and complex school-age population, which is currently experiencing profound changes to its social development and demographic structure [1,2]. Moreover, the educational space is diverse and unique [3]. The migrant school-age population of China refers to children and adolescents who have registered their household in other provinces (districts and cities) and counties (districts) and travel to urban areas or towns with their parents for compulsory education [4]. According to the "Statistical Bulletin of the National Education Development in 2020", there were 156 million students at the compulsory education stage nationwide (including 107.3 million elementary school students and 49.1 million junior high school students). A total of 14.3 million children were classed as relocated children, with 10.3 million enrolled in elementary schools and 3.9 million enrolled in junior high schools, accounting for 9.60% and 8.04% of the total school-age population, respectively [4]. With the increasing population movement in China and the widespread phenomenon of "children moving with them", the education of migrant children has received increasing attention from central and local governments at all levels. As early as 1998, the former State Education Commission and the Ministry of

Public Security jointly issued the "Interim Measures for the Schooling of Migrant Children and Adolescents", requesting local governments to actively solve the problem of schooling for migrant children and adolescents. Article 12 of the "Compulsory Education Law of the People's Republic of China" stipulates the right of migrant children and adolescents to receive compulsory education on an equal basis in the place where they enter. In 2011, the State Council issued the "China Children's Development Program (2011–2020)", which demands measures to ensure that migrant children receive equal access to compulsory education. In 2012, the "Opinions of the State Council on Further Promoting the Balanced Development of Compulsory Education" stated the need to ensure equal access to compulsory education for special groups and to ensure equal access to compulsory education for children of migrant workers in cities. However, owing to the limitations of the education system and the urban–rural dual socioeconomic structure, the educational integration of migrant children remains a prominent issue in China [5].

Previous research into migrant populations around the world has noted the relationship between labor mobility, human capital accumulation, and regional development [6,7]. In China, scholars have conducted detailed analyses of the evolution and geographical patterns of migrant populations [8–10], the typical characteristics and distribution of migrant populations in coastal and inland areas [11,12], and the temporal and spatial characteristics of migrant populations in cities, suburbs, and fringe areas [13,14]. The extensive flow of labor is also accompanied by a large increase in the school-age migrant population, whose spatial distribution was first investigated in the 1960s [15,16]. This revealed a close relationship between population mobility and the allocation of regional compulsory education resources [17], which is reflected by research into the impact of the allocation of educational resources (such as the spatial layout of schools, the use of appropriate education scales, and economic benefits) on the spatial distribution of school-age migrant populations [18]. Increasing attention has also been paid to the temporal and spatial characteristics of the research objects, exploring the relationship between population pressure, residential differentiation, and other factors [19] as well as the allocation of educational resources [20] by introducing theories and methods relating to urban sociology and educational economics.

Domestic research on the Chinese school-age migrant population has focused on changes in the spatial structure of this population, the characteristics of spatial agglomeration and differentiation, and the factors driving these changes. For example, in the three major regions of eastern, central, and western China as well as coastal and inland regions, the spatial distribution of the school-age migrant population shows large regional differences [21]. Based on the uncertain nature of migrant children from urban and rural areas, the distribution of education in China is divided into three integration domains, namely urban areas, rural areas, and urban–rural areas where a large number of school-age migrant populations gather, to describe the distribution of the school-age migrant population and the state of schooling [22]. These domains also enable in-depth analysis of the regional differences in the school-age migrant population, with previous research focusing on super large cities, large cities, national-level new districts, and small and medium-sized cities among others, in order to reveal the distribution of the school-age migrant population in different types of regions [23,24]. According to population flows and distributions, cities can be divided into net inflow cities, approximately stable cities, and net outflow cities [25] to further evaluate the scale and structure of the school-age migrant population. It should be noted that research on the spatial distribution of the school-age migrant population is typically based on data analysis at the prefecture level [26]. Thus, although these findings are significant for guiding the allocation and planning of compulsory education resources, studies should also be performed at the county level to achieve a more in-depth understanding of the spatial patterns and driving factors of the school-age migrant population.

Existing county-level research has analyzed the influence of individual and family factors on the choice of education location [27], with particular attention on the impact of the family's ability and willingness to move with the children's school location [28]. How-

ever, relatively little attention has been paid to the factors driving the spatial distribution of the school-age migrant population. The factors driving the spatial mobility characteristics of school-age children are typically the same as those for their parents [29], which include factors such as the level of economic and social development, policy environment, urban administrative hierarchy, location advantages, occupational types, and employment opportunities [30]. The driving factors behind the formation and evolution of the spatial distribution of migrant populations also vary over time. As the two key driving forces, the government and the market promote each other, maintain checks and balances with each other, and exert a continuous influence on migrant populations [31–33]. Thus, the flow and spatial distribution of the school-age migrant population will inevitably be affected by factors, such as the economic and social development level and policy environment of the inflow area, and will be both promoted and restricted by government and market forces.

Therefore, research on the school-age migrant population in China has mainly focused on the spatial distribution and evolution of the school-age migrant population, the implementation of educational policies for floating children and educational equity [34], and the redistribution of educational resources for the school-age migrant population [35]. Moreover, the research perspective has shifted from the macro scale to the meso- and micro-scales, reflecting the need for more in-depth analysis as well as an understanding of the macroscopic distribution and dynamic trends of the school-age migrant population [36]. More importantly, we must start from the meso- and micro-scales, reducing a wide range of statistical data on the effect of specific differences within the region, and carefully analyze the flow characteristics and driving factors of the school-age migrant population within regions and the characteristics of differences within regions. Therefore, this study uses spatial autocorrelation and other methods to quantitatively explore the temporal and spatial evolution of the school-age migrant population in Liaoning Province, China, from 2008 to 2020 from two aspects: the number and the proportion of school-age migrants. Then, a multiscale geographic weighted regression (MGWR) model is used to analyze the underlying driving factors.

2. Materials and Methods

2.1. Research Area

From 2008 to 2020, the number of students in compulsory education in Liaoning Province, Northeast China, dropped from 3.8 million to 2.97 million, whereas the number and proportion of school-age migrants rose from 200,000 to 263,000 and from 5.26% to 8.85%, respectively. The school-age population continues to exhibit both spatial and temporal differentiation. Changes in the size, structure, and distribution of the school-age population have a significant impact on the allocation of compulsory education resources. Compulsory education resource allocation exhibits clear urban–rural differences, regional differences, and redistribution processes. Liaoning Province has 14 prefecture-level cities, 100 municipal districts, counties (autonomous counties), and county-level cities as well as functional parks, such as the Dalian Huayuankou Economic Zone, Anshan Economic Development Zone, and Jinzhou Binhai New Area. To maintain the unity of administrative divisions, the research object was set to 100 county-level administrative units in Liaoning Province (Figure 1).

2.2. Data and Processing

The student data employed in this study were predominantly derived from the statistical data of government agencies and included the number of students in each school in the province from 2008 to 2020, the number of children of migrant workers in cities, and other statistical information, which provides detailed and reliable data support for studying the school-age migrant population. Geographical data were obtained from the Resource and Environmental Science Data Center of the Chinese Academy of Sciences. ArcGIS 10.7 software was used to link the above-mentioned 12 periods (years) of student system data and corresponding annual statistical data to the administrative division maps

of the counties in Liaoning Province. Thus, we established a research database of the school-age migrant population in Liaoning Province.

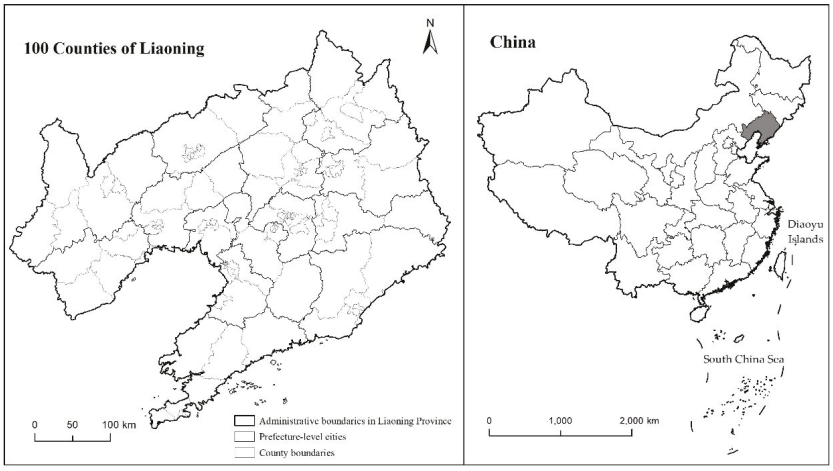

Figure 1. Location of the study area.

2.3. Research Methods

Two measurement indicators were employed to reflect the status of the school-age migrant population in a region. One was the number of school-age migrants, which expresses the scale of this population, and the other was the proportion of school-age migrants, which expresses the relative magnitude of this population.

2.3.1. Spatial Autocorrelation

Global spatial autocorrelation is typically used to determine whether a certain geographic phenomenon exhibits agglomeration characteristics in space and reflects the similarity of the attribute values of spatially adjacent research units. Global Moran's I is the most common measure of global spatial autocorrelation [37,38]. Its value range is [−1, 1], which indicates negative, positive, or no spatial correlation. Local spatial autocorrelation is typically used to measure the degree of similarity or difference between the attributes of a unit and its surrounding units and can reveal how spatial dependence varies with the location. Based on the Queen adjacency principle of GeoDa software, the spatial weight matrix is determined. If there is a common edge or point between two spatial objects, they are considered to be adjacent and a weight of 1 is assigned; otherwise, a weight of 0 is assigned. The Queen adjacency principle can express the distance between two regions and the neighbor relationship with more detail.

2.3.2. Local G Coefficient

Among local spatial autocorrelation measures, the local G coefficient has a very significant effect on the recognition of high-value agglomeration areas and can detect cold spots and hot spots in different areas [39]. Considering that the areas of the counties and districts in Liaoning Province are substantially different, this study adopts the Queen adjacency principle to determine the spatial weight matrix in order to avoid an uneven distribution of neighboring counties and districts caused by a large distance threshold. Furthermore, in order to avoid the island of Changhai County having no neighbors, Jinzhou District, Pulandian City, and Zhuanghe City were set as the neighbors of Changhai County.

2.3.3. MGWR Model

The basic formula for the MGWR model is as follows [40]:

$$y_i = \sum_{j=1}^{k} \beta_{bwj}(u_i,\ v_i)x_{ij} + \varepsilon_i \quad (1)$$

where y_i is the dependent variable of element i; x_{ij} is the attribute value of the independent variable j at position i; β_{bwj} is the bandwidth used by the regression coefficient of the *j-th* variable; $(u_i,\ v_i)$ are the spatial coordinates of the i element points; and ε_i is the residual. The MGWR model can be regarded as a generalized additive model [41], as follows:

$$y_i = \sum_{j=1}^{k} f_i + \varepsilon\left(f_i = \beta_{bwj}x_i\right) \quad (2)$$

in which the back-fitting algorithm can be used to fit each smoothing item. The back-fitting algorithm first needs to initialize all the smoothing terms; therefore, it is necessary to make a preliminary estimate of each coefficient in the MGWR model in advance. There are generally four choices for initialization: classic GWR estimation; semiparametric GWR estimation; least-square estimation; or setting all coefficients to zero. This study chose the classic GWR estimate as the initial estimate. After the initial setting was determined, the difference between the real and predicted values obtained by the initial estimation was calculated, giving the initial residual.

3. Results

3.1. Overall Distribution of the School-Age Migrant Population

According to the distribution of the school-age migrant population in Liaoning Province, combined with the manual classification method in ArcGIS 10.7, the 100 counties in this study were divided into five categories (Figure 2). In general, the spatial distribution of the school-age migrant population in Liaoning Province was extremely unbalanced over the study period. The absolute number of school-age migrants was high in several counties (districts), and the relative proportion of school-age migrants was high in municipal districts, neighboring counties, and cities. However, for most counties and districts, the number and proportion of school-age migrants were relatively low, and decreased in the following order: municipal districts > county-level cities > counties (autonomous counties).

3.1.1. Number of School-Age Migrants

In 2008, areas with a large number of school-age migrants were concentrated in the suburbs of metropolitan areas, such as Shenyang and Dalian, Ganjingzi District, Jinzhou District, Hunnan District, Yuhong District, and Lushunkou District. By 2013, counties and districts with a large school-age migrant population were still predominantly distributed in municipal districts. Haicheng, Wafangdian, Zhuanghe, Donggang, and other economic and populous cities also exhibited an increase in their school-age migrant populations. The data for 2020 revealed no major changes in the spatial distribution characteristics of the school-age migrant population. Notably, the number of school-age migrants in Jinzhou District, Ganjingzi District, Dadong District, Huanggu District, Lianshan District, Shuangta District, Yinzhou District, and other municipal districts maintained a rapidly increasing trend over the 12-year study period. Conversely, the trend in some districts (such as Xigang District and Bayuquan District) remained approximately stable, whereas that in other districts (such as Yuhong District and Sujiatun District) decreased over the study period.

3.1.2. Proportion of School-Age Migrants

In 2008, the school-age migrant population represented more than 10% of the total school-age population in 18 counties and districts. The 10 counties with the largest proportion of school-age migrants were all municipal districts of Dalian or Shenyang. The only

exception was Changhai County, which is an island county. Most counties (county-level cities and autonomous counties) exhibited a relatively low proportion of school-age migrants, indicating clear spatial differentiation. By 2013, most municipal districts had a high proportion of school-age migrants, whereas most counties (county-level cities and autonomous counties) still had a low proportion, revealing clear differences between urban and rural areas and between regions. In 2020, the spatial distribution of the proportion of school-age migrants was the same as that in 2013, with counties with low proportions enclosing counties with high proportions. Moreover, counties with high proportions were spatially concentrated and contiguous, whereas counties with low proportions were relatively scattered.

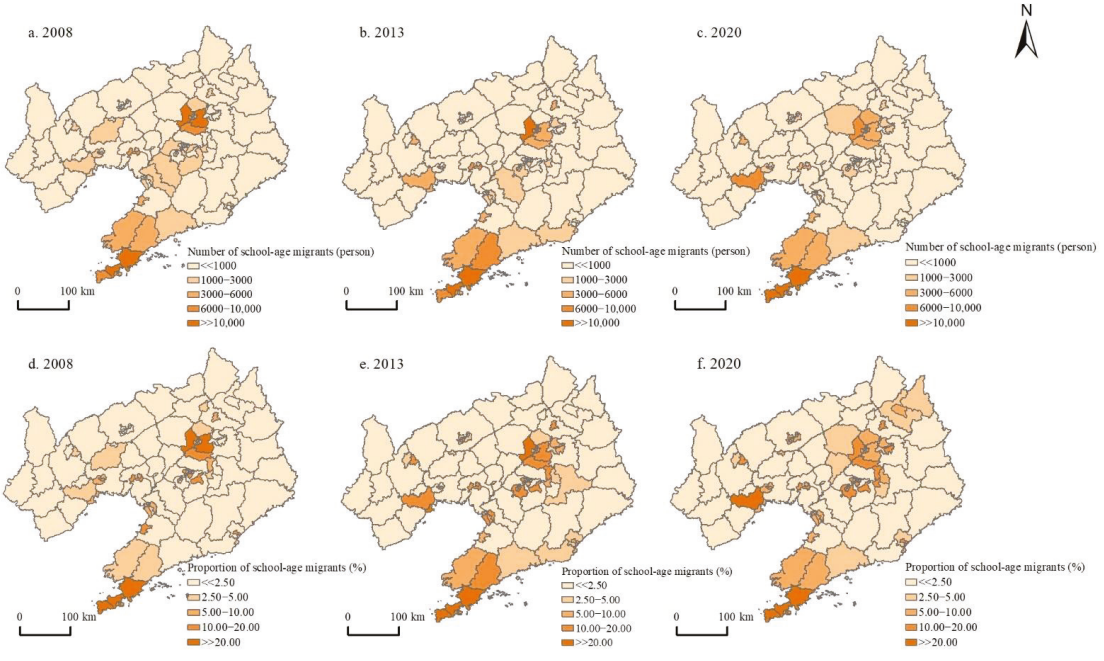

Figure 2. Spatial distribution of the school-age migrant population in Liaoning Province from 2008 to 2020: (**a**–**c**) number of school-age migrants and (**d**–**f**) proportion of school-age migrants.

3.2. Spatial Autocorrelation Characteristics of the School-Age Migrant Population

Figure 3 shows the global Moran's I estimates of the number of school-age children, the number of school-age migrants, and the proportion of school-age migrants among the total school-age population from 2008 to 2020. In the entire study period, all global Moran's I estimates were greater than zero, and all p-values were less than 0.001. This indicates a significant positive global spatial correlation between the proportion of school-age migrants and the school-age migrant population among county units. This proves that spatial differences in the distribution of the school-age migrant population between regions are objective, and that the school-age migrant population has a significant spatial agglomeration effect. Throughout the study period, the global Moran's I estimates of the number and proportion of school-age migrants were approximately consistent, first increasing then decreasing. Inflection points occurred in 2010 and 2012; however, the changes were not very large. This shows that the distribution of the school-age migrant population among counties exhibited a certain degree of spatial diffusion as well as spatial agglomeration; however, the overall spatial correlation pattern remained relatively the same as that in 2008. From 2008 to 2015, despite a similar trend, the global Moran's I estimate of the number of

school-age migrants was lower than that of the proportion of school-age migrants. In 2015, these two areas appeared to overlap, with the global Moran's I estimate of the number of school-age migrants becoming slightly higher from 2015 to 2020. It is worth noting that the global Moran's I estimate of the total school-age population increased significantly over the study period, with the degree of spatial autocorrelation showing an opposite trend to the distribution of the school-age migrant population. Thus, the spatial distribution of the school-age population may have a certain influence on the uneven spatial distribution of the school-age migrant population.

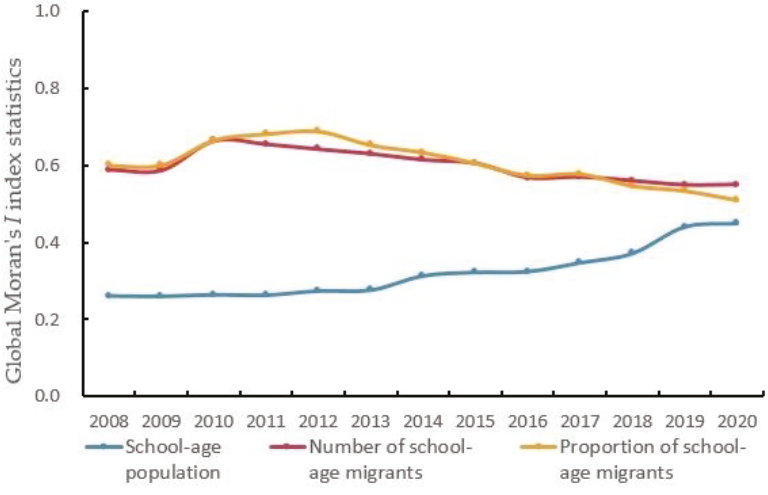

Figure 3. Spatial autocorrelation of the number and proportion of school-age migrants in Liaoning Province according to Global Moran's I.

The local G coefficient method was used to detect the local relevance of the distribution of the school-age migrant population in various counties and districts in Liaoning Province with the aim of analyzing the evolution characteristics of the spatial pattern of cold and hot spots (Figure 4). From 2008 to 2020, the distribution of the school-age migrant population showed strong spatial evolution characteristics and maintained relatively stable regional differences. On the one hand, the hot spots were mainly concentrated in the municipal districts of Dalian and showed a trend of continuous expansion, and the cold spots were mainly distributed in western Liaoning and Liaondong. On the other hand, Shenyang was gradually separated from the cold spots, whereas the size of the cold spot area in Liaodong region expanded. The distribution of both the number and proportion of school-age migrants reflected the obvious spatial differentiation between cold spots and hot spots. However, cold and hot spots related to the number of school-age migrants exhibited gradual expansion and concentration, whereas those related to the proportion of school-age migrants gradually decreased; these are mainly distributed in the municipal districts of most prefecture-level cities.

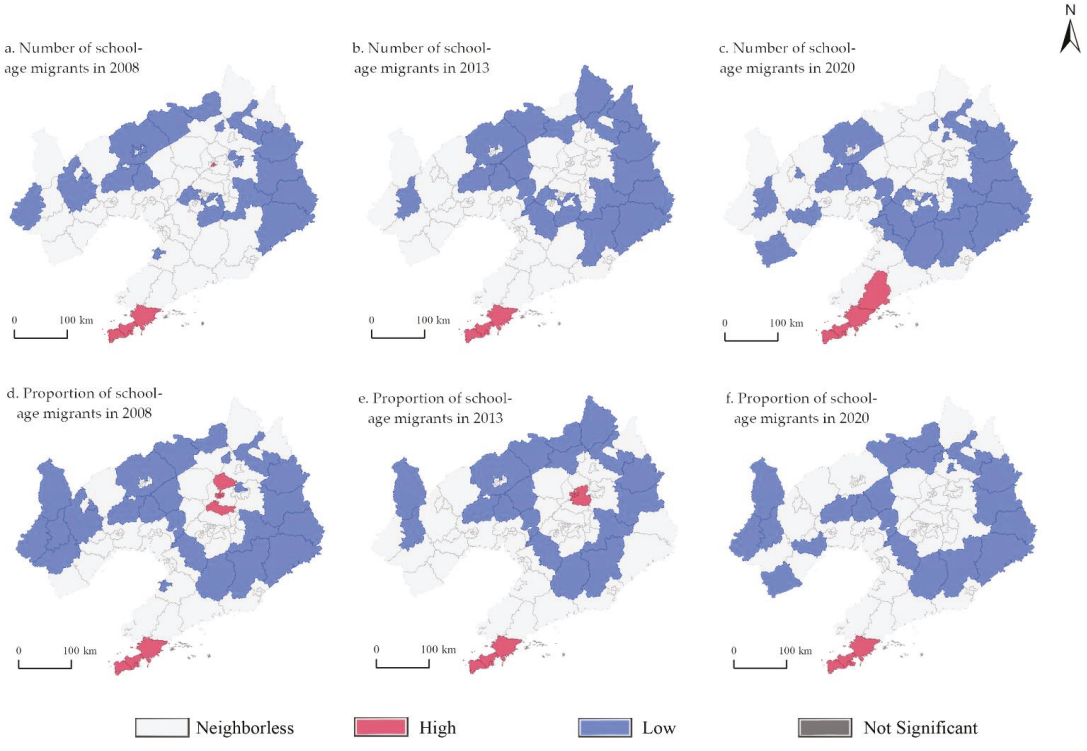

Figure 4. Spatial agglomeration of the school-age migrant population in Liaoning Province from 2008 to 2020: (**a**–**c**) number of school-age migrants and (**d**–**f**) proportion of school-age migrants.

3.3. Factors Driving the Spatial Differentiation of the School-Age Migrant Population

3.3.1. Variable Selection and Preprocessing

According to current literature and statistical data, six driving factors were selected from three categories (Table 1). Among them, the teacher-student ratio and the number of teachers (persons) with intermediate and above professional and technical titles reflect the quantity and quality of teaching staff; the monetary value of teaching equipment (yuan) and the number of books (books) reflect the quality of the teaching equipment and conditions; and the area of green spaces (m^2) and gymnasiums (m^2) reflect the quality of the educational and recreational environment. After standardizing the original data, the goodness of fit indicator, R^2, was 91.7%, and variance inflation factor (VIF) was less than 7.5, which was suitable for regression analysis.

3.3.2. Model Estimation Result

The average value of the regression coefficient of the MGWR model reflects the degree of influence of different driving factors on the school-age migrant population in 2020. The degree of influence decreased in the following order: number of books > teaching equipment value > green area > teacher-student ratio > number of teachers with intermediate and above professional titles > gymnasium area (Table 1). However, the bandwidth of books and teaching equipment was much smaller than that of other variables; thus, they were more sensitive to changes in a regional scale and were considered local variables. All other variables were considered global variables, indicating that their spatial effects were not significant. The results showed that the signs of the regression coefficients of all independent variables were positive and negative; thus, they were not

spatially stable. Moreover, the regression coefficients showed a large fluctuation trend, indicating an unstable influence on the distribution of the school-age migrant population.

Table 1. Statistical description of the MGWR model regression coefficients, indicating the degree of influence of different variables on the school-age migrant population.

Variable	Bandwidth	Mean	STD	Min	Median	Max
Teacher-student ratio	99.000	−0.024	0.009	−0.038	−0.025	−0.002
Number of teachers	86.000	−0.036	0.037	−0.071	−0.058	0.054
Books	43.000	0.752	0.276	0.555	0.685	1.613
Teaching equipment	68.000	0.081	0.079	0.023	0.034	0.305
Greening land area	79.000	−0.019	0.044	−0.072	−0.029	0.117
Gymnasium area	93.000	−0.445	0.011	−0.466	−0.445	−0.414
Intercept	47.000	−0.112	0.057	−0.255	−0.113	0.009

3.3.3. Analysis of Model Estimation Results

In this study, a Gaussian MGWR model type, adaptive bisquare spatial kernel, golden section bandwidth searching, and AICc optimization criterion were used. In the MGWR model, the research units exhibited spatial and temporal differences in their undetermined coefficient estimates. The larger the value, the greater the driving strength of the explanatory variable on the dependent variable, and vice versa. To more intuitively reflect the relationship between the proportion of school-age migrants and the driving factors, the ArcGIS natural breakpoint method was used to show the degree of influence of the driving factors (Figure 5).

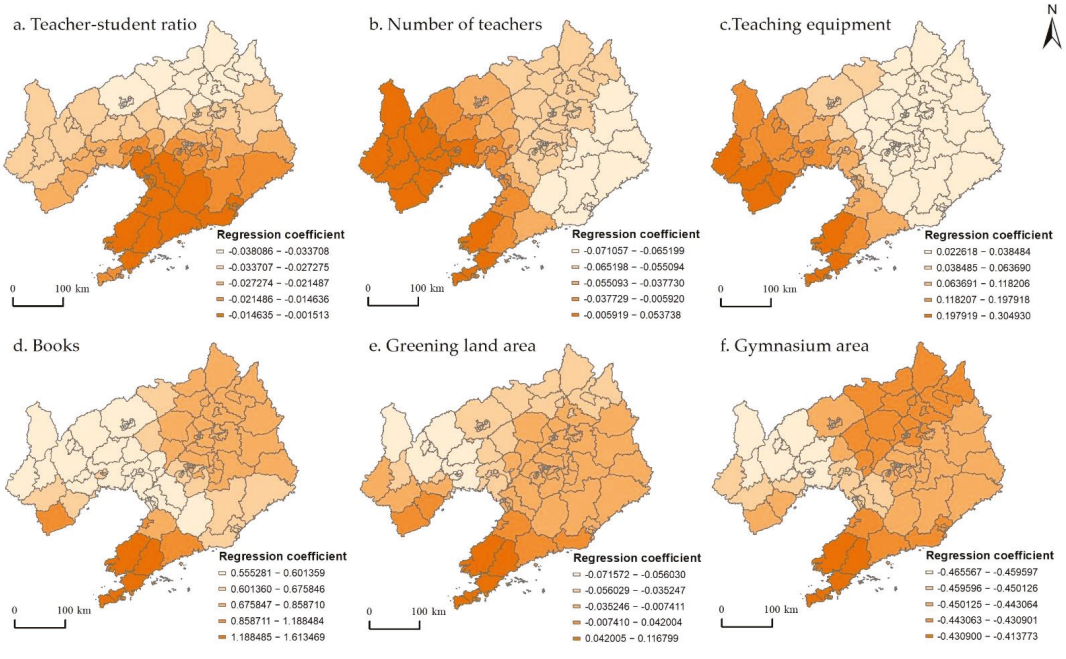

Figure 5. Spatial distribution of regression coefficients in the GTWR model in 2020: (**a**) teacher-student ratio, (**b**) number of teachers, (**c**) monetary value of teaching equipment, (**d**) number of books, (**e**) area of green spaces and (**f**) area of gymnasiums.

Regarding the influence of teachers on the distribution of the school-age migrant population, the regression coefficient of the teacher-student ratio decreased from the southeast to the northwest of Liaoning Province. The spatial distribution trend of the regression coefficient of the number of teachers with intermediate and above professional and technical

titles was approximately opposite to that of the teacher-student ratio, indicating an opposite influence of the quantity and quality of teachers. Therefore, the metropolises represented by Dalian and Shenyang should optimize the structure of the teaching team according to differences between the central city, suburbs, and counties under the jurisdiction of the outer suburbs. Overall, compared with the number of teachers, the quality of teachers attracts a greater school-age migrant population.

As for the impact of teaching equipment and conditions on the distribution of the school-age migrant population, the spatial trends of the regression coefficients of the value of teaching equipment and the number of books indicated restraining and promoting roles on the agglomeration and distribution of school-age migrants, respectively. However, the opposite trend was observed in Chaoyang and Fuxin City, whereas Dalian showed a double promotion effect. Thus, the teaching conditions of Dalian's primary and secondary schools are highly attractive for the school-age migrant population. Therefore, Chaoyang and Fuxin City are advised to make corresponding adjustments to attract more school-age migrants. Overall, the better the teaching conditions, the higher the proportion of school-age migrants. The quality of the teaching conditions is an important driving factor promoting the spatial agglomeration and distribution of the school-age migrant population.

Lastly, the spatial variation characteristics of the influence of the educational and recreational environment on the distribution of the school-age migrant population are shown in Figure 5. According to the spatial trend of the regression coefficient of the area of green land, green areas in Dalian, Dandong, Shenyang, and other cities promoted the school-age migrant population. Conversely, in Chaoyang City, Jinzhou City, Fuxin City, and other cities, green areas reduced the school-age migrant population. Regarding the area of gymnasiums, a dividing line was observed from Fuxin City and Dalian City, where the distribution of gymnasiums promoted and restricted the school-age migrant population on the east and west sides of this line, respectively. Overall, the amount of green space in the educational environment had a greater impact than recreation on attracting school-age migrants.

4. Discussion

Against the background of population migration in China, limitations in the education management system have led to the insufficient, untimely, and unreasonable allocation of educational resources in the territories. Therefore, it is necessary to guide compulsory education resource allocation to adapt to changes in the school-age population and achieve a truly balanced allocation of compulsory education resources [42,43]. This should involve implementation of a dynamic balance plan for dealing with changing trends in the school-age population, especially the school-age migrant population, strengthening reforms of the educational resource supply side, adjusting the supply of primary and secondary school degrees in a timely manner, promoting "spatial matching" between the school-age population and educational resources, and formulating reasonable compulsory education development planning and spatial layouts [44].

4.1. Overall Distribution of the School-Age Migrant Population

With large-scale population movement, educational issues related to the influx of school-age migrant populations require urgent attention. Thus, the research perspective must change from external to internal, from superficial to in-depth, and from a macro- to meso-scale in order to analyze specific regional differences in the school-age migrant population. However, the regularity of large-scale data may not be universal for small-scale spatial regions. This study used government agency student data from 2008 to 2020 to reveal the temporal and spatial differentiation characteristics of the school-age migrant population on the county scale and to analyze the detailed flow characteristics of the school-age migrant population within the region. The results of this study provide insights into the reasonable distribution of educational resources in the study region and the development planning and spatial layout of compulsory education.

4.2. Factors Driving the Spatiotemporal Differentiation of the School-Age Migrant Population

The driving factors of the school-age migrant population govern changes in the school-age population and the balanced allocation of educational resources. This study used the MGWR model to analyze the degree of influence of the teaching staff, school conditions, and educational/recreational environment. The results revealed significant spatial differences in the strength and trends of factors affecting the distribution of the school-age migrant population. The traditional geographic weighted regression model uses a local regression fitting method to estimate the parameter vector at each observation point and detect the spatial variation in the regression coefficients of various factors; however, it does not directly consider the spatial dependence between factors [45,46]. Conversely, the MGWR model represents an improvement on the traditional model as it cancels the assumption that all modeling processes are on the same spatial scale. By deriving the optimal bandwidth vector, different modeling runs can be performed on different spatial scales, which solves the requirements of multivariate spatial data for different spatial scales, and more effectively recognizes the heterogeneity of multivariate data in spatial dimensions [47,48].

4.3. Study Limitations

In this study, subjective factors inevitably affected the selection of driving factors. Moreover, cultural, economic, and policy factors are difficult to quantify, and some influencing factors were inevitably omitted, which should be addressed in future research. Furthermore, the distribution of the school-age migrant population exhibited significant urban–rural and regional differences. According to this small-scale survey of differences in the distribution of the school-age migrant population between major urban areas, suburbs, and the outer suburbs of metropolises, the findings of this study have significant implications for the balanced allocation of urban compulsory education resources. Therefore, followup research will be conducted in the future.

5. Conclusions

This study analyzed the spatial distribution characteristics of the school-age migrant population in 100 counties and districts in Liaoning Province using spatial autocorrelation methods. We also selected six representative driving factors from three categories, i.e., the quality and quantity of teachers, the quality of teaching conditions, and the amount of green land and recreational facilities, and used a multiscale geographically weighted regression model to analyze the driving force behind the distribution of the school-age migrant population in a multidimensional manner. The main conclusions are as follows. Both the number and proportion of school-age migrants in Liaoning Province exhibited highly uneven spatial distribution characteristics and were concentrated in the districts of various cities, especially Dalian and Shenyang. From 2008 to 2020, the school-age migrant population continued to increase in the suburbs of large and medium-sized cities; however, the number and proportion of school-age migrants in many counties remained relatively low. Additionally, over the 12-year study period, the distribution of the school-age migrant population in Liaoning Province exhibited significant spatial autocorrelation. Regarding the number of school-age migrants, hot spots were mainly concentrated in the municipal district of Dalian, whereas cold and hot spots exhibited continuous expansion and concentration. Conversely, regarding the proportion of school-age migrants, cold and hot spots decreased in area, whereas cold spots became more diffuse. The MGWR model results revealed spatial differences in the factors affecting the distribution of the school-age migrant population. The different driving factors exhibited different degrees of influence and different influence trends on the distribution of the school-age migrant population in Liaoning Province.

Author Contributions: W.X. contributed to all aspects of this work; C.S. wrote the main manuscript text, D.S. and B.Y. conducted the experiment and analyzed the data. All authors have read and agreed to the published version of the manuscript.

Funding: This study was supported by the 2018 National Social Science Fund of China Project: Research on Resources Allocation of Compulsory Education Based on School-age Population Flow Trend Prediction (Grant No. 18BRK037).

Institutional Review Board Statement: Not applicable.

Informed Consent Statement: Not applicable.

Data Availability Statement: The data supporting this study are available from the first author upon reasonable request.

Acknowledgments: The authors would like to acknowledge all colleagues and friends who have voluntarily reviewed the translation of the survey and the manuscript of this study.

Conflicts of Interest: The authors declare no conflict of interest.

References

1. You, H.; Yang, J.; Xue, B.; Xiao, X.; Xia, J.; Jin, C.; Li, X. Spatial evolution of population change in northeast China during 1992–2018. *Sci. Total Environ.* **2021**, *776*, 146023. [CrossRef]
2. Jina, S.; Yangab, J.; Wangb, E.; Liuc, J. The influence of high-speed rail on ice–snow tourism in northeastern China. *Tour. Manag.* **2020**, *78*, 104070. [CrossRef]
3. Yu, S.; Chen, B.; Levesque-Bristol, C.; Vansteenkiste, M. Chinese education examined via the lens of self-determination. *Educ. Psychol. Rev.* **2018**, *30*, 177–214. [CrossRef]
4. Ministry of Education of the People's Republic of China. *National Statistical Bulletin on Educational Development [EB/OL]*; Ministry of Education of the People's Republic of China: Beijing, China. Available online: http://www.moe.gov.cn/jyb_sjzl/sjzl_fztjgb/ (accessed on 10 September 2021).
5. Yu, M.; Crowley, C.B. The discursive politics of education policy in China: Educating migrant children. *China Q.* **2020**, *241*, 87–111. [CrossRef]
6. Bosker, M.; Brakman, S.; Garretsen, H.; Schramm, M. Relaxing hukou: Increased labor mobility and China's economic geography. *J. Urban Econ.* **2012**, *72*, 252–266. [CrossRef]
7. Fu, Y.; Gabriel, S.A. Labor migration, human capital agglomeration and regional development in China. *Reg. Sci. Urban Econ.* **2012**, *42*, 473–484. [CrossRef]
8. Chen, L.; Xi, M.; Jin, W.; Hu, Y. Spatial pattern of long-term residence in the urban floating population of China and its influencing factors. *Chin. Geogr. Sci.* **2021**, *31*, 342–358. [CrossRef]
9. Wang, Y.; Wang, Z.; Zhou, C.; Liu, Y.; Liu, S. On the settlement of the floating population in the pearl river delta: Understanding the factors of permanent settlement intention versus housing purchase actions. *Sustainability* **2020**, *12*, 9771. [CrossRef]
10. Zhao, M.; Liu, S.; Qi, W. Exploring the differential impacts of urban transit system on the spatial distribution of local and floating population in Beijing. *J. Geogr. Sci.* **2017**, *27*, 731–751. [CrossRef]
11. Dong, X.; Jiang, X. Population mobility model & floating growth spatial types and their influencing factors in southwest China. In *2019 International Conference on Management, Finance and Social Sciences Research (MFSSR 2019)*; Francis Academic Press: London, UK, 2019.
12. Xu, J.; Takahashi, M. Progressing vulnerability of the immigrants in an urbanizing village in coastal China. *Environ. Dev. Sustain.* **2021**, *23*, 8012–8026. [CrossRef]
13. Karachurina, L.B.; Mkrtchyan, N.V. Intraregional population migration in Russia: Suburbs outperform capitals. *Reg. Res. Russ.* **2021**, *11*, 48–60. [CrossRef]
14. Ma, W.; Jiang, G.; Wang, D.; Li, W.; Guo, H.; Zheng, Q. Rural settlements transition (RST) in a suburban area of metropolis: Internal structure perspectives. *Sci. Total Environ.* **2018**, *615*, 672–680. [CrossRef]
15. O'Brien, R.J. Model for planning the location and size of urban schools. *Socio-Econ. Plan. Sci.* **1969**, *2*, 141–153. [CrossRef]
16. Morrill, R.L. Efficiency and equity of optimum location models. *Antipode* **1974**, *6*, 41–46. [CrossRef]
17. Butler, T.; Hamnett, C. Praying for success? Faith schools and school choice in east London. *Geoforum* **2012**, *43*, 1242–1253. [CrossRef]
18. Mustapha, O.-O.; Akintunde, O.; Alaga, A.; Badru, R.; Ogbole, J.; Samuel, P.; Samuel, S. Spatial distribution of primary schools in Ilorin West local government area, Kwara State, Nigeria. *J. Sci. Res. Rep.* **2016**, *9*, 1–10. [CrossRef]
19. Andersson, E.; Malmberg, B.; Östh, J. Travel-to-school distances in Sweden 2000–2006: Changing school geography with equality implications. *J. Transp. Geogr.* **2012**, *23*, 35–43. [CrossRef]
20. Chi, G.Q.; Ho, H.C. Population stress: A spatiotemporal analysis of population change and land development at the county level in the contiguous United States, 2001–2011. *Land Use Policy* **2018**, *70*, 128–137. [CrossRef] [PubMed]

21. Gao, Y.; He, Q.; Liu, Y.; Zhang, L.; Wang, H.; Cai, E. Imbalance in spatial accessibility to primary and secondary schools in China: Guidance for education sustainability. *Sustainability* **2016**, *8*, 1236. [CrossRef]
22. Lu, S.; Rios, J.A.; Huang, C.-C. Mindfulness, emotion and behaviour: An intervention study with Chinese migrant children. *Child. Soc.* **2018**, *32*, 290–300. [CrossRef]
23. Zhang, W.; Chong, Z.; Li, X.; Nie, G. Spatial patterns and determinant factors of population flow networks in China: Analysis on Tencent location big data. *Cities* **2020**, *99*, 102640. [CrossRef]
24. Zhang, D.; Zhou, C.; Xu, W. Spatial-temporal characteristics of primary and secondary educational resources for relocated children of migrant workers: The case of Liaoning province. *Complexity* **2020**, *2020*, 1–13. [CrossRef]
25. Li, C.; Wu, Z.; Zhu, L.; Liu, L.; Zhang, C. Changes of spatiotemporal pattern and network characteristic in population flow under COVID-19 epidemic. *ISPRS Int. J. Geo-Inf.* **2021**, *10*, 145. [CrossRef]
26. Chan, K.W.; Ren, Y. Children of migrants in China in the twenty-first century: Trends, living arrangements, age-gender structure, and geography. *Eurasian Geogr. Econ.* **2018**, *59*, 133–163. [CrossRef]
27. Ye, B. Reform of compulsory education system and urban integration of floating population. *World Sci. Res. J.* **2021**, *7*, 184–197.
28. Zhao, M.; Hannum, E. Stark choices: Work-family tradeoffs among migrant women and men in urban China. *Chin. Sociol. Rev.* **2019**, *51*, 365–396. [CrossRef] [PubMed]
29. Huijsmans, R. Child migration and questions of agency. *Dev. Chang.* **2011**, *42*, 1307–1321. [CrossRef]
30. Tan, S.; Li, Y.; Song, Y.; Luo, X.; Zhou, M.; Zhang, L.; Kuang, B. Influence factors on settlement intention for floating population in urban area: A China study. *Qual. Quant.* **2017**, *51*, 147–176. [CrossRef]
31. Luo, J.; Zhang, X.; Wu, Y.; Shen, J.; Shen, L.; Xing, X. Urban land expansion and the floating population in China: For production or for living? *Cities* **2018**, *74*, 219–228. [CrossRef]
32. Liu, Z.; Wang, Y.; Chen, S. Does formal housing encourage settlement intention of rural migrants in Chinese cities? A structural equation model analysis. *Urban Stud.* **2016**, *54*, 1834–1850. [CrossRef]
33. Yu, D.; Zhang, Y.; Wu, X. Correction to: How socioeconomic and environmental factors impact the migration destination choices of different population groups in China: An eigenfunction-based spatial filtering analysis. *Popul. Environ.* **2020**, *41*, 396. [CrossRef]
34. Liu, S.; Zhao, X. How far is educational equality for China? Analysing the policy implementation of education for migrant children. *Educ. Res. Policy Pract.* **2018**, *18*, 59–74. [CrossRef]
35. Stiefel, L.; Elbel, B.; Prescott, M.P.; Aneja, S.; Schwartz, A.E. School wellness programs: Magnitude and distribution in New York city public schools. *J. Sch. Health* **2017**, *87*, 3–11. [CrossRef] [PubMed]
36. Fan, C.C.; Li, T. Split households, family migration and urban settlement: Findings from China's 2015 national floating population survey. *Soc. Incl.* **2020**, *8*, 252–263. [CrossRef]
37. Goodchild, M.F. What problem? Spatial autocorrelation and geographic information science. *Geogr. Anal.* **2009**, *41*, 411–417. [CrossRef]
38. Getis, A.; Ord, J.K. The analysis of spatial association by use of distance statistics. In *Advances in Spatial Science*; Springer: Berlin/Heidelberg, Germany, 2010; pp. 127–145.
39. Wulder, M.; Boots, B. Local spatial autocorrelation characteristics of remotely sensed imagery assessed with the Getis statistic. *Int. J. Remote Sens.* **1998**, *19*, 2223–2231. [CrossRef]
40. Fotheringham, A.S.; Yang, W.; Kang, W. Multiscale geographically weighted regression (MGWR). *Ann. Am. Assoc. Geogr.* **2017**, *107*, 1247–1265. [CrossRef]
41. Hastie, T.; Tibshirani, R. Generalized additive models: Some applications. *J. Am. Stat. Assoc.* **1987**, *82*, 371–386. [CrossRef]
42. Reis, J.; Ballinger, R.C. Creating a climate for learning-experiences of educating existing and future decision-makers about climate change. *Mar. Policy* **2020**, *111*. [CrossRef]
43. Li, J.; Shi, Z.; Xue, E. The problems, needs and strategies of rural teacher development at deep poverty areas in China: Rural schooling stakeholder perspectives. *Int. J. Educ. Res.* **2020**, *99*, 101496. [CrossRef]
44. Boldermo, S.; Ødegaard, E.E. What about the migrant children? The state-of-the-art in research claiming social sustainability. *Sustainability* **2019**, *11*, 459. [CrossRef]
45. Kumar, S.; Lal, R.; Liu, D. A geographically weighted regression kriging approach for mapping soil organic carbon stock. *Geoderma* **2012**, *189–190*, 627–634. [CrossRef]
46. Yang, J.; Bao, Y.; Zhang, Y.; Li, X.; Ge, Q. Impact of accessibility on housing prices in Dalian city of China based on a geographically weighted regression model. *Chin. Geogr. Sci.* **2018**, *28*, 505–515. [CrossRef]
47. Fotheringham, A.S.; Yue, H.; Li, Z. Examining the influences of air quality in China's cities using multi-scale geographically weighted regression. *Trans. GIS* **2019**, *23*, 1444–1464. [CrossRef]
48. Li, Z.; Fotheringham, A.S. Computational improvements to multi-scale geographically weighted regression. *Int. J. Geogr. Inf. Sci.* **2020**, *34*, 1378–1397. [CrossRef]

land

MDPI

Article

Application of the Adapted Approach for Crop Management Factor to Assess Soil Erosion Risk in an Agricultural Area of Rwanda

Albert Poponi Maniraho [1,2,3,4], Richard Mind'je [1,2,3,4], Wenjiang Liu [5], Vincent Nzabarinda [1,3], Patient Mindje Kayumba [1,3,4], Lamek Nahayo [4], Adeline Umugwaneza [1,3,4], Solange Uwamahoro [1,3] and Lanhai Li [1,2,3,5,6,*]

[1] State Key Laboratory of Desert and Oasis Ecology, Xinjiang Institute of Ecology and Geography, Chinese Academy of Sciences, 818 South Beijing Road, Urumqi 830011, China; albapoponi@mails.ucas.ac.cn (A.P.M.); mindjerichard@mails.ucas.ac.cn (R.M.); vincentzabarinda@mails.ucas.edu.cn (V.N.); patientestime001@mails.ucas.ac.cn (P.M.K.); umugwaneza15@mail.ucas.ac.cn (A.U.); uwamaharoso@mails.ucas.ac.cn (S.U.)
[2] Ili Station for Watershed Ecosystem Research, Chinese Academy of Sciences, Urumqi 835800, China
[3] University of Chinese Academy of Sciences, Beijing 100049, China
[4] Faculty of Environmental sciences, University of Lay Adventists of Kigali (UNILAK), Kigali 6392, Rwanda; lameknahayo@unilak.ac.rw
[5] CAS Research Center for Ecology and Environment of Central Asia, 818 South Beijing Road, Urumqi 830011, China; wjliu@ms.xjb.ac.cn
[6] Xinjiang Key Laboratory of Water Cycle and Utilization in Arid Zone, Urumqi 830011, China
* Correspondence: lilh@ms.xjb.ac.cn; Tel.: +86-991-7823125

Citation: Maniraho, A.P.; Mind'je, R.; Liu, W.; Nzabarinda, V.; Kayumba, P.M.; Nahayo, L.; Umugwaneza, A.; Uwamahoro, S.; Li, L. Application of the Adapted Approach for Crop Management Factor to Assess Soil Erosion Risk in an Agricultural Area of Rwanda. *Land* **2021**, *10*, 1056. https://doi.org/10.3390/land10101056

Academic Editor: Baojie He

Received: 25 September 2021
Accepted: 4 October 2021
Published: 8 October 2021

Abstract: Land use and land cover (LULC) management influences the severity of soil erosion risk. However, crop management (C) is one factor of the Revised Universal Soil Loss Equation (RUSLE) model that should be taken into account in its determination, as it influences soil loss rate estimations. Thus, the present study applied an adapted C-factor estimation approach (CvkA) modified from the former approach (Cvk) to assess the impact of LULC dynamics on soil erosion risk in an agricultural area of Rwanda taking the western province as a case study. The results disclosed that the formerly used Cvk was not suitable, as it tended to overestimate C-factor values compared with the values obtained from t CvkA. An approximated mean soil loss of 15.1 t ha^{-1} yr^{-1}, 47.4 t ha^{-1} yr^{-1}, 16.3 t ha^{-1} yr^{-1}, 66.8 t ha^{-1} yr^{-1} and 15.3 t ha^{-1} yr^{-1} in 2000, 2005, 2010, 2015 and 2018, respectively, was found. The results also indicated that there was a small increase in mean annual soil loss from 15.1 t ha^{-1} yr^{-1} in 2000 to 15.3 t ha^{-1} yr^{-1} in 2018 (1.3%). Moreover, the soil erosion risk categories indicated that about 57.5%, 21.8%, 64.9%, 15.5% and 73.8% had a sustainable soil erosion rate tolerance ($\leq$10 t ha^{-1} yr^{-1}), while about 42.5%, 78.2%, 35.1%, 84.5% and 16.8% had an unsustainable mean soil erosion rate (>10 t ha^{-1} yr^{-1}) in 2000, 2005, 2010, 2015 and 2018, respectively. A major portion of the area fell under the high and very high probability zones, whereas only a small portion fell under the very low, low, moderate and extremely high probability zones. Therefore, the CvkA approach presents the most suitable alternative to estimate soil loss in the western province of Rwanda with reasonable soil loss prediction results. The study area needs urgent intervention for soil conservation planning, taking into account the implementation of effective conservation practices such as terracing for soil erosion control.

Keywords: GIS; modeling; probability zones; remote sensing; RUSLE; Rwanda; soil loss

1. Introduction

Globally, soil erosion incidences enhanced by human activities have been a serious environmental problem since the last century [1]. They are a known risk factor to an ecosystem's integrity and cause major environmental impacts, including a reduction in

agricultural productivity; they can even affect the freshwater ecology of different regions. Previous studies have reported a soil loss of approximately 73.5 Pg yr^{-1} in agricultural land [2,3]. Topography, soil characteristics, local climatic conditions and land use are considered as the main influencing factors of increasing soil erosion risks [3–5].

However, it is not easy to estimate soil loss without relating it to various human, natural or physical processes. Quantitative and qualitative descriptions of soil erosion have been executed by field observations and measurements and via meta-analyses of soil erosion levels [6]. Owing to the scarcity of in situ or field data, as well as their expensiveness and time-consuming aspects, researchers have established quantitative soil-erosion modeling approaches that apply physical factors including topography, climate, soil features and vegetation type, with the aim of mapping spatial distribution rates to better understand the mechanisms of soil erosion. Moreover, these erosions provide a clear understanding of natural phenomena such as the transportation and deposit of sediment, including soil erosion prediction [7,8].

It is difficult to find a model that matches all types of erosion. This situation contributes to the intricacy in identifying areas prone to practicing soil conservation measures in terms of a reduction in soil loss. Therefore, the development and planification of numerous alternative land-use scenarios are of great significance as far as the management of soil erosion risk is concerned [9].

The primary challenge in modeling soil erosion risk is mostly associated with accuracy assessments, especially in data-scarce regions such as Rwanda [4]. Therefore, it is challenging to determine the degree of risk without the existence of numerous soil erosion models. For the prediction of soil erosion, different approaches have been proposed by different authors depending on study objectives, time, data availability and spatial scales [10–12]. The approaches for modeling soil erosion are easily understandable because of their powerful reliance on geospatial techniques that include remote sensing (RS) and geographic information system (GIS) platforms [11]. To this end, the USLE (Universal Soil Loss Equation) and its modified form, RUSLE (the Revised Universal Soil Loss Equation), proposed by [13], are largely applied due to their ability to integrate the aforementioned geospatial techniques. The integrated application of RUSLE and GIS combined with RS technology has been verified as an effective approach for assessing the spatial variability of soil erosion occurrence and its drivers [11,14–17].

In Rwanda, studies have applied the RUSLE model to simulate soil erosion at both national and local scales. However, those considering agricultural areas are still understudied. Among the few existing studies, Nyesheja and Chen [18] modeled soil erosion in the Congo Nile Ridge region of Rwanda by estimating serious soil loss from different land use/land cover (LULC) types such as grasslands, forestlands and farmlands that expressed impaired ecosystems. Additionally, Byizigiro et al. [19] estimated soil erosion in the Ngororero district taking the Satinskyi Catchment as a case and disclosed the geomorphological features and processes of the area to be the major natural factors that aggravated increased soil erosion rates pronounced in the area. In conjunction with its seven-year development strategies on the sensitization of the population regarding aspects related to soil conservation, Niyonsenga et al. [20] considered the Nyamasheke district to spatially analyze the unknown sensitivity of soil erosion. They reported that soil erosion and the associated high level of land degradation caused by vegetation cover change are leading to a loss in fertile soil in the area.

Nevertheless, keeping the basic form of the RUSLE equation, these studies presented the overestimation of the crop management (C) factor, which seemed to provide unsatisfactory results in the considered areas [21,22]. In addition, all the above-mentioned studies were limited to only the district and catchment scales of the province opposite this study, which considered the agricultural areas of the entire western province. Useful information related to LULC change, erosional features such as rainfall interception and gullies has been delivered by multi-temporal satellite images to analyze the LULC change in relation to soil erosion hazards at a regional scale [23]. LULC change is central to the study of

global environmental change, including land degradation [24]. It is the most significant indicator between a natural environment and human activity. Rwanda is considered one of the regions highly vulnerable to water-induced soil erosion [25]. This is because of its rapid population growth with a low economic base, poor agricultural practices, fragile soil [26] and steep topography, which contributes to heavy rainfall [27]. Similarly, the effects of LULC change studies have been conducted at different small watersheds at district, national, regional and global levels [11,28–30]. All these studies agree on the strong influence of land-use change on soil erosion.

Rwanda has experienced a significant regional change in its land-use patterns, especially in the western province, with limited scientific studies tackling this issue. In line with this, Nambajimana and He [21] used the RUSLE model for Land-Use Change Impacts on water erosion in Rwanda and identified the driving forces of soil erosion; however, this study was limited by its inability to capture degraded areas in its impact assessment. This can have some unforeseen significant impacts on land area and the wellbeing of local residents. Based on this background and the context of evolving land-use changes in Rwanda, this present study intends to address all of the above-mentioned shortcomings in the previous studies, and establish an adapted approach that is suitable for the estimation of C-factor in the RUSLE model that exhibits overestimated values. Thus, the objectives of this study are to: (a) examine the adapted approach for the estimation of the crop management (C) factor in the western province of Rwanda; (b) analyze the LULC changes and their impacts on soil erosion risk; (c) estimate the potential annual soil loss rate for the study area; and (d) delineate the spatial distribution of soil erosion probability zones. Addressing these objectives will fill the knowledge gap in identifying the most degraded parts of agricultural lands in the study area, which is crucial for effective soil conservation planning and environmental management.

2. Datasets and Methods

2.1. Study Area

The study covers the entire western part of Rwanda with −2° 22′″ and 17.99″ south latitude and 29°12″ and 21°00″ east longitude spatial coordinates. It is made of seven districts, namely Ngororero, Karongi, Rubavu, Nyabihu, Rutsiro, Rusizi and Nyamasheke (Figure 1). The area is mountainous and covers 5883 km^2, with the highest altitude in the country. It has an elevation ranging between 921 m and 4492 m, with an annual average temperature of 18°C. The country's climate is made up of four seasons, namely the long dry (June–September), short dry (mid-December–mid-February), long rainy (late February–late May) and short rainy (late September–early December) seasons [31]. The area receives up to 1800 mm annual rainfall, which usually contributes to high average runoff [18]. High annual precipitation and steep topography (> 26°) constitute major natural factors that influence morphological developments in the area. The latter is aggravated by agriculture and mining operations, which contribute to increased soil erosion rates observed in the area.

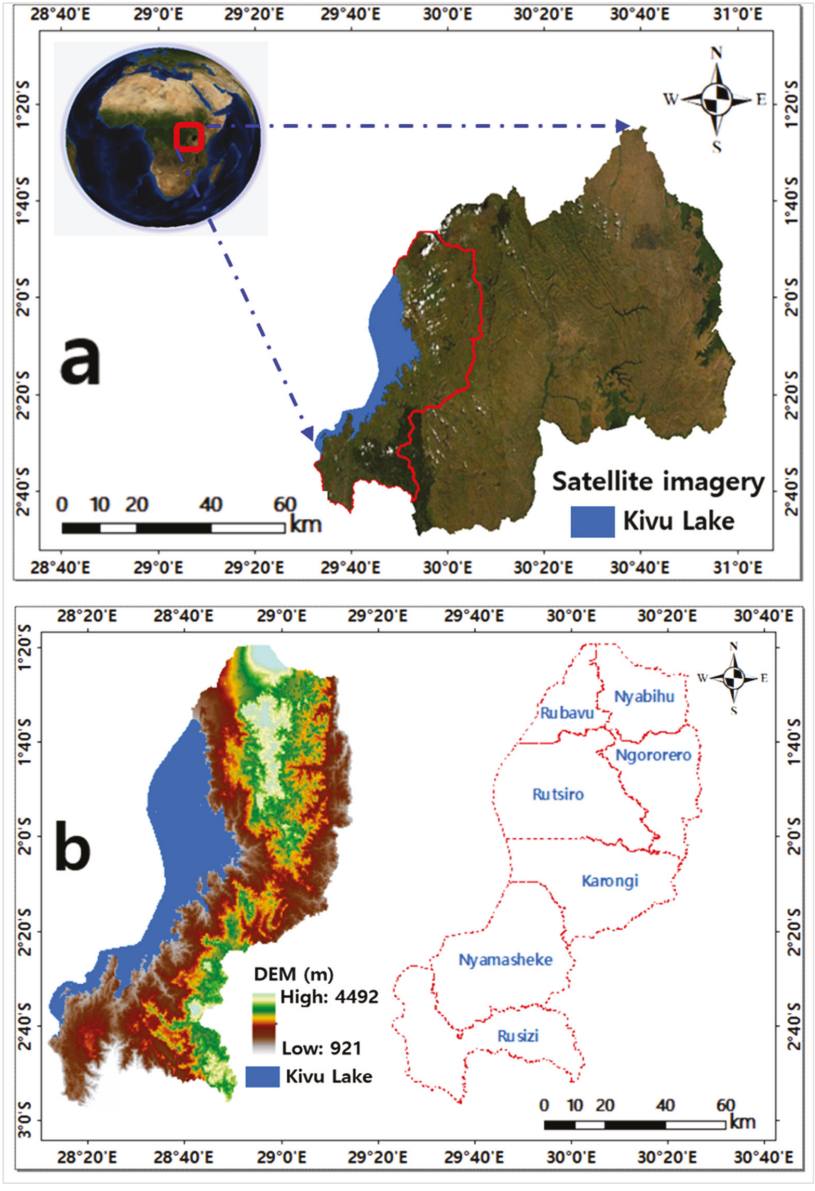

Figure 1. Location of the study area: (**a**) delimitation of the western province in Rwanda using satellite imagery; (**b**) digital elevation model with district boundaries of the study area.

2.2. Data and Preprocessing

For the successful application of the RUSLE model in this study, GIS and RS techniques were used for satellite data processing and analysis. The Landsat 7 ETM+ and Landsat 8 OLI-TIRS images (30 m × 30 m, WRS path 172 and rows 61) products were acquired from the United States Geological Survey (USGS) EROS data center. These images were pre-processed for radiometric and atmospheric rectification [32] and then used for calculating the vegetation index, as well as LULC classification using a supervised maximum classification algorithm

supported by expert judgment and ground truth observation. The main land-cover classes were water bodies, forest, grassland, cropland, wetland and settlements. In addition, the Digital Elevation Model (SRTM-DEM) at 30 m resolution (http://www.earthexplorer.usgs.gov, accessed on 4 October 2021) was acquired to calculate the flow accumulation and the slope gradient (degrees), which were both used to generate the factors representing the length of the slope and its steepness (LS). Moreover, a soil-type map from the Food and Agriculture Organization of the United Nations (FAO) was used in addition to meteorological data (rainfall) acquired from the Rwanda Meteorological Agency. Further details of the datasets are illustrated in Table 1.

Table 1. Summary of datasets and their sources.

Datasets	Sources	Path and Row
Landsat 7 ETM+/Landsat 8 OLI-TIRS	USGS earth Explorer/ Earthexplorer.usgs.gov accessed on 4 October 2021	172-61
DEM	Earthexplorer.usgs.gov accessed on 4 October 2021	
Meteorological data (Rainfall)	Rwanda Meteorological agency	
Soil map	Food and Agriculture Organization (FAO)	

2.3. Estimations Based of RUSLE Model

RUSLE is an erosion empirical model aiming to predict the long-term averages of soil loss per year caused by runoff from specific slopes area in specified cropping and management systems. The RUSLE model collects many factors on the process of soil erosion into different groups (relief, climate, vegetation, land use, soil profile and the practice of land management). These five groups are subdivided as soil erosion factors, including the rainfall erosivity (R) factor, the soil erodibility (K) factor, the slope length and slope steepness (LS) factor, the crop management (C) factor and the erosion management practice (P) factor. The expected soil loss in t/ha/yr was estimated by multiplying these factors' values based on the dimensions used in the climate and soil factor.

The RUSLE equation is given below:

$$A = R \times K \times LS \times C \times P \quad (1)$$

where A is the estimated spatial average soil loss and temporal average soil loss per unit area, expressed in t/ha/yr.

2.3.1. Rainfall Erosivity (R) Factor

Rainfall is a key factor triggering soil erosion in the tropic region. The R factor defines the erosive power of precise rainfall or the intensity of rainfall as the factor causing soil erosion [33]. The understanding of this factor relies on the kinetic force of raindrops on the soil's surface [34]. In the RUSLE model, R factor estimation depends on the product given by the storm power based on a rainfall intensity of 30 min, expressed as R = EI30 [34]. The R factor (Figure 2a) was estimated using Equation (2) proposed by [35]:

$$R = 38.5 + 0.35P \quad (2)$$

where R represents the rainfall erosivity factor while the mean annual rainfall (mm) is represented by P.

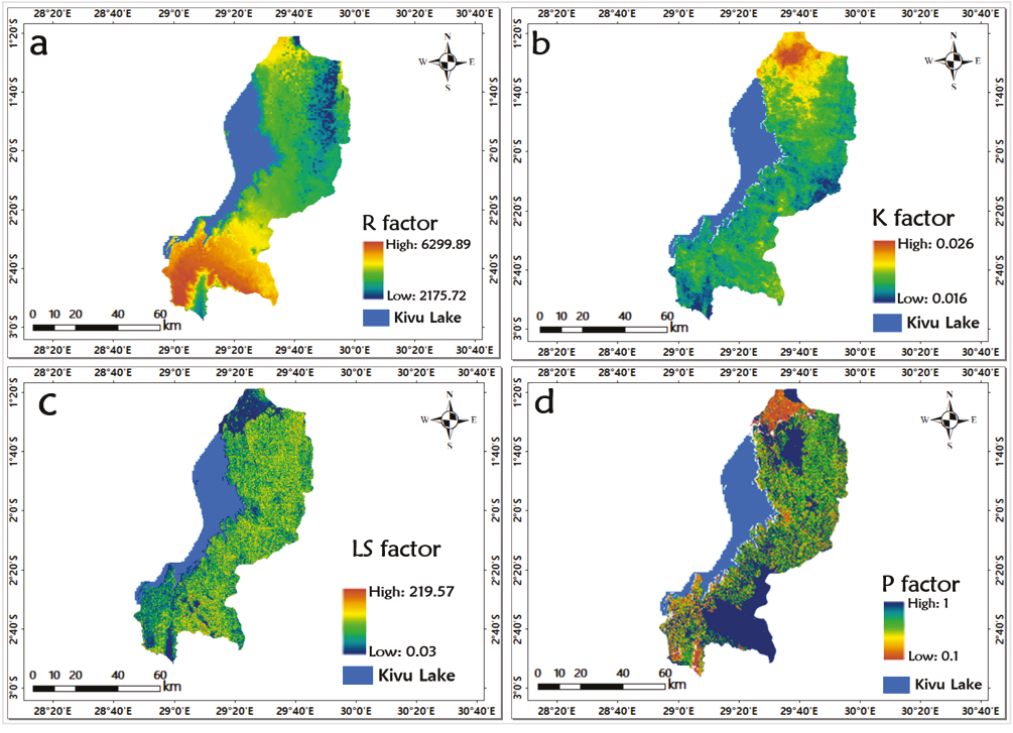

Figure 2. RUSLE factor maps for the western province of Rwanda: (**a**) rainfall erosivity (R) factor; (**b**) soil erodibility (K) factor; (**c**) slope length and its steepness (LS) factor; (**d**) support practice (P) factor.

2.3.2. Soil Erodibility (K) Factor

The K-factor expresses the susceptibility of soil-to-soil erodibility. K-factor (Figure 2b) was computed based on the soil properties, including a fraction of sand, clay, silt and organic carbon using the Equation (3):

$$K = A * B * C * D * 0 \quad (3)$$

where A represents the soils with high-and rough-sand contents and those with less sand (Equation (3a)), B specifies the soils with high clay-to-silt fractions (Equation (3b)), C is soils rich in organic carbon (Equation (3c)) and D defines soils very rich in sand (Equation (3d)). Practically, A, B, C and D were multiplied with 0.1317 values to convert the K-factor from the American system to the metric system unity/International System of Units (SI).

$$A = \left(0.2 + 0.3.\exp\left[-0.256.SAN.\left(1 - \frac{SIL}{100}\right)\right]\right) \quad (3a)$$

$$B = \left(\frac{SIL}{CLA + SIL}\right)^{0.3} \quad (3b)$$

$$C = \left(1 - \frac{0.0256C}{C + \exp(3.72 - 2.95C)}\right) \quad (3c)$$

$$D = \left(1 - \frac{0.7SN1}{SN1 + \exp(-5.51 + 22.9SN1)}\right) \quad (3d)$$

where SAN is the sand content percentage (0.05–2.00 mm diameter); SIL specifies the silt content percentage (0.002–0.05 mm diameter); CLA specifies the clay content percentage (<0.002 mm diameter); C is the organic carbon content percentage; and SN1 = 1 − (SAN/100).

2.3.3. Slope Length and Its Steepness (LS) Factor

LS is a factor derived from DEM obtained by multiplying the length (L) and steepness (S) of a slope. L is the fraction of soil loss from the ground to soil loss from 22.1 meters under similar conditions, while S is the fraction of soil loss from the ground slope gradient to the loss of soil from 9% under similar conditions. L was derived from an algorithm (Equation (4)) developed by Desmet and Govers [36], while the S factor was computed using the McCool and Brown [37] method (Equation (5)). Finally, the LS (Figure 2c) was calculated using the equations below:

$$L = \left(\frac{\lambda}{22.13}\right)^{m} \tag{4}$$

$$\mathrm{m} = \left(\frac{\mathrm{E}}{1+\mathrm{E}}\right) \tag{4a}$$

$$\mathrm{E} = \frac{\mathrm{Sin}\theta/0.0896}{3\ (\mathrm{Sin}\theta)0.8 + 0.56\prime} \tag{4b}$$

$$S1 = 10.8 * +0.03 \tag{4c}$$

$$S2 = 16.8 * -0.05 \tag{4d}$$

where L and S indicate the slope length and steepness factor (dimensionless); λ is the slope length (in m); m denotes the variable power based on E; E denotes the rill to interrill erosion fraction; and θ is the slope angle (in degrees). S1 and S2 represent the slope percentage <9% and slope percentage ≥ 9%, respectively.

2.3.4. Crop Management (C) Factor

C is a factor representing crop management as a fraction of soil loss from land collected under specified conditions to the soil loss from the same area in tilled unceasing fallow land. It represents the effects of vegetation and other ground covers [38]. The traditional approach for the calculation of the C-factor in space is allocating values to LULC classes. The effects of vegetation are generally expressed using different vegetation indices, whereby each index has its specific expression of green vegetation and its particular suitability for specific applications. Therefore, the choice of a specific vegetation index or soil biophysical indices needs to be made cautiously by widely considering and analyzing their prevailing advantages and shortcomings. For this specific study, the Normalized Difference Vegetation Index (NDVI) was deemed worthy of being used for the estimation of the RUSLE-based C-factor due to its important advantages such as its ability to indicate green vegetation potency [39], show fluctuations in LULC [40] and estimate values that represent the utmost heterogeneity in the stage of crop growth [41]. Different researchers developed many techniques to calculate the C-factor using the NDVI for assessing soil loss with the USLE/RUSLE model. This index can be derived from the spectral reflectance difference between near infrared (NIR) and red. It ranges between −1 and +1, with the highest values accredited to areas with higher vegetation cover [42,43], and it is estimated using the equation below:

$$\mathrm{NDVI} = \frac{\mathrm{NIR} - \mathrm{RED}}{\mathrm{NIR} + \mathrm{RED}} \tag{5}$$

We used NDVI and two approaches for determining the soil cover management factor. The first (Equation (6)) was proposed by Van der Knijff and Jones [22], and the second

was suggested as an adapted version of the first approach (Equation (7)). In the approach proposed by Van der Knijff and Jones [44] (Cvk), the C-factor is calculated as:

$$\text{Cvk} = \exp\left(-\alpha\frac{\text{NDVI}}{(\beta - \text{NDVI})}\right) \quad (6)$$

where α and β are the parameters that determine the shape of the curve that links NDVI with the C-factor. Van der Knijff and Jones [22] used values 2 and 1 for European climate conditions as the best representatives of the equation parameters α and β, respectively. Nevertheless, for tropical climate conditions with high intensities of rainfall, the C-factor tends to be overestimated compared to that calculated using the approach by Van der Knijff and Jones [22] for the same vegetation cover. Hence, a newly adapted approach for calculating the RUSLE C-factor was presented in this study in comparison to the former one. Due to the bias identified in the previous studies, this study recommends an adjustment factor of 2, which has been divided by the aforementioned equation (Equation (6)) to minimize the bias for the tropical climate conditions. Therefore, the adapted C-factor (CvkA) was proposed as follows:

$$\text{CvkA} = \frac{\exp[-\alpha(\text{NDVI}/(\beta - \text{NDVI}))]}{2} \quad (7)$$

To establish the adequacy of the used index (NDVI) in the estimation of the RUSLE-based C-factor, a linear regression analysis was then executed using the extracted values against the related NDVI-based C-factor values [42]. Additionally, the shape of the mean cover management factor values calculated for all images was compared to determine the relationship between the two approaches (Cvk and CvkA). To achieve this, a sample of spatially distributed random points within the study area was produced in the ArcGIS 10.8 platform, and then its tool was applied to extract multi-values to points from both variables (NDVI and C-factor). To quantify the sensitivity of NDVI-derived CvkA values to biophysical variables, the influence of biophysical variables (Table 2) on CvkA (adapted C-factor) in Equation (7) with regard to this NDVI was carried out.

Table 2. Variables and their description used for regression analysis to investigate their influence on NDVI-derived C-factor (CvkA) values.

Variables	Description	Data Type
Dependent variable		
Improved C-factor (CvkA)	Adapted cover management factor from equation proposed by Van der Knijff, Jones and Montanarella (2000) derived from satellite images (Equation (3))	Continuous
Biophysical variables		
Rainfall	Rainfall erosivity (R value) (Equation (2))	Continuous
Elevation	Digital elevation model (30 m spatial resolution, from the USGS)	Continuous
Soil	Soil erodibility (K value) (Equation (3))	Continuous

2.3.5. Support Practice (P) Factor

P is a factor that represents the support practice to express the rate of soil loss with erosion control practices such as strip-cropping, terracing and contouring [18]. The P factor (Figure 2d) can be computed for the croplands of different slope classes. Depending on the slope grades, either erosion control practice can be used. However, the values of the P factor were not estimated as part of the equation due to the unavailability of data. Therefore, this study adopted the P factor values (Table 3) suggested by Shin and Noh [45].

Table 3. Support practice factor values as per soil conservation practice by Shin and Noh [45].

Slope %	Strip-Cropping	Contouring	Terracing
0–7.0	0.27	0.55	0.10
7.0–11.3	0.30	0.60	0.12
11.3–17.6	0.40	0.80	0.16
17.6–26.8	0.45	0.90	0.18
>26.8	0.50	1.0	2.0

2.4. Soil Erosion Probability Zones Delineation

For the identification and generation of the areas with a probability of soil erosion, maps were prepared using ArcGIS 10.8 version. Key factors including slope, rainfall intensity, LULC and soil properties were utilized as the most influential factors on soil erosion. Weights were assigned to each theme taking into consideration its role in soil erosion. A raster overlay analysis process (weighted index overlay) was used to generate the zones with the highest probability of soil erosion occurrence. Therefore, the feature with the highest susceptibility was given the maximum value, while the minimum value was assigned to the feature with the lowest susceptibility.

3. Results

3.1. Adapted Approach ($C_{vk}A$) for C-Factor Estimation

By comparing the C-factor values from both methods (Cvk and its adapted version CvkA), the results exhibited Cvk with higher overestimations for the mean value in different LULCs (forestland, cropland, grassland and wetland) than CvkA in all the periods studied (Figure 3). The results estimated from the adapted C-factor (CvkA) presented greater consistent values compared with those of the Cvk approach, which makes the estimation of soil loss more reliable. Figure 4 shows the spatial distribution of C-factor values estimated from two approaches for the LULC in the western province of Rwanda.

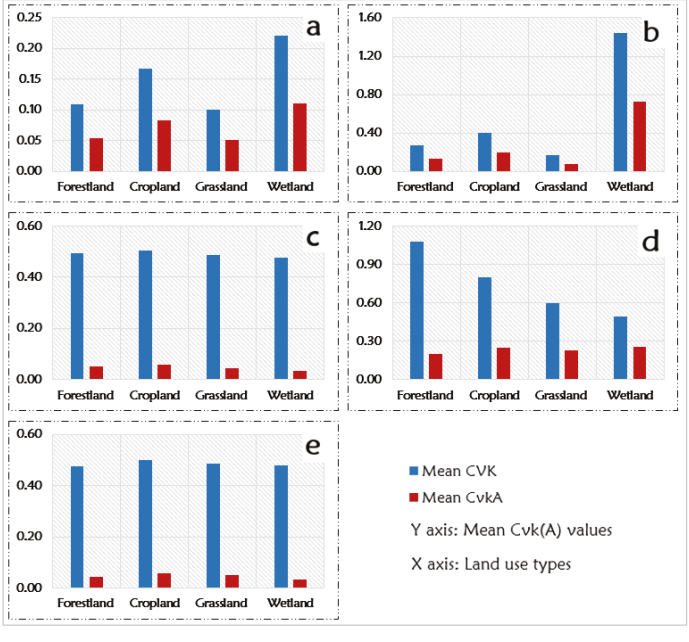

Figure 3. Annual mean C-factor comparisons between Cvk and $C_{vk}A$ values among different LULCs for five considered years: (**a**) 2000, (**b**) 2005, (**c**) 2010, (**d**) 2015 and (**e**) 2018.

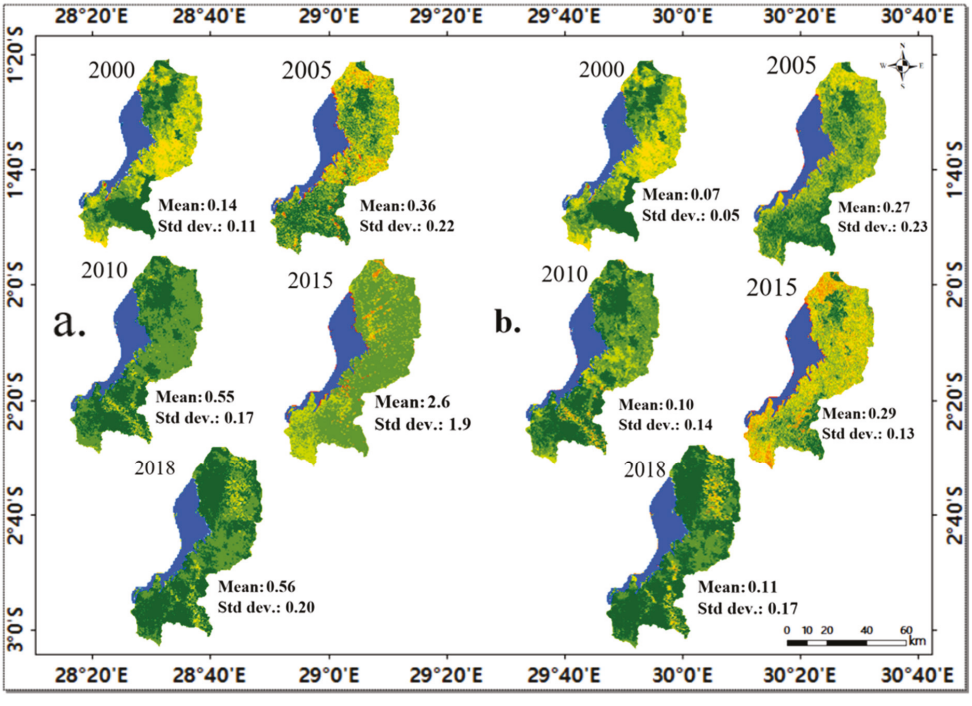

Figure 4. Comparison between the RUSLE cover management (C) factor maps: (**a**) using the formerly used approach (Cvk);and (**b**) using the adapted approach (CvkA) for the considered years.

The mean and standard deviation values of CvkA are 0.068 ± 0.054 in 2000, 0.27 ± 0.23 in 2005, 0.10 ± 0.14 in 2010, 0.29 ± 0.13 in 2015 and 0.11± 0.17 in 2018, respectively, while Cvk values are 0.14 ±0.11, 0.36 ± 0.22, 0.55 ± 0.17, 2.6 ± 1.9 and 0.56 ± 0.20 in 2000, 2005, 2010, 2015 and 2018, respectively (Figure 4). Cvk was found not to be suitable for estimating the C-factor in the study area, as it presented overestimated values compared to those from its adapted equation. CvkA was the most suitable based on the spatial variability of vegetation coverage of the area and the obtained C-factor values.

In general, NDVI is one of the several numerical combinations of satellite bands reported to be sensitive indicators in the existence and state of green vegetation considering the LULC of an area. For this, based on the spatial variability of soil coverage in the study area, the method using NDVI to obtain the C-factor was the most suitable. It was applied with an assumption that there was a linear relationship between NDVI and the C-factor linear model (Figure 5). The two variables have shown a tendency to move in the opposite direction from one another, such that when NDVI increased, C-factor decreased, and vice versa. The study achieved the highest correlation coefficient between the NDVI and C-factors in all the considered periods, with an R^2 higher than 85% (Figure 5). Thus, NDVI was judged to be relevant in the estimation of the C-factor in the adapted equation.

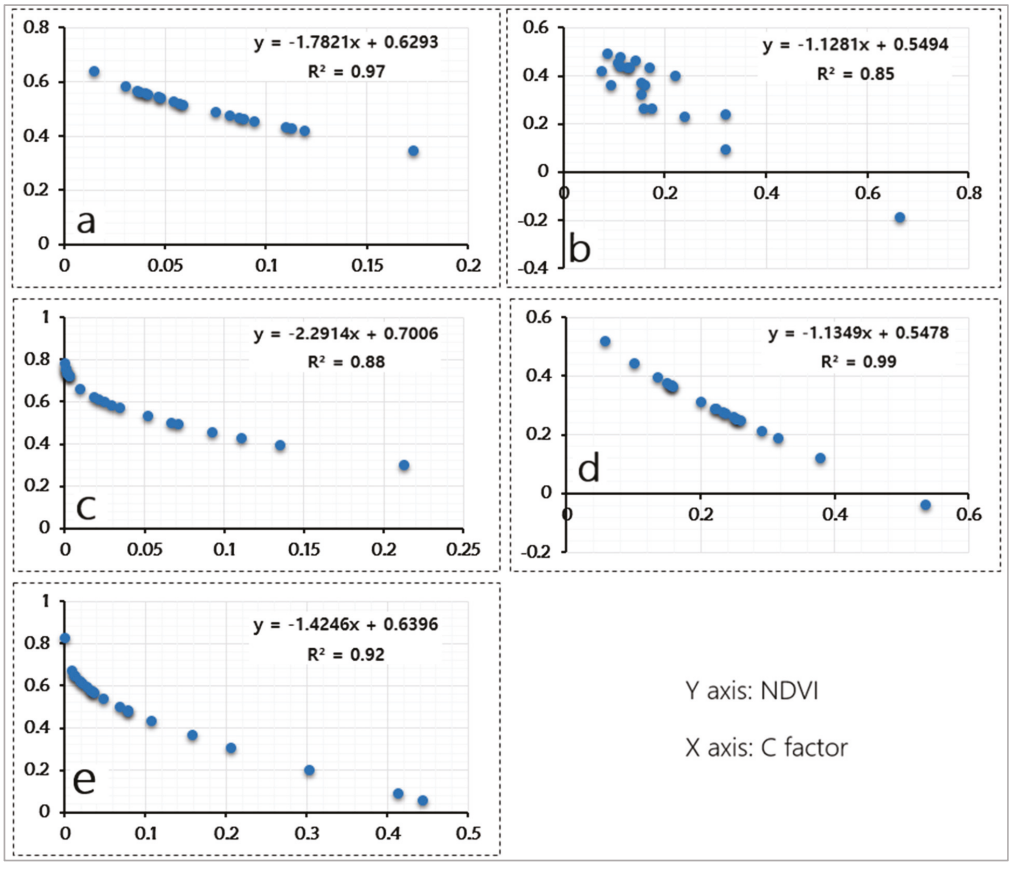

Figure 5. Correlation between NDVI and C-factor ($C_{vk}A$) for each year: (**a**) 2000, (**b**) 2005, (**c**) 2010, (**d**) 2015 and (**e**) 2018.

3.2. Influence of Soil Erodibility on NDVI-Derived C-Factor (CvkA)

The executed regression analysis revealed that the vegetation index-derived C-factor values were affected by the soil erodibility (K) values (Figure 6). The correlation analysis varied from 0.77 to 0.86. The sensitivity of the adapted C-factor estimation (CvkA) to the variation of soil background can be clarified through the spatial variability of soil erodibility (K) values in the study area. In the current study, an increase in the value of soil erodibility led to an increase in the values of NDVI-derived C-factor (Figure 6), while the magnitude probably changed following different seasons of a year. A higher value in the K-factor resulted in a higher near-infrared reflectance (NIR) band, while the lower the NIR reflectance, the lower NDVI values. This fact can explain the possible overestimation of the values in the prediction of soil erosion risk using the Cvk method under certain climate conditions, which may generate different K-factor values that compound the impact of the K-factor and NDVI-derived C-factor values in the RUSLE model (Figure 8).

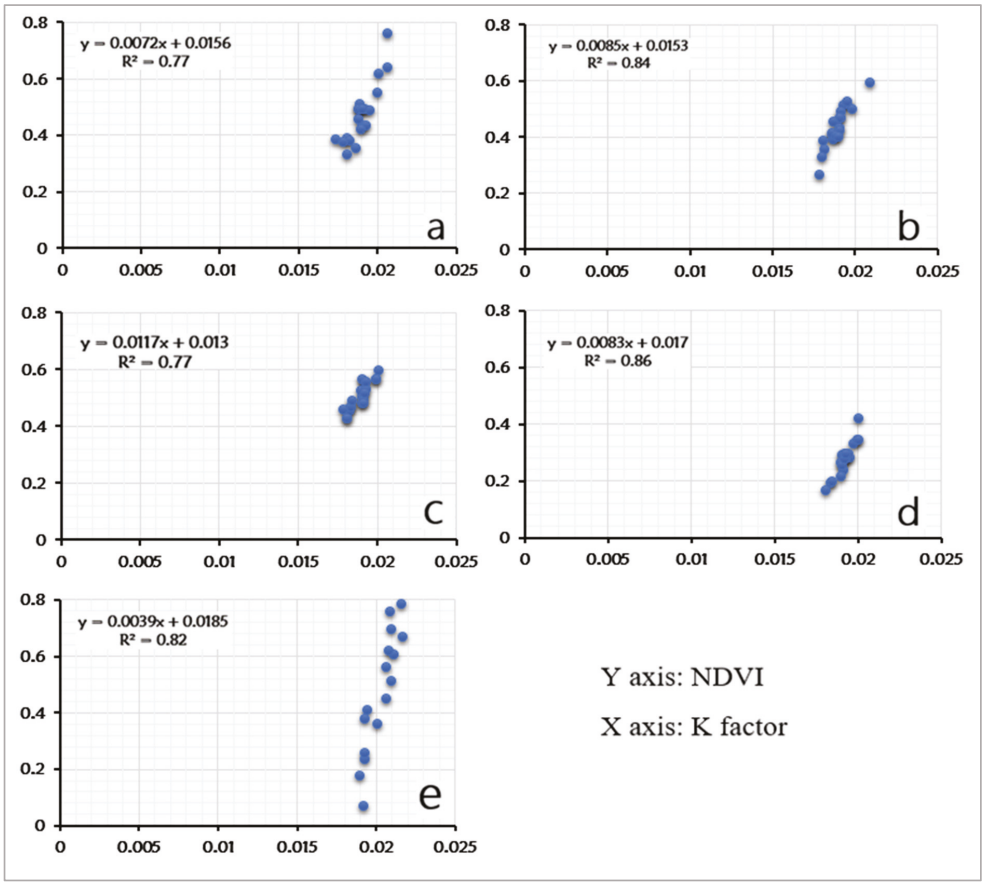

Figure 6. Impact of soil heterogeneity (classified as 1, K = 0.016 to 0.018; 2, K = 0.018 to 0.019; 3, K = 0. 019 to 0.02 and 4, K ≥ 0.02) on NDVI values for the period of study: (**a**) 2000, (**b**) 2005, (**c**) 2010 (**d**) 2015 and (**e**) 2018.

3.3. Influence of Rainfall on NDVI-Derived C-Factor (CovkA)

The correlation between annual mean NDVI and rainfall variable is shown in Figure 7. The studied period (2000–2018) clearly showed the geographical distribution of the relationship between NDVI and rainfall. The results revealed NDVI to be closely interacting with rainfall erosivity (Figure 7). The R^2 values were 0.83 in 2000, 0.79 in 2005, 0.71 in 2010, 0.74 in 2015 and 0.73 in 2018 (Figure 7). When the annual rainfall erosivity increased, the values of NDVI also increased at the same time. The analyses proved that more rainfall would definitely lead to higher NDVI value, which might affect the estimation of C-factor for accurate soil erosion predictions. The variation in annual NDVI was determined by climate variable including rainfall. The correlation between NDVI and rainfall is stronger due to the fact that rainfall is the dominant factor influencing vegetation growth in the area.

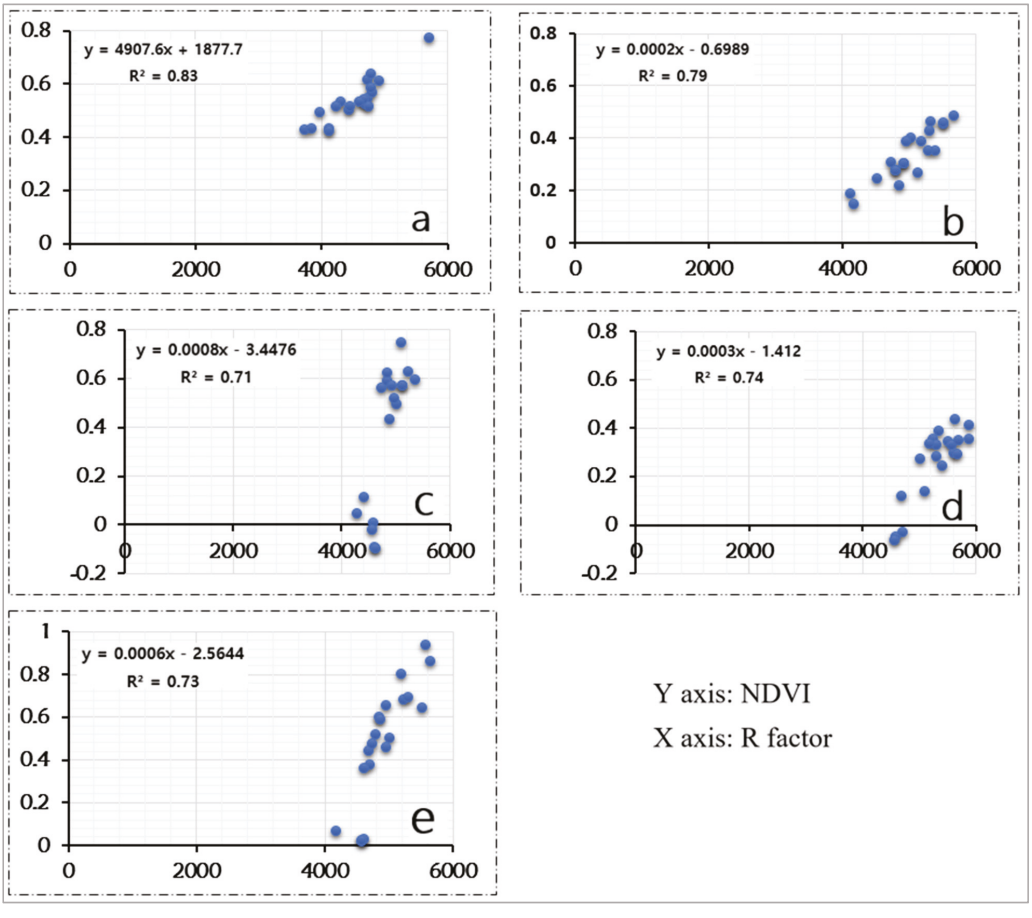

Figure 7. Correlation coefficients between NDVI and rainfall for the considered years: (**a**) 2000, (**b**) 2005, (**c**) 2010 (**d**) 2015 and (**e**) 2018.

3.4. Influence of Topographic Features on NDVI-Derived C-Factor ($C_{vk}A$)

The results showed that NDVI-derived $C_{vk}A$ values had a significant impact on the varying elevation of the area (Figure 8). The increase in NDVI values increased with elevation, mainly in high-elevation areas. NDVI values increased fast within elevation ranges between 1500 and 2000 m in 2000, 1800 and 2200 m in 2005, 1600 and 2400 m in 2010, 2000 and 2600 in 2015 and 1600 and 2000 m in 2018 (Figure 8). This latter point shows that topographic features have significant effects on the vegetation distribution in the study area.

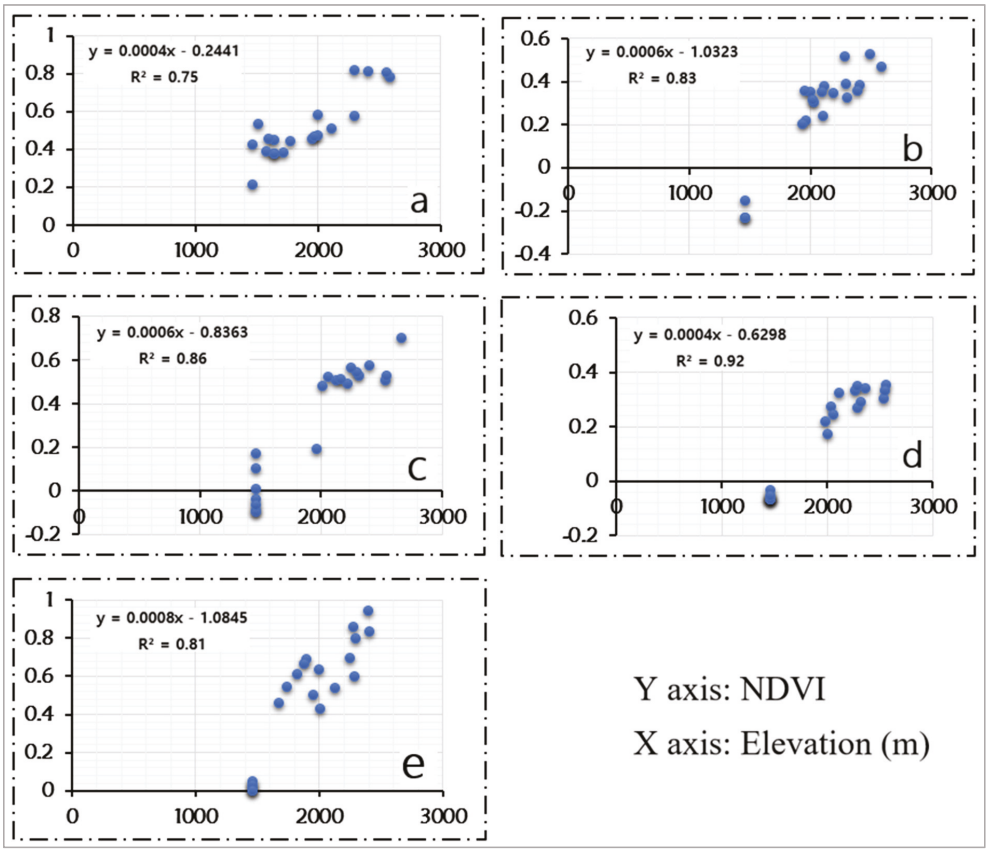

Figure 8. The relationships between NDVI and elevation for different considered years: (**a**) 2000, (**b**) 2005, (**c**) 2010, (**d**) 2010 and (**e**) 2018.

3.5. Soil Loss Rate Estimation

To facilitate the analysis and identify soil erosion severity classes that are of high priority for conservation practices, the estimated soil erosion maps (Figure 9) were classified into six categories. From total surface area (5883 km^2), erosion-prone areas were estimated at 4670.8 km^2 (79.4%). Based on the LULC, the remaining 20.6% in each was occupied by non-erosive lands. The results revealed a mean soil loss of 15.1 t ha^{-1} yr^{-1} in 2000, 47.4 t ha^{-1} yr^{-1} in 2005, 16.3 t ha^{-1} yr^{-1} in 2010, 66.8 t ha^{-1} yr^{-1} in 2015 and 15.3 t ha^{-1} yr^{-1} in 2018 for entirely erosive lands.

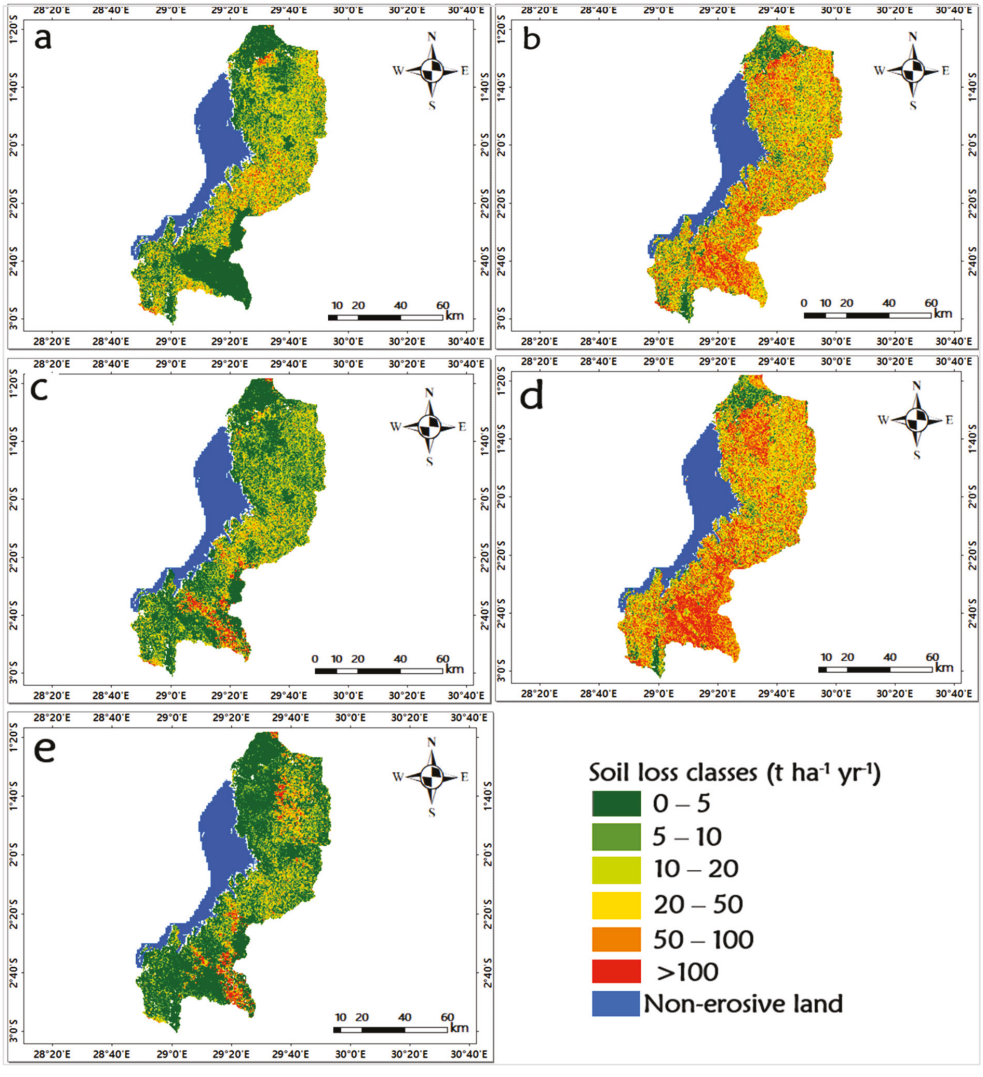

Figure 9. Spatial distribution of estimated soil erosion rates in the study area: (**a**) 2000, (**b**) 2005, (**c**) 2010, (**d**) 2015 and (**e**) 2018.

An estimated soil loss rate of ≤10 t ha^{-1} yr^{-1} was considered as a threshold for soil erosion rate tolerance; however, an area that experiences a soil erosion rate of >10 t ha^{-1} yr^{-1} occupied by the area with high erosion susceptibility requires urgent soil erosion control measures (Figure 9). Analyses showed that an area of about 2684.16 km^2 (57.5%) in 2000, 1017.2 Km^2 (21.8%) in 2005, 3033.86 km^2 (64.9%) in 2010, 724.32 km^2 (15.5%) in 2015 and 3445.87 km^2 (73.8%) in 2018 had a sustainable soil erosion rate tolerance (≤10 t ha^{-1} yr^{-1}). However, 1,985.84 km^2 (42.5%) in 2000, 3,652.8 km^2 (78.2%) in 2005, 1636.14 km^2 (35.1%) in 2010, 3945.68 km^2 (84.5%) in 2015 and 1224.13 km^2 (16.8%) had an unsustainable mean rate of soil loss tolerance (>10 t ha^{-1} yr^{-1}) (Figure 9 and Table 4). However, our study found a high increase in annual mean soil loss by 68.1% (15.11 t ha^{-1} yr^{-1} to 47.4 t ha^{-1} yr^{-1}) from 2000 to 2005 and 75.5% (16.3 t ha^{-1} yr^{-1} to 66.8 t ha^{-1} yr^{-1}) from 2010 to 2015, while the

small percentage increase in annual mean soil loss was found to be 1.3% (15.1 t ha^{-1} yr^{-1} to 15.3 t ha^{-1} yr^{-1}) from 2000 to 2018.

Table 4. The rates of estimated soil loss per class (of entire erosive lands of 4,670.8 km^2) corresponding to Figure 9.

Severity Categories	Soil Loss Classes	Area %					Mean Soil Loss Per Class (t ha^{-1} yr^{-1})				
		2000	2005	2010	2015	2018	2000	2005	2010	2015	2018
Very low	0–5	40.7	11.66	45.38	8.00	59.20	1.61	2.56	1.95	2.65	1.53
Low	5–10	16.8	10.12	19.58	7.51	14.60	7.34	7.42	7.24	7.47	7.14
Moderate	10–20	19.4	16.49	16.47	12.39	10.90	14.35	14.82	14.07	14.89	14.07
High	20–50	16.1	29.92	12.14	28.91	8.60	31.04	32.63	31.23	33.84	31.48
very High	50–100	5.9	18.29	3.89	19.59	3.50	67.89	70.96	67.63	71.55	68.49
Extremely High	>100	1.1	13.52	2.54	23.60	3.20	127.53	156.42	209.54	171.99	209.98

A soil erosion severity map was developed from the estimated soil erosion of the western province of Rwanda (Figure 9). The result showed that about 40.7% (1900.12 km^2), 45.4% (2119.3 km^2) and 59.2% (2764.44 km^2) of the total erosive land highly was in the very low category (0–5 t ha^{-1} yr^{-1}) of soil erosion risk in 2000, 2010 and 2018, which contributed to about 0.64%, 0.58% and 0.45% of the mean annual estimated soil loss, respectively. These results also show that only about 30% (1397.3 km^2) and 29% (1350.06 km^2) of the total erosive land was mostly covered by the category of high soil erosion rate (20–50 t ha^{-1} yr^{-1}) in 2005 and 2015, respectively (Table 3). High, very high and extremely high soil loss categories experienced increases of 13.8%, 12.4% and 12.42% in terms of total erosive land from 2000 to 2005 (Figure 9a,b), respectively, while increases of about 16.77%, 15.7 % and 21.06% were recorded from 2010 to 2015 (Figure 9c,d), respectively. Therefore, the high (20–50 t ha^{-1} yr^{-1}), very high (50–100 t ha^{-1} yr^{-1}) and extremely high (>100 t ha^{-1} yr^{-1}) erosion categories were found mainly in a small part of the Rusizi district (Bweyeye and Butare sectors), Nyamasheke district (Karambi, Mahembe, Cyato, Rangiro and Bushekeri sectors), Ngororero district (Muhanda sector) and in Nyabihu district (in Muringa Sector and north-east part of Kabatwa sector (Figure 9b,d,e). Commonly, this was mainly influenced by steep slopes in the area, rainfall intensity and land-cover management factors.

3.6. LULC Change and Its Impacts on Soil Erosion Rate

Classification and statistical results are presented in Figure 10 and Table 4, while estimated soil erosion rates per each LULC are shown in Table 5. We assessed the dynamics in LULC over eighteen years subdivided into different time intervals (2000, 2005, 2010, 2015 and 2018). The forest area revealed the most significant change. The significant decrease in forestland, which was closely doubled, reduced from 46.5% to 21.84% in 2000 and 2005, and from 42.14% to 23.99% in 2010 to 2015, respectively. This decreasing trend from forestland occurred due to the expense of the increase in cropland from 32.2% in 2000 to 57.29% in 2005, as well as from 33.79% in 2010 to 46.18 % in 2015, respectively. The estimated grassland cover was about 3.28%, 3.6%, 5.76%, 9.75% and 9.23% of the total area in 2000, 2005, 2010, 2015 and 2018, respectively.

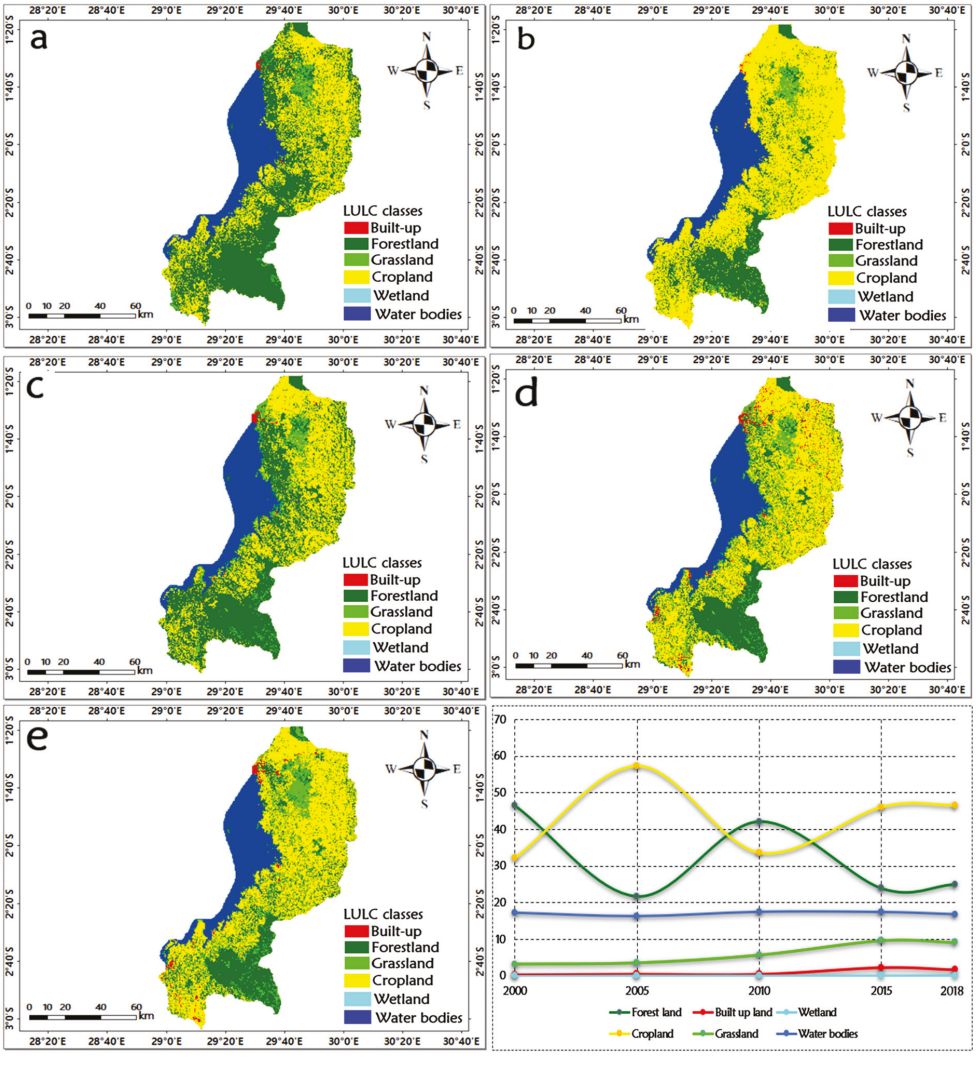

Figure 10. Change detection in LULC: (**a**) 2000, (**b**) 2005, (**c**) 2010, (**d**) 2015 and (**e**) 2018.

Table 5. Statistical changes for LULC (2000–2018).

LULC Types	2000	2005	2010	2015	2018
Forest land	46.5	21.84	42.14	23.99	25.12
Built up land	0.43	0.6	0.57	2.39	1.8
Wetland	0.23	0.24	0.24	0.24	0.25
Cropland	32.28	57.29	33.79	46.18	46.7
Grassland	3.28	3.6	5.76	9.75	9.23
Water bodies	17.28	16.43	17.5	17.45	16.9

Considering the entire surface area, the net annual forest loss was 53% from 2000 to 2005, and 43% from 2010 to 2015, respectively (Table 5). The built-up area had less significant land cover, but steadily increased from 0.43% to 0.6 and 0.57 to 2.39% between

2000 and 2005, and between 2010 and 2015, respectively. This increase is due to a decrease in forestland, resulting in an increase of mean soil loss in the cropland from 15.6 t/ha/yr to 34.3 t/ha/yr between 2000 and 2005 and from 10.4 t/ha/yr to 45.41 t/ha/yr between 2010 and 2015 (Table 6). Therefore, there was a mean increase of 18.7 t/ha/yr (about 120%) and 35.01 t/ha/yr (about 337%) from 2000 to 2005 and 2010 to 2015 in cropland, respectively; these values were generated at the expense of a high decrease in forest cover (Table 5).

Table 6. Mean soil erosion (t/ha/yr) per each LULC class.

LULC	Mean Soil Loss in 2000	Mean Soil Loss in 2005	Mean Soil Loss in 2010	Mean Soil Loss in 2015	Mean Soil Loss in 2018
Forestland	14.7	69.8	21.4	111.7	22.6
Grassland	15.6	34.3	12.3	64.7	24.1
Cropland	15.7	39.7	10.4	45.41	9.5
Built up	4.7	45.4	7.8	27.5	4.1

3.7. Estimated Mean Soil Loss for Each LULC Category

Comparing the soil erosion based on land-use types, the results showed a significant increase in the estimated soil erosion rates in cropland in 2005 and 2015 (Table 6). A decline in this type of land was found in 2010 and 2018. Cropland covered about 32.2%, 57%, 33.7%, 46.1% and 46% of the total studied area in 2000, 205, 2010, 2015 and 2018. However, it is responsible for about 31%, 21%, 20%, 18.2%, and 16% of the total predicted soil loss in 2000, 2005, 2010, 2015 and 2018, respectively. From 2000 to 2005 and 2010 to 2015, the predicted mean soil erosion in cropland is more than two times (15.6 t/ha/yr to 34.3 t/ha/yr) and more than four times (10.4 t/ha/yr to 45.41 t/ha/yr) higher than mean soil erosion rates, respectively (Table 6). Water bodies are considered as non-erosive land. The forestland and grassland are expected to have low erosion rates, but the results show that meant soil loss increased. Therefore, the poor coverage of trees due to a decline in forestland in the steep slopes accelerates soil erosion rates in the area.

3.8. Soil Erosion Probability Zones

The zones with a probability of soil erosion have been classified into six categories, including very low, low, moderate, high, very high and extremely high risk. It was observed that approximately 44.9% of the total eroded land produced a very high mean soil erosion of 697.6 t ha^{-1} yr^{-1} (Figure 11), while zones with high probability occupied 42.9% of the total eroded land, with 315 t ha^{-1} yr^{-1} mean soil loss. That said, zones of extremely high probability were found to cover 5.03% of the total eroded land, producing a mean soil loss of 1164.6 t ha^{-1} yr^{-1}. Therefore, the three smallest probability zones were very low, low and moderate, which covered about 0.46%, 2.10% and 4.5% of the total eroded area and produced a mean soil loss of 3.47 t ha^{-1} yr^{-1}, 32.79 t ha^{-1} yr^{-1} and 75.8 t ha^{-1} yr^{-1}, respectively.

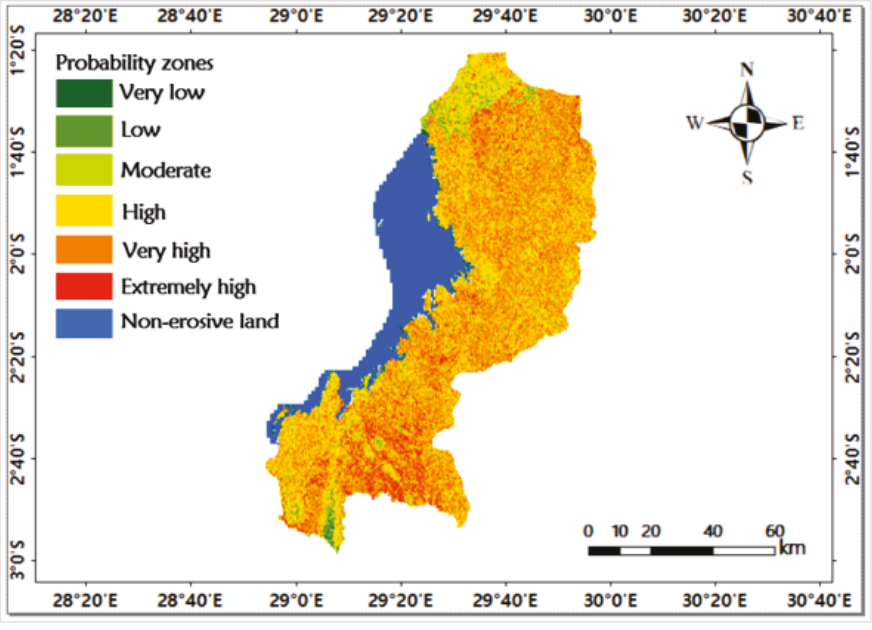

Figure 11. Zones with probability of soil erosion.

4. Discussion

4.1. Cover Management (C) Factor and Biophysical Variables

The change in soil loss prediction can be reflected by NDVI with some variation in the values of cover management practices. The C-factor is one of the decisive parameters of the RUSLE, preventing bias from any C-factor estimation approach, which affects the prediction of soil erosion rate estimations [46]. For this, estimating the C-factor using NDVI by considering biophysical variables should be taken into account, as the applied equation has an influence on the estimated values. For this reason, the NDVI used to estimate C-factor was analyzed by checking its sensitivity to some biophysical factors such as rainfall, elevation and soil erodibility. The results revealed a good agreement between both variables (NDVI and biophysical factors) with acceptable and good correlation coefficients (Figures 5–8). This is in agreement with a previous study [42] reporting that the NDVI-derived C-factor used to estimate soil erosion can be sensitive to different biophysical variables, such as soil condition, topographic features and vegetation phenology. In this sense, Jin and Zhang [47] argued that the spatial distribution of vegetation cover through NDVI was usually affected by elevation, concluding that elevation was the main controlling factor in vegetation growth in their study area. The result of this study revealed that variation in annual NDVI was determined by climate variable including rainfall; this is aligned with an earlier study [48] that reported that various climate factors, including rainfall, played a vital role in vegetation growth. Moreover, topographic reasons also conformed with an earlier study [19] that argued that highly mountainous and elevated sites are susceptible to soil erosion due to the domination of high inclination slopes and heavy rainfall distribution. Ayalew and Deumlich [42] revealed that a higher erodibility condition was associated with higher C-factor values which, in turn, might affect the prediction of soil erosion. To this end, this study found that the Van der Knijff and Jones [44] approach (Cvk) was not fit to estimate the C-factor in the study area, as it overestimated the values [18]. This can be clarified by the fact that this approach assessed the monthly C-factor based on NDVI and then calibrated the factor in a European study area that was totally different from the current study area (tropical) in terms of climate conditions

and vegetation features. This is in agreement with Almagro and Thomé [43], who found underestimated Cvk values and concluded that this method was not suitable for tropical regions such as Rwanda; thus, this approach should be changed to CvkA. Generally, this study adapted the aforementioned equation by also performing a correlation analysis between the used NDVI and the produced C-factor (Figure 5), leading to a good result in the prediction of soil loss in the study area without overestimation.

4.2. Variation in Land Use Land Cover and Soil Erosion

This study found that the main reason behind an accelerated soil erosion rate is attributable to changes in LULC (Figure 10). The changes were depicted by the expansion of agricultural areas resulting from the decrease in forestland, steep slopes and high annual rainfall, which are also considered to be core soil erosion risk factors. Compared with different parts of the world, studies [49–51] have disclosed different rates of mean soil erosion under different land uses. The same conclusion was reached for the average annual soil losses following the fluctuation of land-use types triggered by changing rainfall patterns, while the highest estimated average annual soil loss per LULC has been accredited to seasonal agricultural land [52]. Moreover, based on global circulation models (GCMs) data, projected future storm rainfall and soil erosion rates in a monsoon-dominated region of eastern India showed that these regions were challenged by relatively greater erosion problems triggered by intense precipitation. They concluded that the loss of soils during erosion processes leads to decline in soil fertility, and thus the deterioration of soil resources in the region; this consequence should be expected in the study area examined in this paper. All the aforementioned drivers could be accelerated by LULC change, as the area showed dynamism. In the study area, the LULC change affecting soil erosion can be depicted clearly in the areas where a decrease in forestland and expansion of cropland areas resulted in an increase in the mean soil erosion of cropland cover from 2000 to 2005 and from 2010 to 2015 (Table 6). Previous studies found that the LULC change affects soil erosion rates by producing higher mean soil loss [18,25,30]. In the temperate forest zone of Russia characterized by multifaceted levels of land-use history, Zhidkin and Fomicheva [53] compared the simulated rates of soil erosion given by two models based on the type of precipitation (rainfall and snow erosion). Concerning rainfall acting as a trigger and the same types of land-use cover as examined in this present study, they found that variations in arable land (cropland) area and cropping structure were factors that determined changes in soil erosion to a greater extent, while other factors had no directional trend. This latter point is in accordance with the findings of this study, where the risk of erosion increases when land use changes from forestland in 2000 and 2010 to cropland in 2005 and 2015, respectively (Figure 10). The features of each LULC category could be considered in changing the average soil loss estimated from one land-use class to another [54,55]. Similar to this study, some LULC types such as cropland and built-up land increased, while others, including forestland, decreased (Figure 10). The change in forestland to uncontrolled agricultural lands is the main cause blamed for the increase in soil erosion, with triggers such as heavy rainfall and the length and steepness of slopes (Figure 9); these results are in accordance with a study [52] conducted in Kenya located in the same region as our case study disclosing that the increment of slope steepness and its length (LS-factor) increases the level of soil erosion due to the high velocity and erosivity of runoff. Generally, in rural areas of the western province, a large number of the residents depends on agriculture as a means of livelihood [56]. Land scarcity for agriculture and the continuous increase in demand for agricultural commodities are the main reasons pushing communities to convert forest and grasslands into cultivated lands [56]. Unfortunately, unprecedented climate changes are expected in the region, and the most prominent climatic change impact on rain-fed agriculture results in a reduction in crop productivity [57,58]. Thus, areas with a considerable conversion from forest to less vegetated areas, coupled with steep slopes and rainfall intensity, in the study area should expect higher soil erosion potential [25,59–61].

4.3. Estimation of Soil Loss and Probability Zones

Table 4 shows the estimated soil erosion intensity classes and the mean soil erosion rate of a certain magnitude of soil loss and its area coverage over the previous two decades. In the entire study area, soil erosion severity was classified from very low to extremely high. These classes were concentrated in cultivated land and steep slope areas, which indicated that areas in these categories were highly susceptible to soil erosion. These findings are in accordance with a previous study [62] providing details on the intensity of soil erosion in different slope gradients, whereby the analysis of soil erosion intensity exhibited a slightly intense erosion on largely gentle (<5°) slope terrains and steep terrains (15–25°), while severe soil erosion was found to be on moderate (5–15°) slopes. However, the very low and low soil erosion classes fell under a <10 t ha^{-1} yr^{-1} severity class, making them less susceptible to soil erosion based on slope gradient [25,30]. This study also indicates a significant increase in high, very high and extremely high soil erosion severity classes of about 13.85, 12.3% and 12.42%, respectively, between 2000 and 2005. Increases of about 16.77%, 15.7% and 21.06%, were found in high, very high and extremely high soil erosion severity class, respectively, from 2010 to 2015, accelerated by the expansion of cropland in steep slopes. Nevertheless, a small decline in three severity classes (very low, low, moderate) from 2005 to 2010 and from 2015 to 2018 resulted from various conservation activities implemented by local leaders and sector land officers in the study area for sustainable land-use management [25,29]. The activities include the implementation of bench terraces on steep cultivated land and afforestation campaigns. While this optimistic initiative to lessen the soil loss caused by erosion has proven popular, problems related to clearing natural forests and unsuitable cultivation on steep slopes still exist. Therefore, rainfall intensity and forest clearance become core factors for increasing zones prone to soil erosion within the study area. It was also demonstrated that about 44.9 % of the study area fell under very high soil erosion risk, while high-probability zones covered 42.9% of the study areas (Figure 11). Compared with an earlier study [63] in the Urmodi river watershed (India), a significant output regarding increased conversion was obtained from very slight to very severe risk zone; research concluded the existence of extensive variation in very severe soil vulnerable risk zones over the study period. Overall, the findings of this study and other studies carried out in Rwanda and east African regions similar to results reported by Karamage [30,62], which seem to overestimate soil loss rates.

The conversion of lower to higher risk category areas of soil erosion was detected all over the study area. Hence, croplands and grasslands, with their related conversions as the main LULC classes, should lead the immediate execution of more suitable agricultural practices; terracing integrated with surface residue mulching and cover-cropping and cross-slope farming should be suggested for reducing soil erosion potential within agricultural areas in the western province of Rwanda.

5. Conclusions

In this study, an adapted approach (CvkA) for the estimation of cover management (C) factor from RUSLE was explored in comparison with the formerly used approach (Cvk) based on NDVI. We also analyzed the correlation between the adapted C-factor (CvkA), NDVI and different biophysical variables such as the rainfall, elevation and soil erodibility. The Cvk approach presented an overestimation of the C-factor values, making it unsuitable for the study area. Therefore, using the adapted C-factor, which was found to be suitable for this study, we analyzed the impacts of LULC dynamics on soil erosion risk in agricultural areas of the western province of Rwanda. The results showed significant correlations between the NDVI and the biophysical variables, which implied that using remote sensing data to capture the spatial and temporal changes in C-factor estimation can serve as an input factor for soil erosion modeling procedures that can themselves be enhanced by considering the quantified sensitivity of NDVI-based C-factor estimations.

Moreover, the results revealed that the area experienced estimated annual mean soil losses of about 15.1 t ha^{-1} yr^{-1}, 47.4 t ha^{-1} yr^{-1}, 16.3 t ha^{-1} yr^{-1}, 66.8 t ha^{-1} yr^{-1} and

15.3 t ha^{-1} yr^{-1} in 2000, 2005, 2010, 2015 and 2018, respectively. However, cropland experienced a great increase in soil loss during the period when there was a decline in forests (2000–2005 and 2010–2015). It was also observed that the rate of erosion varied based on steep slopes and LULC changes. The noted differences in the studied period indicated that LULC changes affected the rate of soil erosion significantly. The application of the weighted index overlay (WIO) method supported the categorizing of areas into different probable zones of soil erosion risk, which was useful for developing sustainable soil conservation measures. The estimated amount of soil loss suggests the urgent implementation of conservation practices such as terracing, integrated with surface residue mulching and cover cropping and cross-slope farming in the study area. The results of this study may be useful for soil and water conservation planning and soil loss estimations. However, the application of the adapted C-factor (CvkA) approach can be used in similar tropical regions after evaluating its performance. Future research should attempt to compare NDVI with other spectral indices such as the soil adjusted vegetation index and enhanced vegetation index in the context of C-factor estimation.

Author Contributions: Conceptualization, A.P.M., L.L. and W.L.; methodology and data curation, A.P.M. and R.M.; software and visualization, P.M.K. and V.N.; formal analysis and writing the original draft preparation, A.P.M.; review and editing previous draft versions, L.N., R.M., A.U., S.U.; supervision and funding acquisition, L.L. All authors have read and agreed to the published version of the manuscript.

Funding: This research funded by the key program for international cooperation of the Bureau of International Cooperation, Chinese Academy of Sciences: 151542KYSB20200018; Sino-Africa Joint Research Center of Chinese Academy of Sciences: SAJC202107.

Acknowledgments: This study was funded and supported by the key program for international cooperation of the Bureau of International Cooperation, Chinese Academy of Sciences (Grant No.151542KYSB20200018) and the Sino-Africa Joint Research Center of Chinese Academy of Sciences (Grant Number: SAJC202107). The authors are also thankful to Tianshan Station for Snow cover and Avalanche Research for its remarkable assistance in the data collection and processing.

Conflicts of Interest: The authors declare no conflict of interest.

References

1. Nunes, A.N.; de Almeida, A.C.; Coelho, C.O. Impacts of land use and cover type on runoff and soil erosion in a marginal area of Portugal. *Appl. Geogr.* **2011**, *31*, 687–699. [CrossRef]
2. Crosson, P.; Pimentel, D.; Harvey, C.; Resosudarno, P.; Sinclair, K.; Kurz, D.; Fitton, L. Soil erosion estimates and costs. *Science* **1995**, *269*, 461–466.
3. Borrelli, P.; Robinson, D.A.; Fleischer, L.R.; Lugato, E.; Ballabio, C.; Alewell, C.; Ferro, V. An assessment of the global impact of 21st century land use change on soil erosion. *Nat. Commun.* **2017**, *8*, 2013. [CrossRef]
4. Ganasri, B.; Ramesh, H. Assessment of soil erosion by RUSLE model using remote sensing and GIS-A case study of Nethravathi Basin. *Geosci. Front.* **2016**, *7*, 953–961. [CrossRef]
5. Zare, M.; Panagopoulos, T.; Loures, L. Simulating the impacts of future land use change on soil erosion in the Kasilian watershed, Iran. *Land Use Policy* **2017**, *67*, 558–572. [CrossRef]
6. García-Ruiz, J.M.; Beguería, S.; Nadal-Romero, E.; González-Hidalgo, J.C.; Lana-Renault, N.; Sanjuán, Y. A meta-analysis of soil erosion rates across the world. *Geomorphology* **2015**, *239*, 160–173. [CrossRef]
7. De Vente, J.; Poesen, J.; Verstraeten, G.; Govers, G.; Vanmaercke, M.; Van Rompaey, A.; Arabkhedri, M.; Boix-Fayos, C. Predicting soil erosion and sediment yield at regional scales: Where do we stand? *Earth Sci. Rev.* **2013**, *127*, 16–29. [CrossRef]
8. Shi, Z.H.; Ai, L.; Fang, N.F.; Zhu, H.D. Modeling the impacts of integrated small watershed management on soil erosion and sediment delivery: A case study in the Three Gorges Area, China. *J. Hydrol.* **2012**, *438*, 156–167. [CrossRef]
9. Fistikoglu, O.; Harmancioglu, N.B. Integration of GIS with USLE in assessment of soil erosion. *Water Resour. Manag.* **2002**, *16*, 447–467. [CrossRef]
10. Li, P.; Mu, X.; Holden, J.; Wu, Y.; Irvine, B.; Wang, F.; Gao, P.; Zhao, G.; Sun, W. Comparison of soil erosion models used to study the Chinese Loess Plateau. *Earth -Sci. Rev.* **2017**, *170*, 17–30. [CrossRef]
11. Alkharabsheh, M.M.; Alexandridis, T.K.; Bilas, G.; Misopolinos, N.; Silleos, N. Impact of land cover change on soil erosion hazard in northern Jordan using remote sensing and GIS. *Procedia Environ. Sci.* **2013**, *19*, 912–921. [CrossRef]
12. De Vente, J.; Poesen, J. Predicting soil erosion and sediment yield at the basin scale: Scale issues and semi-quantitative models. *Earth Sci. Rev.* **2005**, *71*, 95–125. [CrossRef]

13. Renard, K.G. *Predicting Soil Erosion by Water: A Guide to Conservation Planning with the Revised Universal Soil Loss Equation (RUSLE)*; United States Government Printing: Washington, DC, USA, 1997.
14. Karamage, F.; Zhang, C.; Liu, T.; Maganda, A.; Isabwe, A. Soil erosion risk assessment in Uganda. *Forests* **2017**, *8*, 52. [CrossRef]
15. Erdogan, E.H.; Erpul, G.; Bayramin, I. Use of USLE/GIS Methodology for Predicting Soil Loss in a Semiarid Agricultural Watershed. *Environ. Monit. Assess.* **2006**, *131*, 153–161. [CrossRef] [PubMed]
16. Chandramohan, T.; Durbude, D.G. Estimation of soil erosion potential using universal soil loss equation. *J. Indian Soc. Remote Sens.* **2002**, *30*, 181–190. [CrossRef]
17. Da Silva, R.M.; Montenegro, S.M.G.L.; Santos, C.A.G. Integration of GIS and remote sensing for estimation of soil loss and prioritization of critical sub-catchments: A case study of Tapacurá catchment. *Nat. Hazards* **2012**, *62*, 953–970. [CrossRef]
18. Nyesheja, E.M.; Chen, X.; El-Tantawi, A.M.; Karamage, F.; Mupenzi, C.; Nsengiyumva, J.B. Soil erosion assessment using RUSLE model in the Congo Nile Ridge region of Rwanda. *Phys. Geogr.* **2019**, *40*, 339–360. [CrossRef]
19. Byizigiro, R.V.; Rwanyiziri, G.; Mugabowindekwe, M.; Kagoyire, C.; Biryabarema, M. Estimation of Soil Erosion Using RUSLE Model. and GIS: The Case of Satinskyi Catchment, Western Rwanda. *Rwanda, J. Eng. Sci. Technol. Environ.* **2020**, *3*, 20–56. [CrossRef]
20. Niyonsenga, J.D.; Mugabowindekwe, M.; Mupenzi, C. Spatial analysis of soil erosion sensitivity using the revised universal soil loss equation model in Nyamasheke District, Western Province of Rwanda. *Trans. GIS* **2021**, *25*, 735–750. [CrossRef]
21. Bosco, C.; de Rigo, D.; Dewitte, O.; Poesen, J.; Panagos, P. Modelling soil erosion at European scale: Towards harmonization and reproducibility. *Nat. Hazards Earth Syst. Sci.* **2015**, *15*, 225–245. [CrossRef]
22. Van der Knijff, J.; Jones, R.; Montanarella, L. *Soil Erosion Risk: Assessment in Europe*; European Soil Bureau, European Commission Brussels: Brussels, Belgium, 2000.
23. Jordan, G.; Van Rompaey, A.; Szilassi, P.; Csillag, G.; Mannaerts, C.; Woldai, T. Historical land use changes and their impact on sediment fluxes in the Balaton basin (Hungary). *Agric. Ecosyst. Environ.* **2005**, *108*, 119–133. [CrossRef]
24. Hassan, Z.; Shabbir, R.; Ahmad, S.S.; Malik, A.H.; Aziz, N.; Butt, A.; Erum, S. Dynamics of land use and land cover change (LULCC) using geospatial techniques: A case study of Islamabad Pakistan. *SpringerPlus* **2016**, *5*, 812. [CrossRef] [PubMed]
25. Nambajimana, J.d.D.; He, X.B.; Zhou, J.; Justine, M.F.; Li, J.L.; Khurram, D.; Mind'je, R.; Nsabimana, G. Land use change impacts on water erosion in Rwanda. *Sustainability* **2020**, *12*, 50. [CrossRef]
26. Twagiramungu, F. Environmental profile of Rwanda. *Consult. Rep.* **2006**, 78–254.
27. Clay, D.C.; Lewis, L.A. Land use, soil loss, and sustainable agriculture in Rwanda. *Case Stud. Hum. Ecol.* **1996**, 271–287.
28. Sharma, A.; Tiwari, K.N.; Bhadoria, P. Effect of land use land cover change on soil erosion potential in an agricultural watershed. *Environ. Monit. Assess.* **2011**, *173*, 789–801. [CrossRef] [PubMed]
29. Kabirigi, M.; Mugambi, S.; Musana, B.S.; Ngoga, G.T.; Muhutu, J.C.; Rutebuka, J.; Ruganzu, V.; Nzeyimana, I.; Nabahungu, N.L. Estimation of soil erosion risk, its valuation and economic implications for agricultural production in western part of Rwanda. *J. Exp. Biol. Agric. Sci.* **2017**, *5*, 525–536. [CrossRef]
30. Karamage, F.; Zhang, C.; Ndayisaba, F.; Shao, H.; Kayiranga, A.; Fang, X.; Nahayo, L.; Muhire Nyesheja, E.; Tian, G. Extent of cropland and related soil erosion risk in Rwanda. *Sustainability* **2016**, *8*, 609. [CrossRef]
31. Muhire, I.; Ahmed, F.; Elbasit, M.A. Spatio-temporal variations of rainfall erosivity in Rwanda. *J. Soil Sci. Environ. Manag.* **2015**, *6*, 72–83.
32. Kayumba, P.M.; Chen, Y.; Mind'je, R.; Mindje, M.; Li, X.; Maniraho, A.P.; Umugwaneza, A.; Uwamahoro, S. Geospatial land surface-based thermal scenarios for wetland ecological risk assessment and its landscape dynamics simulation in Bayanbulak Wetland, Northwestern China. *Landsc. Ecol.* **2021**, *36*, 1699–1723. [CrossRef]
33. Prasannakumar, V.; Vijith, H.; Abinod, S.; Geetha, N.J. Estimation of soil erosion risk within a small mountainous sub-watershed in Kerala, India, using Revised Universal Soil Loss Equation (RUSLE) and geo-information technology. *Geosci. Front.* **2012**, *3*, 209–215. [CrossRef]
34. Van Dijk, A.; Bruijnzeel, L.; Rosewell, C. Rainfall intensity–kinetic energy relationships: A critical literature appraisal. *J. Hydrol.* **2002**, *261*, 1–23. [CrossRef]
35. Morgan, R. Assessment of soil erosion risk in England and Wales. *Soil Use Manag.* **1985**, *1*, 127–131. [CrossRef]
36. Desmet, P.; Govers, G. A GIS procedure for automatically calculating the USLE LS factor on topographically complex landscape units. *J. Soil Water Conserv.* **1996**, *51*, 427–433.
37. McCool, D.K.; Brown, L.C.; Foster, G.R.; Mutchler, C.K.; Meyer, L.D. Revised slope steepness factor for the Universal Soil Loss Equation. *Trans. ASAE* **1987**, *30*, 1387–1396. [CrossRef]
38. Patil, R.; Sharma, S. Remote Sensing and GIS based modeling of crop/cover management factor (C) of USLE in Shakker river watershed. In Proceedings of the 2nd International Conference on Chemical, Agricultural and Medical Sciences (CAMS-2013), Kuala Lumpur, Malaysia, 29–30 December 2013.
39. Onyia, N.N.; Balzter, H.; Berrio, J.-C. Normalized difference vegetation vigour index: A new remote sensing approach to biodiversity monitoring in oil polluted regions. *Remote Sens.* **2018**, *10*, 897. [CrossRef]
40. Aburas, M.M.; Abdullah, S.H.; Ramli, M.F.; Ash'aari, Z.H. Measuring land cover change in Seremban, Malaysia using NDVI index. *Procedia Environ. Sci.* **2015**, *30*, 238–243. [CrossRef]
41. Ding, Y.; Zhao, K.; Zheng, X.; Jiang, T. Temporal dynamics of spatial heterogeneity over cropland quantified by time-series NDVI, near infrared and red reflectance of Landsat 8 OLI imagery. *Int. J. Appl. Earth Obs. Geoinf.* **2014**, *30*, 139–145. [CrossRef]

42. Ayalew, D.A.; Deumlich, D.; Šarapatka, B.; Doktor, D. Quantifying the sensitivity of NDVI-based C factor estimation and potential soil erosion prediction using Spaceborne earth observation data. *Remote Sens.* **2020**, *12*, 1136. [CrossRef]
43. Almagro, A.; Thomé, T.C.; Colman, C.B.; Pereira, R.B.; Junior, J.M.; Rodrigues, D.B.; Oliveira, P.T. Improving cover and management factor (C-factor) estimation using remote sensing approaches for tropical regions. *Int. Soil Water Conserv. Res.* **2019**, *7*, 325–334. [CrossRef]
44. Van der Knijff, J.; Jones, R.; Montanarella, L. *Soil Erosion Risk Assessment in Italy*; CiteSeer: Princeton, NJ, USA, 1999.
45. Shin, S.K.; Noh, H.; Kang, S.W.; Seo, B.J.; Lee, I.H.; Song, H.Y.; Choi, K.H.; Ha, S.K.; Lee, H.Y.; Han, D.S. Risk factors influencing the decline of residual renal function in continuous ambulatory peritoneal dialysis patients. *Perit. Dial. Int.* **1999**, *19*, 138–142. [CrossRef]
46. Tanyaş, H.; Kolat, Ç.; Süzen, M.L. A new approach to estimate cover-management factor of RUSLE and validation of RUSLE model in the watershed of Kartalkaya Dam. *J. Hydrol.* **2015**, *528*, 584–598. [CrossRef]
47. Jin, X.M.; Zhang, Y.K.; Schaepman, M.E.; Clevers, J.G.; Su, Z.; Cheng, J.; Jiang, J.; van Genderen, J. Impact of elevation and aspect on the spatial distribution of vegetation in the Qilian mountain area with remote sensing data. In Proceedings of the 21st ISPRS Congress, Beijing, China, 3–11 July 2008.
48. Pei, Z.; Fang, S.; Yang, W.; Wang, L.; Wu, M.; Zhang, Q.; Han, W.; Khoi, D.N. The relationship between NDVI and climate factors at different monthly time scales: A case study of grasslands in inner Mongolia, China (1982–2015). *Sustainability* **2019**, *11*, 7243. [CrossRef]
49. Koirala, P.; Thakuri, S.; Joshi, S.; Chauhan, R. Estimation of soil erosion in Nepal using a RUSLE modeling and geospatial tool. *Geosciences* **2019**, *9*, 147. [CrossRef]
50. Ajibade, F.O.; Nwogwu, N.A.; Adelodun, B.; Abdulkadir, T.S.; Ajibade, T.F.; Lasisi, K.H.; Fadugba, O.G.; Owolabi, T.A.; Olajire, O.O. Application of RUSLE integrated with GIS and remote sensing techniques to assess soil erosion in Anambra State, South-Eastern Nigeria. Journal of Water and Climate Change. 2020 Dec 1;11(S1):407-22. Application of RUSLE integrated with GIS and remote sensing techniques to assess soil erosion in Anambra State, South.-Eastern Nigeria. *J. Water Clim. Chang.* **2020**, *11*, 407–422.
51. Thapa, P. Spatial estimation of soil erosion using RUSLE modeling: A case study of Dolakha district, Nepal. *Environ. Syst. Res.* **2020**, *9*, 1–10. [CrossRef]
52. Kogo, B.K.; Kumar, L.; Koech, R. Impact of Land Use/Cover Changes on Soil Erosion in Western Kenya. *Sustainability* **2020**, *12*, 9740. [CrossRef]
53. Zhidkin, A.; Fomicheva, D.; Ivanova, N.; Dostál, T.; Yurova, A.; Komissarov, M.; Krása, J. A detailed reconstruction of changes in the factors and parameters of soil erosion over the past 250 years in the forest zone of European Russia (Moscow region). *Int. Soil Water Conserv. Res.* **2021**, in press. [CrossRef]
54. Gessesse, B.; Bewket, W.; Bräuning, A. Model.-based characterization and monitoring of runoff and soil erosion in response to land use/land cover changes in the Modjo watershed, Ethiopia. *Land Degrad. Dev.* **2015**, *26*, 711–724. [CrossRef]
55. Kidane, M.; Bezie, A.; Kesete, N.; Tolessa, T. The impact of land use and land cover (LULC) dynamics on soil erosion and sediment yield in Ethiopia. *Heliyon* **2019**, *5*, e02981. [CrossRef]
56. Mind'je, R.; Li, L.; Amanambu, A.C.; Nahayo, L.; Nsengiyumva, J.B.; Gasirabo, A.; Mindje, M. Flood susceptibility modeling and hazard perception in Rwanda. *Int. J. Disaster Risk Reduct.* **2019**, *38*, 101211. [CrossRef]
57. Karimi, V.; Karami, E.; Keshavarz, M. Climate change and agriculture: Impacts and adaptive responses in Iran. *J. Integr. Agric.* **2018**, *17*, 1–15. [CrossRef]
58. Rowhani, P.; Lobell, D.B.; Linderman, M.; Ramankutty, N. Climate variability and crop production in Tanzania. *Agric. For. Meteorol.* **2011**, *151*, 449–460. [CrossRef]
59. Kagabo, D.M.; Stroosnijder, L.; Visser, S.M.; Moore, D. Soil erosion, soil fertility and crop yield on slow-forming terraces in the highlands of Buberuka, Rwanda. *Soil Tillage Res.* **2013**, *128*, 23–29. [CrossRef]
60. Karamage, F.; Shao, H.; Chen, X.; Ndayisaba, F.; Nahayo, L.; Kayiranga, A.; Omifolaji, J.K.; Liu, T.; Zhang, C. Deforestation effects on soil erosion in the Lake Kivu Basin, DR Congo-Rwanda. *Forests* **2016**, *7*, 281. [CrossRef]
61. Karamage, F.; Zhang, C.; Kayiranga, A.; Shao, H.; Fang, X.; Ndayisaba, F.; Nahayo, L.; Mupenzi, C.; Tian, G. USLE-based assessment of soil erosion by water in the Nyabarongo River Catchment, Rwanda. *Int. J. Environ. Res. Public Health* **2016**, *13*, 835. [CrossRef]
62. Rajbanshi, J.; Bhattacharya, S. Assessment of soil erosion, sediment yield and basin specific controlling factors using RUSLE-SDR and PLSR approach in Konar river basin, India. *J. Hydrol.* **2020**, *587*, 124935. [CrossRef]
63. Bagwan, W.A.; Gavali, R.S. Delineating changes in soil erosion risk zones using RUSLE model based on confusion matrix for the Urmodi river watershed, Maharashtra, India. *Modeling Earth Syst. Environ.* **2021**, *7*, 2113–2126. [CrossRef]

land

MDPI

Article

Spatial Distribution Equilibrium and Relationship between Construction Land Expansion and Basic Education Schools in Shanghai Based on POI Data

Zhenchao Zhang, Weixin Luan *, Chuang Tian , Min Su and Zeyang Li

School of Maritime Economics and Management, Dalian Maritime University, Dalian 116026, China; zhenchao_zhang@dlmu.edu.cn (Z.Z.); sumin@dlmu.edu.cn (C.T.); tcyeah@dlmu.edu.cn (M.S.); lzy207@dlmu.edu.cn (Z.L.)

* Correspondence: weixinl@dlmu.edu.cn

Abstract: Basic education is about improving the quality of life of a country's population and promote social cohesions, and it is also an important factor in shaping a country and region's person-to-person relationship. This study analyzes the spatial morphological patterns, aggregation characteristics, and distribution inequality among kindergarten, elementary, and junior high schools within districts in Shanghai, using point of interest data, kernel density estimation, Ripley's K-function, location quotient, and grid analysis to investigate the effect on the distribution of schools using construction land growth data. The findings were as follows. (1) There was little difference in the spatial distribution characteristics of the three school types. They all exhibited the spatial distribution characteristics of core area clustering and the coexistence of multiple circadian layers, in which both the agglomeration size and the aggregation intensity showed the order of kindergarten > elementary school > junior high schools. The spatial distribution characteristics of the three types of schools are highly positively correlated with the population distribution. (2) Spatially, low-level schools were adjacent to high-level schools, and the structure of the three school types showed an uneven distribution overall. The aggregation characteristics of the seven inner districts within Shanghai were relatively balanced, while Pudong District showed the phenomenon of being "high in the southeast and low in the northeast", and the suburban areas showed an uneven distribution of core district aggregation overall. (3) The longer the construction land growth cycle, the greater the density of school points, and the more consistent the distribution of school points with the direction of construction land expansion.

Keywords: point of interest; school; spatial inequality; construction land; Shanghai

Citation: Zhang, Z.; Luan, W.; Tian, C.; Su, M.; Li, Z. Spatial Distribution Equilibrium and Relationship between Construction Land Expansion and Basic Education Schools in Shanghai Based on POI Data. *Land* **2021**, *10*, 1059. https://doi.org/10.3390/land10101059

Academic Editors: Baojie He, Ayyoob Sharifi, Chi Feng, Jun Yang and Richard C. Smardon

Received: 3 September 2021
Accepted: 6 October 2021
Published: 8 October 2021

1. Introduction

Education, as a practical activity to improve the comprehensive quality of human beings, has an important effect on the continuous development of the social economy. Ensuring inclusive and equitable quality education is one of the United Nation's Sustainable Development Goals [1], and the scarcity of resources and the imbalance in the allocation of basic education resources remain substantial barriers to achieving this goal [2,3]. At present, the proximate admission model, which assigns students to schools based on their home residence, has been widely adopted worldwide in many developed countries such as the United States [4], the United Kingdom [5], and Japan [6], as well as in developing countries such as China [7]. Ensuring the inclusion and equality of basic education can improve the quality of the whole nation, promote social cohesion, and encourage economic competitiveness [8,9]. Schools are the basic units of education resource allocation. Their spatial pattern, along with all levels of school resource configuration, will affect the resource allocation in these regions [10], as their spatial distribution decides whether students can get education near their place of residence [11]. Besides, the inequality of the area is

exacerbated by this situation to some extent [12,13]. Therefore, focusing on the spatial distribution laws between kindergarten, elementary, and junior high schools as the main basic education types can help achieve the equilibrium distribution of resources in basic education.

The uneven allocation of educational resources problem has received extensive attention in recent years [14–16]. The extant literature has mostly been dominated by studies on the imbalance of educational resources caused by urban population growth and rapid urbanization-related policies. These studies have shown that first, the rapid growth of the urban population and the greatly increased need for land use for urban construction have created a demand for infrastructure that far exceeds the service capacity of the existing service facilities [17,18]. The lack of space in the urban center and the shortage of educational facilities in the suburbs often leads to the uneven distribution of schools in the core and peripheral areas of a city [19], thus exacerbating the inequities in educational resource distribution. Liu et al. [20] used quantitative methods, such as spatial interpolation and cluster analysis, based on resource data such as elementary school building conditions, faculty, and the total amount of educational resources in Dalian City, and found that its elementary school resources exhibited a "center edge" circled layout; that is, the central urban areas were dominated by high-level secondary schools while the peripheral county cities were dominated by elementary schools, exhibiting a circled "decay" pattern. Tu et al. [21] used a log model to analyze the spatial evolution of compulsory educational facilities in Nanjing City, and found that the "core edge" structure of educational resources was still obvious and that the educational resources were highly spatially clustered.

Second, China's school merging policies have greatly advanced the educational urbanization process [22]. Unlike the demographic changes that accompany school closures and urbanization in developed countries [23], school merging policies in China stem from a top-down administrative push. These were adopted to optimize the allocation of rural educational resources, comprehensively improve the investment efficiency and quality of primary and secondary education, and promote the healthy and sustainable development of rural basic education. China has integrated rural educational resources to abandon the way of "running schools in villages" and merge resources of adjacent schools. However, due to improper operation in some areas, students' living conditions have decreased and have dropped out of school in some areas. Therefore, the implementation of these policies has generated greater controversy [24].

To some extent, the scale expansion caused by the school merging policy could improve students' academic performance and enable them to obtain better academic opportunities in the long term, but the merger has resulted in the concentration of more spatially distributed schools, which has resulted in increased commuting times for students in less accessible suburban areas and the more uneven distribution of schools between urban and rural areas. Due to the lack of education data at the micro-level, most studies have focused on educational inequalities at different prefectural or provincial levels [25,26] and between rural and urban areas [27,28], rather than between urban and suburban areas. Although a few studies have been based within cities [29], there is a notable paucity of research on the overall urban and peri-urban school distribution disequilibrium and its spatial structure composition.

Scholars have mostly analyzed and evaluated the spatial layout and inequality of educational resources on different scales from a geographic perspective, using methods such as 3S technology and spatial model simulation, which reflect both the social reality of the spatial outcomes and the products of the sociopolitical and economic operation of education resources [30,31]. In addition, mixed quantitative and qualitative research methods [32] have been used to analyze the relationship between the spatial pattern of educational resources and the spatial process of different scales and scenarios, such as the urbanization process [33–35], regional planning [36,37], population migration, and social-spatial differentiation [38,39].

In terms of data, points of interest (POI) data, as important urban space geographic big data [40], can describe the spatial and attribute information of geographical entities in real-time, such as name, address, and coordinates; has the advantage of large sample sizes; covers information meticulously, and so on. POI-based research has been fruitful in areas such as business spatial distribution [41], urban functional area identification [42], and urban built-up area identification [43,44]. The combination of POI data and GIS technology has facilitated better analysis of the spatial structure composition of schools within cities. At present, there are relatively few studies that have combined POI data to study the spatial distribution of schools via GIS visualization, and have mainly explored the spatial distribution of schools at a single level [45] to study the equilibrium of single educational resources with urban and rural origins [46,47]. Fewer studies have analyzed the spatial distribution of school resources based on a comprehensive consideration of intrinsic connections among the different levels of schools. Meanwhile, there is also relatively scant literature on the spatial relationship among kindergarten, elementary, and junior high schools under the mechanism of the ascending studies that use schools as the entry point.

At present, the number and size of elementary schools in China have ranked among the top in the world. The 2019 data for educational and career development in China show that there are 247, 105, and 148 million students in kindergarten, elementary, and junior high schools, respectively, which correspond to school sizes of 281,000, 160,000, and 52,000 [48]. In the past few decades, China has experienced extremely drastic land-use changes [49]. Cities need to expand the land area to seek new development space as part of the process of urbanization. The primary manifestation of urbanization is the phenomenon of urban spatial expansion, the direct embodiment of urbanization development. Urban expansion has become one of the important contents of land-use change research with the continuous advancement of urbanization in the world [50]. As such, the trend of population concentration to the urban center is becoming more and more obvious, expanding the urban scale and resulting in the continuous expansion of urban construction land [51]. Through the superposition analysis of the geographical location of construction land expansion in different growth cycles and school POI points, we can better understand the main trend of school distribution and explore the rationality of its spatial distribution. Moreover, construction land, as the most active area of urban space, tends to agglomerate resources such as population, capital, and information [52]. As schools are an important part of the social infrastructure whose land types are on construction land, the expansion of construction land will have a large impact on the distribution of schools within a city. Shanghai, as a megacity in China, has a rapid expansion of urban space [53,54] and extremely representative educational career development, and the expansion of construction land is also evident. In 2020, there were 2978 school points on construction land in Shanghai, accounting for 82% of the total number of schools.

Due to the limitation of data, we only have POI data in 2020, which cannot match the time of study of the construction land. However, schools are built on construction land, and the distribution of schools is inseparable from the construction land's expansion. Therefore, by studying the impact of the expansion of construction land in Shanghai and the change of spatial distribution of school points in different growth cycles, we can evaluate the spatial relevance under the circumstance of this timing mismatch. The research on the balance of school spatial distribution has important practical significance. The growth cycle of construction land refers to the expansion of construction land area with time growth, taking ten years as a cycle. The paper refers to 30 years from 1990 to 2020, 20 years from 2000 to 2020, and so on.

In sum, this study focuses on the following three issues. (1) Using 2019 Shanghai POI data, this study analyzes the spatial distribution laws of kindergarten, elementary, and junior high schools using GIS spatial analysis. (2) The spatial proportional relationship between the number of the three school types is analyzed using a grid net to illustrate the status of the spatial distribution of education in Shanghai. (3) Construction sites are combined with school POI points to analyze the effects of the maturity of construction

sites on the distribution state and density of school POI points in different growth periods between 1990 and 2020. This study can provide a new perspective for research on the spatial balance of educational resources.

2. Materials and Methods

2.1. Study Area

As shown in Figure 1: Shanghai is located in the Yangtze River Delta region, East China, at the estuary of the Yangtze River and the East China Sea. It borders Jiangsu and Zhejiang Provinces in the North and West and is between 120°52′–122°12′ E and 30°40′–31°53′ N. Shanghai is a central and megacity in China, and it is an international economic, financial, trade, education, science, and technology innovation center. The education development of Shanghai is already among the highest levels of education in China. Among them, the balanced proportion of basic education, the consolidation rate of basic education, and the number of international students are higher than the average level of China, and the education infrastructure in economically developed areas is also relatively perfect. However, there are still some differences between the main urban area and the suburbs. Therefore, the study area of this research was based on the following 16 main districts in Shanghai: Huangpu, Xuhui, Changning, Jingan, Putuo, Hongkou, Yangpu in the main city; and Pudong in the semi-urban and semi-suburban areas; and Minhang, Baoshan, Jiading, Jinshan, Songjiang, Qingpu, Fengxian, and Chongming District in the suburban areas. This study focused on the spatial distribution pattern characteristics of kindergarten, elementary, and junior high schools in Shanghai and these three school types' overall spatial distribution proportions to explore the imbalance of their spatial distribution.

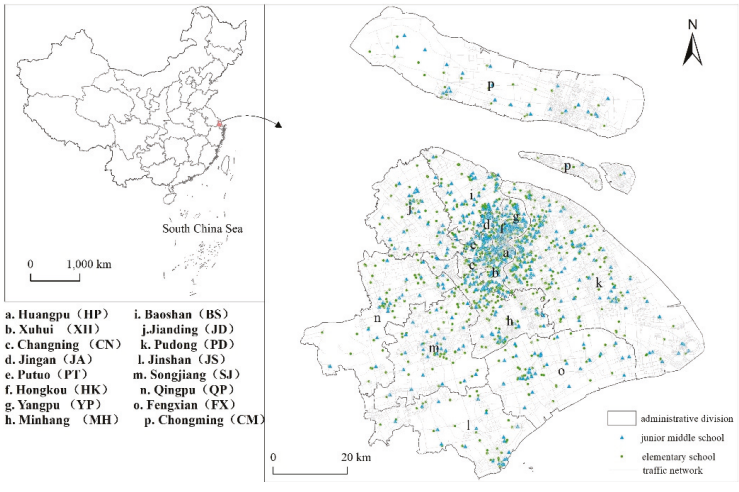

Figure 1. The distribution of three types of schools in 16 districts of Shanghai.

2.2. Data Source and Processing

This study used Baidu Maps as the data source. The "POI query" function (Maice Data Technology) was used to input the keywords "Shanghai kindergarten" and "Shanghai elementary school", and the deadline was set to 24 March 2020. The POI data points found 2121 kindergartens, 945 elementary, and 534 junior high schools in Shanghai, and included the schools' names, latitude and longitude coordinates, and addresses. The data preprocessing included coordinate correction, coordinate point reverse search, and address information correction and completion, which were used to construct the Shanghai school POI basic database. Data post-processing included district name extraction and street name determination. In addition to the POI data, the supporting data also included the

administrative divisions of the study area from the national basic geographic information system database. The construction land data for Shanghai between 1990 and 2020 were from the Institute of Geographical Sciences and Resources, the Chinese Academy of Sciences. Because the POI data is only in 2020, to study the influence of construction land expansion on school distribution in different periods, the construction land was divided into four growth cycles and superimposed with the POI data. 100 m × 100 m Shanghai population data is taken from WorldPop (https://www.worldpop.org/accessed on 26 September 2020).

2.3. Method

2.3.1. Kernel Density Estimation (KDE)

KDE is a nonparametric estimation method that is widely used in the spatial analysis of point data. Its purpose is mainly to estimate the density of point patterns with the help of a moving cell, obtain diagrams of the change of element density, output the continuous spatial distribution results, and reflect the relative agglomeration degree of the point distribution [55]. This study used ArcGIS software to both obtain the KDE distribution of all kinds of outlets and extract the KDE grid value of three school types. The natural segment method was used to divide them into five categories for comparative study.

2.3.2. Nearest Neighbor Indicator (NNI)

NNI counts the mean value of the closest distance between different points. This method is based on the distance of the points and is mainly used to measure the overall agglomeration and dispersion of the point distribution [56]. The calculation formula is:

$$d(NNO) = \sum_{i=1}^{n} \frac{\min(d_{ij})}{n} \quad (1)$$

$$d(NNE) = 0.5\sqrt{\frac{A}{n}} \quad (2)$$

$$NNI = \frac{d(NNO)}{d(NNE)} \quad (3)$$

where n is the number of points, min (d_{ij}) is the distance from point i to the nearest neighbor, d(NNO) is the observed average nearest neighbor distance, d(NNE) is the theoretical average distance under the condition of random spatial distribution, and NNI is the standardized nearest neighbor distance index. NNI < 1 tends to agglomerate points, NNI > 1 tends to disperse points, and NNI = 1 is the random distribution. The results were tested for reliability using the z-test.

2.3.3. Ripley's K-Function Analysis

The NNI can judge the overall spatial agglomeration characteristics of various outlet types but cannot judge the agglomeration characteristics on different spatial scales. Ripley's K function is a multi-distance spatial clustering analysis. It is a common method for point pattern analysis, and the number of points is counted according to the search circle range of a certain radius distance [57]. This study used it to analyze the spatial agglomeration patterns of Shanghai's kindergartens, elementary, and junior high schools on different spatial scales. The calculation formula is:

$$K(t) = A\sum_{i=1}^{n}\sum_{j=1}^{n} \frac{w_{ij}(t)}{n^2} \quad (4)$$

$$L(t) = \sqrt{\frac{K(t)}{\pi}} - t \quad (5)$$

This paper uses a common transformation of Ripley's K function analysis, i.e., L (t), where A represents the area of the study area, n represents the number of school points, and $w_{ij}(t)$ represents the actual distance between schools i and j within distance t. L (t) is the observed value of K, if L(t) is less than the expected value of the random distribution (that is, a negative value), then schools have the trend of discrete distribution. If L(t) is greater than the expected value (that is, a positive value), then the school has a trend of agglomeration distribution. The larger the gap between the observed L(t) and the expected value of random distribution, the higher the degree of clustering, and the corresponding t-value represents the distance used to measure the agglomeration scale.

2.3.4. Colocation Quotient Analysis (CLQ)

CLQ is usually used to judge whether an industry constitutes a specialized department of a region [58]. It is widely used in regional economics and geography. CLQ is a derivative form of the location quotient, which can be used to measure the proximity degree of distribution between different types of points. Leslie et al. verified and improved the formula for CLQ, taking Phoenix as an example to analyze the relationship between different industries [59]. The current study used it to study the proximity of the different school spaces, and the calculation formula is:

$$CLQ_{A \to B} = \frac{C_{A \to B}/N_A}{N_B/(N-1)} \quad (6)$$

where $CLQ_{A \to B}$ refers to the CLQ of A "attracted" by B, $C_{A \to B}$ refers to the number of A-type outlets close to B-type outlets (relative to A-type outlets themselves), NA and NB refer to the number of dot types A and B, respectively, and N is the total number of two outlets. When $CLQ_{A \to B}$ is less than 1, A tends to be far away from B; when $CLQ_{A \to B}$ is more than 1, A tends to be close to B. This study used CLQ to measure the spatial proximity relationship of POI points between kindergarten and elementary schools and junior high schools.

3. Results

3.1. Characteristics of the Spatial Distribution of Schools

From the results of the kernel density analysis presented in Figure 2, I used "the three school types" here as this paragraph contains the results for the three school types here. The spatial distribution of the three school types showed the characteristics of core area clustering and multiple circadian distributions. The morphological consistency of the distribution among the kindergarten, elementary, and junior high schools in Shanghai was significant, while the difference was not very significant. For consistency, the high-density KDE values of the kindergarten, elementary, and junior high schools were mainly concentrated in the inner seven districts of Shanghai (Yangpu, Hongkou, Jingan, Putuo, Changning, Xuhui, and Huangpu District) and in the outer ring of Pudong District, showing a circled distribution pattern and a pooling of consecutive slices. In addition to the high KDE value, there were eight gathering centers located in Jiading, Qingpu, Songjiang, Jinshan, Fengxian, Baoshan, and Minhang District, as well as the central area of Pudong District. Overall, the distribution showed a "circled + multicentric" morphology. Differentially, the KDE's extremely high values were ranked from high to low as kindergarten > elementary > junior high schools. The area covered by the KDE's high values also conformed to this rule, with the extremely high values in the inner seven districts being larger than the kernel density's extremely high values in the outer eight centers, and the peripheral distribution was also more sparse.

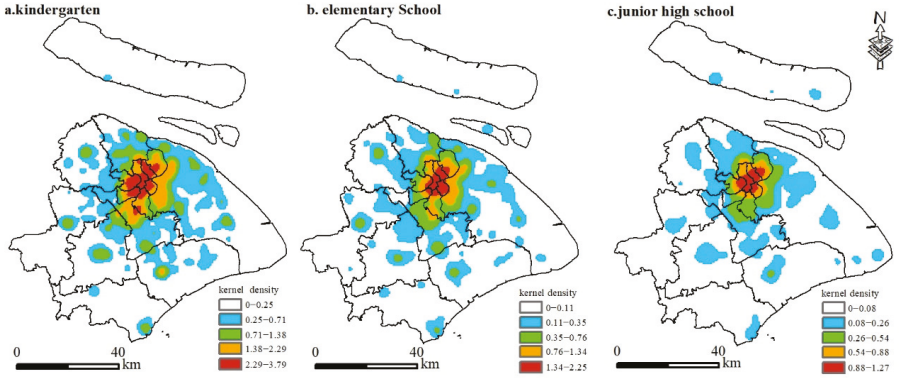

Figure 2. The spatial distribution of kernel density in the school types in Shanghai. (**a**) stands for kindergarten, (**b**) for elementary school and (**c**) for junior high school.

At the same time, this paper superimposes the three types of schools with the 100 m × 100 m grid population distribution data of Shanghai, and carries out the correlation test through SPASS software. Figure 3 shows that the population distribution is consistent with the distribution of POI, with typical core area agglomeration and multi circle spatial distribution characteristics, where the correlation coefficient reaches 0.7. It proves that the distribution of schools is highly positively correlated with the distribution of the population. This imbalance of population distribution will aggravate the imbalance of school distribution because schools are mainly established to meet people's needs.

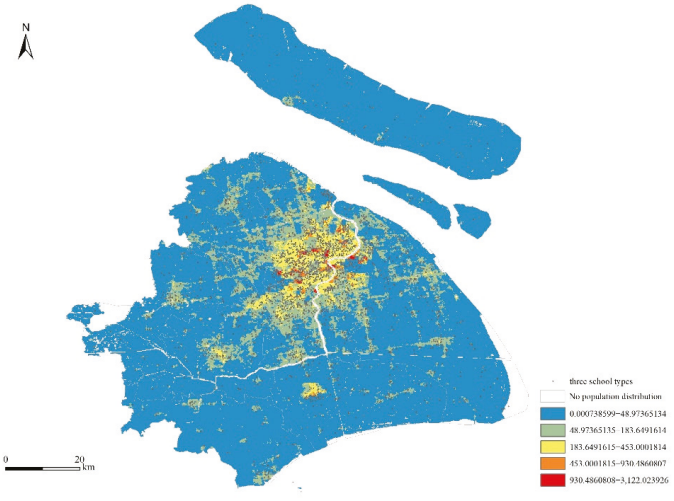

Figure 3. The population and school distribution in Shanghai.

Combined with the NNI distance (see Table 1), the spatial distribution of the kindergarten, elementary, and junior high schools in Shanghai all exhibited significant spatial clustering characteristics. Table 1 shows that the NNI values of the three school types in the overall range are all less than 1.0, the confidence level is 99%, and they all show a significant agglomeration distribution pattern. However, the degree of agglomeration differs, and is ordered as follows: kindergarten > elementary > junior high schools. The clustering characteristic of this decreasing trend, mainly influenced by the radiation range

of the schools, is that the area served by junior high schools has the largest number of elementary schools followed by the smallest number of kindergartens, thus leading to a higher number of kindergartens than elementary schools in the same area and a higher number of elementary schools than junior high schools. Moreover, kindergartens, elementary, and junior high schools are significantly regulated by the government in their spatial configuration, and their distribution in the central urban area is relatively dense.

Table 1. The nearest neighbor indicator of kindergartens, elementary schools, and junior high schools in Shanghai.

Type	Kindergarten	Elementary School	Junior High School
NNI	0.515	0.631	0.69
z	−42.771	−21.645	−13.552
P	<0.01	<0.01	<0.01

Although all three school types appear to be significantly spatially clustered, there is a significant difference between aggregate intensity and size, reflecting the differential characteristics of spatial distribution among the three types. To describe the clustering patterns across the schools in more detail, this study used Ripley's K-function in ArcGIS software. As shown in Figure 4, the results found that the overall observed value of the L(t) curve was larger than the expected value for all types of outlets, in an agglomerated distribution pattern, and all passed the examination at a 99% confidence rate. From the spatial feature scale of agglomeration, the difference between the observed and predicted values at the peak and the corresponding distance at the peak showed that the agglomeration degree of the three school types first increased but then decreased as the spatial scale increased. From the aggregated spatial feature scale, the three school types were showed the following order: kindergarten (20,387 m) > elementary (19,633 m) > junior high school (16,868 m). The corresponding L(t) peak represented the aggregation intensity and showed the following order: kindergarten (18,008 m) > elementary (17,249 m) > junior high school (15,936 m). The aggregation size and the aggregation intensity showed the following order: kindergarten > elementary > junior high school, which is consistent with the results obtained from the KDE and the nearest neighbor analysis because there was a hierarchy variability in the schools themselves, and this variability was also spatial in the same case.

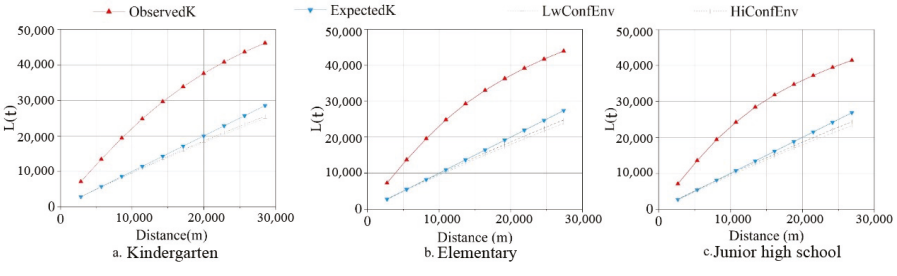

Figure 4. The Ripley's K of (**a**) kindergartens, and (**b**) elementary and (**c**) junior high schools in Shanghai.

3.2. Spatial Structure Distribution Equilibrium among School Types in Shanghai

To study the spatial structure composition of the kindergarten, elementary, and junior high schools, a buffer was created with a radius of 2500 m to analyze the intersection of the three schools. As shown in Table 2, 1723 kindergartens were clustered in the elementary school-centered buffer, while 626 elementary schools were clustered in the junior high school-centered buffer. The calculated results were used as input values to analyze the spatial proximity among the kindergarten, elementary, and junior high schools in Shanghai

using the same CLQ method. The results showed that C kindergarten → elementary school = 2.30, C elementary school → junior high school = 1.85, and the values of the same CLQ were all greater than 1, showing the proximity of the spatial distribution of schools. In turn, C elementary → kindergarten = 0.81 and C junior → elementary = 0.63 were all less than 1, showing discrete state distribution. Schools that were spatially distributed with low levels tended to resemble the characteristics of high-level schools.

Table 2. The Colocation quotient analysis of kindergartens, elementary schools, and junior high schools in Shanghai.

Proximity	Number of Coverage	Colocation Quotient
kindergarten → elementary school	1723	2.31
elementary school → junior high school	626	1.85
elementary school → kindergarten	2120	0.81
junior high school → elementary school	944	0.63

Since the distribution of schools tended to go from low levels to high levels, a 2500 m × 2500 m grid was constructed based on the administrative divisions in Shanghai, resulting in 1233 grids, of which 589 showed the school point distribution. The different classes within each grid were obtained by the spatial linkage function of ArcGIS software in order to visualize the regional-level relationships spatially for the number of school type points, and the proportional relationship was constructed based on junior high schools. From the average proportional relationship between the number of the three school types in Shanghai, the junior high school: elementary school: kindergarten ratio was 1:1.77:3.89, which indicates that there were 1.77 elementary schools and 3.89 kindergartens for every one area near a junior high school. The number of the three school types within each grid was statistically analyzed and contrasted with the average proportional relationship, as shown in Table 3. Four levels were divided according to how many schools were distributed and used to indicate the equality of spatial distribution. Quantitatively, the imbalance of the spatial structure distribution among the schools in Shanghai was significant and lower than the average proportional relationship in Shanghai overall, where the number of meshes with the high-high, high-low, low-high aggregation types was only 18.47%, and the total number of meshes with the low-low aggregation types was 81.53%.

Table 3. The level of agglomeration in Shanghai.

Level	Rationale for Classification	Number
High-High	Junior high school existed, and the proportions in elementary school and kindergarten were higher than the average proportion in Shanghai	60
High-Low	Junior high school existed, elementary school was higher than the average proportion in Shanghai, and kindergartens were lower than the average proportion in Shanghai	27
Low-High	Junior high school existed, elementary school was lower than the average proportion in Shanghai, and kindergartens were higher than the average proportion in Shanghai	22
Low-Low	Junior high school, elementary school, kindergartens were lower than the average proportion in Shanghai	480

Figure 5 shows that for the spatial distribution of schools in Shanghai, kindergarten, elementary, and junior high schools have an unbalanced distribution overall. The agglomeration characteristics of the seven districts within Shanghai are significant, while the polarization distribution of Pudong District obviously shows the phenomenon of being

"high in the northeast and low in the southeast", and the suburban areas have an unbalanced distribution in the core areas overall; that is, the distribution of the three school types are all lower than the average for Shanghai. From the distribution of different levels in the administrative region (Figure 6), high-high agglomeration is mainly distributed in the main urban area, with 10 grids and 22 grids in Pudong District. The most distributed district in the suburbs is Minhang, with nine grids. The other districts (in order) are: Qingpu, Jiading, Baoding, Songjiang, Baoshan, Jinshan, and Fengxian. There is no high-high agglomeration in Chongming District; however, high-low agglomerations and low-high agglomerations are mainly distributed in the west Pudong District, southeast Baoshan District, and north Minhang District because the development of the main city district has reached a certain scale. As these districts are relatively close to the main city district, there will be a certain phenomenon of population migration. Thus, the required number of schools will increase, and the agglomeration state will be more obvious with a relatively high level of agglomeration and reasonable distribution. Low-low agglomeration is mainly distributed in the suburbs and in Pudong District, which has the largest number (104), while most districts are distributed in the middle and in the southeast, close to Fengxian District. Overall, there is a trend of increasing distribution from northeast to southeast. In the future, the investment and development of education should be carried out in this direction to improve the unbalanced spatial distribution of schools in the southeast. Since the proportion of the low agglomeration grids is large, this distribution state leads to the imbalance of the spatial distribution of basic education in Shanghai overall.

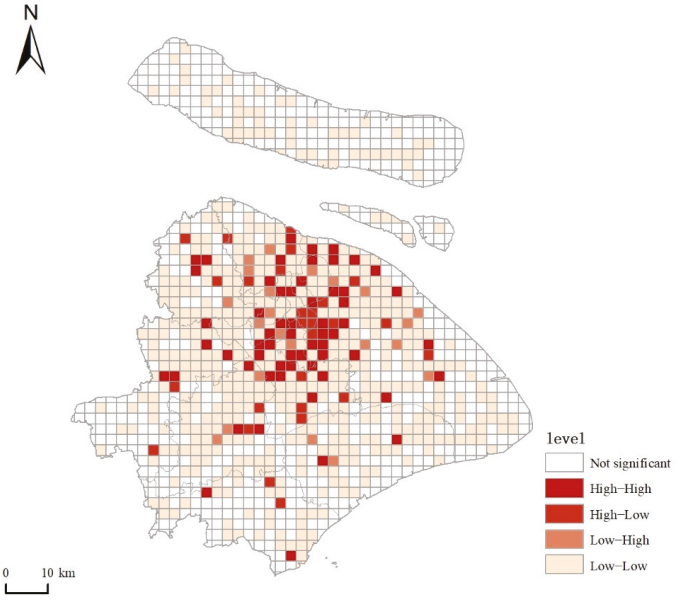

Figure 5. The proportional relationship of kindergartens, elementary, and junior high schools in Shanghai.

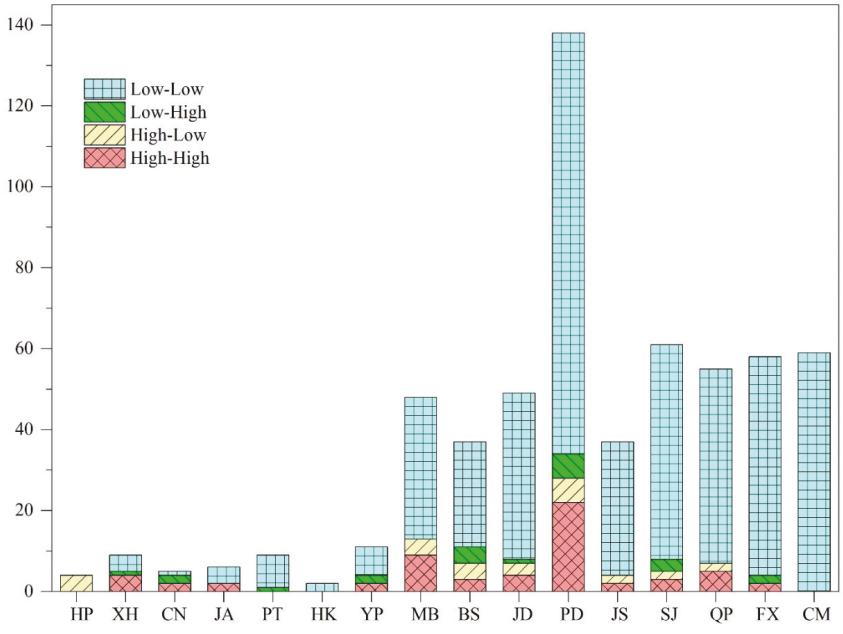

Figure 6. The proportional relationship of kindergartens, elementary, and junior high schools in the 16 districts in Shanghai.

3.3. Impact of the Cycle of Construction Land Growth on the Distribution of Schools

Since the change in location will not be obvious after a school is built and the expansion of construction land will have an effect on the density of its distribution, the data from the newly-added construction land between 1990 and 2020 were selected to be superimposed with school POI points, and the expansion area of the construction land and the change in the distribution of the school sites in different growth periods were obtained.

The combination of the construction land plots with the point density distribution of the three school types (see Figure 7) and the specific number of distributions (see Table 4) yielded the following results. Between the 20-year and 30-year growth cycle periods, the construction land expansion trend was mainly driven by the inner seven districts of Shanghai to the surrounding adjacent areas and was particularly prominent in the Minhang and Baoshan Districts. Pudong District was spread eastward from the outer ring area, and the other areas were all expanded and connected on the basis of the original construction land blocks, with a total growth area of 215.58 km^2. There were 397 schools on the newly-constructed land during this period. The expansion of the construction land between the 10-year and 20-year growth cycles was similar to the expansion in the previous period. However, it is obvious that the seven districts within the city did not significantly expand to reach certain saturation. There were 205 schools on the newly constructed land during this period. There were 1053 km^2 of newly-constructed land between the 10-year growth cycle and the current stage, increasing the number of schools (686). The expansion of construction land from the city center to the suburbs had a significant trend. Jiading, Qingpu, and Songjiang District had a large growth area, and Pudong District continued to expand to the southeast. Although the expansion of the construction land area was positively correlated with the distributed number of schools, the density of the school points within the construction land expansion continuously decreased. This can be seen by comparing the density of the school POI points between the 30-year growth cycle and the current stage, where the density of school points under the 30-year construction land formation cycle was 3.06/km^2, which was much higher than the current phase of 1.47/km^2.

With the shortening of the growth cycle of construction land, the distribution direction of school sites was consistent with the expansion direction of construction land, which was extended from inside to outside of the city. Although the construction land area gently increased, the distribution of school sites was increasingly sparse, and most were located in the suburbs with a relatively low degree of development.

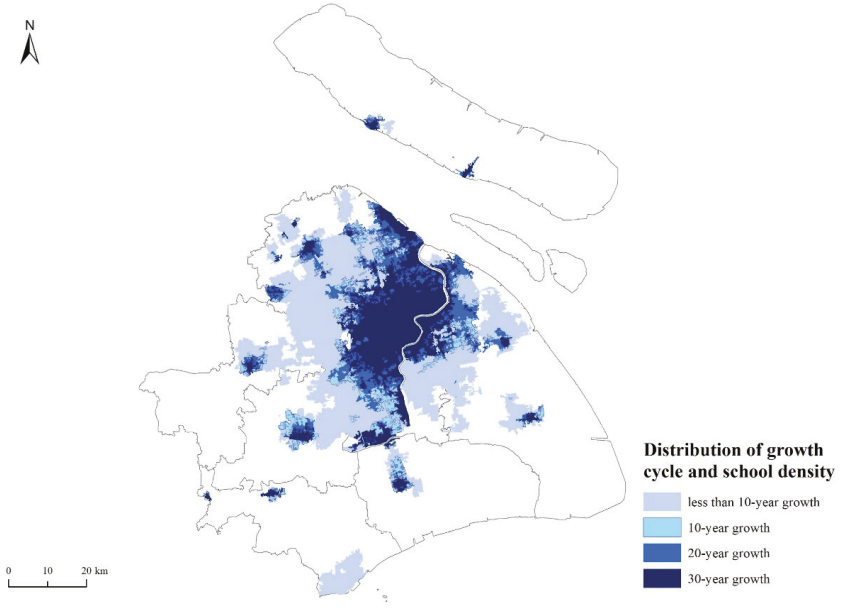

Figure 7. The growth cycle of new construction land and density distribution of school sites in Shanghai.

Table 4. Land area and school density for growth cycle construction in Shanghai.

Growth Cycle	Junior High School	Elementary School	Kindergarten	Constructed Land Area (km^2)	Density (Unit/km^2)
30 Year	261	482	964	556.26	3.06
20 Year	317	575	1211	777.87	2.71
10 Year	347	618	1343	1053.63	2.33
Less Than 10 Year	429	775	1774	2031.63	1.47

4. Conclusions and Discussion

This study constructed a 2500-m grid based on POI point data from kindergarten, elementary, and junior high schools in Shanghai using CLQ and Ripley's K-function. A variety of spatial point pattern analysis methods comparatively analyzed the spatial distribution pattern and the spatial aggregation characteristics of the kindergarten, elementary. Junior high schools in Shanghai, the grade of the spatial distribution of schools within the grid, and the impact of different long-term construction sites in combination with the school POI point to explore the distribution patterns of the schools. The following conclusions are drawn.

(1) The distribution of kindergarten, elementary, and junior high schools in Shanghai show remarkable consistency and little difference; overall, they show the spatial distribution characteristics of core area clustering and the coexistence of multiple circadian layers. The extremely high KDE values and covered areas rank as follows (from large to small): kindergarten > elementary > junior high school. The NNI values of the three school

types are less than 1.0, with a confidence level of 99%, showing a significant clustering distribution pattern. The degree of aggregation is as follows: kindergarten > elementary > junior high school, while the aggregation size and agglomeration intensity of the three school types is as follows: kindergarten > elementary > junior high school, the spatial distribution characteristics of the three types of schools are highly positively correlated with the population distribution. This phenomenon is not only influenced by government planning but also has remarkable historical development inertia, with the seven districts within Shanghai persisting as the regions where the educational facilities are concentrated, and, with these excellent educational resources, they belong in the core region. However, the eight aggregation centers outside the core area result in a "inside high and outside low" center edge structure of schools due to the lack of relevant supporting resources, such as population migration, lagged economic development, and transportation conditions [2,3]. In the context of China's rapid urbanization [60], the development of large cities have had an expanding morphology, from a concentric layer format to a decentralized group format [61], and this urban morphology can also directly affect the allocation of basic educational resources, resulting in a relatively perfect distribution of basic educational resources in urban areas and a relative lag in peri-urban areas. Therefore, the rational allocation of educational resources in Shanghai should be coalesced in the future and should focus on more developmentally lagged suburban areas to reduce the gap in peri-urban educational development.

(2) The structural composition of the schools in Shanghai shows uneven distribution. From the spatial relationship, C kindergarten → elementary school = 2.30, C elementary school → junior high school = 1.85, and the values of the same CLQ are all larger than 1. This indicates that low-level schools are close to the distribution of high-level schools, and that the overall distribution of kindergarten, elementary, and junior high schools in Shanghai is unbalanced. The agglomeration characteristics of the seven districts in Shanghai are significant and relatively balanced. The polarization distribution of Pudong District shows the phenomenon of being "high in the northeast and low in the southeast". The suburban area shows the overall unbalanced distribution of the core area. In the context of high-speed development, government planning and school consolidation can lead to an imbalance in the allocation of regional resources, with consequences for the structure of schools. The results show that schools in the suburban areas of Shanghai basically have low aggregation and an uneven distribution state, which is due to both the implementation of the school merging policy and the rapid urbanization background. Transportation and other infrastructure in the suburban areas are undeveloped, leading to an increase in students' commuting distance, which, in turn, aggravates the imbalance in the distribution of educational resources. The results show that educational infrastructure is relatively well-established, in contrast to the urban areas, and the distribution of schools presents a state of high clustering overall. Students are not restricted by distance, and the number of the three school types is also more evenly distributed. Therefore, special attention should be paid to the layout adjustment of educational resources to students' education problems in remote suburban areas in order to prevent the blind "school merging policy" from causing an expansion of the educational gap within the city, which, in turn, may affect the intergenerational flow and opportunity fairness.

(3) The longer the construction land growth cycle, the greater the school point density, and the more consistent the school point distribution is with the construction land expansion direction. Although construction land has grown enormously, after three decades of evolution, the distribution of school sites is becoming more sparse, and the vast majority of schools are located in suburban areas where the degree of development is relatively low. The results show that, against the background of rapid urbanization in Shanghai, the distribution of schools in suburban areas is extremely uneven, with more schools concentrated in the core areas [62]. This is strongly associated with the School merging policy, as well as population migration [63,64], and the uneven distribution of schools in

the peri-urban areas is also an important problem regarding educational development in Shanghai.

As this study's research area was more refined, the research needs were difficult to meet using data from traditional census statistics or fieldwork, and the data are less time-consuming, while the use of POI data made it easy to achieve a more detailed study using different scales because of the advantages of a large volume of data, easy acquisition, and spatial attributes. This leads to new research content and methods for the study of spatial balance in urban education. Previous studies on the equilibrium of basic education have mostly focused on the resource fairness and spatial equality of education [65,66], while most of the research scales that have focused on the provincial level [67–69] lack the meticulous analysis of the intra-urban and peri-urban contrast from the prefectural-level urban scale. Further, many studies have focused on a single educational resource, while few have focused on the analysis of kindergarten, elementary, and junior high schools. Therefore, the current study is innovative from its research data and perspective, specifically from the combination of spatial POI big data to analyze the distribution of the three school types in Shanghai. In addition to studying the spatial distribution pattern characteristics of the three school types, this study also divided the grid to assess their overall spatial structure composition relationship. It then analyzed the imbalance of their spatial distribution and the superimposition between the growth cycle of construction land and the school points to study the impact of the construction land expansion on the distribution of schools, which provides a new perspective for studying the spatial equilibrium of basic educational resources.

This study included some limitations. First, it considered the characteristics of the distribution pattern and the spatial distribution equilibrium of schools but did not provide an in-depth exploration of the balanced influencing mechanisms and the resulting social effects. Further, the data are limited from only using 2020 POI data, which cannot make a perfect fit with the construction land data. Future studies should combine POI and construction land-use data with data on economic statistics, traffic networks, and others, based on the existing research. They should also discuss the coupling mechanisms and mechanisms of the uneven spatial distribution of schools within cities and should focus on considering the service radius of schools in basic education to provide relevant recommendations for spatial planning in basic education.

Author Contributions: Conceptualization, Z.Z. and W.L.; methodology, Z.Z.; software, Z.Z.; validation, Z.Z., W.L.; formal analysis, Z.Z.; investigation, Z.Z.; resources, Z.Z.; data curation, Z.Z.; writing—original draft preparation, Z.Z.; writing—review and editing, Z.Z.; visualization, Z.Z. and Z.L.; supervision, Z.Z. and C.T.; project administration, Z.Z.; funding acquisition, W.L. and M.S. All authors have read and agreed to the published version of the manuscript.

Funding: This research was funded by the Key Program of National Natural Science Foundation of China, grant number [42030409].

Institutional Review Board Statement: Not applicable.

Informed Consent Statement: Not applicable.

Data Availability Statement: The collection and preprocessing of data are in Section 2.2.

Acknowledgments: The authors would like to acknowledge all experts' contributions in the building of the model and the formulation of the strategies in this study.

Conflicts of Interest: The authors declare no conflict of interest.

References

1. Norman, C. Francis quality education and equality of educational opportunity. *NASSP Bull.* **1977**, *61*, 16–25.
2. Burger, K. The socio-spatial dimension of educational inequality: A comparative European analysis. *Stud. Educ. Eval.* **2019**, *62*, 171–186. [CrossRef]

3. Hu, L.; He, S.; Luo, Y.; Su, S.; Xin, J.; Weng, M. A social-media-based approach to assessing the effectiveness of equitable housing policy in mitigating education accessibility induced social inequalities in Shanghai, China. *Land Use Policy* **2020**, *94*, 104513. [CrossRef]
4. Dhar, P.; Ross, S.L. School district quality and property values: Examining differences along school district boundaries. *J. Urban Econ.* **2012**, *71*, 18–25. [CrossRef]
5. Allen, R. Allocating pupils to their nearest secondary school: The consequences for social and ability stratification. *Urban Stud.* **2007**, *44*, 751–770. [CrossRef]
6. Yuta, K. The effect of school quality on housing rents: Evidence from Matsue city in Japan. *J. Jpn. Int. Econ.* **2018**, *50*, 16–25.
7. Wen, H.; Xiao, Y.; Zhang, L. School district, education quality, and housing price: Evidence from a natural experiment in Hangzhou, China. *Cities* **2017**, *66*, 72–80. [CrossRef]
8. Organisation for Economic Cooperation and Development (OECD). *Equity and Quality in Education: Supporting Disadvantaged Students and Schools*; Organisation for Economic Cooperation and Development (OECD): Paris, France, 2012.
9. Xiang, L.; Stillwell, J.; Burns, L.; Heppenstall, A.; Norman, P. A geodemographic classification of sub-districts to identify education inequality in Central Beijing. *Comput. Environ. Urban Syst.* **2018**, *70*, 59–70. [CrossRef]
10. Wen, J.; Chudan, G.U. The rural-urban differences in resources allocation of basic education and its social consequence: Base on the analysis of China's education statistics. *J. East China Norm. Univ. Educ. Sci.* **2017**, *35*, 33.
11. Yang, J.; Huang, X.; Liu, X. An analysis of education inequality in China. *Int. J. Educ. Dev.* **2014**, *37*, 2–10. [CrossRef]
12. Wei, Y.D. Spatiality of regional inequality. *Appl. Geogr.* **2015**, *61*, 1–10. [CrossRef]
13. Liu, R.; Li, T.; Greene, R. Migration and inequality in rental housing: Affordability stress in the Chinese cities. *Appl. Geogr.* **2020**, *115*, 102138. [CrossRef]
14. Qian, X.; Smyth, R. Measuring regional inequality of education in China: Widening coast–inland gap or widening rural–urban gap? *J. Int. Dev.* **2008**, *20*, 132–144. [CrossRef]
15. Li, W. Education inequality in China: Problems of policies on access to higher education. *J. Asian Public Policy* **2008**, *1*, 115–123. [CrossRef]
16. Rodríguez, C.; Amador, A.; Tarango, B.A. Mapping educational equity and reform policy in the borderlands: LatCrit spatial analysis of grade retention. *Equity Excel. Educ.* **2016**, *49*, 228–240. [CrossRef]
17. Li, Z.; Luan, W.; Zhang, Z.; Su, M. Relationship between urban construction land expansion and population/economic growth in Liaoning Province, China. *Land Use Policy* **2020**, *99*, 105022. [CrossRef]
18. Wu, Y.; Zhang, T.; Zhang, H.; Pan, T.; Ni, X.; Grydehøj, A.; Zhang, J. Factors influencing the ecological security of island cities: A neighborhood-scale study of Zhoushan Island, China. *Sustain. Cities Soc.* **2020**, *55*, 102029. [CrossRef]
19. Wu, Y.; Zheng, X.; Sheng, L.; You, H. Exploring the equity and spatial evidence of educational facilities in Hangzhou, China. *Soc. Indic. Res.* **2020**, *151*, 1075–1096. [CrossRef]
20. Tianbao, L.; Liwen, Z.; Du, P. Spatial characteristics and distribution pattern of the equilibrium level of municipal compulsory education resources —Take Dalian primary school as an example. *Econ. Geogr.* **2018**, *7*, 67–74.
21. Tangqi, T.; Dongsheng, Y.; Jianglong, C. Evolution of compulsory educational facilities in urban Nanjing. *Sci. Geogr. Sin.* **2019**, *3*, 433–441.
22. Hannum, E.; Liu, X.; Wang, F. Estimating the effects of educational system contraction: The case of China's rural school closure initiative. *Econ. Dev. Cult. Chang.* **2021**, *70*, 485–528. [CrossRef]
23. Howley, C.; Johnson, J.; Petrie, J. Consolidation of schools and districts: What the research says and what it means. *Natl. Educ. Policy Cent.* **2011**.
24. Chao, L. The impact of educational public goods allocation adjustment on human capital. *Econ. Res. J.* **2020**, *55*, 140–156.
25. Wang, W. Decomposing inequality in compulsory education finance in China: 1998–2008. *Public Finance Manag.* **2014**, *14*, 437–458.
26. Xie, T. Analysis on inter-provincial disparities of China's rural education and convergence rate: Empirical analysis on 31 provinces' (municipalities') panel data from 2001 to 2008. *Int. J. Educ. Manag.* **2011**, *25*, 714–723. [CrossRef]
27. Rao, J.; Ye, J. From a virtuous cycle of rural-urban education to urban-oriented rural basic education in China: An explanation of the failure of China's Rural School Mapping Adjustment policy. *J. Rural Stud.* **2016**, *47*, 601–611. [CrossRef]
28. Zhang, D.; Li, X.; Xue, J. Education inequality between rural and urban areas of the People's Republic of China, migrants' children education, and some implications. *Asian Dev. Rev.* **2015**, *32*, 196–224. [CrossRef]
29. Liu, J.; Jacob, W.J. From access to quality: Migrant children's education in urban China. *Educ. Res. Policy Pract.* **2013**, *12*, 177–191. [CrossRef]
30. Pacione, M. The geography of educational disadvantage in Glasgow. *Appl. Geogr.* **1997**, *17*, 169–192. [CrossRef]
31. Mulaku, G.; Nyadimo, E. GIS in education planning: The Kenyan school mapping project. *Surv. Rev.* **2011**, *43*, 567–578. [CrossRef]
32. Yoon, E.S.; Lubienski, C. Thinking critically in space: Toward a mixed-methods geospatial approach to education policy analysis. *Educ. Res.* **2018**, *47*, 53–61. [CrossRef]
33. Butler, T.; Robson, G. Social capital, gentrification and neighbourhood change in London: A comparison of three south London neighbourhoods. *Urban Stud.* **2001**, *38*, 2145–2162. [CrossRef]
34. Thrupp, M. School admissions and the segregation of school intakes in New Zealand cities. *Urban Stud.* **2007**, *44*, 1393–1404. [CrossRef]

35. Lubienski, C.; Lee, J. Geo-spatial analyses in education research: The critical challenge and methodological possibilities. *Geogr. Res. J. Inst. Aust. Geogr.* **2017**, *55*, 89–99. [CrossRef]
36. Yong, W.; Change, L.U.; Education, S.O. Analysis on the regional proportionality of preschool educational resources allocation: With the technical supporting of GIS. *J. Mianyang Teach. Coll.* **2018**, *37*, 27–32.
37. Xie, C.D.; University, Y.Z.N. Analysis on the equilibrium degree of regional allocation of educational resources in weaker schools of compulsory education. *J. Nanchang Coll. Educ.* **2019**.
38. Yuan, Z.; Qian, J.; Zhu, H. The Xinjiang class: Multi-ethnic encounters in an eastern coastal city. *China Q.* **2017**, *232*, 1094–1115. [CrossRef]
39. Glorius, B. Transnational social capital in migration: The example of educational migration between Bulgaria and Germany. *Soc. Incl.* **2019**, *7*, 232–242. [CrossRef]
40. Liu, K.; Yin, L.; Lu, F.; Mou, N. Visualizing and exploring POI configurations of urban regions on POI-type semantic space. *Cities* **2020**, *99*, 102610. [CrossRef]
41. Lan, T.; Yu, M.; Xu, Z.; Wu, Y. Temporal and spatial variation characteristics of catering facilities based on POI data: A case study within 5th ring road in Beijing. *Procedia Comput. Sci.* **2018**, *131*, 1260–1268. [CrossRef]
42. Zhai, W.; Bai, X.; Shi, Y.; Han, Y.; Peng, Z.-R.; Gu, C. Beyond Word2vec: An approach for urban functional region extraction and identification by combining Place2vec and POIs. *Comput. Environ. Urban Syst.* **2019**, *74*, 1–12. [CrossRef]
43. He, Q.; He, W.; Song, Y.; Wu, J.; Yin, C.; Mou, Y. The impact of urban growth patterns on urban vitality in newly built-up areas based on an association rules analysis using geographical 'big data'. *Land Use Policy* **2018**, *78*, 726–738. [CrossRef]
44. Yang, J.; Ren, J.; Sun, D.; Xiao, X.; Xia, J.; Jin, C.; Li, X. Understanding land surface temperature impact factors based on local climate zones. *Sustain. Cities Soc.* **2021**, *69*, 102818. [CrossRef]
45. Zeng, J.; Yuanyuan, Y.E.; Zhong, Z. Research into the equalization of public service formats based on POI big data. *J. West Anhui Univ.* **2018**, *34*, 72–75.
46. Su, F.; Mo, X.; Min, W.; Li, B. The equalization of the general high school education and its obstacle factors in China. *Sci. Geogr. Sin.* **2017**, *10*, 1478–1485.
47. Zhao, C.; Shao, J.A.; Guo, Y.; Xu, X. Spatial pattern evolvement characteristics of rural schools and their development level in the mountainous area. *Geogr. Res.* **2016**, *35*, 455–470.
48. Development of National Education in 2019. Available online: www.moe.gov.cn/jyb_sjzl/s5990/202008/t20200831_483697.html (accessed on 3 October 2019).
49. Yang, J.; Xie, P.; Xi, J.; Ge, Q.; Ma, Z. LUCC simulation based on the cellular automata simulation: A case study of Dalian Economic and Technological Development Zone. *Acta Geogr. Sin.* **2015**, *70*, 461–475.
50. Yang, J.; Wang, Y.; Xue, B.; Li, Y.; Xiaog, X.; Xia, J.; He, B. Contribution of urban ventilation to the thermal environment and urban energy demand: Different climate background perspectives. *Sci. Total Environ.* **2021**, *795*, 148791. [CrossRef]
51. Luo, X.; Yang, J.; Sun, W.; He, B. Suitability of human settlements in mountainous areas from the perspective of ventilation: A case study of the main urban area of Chongqing. *J. Clean. Prod.* **2021**, *310*, 127467. [CrossRef]
52. Dong, L.; Li, J.; Xu, Y.; Yang, Y.; Li, X.; Zhang, H. Study on the spatial classification of construction land types in Chinese cities: A case study in Zhejiang province. *Land* **2021**, *10*, 523. [CrossRef]
53. Yang, J.; Guo, A.; Li, Y.; Zhang, Y.; Li, X. Simulation of landscape spatial layout evolution in rural-urban fringe areas: A case study of Ganjingzi District. *GIScience Remote Sens.* **2019**, *56*, 388–405. [CrossRef]
54. Zhu, J.; Li, B.; He, B.-J. Is linked migration overlooked in peri-urban Shanghai? Uncovering the domino effect of driving away interregional migrants. *Habitat Int.* **2019**, *94*, 102046. [CrossRef]
55. Silverman, B.W. *Density Estimation for Statistics and Data Analysis*; Routledge: Abingdon, UK, 1986.
56. Xue, B.; Xiao, X.; Li, J. Identification method and empirical study of urban industrial spatial relationship based on POI big data: A case of Shenyang City, China. *Geogr. Sustain.* **2020**, *1*, 152–162. [CrossRef]
57. Shen, Q.X.; Li, C.G.; Liu, Z.Y. Spatial pattern of public service facilities space and living space in Changchun. *Geogr. Res.* **2018**, *37*, 127–136.
58. Hao, F.; Shi, X.; Xue, B.; Wang, S. Geographic detection and multifunctional land use from the perspective of urban diversity: A case study of Changchun. *Geogr. Res.* **2019**, *38*, 247–258.
59. Leslie, T.F.; Kronenfeld, B.J. The colocation quotient: A new measure of spatial association between categorical subsets of points. *Geogr. Anal.* **2011**, *43*, 306–326. [CrossRef]
60. Yang, J.; Yang, Y.; Sun, D.; Jin, C.; Xiao, X. Influence of urban morphological characteristics on thermal environment. *Sustain. Cities Soc.* **2021**, *72*, 103045. [CrossRef]
61. Lin, J.; Huang, B.; Chen, M.; Huang, Z. Modeling urban vertical growth using cellular automata—Guangzhou as a case study. *Appl. Geogr.* **2014**, *53*, 172–186. [CrossRef]
62. Li, C.; Wu, K.; Gao, X. Manufacturing industry agglomeration and spatial clustering: Evidence from Hebei Province, China. *Environ. Dev. Sustain.* **2020**, *22*, 2941–2965. [CrossRef]
63. Haepp, T.; Lyu, L. The impact of primary school investment reallocation on educational attainment in rural China. *J. Asia Pac. Econ.* **2018**, *23*, 606–627. [CrossRef]
64. Zhao, Z.Q.; He, B.J.; Li, L.G.; Wang, H.B.; Darko, A. Profile and concentric zonal analysis of relationships between land use/land cover and land surface temperature: Case study of Shenyang, China. *Energy Build.* **2017**, *155*, 282–295.

65. Sherman, J.D.; Poirier, J.M. *Educational Equity and Public Policy: Comparing Results From 16 Countries*; UNESCO Institute for Statistics: Montreal, QC, Canada, 2007.
66. Malczewski, J.; Jackson, M. Multicriteria spatial allocation of educational resources: An overview. *Socio-Econ. Plan. Sci.* **2000**, *34*, 219–235. [CrossRef]
67. Peng, Y.; Wang, Z. Space operation of rural primary and secondary school location. *Acta Geogr. Sin.* **2013**, *68*, 1411–1417.
68. Li, C.; Gao, X.; Wu, J.; Wu, K. Demand prediction and regulation zoning of urban-industrial land: Evidence from Beijing-Tianjin-Hebei Urban Agglomeration, China. *Environ. Monit. Assess.* **2019**, *191*, 412. [CrossRef] [PubMed]
69. He, B.J.; Zhao, Z.Q.; Shen, L.D.; Wang, H.B.; Li, L.G. An approach to examining performances of cool/hot sources in mitigating/enhancing land surface temperature under different temperature backgrounds based on Landsat 8 image. *Sustain. Cities Soc.* **2018**, *44*, 416–427. [CrossRef]

land

MDPI

Article

Assessment and Estimation of the Spatial and Temporal Evolution of Landscape Patterns and Their Impact on Habitat Quality in Nanchang, China

Yanan Li [1,2,3], Linghua Duo [1,2,3,*], Ming Zhang [2], Zhenhua Wu [4] and Yanjun Guan [5]

[1] Research Center of Geological Resource Economics and Management, East China University of Technology, Nanchang 330013, China; 201911204013@ecut.edu.cn
[2] Faculty of Geomatics, East China University of Technology, Nanchang 330013, China; mzhang@ecut.edu.cn
[3] Key Laboratory of Mine Environmental Monitoring and Improving around Poyang Lake, Ministry of Natural Resources, Nanchang 330013, China
[4] School of Economics and Management, China University of Mining and Technology, Xuzhou 221116, China; wuzhenhua@cumt.edu.cn
[5] School of Land Science and Technology, China University of Geosciences, Beijing 100083, China; guanyj@cugb.edu.cn
* Correspondence: dlh_123@ecut.edu.cn; Tel.: +86-133-6163-8558

Abstract: Assessing and predicting the evolution of habitat quality based on land use change under the process of urbanization is important for establishing a comprehensive ecological planning system and addressing the major challenges of global sustainable development. Here, two different prediction models were used to simulate the land use changes in 2025 based on the land use distribution data of Nanchang city in three periods and integrated into the habitat quality assessment model to specifically evaluate the trends and characteristics of future habitat quality changes, explore the impact of landscape pattern evolution on habitat, and analyze the differences and advantages of the two prediction models. The results show that the overall habitat quality in Nanchang declined significantly during the period 1995–2015. Habitat degradation near cities and in various watersheds is relatively significant. During the period 2015–2025, the landscape pattern and habitat quality of Nanchang will continue to maintain the trend of changes observed between 1995 and 2015, i.e., increasing construction land and decreasing habitat quality, with high pressure on ecological restoration. This study also identified that CA-Markov simulates the quantity of land use better, while FLUS simulates the spatial pattern of land use better. Overall, this study provides a reference for exploring the complex dynamic evolution mechanism of habitats.

Keywords: CA-Markov model; FLUS model; InVEST model; land use change; habitat quality

Citation: Li, Y.; Duo, L.; Zhang, M.; Wu, Z.; Guan, Y. Assessment and Estimation of the Spatial and Temporal Evolution of Landscape Patterns and Their Impact on Habitat Quality in Nanchang, China. *Land* **2021**, *10*, 1073. https://doi.org/10.3390/land10101073

Academic Editors: Baojie He, Ayyoob Sharifi, Chi Feng and Jun Yang

Received: 19 September 2021
Accepted: 6 October 2021
Published: 12 October 2021

1. Introduction

China's urbanization process has been accelerating in recent years, with China's urbanization rate increasing significantly to 63.89% by 2020 and expected to reach 70% by 2030 [1]. On the one hand, changes in land use/land cover and rapid urban expansion inevitably transform a large amount of ecological land, such as forests, grasslands and waters, into construction land, resulting in the fragmentation of habitats that are suitable for biological survival, which not only affects the changes in ecosystem structure but also influences the content of greenhouse gases in the atmosphere and changes the regional atmospheric chemistry [2]. Then, this destroys ecosystem climate regulation and other service functions, leading to a series of climate change problems, such as ozone layer holes, glacier melting and frequent extreme weather, and the sustainable development of cities is threatened and challenged [3]. On the other hand, climate change, such as global temperature increases, also leads to the degradation of ecosystem functions and habitat fragmentation, thus affecting the quality of ecosystem habitats [4]. According to the results

of the Millennium Ecosystem Assessment published by the United Nations, climate change is already one of the most important factors threatening biodiversity and is expected to have an increasing proportion of its impact in the coming decades, changing the quality of the original habitats to varying degrees. Therefore, assessing and predicting the evolution of habitat quality based on land use change in the process of urbanization is of practical significance for establishing a comprehensive ecological planning system and coping with the great challenge of climate change. Therefore, assessing and predicting the evolution of habitat quality based on land use change under the process of urbanization is of practical importance for establishing a comprehensive ecological planning system and addressing the major challenges of climate change. The Integrated Valuation of Ecosystem Services and Trade-offs (InVEST) model, developed by Stanford University and the WWF, has been widely used due to its accurate quantification, visualization of results, and low application cost [5,6]. Nelson et al. applied the model to study different land use scenarios in the Willamette Basin, Oregon, North America, and explored the value and spatial distribution of ecosystem services in different scenarios [7]. Leh, Mansoor, D.K. et al. studied the evolution of habitat quality in Ghana and Cote d'Ivoire in different periods, and the authors elaborated on the general situation of habitat quality in these two countries [8]. Kovacs. et al. and Shaw. et al. quantitatively assessed ecosystems in the Minnesota and Sierra Nevada regions of the USA in the form of thematic maps and derived core areas for investment and conservation [9,10].

However, recent studies have generally concentrated on assessing the historical and current habitat quality in the study area, and few have explored future trends in habitat quality. There are many models currently available to estimate future land use variation [11–15], among which the cellular automata (CA)-Markov model integrates the properties of CA model to simulate the evolution of spatial patterns [16] and the superiorities of the Markov model for long-term quantitative estimation [17]; thus, the CA-Markov model has good results for the prediction of spatiotemporal evolution, while the future land use simulation (FLUS) model can better address the complex intertransformation of landscape types occurring under the combined action of natural factors and socioeconomic factors, which makes the simulation results match better with real land use conditions [18]. Consequently, the above two prediction models are commonly used in land use simulations. Jenerette et al. applied the CA-Markov model to the vicinity of Phoenix, Arizona, USA, to explore the effects of urbanization and population growth on land-use change [19]. Nourqolipour et al. used CA-Markov and multicriteria evaluation (MCE) models to estimate landscape variations in oil palm plantations in Kualalangat, Malaysia, and successfully predicted the land-use evolution trend in 2020 [20]. Liang Xun used the FLUS model to predict the urban form of the Pearl River Delta (PRD) area from 2020 to 2050 to establish urban growth boundaries [21]. Taking Hubei Province of China as an example, Wang Xu predicted the ecological spatial distribution of the province in 2035 by using the FLUS model [22]. All the above explorations indicate that CA-Markov and FLUS have good generalizability for the realistic simulation of land use development trends.

The models mentioned above have a long history of use and have achieved good results in their respective fields [23–26]. If predictive models and the habitat assessment models can be combined to predict future habitat quality, they will improve the understanding of the complex dynamic evolution mechanism of habitats and provide a reference for the government to implement land and ecological regulation strategies. However, there are few studies on future habitat quality, and most of the studies on future habitat quality simulation apply a single prediction method, lack a reference mechanism, and are unable to verify future land use patterns [27,28]. In this paper, given the abovementioned insufficiencies, two different prediction models (CA-Markov and FLUS) are combined with the habitat assessment model (InVEST). The results of the two prediction models can validate and support each other. Compared with the single-line model combination, this double-line model combination improves the reliability of prediction.

As a large provincial capital city, Nanchang plays an essential role in the Yangtze River economic zone. In recent years, the economic level of Nanchang has rapidly developed in all directions, and a series of problems related to urban expansion have occurred, which may lead to the urban heat island effect, deterioration of the habitat environment and frequent occurrence of extreme weather. Therefore, evaluating and predicting the characteristics of habitat evolution from the perspective of land use evolution is of great significance to maintain the balance of the ecosystem and achieve the goal of sustainable development in Nanchang city. This study took Nanchang city as the research area, two different prediction models (CA-Markov and FLUS) were used to model past, current and future land-use changes, and the InVEST model was introduced to integrate each of these two prediction models into habitat quality modeling to explore the effects of the evolution of landscape patterns on habitats. Specifically, the research can achieve the following three objectives: (1) assess and predict trends and characteristics of habitat quality from the perspective of land use variation; (2) analyze the differences between the two prediction models (CA-Markov and FLUS) and explore their respective advantages; and (3) obtain new information and measures for optimizing landscape patterns and improving habitat quality in Nanchang.

The main contributions of this paper are as follows. In terms of theory, on the one hand, the introduction of habitat evaluative indicators reflecting regional biodiversity allows for a multidimensional and comprehensive analysis of habitats, providing a novel approach and perspective for the diversified development of habitat assessment systems. On the other hand, this study uses the double-line combination of two prediction methods and the habitat assessment model to reduce the uncertainty associated with the model, thus enhancing the reliability of the simulation results. This approach is more reasonable and effective than relying only on a single prediction model. In terms of practical implications, exploring the impact of landscape pattern evolution on habitat can help people to understand the complex mechanisms of habitat quality change to better optimize landscape patterns to improve the current ecological environment and provide a reference for territorial spatial planning and the implementation of ecological control strategies.

2. Materials and Methods

2.1. Study Area

Nanchang (115°27′–116°35′ E, 28°10′–29°11′ N), as the capital of Jiangxi Province, occupies a large area of plains, with relatively flat terrain in the southeast, rolling hills in the northwest, and plains, water bodies, and mountainous hilly terrain, each accounting for approximately one third of the area (Figure 1). The total area of the city is 7402 square kilometers. As a major transportation hub in the central part of China, with transportation running east–west and north–south, and as a major ecological barrier in southern China, Nanchang has undergone rapid population growth and the expansion of construction land. Therefore, maintaining regional ecological security should be the focus of future efforts.

2.2. Data Sources and Processing

The land use data of this research are obtained based on Landsat TM/ETM+ images from the NASA scientific data service platform (https://earthdata.nasa.gov/, accessed on 9 September 2021). The Landsat images with 30 m resolution from July to August in 1995, 2005 and 2015 were preprocessed by cloud mask, atmospheric correction and clipping to form three full coverage images of Nanchang city. By applying the method of combining supervised classification with manual visual interpretation, the land use categories in Nanchang were divided into six categories: cultivated land, forestland, grassland, water area, construction land and unused land. The DEM data come from the geospatial data cloud platform (http://www.gscloud.cn/, accessed on 9 September 2021), and the slope is extracted by using the slope function of ArcGIS. The auxiliary gridded GDP, population density data with 1 km resolution and road data of the corresponding time period are

downloaded from the Resource and Environmental Science Data Center of the Chinese Academy of Sciences (http://www.resdc.cn/, accessed on 9 September 2021).

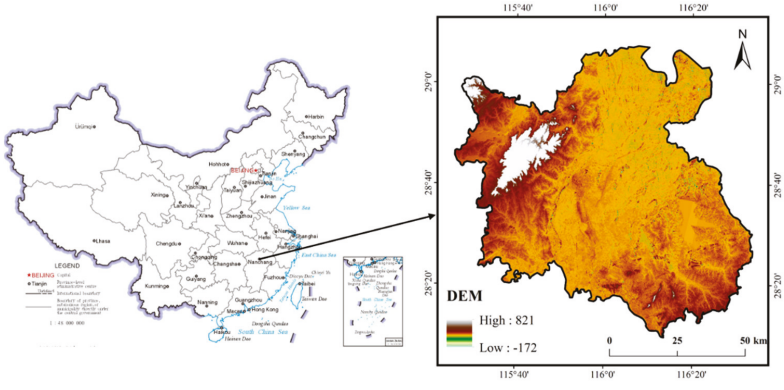

Figure 1. The study area.

2.3. Methodology

Based on the data collection and processing, we first analyzed the characteristics of land use dynamics in the study area from 1995 to 2015, applied the InVEST model to determine the habitat quality index, habitat rarity index and habitat degradation index in this time period, and assessed the ecological and environmental conditions of Nanchang in the past 20 years from these three aspects. Second, two different prediction models (CA-Markov and FLUS) are used to simulate the future land use changes in the region to verify and support each other's simulation results and to compare the differences between the two prediction models and explore their respective advantages. Finally, based on the future land use cover map predicted by the two prediction models, the characteristics and trends of future habitat quality evolution are predicted and evaluated by the InVEST model.

2.3.1. CA-Markov Model

The CA-Markov model is a combination of a temporal prediction model (Markov chain) and a spatially dynamic model (Cellular Automata) with discrete time, space and state [29,30]. The Markov model cannot predict spatial variation, while the CA model has the advantage of simulating the spatiotemporal dynamic development of complex systems; thus, combining the two models could effectively simulate the spatiotemporal changes in land-use patterns [31,32].

A Markov model is first run to obtain the transition matrices (including the transition area, transition probability and a series of auxiliary maps). The land-use status $S_{(t+1)}$ is forecasted through the status $S_{(t)}$ at a given moment with a transition probability matrix P_{ij} in the Markov process. Therefore, the land-use status can be forecasted using the following equation [33]:

$$S_{(t+1)} = P_{ij} \times S_{(t)}, \quad (1)$$

In the second step, the CA model is a lattice dynamics model in which spatial interactions and temporal connections are localized and spatiotemporal relationships and morphological conditions are discrete [34,35]; it can be expressed using the following equation [36]:

$$S_{(t+1)} = f\left(S_{(t)}, N\right), \quad (2)$$

where S represents the set of finite and discrete cellular situations, t and $t+1$ are diverse moments, N is the cellular neighborhood, and f is the cellular transition rules.

The suitability image set is generated to define evolutionary rules or criteria based on the MCE model [20], and the state of the metacell at the next moment is determined based

on the suitability image set. Based on the economic and ecological conditions of the study area, eight suitability factors, including elevation, slope, slope direction, distance from road, distance from water, distance from construction land, per capita GDP and population density, are selected to generate transfer suitability images, and finally, the Collection Editor tool is used to package the transfer suitability image set to participate in the later land use change prediction.

The kappa coefficient can check the consistency between simulation results and observation data as a whole and is widely used in studies on the accuracy of land use change simulations, which can be expressed by the following formula [37,38]:

$$Kappa = (P_0 - P_c)/(P_p - P_c), \quad (3)$$

where P_0 denotes the probability of correct prediction; P_c denotes the probability of correct prediction in the random case; and P_p denotes the probability of correct prediction under ideal classification. The Kappa coefficient for 2015 was 0.86, as calculated by IDRISI software, indicating that the model had a good prediction effect, and the prediction results were credible. Based on this result, this study further simulated the land use in 2025 in the study area.

2.3.2. FLUS Model

The FLUS (future land use simulation) model mainly includes three major components: ANN-based probability-of-occurrence estimation [39], self-adaptive inertia and competition mechanism, and Markov chain. This is a land-use simulation model based on the probability of occurrence and land competition mechanism. The formula is expressed as follows [18]:

$$TPS_{k,t}^{l} = p(k,t,l) \times \Omega_{k,t}^{l} \times Inertia_{t}^{l} \times (1 - sc_{c \to t}), \quad (4)$$

where $TPS_{k,t}^{l}$ is the total probability of conversion of raster k to land category t at moment l; $p(k,t,l)$ is the probability of suitability of land category t on raster k at moment l; $\Omega_{k,t}^{l}$ is the meta-neighborhood influence factor; $Inertia_{t}^{l}$ is the adaptive inertia coefficient of land category t at moment l; $sc_{c \to t}$ is the cost required to convert land use category c to category t; and $1 - sc_{c \to t}$ is the ease of land category conversion.

After obtaining suitability probabilities, the roulette selection mechanism is used to simulate the future evolution characteristics of land use [40]. The future demand for each land use category is obtained through expert empirical methods or other land type quantity forecasting methods [21]. In this study, we obtained land use demand data for each year from 2015–2025 by expert empirical methods and Markov chains. The following driving factors are selected: elevation, slope, slope direction, distance to road, distance to water, distance to construction land, regional gross domestic product (GDP) and population density.

The precision validation module in FLUS software estimated that the Kappa coefficient for 2015 was 0.90, which confirms that the model has a good prediction effect and reliable prediction results. On this basis, the simulation of the evolution of land patterns in the study area in 2025 was further carried out.

2.3.3. Establishment of Habitat Evaluative Indicators

The habitat quality module of the InVEST model habitat quality evaluation is based on land use/cover information and biodiversity stressors and thus assesses the function of biodiversity maintenance [41]. The module assumes areas with better habitat quality have better biodiversity and that a decrease in habitat extent and habitat quality indicates a decrease in biodiversity in the area. By analyzing the impact of ecological threat factors related to human activities on land use, the degree of habitat degradation (degradation), habitat quality (habitat quality) and habitat rarity (habitat rarity) are evaluated in general.

(1) Habitat Degradation Index

The value of the habitat degradation index represents the impact level of threat factors on habitat and, thus, the potential for habitat destruction and the degradation of habitat quality. The habitat degradation index takes values from 0 to 1; the closer the value is to 1, the greater the potential damage caused by the threat source to the regional habitat and the more detrimental the maintenance of biodiversity [42]. The habitat degradation index is calculated by the following equation:

$$D_{xj} = \sum_{r=1}^{R} \sum_{y=1}^{Y_r} \left(\frac{w_r}{\sum_{r=1}^{R} w_r} \right) r_y i_{rxy} \beta_x S_{jr} \tag{5}$$

where D_{xj} is the habitat degradation index; R is the total number of threat factors; w_r is the weight; the number of grids in the threat factor r is Y_r; r_y is the threat factor r in grid y; β_x denotes the accessibility of the threat source to grid x under the protection of society and law; S_{jr} is the sensitivity of land use type j to threat r; and i_{rxy} is the threat effect of threat factor r in grid y on the habitat in grid x.

(2) Habitat Rarity Index

The habitat rarity index refers to the degree of fragmentation and ecological stability of the habitat patches in a region. The higher the habitat rarity index is, the more unstable the ecological structure and function of the area and the greater the possibility of ecological environment damage [43]. The lower the habitat rarity index, the more stable the ecosystem, and the material and energy cycles are not easily broken. Habitat scarcity is calculated by the equation:

$$R_x = \sum_{x=1}^{X} \sigma_{xj} R_j \tag{6}$$

where R_x is the habitat rarity index; R_j is the discriminant index of land use category j of the raster cell; and σ_{xj} indicates whether the current land cover category of raster cell x is j. If yes, then σ_{xj}=1; if not, then σ_{xj}=0.

(3) Habitat Quality Index

Habitat quality refers to the ability of an ecosystem to provide suitable conditions for the survival of individual organisms and populations. In the grid layer, the habitat quality index changes continuously from 0 to 1. The closer the value is to 1, the more favorable the maintenance of biodiversity [44]. The specific calculation equation is as follows:

$$Q_{xj} = H_j \left[1 - \left(\frac{D_{xj}^z}{D_{xj}^z + k^z} \right) \right] \tag{7}$$

where Q_{xj} represents the habitat quality of grid x in land cover category j; H_j denotes the habitat suitability of land cover category j; and k is the half-saturation factor, whose value is equal to half the resolution size of the raster cell.

(4) Parameter requirement analysis of the InVEST model

The main parameters required to run the InVEST model include the weights and effective distances of the threat factors as well as the suitability and sensitivity of the habitat for each threat factor.

According to the review of relevant literature [6,28,42–45], reference to the application examples in the InVEST User's Guide [46], expert consultation and analysis of field survey for Nanchang area, the region has higher population, arable land and villages and towns, human activity disturbance has a greater impact on the change of landscape pattern in the study area, construction land and agricultural land reflect the threat of human activity to habitat, while traffic roads also have an impact on the evolution of habitat with the modification of the surface by human activity. The habitat quality evolution of the

agricultural land, rural residential land, urban land, other construction land, highway and railroad, which have more population activities and greater influence on ecological landscape, were selected as threat factors, and the influence distance and weight of each threat factor (Table 1) and the suitability and sensitivity of each landscape type (Table 2) were assigned.

Table 1. Attributes of threat data.

Threat Factor	Maximum Distance	Weight	Spatial Decay Type
Farmland	1.5	0.6	Linear
Rural Resident Land	2.5	0.4	Exponential
Urban Land	6	0.8	Exponential
Other Construction Land	4	0.5	Exponential
Highway	6	0.6	Linear
Railway	5	0.3	Linear

Table 2. Sensitivity of land-use types to each threat.

Landscape Types	Habitat Suitability	Farmland	Rural Resident Land	Urban Land	Other Construction Land	Highway	Railway
Farmland	0.4	0	0.35	0.5	0.3	0.5	0.5
Woodland	1	0.8	0.85	1	0.8	0.9	0.8
Grassland	0.6	0.5	0.35	0.6	0.5	0.7	0.7
Waters	1	0.7	0.75	0.9	0.9	0.75	0.6
Construction Land	0	0	0	0	0	0	0
Unutilized Land	0	0	0	0	0	0	0

3. Results

3.1. Land Use and Its Transfer Changes in the Study Area

Woodland, farmland and waters are the major land categories in Nanchang city, accounting for 70% of the total area, of which 50% is farmland (Figure 2). The land-use pattern changed considerably between 1995 and 2015, with the greatest changes occurring in farmland and construction land. The area change of each land type was mainly reflected in the decreases in farmland, woodland and grassland each year. Among them, farmland has been decreasing at a rate of 0.2% per year, with a total reduction of 293,550 ha, and the pressure on farmland has been increasing. Woodland and grassland also showed declines, with more moderate rates of reduction. The area of construction land has increased each year, with a growth rate of 96.44% and an overall increase in area of 2,951,500 ha in the past 20 years, which reflects the increasing demand for the expansion of construction land under the background of an increasing level of urbanization, an increase in population pressure and continuous economic development. The rate of decline in unused land was more moderate. A slight increase is observed in the water area (Figure 3).

As shown in Table 3, from 1995 to 2005, the most transferred land type in the study area was farmland, with a net transfer of 58,403 ha, shifting mainly to 32,878 ha of waters and 47,612 ha of construction land, with the transfer of farmland being influenced by the return of farmland to lakes and the expansion of urban construction land. The next largest land type transferred out was woodland, with a net transfer of 17,475 ha, and the majority transferred to farmland (4202 ha) and construction land (14,291 ha), indicating that the clearance of woodland for farmland and construction land expansion still occurs. The land types that significantly increased were water (16,657 ha) and construction land (59,513 ha), with the increase in water mainly coming from farmland (32,878 ha), reflecting the achievements of returning farmland to lakes. At the same time, the most transferred

land type was construction land, with 69.9% of the transferred construction land coming from farmland, indicating that the main land type occupied by urban expansion is still farmland. The areas of grassland and unused land did not change much.

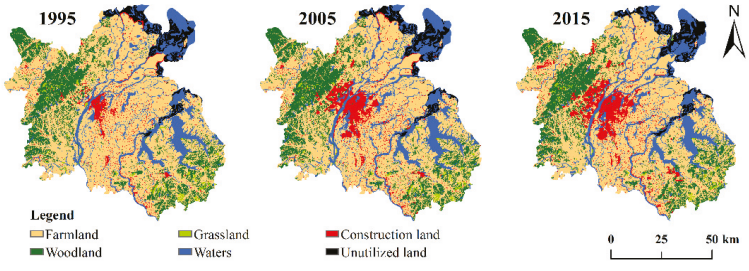

Figure 2. Spatial distribution patterns of landscape types in 1995, 2005, and 2015.

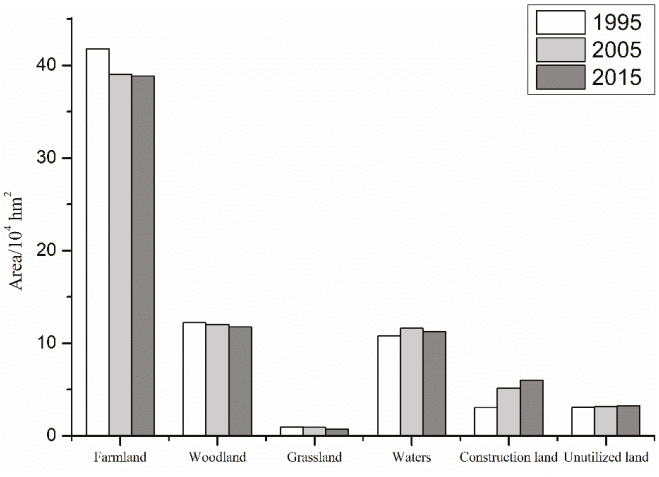

Figure 3. Land-use area of the first classes in 1995, 2005, and 2015.

From 2005 to 2010, farmland was still the most transferred land type, and its area continued to decrease by 35,344 ha, with the rate of reduction tending to be smaller and the main shifts to construction land (46,976 ha), followed by water (11,669 ha) and woodland (9873 ha); additionally, the conversion of farmland and the conversion of grassland largely offset one another. The decrease in woodland also tended to be smaller, with a reduction of 8894 ha and the main shifts to farmland (15,815 ha) and unused land (6519 ha). The area of grassland decreased slightly. The waters were significantly different from the previous period, from a net transfer of 32,878 ha to a net transfer of 1823 ha, mainly due to the shrinkage of Poyang Lake and the transfer of water out to unused land. The construction land continued to increase, with a net transfer of 5,699,300 ha, but the growth rate was lower than that of the previous period. Farmland was still an important source of construction land, with a net transfer of 46,977 ha of farmland to construction land. The net transfer of unused land was 2605 ha, with a clear interconversion between and water.

Table 3. Land use transfer matrix in the study area (ha).

Period	Landscape Types	Farmland	Woodland	Grassland	Waters	Construction Land	Unutilized Land	Transfer Out	Net Transfer Out
1995~2005	Farmland	305,595	1238	916	32,878	47,612	1166	83,811	58,403
	Woodland	4202	99,495	334	1423	14,291	54	20,304	17,475
	Grassland	310	662	7227	444	603	0	2019	656
	Waters	14,146	778	112	93,473	5588	1261	21,885	−16,657
	Construction land	3551	82	1	2118	43,069	2837	8589	−59,513
	Unutilized land	3200	69	0	1679	8	26,124	4956	−362
	Transfer in	25,408	2829	1363	38,542	68,102	5318		
2005~2015	Farmland	318,526	9873	659	11,669	46,976	43	69,220	35,344
	Woodland	15,814	93,681	642	463	6518	6	23,443	8893
	Grassland	805	1714	4921	93	49	0	2661	781
	Waters	9033	2631	98	86,935	3368	9548	24,678	1822
	Construction land	8169	331	46	4179	47,333	32	12,756	−44,235
	Unutilized land	54	1	434	6453	81	25,352	7025	−2604
	Transfer in	33,876	14,550	1879	22,857	56,992	9629		

3.2. Analysis of Habitat Degradation

The value of the habitat degradation index represents the impact level of threat factors on habitat and, thus, the potential for habitat destruction and the degradation of habitat quality. The habitat degradation index takes values from 0 to 1; the closer the value is to 1, the greater the potential damage caused by the threat source to the regional habitat and the more detrimental the maintenance of biodiversity.

As shown in Figure 4, the maximum values of the habitat degradation index at each time point were 0.1411, 0.1422 and 0.1473, respectively, with a gradual increasing trend from 1995 to 2015. The areas with a high degree of habitat degradation were around the city and in various watersheds, indicating that their habitats had high degradation potential. The expansion of cities has resulted in the conversion of farmland and other land types around cities into construction land, which causes the most serious damage to the ecological environment. The ecosystem around the watershed is vulnerable to external disturbance, and the level of habitat degradation is significant. In addition, habitat degradation at the junction of the plain and Meiling is very prominent, presenting almost a linear trend. The areas with a low degree of habitat degradation were located in the Poyang Lake area in the northeastern portion of Nanchang city, where the corresponding land types were mainly water and mudflat swamps, and the land types were relatively singular and less disturbed by humans; thus, the habitat quality was not significantly degraded. Generally, the urbanization of Nanchang city developed rapidly from 1995 to 2015, which led to the increasing trend of habitat degradation.

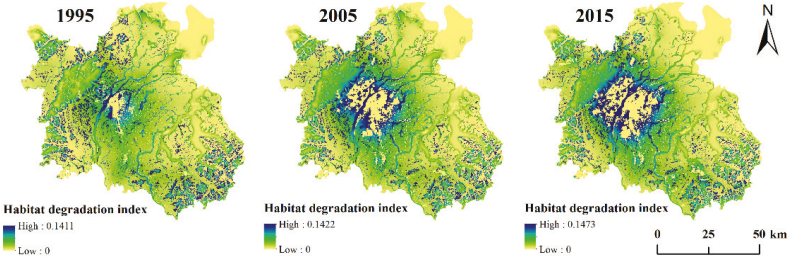

Figure 4. Spatial distribution pattern of the habitat degradation index in 1995, 2005, and 2015.

3.3. Analysis of Habitat Rarity

The habitat rarity index refers to the degree of fragmentation and ecological stability of the habitat patches in a region. The higher the habitat rarity index, the more unstable the ecological structure and function of the area are, and the greater the possibility of ecological environment damage. The lower the habitat rarity index, the more stable the ecosystem, and the material and energy cycles are not easily broken.

The minimum value of the habitat rarity index in Nanchang decreased from −0.6888 to −0.9644 (Figure 5), and the maximum value increased from 0.0663 to 0.2094 in both periods, indicating that the range of the habitat rarity index in the study area expanded; i.e., the stability of landscape patches became more variable. A comparative analysis of Figure 5 and the land use types in Nanchang showed that the red area in Figure 5 indicates the highest habitat rarity index, and the land-use type is mainly farmland. Due to the expansion of construction land, the farmland was relatively more damaged and became more fragmented and less stable. The woodland landscape (orange) in the western and southeastern parts of the study area had a high habitat rarity, which may be due to the influence of the surrounding construction land as well as human factors; in addition, the landscape integrity of the woodland suffered some disturbances, and the woodland cover tended to be unstable. The land use types with low habitat rarity (blue) were mainly construction land and water. Moreover, the habitat rarity of unutilized land, such as the mudflats and marshes of Poyang Lake in the northeastern part of the study area, changed from medium (yellow) to low (blue), and the decrease in the habitat rarity index in this area reflected the effectiveness of ecological restoration and the construction of the Poyang Lake Nature Reserve in recent years. There is an urgent need for governments and ecological managers to take certain initiatives to enhance the regulation and protection of farmland, woodland, and grassland to prevent further habitat degradation.

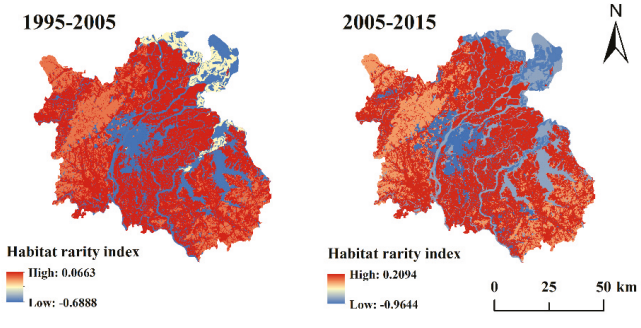

Figure 5. Spatial distribution pattern of the habitat rarity index in 1995–2005 and 2005–2015.

3.4. Analysis of Habitat Quality

To further investigate the influence of land-use change on habitat quality in the study area, the results of the habitat quality index calculations for the three periods were classified into five levels: low (0–0.2), relatively low (0.2–0.3), medium (0.3–0.4), relatively high (0.4–0.8) and high (0.8–1) (Table 4), and the habitat quality area and its percentage of each level in the three periods were calculated (Table 5, Figure 6). The results showed the following:

1. In terms of temporal change, the proportion of low-grade habitats has been increasing over 20 years, while the proportion of relatively low-grade habitats has been decreasing over 20 years; however, both types of habitat have changed more in the last 10 years than in the first 10 years. The proportion of medium-grade habitats decreased significantly and then increased slightly, showing an overall decreasing trend. The proportion of relatively high-grade habitat also showed a decreasing trend. The proportion of high-grade habitat experienced a slight fluctuation of increasing

and then decreasing, with no significant overall change. The above changes represent a process of transition from relatively high-grade, middle-grade and relatively low-grade habitats to low-grade habitats, and the habitat quality is in the process of being degraded. Finally, the degradation was more serious in the first 10 years than in the last 10 years.

2. In terms of spatial pattern, the change in the spatial pattern in Nanchang had a certain amount of regularity. The area with high habitat quality accounted for a small proportion and was mainly distributed in Meiling in northwestern Nanchang, Poyang Lake in the northeast, and Junshan Lake and Qinglan Lake in the southeast. The famous Meiling National Forest Park is located in Meiling, and this zone is mainly woodland, rich in biodiversity, with little human activity and a high degree of ecological protection; thus, the habitat quality of this zone is high. Poyang Lake, Junshan Lake and Qinglan Lake have the ecological function of maintaining the biodiversity of the wetland landscape and replenishing groundwater. The habitat quality in this area is also relatively high under the protection of the local government. Areas of low habitat quality were mainly located in the Honggutan, East Lake, West Lake and Qingshan Lake districts on both sides of the Ganjiang River in central Nanchang, which are the central urban areas of Nanchang; these areas have rapid economic development, commercial development, rapid expansion of construction land, massive occupation of farmland resources and serious disturbances by human activities, resulting in poor habitat quality in this area. Areas of relatively low habitat quality were concentrated in most of the plain areas, where the land type is mainly farmland. These regions also have concentrations of rural settlements, and human activity is frequent; thus, ecological damage has occurred.

Table 4. Classification value of habitat quality.

Grade	Value Range	Description
Low	0~0.2	Poor habitat quality
Relatively low	0.2~0.3	Relatively poor habitat quality
Medium	0.3~0.4	Medium habitat quality
Relatively high	0.4~0.8	Relatively high habitat quality
High	0.8~1	High habitat quality

Table 5. Area and percentage of habitat quality at all grades (10^4 ha, %).

Grade	1995		2005		2015	
	Area	Percentage	Area	Percentage	Area	Percentage
Low	6.1491	8.56	8.3151	11.57	9.2899	12.93
Relatively low	39.5481	55.05	37.4760	52.16	37.1181	51.66
Medium	2.2179	3.09	1.5215	2.12	1.7134	2.38
Relatively high	0.9609	1.34	0.9260	1.29	0.7484	1.04
High	22.9699	31.97	23.6073	32.86	22.9761	31.98

3.5. Comparison of Land Use Pattern Projections

Both the CA-Markov model and the FLUS model found that the simulated land use category in Nanchang in 2025 (Figure 7) is dominated by farmland, woodland land and water bodies, with these three types together accounting for more than 79% of the study area. In 2025, there were differences in the area of different land types simulated by the two models (Figure 8), but the characteristics of future land use change were similar. From 2015 to 2025, the area of construction land continued to increase significantly, and the area of watershed and unutilized land increased slightly, with construction land increasing by 4% compared to 2015, and the situation of construction land expansion was serious. The area of other land types decreased compared with 2015, including farmland, which decreased

by at least 20,000 ha, reflecting the pressure on farmland conservation, while the areas of woodland and grassland both shrank to different degrees. These changes are mainly due to the impact of urban expansion. The differences in the spatial distribution by the two simulated models are reflected in the following two regions.

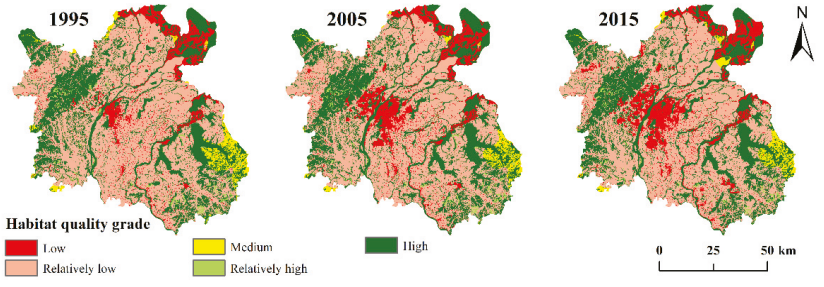

Figure 6. Spatial distribution pattern of habitat quality in 1995, 2005, and 2015.

One region is located in the Poyang Lake area in the northeastern part of the study area, and the grassland and water bodies predicted by the above two models differ significantly in quantity and spatial distribution. Compared with the distribution in 2015, the grassland in 2025 predicted by the CA-Markov model is significantly larger, and the watershed area is smaller, while the grassland and watershed areas predicted by the FLUS model change little. In recent years, many sand mining vessels have entered Poyang Lake and carried out sand mining operations due to the increased crackdown on sand mining in the Yangtze River and the interest driven by the high price of natural sand. Sand mining has caused the riverbed to be dug deeper and the volume of the river channel to be enlarged continuously, resulting in a drop in the water level, a reduction in water, and the exposure and expansion of grassy patches [47]. Hence, the prediction of FLUS in this area is error, and the CA-Markov model performs better in this region.

The other region is the Meiling area, located in the northwestern part of the study area, where the two models predict a significant difference in the area of construction land. CA-Markov predicts a significant expansion of construction land in 2025 compared to 2015, while FLUS predicts a smaller change in construction land. The region is located in Meiling National Forest Park, and the land use type is mainly woodland, which is a pivotal ecological security barrier in Nanchang and is protected by the government and ecological managers. The area is less likely to be developed for building land, so the prediction of the CA-Markov model is biased in this area, and the FLUS model performs better in this region. In general, the two models are well applied overall, but there are still deviations and shortcomings in individual regions.

3.6. Prediction of Habitat Quality

The future land use cover maps simulated by the two prediction models in Section 3.5 were input into the InVEST model, and the parameters were set according to Section 2.3.3 to obtain the spatial distribution patterns of habitat quality in 2025 predicted by CA-Markov and FLUS.

The spatial and temporal variation characteristics of habitat quality in Nanchang in 2025 simulated by the CA-Markov and FLUS combined with the InVEST model are basically consistent with those in the previous period. From the spatial pattern (Figure 9), there is an overall pattern of high habitat quality in the Meiling belt in the northwest and in the Poyang Lake area in the northeast, a dense lake network in the southeast, and a gradual decrease in habitat quality toward the central area. From the temporal variation (Table 6), the combination of the CA-Markov and InVEST models predicts an average habitat quality index of 0.4236 in 2025, and the combination of the FLUS and InVEST models predicts an average habitat quality index of 0.4359 in 2025. Compared with the values in 2015, the two

averages in 2025 decreased by 0.0209 and 0.0086, respectively, suggesting that in the context of the continuous expansion of construction land, the habitat quality of Nanchang City in 2025 will further decline. Although the percentages of future habitat quality predicted by the combination of the two models differed slightly for different classes, the trends in habitat quality were consistent with those observed in 2015 (Table 6). By 2025, the percentage of high-grade and higher-grade habitats continues to decrease, shifting mainly to low-grade and mid-grade habitats. Areas with low-grade habitats are mostly construction land, and habitat quality in these areas declines further. Although the percentage of relatively low-grade habitats in 2025 is lower than that in 2015, the percentage of low-grade habitats increases significantly, with an area increase of at least 4%. The above phenomenon reflects that the habitat quality in the region is expected to deteriorate significantly from 2015 to 2025, mainly due to the significant expansion of land use types with poor habitat suitability, such as construction land and unutilized land, and the decreases in the areas of woodland and grassland with good habitat suitability during that period.

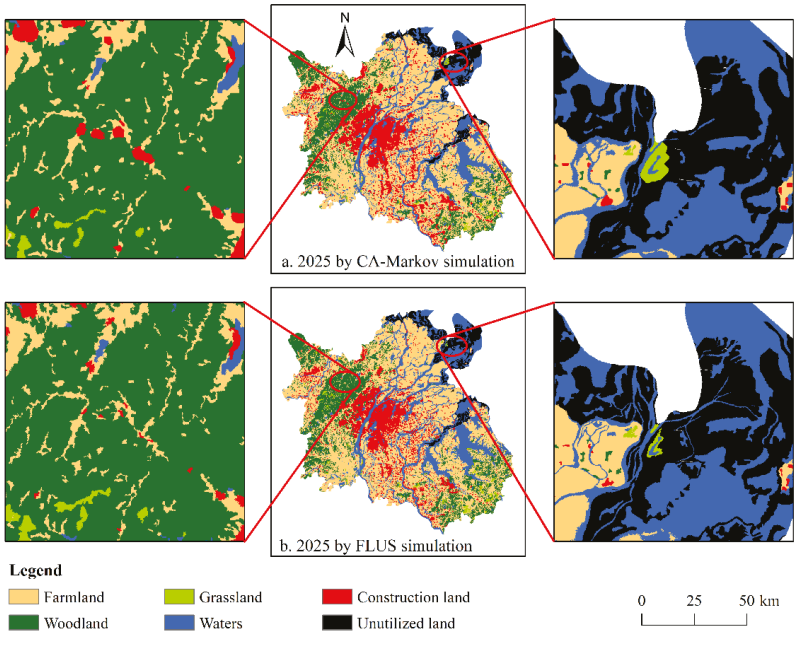

Figure 7. Spatial distribution patterns of land-use types in 2025 projected by CA-Markov and FLUS.

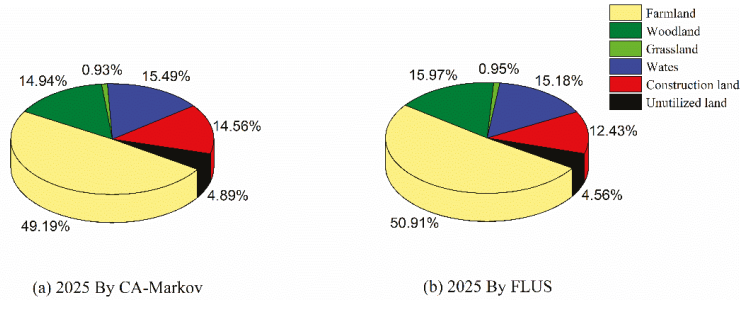

Figure 8. Percentage of each land-use type in 2025 projected by CA-Markov and FLUS.

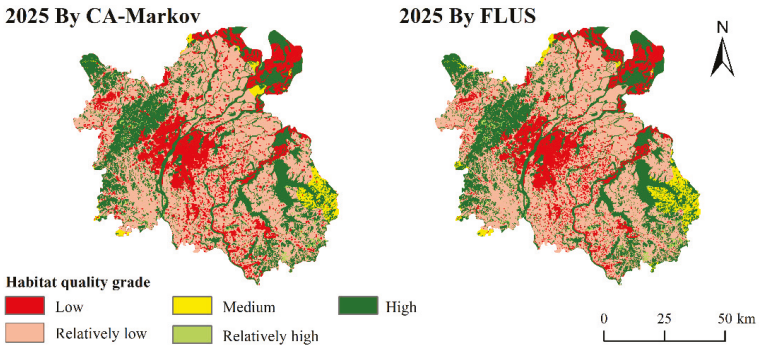

Figure 9. Spatial distribution patterns of habitat quality in 2025 projected by CA-Markov and FLUS.

Table 6. Changes in area and percentage of different classes of habitat quality in 2015–2025 (10^4 ha, %).

Grade	2015		2025 by CA-Markov		2025 by CA-Markov	
	Area	Percentage	Area	Percentage	Area	Percentage
Low	9.2899	12.93	14.1289	19.67	12.2113	17.00
Relatively low	37.1181	51.66	33.5012	46.63	34.4019	47.88
Medium	1.7134	2.38	1.7451	2.43	2.1673	3.02
Relatively high	0.7484	1.04	0.6250	0.87	0.6750	0.94
High	22.9761	31.98	21.8461	30.41	22.3909	31.17

4. Discussion

4.1. Analysis of the Causes of Changes in Habitat Quality

With the accelerated urbanization of Nanchang, issues such as increased population and town expansion can cause a certain amount of damage to the regional ecological environment, and the protection of the ecological environment must not be neglected in the pursuit of social and economic development. The prediction and evaluation of landscape patterns and habitat quality are important tools for optimizing regional landscape patterns and maintaining regional ecological security, which fits with the results of other case studies listed in the first section [5–10]. In this paper, two different prediction models (CA-Markov and FLUS) are used to model historical, present and future land use variations, and the InVEST model is introduced to integrate each of these two prediction models into habitat quality modeling to explore the effects of the evolution of landscape patterns on habitats. This study found a significant decline in habitat quality in Nanchang during 1995–2025.

From a land use perspective, the main variations in Nanchang were the high rate of expansion of construction land and the significant reductions in woodland, grassland and water areas with high habitat suitability. The area of construction land, which is a source of habitat quality threat, increased dramatically during the research period, especially around the central urban areas represented by the Honggutan, East Lake, West Lake and Qingshan Lake districts on both sides of the Ganjiang River. Furthermore, the abovementioned areas have continuously encroached on woodlands, waters and grasslands with high habitat suitability, thus expanding the area and impact of the threat source and leading to a continuous decline in the habitat quality of the study area. These findings coincide with those of other case studies indicating that urban expansion is the primary cause of habitat quality decline [48,49].

From a topographical perspective, the landform of Nanchang city is mainly plain, with a wider water area and a large number of hills and low hills. The Ganjiang River and the Fuxiang River flow through Nanchang from south to north. The study area also has the famous Gan-Fu Plain with relatively flat topography, and the only hilly area in the

study area is in Meiling National Forest Park in the northwest. In terms of topography, it is less difficult to develop construction land, and the area is prone to unrestricted sprawl, while hilly areas have always maintained a high habitat quality due to the low impact of human activity.

From the spatial distribution of habitat quality, the areas with a habitat quality index above 0.8 were mainly distributed in Meiling in the northwest, Poyang Lake in the northeast, the watersheds of Ganjiang River and Fuxiang River running through the study area, and Junshan Lake and Qinglan Lake in the southeast; specifically, the areas with a high index included Meiling National Forest Park, which is dominated by woodlands and rich in biodiversity, and Poyang Lake, Junshan Lake and Qinglan Lake, which are important wetland areas in Nanchang with a superior natural environment. At the same time, the government has paid great attention to the ecological protection of these areas, and as a result, they have a high habitat quality. The increase in ecological land, such as woodland and water, can offset the negative effects of urbanization [50].

In the pursuit of socioeconomic development in Nanchang, if the existing land-use pattern is not changed, the dramatic increase in construction land and the decreases in woodland and grassland, such as industrialization and urbanization acceleration, will lead to a continued decline in the overall habitat quality. By 2025, the proportion of low-grade habitats in Nanchang will rise significantly, with an increase of at least 4% in area, and most of the low-grade habitat areas will be construction land. The government should strengthen the risk monitoring and the assessment of these areas to avoid habitat deterioration as much as possible.

4.2. Comparison and Suitability Analysis of the CA-Markov and FLUS

In general, the future land use distributions predicted by CA-Markov and FLUS have a high consistency, with a few differences in the edges of the land types. The edges of the land type patches predicted by CA-Markov are smoother, especially for construction land with more intense expansion, and the land type shapes are distributed in clusters, mainly due to the more aggressive simulation mechanism. The edges of the land type patches predicted by FLUS are more fragmented, and the land type shapes are more irregular, thereby portraying the spatial morphological evolution of land use more precisely.

In terms of quantitative land-use change, CA-Markov predicts a more radical evolution of the landscape pattern than FLUS. In particular, the growth rate of construction land and the shrinkage rates of woodland and grassland increase significantly, which is more in line with the observed situation of land use evolution in Nanchang. In terms of spatial land-use change, the kappa coefficient of CA-Markov was lower than that of FLUS, proving that the simulation results of FLUS in this study are better than those of CA-Markov in terms of spatial pattern. Through comparison, this paper finds that CA-Markov is better at predicting land use quantities, while FLUS is closer to the real land use pattern in terms of spatial morphology and overall structure. The CA-Markov model is more suitable when focusing on the prediction of quantitative land-use changes, especially for construction land, and the FLUS model is relatively more suitable when putting particular emphasis on the spatial morphology and overall structure of land use.

By conducting spatial and quantitative comparisons, the prediction results of the two models are mutually supported and indirectly verified, and the above findings provide a more accurate reference for land use simulation for different needs. In practical applications, the corresponding models should be selected according to specific requirements and purposes to achieve better simulation results.

4.3. Implications

The implications of this paper can be described from both theoretical and practical aspects.

In terms of theory, on the one hand, the introduction of habitat evaluative indicators reflecting regional biodiversity provides a novel approach and perspective for the diversification of habitat assessment systems. On the other hand, the method of this study

is more reasonable and effective than the traditional single-line model combination of a single prediction method and the habitat assessment model. Although this study provides some references for helping to understand the complex dynamic evolution mechanism of habitats under global urbanization and provides a guide for habitat assessment and prediction in other areas with rapid urbanization, there are still some shortcomings. There are many models currently available to estimate future land-use variation, such as the gray model, logistic regression model, conversion of land-use and its effects (CLUE)-S model and composite models based on CA. [11–15]. All of these models are now widely used in the field, yet we did not study whether there are some models with higher simulation accuracy available. Exploring whether higher precision models are available will be a direction for future improvement and effort. Since the evolution of land use patterns is a complex process influenced not only by the geographical conditions of the region but also by human interventions such as land use policies, it will be essential to explore the role of policy interventions on the evolution of land types to improve the prediction accuracy [51]. In addition, the InVEST model only considers the influence of threat factors on habitats within the study area, while habitats at the edge of the study area are also influenced by other threat factors outside the study area boundary, which might make the assessment results inaccurate. In the future, attention should be given to collecting data on threat factors at the edge of the study area [27]. These shortcomings provide a direction for future theoretical development.

In terms of practice, by studying the impact of land use evolution on habitat quality in Nanchang city, we obtained the following measures that are crucial for optimizing the landscape pattern of Nanchang city and maintaining regional ecological security: (1) The dramatic expansion of construction land is the primary cause for the decline in habitat quality, and the scale of construction land should be managed to avoid the disorderly expansion of urban construction land. (2) The reduction in the area of ecological land, such as woodland and grassland, can also directly lead to a decrease in habitat quality, so it is necessary to set up a forest manager system; implement the zoning management of woodland, grassland and other types of land with high habitat suitability; and establish a system of responsibility for resource targets in ecological barrier areas [52]. (3) From the perspective of habitat degradation, habitat degradation is especially obvious near the city and around the watershed. On the basis of controlling the scale of construction land, it is also crucial to strengthen watershed protection to achieve the goal of ecological security [53]. The above measures are of practical significance for territorial development plans and the construction of ecological security. In the future, the impact of land use/land cover changes on ecological and environmental quality should be fully considered, a constraint mechanism between environmental protection and economic development should be established, and scientific decisions and reasonable planning should be made for rapidly urbanizing areas to promote the win-win development of the social economy and ecological protection.

5. Conclusions

Evaluating and predicting the spatial and temporal evolution of habitat quality under land-use change provides a scientific reference for carrying out ecological conservation and sustainable development. In this paper, two different prediction models (CA-Markov and FLUS) were used to simulate past, current and future land use changes based on the land use distribution data of Nanchang city in three periods of 1995, 2005 and 2015, and the InVEST model was introduced to integrate each of these two prediction models into habitat quality modeling to analyze the effects of the spatial and temporal evolution of landscape patterns on habitats. The results indicate that the habitat quality of the study area is expected to decline significantly from 1995 to 2025, and low-grade habitats will continue to increase. By 2025, the percentage of high-grade and relatively high-grade habitats continues to decrease, shifting mainly to low-grade and middle-grade habitats. Areas with low-grade habitats are mostly construction land. With accelerated industrialization and urbanization, the high rate of expansion of land types with low habitat suitability, such as construction

land, will in turn interfere with areas with high habitat quality, such as woodlands, water bodies and grasslands, resulting in the expansion of the scale and sphere of influence of threat sources, greater landscape fragmentation and reduced stability, which will cause a continuous decline in habitat quality in Nanchang city. This study also identified that the future land use distributions predicted by the CA-Markov and FLUS models have a high consistency, with a few differences in the edges of the land types.

Author Contributions: Conceptualization, Y.L. and L.D.; methodology, Y.L. and L.D.; software, Y.L.; validation, L.D. and M.Z.; formal analysis, Z.W. and Y.G.; investigation, M.Z. and Z.W.; writing—original draft preparation, Y.L.; writing—review and editing, L.D.; visualization, Y.L. and L.D.; supervision, M.Z. and Y.G.; funding acquisition, L.D., M.Z. and Y.L. All authors have read and agreed to the published version of the manuscript.

Funding: This research was funded by the Research Center of Geological Resource Economics and Management of East China University of Technology, grant number 20GL02, the Institutional Research Centers of Jiangxi Provincial of Ecological Civilization Construction, grant number JXST2103, the Doctoral Research Initiation fund of East China University of Technology, grant number DHBK2019184, Science and Technology Projects of Jiangxi Provincial Department of Education, grant number GJJ200770, the National Natural Science Foundation of China, grant number 11465002, and the Graduate Innovation Fund of East China University of Technology, grant number DHYC-202123.

Data Availability Statement: Not applicable.

Acknowledgments: The authors are grateful to the editor and reviewers for their valuable comments and suggestions.

Conflicts of Interest: The authors declare no conflict of interest.

References

1. Lai, Y.; Jiang, L.; Xu, X. Exploring Spatio-Temporal Patterns of Urban Village Redevelopment: The Case of Shenzhen, China. *Land* **2021**, *10*, 976. [CrossRef]
2. He, B.J.; Zhao, Z.Q.; Shen, L.D.; Wang, H.B.; Li, L.G. An approach to examining performances of cool/hot sources in mitigating/enhancing land surface temperature under different temperature backgrounds based on landsat 8 image. *Sustain. Cities Soc.* **2019**, *44*, 416–427. [CrossRef]
3. Zhao, Z.Q.; He, B.J.; Li, L.G.; Wang, H.B.; Darko, A. Profile and concentric zonal analysis of relationships between land use/land cover and land surface temperature: Case study of Shenyang, China. *Energy Build.* **2017**, *155*, 282–295. [CrossRef]
4. Li, W.; Qi, J.; Huang, S.; Fu, W.; Zhong, L.; He, B. A pressure-state-response framework for the sustainability analysis of water national parks in China. *Ecol. Indic.* **2021**, *131*, 108127. [CrossRef]
5. De Simone, S.; Sigura, M.; Boscutti, F. Patterns of biodiversity and habitat sensitivity in agricultural landscapes. *J. Environ. Plan. Manag.* **2017**, *60*, 1173–1192. [CrossRef]
6. Terrado, M.; Sabater, S.; Chaplin-Kramer, B.; Mandle, L.; Ziv, G.; Acuña, V. Model development for the assessment of terrestrial and aquatic habitat quality in conservation planning. *Sci. Total Environ.* **2016**, *540*, 63–70. [CrossRef]
7. Nelson, E.; Mendoza, G.; Regetz, J.; Polasky, S.; Tallis, H.; Cameron, D.R.; Chan, K.M.A.; Daily, G.C.; Goldstein, J.; Kareiva, P.M.; et al. Modeling multiple ecosystem services, biodiversity conservation, commodity production, and tradeoffs at landscape scales. *Front. Ecol. Environ.* **2009**, *7*, 4–11. [CrossRef]
8. Leh, M.D.K.; Matlock, M.D.; Cummings, E.C.; Nalley, L.L. Quantifying and mapping multiple ecosystem services change in West Africa. *Agric. Ecosyst. Environ.* **2013**, *165*, 6–18. [CrossRef]
9. Kovacs, K.; Polasky, S.; Nelson, E.; Keeler, B.L.; Pennington, D.; Plantinga, A.J.; Taff, S.J. Evaluating the Return in Ecosystem Services from Investment in Public Land Acquisitions. *PLoS ONE* **2013**, *8*, e62202. [CrossRef]
10. Shaw, M.R.; Pendleton, L.; Cameron, D.R.; Morris, B.; Bachelet, D.; Klausmeyer, K.; MacKenzie, J.; Conklin, D.R.; Bratman, G.N.; Lenihan, J.; et al. The impact of climate change on California's ecosystem services. *Clim. Change* **2011**, *109*, 465–484. [CrossRef]
11. Tong, S.T.Y.; Sun, Y.; Ranatunga, T.; He, J.; Yang, Y.J. Predicting plausible impacts of sets of climate and land use change scenarios on water resources. *Appl. Geogr.* **2012**, *32*, 477–489. [CrossRef]
12. Tang, F.; Fu, M.; Wang, L.; Zhang, P. Land-use change in Changli County, China: Predicting its spatio-temporal evolution in habitat quality. *Ecol. Indic.* **2020**, *117*, 106719. [CrossRef]
13. El-Tantawi, A.M.; Bao, A.; Chang, C.; Liu, Y. Monitoring and predicting land use/cover changes in the Aksu-Tarim River Basin, Xinjiang-China (1990–2030). *Environ. Monit. Assess.* **2019**, *191*, 480. [CrossRef]
14. Huang, D.; Huang, J.; Liu, T. Delimiting urban growth boundaries using the CLUE-S model with village administrative boundaries. *Land Use Policy* **2019**, *82*, 422–435. [CrossRef]

15. Varga, O.G.; Pontius, R.G.; Singh, S.K.; Szabó, S. Intensity Analysis and the Figure of Merit's components for assessment of a Cellular Automata—Markov simulation model. *Ecol. Indic.* **2019**, *101*, 933–942. [CrossRef]
16. Riccioli, F.; El Asmar, T.; El Asmar, J.P.; Fratini, R. Use of cellular automata in the study of variables involved in land use changes: An application in the wine production sector. *Environ. Monit. Assess.* **2013**, *185*, 5361–5374. [CrossRef]
17. Guan, D.; Gao, W.; Watari, K.; Fukahori, H. Land use change of Kitakyushu based on landscape ecology and Markov model. *J. Geogr. Sci.* **2008**, *18*, 455–468. [CrossRef]
18. Li, X.; Chen, G.; Liu, X.; Liang, X.; Wang, S.; Chen, Y.; Pei, F.; Xu, X. A New Global Land-Use and Land-Cover Change Product at a 1-km Resolution for 2010 to 2100 Based on Human–Environment Interactions. *Ann. Am. Assoc. Geogr.* **2017**, *107*, 1040–1059. [CrossRef]
19. Jenerette, G.D.; Wu, J. Analysis and simulation of land-use change in the central Arizona—Phoenix region, USA. *Landsc. Ecol.* **2001**, *16*, 611–626. [CrossRef]
20. Nourqolipour, R.; Mohamed Shariff, A.R.B.; Balasundram, S.K.; Ahmad, N.B.; Sood, A.M.; Buyong, T.; Amiri, F. A GIS-based model to analyze the spatial and temporal development of oil palm land use in Kuala Langat district, Malaysia. *Environ. Earth Sci.* **2015**, *73*, 1687–1700. [CrossRef]
21. Liang, X.; Liu, X.; Li, X.; Chen, Y.; Tian, H.; Yao, Y. Delineating multi-scenario urban growth boundaries with a CA-based FLUS model and morphological method. *Landsc. Urban Plan.* **2018**, *177*, 47–63. [CrossRef]
22. Wang, X.; Ma, B.W.; Li, D.; Chen, K.; Yan, H. Multi-scenario simulation and prediction of ecological space in Hubei province based on FLUS model. *J. Nat. Resour.* **2020**, *35*, 230–242. [CrossRef]
23. Azizi, A.; Malakmohamadi, B.; Jafari, H.R. Land use and land cover spatiotemporal dynamic pattern and predicting changes using integrated CA-markov model. *Glob. J. Environ. Sci. Manag.* **2016**, *2*, 223–234. [CrossRef]
24. Ramezani, N.; Jafari, R. Land Use/Cover Change Detection in 2025 with CA-Markov Chain Model (case study: Esfarayen). *Geogr. Res.* **2014**, *29*, 87–101.
25. Lin, W.; Sun, Y.; Nijhuis, S.; Wang, Z. Scenario-based flood risk assessment for urbanizing deltas using future land-use simulation (FLUS): Guangzhou Metropolitan Area as a case study. *Sci. Total Environ.* **2020**, *739*, 139899. [CrossRef] [PubMed]
26. Sallustio, L.; De Toni, A.; Strollo, A.; Di Febbraro, M.; Gissi, E.; Casella, L.; Geneletti, D.; Munafò, M.; Vizzarri, M.; Marchetti, M. Assessing habitat quality in relation to the spatial distribution of protected areas in Italy. *J. Environ. Manag.* **2017**, *201*, 129–137. [CrossRef]
27. Chu, L.; Zhang, X.R.; Wang, T.W.; Li, Z.X.; Cai, C.F. Spatial-temporal evolution and prediction of urban landscape pattern and habitat quality based on CA-Markov and InVEST model. *Chin. J. Appl. Ecol.* **2018**, *29*, 4106–4118. [CrossRef]
28. He, J.; Huang, J.; Li, C. The evaluation for the impact of land use change on habitat quality: A joint contribution of cellular automata scenario simulation and habitat quality assessment model. *Ecol. Model.* **2017**, *366*, 58–67. [CrossRef]
29. Van Hulst, R. On the dynamics of vegetation: Markov chains as models of succession. *Vegetatio* **1979**, *40*, 3–14. [CrossRef]
30. Yang, X.; Zheng, X.Q.; Chen, R. A land use change model: Integrating landscape pattern indexes and Markov-CA. *Ecol. Model.* **2014**, *283*, 1–7. [CrossRef]
31. Sang, L.; Zhang, C.; Yang, J.; Zhu, D.; Yun, W. Simulation of land use spatial pattern of towns and villages based on CA-Markov model. *Math. Comput. Model.* **2011**, *54*, 938–943. [CrossRef]
32. Vaz, E.; Arsanjani, J.J. Predicting urban growth of the greater toronto area—Coupling a markov cellular automata with document meta-analysis. *J. Environ. Inform.* **2015**, *25*, 71–80. [CrossRef]
33. Mondal, B.; Das, D.N.; Bhatta, B. Integrating cellular automata and Markov techniques to generate urban development potential surface: A study on Kolkata agglomeration. *Geocarto Int.* **2017**, *32*, 401–419. [CrossRef]
34. Baqa, M.F.; Chen, F.; Lu, L.; Qureshi, S.; Tariq, A.; Wang, S.; Jing, L.; Hamza, S.; Li, Q. Monitoring and Modeling the Patterns and Trends of Urban Growth Using Urban Sprawl Matrix and CA-Markov Model: A Case Study of Karachi, Pakistan. *Land* **2021**, *10*, 700. [CrossRef]
35. Guan, D.J.; Li, H.F.; Inohae, T.; Su, W.; Nagaie, T.; Hokao, K. Modeling urban land use change by the integration of cellular automaton and Markov model. *Ecol. Model.* **2011**, *222*, 3761–3772. [CrossRef]
36. Kamusoko, C.; Gamba, J. Simulating urban growth using a random forest-cellular automata (RF-CA) model. *ISPRS Int. J. Geo-Inf.* **2015**, *4*, 447–470. [CrossRef]
37. Wang, S.Q.; Zheng, X.Q.; Zang, X.B. Accuracy assessments of land use change simulation based on Markov-cellular automata model. *Procedia Environ. Sci.* **2012**, *13*, 1238–1245. [CrossRef]
38. Ku, C.A. Incorporating spatial regression model into cellular automata for simulating land use change. *Appl. Geogr.* **2016**, *69*, 1–9. [CrossRef]
39. Lin, Y.P.; Chu, H.J.; Wu, C.F.; Verburg, P.H. Predictive ability of logistic regression, auto-logistic regression and neural network models in empirical land-use change modeling—A case study. *Int. J. Geogr. Inf. Sci.* **2011**, *25*, 65–87. [CrossRef]
40. Chen, Y.; Li, X.; Liu, X.; Ai, B.; Li, S. Capturing the varying effects of driving forces over time for the simulation of urban growth by using survival analysis and cellular automata. *Landsc. Urban Plan.* **2016**, *152*, 59–71. [CrossRef]
41. Moreira, M.; Fonseca, C.; Vergílio, M.; Calado, H.; Gil, A. Spatial assessment of habitat conservation status in a Macaronesian island based on the InVEST model: A case study of Pico Island (Azores, Portugal). *Land Use Policy* **2018**, *78*, 637–649. [CrossRef]
42. Xu, L.; Chen, S.S.; Xu, Y.; Li, G.; Su, W. Impacts of land-use change on habitat quality during 1985–2015 in the Taihu Lake Basin. *Sustainability* **2019**, *11*, 3513. [CrossRef]

43. Li, F.; Wang, L.; Chen, Z.; Clarke, K.C.; Li, M.; Jiang, P. Extending the SLEUTH model to integrate habitat quality into urban growth simulation. *J. Environ. Manag.* **2018**, *217*, 486–498. [CrossRef] [PubMed]
44. Sun, X.; Jiang, Z.; Liu, F.; Zhang, D. Monitoring spatio-temporal dynamics of habitat quality in Nansihu Lake basin, eastern China, from 1980 to 2015. *Ecol. Indic.* **2019**, *102*, 716–723. [CrossRef]
45. Seabrook, L.; Mcalpine, C.; Rhodes, J.; Baxter, G.; Bradley, A.; Lunney, D. Determining range edges: Habitat quality, climate or climate extremes? *Divers. Distrib.* **2014**, *20*, 95–106. [CrossRef]
46. Tallis, H.; Ricketts, T.; Nelson, E.; Ennaanay, D. *InVEST 1.005 Beta Users Guide*; The Natural Capital Project; Stanford University: Stanford, CA, USA, 2009.
47. Pan, Y.; Ying, Z.; Li, H.; Liu, C.; Zhang, X.; Guan, B.; Liu, Y.; He, L.; Ge, G. Landscape Patterns and Their Changes of Poyang Lake Wetlands under Hydrological Process and Sand Mining Activities. *Chin. J. Wetl. Sci.* **2019**, *17*, 286–294. [CrossRef]
48. Liu, C.; Wang, C. Spatio-temporal evolution characteristics of habitat quality in the Loess Hilly Region based on land use change: A case study in Yuzhong County. *Shengtai Xuebao/Acta Ecol. Sin.* **2018**, *38*, 7300–7311. [CrossRef]
49. Zhu, C.; Zhang, X.; Zhou, M.; He, S.; Gan, M.; Yang, L.; Wang, K. Impacts of urbanization and landscape pattern on habitat quality using OLS and GWR models in Hangzhou, China. *Ecol. Indic.* **2020**, *117*, 106654. [CrossRef]
50. Choi, Y.; Lim, C.H.; Chung, H.I.; Kim, Y.; Cho, H.J.; Hwang, J.; Kraxner, F.; Biging, G.S.; Lee, W.K.; Chon, J.; et al. Forest management can mitigate negative impacts of climate and land-use change on plant biodiversity: Insights from the Republic of Korea. *Environ. Manag.* **2021**, *288*, 112400. [CrossRef]
51. Chape, S.; Harrison, J.; Spalding, M.; Lysenko, I. Measuring the extent and effectiveness of protected areas as an indicator for meeting global biodiversity targets. *Philos. Trans. R. Soc. B Biol. Sci.* **2005**, *360*, 443–455. [CrossRef]
52. Dutta, S.; Dutta, I.; Das, A.; Guchhait, S.K. Quantification and mapping of fragmented forest landscape in dry deciduous forest of Burdwan Forest Division, West Bengal, India. *Trees For. People* **2020**, *2*, 100012. [CrossRef]
53. Gu, X.; Long, A.; Liu, G.; Yu, J.; Wang, H.; Yang, Y.; Zhang, P. Changes in Ecosystem Service Value in the 1 km Lakeshore Zone of Poyang Lake from 1980 to 2020. *Land* **2021**, *10*, 951. [CrossRef]

land

MDPI

Article

The Evolution of the Urban Residential Space Structure and Driving Forces in the Megacity—A Case Study of Shenyang City

He Sun [1,2,*], Xueming Li [1,2,3], Yingying Guan [1,2], Shenzhen Tian [1,2,4] and He Liu [1,2]

[1] School of Geography, Liaoning Normal University, Dalian 116029, China; lixueming@lnnu.edu.cn (X.L.); gyy9418@126.com (Y.G.); tsz999@lnnu.edu.cn (S.T.); liuhe1581@163.com (H.L.)
[2] Human Settlements Research Center, Liaoning Normal University, Dalian 116029, China
[3] Center for Studies of Marine Economy and Sustainable Development, Liaoning Normal University, Dalian 116029, China
[4] Institute of Geographic Sciences and Natural Resources Research, Beijing 100101, China
* Correspondence: 18642838980@163.com; Tel.: +86-186-4283-8980

Abstract: For megacities, they are in a period of transformation from extensive development to smart growth. Recognizing new characteristics and new changes of the residential space in megacities under the backdrop of new development has great practical significance for realizing the sustainable development of the city. As the only megacity in Northeast China, Shenyang was selected to be the research object, with 1989–2018 as the research period. The research comprehensively used multiple spatial representation methods and statistical methods to study the residential space pattern and driving factors in Shenyang City. The results showed that: (1) Residential space expansion can be divided into four stages: slow development, rapid expansion, speedy expansion, and stable extension. (2) The residential space structure presented a spatial evolution characteristic of overall expansion, forming multiple secondary core density centers. The east-west direction had a larger extension range than the northeast-southwest direction. There was an axisymmetric zonal distribution on both sides of the Hun River. (3) The agglomeration of different residential forms was obvious, and the spatial heterogeneity was increasingly stronger. (4) Urban planning measures and economic strength were the main driving forces of residential space expansion.

Keywords: residential space; structural evolution; multiple linear regression analysis; Shenyang City

Citation: Sun, H.; Li, X.; Guan, Y.; Tian, S.; Liu, H. The Evolution of the Urban Residential Space Structure and Driving Forces in the Megacity—A Case Study of Shenyang City. *Land* **2021**, *10*, 1081. https://doi.org/10.3390/land10101081

Academic Editors: Baojie He, Ayyoob Sharifi, Chi Feng and Jun Yang

Received: 8 September 2021
Accepted: 11 October 2021
Published: 13 October 2021

1. Introduction

As an important aspect of improving people's livelihood, housing has long attracted widespread attention from the country and the wider society [1,2]. Since China's reform and opening up, urbanization and industrialization have developed rapidly, and the scale and spatial structure of cities has expanded significantly [3,4]. Many megacities have been born, and the expansion structure and form of residential space are constantly changing [5,6]. However, with the increase in urban land saturation, some cities have encountered unsustainable development problems such as disorderly expansion, low land-use efficiency, and so on [7]. The national "13th Five-Year Plan" outline put forward the goal of "optimizing the spatial layout of housing construction, significantly improving living quality, transforming and upgrading housing construction mode". In the context of rapid urbanization, it is a top priority for China in the transitional period to systematically analyze the status quo of housing, implement refined management of urban development, and realize the sustainable development of residential space [8]. Urban residential space as people's living communication activities carrier is an important part of urban space. It is not only the spatial combination of buildings but also the social system of human activities [9]. Its evolution process and form are complementary to the evolution of the whole city, deeply affecting the quality of the human settlement environment.

The unprecedented activity of global urban construction has made scholars generally pay attention to the impact on residential space [10]. The study of residential space originated after the Western Industrial Revolution. With the acceleration of industrialization, a huge number of people gathered into cities, and urban functions were complicated, which also brought about urban problems such as housing congestion, environmental deterioration, as well as serious social problems such as the slums and social polarization [11,12]. Therefore, theoretical exploration and practical problem solving emerged. Research on the theory of residential space mainly began in the late 19th century. Social activists led to utopian socialist urban planning ideas, such as the "Pastoral City Theory", "Union New Village" and "Daylight Port" [13]. Developed in the 1980s, five schools gradually formed: ecological [14,15], neoclassical [16,17], behavioral [18], Marxist structural [19], and institutional [20]. According to the existing international theoretical models, Chinese scholars relied on the Marxist Structural School to deepen and put forward the theory of "social-spatial unity", which has been widely recognized as the theoretical basis of Chinese urban residential space differentiation [21]. At the same time, there were theoretical studies based on the comparative analysis of the social space differences of countries with different systems, such as the social-spatial differences of "socialist transition countries" and "post-socialist cities", such as in Eastern Europe and the former Soviet Union [22,23]. The practical research of urban residential space was mostly related to practical issues such as energy, economic society, ethnic and economic system influencing factors, which can diversify the research perspectives and deepen the content. For example, there were studies on the impact of residential buildings and urban forms on energy consumption, the compactness of urban forms affected urban traffic, energy, and the formation of urban heat islands [24,25]. Residential space differentiation characteristics and suburbanization of different income groups, segregation in urban poverty-stricken areas, and mixed living conditions among different races had also been studied [26–31]. The evolution of world urban networks, urban shrinkage, and spatial evolution of human settlements are also hot spots by scholars [32–39]. With the rapid development of science and technology, data collection is more extensive, such as questionnaires, night light data, land cover data, real estate network data, etc. Research methods are gradually diversified, such as principal component analysis, structural equation model, spatial measurement model, etc. Scholars have conducted a large number of empirical studies on the status quo of spatial layout, evolution processes, spatial differentiation, spatial expansion, and driving mechanism through multiple technical means and multi-data fusion [40–43].

China's political and economic system is in a period of transformation, shifting from a socialist planned economy to a socialist market-oriented economy. The housing system has gradually shifted from "a plan" to "a market". The expansion and evolution of residential space closely revolve around the housing system. Due to the derailment of the economic system and marketization, the Northeast China development was once in trouble [44]. Shenyang, the capital of Liaoning Province, is one of the national heavy industrial bases mainly built by the state in the early days of the founding of the People's Republic of China and is an important central city in Northeast China [45]. As a typical megacity in China, Shenyang is the only megacity in China's Bohai Rim region and the three northeastern provinces. It has invested heavily in the real estate market in recent years, and the urban space has been sprawling disorderly, which has kept housing prices at a relatively low level among cities of the same scale, which indicates unreasonable problems in its residential space structure. Therefore, it is particularly important to reveal and summarize the expansion mechanism of residential space in megacities. Shenyang is currently experiencing urban development challenges combining internal and external renewal. Research in this area is very typical and representative. Clarifying the evolution mode and driving mechanism of the expansion of residential space in Shenyang City in the new development period is of great practical significance for exploring the sustainable development of residential space in megacities around the world.

2. Study Area and Data

2.1. Study Area

Shenyang is located in the central part of Liaoning Province, in the transition zone between Changbai Mountain and the Liaohe River alluvial plain [46]. It covers an area of 12,948 km^2 and is rich in water resources, belonging to two major water systems, namely Liaohe River and Hun River. The terrain is flat, the east and north are mostly hilly mountains. The overall terrain has a trend of sloping from northeast to southwest and both sides to the middle. There is a temperate semi-humid continental climate with four distinct seasons [47]. By the end of 2019, Shenyang had a permanent resident population of 8.322 million and an urbanization rate of 81%. In 2019, the GDP of the region was 647.93 billion CNY. Referring to the definition of a central city in Shenyang City Master Plan (2011–2020), this study limited its research scope within the fourth ring road of Shenyang, including nine districts: Tiexi, Dadong, Heping, Shenhe, Huanggu, Sujiatun, Yuhong, Shenbei New, and Hunnan Districts, covering an area of approximately 1545 km^2 (Figure 1).

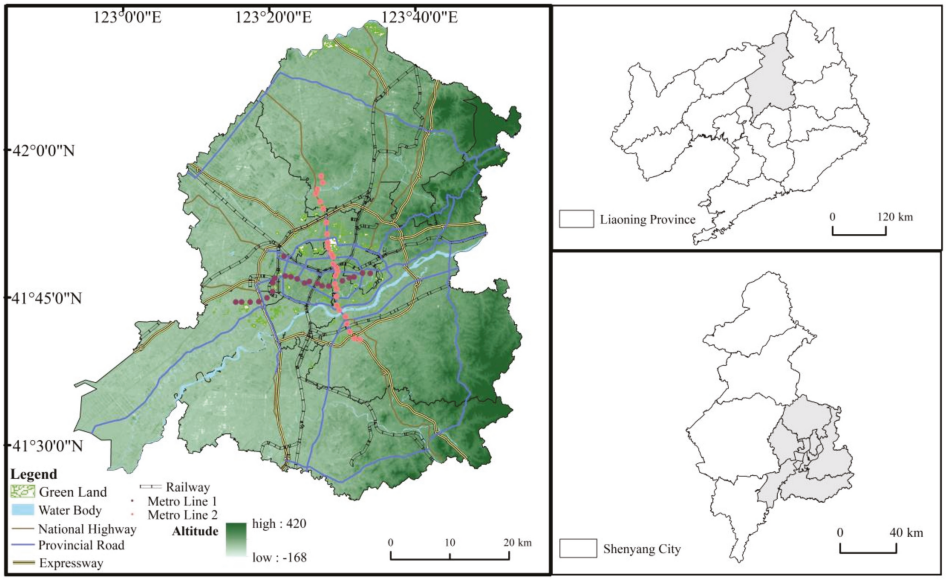

Figure 1. Administrative division and basic elements map of Shenyang.

Due to its basic plain terrain features, Shenyang has had a spatial form reflecting an inner square and outer circle since ancient times. Shenyang was positioned as an industrial city, the railway runs through the city center, and each functional interval is distinctly separated. In the urban fringe area, after successive measures, such as the expansion of the industrial park and workers village, promoting a large agglomeration and transfer of population, planning layout structure across the river development, which has greatly extended and changed the living space.

2.2. Data Source

The residence data from nine districts of Shenyang was collected on 31 December 2018, including the administrative district, business district, completion time, property, and real estate development companies, the average price of housing, number of buildings, building type, and longitude and latitude. 2768 samples were obtained. After data cleaning and correction, 2255 sets of valid data were filtered out. ArcGIS10.2 was used for spatial

processing of other basic elements, and classification and registration were supervised by remote sensing images (Table 1).

Table 1. Data description.

Data Type	Year	Source	Pretreatment
Residence data	2018	Main https://dl.ke.com Others (anjuke.com, soufang.com, fang.com, and 58.com)	Collect other four websites to eliminate incorrect data, combine with high-resolution remote sensing images and Baidu's online map to spatially correct data, carry out a geographical trend surface analysis.
Natural element data	2019	https://www.earthol.com/	Use the same Google Earth image to further correct and supplement the data.
Traffic network data	2019	https://map.baidu.com/ www.gscloud.cn/	
Administrative division data	2019	http://www.lnditu.gov.cn/main/index.html	
Statistical panel data	2019	Shenyang Urban Statistical Yearbook (2002–2018)	Obtain other relevant official publications, and official websites to ensure the accuracy of the data.

3. Models and Methods

3.1. Spatially Extended Feature Model

3.1.1. Classification Standard of Residential Community Form

Previous studies on residential space differentiation are mainly based on housing price or property right type. However, with the reform of the housing system and the growth of the national economy, people are no longer concerned about whether they have a place to live in, but about living more comfortably and improving their quality of life. During residential space expansion in Shenyang, studying the residential form can directly reflect the development quality of each stage, help the rational layout of the city, and provide a deeper understanding of the construction characteristics of each administrative unit. This study referenced the classification method by Sun, combined with five elements: district closure, property right years, building structure, property type, and building volume ratio [48]. The residential district form was divided into five categories: dispersed communities, single closed communities, villas, mixed communities, and integrated commercial and residential communities (Table 2).

Table 2. Classification standard of the residential communities.

	Property Right Years	District Closure	Building Structure	Building Type	Property Type	Floor Area Ratio Grade
Dispersed community	70	Open	Brick mix, steel mix	Low-rise, multi-story	Residence	Medium low, medium
Single closed community	70	Closed	Brick mix, steel mix, Frame	Multi-story, small high-rise, high-rise	Residence, apartments	Medium, medium high, High
Villa	70	Closed	Brick mix, steel mix, frame	Low-rise	Villas	Very low
Mixed community	Residence: 70 Villa: 40 Apartment: 40	Closed; Semi-closed	Brick mix, steel mix, frame	Low-rise, multi-story, small high-rise, high-rise mixed	Residence Villas Apartment	Medium, medium high, High Low, very low High
Integrated commercial and residential community	40	Open	Steel mix, frame	High-rise, super high-rise	Residence, commercial and residential buildings, street buildings	High, super high

3.1.2. Spatial Expansion Intensity Index

In the study of the driving factors affecting the expansion of residential space, the spatial expansion intensity index was introduced. Current research on urban spatial expansion mainly obtains the spatial growth area in different periods through remote sensing image processing and calculates the land expansion speed or land expansion intensity, to compare the temporal differences [49,50]. This method was used to calculate the annual expansion intensity index by selecting the number of newly added communities as the basic data, which reflects the evolution process of residential space expansion in the

study area over time. The index refers to the percentage of the number of newly added residential communities to the total number of the overall residential communities in a certain spatial unit during the study period, and the formula is as follows:

$$\beta_{i,t-t+n} = (N_{i,t} - N_{i,t-1})/N_i * 100\% \quad (1)$$

where $\beta_{i,t-t+n}$ represents the expansion strength index during the study period of t to $t+n$ within the study unit of i; $N_{i,t}$, $N_{i,t-1}$ represent the number of existing residential communities in i spatial unit in year t, year $t-1$, and N_i represents the total number of the overall residential communities in i unit; t represents the research year, and i represents the research spatial unit. In this study, Shenyang as the research unit (i), and 15 years (n) as the research period.

3.1.3. Kernel Density Estimation Method

The kernel density estimation method solves the distribution density of the residential space according to the point dataset of the residential district [51–53]. The spatial distribution characteristics of the data were studied starting from the kernel density estimation sample itself. This method mainly calculates the magnitude value of each unit area according to the data point elements of the residential district and fits each point or broken line into a smooth cone surface. Let the random sample points $X_1 ... X_n$ distribute in the density function f and estimate the function value $f(x)$ at point X. The Rosenblatt Parzen kernel is usually used to estimate:

$$fn(x) = \frac{1}{nh}\sum_{i=1}^{n} K\frac{x - xi}{h} \quad (2)$$

K is the kernel function, h is the bandwidth, and $h > 0$; n is the sample number; $(x\text{-}x_i)$ represents the distance between the estimated point x and the sample x_i. By using ArcGIS to conduct spatial interpolation analysis on the obtained function values, the location, shape, and ductility of the distribution of each housing type can be clearly and intuitively obtained. Among them, different h bandwidths caused different results. This study determined the bandwidth to be 1000 m after several tests and calculations, which is consistent with the spatial pattern of the residential community.

3.1.4. Multi-Distance Spatial Clustering Analysis

The spatial clustering pattern of the point elements in the residential community changed with the change in scale, which is a distance-based technique based on dispersity. It is widely used because it can effectively solve the dependence of the spatial agglomeration pattern on the scale. This study used Ripley's k function to study the spatial distribution pattern and laws of different housing types in nine districts of Shenyang [54,55]. Ripley's $K(d)$ estimation function is:

$$K(d) = \sqrt{\frac{A\sum_i^n \sum_{j(i\neq j)}^n wij(d)}{\pi n(n-1)}} \quad (3)$$

where d is the spatial scale, A represents the area of the study area, n represents the number of communities, and $w_{ij}(d)$ is the weight. If the distance between point i and point j within the range of d is $\leq d$, the value is 1; if the distance is >1, the value is 0.

The simulation method was adopted, and the calculation results were compared with the random distribution model (CSR) obtained by simulation. Under this formula, the obtained function $K(d)$ is the observed value of K, and the expected value of K is d. If the observed value of K is greater than the expected value of K, then the spatial distribution clustering degree of this type of community in Shenyang is higher. If the observed value of K is less than the expected value of K, the spatial dispersion of this type of community is stronger. If the observed value of K is greater than the confidence interval of the high value, then this type of community has a significant agglomeration. If the observed value

of *K* is less than the confidence interval of the low value, then this type of community has significant dispersion.

3.2. Driving Force Analysis Model

3.2.1. Driving Factors Selection

During the selection of indicators, the factors that have a greater impact on the expansion of residential space were summarized. Residential space evolution was the result of the joint action of several aspects. The policy support of the state and the overall planning of the government guide social behavior. Real estate development enterprises built the housing and responded to the housing development behavior through macro-control. Moreover, the overall economic situation of the city also affected the change in population structure and individual consumption behavior. Social behavior is an intermediate process between policy and planning.

From macro and micro perspectives, supply-side and demand-side, the influencing factors were screened by six driving factors: policy, planning, economy, population, the housing market, and transportation externality [56–59]. The panel data of Shenyang from 2002 to 2017 was selected, and all the data were from the Shenyang Yearbook (2002–2018) provided by Shenyang Statistical Information Network (Table 3).

Table 3. Driver selection and construction.

Factor	Indicator	Unit	Variable	Direction
Policy	Investment in fixed assets	10^8 yuan(RMB)	X_1	+
	Total tax revenue	10^4 yuan(RMB)	X_2	-
Planning	Expenditure on urban and rural community public facilities	10^4 yuan(RMB)	X_3	+
	Number of schools at all levels	person	X_4	+
	Green-covered area in the built-up area	hm^2	X_5	+
Economy	GDP	10^8 yuan(RMB)	X_6	+
	Engel coefficient	%	X_7	-
	Average wage of employees	yuan(RMB)	X_8	+
	Percapita income-expenditure ratio	%	X_9	+
	Total floor area of housing per capita	m^2	X_{10}	+
Population	Permanent resident population	10^4 person	X_{11}	+
	Urbanization rate	%	X_{12}	+
	Average population per household	person	X_{13}	-
Estate	Housing development efficiency	%	X_{14}	+
	Residential completed investment	10^8 yuan(RMB)	X_{15}	+
	Residential investment and construction rate of return	%	X_{16}	+
Traffic	Road length	km	X_{17}	+
	Number of civilian cars	number	X_{18}	+

Engel's coefficient is the ratio of per capita consumption of food, tobacco, and alcohol to current consumption expenditure. The ratio of per capita income to expenditure is the ratio of per capita annual income to per capita consumption; the urbanization rate is the proportion of the urban population to total population; residential development efficiency is the proportion of the construction area to the completed area in the real estate development of the year, and the rate of return on residential investment and construction is the proportion of residential sales and completed value in real estate development.

3.2.2. Multiple Linear Regression Analysis Based on PCA

In the study of practical problems of urban development, the change in an urban phenomenon is often determined by the influence of several factors. In this case, two or more influential factors must be used as independent variables to explain the change in dependent variables. When multiple independent variables have a linear relationship

with the dependent variable, multiple linear regression analysis is performed; therefore, to explore the driving force of residential space evolution in Shenyang, a multiple linear regression analysis method was conducted [60,61].

$$\beta = \alpha_1 X_1 + \alpha_2 X_2 + \ldots + \alpha_n X_n + D \quad (4)$$

where β represents the expansion strength index; X_1,X_2,...,X_n represent the driving factors; α_1,α_2,...,α_n represent the importance degree of driving factors; D is the constant.

Due to the large number of impact factors selected in this study, principal component analysis (PCA) was used to reduce the dimensionality of these factors first and extract the main driving factors with greater impact.

4. Results

4.1. Evolution Stage and Characteristics of Residential Spatial Pattern in Shenyang

Shenyang's existing residences were first built in 1989. From 1989 to 2018, the number of residences continued to increase, and the incremental amount differed in different stages. According to the trend and characteristics, with an annual increase of 50 residences and 100 residences as a cut-off point, residential space expansion in Shenyang was divided into four stages: (1) slow development (1989–1994), (2) rapid expansion (1995–2003), (3) high-speed development (2004–2013), and (4) stable extension (2014–2018) (Figure 2). The distribution characteristic was shown in Figure 3.

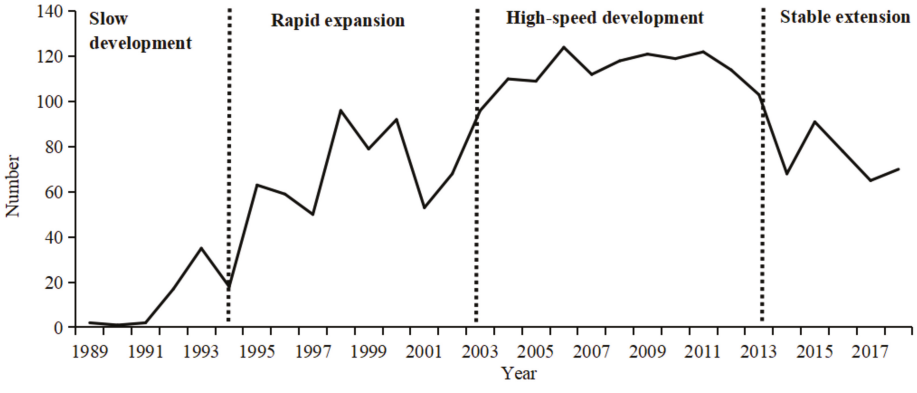

Figure 2. Number of new communities over the years.

Slow development stage: here, a total of 75 new communities were built, and most were built after 1992, indicating that the demolition work in Shenyang was carried out well. The residential areas were mainly located in Shenhe District, followed by Heping and Huanggu Districts. There were no new residential areas in Shenbei New and Hunnan Districts in this stage. The plot distribution was not uniform, and the overall spatial distribution was the pattern of "one core, one ring, and one point". The "One Core" was the high-density area, extending from northwest to southeast, and was mainly located in the center of Shenyang Railway Station, Shenyang North Railway Station, and Huanggutun Railway Station. "Yihuan" was the position between the first ring and the second ring and was distributed in a concentric ring, extending farther in the east-west direction than in the north-south direction, with a long history of construction. "One point" refers to the Sujiatun that had formed an independent residential area, which was farther from the main urban area. During this period, Shenyang developed to the west, north, and south, with a slightly longer distance from east to west. This is because, during this period, Shenyang's export-oriented economy pushed the city into the stage of overall scale expansion (Figure 3a).

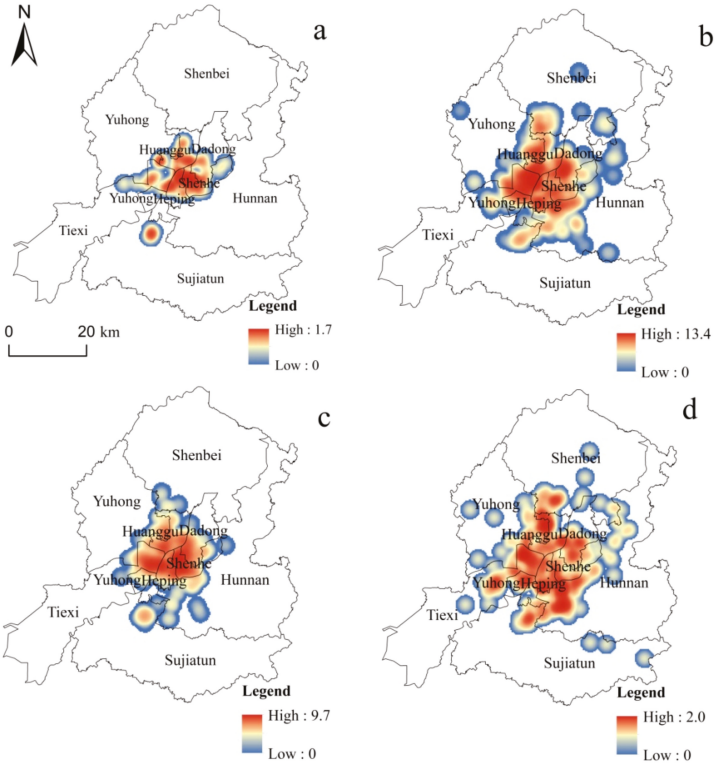

Figure 3. New communities distribution in different stages. (**a**) Slow development stage. (**b**) Rapid expansion stage. (**c**) High-speed development stage. (**d**) Stable extension stage.

Rapid expansion stage: There were 656 new communities built in this stage, 8.7 times that of the previous stage. Shenhe District was still the administrative unit with the most newly built communities, and the increase was different from other districts. Shenhe, Heping, Huanggu, Tiexi, and Dadong Districts were still the center of residential district construction. The new communities of Hunnan and Shenbei New Districts were built around 2000 with good development; while Sujiatun District had relatively weak development power and the total increase is small. Regarding spatial distribution, the city expanded outward from the core in this period. The expansion mode was a linear extension of the main roads with low density, and the filling development was still dominated by the old city. The overall pattern was a ring-radial combination. The eastern part of the First Ring Road and the southern part of the Second Ring Road were still the focus of the construction, with a concentration in the center. The city mainly expanded to the north, south, northeast-southwest, and southeast, along both sides of the main road, albeit on a small scale. The universities originally located in the core area of Shenyang responded to the call of the government, moved to the Shenbei New District and Hunnan New District, forming the present Shenbei University Town and Hunnan University Town (Figure 3b).

High-speed development stage: During this period, with the improvement of urban space, the real estate industry in Shenyang developed rapidly, and the total number of residential areas was 1.7 times that of the last stage. The number of new residential areas in Tiexi District was significantly different from that of other districts. The number of residential areas in Yuhong and Hunnan New Districts increased rapidly. Regarding the spatial distribution, the external expansion of Shenyang during this period was rapid, and the area of living space greatly increased, extending to the third ring road, areas beyond the

third ring road the north and south, and east and west in a cross shape. The north-south direction reflected gradual expansion from Huanggu District to the north of Shenbei New District. The southern Sujiatun District gradually became closer to the main urban area and was connected with Hunnan District. In the east-west direction, the Tiexi Economic Development Zone, Tiexi New District, Yuhong District, and other places built a large number of new communities, extending to the west and southwest. Furthermore, the east also expanded along the two sides of the Hunhe River to form a strip symmetrical distribution. Additionally, villas were constructed around Qipanshan Scenic Area in the northeast area, and high-grade residential buildings began to form in the areas with a good ecological environment. The establishment of the airport formed a linear residential layout pattern along the road from the main urban area to the airport (Figure 3c).

Stable extension stage: during this stage, every year, the number of new residential communities was effectively controlled, there were fewer new main urban areas, and the main construction was in Hunnan District. At this stage, the residential space in Shenyang followed the polycentric distribution pattern of "one main body and four secondary bodies". With the relocation of Shenyang municipal government, Shenyang Olympic Sports Center, the establishment of several large businesses, and the completion of the main road, the new Hunnan New District began to attract developers' investment, and residential living space was transferred. Sujiatun District is connected with Hunnan District, along each of Hun River, forming a unique urban landscape, and forming more high-grade new urban complexes. In Puhe New Town, because of the attraction of several large amusement parks, such as Font Joy World and Seven Star Sea World Theme Park, the north exhibition continued based on the original living space on both sides of the Puhe River. Since the northwest formed a regional logistics and trade base and equipment manufacturing industry base, it also drove the reintegration of residential space in Yuhong District. To realize new-type urbanization and achieve urban-rural integration, new-type urban construction around cities was distributed in points. Traffic was the main factor affecting the expansion of residential space in this stage. The construction of Shenyang South Railway Station, East Railway Station, and the Fourth Ring Road, expressways to surrounding cities were gradually improved, all of which drove the orderly expansion of residential space in Shenyang (Figure 3d).

4.2. Current Residential Space Distribution Pattern in Shenyang

After four urban planning, the overall urban layout and distribution of various types of land are becoming more and more perfect. The overall layout of the living space has obvious agglomeration characteristics, and the single-center phenomenon is still obvious and closely related to the distribution of underground traffic lines (Figure 4).

The high-value region of the core density was a hollow ring, which gradually decreased to the periphery and the interior; there were multiple secondary core density centers in the east-west and northeast-southwest directions, among which the east-west direction expansion was stronger and the northeast-southwest direction expanded farther. The two sides of the Hunhe River had axisymmetric zonal distribution.

Core high-value area: the two high-value areas were Tiexi Square and Youth Street, which are located on the east and west sides of the ring, respectively, and are symmetrically distributed. This form was closely related to the construction of Metro Line 1 and was the result of the coordination between traffic and residential space construction; Metro Line 1 fully opened in 2010. In the early stage, the site selection must be combined with the existing densely inhabited areas, and the opening of the subway motivates the development of the surrounding communities, making the living space more concentrated. To the east, it is connected with commercial areas such as Zhongjie, Joy City, Huaiyuan Men, and other historical and cultural protection areas. The west connects Tiexi Plaza, Yuhong Plaza, Wanda Plaza, and other central CBD areas, and gradually extends to the Developing Avenue, Industrial Development Zone such as Zhang Industrial Zone, all of which are densely populated areas and high - density urban buildings. It has convenient

transportation facilities and relatively compact living spaces. Several core areas were formed along the line. The construction of subway line 2 was distributed in a north–south direction, mainly to connect Shenbei New District and Hunnan New District, drive the development of the two new districts, and accelerate population flow.

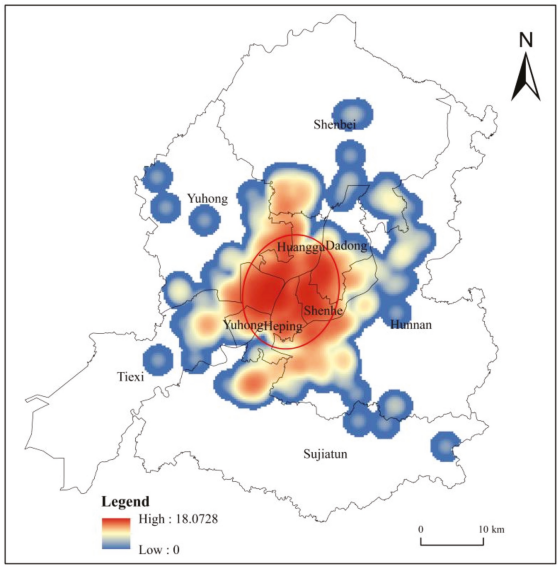

Figure 4. Overall residential communities distribution in Shenyang.

Low center area: located in the urban area in the middle of Beijing and Harbin road, near three around the railway stations, namely Shenyang, Shenyang North, and Huanggu District railway stations, and rail tracks across the city center. Therefore, the internal form of the core of the triangle kernel density value was low; it also benefited from overall planning and layout and urban renewal projects, etc.

The axisymmetric zone distribution on both sides of the Hunnan River: with the continuous attention of the municipal government to the ecological environment and to create a livable Hunnan New City, the landscape was optimized on both sides of the Hunnan River and additional development was conducted on the Hunnan District in the heyday. This caused substantial migration to the south bank of the Hunhe River. Cluster areas had been formed on both sides.

Group distribution of peripheral new towns: the tilt of planning policy significantly improved the development of the four sub-cities. With the development of the industry, Puhe New City in the north, Tiexi West Industrial New City in the west, Hunhe New City in the south of Hunnan District, and Yong'an New City in the northwest of Yuhong District also obtained the surrounding resources and population flows.

4.3. Characteristics of Various Types of Residential Forms

The order of residential forms in Shenyang was as follows: single closed communities (1031, 45.72%) > mixed communities (615, 27.27%) > dispersed communities (465, 20.62%) > integrated commercial and residential communities (79, 3.50%) > villas (65, 2.88%), indicating that the quality of residential communities in Shenyang is generally high, and most are single enclosed communities with obvious differentiation in living space.

Regarding the development stage: in the slow development stage, the new residential buildings were mainly dispersed communities. Single closed communities, mixed communities, and villas appeared. At this time, there was no integrated commercial or residential

community. During the rapid expansion stage, dispersed communities still dominated; however, the number of single closed communities increased significantly, while integrated commercial and residential communities also appeared, and villas began growing slowly. In the high-speed development stage, the single enclosed community was the main type of residence. Along with the construction of mixed communities, the dispersed community gradually faded out of the historical stage, and the new number of integrated commercial and residential communities exceeded the new number of villas. In the stable extension stage, the construction of dispersed residential areas stopped, and this kind of form was replaced by other residential areas. The new number of single closed communities and mixed communities was equal, and the construction of villas and integrated commercial and residential communities slowed.

From the perspective of each administrative unit, Shenhe District was the only district in which there were more dispersed communities than single closed communities, indicating that the overall construction of Shenhe District has a long history and the urban construction work must be improved. Moreover, Shenhe District had more integrated commercial and residential communities, which is closely related to the financial center and other CBD core business districts in this area. The number of single closed communities in Tiexi District was more than that in other districts, which is associated with the vigorous planning and development work later. The overall building age was relatively young. The distribution of Taiyuan Street, Tiexi Square, and Wanda Plaza promoted the concentration of residential space in Tiexi District, and the integrated commercial and residential communities in Tiexi District were the largest among the five old districts. The residential forms of Heping, Huanggu, and Dadong Districts were similar. Regarding the number of residential areas, the number of single closed communities was the highest, followed by dispersed communities and mixed communities. Furthermore, the number of villas and integrated commercial and residential communities was lower, which is a common feature of the old city. Yuhong District developed later than the five districts of the old city, and the single closed and mixed communities occupied the main position in the number. The number of single closed and mixed communities in Hunnan District was more, which is closely related to the construction of infrastructure. The villas and integrated commercial and residential communities dominated in several districts, which is closely related to its excellent natural environment, convenient traffic conditions, and the settlement of several large commercial supermarkets. The development of the Shenbei New District was relatively slow, while Sujiatun District built new residential areas based on the original old city, with fewer villas and integrated commercial and residential communities (Figure 5).

From the perspective of residential forms: (1) Agglomeration: according to the results of the multi-distance spatial clustering analysis, several residential forms show agglomeration characteristics on the short distance scales. With the increase in scale, the agglomeration characteristics of dispersed communities and single closed communities becoming more obvious, the concentrating effect of mixed communities and integrated commercial and residential communities basic remains unchanged. However, the villa was gradually transformed from agglomeration in close scale, uniform distribution in medium-distance scale to dispersion in long-distance scale. These cluster analyses passed 99% confidence intervals. (2) Regarding the distribution area, the distribution shapes of dispersed, single closed, and mixed communities were similar; however, the dispersed communities were distributed within the second ring road area, with fewer surrounding areas and a smaller area. The distribution area of the single closed communities was larger than that of the former, and it was mainly distributed within the second ring road; however, it extended more around. Mixed communities had the largest area, and the distribution was more scattered than dispersed and single closed communities. There were fewer areas of integrated commercial and residential communities and villas, with a center or surrounding scattered distribution. (3) Regarding distribution characteristics, the high-density area of the dispersed communities was mainly located in Shenhe District, showing a mononuclear distribution. The high-density area of the single closed community was located in Tiexi District and formed

a cluster distribution of several small clusters. The overall range of the mixed communities was relatively dispersed, forming multiple high-value areas of core density, which were evenly distributed and had a multi-core distribution. The linear pattern of integrated commercial and residential communities was the most obvious, extending along subway line 1 to the east and west, and extending along subway line 2 to the south, showing a T-shaped distribution. Villas were distributed around the second ring road in the periphery of the main city distribution, showing suburbanization; its distribution depended on the northeast Qipan Mountain Scenic Area and the suburban radial main road distribution (Figure 6).

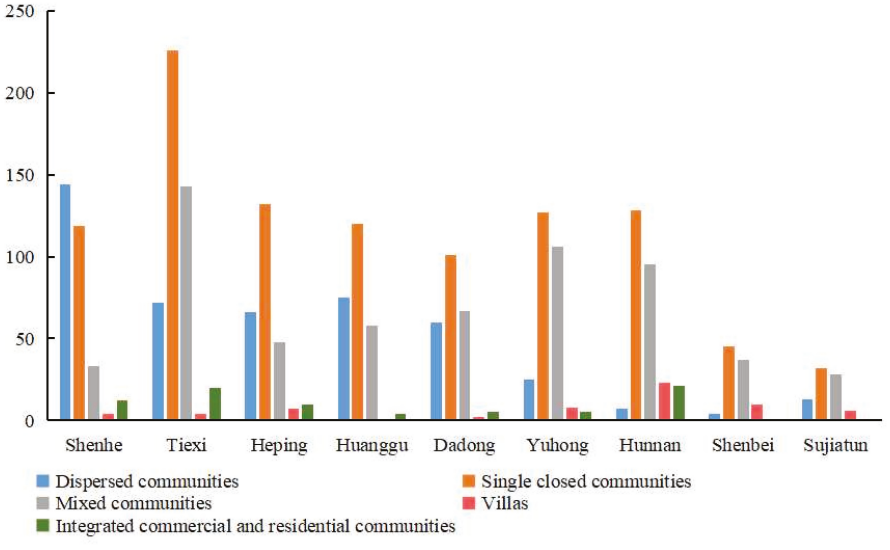

Figure 5. Residential communities number in different regions.

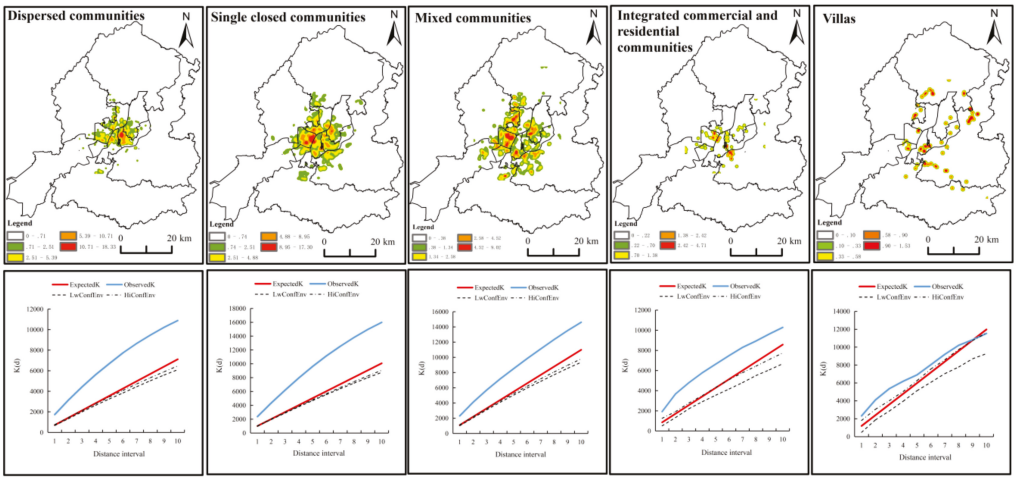

Figure 6. Nuclear density distribution and multi-distance spatial cluster diagram of all kinds of communities.

4.4. Driving Forces of Residential Space Evolution Based on Multiple Linear Regression

To ensure the accuracy and validity of the data, the 18 impact factors from 2002 to 2017 were preprocessed by range standardization. According to eigenvalues >1 as the basis for the selection of the main component, three principal components were selected. The cumulative variance contribution rate of variance reached 94.67%, which can reflect the characteristics of the original 18 variables, which was enough to reflect the expression in the original data (Table 4).

Table 4. Eigenvalues and squared loading of the principal components.

Principal Component	Eigenvalues	% of Variance	Cumulative %
1	12.841	71.341	71.341
2	3.060	16.998	88.338
3	1.139	6.330	94.668

The principal component load matrix can explain the relationship between each principal component and the associated variables. The greater a load of each index in the principal component, the more able to characterize the characteristics of the index variable. The main characteristic factors in the first main component: permanent resident population(X_{11}), road length(X_{17}), urbanization rate(X_{12}), total floor area of housing per capita(X_{10}). It reflected the population characteristic, the status quo of economic development, and transportation. It can be summarized as the residents' behavior. The second main component included expenditure on urban and rural community public facilities(X_3) and Engel coefficient(X_7), reflecting the planning and economic development. It can be summed up as government functions. The third main component included total tax revenue(X_2), reflecting the national policy impact (Table 5).

Table 5. Principal component load matrix.

	Component				Component		
	1	2	3		1	2	3
X1	0.634	0.601	0.34	X10	0.984 *	−0.036	0.118
X2	−0.321	−0.615	0.636 *	X11	0.990 *	−0.062	0.083
X3	0.432	0.896 *	0.042	X12	0.979 *	−0.111	−0.151
X4	−0.915	−0.224	0.331	X13	0.921	−0.143	−0.331
X5	0.957	0.203	−0.092	X14	0.972	−0.098	0.191
X6	0.972	0.011	0.166	X15	0.812	0.502	0.275
X7	−0.461	0.856 *	−0.073	X16	0.749	0.045	0.23
X8	0.947	−0.318	−0.017	X17	0.980 *	−0.048	0.175
X9	0.812	−0.298	−0.339	X18	0.894	−0.446	−0.045

* It refers to the driving factor that with the large load weight in each principal component.

The spatial expansion intensity index was used as the dependent variable Y, FAC1_1, FAC2_1, and FAC3_1 were the independent variables. Use the "linear" in the SPSS "regression analysis" to perform multiple linear regression analysis. After calculation, $R^2 = 0.991$. The Durbin–Watson test was used to test the independence of the model residuals, DW = 1.578. The value of DW was in the range without autocorrelation. Therefore, the residual independence was determined and passed the test, with a significance level of $0.013 \in (0.01, 0.05)$. It indicated that it passed the 0.05 significance test but failed the 0.01 significance test, demonstrating that the regression model has significant statistical significance. The linear relationship between the expansion strength index and the three principal components was significant. The various regression coefficient results are shown in Table 6.

Table 6. Regression coefficient.

Model	Non-Standardized Factor B	Non-Standardized Factor Standard Error	Standardized Factor Beta	T	Significance
(Constant)	4.095	0.052		78.129	0
First primary component	−0.305	0.057	−0.349	−5.315	0.014
Second primary component	0.815	0.057	0.932	14.194	0.005
Third primary component	0.024	0.057	0.028	0.425	0.012

The significance values were all less than 0.05, indicating that the regression coefficients B were present and significant. The regression linear equation of this model can be obtained as follows:

$$\beta = -0.305FAC1\_1 + 0.815FAC2\_1 + 0.024FAC3\_1 + 4.095 \quad (5)$$

Since the coefficient of the second principal component in the formula was relatively large (0.815). It indicated that the second principal component had a greater correlation with β. That is, planning and urban economic development have a greater impact on the intensity of urban expansion. Based on the prediction of this model, the spatial expansion intensity in 2018 was 2.933–5.213, while the actual spatial expansion index in 2018 was 3.104$\in$ (2.933, 5.213). The actual value was consistent with the predicted results, indicating that the accuracy of this statistical model was high (Table 7).

Table 7. Residual statistics.

	Minimum	Maximum	Average	Standard Deviation	N
Forecast Value	2.933	5.213	4.095	0.870	15
Residual Difference	−0.098	0.122	0.000	0.081	15
Standard forecast value	−1.335	1.285	0.000	1.000	15
Standard residual	−0.765	0.952	0.000	0.632	15

The results show that Engel's coefficient, urban and rural community expenditure on public facilities, and fixed asset investment are the three primary factors affecting urban expansion intensity, which correspond to planning and economic development which are the two primary driving factors affecting urban expansion. Meanwhile, other factors have a relatively small influence. Urban planning is the main driving force affecting the expansion of residential space. It guides real estate enterprises and residents to choose residential space by combining the overall development direction of the country. Economic strength is an important basis for the construction of urban vitality.

5. Discussion

5.1. Findings

The continuous optimization of residential space is an important content to improve the quality of urban human settlements. Shenyang is the only megacity in Northeast China, located in the old industrial heartland. It is of great research significance to grasp the evolution model of its overall residential space, grasp the actual problems that its residential space needs to solve, and put forward specific optimization opinions. It is not only an exploration of the development characteristics of urban residential space itself but also a supplement to the research on the development process of megacities in developing countries. Compared with existing research results in the world, the spatial expansion of megacities is mostly in developing countries, mainly in Asia and Africa. In developed countries, this phenomenon rarely exists, such as Europe, Oceania, and North America [62]. Many scholars raise that urban problems are due to urban expansion and urbanization, such

as the sacrifice of green land and farmland, and the deterioration of climatic conditions [6]. However, some scholars have proposed that in the process of urban development, if orderly planning and reasonable ecological protection are obtained, and resource waste is reduced, then it can also be defined as the sustainable development of human society [63]. Studies have shown that economic development is the main driving force for urban expansion [5,33]. Areas with relatively good economic development develop faster, while areas with less economic development are mainly still filled open spaces within boundaries. At the same time, rates of urban expansion in most developing countries are greatly affected by the structural transformation of societies [64–66]. According to the results of this study, Shenyang's residential space expansion characteristics are also closely related to China's economic system reform, and it is undergoing a transition from a planned economy to a market economy, which has greatly expanded the residential space. At the same time, as the capital of Liaoning Province, the urbanization of Shenyang has accelerated. It has realized the importance of orderly expansion and sustainable development. Over the past 40 years, there has been a continuous transformation of Shenyang, from the initial center to the surrounding disorderly spread, to the later planning of industrial, commercial, university town, economic, and technological development zones, and other multi-core cluster modes. It has been in the stage of transition from boundary expansion to internal filling. With the development of the city, the overall residential space in Shenyang has higher vitality and potential. All these indicate that compared with other megacities, Shenyang has made beneficial control and exploration in the overall development of the city.

In this study, we found that economic development and urban planning are the primary driving forces for the intensity of residential space expansion. The development of residential space cannot be separated from the macro-control and micro-transformation of government department planning. The stable development of an urban economy, the guarantee of per capita income, and improvement of consumption level can improve people's willingness to choose a living environment and promote the improvement of living quality and development of the real estate. Moreover, the change of population number and structure, accessibility of traffic layout, the regulation of the real estate market, and national policy support will have a direct or indirect impact on the residential space in terms of supply and demand. At the same time, the research also carried out an in-depth analysis based on the five planning documents of Shenyang City's urban space and found that the results of this paper are consistent with the overall planning direction of Shenyang City.

In the process of development, there were several problems, such as a waste of energy, land, and public resources and an oversupply of housing. Smart growth and intensive use were gradually integrated into urban planning. According to the research results, there are still three practical problems in the development process of residential space in Shenyang: crowded roads, obvious monopolization, and the small green coverage rate of built-up areas. The specific optimization suggestions are as follows: to guide the transfer of the residential population to the sub-cities, to form a complete high-speed road system as soon as possible, and to strengthen the emphasis on ecological construction. The control of residential space in Shenyang should give full play to the government's macro-control ability, weaken the phenomenon of single-polarization and obvious circle structure, and reconstruct old residential areas. Urban construction work should give full consideration to the livability of residents, improve the quality of the living environment, enhance the happiness of residents. It should improve the construction of infrastructure, promote the equal development of the city, and improve the fairness of urban areas. In future development, planning and economic development should be coordinated to jointly promote the high-quality development of urban residential space.

5.2. Contributions

The evolution model of residential space in China has unique Chinese characteristics. It is not appropriate to directly quote the basic hypothetical theories of western countries.

There are few theoretical studies on this in China, and the system is not perfect enough. Firstly, due to the difficulties in collecting historical data, most of the research is based on housing statistics obtained from historical materials such as census data [67], statistical yearbook data, real estate information magazines, newspapers, and city chronicles [68]. With the further strengthening of technology, remote sensing data of land use in interval years was introduced [69]. The acquisition method cannot be unified and the data lacks continuity, so research can only be conducted through limited data. This research mainly uses the data of existing residential quarters to analyze the development process and status quo of residential space in Shenyang in recent years. Although the use of newly added data each year cannot reflect the overall picture of the urban residential space at that time, the urban planning process and direction information can be analyzed at the location of the newly added communities. Divide the development stages according to the characteristics of the number of newly-added communities, describe the change process in different stages, and describe the dynamic evolution expansion process of residential space structure.

At the same time, in the qualitative description and analysis of the current situation of the spatial structure, the evolution law of the housing form is introduced. Different levels of cities have different phenomena at different development stages, and it is difficult to have a unified theoretical model for their evolution laws. Existing morphological studies mostly classify residential space according to single factors such as land use type or building attributes, such as property type [70], floor area ratio [41], housing price [71], and lack of specific analysis of residential morphology. The research describes the differentiation characteristics and structural changes of the urban residential space form and analyzes the overall residential space evolution in Shenyang qualitatively and quantitatively. Based on this, the study enriches and expands the theory of urban space through practical research, and furthers the theoretical research on the evolution mechanism of the urban residential space structure in China.

5.3. Limitation

Due to the difficulty of accurately obtaining historical data and the lack of long-term quantitative research, the comparative analysis should be strengthened in future research. Moreover, more effective methods should be used to refine the research on the differences in the driving factors of the expansion of residential space in various regions in future studies.

6. Conclusions

In this study, the characteristics of urban residential space evolution in Shenyang were the research object. Based on the data of newly added residential from 1989 to 2018, the spatiotemporal characteristics of Shenyang were analyzed using various spatial analysis methods in ArcGIS and classified according to residential area morphology. The overall internal characteristics and existing residential differentiation phenomenon of Shenyang were described in detail. Finally, principal component analysis and multiple linear regression analysis were used to explore the driving mechanism affecting the intensity of urban residential space expansion in Shenyang. The following conclusions were obtained:

(1) From to 1989–2018, Shenyang experienced four stages of slow development, rapid expansion, high-speed expansion, and stable spread. In the process of evolution, the main scope expanded continuously, the circle structure continuously improved, spatial heterogeneity increased, and morphology had obvious spatial agglomeration features.

(2) The number of residential areas among administrative units in Shenyang was different. The residential space of the whole city was large and distributed in a cross-shaped multi-core group. However, there was still a generally circular structure, and according to the results of the standard deviation ellipse, the length from the northeast to southwest of the city is larger than that from the northwest to southeast.

(3) Based on the basic properties of residential areas, the residential areas were classified into five categories: dispersed communities, single closed communities, mixed communities, integrated commercial and residential communities, and villas, and each

residential form had a different degree of spatial agglomeration. The distribution of dispersed communities was mononuclear. The single closed communities are distributed with Tiexi Square as the single core multi-group. Mixed communities were more uniform, showing a multi-core distribution. The integrated commercial and residential buildings were distributed along the subway line in a "T" shape. Villas were mainly distributed in the vicinity of the Qipan Mountain Scenic Area or around the periphery of the main urban area, and the phenomenon of suburbanization was obvious.

(4) Selecting 18 indicators as driving factors and using a multiple linear regression model to analyze the spatial expansion intensity index of Shenyang from 2002 to 2017, it was shown that this theoretical model has a good explanatory ability. According to the influence of each factor on the spatial expansion intensity, six driving factors were ranked in order: urban planning > economic strength > population > transportation > housing market > national policy.

Author Contributions: Conceptualization, X.L.; methodology, H.S.; software, H.S.; validation, H.S., Y.G. and S.T.; formal analysis, H.S.; investigation, H.L.; resources, H.S.; data curation, H.S.; writing—original draft preparation, H.S.; writing—review and editing, X.L.; visualization, H.S.; supervision, X.L.; project administration, X.L.; funding acquisition, X.L. All authors have read and agreed to the published version of the manuscript.

Funding: This research was funded by the National Natural Science Foundation of China (Grant no. 41671158).

Data Availability Statement: The primary data used to support the findings of this study are available from the corresponding author upon request.

Conflicts of Interest: The authors declare no conflict of interest.

References

1. Weimann, A.; Kabane, N.; Jooste, T.; Hawkridge, A.; Smit, W.; Oni, T. Health through human settlements: Investigating policymakers' perceptions of human settlement action for population health improvement in urban South Africa. *Habitat. Int.* **2020**, *103*, 102203. [CrossRef]
2. Wang, Y.; Jin, C.; Lu, M.; Lu, Y. Assessing the suitability of regional human settlements environment from a different preferences perspective: A case study of Zhejiang Province, China. *Habitat. Int.* **2017**, *70*, 1–12. [CrossRef]
3. Li, G.; Fang, C.; Qi, W. Different effects of human settlements changes on landscape fragmentation in China: Evidence from grid cell. *Ecol. Indic.* **2021**, *129*, 107927. [CrossRef]
4. Li, C.; Wu, K.; Gao, X. Manufacturing industry agglomeration and spatial clustering: Evidence from Hebei Province, China. *Environ. Dev. Sustain.* **2020**, *22*, 2941–2965. [CrossRef]
5. Yeh, A.G.; Chen, Z. From cities to super mega city regions in China in a new wave of urbanisation and economic transition: Issues and challenges. *Urban Stud.* **2020**, *57*, 636–654. [CrossRef]
6. Matsa, M.; Mupepi, O.; Musasa, T. Spatio-temporal analysis of urban area expansion in Zimbabwe between 1990 and 2020: The case of Gweru city. *Environ. Chall.* **2021**, *4*, 100141. [CrossRef]
7. Wang, M.; Feng, C. The inequality of China's regional residential CO_2 emissions. *Sustain. Prod. Consum.* **2021**, *27*, 2047–2057. [CrossRef]
8. Yang, J.; Wang, Y.; Xiu, C.; Xiao, X.; Xia, J.; Jin, C. Optimizing local climate zones to mitigate urban heat island effect in human settlements. *J. Clean. Prod.* **2020**, *275*, 123767. [CrossRef]
9. Mao, S.; Chen, J. Residential Mobility and Post-Move Community Satisfaction: Empirical Evidence from Guangzhou, China. *Land* **2021**, *10*, 741. [CrossRef]
10. Luo, X.; Yang, J.; Sun, W.; He, B. Suitability of human settlements in mountainous areas from the perspective of ventilation: A case study of the main urban area of Chongqing. *J. Clean. Prod.* **2021**, *310*, 127467. [CrossRef]
11. Yang, J.; Yang, Y.; Sun, D.; Jin, C.; Xiao, X. Influence of urban morphological characteristics on thermal environment. *Sustain. Cities Soc.* **2021**, 103045. [CrossRef]
12. Kim, J.H.; Li, X. Building more housing near transit: A spatial analysis of residential densification dynamics. *Transport. Policy* **2021**, *114*, 15–24. [CrossRef]
13. Howard, E. *Garden Cities of To-Morrow*; The Commercial Press: Beijing, China, 2009; ISBN 9780262580021.
14. Park, R.E. Human ecology. *Am. J. Sociol.* **1936**, *13*, 1–15. [CrossRef]
15. Hoyt, H. The structure and growth of residential areas in American cities. *Development* **1941**, *19*, 453–454. [CrossRef]
16. Muth, R.F. *Cities and Housing*; The University of Chicago Press: Chicago, IL, USA, 1969; ISBN 8170220300.
17. Alonso, W. Location and land use: Toward a general theory of land rent. *Econ. Geogr.* **1964**, *42*, 11–26. [CrossRef]

18. Michelson, W.M. *Environmental Choice, Human Behavior, and Residential Satisfaction*; Oxford University Press: New York, NY, USA, 1977; ISBN 0195021452.
19. Liu, W.; Zhang, W. Review and prospect of the research on urban residential spatial structure. *Hum. Geogr.* **2004**, *3*, 6–11. [CrossRef]
20. Shapely, P. *The Politics of Housing: Power, Consumers and Urban Culture*; Manchester University Press: Manchester, UK, 2007; ISBN 9781526130686.
21. Wu, Q.; Ren, D.; Yang, Y.; Shu, X. The theoretical basis of urban residential differentiation and its research field. *Hum. Geogr.* **2000**, *3*, 1–5. [CrossRef]
22. Wei, L.; Yan, X. Summaries and analysis on the studies about urban social space in the socialist transitional countries. *Hum. Geogr.* **2006**, *4*, 13–18.
23. Li, Z.; Wu, F.; Xue, D. A review of sociospatial differentiation in 'post-socialist' cities. *Hum. Geogr.* **2006**, *5*, 1–5.
24. Moura, M.; Smith, S.; Belzer, D.B. 120 years of U.S. residential housing stock and floor space. *PLoS ONE* **2015**, *10*, e0134135:1–e0134135:18. [CrossRef] [PubMed]
25. He, B.; Zhao, Z.; Shen, L.; Wang, H.; Li, L. An approach to examining performances of cool/hot sources in mitigating/enhancing land surface temperature under different temperature backgrounds based on landsat 8 image. *Sustain. Cities Soc.* **2019**, *44*, 416–427. [CrossRef]
26. Wang, D.; Schwanen, T.; Mao, Z. Does exposure to richer and poorer neighborhoods influence wellbeing. *Cities* **2009**, *95*, 102401–102408. [CrossRef]
27. Glaeser, E.L.; Kahn, M.E.; Rappaport, J. Why do the poor live in cities? The role of public transportation. *J. Urban Econ.* **2008**, *63*, 1–24. [CrossRef]
28. Mansour, S. Spatial concentration patterns of South Asian low-skilled immigrants in Oman: A spatial analysis of residential geographies. *Appl. Geogr.* **2017**, *88*, 118–129. [CrossRef]
29. Yang, J.; Yang, R.; Chen, M.; Su, C.J.; Zhi, Y.; Xi, J. Effects of rural revitalization on rural tourism. *J. Hosp. Tour. Manag.* **2021**, *47*, 35–45. [CrossRef]
30. Sharma, M.; Brown, L.A. Racial/ethnic intermixing in intra-urban space and socioeconomic context: Columbus, Ohio and Milwaukee, Wisconsin. *Urban Geogr.* **2012**, *33*, 317–347. [CrossRef]
31. Rémi, L.; Marc, B.; Chen, Y. Patterns of residential segregation. *PLoS ONE* **2016**, *11*, e0157476:1–e0157476:20. [CrossRef]
32. Xue, B.; Zhang, L.; Geng, Y.; Mitchell, B.; Ren, W. Extended land-use coding system and its application in urban brown field redevelopment: A case study of Tiexi district in Shenyang, China. *J. Urban Plan. Dev.* **2016**, *142*, 5015014:1–5015014:11. [CrossRef]
33. Small, C.; Sousa, D.; Yetman, G.; Elvidge, C.; MacManus, K. Decades of urban growth and development on the Asian megadeltas. *Glob. Planet. Chang.* **2018**, *165*, 62–89. [CrossRef]
34. Kowalczyk, C.; Kil, J.; Kurowska, K. Dynamics of development of the largest cities—Evidence from Poland. *Cities* **2019**, *89*, 26–34. [CrossRef]
35. Li, X.; Bai, Z.; Tian, S.; Yang, J.; Guo, Y. Human settlement assessment in Jinan from a facility resource perspective. *SAGE Open* **2020**, *10*, 2158244020924056:1–2158244020924056:16. [CrossRef]
36. Yang, J.; Ren, J.; Sun, D.; Xiao, X.; Xia, J.C.; Jin, C.; Li, X. Understanding land surface temperature impact factors based on local climate zones. *Sustain. Cities Soc.* **2021**, *69*, 102818. [CrossRef]
37. Shang, S.; Du, S.; Du, S.; Zhu, S. Estimating building-scale population using multi-source spatial data. *Cities* **2021**, *111*, 103002:1–103002:13. [CrossRef]
38. Zhou, G.; Li, C.; Liu, Y.; Zhang, J. Complexity of functional urban spaces evolution in different aspects: Based on urban land use conversion. *Complexity* **2020**, 9741203. [CrossRef]
39. Tong, Y.; Liu, W.; Li, C.; Zhang, J.; Ma, Z. Understanding patterns and multilevel influencing factors of small town shrinkage in Northeast China. *Sustain. Cities Soc.* **2021**, *2*, 102811:1–102811:11. [CrossRef]
40. Zhou, C.; Luo, R.; Dai, D. Evolution and mechanism of the residential spatial structure from 2000 to 2010 in Guangzhou. *Geogr. Res.* **2015**, *34*, 1109–1124.
41. Li, X.; Zhu, J.; Wang, Y. Spatial differences of residential quarter floor area ratio: A case study of Dalian. *Prog. Geogr.* **2015**, *34*, 687–695.
42. Yang, J.; Guo, A.; Li, Y.; Zhang, Y.; Li, X. Simulation of landscape spatial layout evolution in rural-urban fringe areas: A case study of Ganjingzi District. *Gisci. Remote Sens.* **2019**, *56*, 388–405. [CrossRef]
43. Zhong, Y.; Feng, J. Residential spatial differentiation of migrant population within the city: A case study of Shenzhen. *Prog. Geogr.* **2017**, *36*, 125–135. [CrossRef]
44. You, H.; Yang, J.; Xue, B.; Xiao, X.; Xia, J.; Jin, C.; Li, X. Spatial evolution of population change in Northeast China during 1992–2018. *Sci. Total Environ.* **2021**, *776*, 146023. [CrossRef]
45. Sun, L.; Dong, H.; Geng, Y.; Li, Z.; Liu, Z.; Fujita, T.; Ohnishi, S.; Fujii, M. Uncovering driving forces on urban metabolism—A case of Shenyang. *J. Clean. Prod.* **2016**, *114*, 171–179. [CrossRef]
46. Liu, M.; Xu, Y.; Hu, Y.; Li, C.; Sun, F.; Chen, T. A century of the evolution of the urban area in Shenyang, China. *PLoS ONE* **2014**, *9*, e98847. [CrossRef]
47. Zhao, Z.; He, B.; Li, L.; Wang, H.; Darko, A. Profile and concentric zonal analysis of relationships between land use/land cover and land surface temperature: Case study of Shenyang, China. *Energ. Build.* **2017**, *155*, 282–295. [CrossRef]

48. Li, X.; Sun, H.; Tian, S.; Wang, M.; Zhang, D. Spatio-temporal differentiation of types of urban residential community: A case study of four districts in Dalian city. *Resour. Dev. Mark.* **2019**, *35*, 388–394. [CrossRef]
49. Liu, S.; Wu, C.; Shen, H. A GIS based model of urban land use growth in Beijing. *Acta Geogr. Sin.* **2000**, *4*, 407–416.
50. Xu, Q.; Huang, Y. Analysis of urban expansion measurement and driving mechanism in typical region of pearl river delta. *Sci. Surv. Mapp.* **2018**, *43*, 45–53.
51. Okabe, A.; Kitamura, M. A computational method for market area analysis on a network. *Geogr. Anal.* **1996**, *28*, 330–349. [CrossRef]
52. Anderson, T.K. Kernel density estimation and K-means clustering to profile road accident hotspots. *Accident Anal. Prev.* **2009**, *41*, 359–364. [CrossRef] [PubMed]
53. Nadi, P.A.; Murad, A.K. Modelling Sustainable Urban Transport Performance in the Jakarta city Region: A GIS Approach. *Sustainability* **2019**, *11*, 1879. [CrossRef]
54. Wang, J.; Lu, M.; Yuan, Z.; Rui, Y.; Qian, T. Point pattern analysis of ATMs distribution based on Ripley's K-Function method in Nanjing city. *Sci. Geogr. Sin.* **2016**, *36*, 1843–1849.
55. Ripley, B.D. *Spatial Statistics*; John Wiley: Chichester, UK, 1981; ISBN 047169116X.
56. Chai, Y.; Zhou, Y. The characteristics, mechanisms and tendency of suburbanization of residence in Dalian city. *Sci. Geogr. Sin.* **2000**, *20*, 127–132.
57. Cao, X.; Xue, D.; Yan, X. Development tendency of urban transport geography. *Sci. Geogr. Sin.* **2006**, *26*, 111–117.
58. Li, X.; Du, J. Research on private cars' influence on residential space based on residents' travel behavior: Taking Dalian as an example. *Geogr. Res.* **2007**, *26*, 1033–1042.
59. Zhang, C.; Li, X.; Zhang, X. Expansion of residence distribution and suburbanization research in Dalian. *Areal. Res. Dev.* **2005**, *1*, 66–69.
60. Niu, X.; Ou, M. A Study on driving-force system of regional land-use change: Taking Yangzhou city as an example. *China Popul. Resour. Environ.* **2007**, *1*, 102–108.
61. Hou, J.; Ying, W. *Analysis Methods of Regional Economy*; The Commercial Press: Beijing, China, 2004; ISBN 9787100041256.
62. Ilesanmi, A.O. Urban sustainability in the context of Lagos mega-city. *J. Geogr. Reg. Plan.* **2010**, *3*, 240–252. [CrossRef]
63. Newman, P.; Kenworthy, J. Sustainability and Cities: Summary and Conclusions. In *Designing Cities: Critical Readings in Urban Design*; Cuthbert, A.R., Ed.; Blackwell: Oxford, UK, 2003.
64. Griffiths, P.; Hostert, P.; Gruebner, O.; der Linden, S.V. Mapping megacity growth with multi-sensor data. *Rem. Sens. Environ.* **2010**, *114*, 426–439. [CrossRef]
65. Cheeseman, N.; de Gramont, D. Managing a mega-city: Learning the lessons from Lagos. *Oxf. Rev. Econ. Pol.* **2017**, *33*, 457–477. [CrossRef]
66. Aguilar, A.G.; Ward, P.M.; Smith Sr, C.B. Globalization, regional development, and mega-city expansion in Latin America: Analyzing Mexico City's peri-urban hinterland. *Cities* **2003**, *20*, 3–21. [CrossRef]
67. Xiao, Y.; Chen, S.; Wang, X.; Huang, J. Study on segregation of residential space of new migrants in Shanghai from the perspective of global city. *Plan. Stud.* **2016**, *3*, 25–33. [CrossRef]
68. Xu, Y.; Li, X.; Gao, J.; Guo, J. Research on dynamic changes and evolution model of urban residential quarter of Dalian in past ten years. *Sci. Geogr. Sin.* **2009**, *29*, 825–832.
69. Yang, Y.; Li, T.; Feng, X. Spatial-temporal analysis of residential space in Xi'an metropolis. *Areal. Res. Dev.* **2016**, *35*, 51–57.
70. Song, W.; Wu, Q.; Zhu, X. Residential differentiation of Nanjing in the new period. *Acta Geogr. Sin.* **2010**, *65*, 685–694.
71. Zhang, Y. Study on Spatial Differentiation of Beijing's Second-Hand Housing Prices Based on GWR Model. Master's Thesis, China University of Geosciences, Beijing, China, 2018.

land

MDPI

Article

Impact of Artificial Elements on Mountain Landscape Perception: An Eye-Tracking Study

Suling Guo [1,2], Wei Sun [1,2,*], Wen Chen [1,3], Jianxin Zhang [4] and Peixue Liu [4]

[1] Key Laboratory of Watershed Geographic Sciences, Nanjing Institute of Geography & Limnology, Chinese Academy of Sciences, East Beijing Road 73, Nanjing 210008, China; slguo@niglas.ac.cn (S.G.); wchen@niglas.ac.cn (W.C.)
[2] University of Chinese Academy of Sciences, Yuquan Road 19A, Beijing 100049, China
[3] College of Resources and Environment, University of Chinese Academy of Sciences, Yuquan Road 19A, Beijing 100049, China
[4] School of Geography and Ocean Science, Nanjing University, 163 Xianlin Street, Nanjing 210023, China; bokaimiwu@nju.edu.cn (J.Z.); pixliu@nju.edu.cn (P.L.)
* Correspondence: wsun@niglas.ac.cn

Abstract: The landscape is an essential resource for attracting tourists to a destination, but this resource has long been overused by tourism development. Tourists and scholars have begun noticing the interference of human structures in the natural environment and how this can change the meaning of a landscape. In this study, the impact of artificial elements on mountain landscapes was investigated by measuring the characteristics of visual perception and a landscape value assessment using eye-tracking analysis. Furthermore, this study includes socio-demographic features for testing whether they have an impact on landscape perception. The results show that human structures impact both visual perception and the perceived value of landscapes. Hotels and temples attract more visual attention than a purely natural landscape. Modern hotels appear to have a negative influence on mountain landscape valuation, while temples with unique culture have positive impacts. Socio-demographic groups differ significantly in how they observe landscape images and, to a degree, how they value the landscape therein. Our study should be of value to landscape planning and tourism policy making.

Keywords: landscape perception; artificial element; eye movement; socio-demography; tourism resource conservation

Citation: Guo, S.; Sun, W.; Chen, W.; Zhang, J.; Liu, P. Impact of Artificial Elements on Mountain Landscape Perception: An Eye-Tracking Study. *Land* **2021**, *10*, 1102. https://doi.org/10.3390/land10101102

Academic Editors: Baojie He, Ayyoob Sharifi, Chi Feng, Jun Yang and César Parcero-Oubiña

Received: 25 August 2021
Accepted: 14 October 2021
Published: 17 October 2021

Publisher's Note: MDPI stays neutral with regard to jurisdictional claims in published maps and institutional affiliations.

1. Introduction

A landscape can be defined as a space viewed or appreciated by a person or the scenery of one's daily life. The landscape is endowed with values by its inherent aesthetics, culture, or other merits that can be perceived by people's senses [1]. Continued research on landscapes has altered the way people think about it; a more current conception of the landscape is an environment produced by ongoing interaction between human and the surroundings around them [2–4]. Therefore, a landscape can be recognized by its two features: the landscape is formed by the interaction between human beings and the environment around them, and it is perceived or evaluated by people for its meaning within a place. The unique emotional or physical experience the landscape attracts tourists [5,6]. However, these important tourism resources are being consumed excessively in modern society, resulting in problems such as unsustainable utilization and environmental visual pollution. As one of the fastest-growing economic activities in China, tourism development alters the landscape by shaping its appearance and, therefore, the original meaning of a place. Modern structures or facilities interfering the landscape may alter people's perception and, in turn, their preference for tourism destinations, perhaps leading them to abandon it.

Perception is an intrinsic attribute of the landscape. Expressed in the form of space, the composition and layout of a landscape constitute what it affords; that is to say that

landscape affordance can be received spontaneously by people's sensory organs [7]. Visual sense plays a vital role in landscape perception; studies have demonstrated that people apperceive about 80 percent of outsider information through their visual systems [8]. A large amount of research has been conducted and involves the visual aspects of landscapes, and they are mostly carried out under the psycho-physical paradigm that regards landscape perception as a result of a stimulus-response relationship between human beings and the surrounding environment [1,9–12]. Aesthetic value receives most of the attention in landscape visual studies. Different landscapes show a variety of aesthetic features, yet they share certain underlying concepts in common. An index system for assessing the aesthetic value of a landscape consists of common indicators such as harmony, diversity, and mystery; systems that are similar have been studied, established, and applied in research and projects [4,13–16]. Daniel and Boster (1976) initially came up with the Scenic Beauty Estimation (SBE) method to evaluate the visual quality of a forest landscape [13]. A Semantic Differential (SD) scale is another frequently used method for evaluating landscape visual quality [17]. Related research has been extended to the landscape studies of cities, rural areas, gardens, roads, and more [18–21]. Cultural value is another essential landscape attribute that people perceive. As the most distinct feature in a regional context, culture can be seen as a type of immaterial tourism resource, and its outcomes provide economic benefit [22,23]. Tourists always pursue the sense of place or special experience generated by a unique cultural environment [24–26]. Other related studies have focused on the intrinsic meaning of cultural landscapes or places, the utilization and protection of heritage, the value and management of rural or urban cultural landscapes, and the environmental concerns as a landscape or a place has changed [27–32].

As modernism has globally spread, a question has been raised regarding whether modern architecture truly fits into landscapes with inherent local natural and cultural values. A landscape visual impact would be brought forth if the landscape changed when some entities invaded or moved out, causing a general irritation of emotional or psychological harm to viewers [33–35]. Relevant studies have focused on the harmony of human facilities set in a natural environment, the authenticity of landscape reconstruction, and world heritage protection [36–42]. In recent years, obtrusive man-made facilities and buildings interfering in scenic spots have irritated tourists and earned the notoriety, similarly to a misplaced brushstroke in a painting. Landscape reconstruction and visual threshold can be analyzed via GIS or an evaluation scale questionnaire, and such tools are important for investigating a landscape's visual impact [43–45]. Many studies focus on how man made facilities such as roads, buildings, and renewable-energy farms affect the landscape's natural properties and cause visual pollution [46–49]. There are some studies conducted to discuss the impact of cultural elements on the natural landscape during tourism development [31,50]. Little research has been conducted on modern buildings or facilities installed at natural tourism destinations. Built facility expansion resulting from tourism or other economic activities is the main theme in the impact of artificial elements research, including both positive and negative impacts [51–53]. Visual impact is one of the most common factors that account for the unsustainable utilization of tourism resources, but researchers have long been neglecting it. This study tested the impact of artificial element intervention in natural tourism resources from a perception perspective. Our study tries to fill in these gaps in existing research.

According to environmental cognitive psychology, a landscape as a stimulus can be perceived simultaneously and spontaneously through two processes: a top-down mode and a bottom-up mode. Bottom-up is an 'outside-in' information process, i.e., a variety of information from the external environment stimulates people's feelings and causes them to reflect. The landscape component as external information refers to physical features such as artificial buildings or the entire cultural or natural appearance of a landscape. Top-down means an 'inside-out' target-tracking task driven by the conceptions or established knowledge obtained from previous experience [54–56]. The human component such as internal consciousness encompasses past experience, knowledge, and expectations

shaped by an individual's or a group's socio-cultural context [57,58]. Demographics has been studied as a variable that partly explains the differences among several groups in landscape preference, tourism destination choice, and environmental behavior. Gender, age, education, income, ethnicity, and childhood background are the main characteristic descriptors in such studies [59–65]. Landscape is a discourse constructed from a method of perception that represents an identifiable socio-demographic group owing to a particular cultural mode or collective value [2]. Due to the fact that certain experiences, values, or attitudes shared by one group are different from the others, landscape perception varies between different groups and different levels of certain properties, including expertise and ethnicity [66–68]. Two types of landscape perception and evaluation approach are developed: an expert/design approach and a public perception-based approach [69]. The first focuses on knowledge about landscape attributes that is evaluated by several experts; the latter involves evaluations from public perspectives and is considered a more reliable measure [69–71]. Although the public participation method has been used in urban and tourism planning, a human's perception is still difficult to measure quantitatively, and often a more holistic and innovative method is needed [72,73].

The interaction between the physical landscape and personal knowledge is expressed through visual characteristics, landscape assessment, and attitude. Likewise, visual exploration can be explained as driven by two main factors: environmental stimuli and our own individual interests and intentions. Therefore, landscape value assessment results might be connected to the visual features demonstrated by physical eye movements [74–76]. As a psychological method, eye-tracking has been employed recently in landscape visual perception research. Visual behavior can be measured quantitatively and objectively through eye-tracking experiments, which entails, for example, a direct documentation of the location, duration, and order of the subjects' gazes; all of this can be obtained easily, clearly revealing the visual perceptual process [77,78]. Eye tracking has been applied in research on forest landscape [79], urban green space [73,80,81], landmark landscape [82], and rural landscape [66,75,83] in recent years. Landscape characteristics such as format, color, and openness have been applied as main variables in landscape perception. Some studies focus on the socio-demographic or acoustic variables during the landscape viewing process and demonstrate that humanistic elements do have an impact on landscape visual behaviors [73,79,84,85]. The visual impact of humanistic attributes on the natural landscape is usually discussed in this research area, but a negative or positive value assessment is lacking. Some research focuses on the tourism advertising effect [86,87] and tourism map cognition [88–90]. Little research has been constructed from the utilization of tourism landscapes [84,91,92], and the impact of artificial elements on tourism landscapes is rarely studied. The key point of these studies is the difference in landscape visual attention or landscape attractiveness. The mechanism behind the difference in visual perception still requires future research.

A theory and literature review demonstrates that landscape perception has been studied for a long time, but most analysis is concerned mainly with the separate views of either landscape surface features or different groups of observers; analysis combining external and internal factors as an entire landscape perception system remains to be discussed in depth. We, therefore, found our research conception framework based on the environmental cognitive process (Figure 1). Traditional methods such as a questionnaire survey are generally used in studies of landscape perception. Eye tracking as a more objective method has been applied in landscape studies recently, but there is little research on the impact of artificial elements on tourism landscapes. Modern tourism has been developed along with globalization; the impact of this development on the landscape requires further research. This article quantifies visual perception and value assessments as artificial elements and external stimuli that interfere in a natural landscape. Demographically, we also investigated landscape perception variations between different groups. Finally, the applicability of the eye movement analysis method relative to landscape perception and assessment research is discussed. Our hypotheses are as follows: (1) artificial elements in a natural landscape

cause differences in visual behavior, (2) artificial elements in a natural landscape cause differences in landscape value assessment, and (3) social demographics have an impact on landscape observation and evaluation.

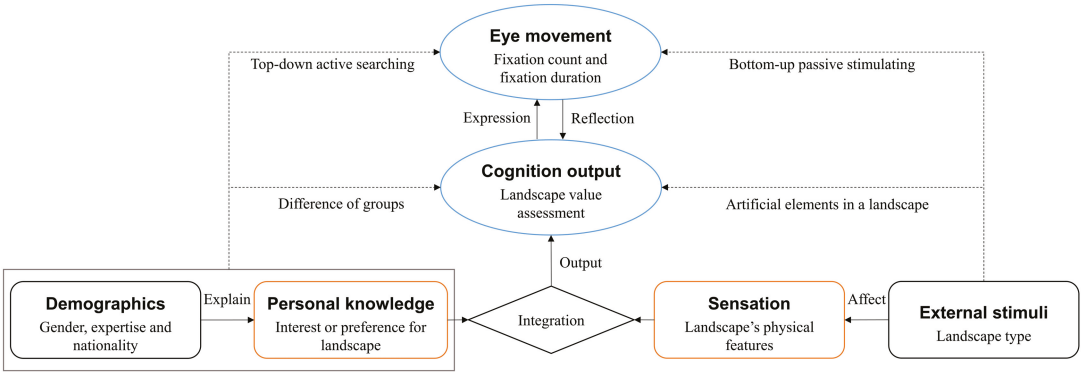

Figure 1. Conceptual framework of landscape perception.

2. Data and Methodology

2.1. Case Selection

As one of the most important resources for tourism, the mountain landscape has long been utilized for leisure purposes. Located in a densely populated area, because of their accessibility with a convenient transportation, the pleasant nature at a comfortable altitude (most of the mountains are below 2000 M in height), and the rich culture of religion and literature, the the mountains of Eastern China were tourist destinations first and only underwent intensive tourism development in recent years [93–95]. It is precisely because of the unique natural and cultural values the mountains are endowed with that many of them are listed as either natural or cultural World Heritage Sites or both. Mount Tai, for example, was listed as a World Cultural and Natural Heritage Site by UNESCO in 1987 as it was "the object of an imperial cult [. . .], and the artistic masterpieces found there are in perfect harmony with the natural landscape" [96]. On such values, the mass tourism development of mountains in Eastern China began, along with China's reform and opening up, and went through rapid development from the late 20th century. Tourism development for mountains is experiencing intense conflicts between utilization and protection. These mountains are always popular scenic spots in holidays. For example, about 166,200 tourists visited Mount Tai in 2019 on the Labor Day holiday, and 5.68 million tourists in total visited over the entire year. Mount Huang has maintained over 3 million tourists per year since 2012, except for the years after the outbreak of the coronavirus pandemic. Unlike the old temples that were shaped in harmony with the landscape, large modern buildings and facilities are being created to accommodate a large number of tourists. Landscape protection gives way to maximizing economic benefit. The mountain landscape has been severely devastated, and people's perception and value assessment of it is changing [94,97]. Accurately assessing the impact of artificial elements on mountain landscape perception and evaluation will contribute to resolving the tourism paradox of protection and exploitation.

2.2. Research Design

2.2.1. Experimental Design

A two by three experimental design was applied in this study. The landscape type is the within-subject variable, and it has three levels: the natural landscape, the temple landscape, and the hotel landscape. The between-subject variables are gender, expertise, and nationality, each of which has two levels: male and female, expert and layman,

and Chinese and foreigner, respectively. The dependent variables are landscape value assessment and eye movement characteristics.

2.2.2. Photograph Stimuli

Landscape photographs have been chosen as experiment stimuli in previous landscape studies and have proven to have the same effect with the real landscape [98–100]. In this study, three similar photos for each landscape type, nine in total, were selected from the official websites of tourism bureaus or scenic spot committees. The images posted on the official website were regarded as the distinctive landscapes in a scenic area. The official websites are always the first and most important info portal for tourists, so the images on official websites are viewed frequently by the masses and are familiar to them. The images on official websites are endowed with the representativeness of the real mountain landscape. With rich natural and cultural connotations, the mountain landscape has experienced a long period of tourism development history, such as those of Mount Tai and Mount Huang (Figure 2). A long shot or a medium shot view was applied when selecting the landscape photos.

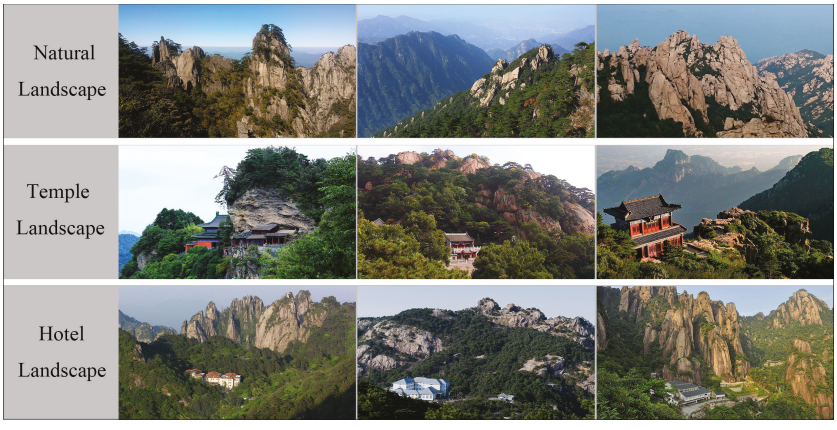

Figure 2. Landscape images. Images were selected from the official websites of tourism bureaus or scenic spot committees, including the Management Committee of Huangshan National Park (http://hsgwh.huangshan.gov.cn/) (accessed on 26 February 2018), the Management Committee of Scenic Spots and Historic Sites of Taishan (http://tsgw.taian.gov.cn/) (accessed on 26 February 2018), the Wudang Mountains Tourism Portal (http://ly.wudangshan.gov.cn/) (accessed on 26 February 2018), the Mount Laoshan tourism Portal (http://www.qdlaoshan.cn/) (accessed on 26 February 2018), and the Committee of Mount Jiuhua (http://www.jiuhuashan.gov.cn/) (accessed on 26 February 2018).

2.2.3. Mountain Landscape Value Assessment Scale

The mountain landscape was evaluated from the perspective of tourists' perceptions. The assessment index system has been well studied. Four indicators of coherence, complexity, legibility, and mystery were chosen in the environmental preference evaluation in Kaplan's research [101]. Tveit, Ode, and Fry presented a framework for analyzing landscape visual characteristics based on nine key visual concepts, namely stewardship, coherence, disturbance, historicity, visual scale, imageability, complexity, naturalness, and ephemera [35,40,102]. Aesthetic values and cultural values are the major components used in mountain landscape evaluation; visitors are attracted to these mountains principally because of these two values in Eastern China [93,94]. In this research, aesthetic and cultural values were emphasized in the mountain landscape value assessment. Five indices for both aesthetics and culture were itemized based on the landscape assessment system of Kaplan, Tveit, Ode, and Fry. Charm, ecology, peace, diversity, and harmony were likewise

selected for the aesthetic value assessment, and peculiarity, typicality, cultural connotation, mystery, and protection value were selected for the cultural value assessment (Table 1). Furthermore, the Outstanding Universal Value (OUV) assessment system set by UNESCO as the main tool in World Heritage Site selection, which includes six cultural and four natural criteria emphasizing uniqueness, historicity, aesthetic, geomorphology, ecology, etc., was also referred to in our mountain landscape value assessment system [103]. The questionnaire consisted of two parts: a five-point Likert scale of value assessment and a demographic information survey.

Table 1. Mountain landscape value assessment scale (Ath means aesthetic value and Cul means cultural value).

Assessment Content	Index	Index Description
Aesthetic value	Ath1	This landscape has graceful charm.
Aesthetic value	Ath2	This landscape is ecologically vibrant.
Aesthetic value	Ath3	This This landscape makes me feel peaceful.
Aesthetic value	Ath4	This landscape contains much diversity.
Aesthetic value	Ath5	This landscape is harmonious.
Cultural value	Cul1	This landscape reflects the peculiar characteristics of a mountain landscape.
Cultural value	Cul2	This landscape represents the characteristics of mountains in China.
Cultural value	Cul3	This landscape has profound cultural connotations.
Cultural value	Cul4	This landscape is full of mystery.
Cultural value	Cul5	This landscape contains significant value and ought to be protected.

2.3. Subjects and Data Collection

2.3.1. Subjects

A total of 106 students with either normal or corrected vision from Nanjing University (NJU) were invited to participate in the experiment by using informative flyers and posters distributed throughout NJU. College students are considered to have a certain level of knowledge in terms of thinking and acting independently. They tend to pay more attention to tourism information. Thus, they can perceive and evaluate the tourism landscape more quickly and accurately. After manually scrutinizing and excluding abnormal values (extreme and zero values), data of 96 subjects were filtered and assessed as effective for analysis in this study. Of the 96 subjects, 51 percent were males and 49 percent were females; students with landscape—or tourism—related expertise (experts) accounted for 37.5 percent, and laymen accounted for 62.5 percent. Chinese subjects accounted for 78.1 percent, and foreigners accounted for 21.9 percent. The foreign participants' countries of origin included Germany, Pakistan, Indonesia, South Korea, Russia, Ukraine, and Vietnam.

2.3.2. Data Collection

During the experiment, an SMI MOBILE eye tracker was used with a laptop (1600 $*$ 900 screen resolution) to track the subjects' eye movements, and an iPad was used for the landscape value assessment questionnaire survey. At first, the subjects were asked to view the photos on the laptop screen in a random order. After finishing one photo, the subjects would press the left arrow to view the next one. Subject-controlled viewing time for each photo prevented insufficient viewing time or observational data that did not reveal real landscape preference and eye movement characteristics. After the eye-tracking experiment, the subjects were asked to complete a landscape value assessment questionnaire about the landscapes they had just viewed on the laptop. Each experiment of the subjects lasted about three minutes.

2.4. Data Analysis

2.4.1. General Analysis of ETM

BeGaze 3.7, the software package provided with the SMI eye-tracker, was used to export the data of eye tracking metrics (ETM) in well-structured Excel files. Fixation count (FC) and fixation duration (FD) were selected as the eye movement indicators based on

which subjects' perception behavior would be analyzed [87,104]. Fixation count (FC) is the number of fixations measured in counts (c). A higher FC indicates that the participants processed more but not necessarily useful information during the viewing time. Fixation duration (FD) is the total duration time of all fixations for an image, measured in seconds (s). The longer the FD, the more interested the participants were [90].

Since each landscape type included three similar landscape images, the subjects' FC and FD for each landscape type were calculated by averaging the values of the three similar landscape images. Multiplying 96 subjects by three landscape types and by two eye movement indicators yielded data containing 576 eye movement records in total. Aesthetic and cultural landscape values were integrated by averaging their five index scores for the three similar landscape pictures. Similarly, the data of the 576 records of landscape value assessment indicators were usually distributed. A log transformation was applied to convert eye movement data into the normal distribution for later analysis.

2.4.2. Creating the Eye-Tracking Maps

A heat map can be created in BeGaze 3.7 directly. The heat map is projected onto the original image to highlight the observed areas. On the heat map, red means a high amount of observations, green means a lower amount, and no color means almost no observation. Our research obtained nine heat maps by positioning fixation points and overlaying viewing time on landscape images (Figure 3). A scan path map can be created by orderly connecting lines between the fixation points in BeGaze 3.7. The scan path map shows the attention process. Subjects in a landscape always notice prominent elements. We, therefore, can obtain the attention sequence by analyzing the scan path. By capturing the scan path characteristics at the 0.1th second and the 0.5th second of the viewing process, we obtained six scan path maps (Figure 4).

Figure 3. Heat maps of landscape images.

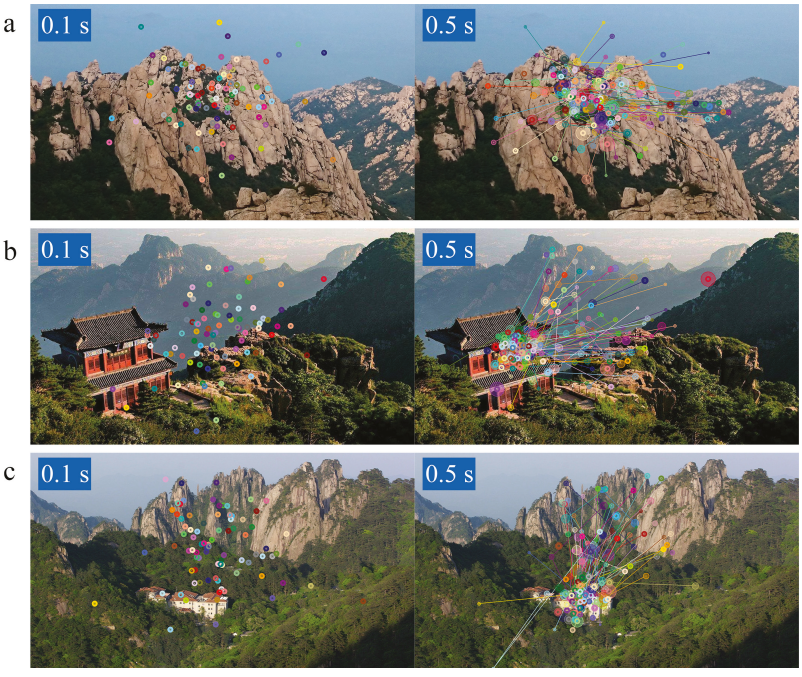

Figure 4. Scan path maps of three types of landscapes at 0.1 s and 0.5 s: (**a**) the natural landscape, (**b**) the temple landscape, and (**c**) the hotel landscape.

2.4.3. Perception Difference of Three Landscapes and Demographics Analysis

The classical difference analysis method was applied in this research. One-way repeated measures ANOVA was conducted to test the difference of visual behavior and landscape value assessment among natural, temple, and hotel landscapes. A least significant difference pairwise comparison method was used to further discuss each difference between the three landscapes. Two variables, landscape type and demographics, were tested by using two-way repeated measures ANOVA to test the demographic differences. Furthermore, the differences in demographic features were also obtained from the tests of the between-subjects effect.

3. Results

3.1. Eye-Tracking Maps of Landscape Images

Heat maps can be created by positioning fixation points and overlaying viewing time on landscape images. By visualizing all the fixation points and the total fixation duration from the 96 subjects, nine heat maps of the landscape images were obtained (Figure 3). The heat maps analysis indicates that natural landscapes encompassed a wider visual scope. For natural landscapes, visual attention not only concentrated on the center of the image but also scattered around the center. Visual attention on the temple landscape and the hotel landscape focused mainly on the artificial elements in the image and was constrained within a relatively smaller area than the natural landscape. The visual difference between the natural landscape and the landscapes with an artificial element is clearly presented in heat maps. Therefore, hypothesis one was demonstrated to be true.

Nearly all the subjects' visual focus was fixed on the image center for all landscape types at the 0.1th second of the experiment. At the 0.5th second, the subjects' second fixation point appeared; viewing paths were drawn by connecting these two points with a line (Figure 4). In the temple and hotel landscapes, nearly all the subjects' second fixation points were located on the artificial elements in the temple and hotel landscapes. This

differs from the natural landscape. In the natural landscape, the second fixation points were still collected near the very center in the visual field (the image center). Fixation changes are clearly revealed in the scan path maps (Figure 4). Thereafter, the subjects' fixation points remained focused on the artificial elements in the temple landscape and the hotel landscape and focused on the image geometric center in the natural landscape for the remainder of the viewing time. The results demonstrate that artificial elements in the natural landscape are more likely to attract subjects' attention.

3.2. Eye Movement and Value Assessment of Three Landscapes

One-way repeated measures ANOVA was conducted to test the visual differences between the natural, temple, and hotel landscapes. The results show that the FCs of the three landscapes are different in terms of statistical significance ($F = 7.532$, $p = 0.001$). The hotel landscape has the highest viewing counts with a mean of 19.858. The FC mean of the temple landscape is 18.792. The natural landscape shows the lowest viewing counts with a mean of 16.962. The hotel and temple landscapes received more information and attention than compared to the natural landscape. The same results were found in FD. For the three landscapes, the hotel landscape shows the highest FD. The FD mean values of the hotel and temple landscapes are 5.033 s and 4.926 s, respectively, which are also higher than that of the natural landscape, which is 4.267 s. There is also a significant difference statistically in FD among the three landscapes ($F = 4.521$, $p = 0.012$). This demonstrates that artificial elements in the natural mountain landscape impact visual perception, further proving Hypothesis 1. The same method was applied to analyze the differences in landscape value assessment. Three landscape types differ significantly in their aesthetic value ($F = 18.285$, $p = 0.000$). Likewise, the cultural values of the three landscapes are also different in terms of statistical significance ($F = 44.770$, $p = 0.000$). The temple landscape obtained the highest score both in aesthetic value (mean = 3.641) and cultural value (mean = 3.719), while the hotel landscape obtained the lowest score both in aesthetic value (mean = 3.260) and cultural value (mean = 2.994). Hypothesis 2 was confirmed. The difference is clearly revealed by the boxplots of eye movement and value assessment for the three landscapes (Figure 5).

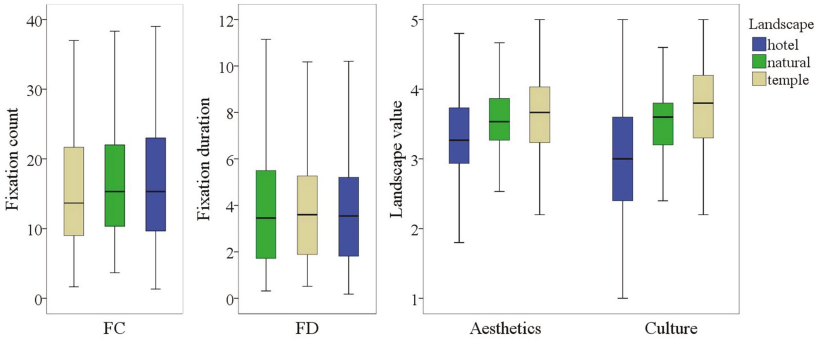

Figure 5. Boxplots of eye movement and value assessment for the three landscapes. The fixation count is measured in counts (c), and the fixation duration is measured in seconds (s).

A least significant difference pairwise comparison method was used to further discuss each difference between the three landscapes; the results are shown in Tables 2 and 3. The results demonstrate that temples and hotels have a significantly higher FC and FD than a purely natural landscape, while there is no significant difference between the temple and hotel landscapes. Natural and temple landscapes differed significantly from the hotel landscape in terms of aesthetic value, while the difference between the natural and temple landscapes was not significant. Compared to the hotel landscape, the natural landscape and temple landscape had higher aesthetic and cultural values. Regarding cultural value,

each landscape differed significantly from one another. The hotel landscape has far less cultural value than the two other landscapes, and the temple landscape received the highest cultural value assessment score (Table 2). The same conclusions can also be drawn from Figure 5.

Table 2. Statistical description of three landscapes in terms of eye movement and landscape values.

Landscape	Fixation Count		Fixation Duration		Aesthetic Value		Cultural Value		N
	Mean	SD	Mean	SD	Mean	SD	Mean	SD	
Natural	16.962	11.372	4.267	3.171	3.580	0.490	3.465	0.578	96
Temple	18.792	14.297	4.926	4.390	3.641	0.611	3.719	0.604	96
Hotel	19.858	14.420	5.033	4.502	3.260	0.735	2.994	0.942	96

Table 3. Least significant difference pairwise comparison of three landscapes.

Landscape Pairs	Fixation Count		Fixation Duration		Aesthetic Value		Cultural Value		N
	p	SD Er.	*p*	SD Er.	*p*	SD Er.	*p*	SD Er.	
Natural-Temple	0.040	0.016	0.010	0.018	0.336	0.063	0.000	0.068	96
Natural-Hotel	0.001	0.018	0.021	0.020	0.000	0.081	0.000	0.101	96
Temple-Hotel	0.406	0.015	0.929	0.016	0.000	0.062	0.000	0.082	96

3.3. Socio-Demographic Differences in Landscape Perception

Two variables, landscape type and demographics, were tested by using two-way repeated-measures ANOVA. Tests of the within-subjects effect indicated that the differences of eye movement and value assessment between the three landscapes (natural, temple, and hotel) were significant, consistent with the analysis above. All three demographic features (gender, expertise, and nationality) have no interaction effect on landscape type. This means that whether demographic features show a significant difference in eye movement or landscape value assessment had no significant relevance to the variable of landscape type. We directly obtained the difference between demographic features from the tests of the between-subjects effect (Table 4). Eye movement, i.e., both FC and FD, shows significant differences between men and women. Gender, expertise, and nationality are the demographic reasons for the differences in landscape value assessment.

Table 4. Demographic differences in eye movement and landscape value assessment.

Demographic Feature	Fixation Count		Fixation Duration		Aesthetic Value		Cultural Value		N
	F	*p*	F	*p*	F	*p*	F	*p*	
Gender	9.682	0.002	7.743	0.007	5.075	0.027	0.170	0.681	F47, M49
Expertise	0.831	0.364	0.425	0.516	3.012	0.086	4.611	0.034	E36, L60
Nationality	2.282	0.134	2.576	0.112	10.869	0.001	7.973	0.006	C75, F21

There are significant gender differences in visual perception, with higher FC and FD in males than females. Men tended to observe the landscape images in more detail and for a longer duration. Likewise, men generally showed higher landscape value assessment scores, whereas women showed higher cultural value assessment. Compared to laymen, experts have higher FCs and longer viewing times but lower landscape value assessment scores. Foreigners appeared to score higher than Chinese participants in terms of both eye movement and landscape value assessments. Although eye movement differences in expertise and nationality showed no statistical significance, the obvious gaps were indicated by comparing the mean values of FC and FD between experts and laymen and between Chinese and foreigners. Women scored a higher average cultural value than men in terms of natural landscapes, which may account for the insignificant difference. Figure 6 illustrates the difference in the mean values in gender, expertise, and nationality, which solidly supports our analysis above. Therefore, we claim that demographic features such

as gender, expertise, and nationality show differences in general. That is, demographic features have impacts on landscape observation and evaluation. The validity of Hypothesis 3 is thereby demonstrated.

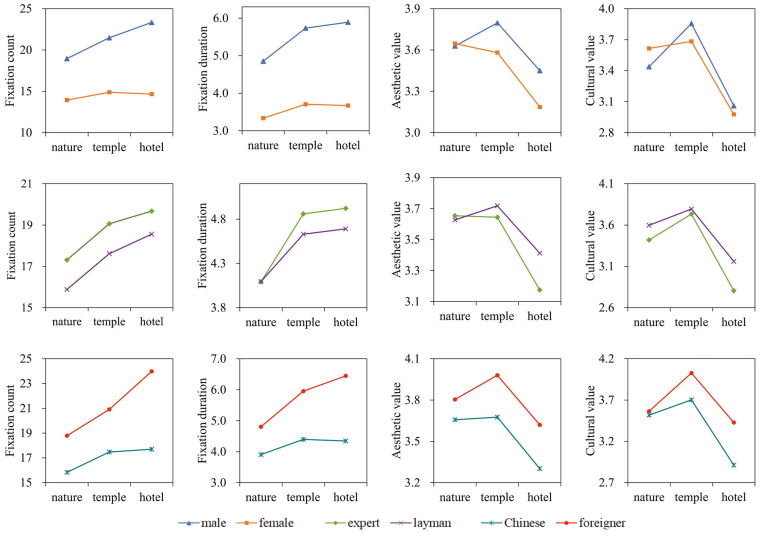

Figure 6. Mean values of eye movement and landscape assessment under gender, expertise, and nationality. The fixation count is measured in counts (c), and the fixation duration is measured in seconds (s).

4. Discussion

Landscape perception is an integrated outcome of the intrinsic physical appearance of the landscape and a posteriori knowledge of social demographics [1,105]. In the present study, we applied a systematic method to verify this landscape perception process by combining eye movement and value assessment. Both eye movement and value assessment can be regarded as the outcome of human–landscape interactions, both of which can manifest landscape perception. Based on the philosophical ideologies of his time, Lothian (1999) [105] compared the objectivist and subjectivist paradigms in landscape assessment. He concluded that the subjective method is a more reasonable method for evaluating the landscape. In this research, we found that the physical features of a landscape are as important as the eye of the beholder because they are prerequisites for capturing people's attention. Objectivity, in this study, refers to the type of data we obtained that owe less to individual subjectivity; therefore, such methods more realistically reflect the underlying laws of landscape perception. Some studies have been conducted by combining objective and subjective methods to evaluate landscape [49,106,107]. Our results indicate that eye tracking might be feasible as an alternative or complementary method in landscape research to enable a more objective and scientific study, which corresponds to the conclusions in other studies in this field [75,76].

Here, we emphasize that artificial elements impact landscape visual perception and value assessment and that gender, expertise, and nationality, because of the different experience and knowledge, also show different perceptual modes and characteristics. Eye-tracking has been used in tourism studies mainly on advertisement effectiveness, with few studies on rural or urban landscape research and almost none on tourism landscape research [87,91,108]. However, visual characteristics are essential for tourism landscape because tourists first visually receive sensory information of the surrounding environment. Our observations contribute to a better understanding of landscape perception and the

impact of artificial elements on landscape theoretically by combining visual behavior with value assessment, providing, therefore, proper and practical guidance for landscape utilization and tourism planning.

4.1. The Impact of Artificial Elements on Mountain Landscape Perception

The landscape has played a crucial role in attracting tourists. As pointed out in the existing literature, aesthetics and culture are two of the most palpable features of the landscape embedded in a particular place [9,11,14,15,22–26,93,94]. Our research results further confirmed this: the temple landscape received the highest assessment score both in aesthetic and cultural value, and the natural landscape received a higher aesthetic value score because of their ecological traits and restorative and recreational benefits [4,109].

Harmony has long been used as a major criterion in landscape value assessment [36–42]. Existing research has shown that a landscape without artificial elements is perceived as harmonious [42]. However, our study shows that special artificial structures may be equally coherent with their natural surroundings. This is indicated by the temple landscape, which tends to have a more traditional structure, scoring higher on harmony than the natural landscape, which is consistent with the results of existing research [31,50,93]. Temples, especially Taoist temples, are places where people seek peace, relaxation, and spiritual solace, and such temples are built explicitly by integrating human and natural elements. The features of such places are appealing to stressed people living in modern cities with busy lives [32,68,110]. Traditional elements such as temples have long been perceived as coexisting with mountain landscapes or being rooted in the mountains for thousands of years. Thus, people may tend to perceive temples as harmonious with its mountainous surroundings. On the contrary, modern hotels appeared relatively recently with industrialization and globalization. People might have a more traditional perspective and may not be used to such modern objects visually and cognitively [111,112], and such man-made structures may be considered disharmonious or intrusive elements.

Existing research shows that artificial elements are given more visual sensitivity in a landscape. The more visually sensitive the landscape is, the more visual pollution will be caused, and the more disharmonious the landscape will be [45,48,85,113]. This is reflected in this study. Hotels are the most obtrusive element and are perceived first and foremost. Temples received more attention from the subjects than their natural surroundings. Although temple landscapes received the highest assessment value (both in aesthetics and culture), they received less viewing time and attention than hotels. Similarly, hotel landscapes had the lowest value but received the most visual attention; natural landscapes had a moderate value and received the least visual attention. Therefore, landscape surface features and people's interests could be implied by the visual attention to some extent, but not all aspects. In this study, the subjects' landscape value assessment only partially reflected their visual characteristics. The mechanism between visual behavior and value assessment during landscape perception requires further investigation.

4.2. Demographic Differences in Mountain Landscape Perception

As research has shown a preference for the empiricism paradigm recently, knowledge acquired from experience in a particular circumstance (a posteriori knowledge) is recognized as an essential factor affecting landscape perception. Gender, expertise, and nationality are three of the variables most often studied [59–63]. In this study, men showed higher value assessment scores and paid more visual attention to landscapes than women, with the exception of natural landscapes. Men had lower value assessment scores for the natural landscape and higher value assessment scores for the temple and hotel landscapes. This significant gender difference is consistent with the studies of Li et al. [82] and Wang et al. [84] which have shown that men are more likely to perceive the humanistic attribute than compared to women. As revealed by many studies, gender also significantly affects attribute recognition of tourism destinations, value assessment, and travel behavior [64,114]. Personality differences between men and women may emerge as the cause of the land-

scape perception differences. Moreover, the reason people stay in an area with a particular landscape or environment also affected landscape assessment [65,115].

One exciting finding in this study is that the three types of landscapes were paid a greater amount of visual attention but were given lower value assessment scores by experts than laymen. One possible explanation is that experts tend to spend more time scrutinizing the landscape and carry out a stricter standard for value assessment from a professional perspective [66,116]. Furthermore, location also plays an important role in landscape perception. This research shows that people from different countries may hold various opinions about a landscape, consistent with previous studies [68,98,117]. In the study presented by Wang et al. (2016) [68], Australian participants fixated more frequently and for longer durations on tourism images than Chinese participants. Fixation also varied with image conditions, with the Chinese group having particularly low fixation durations and counts for the low arousal or natural condition. Perhaps because of their curiosity or yearning for novelty, foreigners might have longer visual attention span and provide higher value assessment scores of the landscapes than native subjects.

4.3. Limitations and Future Research

This paper has certain limitations. First, using landscape images may have been resulted in conclusions that are similar to those made using actual landscapes; however, the limited number of images and photographic techniques cannot completely replace an actual landscape. Additionally, landscape information may be omitted from the images. Panoramic photos or virtual reality might be a better alternative in obtaining research results accurately [104,118]. Second, this study included only college students as subjects. In future research, a more diversified sample, with different educational backgrounds and age groups, is needed in order to improve the validity of the research. The number of participants is a key factor for validity and efficacy in a study. Although a sample containing over 30 participants has been reported as a valid sample size in previous eye movement studies [68,87,104], social surveys such as the landscape assessment used in this study generally required a larger sample size, around 300–500 participants [16]. It is essential to connect psychological experiments and social surveys properly to discover the underlying implications. Eye-tracking still remains a new tool in landscape research, and it might be more appropriate to use it as an assisted method functioning together with questionnaires. Finally, human visual perception and psychological cognition are two mutually influenced processes; the interaction between subjects' visual attention to landscapes and their real interest in it requires further discussion. Visual fixations are selected according to visual acuity and color sensitivity in a human vision system. The visual–cognitive system patterns the viewing process by actively controlling fixations directly relative to important and informative visual cues [119]. In addition, layout, colors, lighting, and other attributes of landscape photos require thorough consideration in future research.

5. Conclusions

This study aimed to examine the effect of artificial elements on mountain landscape perception through the eye-tracking method. Our results indicate that artificial elements stand out visually in a natural landscape. The hotel, a modern artificial entity, is considered as visual pollution and received negative landscape value assessments. By contrast, the temple is generally regarded as a traditional and distinctive element that is harmonious with the mountain landscape. Temples have a higher landscape value because of their spiritual significance, which demonstrates that temples should be preserved as valuable tourism resources. Modern artificial facilities such as hotels are considered to have a greater visual impact and should be evaluated before construction. Otherwise, improper construction in a landscape may become a negative intrusion, similarly to a misplaced brushstroke in a painting, resulting in abandoned tourism sites and a waste of tourism resources. More attention should be paid to the negative impact of modern buildings in

already harmonious environments, and more sustainable tourism development in such areas is needed. For mountainous tourism areas, hotels could be located at the foot of or around mountains instead of at the mountainsides or peaks. Architectural design with more harmonious appearance (i.e., in terms of color, shape, materials, etc.) with relative to the surrounding natural landscape should be given more attention in tourism planning and development. For the most famous mountain tourism spots, such as Mount Huang, a two-day trip with a one night stay on a mountain is necessary, causing the demand for accommodation. The academic and practical question of how tourist demand can be balanced with landscape protection remains to be investigated for tourism planners and developers, and more research is needed in the future.

Based on the theories of environmental psychology, this study tested whether socio-demographic factors affect landscape perception in a top-down cognitive mode. The findings indicate that gender, expertise, and nationality affect both landscape visual behaviors and landscape value assessments. Men, in general, observed the landscapes in more detail and for a longer duration; men also had higher landscape value assessment scores than women. Experts were more likely to observe landscapes with greater scrutiny and provide lower landscape value assessment scores, probably due to their professional knowledge on landscapes. In terms of both eye movement and landscape value assessment, foreigners scored higher than Chinese participants. Curiosity is probably the most relevant explanation for this difference.

This study measured landscape visual perception and value assessments by an eye-tracking experiment on artificial elements interfering with mountain landscapes. A systematic research framework combining the external factors of landscape surface features and internal factors of socio-demographics was applied. Eye-tracking as a method recently applied in landscape research can obtain a more objective and quantitative visual behavior data. The feasibility of the eye-tracking method on landscape perception research has been tested in this study, which provides certain theoretical and methodological innovations. Nevertheless, as a primary study, there are still some limitations. The images used were mainly second-hand images. Photographs taken by the researchers themselves might contain more landscape information. Furthermore, panoramic images or virtual reality technologies might reveal more information if applied to landscape research. Additionally, sample selection must be considered more rigorously. The relationship between eye movement and landscape assessment and the underlying mechanism require further discussions.

Author Contributions: Conceptualization, S.G.; methodology, S.G.; software, S.G.; validation, S.G. and P.L.; formal analysis, S.G.; investigation, S.G.; resources, S.G. and J.Z.; data curation, S.G.; writing—original draft preparation, S.G.; writing—review and editing, S.G., W.S., W.C., J.Z. and P.L.; visualization, S.G.; supervision, W.C. and J.Z. All authors have read and agreed to the published version of the manuscript.

Funding: This research was funded by the Strategic Priority Research Program(A) of the Chinese Academy of Sciences, grant number XDA230201, and the Key R&D Program of Jiangsu Province, grant number BE2019773. The Strategic Priority Research Program(A) of the Chinese Academy is funded by the Chinese Academy of Sciences, and the Key R&D Program of Jiangsu Province is funded by the Jiangsu Provincial Department of Science and Technology.

Institutional Review Board Statement: Not applicable.

Informed Consent Statement: Not applicable.

Data Availability Statement: Not applicable.

Conflicts of Interest: The authors declare no conflict of interest.

References

1. Zube, E.H.; Sell, J.L.; Taylor, J.G. Landscape perception: Research, application and theory. *Landsc. Plan.* **1982**, *9*, 1–33. [CrossRef]
2. Cosgrove, D.; Daniels, S. *The Iconography of Landscape: Essays on the Symbolic Representation, Design and Use of Past Environments*; Cambridge University Press: Cambridge, UK, 1988; Volume 9.
3. Cosgrove, D.E. *Social Formation and Symbolic Landscape*; Univ. of Wisconsin Press: Madison, WI, USA, 1998.
4. Kaplan, R.; Kaplan, S. *The Experience of Nature: A Psychological Perspective*; Cambridge University Press: Cambridge, UK, 1989.
5. Qiu, H.; Hsu, C.; Li, M.; Shu, B. Self-drive tourism attributes: Influences on satisfaction and behavioural intention. *Asia Pac. J. Tour. Res.* **2018**, *23*, 395–407. [CrossRef]
6. Tyrväinen, L.; Silvennoinen, H.; Nousiainen, I.; Tahvanainen, L. Rural tourismin Finland: Tourists' expectation of landscape and environment. *Scand. J. Hosp. Tour.* **2001**, *1*, 133–149. [CrossRef]
7. Gibson, J.J. *The Perception of the Visual World*; Houghton Mifflin: Boston, MA, USA, 1950.
8. Anderson, J.R.; Boyle, C.F.; Corbett, A.T.; Lewis, M.W. Cognitive modeling and intelligent tutoring. *Artif. Intell.* **1990**, *42*, 7–49. [CrossRef]
9. Di, F.; Yang, Z.; Liu, X.; Wu, J.; Ma, Z. Estimation on aesthetic value of tourist landscapes in a natural heritage site: Kanas National Nature Reserve, Xinjiang, China. *Chin. Geogr. Sci.* **2010**, *20*, 59–65. [CrossRef]
10. Menatti, L.; Casado da Rocha, A. Landscape and health: Connecting psychology, aesthetics, and philosophy through the concept of affordance. *Front. Psychol.* **2016**, *7*, 571. [CrossRef]
11. Ribe, R.G. A general model for understanding the perception of scenic beauty in northern hardwood forests. *Landsc. J.* **1990**, *9*, 86–101. [CrossRef]
12. Stern, R.M.; Ray, W.J.; Quigley, K.S. *Psychophysiological Recording*; Oxford University Press: Oxford, UK, 2001.
13. Daniel, T.C.; Boster, R.S. *Measuring Landscape Esthetics: The Scenic Beauty Estimation Method*; USDA Forest Service, Rocky Mountain Forest and Range Experiment Station: Fort Collins, CO, USA, 1976; Volume 167.
14. Gobster, P.H.; Nassauer, J.I.; Daniel, T.C.; Fry, G. The shared landscape: What does aesthetics have to do with ecology? *Landsc. Ecol.* **2007**, *22*, 959–972. [CrossRef]
15. Rosley, M.S.F.; Lamit, H.; Rafida, S. Aesthetic and Perception: Indicators of perceiving the rural landscape. *Asian J. Behav. Stud.* **2017**, *2*, 11–22. [CrossRef]
16. Tveit, M.S.; Ode Sang, Å.; Hagerhall, C.M. Scenic beauty: Visual landscape assessment and human landscape perception. *Environ. Psychol. Introd.* **2018**, *2018*, 45–54.
17. Osgood, C.E. Semantic differential technique in the comparative study of cultures 1. *Am. Anthropol.* **1964**, *66*, 171–200. [CrossRef]
18. Arriaza, M.; Cañas-Ortega, J.F.; Cañas-Madueño, J.A.; Ruiz-Aviles, P. Assessing the visual quality of rural landscapes. *Landsc. Urban Plan.* **2004**, *69*, 115–125. [CrossRef]
19. Bulut, Z.; Yilmaz, H. Determination of landscape beauties through visual quality assessment method: A case study for Kemaliye (Erzincan/Turkey). *Environ. Monit. Assess.* **2008**, *141*, 121–129. [CrossRef] [PubMed]
20. Chen, B.; Adimo, O.A.; Bao, Z. Assessment of aesthetic quality and multiple functions of urban green space from the users' perspective: The case of Hangzhou Flower Garden, China. *Landsc. Urban Plan.* **2009**, *93*, 76–82. [CrossRef]
21. Ramírez, Á.; Ayuga-Téllez, E.; Gallego, E.; Fuentes, J.M.; García, A.I. A simplified model to assess landscape quality from rural roads in Spain. *Agric. Ecosyst. Environ.* **2011**, *142*, 205–212. [CrossRef]
22. Knudsen, D.C.; Soper, A.K.; Metro-Roland, M. Commentary: Gazing, performing and reading: A landscape approach to understanding meaning in tourism theory. *Tour. Geogr.* **2007**, *9*, 227–233. [CrossRef]
23. Metro-Roland, M. Interpreting meaning: An application of Peircean semiotics to tourism. *Tour. Geogr.* **2009**, *11*, 270–279. [CrossRef]
24. Davenport, M.A.; Anderson, D.H. Getting from sense of place to place-based management: An interpretive investigation of place meanings and perceptions of landscape change. *Soc. Nat. Resour.* **2005**, *18*, 625–641. [CrossRef]
25. Quinn, T.; Bousquet, F.; Guerbois, C.; Sougrati, E.; Tabutaud, M. The dynamic relationship between sense of place and risk perception in landscapes of mobility. *Ecol. Soc.* **2018**, *23*. [CrossRef]
26. Tuan, Y.F. *Space and Place: The Perspective of Experience*; U of Minnesota Press: Minneapolis, MN, USA, 1977.
27. Taylor, K. The Historic Urban Landscape paradigm and cities as cultural landscapes. Challenging orthodoxy in urban conservation. *Landsc. Res.* **2016**, *41*, 471–480. [CrossRef]
28. Tieskens, K.F.; Schulp, C.J.; Levers, C.; Lieskovskỳ, J.; Kuemmerle, T.; Plieninger, T.; Verburg, P.H. Characterizing European cultural landscapes: Accounting for structure, management intensity and value of agricultural and forest landscapes. *Land Use Policy* **2017**, *62*, 29–39. [CrossRef]
29. Tilley, C. Introduction: Identity, place, landscape and heritage. *J. Mater. Cult.* **2006**, *11*, 7–32. [CrossRef]
30. Wynveen, C.J.; Kyle, G.T.; Sutton, S.G. Natural area visitors' place meaning and place attachment ascribed to a marine setting. *J. Environ. Psychol.* **2012**, *32*, 287–296. [CrossRef]
31. Cartier, C. Megadevelopment in Malaysia: From heritage landscapes to "leisurescapes" in Melaka's tourism sector. *Singap. J. Trop. Geogr.* **1998**, *19*, 151–176. [CrossRef]
32. Jiang, T.; Ryan, C.; Zhang, C. The spiritual or secular tourist? The experience of Zen meditation in Chinese temples. *Tour. Manag.* **2018**, *65*, 187–199. [CrossRef]

33. Chmielewski, S.; Lee, D.J.; Tompalski, P.; Chmielewski, T.J.; Wężyk, P. Measuring visual pollution by outdoor advertisements in an urban street using intervisibilty analysis and public surveys. *Int. J. Geogr. Inf. Sci.* **2016**, *30*, 801–818. [CrossRef]
34. Jana, M.K.; De, T. Visual pollution can have a deep degrading effect on urban and suburban community: A study in few places of Bengal, India, with special reference to unorganized billboards. *Eur. Sci. J.* **2015**, *11*, 1–14.
35. Ode, Å.; Tveit, M.S.; Fry, G. Capturing landscape visual character using indicators: Touching base with landscape aesthetic theory. *Landsc. Res.* **2008**, *33*, 89–117. [CrossRef]
36. Gahwiler, P.; Havitz, M.E. Toward a relational understanding of leisure social worlds, involvement, psychological commitment, and behavioral loyalty. *Leis. Sci.* **1998**, *20*, 1–23. [CrossRef]
37. Nohl, W. Sustainable landscape use and aesthetic perception–preliminary reflections on future landscape aesthetics. *Landsc. Urban Plan.* **2001**, *54*, 223–237. [CrossRef]
38. Palmer, J.F. The perceived scenic effects of clearcutting in the White Mountains of New Hampshire, USA. *J. Environ. Manag.* **2008**, *89*, 167–183. [CrossRef] [PubMed]
39. Rössler, M. World heritage cultural landscapes: A UNESCO flagship programme 1992–2006. *Landsc. Res.* **2006**, *31*, 333–353. [CrossRef]
40. Tveit, M.; Ode, Å.; Fry, G. Key concepts in a framework for analysing visual landscape character. *Landsc. Res.* **2006**, *31*, 229–255. [CrossRef]
41. Zukin, S. Reconstructing the authenticity of place. *Theory Soc.* **2011**, *40*, 161–165. [CrossRef]
42. Sowifska-fwierkosz, B. Index of Landscape Disharmony (ILDH) as a new tool combining the aesthetic and ecological approach to landscape assessment. *Ecol. Indic.* **2016**, *70*, 166–180. [CrossRef]
43. Canter, L.W.; Hill, L.G. *Handbook of Variables for Environmental Impact Assessment*; Ann Arbor Science Publishers: Ann Arbor, MI, USA, 1979.
44. Shang, H.; Bishop, I.D. Visual thresholds for detection, recognition and visual impact in landscape settings. *J. Environ. Psychol.* **2000**, *20*, 125–140. [CrossRef]
45. Palmer, J.F. The contribution of a GIS-based landscape assessment model to a scientifically rigorous approach to visual impact assessment. *Landsc. Urban Plan.* **2019**, *189*, 80–90. [CrossRef]
46. Garré, S.; Meeus, S.; Gulinck, H. The dual role of roads in the visual landscape: A case-study in the area around Mechelen (Belgium). *Landsc. Urban Plan.* **2009**, *92*, 125–135. [CrossRef]
47. Rodrigues, M.; Montañés, C.; Fueyo, N. A method for the assessment of the visual impact caused by the large-scale deployment of renewable-energy facilities. *Environ. Impact Assess. Rev.* **2010**, *30*, 240–246. [CrossRef]
48. Sklenicka, P.; Zouhar, J. Predicting the visual impact of onshore wind farms via landscape indices: A method for objectivizing planning and decision processes. *Appl. Energy* **2018**, *209*, 445–454. [CrossRef]
49. del Carmen Torres-Sibille, A.; Cloquell-Ballester, V.A.; Cloquell-Ballester, V.A.; Ramírez, M.Á.A. Aesthetic impact assessment of solar power plants: An objective and a subjective approach. *Renew. Sustain. Energy Rev.* **2009**, *13*, 986–999. [CrossRef]
50. Fatimah, T. The impacts of rural tourism initiatives on cultural landscape sustainability in Borobudur area. *Procedia Environ. Sci.* **2015**, *28*, 567–577. [CrossRef]
51. Korça, P. Resident perceptions of tourism in a resort town. *Leis. Sci.* **1998**, *20*, 193–212. [CrossRef]
52. Noll, D.; Wiedenhofer, D.; Miatto, A.; Singh, S.J. The expansion of the built environment, waste generation and EU recycling targets on Samothraki, Greece: An island's dilemma. *Resour. Conserv. Recycl.* **2019**, *150*, 104405. [CrossRef]
53. Puczko, L.; Ratz, T. Tourist and resident perceptions of the physical impacts of tourism at Lake Balaton, Hungary: Issues for sustainable tourism management. *J. Sustain. Tour.* **2000**, *8*, 458–478. [CrossRef]
54. Corbetta, M.; Shulman, G.L. Control of goal-directed and stimulus-driven attention in the brain. *Nat. Rev. Neurosci.* **2002**, *3*, 201–215. [CrossRef]
55. Delorme, A.; Rousselet, G.A.; Macé, M.J.M.; Fabre-Thorpe, M. Interaction of top-down and bottom-up processing in the fast visual analysis of natural scenes. *Cogn. Brain Res.* **2004**, *19*, 103–113. [CrossRef]
56. Gerrig, R.J.; Zimbardo, P.G. *Psychology and Life*; Pearson Education: Boston, MA, USA, 2009.
57. Burns, T.R.; Engdahl, E. The social construction of consciousness. Part 1: Collective consciousness and its socio-cultural foundations. *J. Conscious. Stud.* **1998**, *5*, 67–85.
58. Vespestad, M.K.; Lindberg, F. Understanding nature-based tourist experiences: An ontological analysis. *Curr. Issues Tour.* **2011**, *14*, 563–580. [CrossRef]
59. Bruwer, J.; Joy, A. Tourism destination image (TDI) perception of a Canadian regional winescape: A free-text macro approach. *Tour. Recreat. Res.* **2017**, *42*, 367–379. [CrossRef]
60. Buijs, A.E.; Pedroli, B.; Luginbühl, Y. From hiking through farmland to farming in a leisure landscape: changing social perceptions of the European landscape. *Landsc. Ecol.* **2006**, *21*, 375–389. [CrossRef]
61. Gkargkavouzi, A.; Halkos, G.; Matsiori, S. Environmental behavior in a private-sphere context: Integrating theories of planned behavior and value belief norm, self-identity and habit. *Resour. Conserv. Recycl.* **2019**, *148*, 145–156. [CrossRef]
62. Wang, R.; Zhao, J. Demographic groups' differences in visual preference for vegetated landscapes in urban green space. *Sustain. Cities Soc.* **2017**, *28*, 350–357. [CrossRef]
63. Yoo, C.K.; Yoon, D.; Park, E. Tourist motivation: An integral approach to destination choices. *Tour. Rev.* **2018**. [CrossRef]

64. Meng, F.; Uysal, M. Effects of gender differences on perceptions of destination attributes, motivations, and travel values: An examination of a nature-based resort destination. *J. Sustain. Tour.* **2008**, *16*, 445–466. [CrossRef]
65. Perera, D.; Chandrasekara, D. Influence of Gender on Perception of Landscape: A Study of Viharamahadevi Park in Colombo. *Proc. Int. For. Environ. Symp.* **2017**, *22*. [CrossRef]
66. Dupont, L.; Antrop, M.; Van Eetvelde, V. Does landscape related expertise influence the visual perception of landscape photographs? Implications for participatory landscape planning and management. *Landsc. Urban Plan.* **2015**, *141*, 68–77. [CrossRef]
67. Potschin, M.; Haines-Young, R. Landscapes, sustainability and the place-based analysis of ecosystem services. *Landsc. Ecol.* **2013**, *28*, 1053–1065. [CrossRef]
68. Wang, Y.; Sparks, B.A. An eye-tracking study of tourism photo stimuli: Image characteristics and ethnicity. *J. Travel Res.* **2016**, *55*, 588–602. [CrossRef]
69. Daniel, T.C. Whither scenic beauty? Visual landscape quality assessment in the 21st century. *Landsc. Urban Plan.* **2001**, *54*, 267–281. [CrossRef]
70. Peterson, G.L.; Neumann, E.S. Modeling and predicting human response to the visual recreation environment. *J. Leis. Res.* **1969**, *1*, 219–237. [CrossRef]
71. Shafer Jr, E.L.; Brush, R.O. How to measure preferences for photographs of natural landscapes. *Landsc. Plan.* **1977**, *4*, 237–256. [CrossRef]
72. Zhao, J.; Yan, Y.; Deng, H.; Liu, G.; Dai, L.; Tang, L.; Shi, L.; Shao, G. Remarks about landsenses ecology and ecosystem services. *Int. J. Sustain. Dev. World Ecol.* **2020**, *27*, 196–201. [CrossRef]
73. Li, J.; Zhang, Z.; Jing, F.; Gao, J.; Ma, J.; Shao, G.; Noel, S. An evaluation of urban green space in Shanghai, China, using eye tracking. *Urban For. Urban Green.* **2020**, *56*, 126903. [CrossRef]
74. De Lucio, J.; Mohamadian, M.; Ruiz, J.; Banayas, J.; Bernaldez, F. Visual landscape exploration as revealed by eye movement tracking. *Landsc. Urban Plan.* **1996**, *34*, 135–142. [CrossRef]
75. Guo, S.; Zhao, N.; Zhang, J.; Xue, T.; Liu, P.; Xu, S.; Xu, D. Landscape visual quality assessment based on eye movement: College student eye-tracking experiments on tourism landscape pictures. *Resour. Sci.* **2017**, *39*, 1137–1147.
76. Sun, L.; Shao, H.; Li, S.; Huang, X.; Yang, W. Integrated application of eye movement analysis and beauty estimation in the visual landscape quality estimation of urban waterfront park. *Int. J. Pattern Recognit. Artif. Intell.* **2018**, *32*, 1856010. [CrossRef]
77. Duchowski, A.T. A breadth-first survey of eye-tracking applications. *Behav. Res. Methods Instrum. Comput.* **2002**, *34*, 455–470. [CrossRef]
78. Haber, R.N.; Hershenson, M. *The Psychology of Visual Perception*; Holt, Rinehart & Winston: New York, NY, USA, 1973.
79. Liu, Y.; Hu, M.; Zhao, B. Interactions between forest landscape elements and eye movement behavior under audio-visual integrated conditions. *J. For. Res.* **2020**, *25*, 21–30. [CrossRef]
80. Nordh, H.; Hagerhall, C.M.; Holmqvist, K. Tracking restorative components: Patterns in eye movements as a consequence of a restorative rating task. *Landsc. Res.* **2013**, *38*, 101–116. [CrossRef]
81. Amati, M.; Parmehr, E.G.; McCarthy, C.; Sita, J. How eye-catching are natural features when walking through a park? Eye-tracking responses to videos of walks. *Urban For. Urban Green.* **2018**, *31*, 67–78. [CrossRef]
82. Li, X.Q.; Zhao, N.X.; Wang, C.Z.; Wang, M.; Huang, H. A preliminary study on the application of eye tracker to the landmark landscape of campus tourism—Taking the north building of Nanjing University as an example. *Acta Agric. Jiangxi* **2011**, *23*, 148–151.
83. Ren, X.; Kang, J. Interactions between landscape elements and tranquility evaluation based on eye tracking experiments. *J. Acoust. Soc. Am.* **2015**, *138*, 3019–3022. [CrossRef]
84. Wang, P.; Yang, W.; Wang, D.; He, Y. Insights into Public Visual Behaviors through Eye-Tracking Tests: A Study Based on National Park System Pilot Area Landscapes. *Land* **2021**, *10*, 497. [CrossRef]
85. Misthos, L.M.; Pavlidis, A.; Karabassakis, E.; Menegaki, M.; Krassanakis, V.; Nakos, B. Exploring the visual impact from open pit mines applying eye movement analyses on mining landscape photographs. *Int. J. Min. Reclam. Environ.* **2020**, *34*, 609–624. [CrossRef]
86. Scott, N.; Green, C.; Fairley, S. Investigation of the use of eye tracking to examine tourism advertising effectiveness. *Curr. Issues Tour.* **2016**, *19*, 634–642. [CrossRef]
87. Li, Q.; Huang, Z.J.; Christianson, K. Visual attention toward tourism photographs with text: An eye-tracking study. *Tour. Manag.* **2016**, *54*, 243–258. [CrossRef]
88. Wang, J.Y.; Lin, L.; Gao, H.; Feng, Z.L. Differences in college students'spatial symbol cognition of tourism map: Based on experimental data from an eye-movement tracking system. *Tour. Trib.* **2016**, *31*, 97–105.
89. Huang, X.; Li, M.; Yan, S. Research on pattern of eye-tracking behavior based on tourism map. *Tour. Trib.* **2018**, *33*, 87–96.
90. Dong, W.; Liao, H.; Zhan, Z.; Liu, B.; Wang, S.; Yang, T. New research progress of eye tracking-based map cognition in cartography since 2008. *J. Geogr. Sci.* **2019**, *74*, 599–614.
91. Scott, N.; Zhang, R.; Le, D.; Moyle, B. A review of eye-tracking research in tourism. *Curr. Issues Tour.* **2019**, *22*, 1244–1261. [CrossRef]
92. Scott, N.; Le, D.; Becken, S.; Connolly, R.M. Measuring perceived beauty of the Great Barrier Reef using eye-tracking technology. *Curr. Issues Tour.* **2020**, *23*, 2492–2502. [CrossRef]

93. Li, F.M.S. Culture as a major determinant in tourism development of China. *Curr. Issues Tour.* **2008**, *11*, 492–513.
94. Li, M.; Wu, B.; Cai, L. Tourism development of World Heritage Sites in China: A geographic perspective. *Tour. Manag.* **2008**, *29*, 308–319. [CrossRef]
95. Shepherd, R.J. *Faith in Heritage: Displacement, Development, and Religious Tourism in Contemporary China*; Left Coast Press: Walnut Creek, CA, USA, 2013.
96. UNESCO. World Heritage List: Mount Taishan. 1987. Available online: https://whc.unesco.org/en/list/437 (accessed on 25 August 2021).
97. Sofield, T.; Li, F.M.S. China: Ecotourism and cultural tourism, harmony or dissonance. In *Critical Issues in Ecotourism: Understanding a Complex Tourism Phenomenon*; Elsevier, Butterworth Heinemann: Amsterdam, NL, USA, 2007; pp. 368–385.
98. Beza, B.B. The aesthetic value of a mountain landscape: A study of the Mt. Everest Trek. *Landsc. Urban Plan.* **2010**, *97*, 306–317. [CrossRef]
99. Steen Jacobsen, J.K. Use of landscape perception methods in tourism studies: A review of photo-based research approaches. *Tour. Geogr.* **2007**, *9*, 234–253. [CrossRef]
100. Kaplan, S. The restorative benefits of nature: Toward an integrative framework. *J. Environ. Psychol.* **1995**, *15*, 169–182. [CrossRef]
101. Kaplan, S. Aesthetics, affect, and cognition: Environmental preference from an evolutionary perspective. *Environ. Behav.* **1987**, *19*, 3–32. [CrossRef]
102. Fry, G.; Tveit, M.S.; Ode, Å.; Velarde, M. The ecology of visual landscapes: Exploring the conceptual common ground of visual and ecological landscape indicators. *Ecol. Indic.* **2009**, *9*, 933–947. [CrossRef]
103. UNESCO; WHC. Operational Guidelines for the Implementation of the World Heritage Convention, Released on 10 July 2019. Available online: https://whc.unesco.org/en/guidelines/ (accessed on 25 August 2021).
104. Dupont, L.; Antrop, M.; Van Eetvelde, V. Eye-tracking analysis in landscape perception research: Influence of photograph properties and landscape characteristics. *Landsc. Res.* **2014**, *39*, 417–432. [CrossRef]
105. Lothian, A. Landscape and the philosophy of aesthetics: Is landscape quality inherent in the landscape or in the eye of the beholder? *Landsc. Urban Plan.* **1999**, *44*, 177–198. [CrossRef]
106. Aretano, R.; Petrosillo, I.; Zaccarelli, N.; Semeraro, T.; Zurlini, G. People perception of landscape change effects on ecosystem services in small Mediterranean islands: A combination of subjective and objective assessments. *Landsc. Urban Plan.* **2013**, *112*, 63–73. [CrossRef]
107. Atik, M.; Işıklı, R.C.; Ortaçeşme, V.; Yıldırım, E. Exploring a combination of objective and subjective assessment in landscape classification: Side case from Turkey. *Appl. Geogr.* **2017**, *83*, 130–140. [CrossRef]
108. Hernández-Méndez, J.; Muñoz-Leiva, F. What type of online advertising is most effective for eTourism 2.0? An eye tracking study based on the characteristics of tourists. *Comput. Hum. Behav.* **2015**, *50*, 618–625. [CrossRef]
109. Tengberg, A.; Fredholm, S.; Eliasson, I.; Knez, I.; Saltzman, K.; Wetterberg, O. Cultural ecosystem services provided by landscapes: Assessment of heritage values and identity. *Ecosyst. Serv.* **2012**, *2*, 14–26. [CrossRef]
110. Ashton, A.S. Spiritual retreat tourism development in the Asia Pacific region: Investigating the impact of tourist satisfaction and intention to revisit: A Chiang Mai, Thailand case study. *Asia Pac. J. Tour. Res.* **2018**, *23*, 1098–1114. [CrossRef]
111. Long, H.; Woods, M. Rural restructuring under globalization in eastern coastal China: What can be learned from Wales? *J. Rural. Community Dev.* **2011**, *6*, 70–94.
112. Sturken, M.; Cartwright, L. *Practices of Looking: An Introduction to Visual Culture*; Oxford University Press: New York, NY, USA, 2009.
113. Cloquell-Ballester, V.A.; del Carmen Torres-Sibille, A.; Cloquell-Ballester, V.A.; Santamarina-Siurana, M.C. Human alteration of the rural landscape: Variations in visual perception. *Environ. Impact Assess. Rev.* **2012**, *32*, 50–60. [CrossRef]
114. Geng, J.; Long, R.; Chen, H.; Li, W. Exploring the motivation-behavior gap in urban residents' green travel behavior: A theoretical and empirical study. *Resour. Conserv. Recycl.* **2017**, *125*, 282–292. [CrossRef]
115. Feingold, A. Gender differences in personality: A meta-analysis. *Psychol. Bull.* **1994**, *116*, 429. [CrossRef]
116. Conrad, E.; Fazey, I.; Christie, M.; Galdies, C. Choosing landscapes for protection: Comparing expert and public views in Gozo, Malta. *Landsc. Urban Plan.* **2019**, *191*, 103621. [CrossRef]
117. Zhang, C.; Gursoy, D.; Deng, Z.; Gao, J. Impact of culture on perceptions of landscape names. *Tour. Geogr.* **2015**, *17*, 134–150. [CrossRef]
118. Portman, M.E.; Natapov, A.; Fisher-Gewirtzman, D. To go where no man has gone before: Virtual reality in architecture, landscape architecture and environmental planning. *Comput. Environ. Urban Syst.* **2015**, *54*, 376–384. [CrossRef]
119. Henderson, J.M. Human gaze control during real-world scene perception. *Trends Cogn. Sci.* **2003**, *7*, 498–504. [CrossRef] [PubMed]

land

MDPI

Article

Impact of Urbanization and Industrial Structure on Carbon Emissions: Evidence from Huaihe River Eco-Economic Zone

Qinghua Pang, Weimo Zhou, Tianxin Zhao and Lina Zhang *

Business School, Hohai University, Changzhou 213022, China; 20031615@hhu.eud.cn (Q.P.); 181321020005@hhu.edu.cn (W.Z.); txin@hhu.edu.cn (T.Z.)
* Correspondence: 20191001@hhu.edu.cn

Abstract: Rapid urbanization in China greatly contributes to carbon emissions, while the industrial structure greatly contributes to changes in the variation of carbon emissions. This research addresses the impact of urbanization and industrial structure on carbon emissions from 2010 to 2018, by focusing on the Huaihe River Eco-economic Zone, which is an important economic corridor along the north–south division of China. Although many studies have focused on investigating the impact of urbanization or industrial structure on carbon emissions, few studies further addressed an analysis of the impact of both on carbon emissions, using multiple measurement models. This paper reveals the holistic and local impact of industrial structure and urbanization on carbon emissions, by integrating a threshold regression model with geographically weighted regression. The results are as follows: (1) From a holistic point of view, industrial structure and urbanization had both, single threshold, and double threshold effects on carbon emissions in the Huaihe River Eco-economic Zone. (2) From a regional perspective, the coefficients of industrial structure on carbon emissions were all positive, but the rate of increase gradually slowed down. The coefficients of urbanization on carbon emissions were all negative, reaching a maximum value of negative effect in 2013. Understanding the holistic and local impact of urbanization and industrial structure on carbon emissions provides governments with differentiated and forward-looking suggestions for mitigating carbon emissions in the Huaihe River Eco-economic Zone.

Keywords: carbon emissions; industrial structure; urbanization; threshold model; geographically weighted regression

Citation: Pang, Q.; Zhou, W.; Zhao, T.; Zhang, L. Impact of Urbanization and Industrial Structure on Carbon Emissions: Evidence from Huaihe River Eco-Economic Zone. *Land* **2021**, *10*, 1130. https://doi.org/10.3390/land10111130

Academic Editors: Baojie He, Ayyoob Sharifi, Chi Feng and Jun Yang

Received: 29 September 2021
Accepted: 20 October 2021
Published: 25 October 2021

1. Introduction

The increase in carbon emissions has become a serious social problem, because it hinders the development of society and the global economy [1]. The upgrading of industrial structure and urbanization lead to an increase in carbon emissions. According to the World Bank, China's carbon emissions have exceeded the sum of the European Union and the United States; the three territories with the highest carbon emissions in the world [2]. Their total carbon emissions accounted for more than half of the world. China's carbon emissions reached 9.429 Gt in 2018, accounting for 27.8% of global carbon emissions [3]. As the largest developing country and the largest carbon emitter, China strives to achieve its promise to reach the peak of its total carbon dioxide emissions around 2030 and become carbon neutral by 2060 [4].

The Huaihe River Eco-economic Zone (HREZ) covers the provinces of Jiangsu, Henan, and Anhui. Accordingly, tertiary industry in the region accounts for about 10%, and the average annual growth rate of urbanization is about 3.56%. Specifically, the backward production pattern leads to increased carbon emissions in the zone. Furthermore, the carbon emissions of the HREZ are significantly higher than that of other regions. This study is conducive to a reduction of carbon emissions in the region, and even in China as a whole, as well as the early achievement of the carbon neutrality target. Therefore, it is imperative for the HREZ to focus on the impacts of urbanization and industrial structure on carbon

emissions. At the same time, it is important to understand the internal mechanism of carbon emissions in the zone, which would be helpful to achieve China's carbon emissions reduction commitments.

Urbanization and industrialization are the main characteristics of the economic growth in China and promote rapid increases in carbon emissions [5]. Many methods for urbanization and industrial structure, such as the STIRPAT model, the Kaya index method, the LDMI method, and the threshold model, have been used to study the influencing factors on carbon emissions [6]. The panel threshold regression model aims to incorporate a certain threshold value as an unknown variable in the regression model, and to empirically test and estimate the corresponding threshold and the effect of the threshold [7–9]. In addition, the STIRPAT equation helps to disaggregate the factors influencing carbon emissions. Many researchers have proposed the STIRPAT equation, to explore the impact of carbon emissions [10–14]. With the development of spatial measurement in recent years, several scholars have included spatial factors into the framework for consideration of carbon emission driving factors. According to Tobler's first law of geography, all attribute values on a geographic surface are related to each other, but closer values are more strongly related than more distant ones [15]. Geographically weighted regression (GWR) is a local spatial regression technique for modeling the varying relationships in many application domains. Regression is a statistical method used to find the relationship between two or more variables that are interdependent and affected by one another.

Although the economy [16], technology [17], urbanization, industrial structure, trade openness [18–20], energy consumption [21–23], and financial development [11] have been considered in various previous studies, the analysis of both urbanization and industrial structure has not been addressed. Moreover, the optimization of urbanization and industrial structure can help achieve national targets for reducing carbon intensity.

Therefore, although urbanization and industrial structure are two important factors influencing carbon emissions, the combined impact of the two on carbon emissions is not fully understood. Second, the threshold model and GWR were not adequately combined to study carbon emissions in previous studies. The threshold model and GWR are beneficial for studying the carbon emissions of the whole region and each part of the region, respectively. Third, the HREZ has not been adequately addressed. It is one of the most promising areas in the east-central part of China, and the research of carbon emissions is of great value for its long-term development. This paper explores the holistic and local impact of industrial structure and urbanization on the carbon emissions of the HREZ from 2010 to 2018. We aimed to understand how they function, regarding carbon emissions. The main contributions are as follows: (1) This paper combines a threshold model with GWR, to study the impact of urbanization and industrial structure on carbon emissions, from both holistic and local perspectives. (2) Through research on the HREZ, relevant policies can be extended to other regions to mitigate environmental pressure.

With the development of a low carbon economy, the driving factors of carbon emissions have consistently been a research hotspot. Urbanization and industrialization are the main characteristics of economic growth in China and promote rapid increases in carbon emissions. At present, research on carbon emissions in combination with urbanization and industrial structure is mainly concentrated in three strands. The first strand is whether an environmental Kuznets curve (EKC) of carbon emissions exists. Namely, that carbon emissions will eventually appear as an inverted U-shaped curve with the development of urbanization and industrial structure [24–28]. For instance, [10] investigated the heterogeneous dynamic impacts of rural–urban migration and industrial agglomeration on environmental degradation. The combined impacts of both industrial agglomeration and rural–urban migration confirmed EKC in models of the tertiary sector. Reference [29] used the EKC to discuss the relationship between urbanization and carbon emissions in three typical models. The second strand is to use various models or methods to explore the causal relationship and driving factors among urbanization, industrial structure, and carbon emissions, such as cointegration analysis, structural decomposition models, decou-

pling theory, and LMDI [30–34], which showed that urbanization level is the main driving force promoting decoupling elasticity, both in the long-term and short-term, contributing to a significant increase in carbon emissions. Reference [35] explored the threshold effects of industrial structure and urbanization on carbon emissions. With an increase in the level of population aging, industrial structure and urbanization will lead to an increase in carbon emissions, but the relationship fluctuates in three intervals. The last strand is the exploration of carbon emission rights and carbon compensation to establish efficient and stable operations in the carbon market to achieve emissions reduction targets [36,37]. For example, [37] improved the calculation method of the interregional carbon compensation cost, based on the theoretical carbon deficit. While, reference [38] examined how the announcement of an organizational carbon offset program affected consumption in a CO_2-intensive everyday activity. As for the impact of other factors on carbon emissions, foreign direct investment (FDI) has both a promoting and an inhibiting effect on carbon emissions performance [39,40]. There is a relationship among economic growth, energy consumption structure, and carbon emissions [41,42]. In terms of technology, low-carbon technology can increase the potential for carbon emissions reduction [43–45].

In terms of regional measurement, scholars have focused more on studies at the national provincial, national strategic regional, and municipal levels. Among the national strategic regions, scholars have measured the carbon efficiency and influencing factors of the Yangtze River Economic Belt [46–48], Beijing-Tianjin-Hebei Urban Agglomeration [29,49,50], Belt and Road Initiative [40,51], and Pearl River Delta [52]. Although the HREZ is very important to China's economic development and for achieving goals for carbon abatement, there is currently a lack of research on such aspects.

Scholars have studied the influencing factors of carbon emissions more widely, and have made many achievements regarding the influencing factors on carbon emissions. However, there has been very little research on the HREZ. The government has not yet realized the importance of the study of carbon emissions in the HREZ for the national carbon abatement. The HREZ is located between the Yangtze River Economic Belt and the Huanghe River Basin, but its relative overall economic development is lagging. It is one of the regions with the greatest development potentials in the central and eastern part of China. For example, the GDP per capita was 49121 CNY/person in 2018, which is a fraction of the Yangtze River Economic Belt and the Huanghe River Basin. The HREZ, with a planned area of 243,000 square kilometers, has great development potential. This has important strategic significance for promoting the balanced development of China, such as being a bridge connecting the south regions to the north regions, and the east regions to the west regions. It includes several key development areas of heavy industry in China. Therefore, it is valuable to research the factors influencing carbon emissions in the HREZ. The HREZ overlaps with other important strategic regions in China, so its successful experience with carbon abatement could be applied to other geographical regions in China. As the goal of carbon emissions reduction is to set up joint efforts, with emissions mitigation suggestions for each region, it is thus necessary to identify changes of carbon emissions under the consideration of regional variations; however, to our knowledge, corresponding research on the HREZ from a differentiation perspective is absent. Thus, this paper has the following novel features: (1) From multiple perspectives, the article combines industrial structure and urbanization to study their impacts on carbon emissions. (2) The combination of a threshold model and GWR is conducive to analysis and research from both planar and spatial perspectives. (3) The HREZ is the research object, and currently lacks theoretical and empirical studies on improving carbon emissions efficiency in China. This is essential for China's carbon emission reduction and regional development.

2. Methods and Data

2.1. Threshold Regression Model

Following [35], we apply the static panel threshold regression model proposed by [53] to attain the goal of this paper. According to the STIRPAT model, this paper selected

variables of carbon emissions (C, tones), urbanization (U,%), industrial structure (M,%), structure of energy consumption (S,%), energy intensity (Q, tones/million CNY), and GDP per capita (Y, CNY/person) to construct the equation. In addition, industrial structure and GDP per capita reflect economic growth effects, energy intensity and energy consumption structure reflect technological advances, and urbanization reflects social effects. The static panel threshold regression models, in a form of STIRPAT, are as follows:

$$\begin{aligned} LnC_{i,t} &= \mu + \beta_1 LnM_{i,t} I(LnX_{i,t} \le \gamma) + \beta_2 LnM_{i,t} I(LnX_{i,t} > \gamma) + \beta_3 LnS_{i,t} + \beta_4 LnQ_{i,t} + \beta_5 LnY_{i,t} + \beta_6 LnU_{i,t} + \varepsilon \\ LnC_{i,t} &= \mu + \beta_1 LnU_{i,t} I(LnX_{i,t} \le \gamma) + \beta_2 LnU_{i,t} I(LnX_{i,t} > \gamma) + \beta_3 LnS_{i,t} + \beta_4 LnQ_{i,t} + \beta_5 LnY_{i,t} + \beta_6 LnM_{i,t} + \varepsilon \end{aligned} \quad (1)$$

where $C_{i,t}$ denotes carbon emissions (tones), $M_{i,t}$ denotes industrial structure (%), $U_{i,t}$ denotes urbanization (%), $S_{i,t}$ denotes energy consumption structure (%), $Q_{i,t}$ denotes energy intensity (tones/million CNY), $Y_{i,t}$ denotes GDP per capita (CNY/person), μ is a constant term, ε is a random disturbance term, subscripts i, t are prefecture-level administrative unit and year, $LnX_{i,t}$ is a threshold variable, γ is a threshold value, and $I(\cdot)$ is an indicator function; when $LnX_{i,t} \le \gamma$, $I(\cdot) = 1$, when $LnX_{i,t} > \gamma$, $I(\cdot) = 0$.

2.2. GWR Method

GWR relies on standard multiple parameter regression. Unlike classical regression, the coefficients are not constant in this technique. It is an effective technique for exploring spatial nonstationarity. GWR model is specified in the following form:

$$y_i = \beta_0(u_i, v_i) + \sum_{j=1}^{k} \beta_j(u_i, v_i) x_{ij} + \varepsilon_i \qquad i = 1, 2, \ldots, n \quad (2)$$

where y_i is the value at location i, (u_i, v_i) are the geographic coordinates of position i, $\beta_0(u_i, v_i)$ and $\beta_j(u_i, v_i)$ are the intercept and local coefficients at location i, respectively, k is the number of factors, x_{ik} is the explanatory variable at location i, and ε_i accounts for the random error term at location i.

2.3. Data Sources and Processing

Referring to the relevant literature, it was found that scholars in various countries had different emphases in the selection of influencing factors of carbon emissions. This paper selected the variables of carbon emissions, urbanization, industrial structure, structure of energy consumption, energy intensity, and GDP per capita. These were all derived from the statistical yearbooks of cities in the HREZ.

This paper's analysis covers 5 provinces (excluding Henan, Jiangsu, Anhui, Hubei, Shandong) in China. The related data of all variables, spanning 2010 to 2018, were sourced from the China Statistical Yearbook and China Energy Statistical Yearbook [54,55]. To eliminate the impact of price inflation, GDP per capita was converted into constant prices from 2010 using the corresponding indices. A long period can clearly see show an increasing or decreasing trend in carbon emissions. In 2018, the state compiled the "Development Plan of Huaihe River Eco-economic Zone". Therefore, a summary of the development over a long period before 2018 is more conducive for the targeted measures for future carbon abatement.

There are two common methods to calculate carbon emissions. One is based on the reference method provided by the Intergovernmental Panel on Climate Change (IPCC) [56]. The IPCC is the United Nations body for assessing the science related to climate change. IPCC scientists provide a comprehensive summary of the drivers of climate change, its impacts, and future risks, and how adaptation and mitigation can reduce those risks [57]. The other is the input–output (I–O) method. The I–O method represents the economic dependencies between different sectors and uses matrix representations to describe the inter-industry relationships in the economy [58]. While, the input–output method is updated every five years, the method provided by the IPCC can better capture the impact

of factors on regional carbon emissions on a year-by-year basis. The carbon emissions were calculated as follows:

$$C_F = \sum_{i=1}^{8} E_i \times NCV_i \times CEF_i \quad (3)$$

$$CEF_i = CC_i \times COF_i \times (44/12) \times 10^3 \quad (4)$$

where i is the fossil fuel type; E_i is the terminal consumption of the i_{th} fossil fuel (tones); NCV_i is the average low calorific value (kj/kg); CEF_i is the respective carbon emissions coefficient for the 8 fossil fuels (kg/tj); CC_i is the carbon content (t/tj); COF_i is the carbon oxidation factor; and 44 and 12 are the molecular weights of CO_2 and C, respectively.

3. Results

3.1. Results of the Threshold Regression Model

The results of the fixed effects model are as follows. The R^2 value was 0.81 and the p-value also passed the test. The p-value of urbanization, industrial structure, energy intensity, and energy consumption structure were $\leq$1% or lower, and the p-value of GDP per capita was 0.028. Each variable passed the significance test in the model. The details are shown in the following, Table 1.

Table 1. The results of the fixed effect panel model.

	Coef.	95% Confidence Interval
$LnM_{i,t}$	−0.036 *** (−2.14)	(0.67,0.76)
$LnU_{i,t}$	0.054 *** (3.95)	(−0.28, −0.19)
$LnQ_{i,t}$	0.716 *** (30.28)	(−0.02, 0.14)
$LnY_{i,t}$	0.059 ** (1.5)	(−0.07, 0)
$LnS_{i,t}$	−0.241 *** (−11.03)	(0.03, 0.08)
_cons	−1.264 *** (−15.15)	(−1.42, −1.1)

Note: values in parentheses are the T-statistics, **, *** denote significance at 10%, 5%, and 1% levels, respectively.

Then, we tested the threshold effect. We modified the threshold variables and the threshold explanatory variables. The results indicated the existence of single or multiple threshold effects with GDP per capita and energy intensity as threshold variables, respectively. First, the results of GDP per capita as a threshold variable are presented in Table 2. The p-value of urbanization, energy intensity, and energy consumption structure were all $\leq$1% or lower. From the significance of the model, each variable passed the significance test.

From the perspective of industrial structure, the threshold of $LnY_{i,t}$ is −2.725. Before and after the threshold, each unit increase in industrial structure leads to a reduction of 0.35 units followed by an increase of 0.075 units in carbon emissions.

(1) In the early stage of economic development, the HREZ was committed to developing strategic emerging industries. The region made use of new knowledge and technologies to develop the industrial structure in the direction of low consumption, low pollution, and high efficiency. Meanwhile, the HREZ emphasized the development of an ecological industry. Through the introduction of clean energy and advanced technology, the government aimed at transitioning the HREZ from resource-intensive industry to technology-intensive industry.

(2) With the increase of GDP per capita, tertiary industry tended to be saturated. The zone relied on secondary industry, which is the traditionally preponderant industry. The development of secondary industry was more difficult to separate from the

consumption of coal, which has the largest carbon emissions, compared with other kinds of energy. The development of tertiary industry could not make up for the high carbon emissions of secondary industry.

From the perspective of urbanization, the thresholds of $LnY_{i,t}$ are −2.725 and −1.389. When the GDP per capita exceeds the first and second thresholds, each unit of urbanization, first makes carbon emissions decrease by 0.08, then increase by 0.08, and finally decline by 0.001.

(3) Before the first threshold, the GDP per capita of the zone was low and the urbanization process was just beginning. The workforce moved from the countryside to the cities. The gathering of urban population reduced the cost of public goods. Along with the change of lifestyle in the zone, the quality of residents continued to improve. Residents have become more aware of environmental protection. The change of residents has greatly reduced the negative impact of urbanization on the environment.

(4) Between the first and second thresholds, the urbanization process entered the middle stage and became the main driving factor affecting carbon emissions. The consumption structure and level of residents improved rapidly. The increasing use of energy-intensive products, such as cars and appliances led to high carbon emissions in the HREZ.

(5) After the second threshold, the impact of urbanization on carbon emissions slowed down significantly. Despite the advanced economy, the spillover from industrial consumption was compensated by urbanization to a certain extent. The corresponding likelihood ratio function graphs, with GDP per capita as the threshold variable, are shown in Figure 1.

Table 2. Estimation of panel threshold model with GDP per capita as threshold variable.

		IS	**U(1)**	**U(2)**
Threshold estimation	r	−2.725	−2.725	−1.389
	95% confidence interval	[−2.7939, −2.6587]	[−2.794, −2.659]	[−1.422, −1.382]
Other Variables	$LnQ_{i,t}$	0.716 *** (30.41)	0.730 *** (32.24)	
	$LnS_{i,t}$	−0.225 *** (−11.26)	−0.200 *** (−10.20)	
	$LnU_{i,t}$	0.074 *** (5.75)	—	
	$LnM_{i,t}$	—	−0.016 (−1.06)	
Constant terms	$\_cons$	−1.263 *** (−15.13)	−1.210 *** (−14.13)	

Note: values in parentheses are the T-statistics, *** denote significance at the 10%, 5%, and 1% levels, respectively.

Moreover, the results of energy intensity as a threshold variable are shown in Table 3. The p-value of energy intensity and energy consumption structure are ≤1% or lower, and the p-value of urbanization is 0.042. However, the p-value of GDP per capita does not pass the significance test.

From the perspective of industrial structure, the thresholds of $LnQ_{i,t}$ are −2.013 and −2.410. As the energy intensity exceeded the first and the second thresholds, each unit of industrial structure made carbon emissions first decrease by 0.16, then increase by 0.13, and finally decrease by 0.01.

(1) Originally, secondary industry was not the main force of economic development and was less dependent on energy consumption. Due to the low energy intensity, the upgrading of industrial structure meant more production resources were given to tertiary industry. The clean nature of tertiary industry led to a reduction in carbon emissions.

(2) After the energy intensity exceeded the first threshold, the energy dependence of the zone was significantly higher than before. Industries with a high energy consumption and high emissions accounted for a large proportion of economic development. Some regions were relatively backward in technology, so the development of tertiary industry could not offset the high carbon emissions caused by the secondary industry.

(3) With the further increase of energy intensity up to the second threshold, tertiary industry reached its heyday. The regional industrial structure was continuously optimized under the requirements of the new development concept. Green development of secondary industry and the low carbon consumption of tertiary industry compensated for the spillover from the high energy consumption of industry.

From the perspective of urbanization, the thresholds of $LnQ_{i,t}$ are −1.321 and −1.709. As the energy intensity exceeded the first and second thresholds, each unit of urbanization made carbon emissions, first decrease by 0.01, then increase by 0.08, and finally decrease by 0.03.

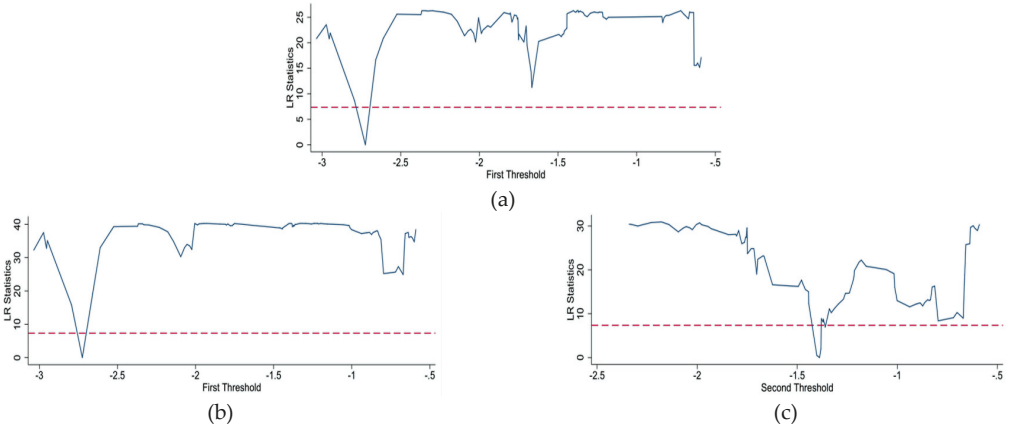

Figure 1. The likelihood ratio function graph with GDP per capita as the threshold variable. (**a**) Industrial structure (1); (**b**) urbanization (1); (**c**) urbanization (2).

Table 3. Estimation of panel threshold model with energy intensity as the threshold variable.

		IS(1)	IS(2)	U(1)	U(2)
Threshold estimation	r	−2.013	−2.410	−1.321	−1.709
	95% confidence interval	[−2.024, −1.998]	[−2.448, −1.721]	[−1.617, −1.271]	[−1.909, −1.673]
Other Variables	$LnY_{i,t}$	0.03		0.056 *	
		(0.85)		(1.64)	
	$LnS_{i,t}$	−0.157 ***		−0.209 ***	
		(−7.65)		(−11.46)	
	$LnU_{i,t}$	0.025 **		—	
		(1.94)			
	$LnM_{i,t}$	—		−0.018	
				(−1.3)	
	$LnQ_{i,t}$	0.704 ***		0.657 ***	
		(32.36)		(29.53)	
Constant terms	_cons	−1.346 ***		−1.418 ***	
		(−18.05)		(−17.55)	

Note: values in parentheses are the T-statistics,***, **, * denote significance at 1%, 5%, and 10% levels, respectively.

(1) At the outset of the urbanization process, the increase of urbanization meant more rural populations moving to the cities. The industrial development of the zone was in the primary stage. A low energy intensity meant low carbon emissions. The positive impact was optimal when the first threshold was reached.

(2) With the increase of energy intensity, energy-intensive industries in the HREZ developed rapidly. The lack of industrial innovation capacity and the pressure of economic transformation were the main problems of the development. With the migration of a large number of people, the economic development relied on high-consumption and high-pollution secondary industry. The high energy intensity led to a significant increase in carbon emissions in the HREZ.

(3) After the energy intensity exceeded the second threshold, the industrial development reached a certain scale. The focus of development shifted to tertiary industry, which is dominated by the service industry. The tertiary sector emits fewer pollutants and has a suppressive effect on carbon emissions. The low carbon consumption of the tertiary sector compensated for the high carbon consumption of the secondary sector. Corresponding likelihood ratio function graphs, with energy intensity as the threshold variable, are shown in Figure 2.

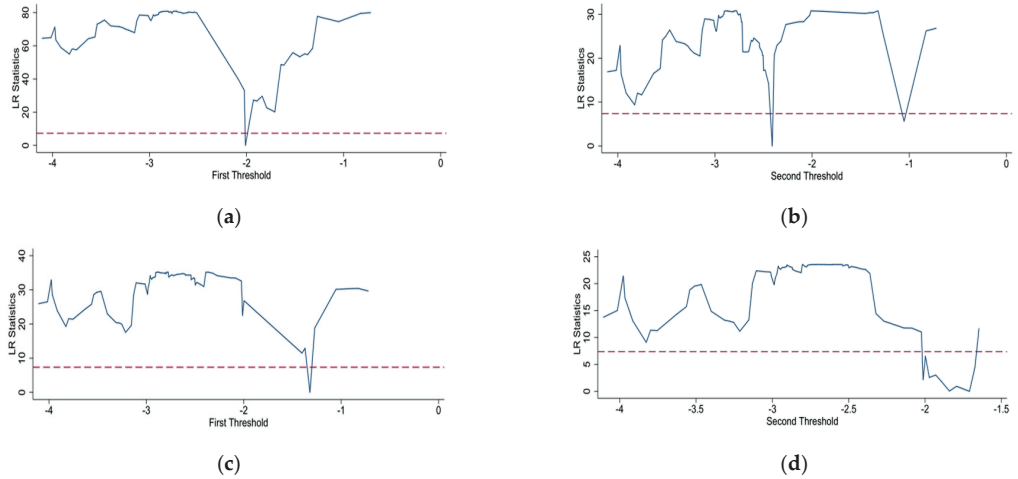

Figure 2. Likelihood ratio function graphs with energy intensity as the threshold variable. (**a**) Industrial structure (1); (**b**) industrial structure (2); (**c**) urbanization (1); (**d**) urbanization (2).

3.2. Estimation Results of GWR Model

The Moran's Index values obtained for all the years are greater than zero, which suggests that there is positive autocorrelation or a highly clustered pattern. The same is seen by looking at the p-values. The obtained p value is less than 0.05 for all the years, ruling out the basic assumption of randomness and independence in the data values. The results of Moran's I are shown in Table 4.

Table 4. Moran's I test.

	Carbon Emissions	Urbanization	Industrial Structure
2010	0.096	0.327	0.345
2011	0.076	0.335	0.430
2012	0.085	0.307	0.433
2013	0.090	0.256	0.486
2014	0.102	0.248	0.323
2015	0.107	0.307	0.244
2016	0.091	0.305	0.202
2017	0.081	0.302	0.159
2018	0.065	0.299	0.105

To show the spatial heterogeneity of the impact of industrial structure on carbon emissions, the spatial impact of industrial structure from 2010 to 2018 is visualized. The results are shown in Figure 3a–d.

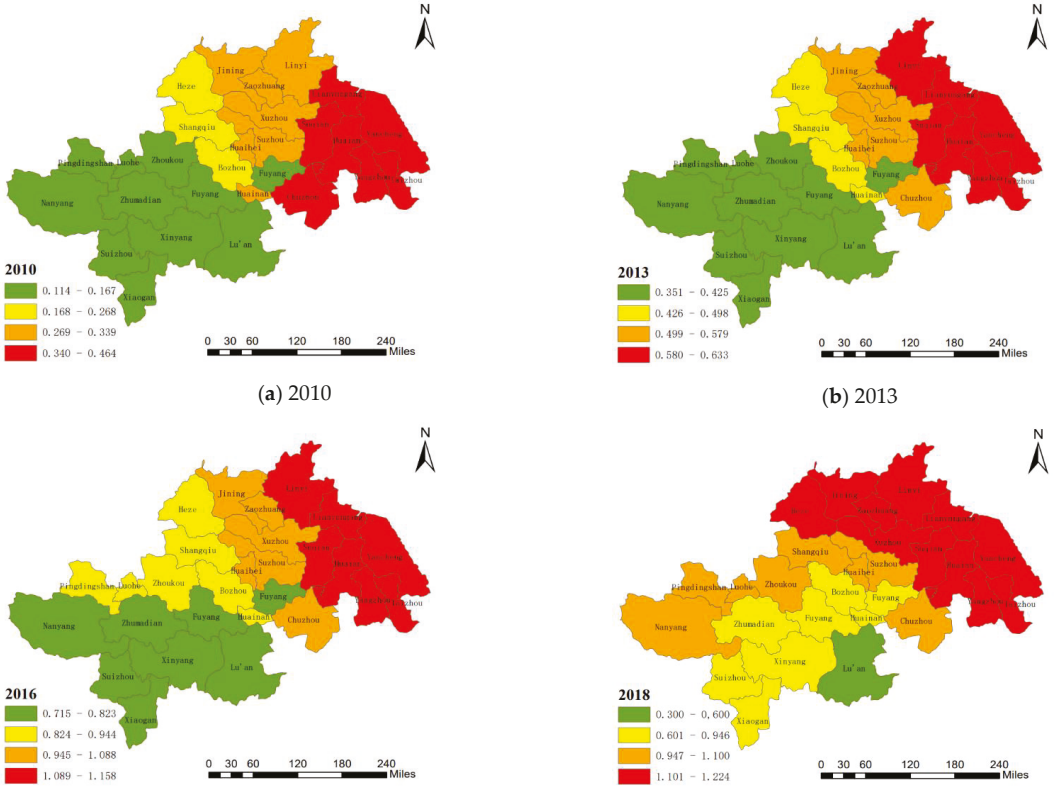

Figure 3. Spatial impact of industrial structure.

The positive influence of industrial structure on carbon emissions in the HREZ from 2010 to 2018 become more and more obvious, but the trend of growth slowed down. In general, it showed a decreasing trend from the northeast to the southwest, and a more obvious east–west gap.

The cities with high coefficients in 2010 were Suqian, Lianyungang, Huai'an, Yancheng, Yangzhou, and Taizhou. The positive influence on carbon emissions was significantly higher in the eastern cities than in the western cities. With their excellent location and resources, these cities seized the opportunity for development. The accelerated development of tertiary industry led to the accelerated flow of production factors to the tertiary industries, such as labor and land. In order to maintain the current scale of other industries, the production relied more on large mechanical production equipment and energy consumption. The coefficient was lower in Xiaogan, Suizhou, Nanyang, Xinyang, Zhumadian, Pingdingshan, Luohe, Zhoukou, Shangqiu, and Bozhou. These cities are deep inland and had a weak foundation in secondary industry. Due to the backwardness of their production, the reliance on mechanical equipment and energy was low. They relied more on labor for production, so the impact on carbon emissions was lower.

From 2012 to 2015, the trend was roughly the same as before. The coefficient increased significantly, especially in Jiangsu and Shandong Provinces, which were significantly higher than those in southwestern cities. Due to the development of transportation and high-tech industries, the rapid growth of the transportation sector made it the largest source of carbon emissions outside of industry. The negative effect of the transportation sector on carbon emissions was less significant in the central region, because of less convenient transportation and a lower population.

However, the cities in the southwestern zone underwent a rapid economic transformation after 2016. The government promoted the introduction of new industries. All cities reshaped industrial structures and promoted industrial clustering. Industrial restructuring drove down the growth rate of carbon emissions. The gap between the southwestern zone and other cities became smaller.

In summary, the government needs to avoid the negative influence of transportation and high-tech industries on carbon emissions. At the same time, traditional industries should be reformed and upgraded to avoid a reliance on large-scale equipment with high energy consumption.

Similarly, the spatial impacts of urbanization are shown in Figure 4a–d. The negative impact of urbanization on carbon emissions increased at first and then decreased. The growth of carbon emissions was inhibited by urbanization in the early stage. When urban development strategies and spatial layouts were adjusted, the energy-saving effects of urbanization became apparent.

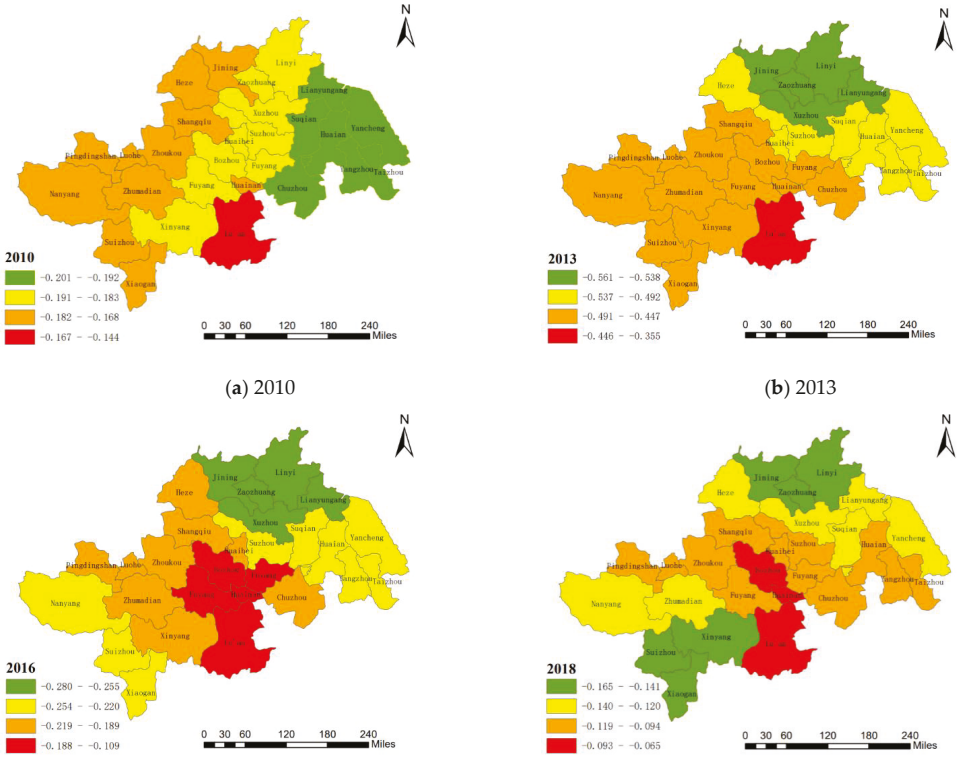

(**a**) 2010 (**b**) 2013

(**c**) 2016 (**d**) 2018

Figure 4. Spatial impact of urbanization.

The cities with low coefficients in 2010 were Xuzhou, Suqian, Lianyungang, Huai'an, Yancheng, Yangzhou, Taizhou, Linyi, Suzhou, and Chuzhou, all of which are located in the coastal region. With the input of production factors from abroad, the increase in urbanization rate made the industries gather in cities. Manufacturing industries with serious environmental pollution were gathered around cities. The increase in urbanization increased carbon emissions. While the northwestern cities, such as Zaozhuang, Huaibei, Fuyang, and Xinyang, had a less negative impact on carbon emissions. The urbanization of these cities started later and the urbanization process was much smaller than the eastern cities. Their development mostly relied on secondary industry, so urbanization could not offset the negative impact of secondary sector on carbon emissions.

The coefficient reached the minimum value in 2013. The coefficients of Jining, Zaozhuang, Linyi, Lianyungang, Xuzhou, Suizhou, Suqian, Huai'an, and Yancheng were significantly lower than the western cities. The distribution in the following two years was consistent with that in 2013. The boundary of Heze, Huaibei, and Suzhou showed a clear east–west gap, in which the correlation of urbanization with carbon emissions in the eastern zone was significantly smaller than in the western zone. The rapid urbanization of eastern cities led to a disorderly development and blind expansion of urban scale, which brought a series of problems in urban land and led to a significant increase in carbon emissions.

The coefficient continued to increase from 2016 to 2018. The zone attached importance to the transportation and tertiary industries. The government solved the problems of employment and resource allocation. However, the coefficient in 2018 was larger than in 2010. The negative effect of urbanization was significantly reduced. The rapid development of urbanization led to the concentration of the urban population and the growth of urban areas, which was a great test for the urban environmental situation. At the same time, urbanization brought an improvement in the living standard of residents and the quality of the population.

In a word, the zone was in the stage of urbanization development, from high speed to high quality. Developed cities should play a radiating role, to avoid the waste of resources and pollution caused by blind expansion. The economically backward regions should accelerate their urbanization process.

4. Discussion

In this paper, we analyzed the factors and spatial patterns influencing carbon emissions in the HREZ from 2010 to 2018. Our findings are summarized as follows:

(1) Urbanization and industrial structure have double and single threshold effects on the carbon emissions, respectively, with GDP per capita as the threshold variable. Urbanization and industrial structure have double threshold effects on the carbon emissions, with energy intensity as the threshold variable.

(2) The coefficients of industrial structure are all positive, but the rate of increase gradually decreases. They show a decreasing trend from northeast to southwest. Before 2016, the positive impact on carbon emissions in Jiangsu and Shandong provinces was significantly higher than in the southwestern cities. Cities bounded by Shangqiu, Huabei, Bengbu, and Huainan had developed tertiary industries and other industries relying on large machinery production equipment in order to compensate for the development of tertiary industry. After 2016, the zone began to move in a favorable direction, towards reducing carbon emissions, gradually meeting the low carbon development targets of the thirteenth Five-Year Plan of China.

(3) The impacts of urbanization are all negative. The coefficients first decreased and then increased, reaching the maximum in 2013. Before 2013, the urbanization of most cities in Jiangsu and Anhui provinces had a significant negative correlation effect on carbon emissions, and the negative coefficient was smaller in the northwest of China, such as in Zaozhuang, Huaibei, Fuyang, and Xinyang. From 2013 to 2016, the negative coefficient of eastern cities was significantly higher than that of western cities, showing a significant east–west gap, bounded by Heze, Huaibei, and Suzhou,

and the negative coefficient effect of urbanization on carbon emissions in some cities in Henan Province increased after 2016.

In order to improve the efficiency of carbon emissions and reduce the regional differences in the HREZ, some suggestions are proposed as follows:

(1) The industrial structure and urbanization development speed of the HREZ need to be adjusted according to the thresholds. Local governments in the HREZ should adjust regional measures and policies according to the marginal benefits of industrial structure and urbanization.
(2) Eastern cities in the zone need to avoid the adverse effects of transportation and high-tech industries on carbon emissions, due to the unreasonable development of industrial structure. In addition, it also needs to reduce the dependence of traditional industries on large equipment with a high energy consumption.
(3) The areas with poor urbanization in the western region need to speed up the rate of urbanization and improve the quality of the population. The developed cities in the east need to control their urban development rate, to avoid the energy consumption caused by large population concentrations.

Author Contributions: Conceptualization, Q.P.; methodology, L.Z.; software, L.Z.; formal analysis, W.Z.; investigation, W.Z.; data curation, W.Z.; writing—original draft preparation, W.Z.; writing—review and editing, Q.P., T.Z. and L.Z.; visualization, T.Z.; supervision, Q.P.; project administration, Q.P.; funding acquisition, Q.P. All authors have read and agreed to the published version of the manuscript.

Funding: This research was funded by the Fundamental Research Funds for the Central Universities (No. B200203175), the Graduate Student Innovation Funds of Jiangsu Province (KYCX20_0524).

Acknowledgments: This research was funded by the Fundamental Research Funds for the Central Universities (No. B200203175), the Graduate Student Innovation Funds of Jiangsu Province (KYCX20_0524).

Conflicts of Interest: The authors declare no conflict of interest.

References

1. Villoria-Sáez, P.; Tam, V.W.; del Río Merino, M.; Arrebola, C.V.; Wang, X. Effectiveness of greenhouse-gas Emission Trading Schemes implementation: A review on legislations. *J. Clean. Prod.* **2016**, *127*, 49–58. [CrossRef]
2. World Bank. CO_2 emissions (kt). 2016. Available online: https://data.worldbank.org/indicator/EN.ATM.CO2E.KT?View=chart (accessed on 21 October 2021).
3. BP. BP Statistical Review of World Energy. Available online: https://www.bp.com/en/global/corporate/energyeconomics/statistical-review-of-world-energy/CO2-emissions.html/ (accessed on 21 October 2021).
4. Xinhua, xinhuanet.com. 2021. Available online: http://www.xinhuanet.com/english/2021-03/20/c_139823518.htm (accessed on 16 October 2021).
5. Tu, Z.; Shen, R. Industrialization's, Urbanization's Dynamic Marginal Carbon Emissions—The Analytical Framework Based on LMDI "Two-Level Perfect Decomposition". *Method. China Ind. Econ.* **2013**, *9*, 31–43.
6. Wang, Z.; Yin, F.; Zhang, Y.; Zhang, X. An empirical research on the influencing factors of regional CO_2 emissions: Evidence from Beijing city. *China Appl. Energy* **2012**, *100*, 277–284. [CrossRef]
7. Du, W.C.; Xia, X. How does urbanization affect GHG emissions? A cross-country panel threshold data analysis. *Appl. Energy* **2018**, *229*, 872–883. [CrossRef]
8. Wang, X.; Shao, Q. Non-linear effects of heterogeneous environmental regulations on green growth in G20 countries: Evidence from panel threshold regression. *Sci. Total Environ.* **2019**, *660*, 1346–1354. [CrossRef] [PubMed]
9. Valadkhani, A.; Smyth, R.; Nguyen, J. Effects of primary energy consumption on CO_2 emissions under optimal thresholds: Evidence from sixty countries over the last half century. *Energy Econ.* **2019**, *80*, 680–690. [CrossRef]
10. Ahmad, M.; Khan, Z.; Anser, M.K.; Jabeen, G. Do rural-urban migration and industrial agglomeration mitigate the environmental degradation across China's regional development levels? *Sustain. Prod. Consum.* **2021**, *27*, 679–697. [CrossRef]
11. Zaidi, S.A.H.; Zafar, M.W.; Shahbaz, M.; Hou, F. Dynamic linkages between globalization, financial development and carbon emissions: Evidence from Asia Pacific Economic Cooperation countries. *J. Clean. Prod.* **2019**, *228*, 533–543. [CrossRef]
12. Hashmi, R.; Alam, K. Dynamic relationship among environmental regulation, innovation, CO_2 emissions, population, and economic growth in OECD countries: A panel investigation. *J. Clean. Prod.* **2019**, *231*, 1100–1109. [CrossRef]
13. Ehrlich, P.R.; Holdren, J.P. Impact of population growth. *Science* **1971**, *171*, 1212–1217. [CrossRef]

14. York, R.; Rosa, E.A.; Dietz, T. STIRPAT, IPAT and ImPACT: Analytic tools for unpacking the driving forces of environmental impacts. *Ecol. Econ.* **2003**, *46*, 351–365. [CrossRef]
15. Tobler, W.R. A Computer Movie Simulating Urban Growth in the Detroit Region. *Econ. Geogr.* **1970**, *46*, 234–240. [CrossRef]
16. Saidi, K.; Omri, A. The impact of renewable energy on carbon emissions and economic growth in 15 major renewable energy-consuming countries. *Environ. Res.* **2020**, *186*, 109567. [CrossRef] [PubMed]
17. Huang, J.; Chen, X.; Yu, K.; Cai, X. Effect of technological progress on carbon emissions: New evidence from a decomposition and spatiotemporal perspective in China. *J. Environ. Manag.* **2020**, *274*, 110953. [CrossRef]
18. Wang, Q.; Zhang, F. The effects of trade openness on decoupling carbon emissions from economic growth—Evidence from 182 countries. *J. Clean Prod.* **2021**, *279*, 123838. [CrossRef]
19. Du, K.; Yu, Y.; Li, J. Does international trade promote CO_2 emission performance? An empirical analysis based on a partially linear functional-coefficient panel data model. *Energy Econ.* **2020**, *92*, 104983. [CrossRef]
20. Khan, Z.; Ali, M.; Jinyu, L.; Shahbaz, M.; Siqun, Y. Consumption-based carbon emissions and trade nexus: Evidence from nine oil exporting countries. *Energy Econ.* **2020**, *89*, 104806. [CrossRef]
21. Nathaniel, S.P.; Adeleye, N. Environmental preservation amidst carbon emissions, energy consumption, and urbanization in selected african countries: Implication for sustainability. *J. Clean. Prod.* **2021**, *285*, 125409. [CrossRef]
22. Salari, M.; Javid, R.J.; Noghanibehambari, H. The nexus between CO_2 emissions, energy consumption, and economic growth in the U.S. *Econ. Anal. Policy* **2021**, *69*, 182–194. [CrossRef]
23. Ehigiamusoe, K.U.; Lean, H.H.; Smyth, R. The moderating role of energy consumption in the carbon emissions-income nexus in middle-income countries. *Appl. Energy* **2020**, *261*, 114215. [CrossRef]
24. Kirikkaleli, D.; Kalmaz, D.B. Testing the moderating role of urbanization on the environmental Kuznets curve: Empirical evidence from an emerging market. *Environ. Sci. Pollut. Res.* **2020**, *27*, 38169–38180. [CrossRef] [PubMed]
25. Chen, Q.; Taylor, D. Economic development and pollution emissions in Singapore: Evidence in support of the Environmental Kuznets Curve hypothesis and its implications for regional sustainability. *J. Clean. Prod.* **2020**, *243*, 118637. [CrossRef]
26. Abdouli, M.; Kamoun, O.; Hamdi, B. The impact of economic growth, population density, and FDI inflows on CO_2 emissions in BRICTS countries: Does the Kuznets curve exist? *Empir. Econ.* **2018**, *54*, 1717–1742. [CrossRef]
27. Xu, Q.; Dong, Y.; Yang, R. Urbanization impact on carbon emissions in the Pearl River Delta region: Kuznets curve relationships. *J. Clean. Prod.* **2018**, *180*, 514–523. [CrossRef]
28. Rahman, M.M.; Kashem, M.A. Carbon emissions, energy consumption and industrial growth in Bangladesh: Empirical evidence from ARDL cointegration and Granger causality analysis. *Energy Policy* **2017**, *110*, 600–608. [CrossRef]
29. Zhou, Y.; Chen, M.; Tang, Z.; Mei, Z. Urbanization, land use change, and carbon emissions: Quantitative assessments for city-level carbon emissions in Beijing-Tianjin-Hebei region. *Sustain. Cities Soc.* **2021**, *66*, 102701. [CrossRef]
30. Li, X.; Wang, J.; Zhang, M.; Ouyang, J.; Shi, W. Regional differences in carbon emission of China's industries and its decomposition effects. *J. Clean. Prod.* **2020**, *270*, 122528. [CrossRef]
31. Wu, Y.; Tam, V.W.; Shuai, C.; Shen, L.; Zhang, Y.; Liao, S. Decoupling China's economic growth from carbon emissions: Empirical studies from 30 Chinese provinces (2001–2015). *Sci. Total Environ.* **2019**, *656*, 576–588. [CrossRef]
32. Feng, J.; Zeng, X.-L.; Yu, Z.; Bian, Y.; Li, W.-C.; Wang, Y. Decoupling and driving forces of industrial carbon emission in a coastal city of Zhuhai, China. *Energy Rep.* **2019**, *5*, 1589–1602. [CrossRef]
33. Zheng, X.; Wang, R.; He, Q. A city-scale decomposition and decoupling analysis of carbon dioxide emissions: A case study of China. *J. Clean. Prod.* **2019**, *238*, 117824. [CrossRef]
34. Wang, Q.; Su, M.; Li, R. Toward to economic growth without emission growth: The role of urbanization and industrialization in China and India. *J. Clean. Prod.* **2018**, *205*, 499–511. [CrossRef]
35. Wang, Q.; Wang, L. The nonlinear effects of population aging, industrial structure, and urbanization on carbon emissions: A panel threshold regression analysis of 137 countries. *J. Clean. Prod.* **2021**, *287*, 125381. [CrossRef]
36. Zhou, H.; Ping, W.; Wang, Y.; Wang, Y.; Liu, K. China's initial allocation of interprovincial carbon emission rights considering historical carbon transfers: Program design and efficiency evaluation. *Ecol. Indic.* **2021**, *121*, 106918. [CrossRef]
37. Yang, G.; Shang, P.; He, L.; Zhang, Y.; Wang, Y.; Zhang, F.; Zhu, L.; Wang, Y. Interregional carbon compensation cost forecast and priority index calculation based on the theoretical carbon deficit: China as a case. *Sci. Total Environ.* **2019**, *654*, 786–800. [CrossRef] [PubMed]
38. Günther, S.A.; Staake, T.; Schöb, S.; Tiefenbeck, V. The behavioral response to a corporate carbon offset program: A field experiment on adverse effects and mitigation strategies. *Glob. Environ. Chang.* **2020**, *64*, 102123. [CrossRef]
39. Song, W.; Mao, H.; Han, X. The two-sided effects of foreign direct investment on carbon emissions performance in China. *Sci. Total Environ.* **2021**, *791*, 148331. [CrossRef]
40. Muhammad, S.; Long, X.; Salman, M.; Dauda, L. Effect of urbanization and international trade on CO_2 emissions across 65 belt and road initiative countries. *Energy* **2020**, *196*, 117102. [CrossRef]
41. Debone, D.; Leite, V.P.; Miraglia, S.G.E.K. Modelling approach for carbon emissions, energy consumption and economic growth: A systematic review. *Urban Clim.* **2021**, *37*, 100849. [CrossRef]
42. Waheed, R.; Sarwar, S.; Wei, C. The survey of economic growth, energy consumption and carbon emission. *Energy Rep.* **2019**, *5*, 1103–1115. [CrossRef]

43. Janzen, R.; Davis, M.; Kumar, A. Greenhouse gas emission abatement potential and associated costs of integrating renewable and low carbon energy technologies into the Canadian oil sands. *J. Clean. Prod.* **2020**, *272*, 122820. [CrossRef]
44. Wang, S.; Tang, Y.; Du, Z.; Song, M. Export trade, embodied carbon emissions, and environmental pollution: An empirical analysis of China's high- and new-technology industries. *J. Environ. Manag.* **2020**, *276*, 111371. [CrossRef]
45. Ganda, F. The impact of innovation and technology investments on carbon emissions in selected organisation for economic Co-operation and development countries. *J. Clean. Prod.* **2019**, *217*, 469–483. [CrossRef]
46. Liu, H.; Nie, J.; Cai, B.; Cao, L.; Wu, P.; Pang, L.; Wang, X. CO_2 emissions patterns of 26 cities in the Yangtze River Delta in 2015: Evidence and implications. *Environ. Pollut.* **2019**, *252*, 1678–1686. [CrossRef] [PubMed]
47. Zhang, S.; Li, H.; Zhang, Q.; Tian, X.; Shi, F. Uncovering the impacts of industrial transformation on low-carbon development in the Yangtze River Delta. *Resour. Conserv. Recycl.* **2019**, *150*, 104442. [CrossRef]
48. Xu, X.; Yang, G.; Tan, Y.; Zhuang, Q.; Tang, X.; Zhao, K.; Wang, S. Factors influencing industrial carbon emissions and strategies for carbon mitigation in the Yangtze River Delta of China. *J. Clean. Prod.* **2017**, *142*, 3607–3616. [CrossRef]
49. Fan, J.; Cao, Z.; Zhang, X.; Wang, J.-D. Comparative study on the influence of final use structure on carbon emissions in the Beijing-Tianjin-Hebei region. *Sci. Total Environ.* **2019**, *668*, 271–282. [CrossRef]
50. Wang, C.; Zhan, J.; Bai, Y.; Chu, X.; Zhang, F. Measuring carbon emission performance of industrial sectors in the Beijing-Tianjin-Hebei region, China: A stochastic frontier approach. *Sci. Total Environ.* **2019**, *685*, 786–794. [CrossRef]
51. Hussain, J.; Khan, A.; Zhou, K. The impact of natural resource depletion on energy use and CO_2 emission in Belt & Road Initiative countries: A cross-country analysis. *Energy* **2020**, *199*, 117409.
52. Chen, L.; Xu, L.; Yang, Z. Accounting carbon emission changes under regional industrial transfer in an urban agglomeration in China's Pearl River Delta. *J. Clean. Prod.* **2017**, *167*, 110–119. [CrossRef]
53. Hansen, B.E. Sample splitting and threshold estimation. *Econometrica* **2000**, *68*, 575–603. [CrossRef]
54. China Statistical Yearbook. 2018. Available online: http://www.stats.gov.cn/tjsj/ndsj/2018/notepyrightch.htm (accessed on 16 October 2021).
55. China Energy Statistical Yearbook. 2018. Available online: https://data.cnki.net/trade/Yearbook/Single/N2019080025?z=Z024 (accessed on 16 October 2021).
56. IPCC. *IPCC Guidelines for National Greenhouse Gas Inventories*; IPCC: Geneva, Switzerland, 2006.
57. The Intergovernmental Panel on Climate Change (IPCC). 2021. Available online: https://www.ipcc.ch/about/.html (accessed on 14 October 2021).
58. Zhou, X.; Gu, A. Impacts of household living consumption on energy use and carbon emissions in China based on the input-output model. *Adv. Clim. Chang. Res.* **2020**, *11*, 118–130. [CrossRef]

land

MDPI

Article

Gross Ecosystem Productivity Dominates the Control of Ecosystem Methane Flux in Rice Paddies

Hong Li [1,2,*,†], Min Zhao [3,†], Changhui Peng [2], Haiqiang Guo [4], Qing Wang [3] and Bin Zhao [4]

[1] State Key Laboratory of Coal Mine Disaster Dynamics and Control, Faculty of Architecture and Urban Planning, Chongqing University, Chongqing 400045, China
[2] Department of Biology Science, Institute of Environment Sciences, University of Quebec at Montreal, Montreal, QC C3H 3P8, Canada; peng.changhui@uqam.ca
[3] Shanghai Academy of Environmental Sciences, Shanghai 200233, China; zhaom@saes.sh.cn (M.Z.); wangq@saes.sh.cn (Q.W.)
[4] Ministry of Education Key Laboratory for Biodiversity Science and Ecological Engineering, Coastal Ecosystems Research Station of the Yangtze River Estuary, Fudan University, Shanghai 200433, China; hqguo@fudan.edu.cn (H.G.); zhaobin@fudan.edu.cn (B.Z.)
* Correspondence: lihom@cqu.edu.cn; Tel.: +86-13193093366
† Hong Li and Min Zhao are equally contributing first authors.

Abstract: Although rice paddy fields are one of the world's largest anthropogenic sources of methane CH_4, the budget of ecosystem CH_4 and its' controls in rice paddies remain unclear. Here, we analyze seasonal dynamics of direct ecosystem-scale measurements of CH_4 flux in a rice-wheat rotation agroecosystem over 3 consecutive years. Results showed that the averaged CO_2 uptakes and CH_4 emissions in rice seasons were 2.2 and 20.9 folds of the wheat seasons, respectively. In sum, the wheat-rice rotation agroecosystem acted as a large net C sink (averaged 460.79 g C m^{-2}) and a GHG (averaged 174.38 g CO_2eq m^{-2}) source except for a GHG sink in one year (2016) with a very high rice seeding density. While the linear correlation between daily CH_4 fluxes and gross ecosystem productivity (GEP) was not significant for the whole rice season, daily CH_4 fluxes were significantly correlated to daily GEP both before (R^2: 0.52–0.83) and after the mid-season drainage (R^2: 0.71–0.79). Furthermore, the *F* partial test showed that GEP was much greater than that of any other variable including soil temperature for the rice season in each year. Meanwhile, the parameters of the best-fit functions between daily CH_4 fluxes and GEP shifted between rice growth stages. This study highlights that GEP is a good predictor of daily CH_4 fluxes in rice paddies.

Keywords: CH_4 flux; eddy covariance; budget; gross ecosystem productivity; rice paddy

Citation: Li, H.; Zhao, M.; Peng, C.; Guo, H.; Wang, Q.; Zhao, B. Gross Ecosystem Productivity Dominates the Control of Ecosystem Methane Flux in Rice Paddies. *Land* **2021**, *10*, 1186. https://doi.org/10.3390/land10111186

Academic Editors: Baojie He, Ayyoob Sharifi, Chi Feng and Jun Yang

Received: 2 October 2021
Accepted: 1 November 2021
Published: 4 November 2021

1. Introduction

Rice paddies provide the dominant staple food crop for over 5 billion people worldwide while acting as a major source of atmospheric methane (CH_4) which is the second most important greenhouse gas following carbon dioxide (CO_2) [1,2]. Thereby, constraint and mitigation of CH_4 emissions from irrigated rice fields emerges as a major scientific and policy issue. Previous studies on global estimation of CH_4 emissions from rice paddies showed that the budget of CH_4 flux remain great uncertainties [2,3], which indicated more efforts are needed to understand the responses of CH_4 flux to biological and environmental factors.

Previous CH_4 flux from rice paddies have predominantly been measured using the manual closed chamber technique [4,5]. Chamber-based measurements can introduce some potential biases due to direct interaction with the near-surface environment and are also limited to estimate annual budgets due to the discrete sampling in time [6,7]. In recent years, the eddy covariance (EC) technique advantaged in measuring CH_4 flux since it provides continuous ecosystem-scale CH_4 flux without interfering with the processes of gas exchange between the surface and the atmosphere [6,8]. Several studies using EC

methods have advantaged our understanding of the dynamics and process of CH_4 flux from rice paddies [9–11]. However, to date few studies have used this method to measure CH_4 flux from rice paddies in China [9,10].

Methane-producing microbes (methanogens) produce CH_4 in soils as the end product of the anaerobic decomposition of organic matter, which would be mineralized to carbon dioxide under aerobic conditions before being released to the atmosphere. Thus, soil water content and soil temperature, which regulate the reduced soil conditions and enzyme-mediated processes, have been widely considered as the most important environmental controlling factors of CH_4 flux. However, rice plants growing in water-saturated soils are also closely associated with the production and transport of CH_4. Recently, several studies revealed that gross ecosystem productivity (GEP) is the dominant cause of the diel pattern of half-hourly CH_4 flux in rice paddies [9,10,12,13], and that GEP represents one of the most important factors regulating seasonal variations in daily CH_4 flux [9,14–16]. However, in some sites, GEP are not that important as temperature for CH_4 flux [10,11].

China has 19% of the global rice field area and provides 30% of the production, in which winter wheat-paddy rice cropping rotation are very common practiced. Over 80% of these rice paddies apply water-saving techniques, such as mid-season drainage and alternate wetting and drying, which has largely decreased the amount of CH_4 emissions [17–20]. In addition to changes in the redox environment, soil water status can influence stomatal conductance and photosynthesis of rice plants [21–23]. While Dai et al. (2019) using EC technique in a rice paddy in China has reported a correlation between GEP and CH_4 flux. How rice plants control CH_4 flux in rice paddies applying water-saving techniques remains unclear. In this study, we measured CH_4 flux using the eddy covariance technique over 3 consecutive rice growing cycles in a rice paddy where water-saving techniques are applied, to: (1) identify factors affecting CH_4 flux during rice season; (2) estimate annual carbon budget and greenhouse gas (GHG) budget for the rice-wheat rotation agroecosystem. We hypothesized that rice plant productivity would exert a strong control on CH_4 flux in the rice season.

2. Methods

2.1. Study Site and Crop Management

The studied rice-wheat rotation agroecosystem is located at the Yuejin Farm on the Chongming Island, Shanghai, China (31°48′37.54″ N, 121°15′0.43″ E, Figure 1a). The farm covers a flat and homogenous area of 18.95 km^2. The climate here is characterized as northern subtropical monsoon climate. The mean air temperature and annual precipitation were 17.1 ± 0.6 °C and 1156.1 ± 190.6 mm (1991 to 2012), respectively. The soil texture is characterized as silt loam. The soil organic carbon and total nitrogen in the topsoil (0–8 cm) are 20 g C kg^{-1} and 1.6 g N kg^{-1}, respectively.

2.2. Crop Establishment

An annual winter wheat-paddy rice cropping rotation was practiced in the field (Figure 1b). Winter wheat was sowed in October or December and rice was direct-seeded in June (Table 1). Seeds of the wheat and rice cultivar were Ningmai 13 and Wuyunjing 31, respectively. Chopped rice and wheat straw at 5–10 cm length is mixed into the soil layer when farmers plow in the cropping systems. The cropping regime and water management at the wheat-paddy field are representative of common practices in southeast China. The cropping regimes are detailed in Li et al. (2019) [16]. Irrigation was only started at a few days before the rice season and ended at about two weeks before the ends of the rice season. During the rice season, alternate wetting and drying regime (AWD) was deployed. The mid-season drainage (MSD) was also applied from late July to early August in each year [16]. In short, a typical water regime of AWD-MSD-AWD-moisture irrigation was practiced in the rice season.

The paddy rice sequentially experienced 3 growth stages related to rice plant phenology, including: vegetative (DOY 164–208, 159–206, 158–202 in 2016, 2017, and 2018,

respectively), reproductive (DOY 209–271, 207–269, 203–271 in 2016, 2017, and 2018, respectively), and ripening stage (DOY 272–315, 270–296, 272–318 in 2016, 2017, and 2018, respectively). Mid-season drainage represents a strong artificial disturbance, and thus the MSD period (DOY 204–222, 200–216, 199–214 in 2016, 2017, and 2018, respectively) was separated from the late vegetative and early reproductive stage in our study. Accordingly, neither the vegetative stage nor the reproductive stage includes the MSD practice in the following analyses.

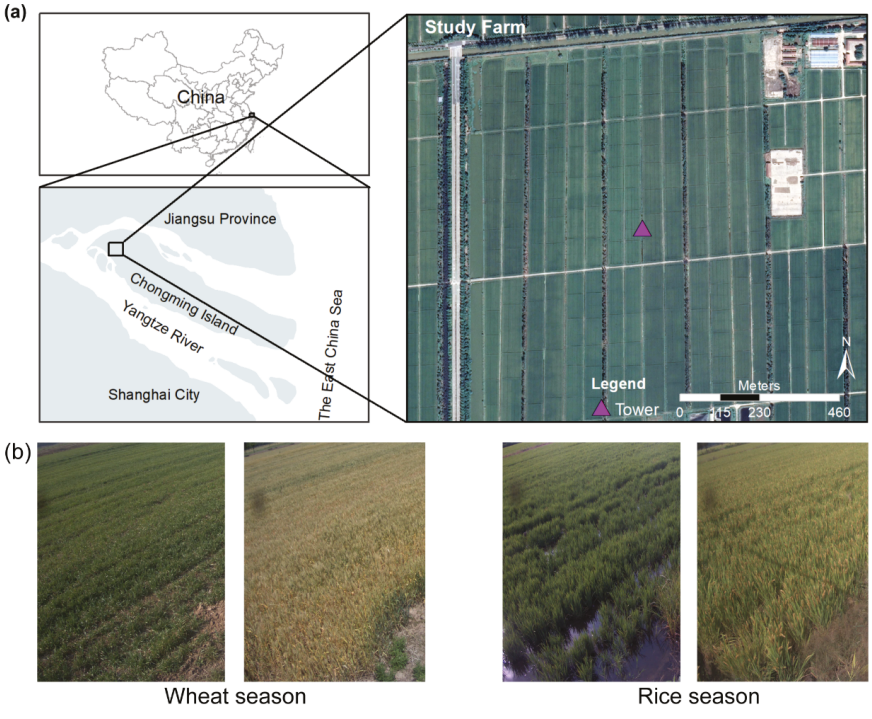

Figure 1. Location and the satellite image from Google Earth taken on 1st October 2018 of the study area (**a**), and the photos of wheat season and rice season, respectively (**b**).

Table 1. Planting and harvest date in the rice-wheat rotation agroecosystem.

Year	2015–2016		2016–2017		2017–2018	
Season	**Wheat**	**Rice**	**Wheat**	**Rice**	**Wheat**	**Rice**
Plant date	28 October	11 June	18 December	7 June	26 October	6 June
Harvest date	30 May	11 November	26 May	24 October	28 May	15 November

2.3. Eddy Covariance Measurements and Data Processing

The eddy covariance (EC) technique was used to continuously collect net CH_4 fluxes and net CO_2 fluxes between the wheat-rice rotation field and the atmosphere from 2016 to 2018. The EC measurement station was in the middle of the farmland (Figure 1). The EC system included an open-path CH_4 gas analyzer (LI-7700, LI−COR), an open-path CO_2/H_2O gas analyzer (EC150, Campbell Scientific), and a sonic anemometer (CSAT3, Campbell Scientific). The turbulence data was sampled with a frequency of 10 Hz.

Fluxes were calculated using the 30 min covariance of gas scalar concentrations of interest and vertical wind velocity after applying a series of standard correction. The

EddyPro 7.0.4 software (LI−COR) was used as outlined in Li et al. (2018, 2019) [16,24]. Briefly, these included a despiking procedure including detecting and eliminating individual out-of-range values [25], time lag detection applying covariance maximization with default, double coordinate rotations [26], compensation of Webb-Pearman-Leuning density fluctuations [27]. The random uncertainty for half-hourly fluxes were estimated [28].

The subsequent QA/QC processing for half-hourly fluxes were performed as detailed in Li et al. (2018, 2019) [16,24]. The data were removed when rainfall events occurred, relative signal strength indicator (RSSI) < 20%, and friction velocity < 0.13 m s^{-1} [29]. The the steady state test and the well-developed turbulence test were used to generate flux quality flags [30]. After QA/QC, data coverage during the rice growing seasons 2016–2018 were 49–56% for CH_4 flux and 52–64% for CO_2 flux. Daily averaged fluxes were only calculated when more than 12 data points were available for both daytime and nighttime.

To estimate seasonal budgets, gaps of CO_2 and CH_4 fluxes were filled using both the marginal distribution sampling method and a random forest algorithm [29,31]. GEP were estimated based on the gap-filling of the marginal distribution sampling method of CO_2 fluxes time series [29]. The uncertainty introduced by the gap-filling procedure were estimated [29,31]. The uncertainty of seasonal budgets was obtained according to Aurela et al. (2002) [32]. The net GHG budget was calculated assuming that 1 g CH_4 is equivalent to 28 g CO_2 with respect to the greenhouse effect over a time horizon of 100 years.

Basic hydrological and micrometeorological data were collected in conjunction with the EC data, including air temperature (3.3 m above ground, HMP155 A, Campbell Scientific), soil temperature (5 cm underground, 109, Campbell Scientific), and volumetric water content (VWC) (5 cm underground, CS616, Campbell Scientific), and water table depth (Pro 30, YSI).

2.4. Statistics

To investigate the seasonal variation in CH_4 flux, a semi-empirical multiplicative model was employed. Based on previous studies, several potential driving factors of the CH_4 flux were included in the model:

$$F_{CH4} = a \times b^{Tg} \times c^{GEP} \times d^{VWC} \times e^{u*} \times f^{P} \quad (1)$$

where F_{CH4} is the daily CH_4 flux, Tg, GEP, VWC, u*, P are the normalized soil temperature, gross ecosystem photosynthesis, volumetric water content, friction velocity, ambient pressure, respectively, and a, b, c, d, e and f are the model parameters. In 2018, water conductivity (g) and water table depth (h) were also tested as model parameters.

To identify the importance of each driving factor in synchronous controls of CH_4 flux, a partial F test was performed to determine whether including the independent variables in the model could significantly increase the model's ability to explain the variation of the dependent variable. A partial F value larger than the threshold F value ($F\alpha$, $\alpha = 0.05$) indicates that the excluded variable can significantly increase the explanation of the dependent variable at the significance level of 5% if it is included in the model. A larger F value suggests that the excluded variable can explain more of the variation of the dependent variable than other independent variables.

3. Results and Discussion

3.1. Seasonal Variations in CH_4 Fluxes and Predictors

Large seasonal variations in daily mean CH_4 fluxes were observed each year in the rice-wheat rotation agroecosystem (Figure 2). Daily CH_4 fluxes during 2016–2018 averaged at 10.57 and 408.07 mg CH_4 m^{-2} d^{-1} in the wheat and rice season, respectively. Daily CH_4 fluxes kept a relatively low range between −52.06 and 199.00 mg CH_4 m^{-2} d^{-1} in the wheat growing season and a range between 0.57 and 1488.70 mg CH_4 m^{-2} d^{-1} in the rice growing season. CH_4 fluxes sharply increased when the field was first flooded for the rice season in June. CH_4 fluxes reach peaks in late July and then gradually decreased to low emissions at the end of the rice season between late October and early November.

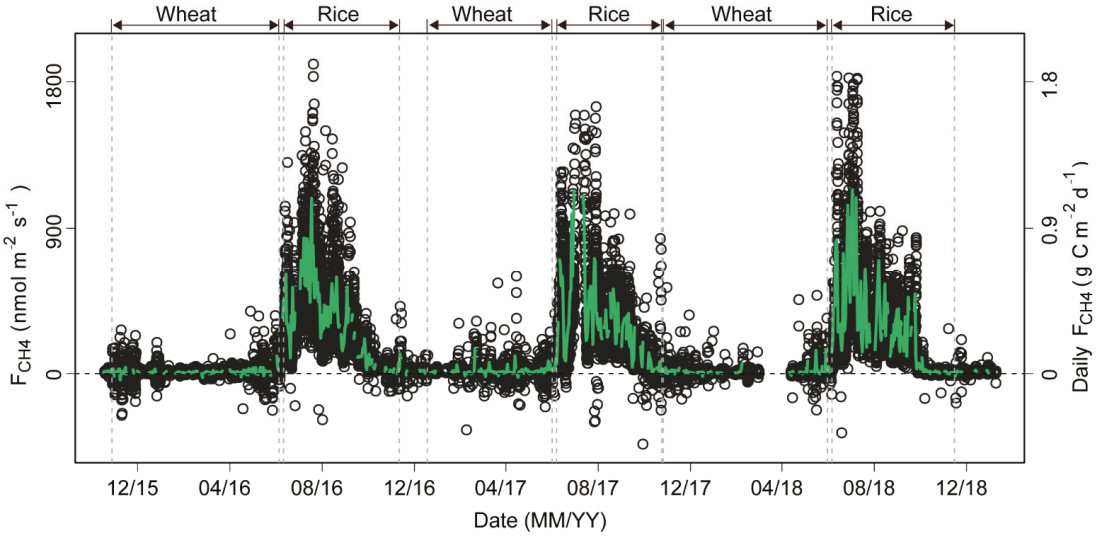

Figure 2. Time series of daily (green lines) and half-hourly (black circles) CH_4 fluxes during the rice growing season in 2016–2018.

For the rice season, daily CH_4 fluxes varied among rice growth stages (Figure 2). In the vegetative stage, daily CH_4 fluxes, as well as GEP and soil temperature, exhibited an increasing trend until the mid-season drainage (Figures 2 and 3). Daily CH_4 fluxes reached peaks of 1.45–1.47g CH_4 m^{-2} d^{-1} at the end of the vegetative stage in middle July of each year. Daily CH_4 fluxes sharply dropped by 81–88% during the mid-season drainage despite GEP and soil temperature continuing to increase (Figures 2 and 3). After the drainage, daily CH_4 flux increased to an average emission of 0.47, 0.42, and 0.44 g m^{-2} d^{-1} in August in 2016, 2017, and 2018, respectively. At the ripening stage, CH_4 flux was much lower compared to other stages (Figure 2). In total, cumulative CH_4 emissions at the vegetative, mid-season drainage, reproductive and, ripening stage were 46–48%, 13–18%, 31–38%, and 1–4%, respectively.

As discussed in Li et al. (2019) [16], CH_4 fluxes in the rice paddy represents a strong CH_4 source for atmosphere CH_4 during the rice growing season. The seasonal pattern (Figure 3) of CH_4 fluxes which was observed to peak before the mid-season drainage with a secondary peak after the mid-season drainage was consistent with previous studies under similar cropping regimes in southeast China [19,33].

During the rice growing season, the linear correlation between daily CH_4 fluxes and GEP were not significant. However, daily CH_4 fluxes were significantly correlated to GEP both before (Figure 4, R^2: 0.52–0.83) and after the mid-season drainage (Figure 4, R^2: 0.71–0.79) in each year. Furthermore, the partial *F* test showed that GEP during all periods were identified as significant variables in each year. Soil temperature during periods except for before the mid-season drainage in 2016 and after the mid-season drainage in 2018 were significant variables. The *F* value of GEP was much greater than that of any other variable including soil temperature in each year (Table 2), which demonstrated that GEP was much more important than any other variable included in the model although when other variables were added, a larger proportion of the variance in CH_4 fluxes could be explained at the seasonal timescale (Table 3, R^2: 0.80–0.98).

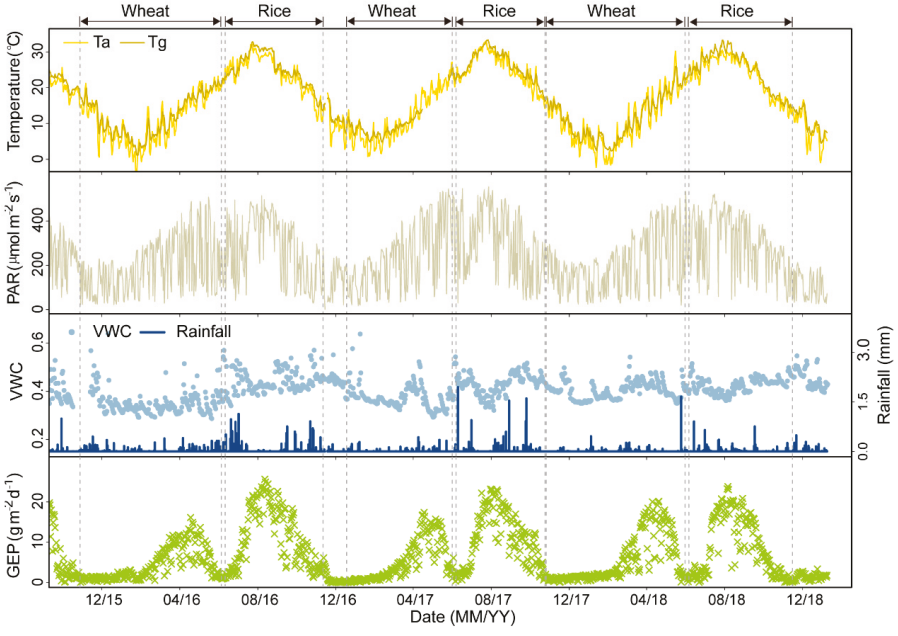

Figure 3. Time series of daily averaged air temperature (yellow lines), 5cm soil temperature (dark yellow lines), photosynthetically active radiation (PAR), volumetric water content (VWC, navy blue lines), rainfall (blue columns), and gross ecosystem productivity (GEP, green forks).

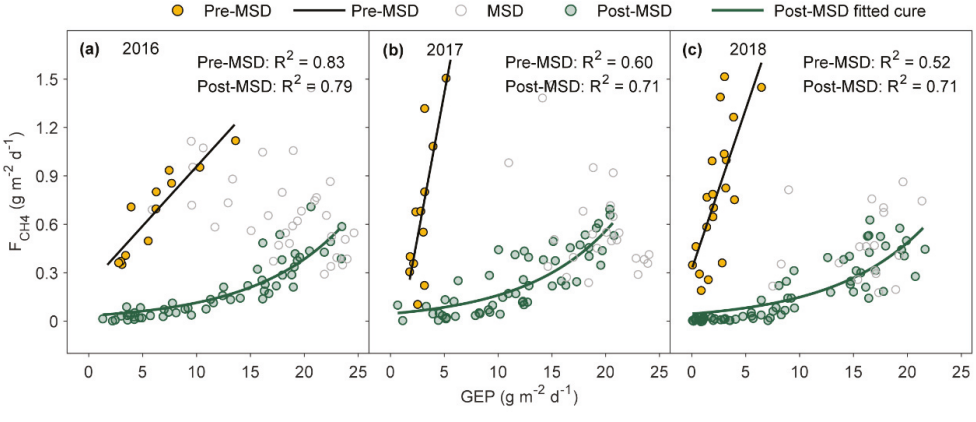

Figure 4. Linear and exponential regression models of daily CH_4 fluxes against GEP for the periods before (yellow points) and after (green points) the mid-season drainage, respectively. The grey circles (**a**–**c**) represent CH_4 fluxes during mid-season drainage each year.

While the linear correlation between daily CH_4 fluxes and GEP were not significant for the whole rice season, the regression (Figure 4) and *F* partial test (Table 2) both before (Figure 4, R^2: 0.52–0.83) and after the mid-season drainage demonstrated that daily GEP was the most important predictor of daily CH_4 fluxes as we hypothesized. This separate analysis for each rice growing stage may be a helpful way to identify the factors of CH_4 fluxes in rice paddies. The close relationship between daily CH_4 fluxes and GEP as well as plant biomass was also reported in a few previous studies [9,15,34,35]. Meanwhile,

the functional relationship between daily CH_4 fluxes and GEP shifted (Figure 4) between growth stages. The linear response of CH_4 fluxes to GEP indicated a direct limitation of substrate supply for methanogenesis in the early cultivation stage while the exponential response might indicate multiple processes associated with GEP controls on CH_4 fluxes in the later stage related to carbon supply and transport processes. The slope of CH_4 flux to GEP becomes smaller after the MSD maybe due to a limited environmental condition for CH_4 production during the AWD period. Overall, the evidence of GEP dominating CH_4 fluxes highlights the importance of rice plant productivity in controlling CH_4 emissions.

Table 2. The results of Partial F test for daily CH_4 fluxes and other variables before and after the mid-season drainage. Signifiant codes: 0 '***' 0.001 '**' 0.01 '*' 0.05 '.' 0.1 ' ' 1.

Year	Period	GEP	Tg	Pa	u*	VWC	WTD	Cond
2016	Before MSD	**66.87** ***	3.91	3.55	8.99 *	0.11		
2017		**18.36** **	24.64 **	0.01	0.54	0.15		
2018		**22.94** ***	8.47 *	9.15	0.60		2.56	4.10
2016	After MSD	**171.29** ***	18.14 ***	5.22 *	4.64 *	2.15		
2017		**157.40** ***	15.88 **	2.54	0.43	5.94 *		
2018		**86.74** ***	1.61	2.07	2.35		0.18	0.05

Table 3. Statistical tests (Coefficient of Determination (R^2) and Akaike Information Criterion (AIC)) for the biophysical drivers in the models of daily CH_4 fluxes in 2016–2018, including stepwise multivariate linear and hierarchical Neural Network Models. Daily CH_4 fluxes were log transformed before being fit with linear models. The results were only presented when the addition of the variable improved the R^2 of the model and was justified by a reduction in the AIC of the model. F_{CH4} is the daily CH_4 flux, Tg, Tw, GEP, VWC, u*, Pa, and spcond are abbreviated soil temperature, water temperature, gross ecosystem photosynthesis, volumetric water content, friction velocity, ambient pressure, and conductivity, respectively.

	Before Mid-Season Drainage			After Mid-Season Drainage		
Year	**Variable**	**R^2**	**AIC**	**Variable**	**R^2**	**AIC**
2016	GEP	0.83	−49.76	GEP	0.79	−25.96
	GEP + Tg	0.87	−50.81	GEP + Tg	0.84	−32.07
	GEP + Tg + u*	0.92	−54.95	GEP + Tg + Pa	0.88	−36.96
	GEP + Tg + u* + Pa	0.98	−68.16	GEP + Tg+ Pa + u*	0.89	−38.74
				GEP + Tg+ Pa + VPD	0.89	−38.75
2017	GEP	0.60	−27.51	GEP	0.71	−42.84
	GEP + Tg	0.91	−43	GEP + Tg	0.73	−44.97
				GEP + Tg + VWC	0.85	−65.39
2018	GEP	0.52	−44.95	GEP	0.71	9.39
	GEP + Tg	0.63	−47.05	GEP + Tw	0.76	−3.18
	GEP + Tg + spcond	0.68	−47.18	GEP + Tw + spcond	0.77	−5.44
	GEP + Tg + spcond + WTD	0.73	−47.7	GEP + Tw + spcond + WTD	0.78	−4.53
	GEP + Tg + spcond + WTD + Pa	0.91	−55.82	GEP + Tw + spcond + WTD + Pa	0.80	−10.45

Water management contributed to the changing magnitude of daily CH_4 fluxes in the rice season. For example, daily CH_4 fluxes sharply increased when the first flooded before the rice season and decreased during the operation of mid-season drainage in each year. Meanwhile, no significant positive correlation between CH_4 fluxes and VWC (even after accounting for possible time lags) was found at each growth stage (Figure 5a–e). CH_4 fluxes was significantly correlated to water table depth only during the ripening stage when water table depth was very low (<0) (Figure 5j). However, daily CH_4 fluxes was significantly correlated with water table depth when analyzing the entire rice growing season even though no significant correlation was observed for the vegetative, mid-season drainage, and reproductive stages (Figure 5f).

Although the results highlight the importance of plants control on CH_4 fluxes in rice paddies, the effect of environmental factors remains important. Higher soil temperature can enhance methanogenesis, molecular diffusion, and transport within plants [36–38]. Although the relative importance was less than GEP, soil temperature was significantly correlated with CH_4 fluxes during some growth stages (Table 2). Anaerobic soil conditions, which depend on soil water content in rice fields, are a prerequisite for CH_4 production by methanogens in rice paddies. This dependence on anaerobic conditions could explain why CH_4 fluxes decreased during the middle season drainage in each year. The significance between daily CH_4 fluxes and water table depth (<0) also indicated the importance of soil water conditions which decides anaerobic conditions of the paddy fields on CH_4 flux.

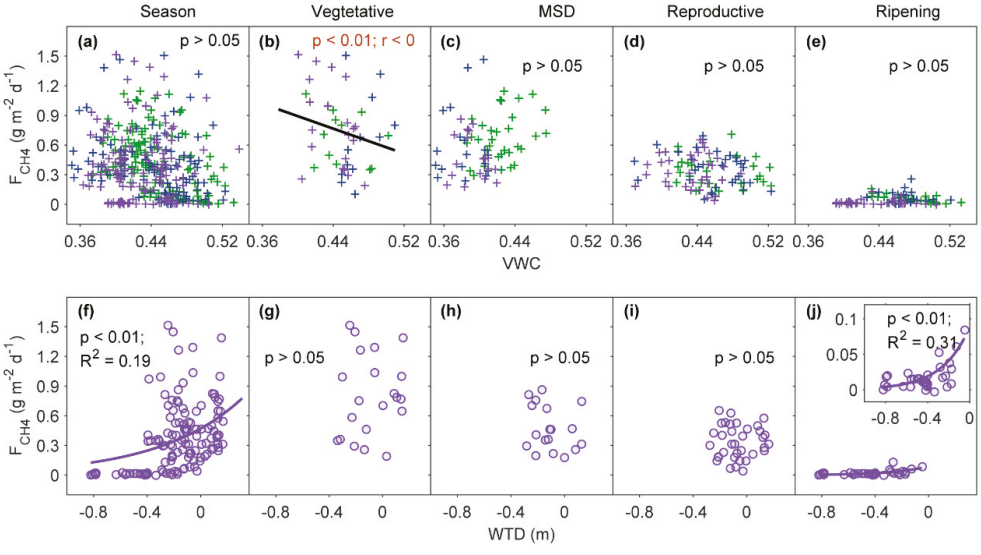

Figure 5. The relationship between daily CH_4 fluxes and volumetric water content (VWC, (**a**–**e**)) in 2016 (green), 2017 (blue) and 2018 (purple), water table depth (WTD, (**f**–**j**)) in 2018 (purple) over the whole rice season (**a**,**f**), during the vegetative stage (**b**,**g**), during the mid-season drainage periods (**c**,**h**), during the reproductive stage (**d**,**i**), during the ripening stage (**e**,**j**). Daily CH_4 fluxes and VWC showed a significant negative correlation only during the vegetative stage (**b**). Daily CH_4 fluxes and WTD showed a significant positive correlation for the whole season (**f**) and during the ripening stage when WTD was very low (**j**).

3.2. Annual C and GHG Budgets

For the wheat season, cumulative CO_2 uptake were estimated at 683.61 ± 43.26, 579.87 ± 50.68, 617.98 ± 4.91 g CO_2 m^{-1} in 2016, 2017, and 2018, respectively (Table 4). Wheat cumulative CH_4 emissions were 3.45 ± 0.40, 2.55 ± 0.13, 4.27 ± 0.21, g CH_4 m^{-1} in 2016, 2017, and 2018, respectively. In total, wheat season acted as both net C and GHG sink (averaged 168.97 g C m^{-2} and 1648.39 g CO_2eq m^{-2}, respectively).

For the rice season, cumulative CO_2 uptake was estimated at −2048.34 ± 193.50, −1299.69 ± 107.91, −839.56 ± 91.62 g CO_2 m^{-1} in 2016, 2017, and 2018, respectively (Table 4). Rice cumulative CH_4 emissions were 59.42 ± 5.11, 57.68 ± 4.90, 56.88 ± 6.29, g CH_4 m^{-1} in 2016, 2017, and 2018, respectively. In total, although rice season acted as a net C sink (averaged 337.20 g C m^{-2}), it existed a GHG source (averaged 227.98 g CO_2eq m^{-2} for 3 years) due to great CH_4 emissions except for the season with very high seeding density in 2016 [16].

Both the wheat and rice season acted as large atmospheric sinks for CO_2 and sources for CH_4. The averaged CO_2 uptakes and CH_4 emissions in rice seasons were 2.2 and 20.9 folds of the wheat seasons, respectively (Table 4). In sum, the rice-wheat rotation

agroecosystem acted as net C sink (averaged 460.79 g C m^{-2}) and GHG source (averaged 174.38 g CO_2eq m^{-2} in 2017–2018) except for 2016. Although the magnitude of CO_2 and CH_4 budget in our study were higher than results reported from other regions [7,12,39–41], they are comparable with EC measurements in the near province of Jiangsu in China [9,10]. The harvest carbon was not accounted for in this study, while rice season might be a C source when harvested carbon was added [42]. The N_2O emissions was not included in the calculation of GHG budget in this study, while N_2O emission especially in the wheat season is a very strong source for atmosphere N_2O.

Table 4. Annual sums of net CO_2 fluxes, GEP, CH_4 fluxes, total ecosystem carbon (C) and greenhouse gas (GHG) budgets in wheat and rice season were estimated. The total C and GHG budget for one year were also calculated.

Season		NEE	GEP	CH_4		C Budget	GHG Budget
		g C m^{-2}	g C m^{-2}	g C m^{-2}	g CO_2eq m^{-2}	g C m^{-2}	g CO_2eq m^{-2}
2016	wheat	−186.44	972.03	2.03	75.91	−184.41	−607.71
	rice	−558.64	1786.52	44.56	1663.74	−514.08	−384.60
	year	−689.13	2743.44	48.86	1824.00	−640.27	−702.81
2017	wheat	−158.15	857.22	1.98	74.03	−156.17	−505.84
	rice	−354.46	1573.59	43.26	1615.06	−311.20	315.37
	year	−407.31	2535.42	46.23	1726.03	−361.08	232.54
2018	wheat	−168.54	1195.16	2.22	83.13	−166.32	−534.84
	rice	−228.97	1474.50	42.66	1592.73	−186.31	753.17
	year	−425.98	2675.04	44.95	1678.14	−381.03	116.21

More than half of the global rice crop experience drought and high temperatures, which are predicted to become more frequent under climate change, resulting that water-saving techniques have been widely employed in rice cropping regimes [17–20]. In some models [18], CH_4 fluxes are often predicted as a function of soil temperature and/or other environmental variables while the importance of rice plant controls on CH_4 fluxes is rarely accounted for. We found daily GEP is a good predictor (R^2: 0.52–0.83) of daily CH_4 fluxes if accounting for growth stage specific responses in water-saving paddy fields. Thus, more studies are needed to further optimize the prediction of CH_4 fluxes in rice paddies under climate change. The strong connection between GEP and CH_4 flux found in this study indicates a possible trade-off in using irrigated ecosystems for carbon capture and sequestration [43,44]. Meanwhile, increasing human population demands for food further increases in rice production. Thus, a balance between increase of photosynthetically fixed carbon for rice grain yield and mitigation of methane emissions is required for irrigated rice fields. In addition to water limiting techniques, practices to control excessive carbon input such as a better-informed management of planting density [16] and to decrease the plant-mediated transport of CH_4 similar to a modified rice plant with low stomatal density has a great potential to limit increases in CH_4 emissions.

4. Conclusions

In this paper, we analyzed 3 consecutive years of eddy covariance measurements of CH_4 fluxes from a rice-wheat rotation agroecosystem located in Southeast China. The wheat-rice rotation agroecosystem acted as a large net C sink (averaged 460.79 g C m^{-2}) and a GHG (averaged 174.38 g CO_2eq m^{-2}) source except for a GHG sink in one year with a very high rice seeding density. The averaged CO_2 uptakes and CH_4 emissions in rice seasons were 2.2 and 20.9 folds of the wheat seasons, respectively. Although daily CH_4 flux and GEP existed not significantly correlated for the whole season, GEP dominates the control of CH_4 flux when the rice season was divided into the periods before and after the mid-season drainage. The reason is that the functional relationship between daily CH_4 flux and GEP shifted between growth stages. The separate analysis for each rice growing stage can be a helpful way to identify the factors of CH_4 flux in rice paddies. We highlight daily GEP was a good predictor of daily CH_4 flux in rice paddies.

Author Contributions: Conceptualization, H.L., C.P. and H.G.; methodology, H.L., M.Z. and C.P.; software, H.L.; validation, Q.W., H.G. and B.Z.; investigation, M.Z.; resources, M.Z.; data curation, H.L.; writing—original draft preparation, H.L.; writing—review and editing, H.L., M.Z., C.P., H.G., Q.W., and B.Z.; visualization, C.P.; supervision, C.P. and B.Z.; project administration, H.L., M.Z. and B.Z.; funding acquisition, H.L., M.Z., Q.W. and B.Z. All authors have read and agreed to the published version of the manuscript.

Funding: This research was funded by the National Natural Science Foundation of China (Grant No. 32101337), the Fundamental Research Funds for the Central Universities (No. 2021CDJQY-023), the Science and Technology Commission of Shanghai Municipality (17DZ1202100 and 20dz1204703).

Informed Consent Statement: Informed consent was obtained from all subjects involved in the study.

Data Availability Statement: All data used in the study are available from the corresponding author by request.

Acknowledgments: Hong Li acknowledges the obtaining postdoctoral fellowship from the University of Quebec at Montreal (UQAM). The authors thank Mengshan Zhang and Shengqi Dai for assistance in the field experiments.

Conflicts of Interest: The authors declare no conflict of interest.

References

1. Myhre, G.; Shindell, D.; Bréon, F.M.; Collins, W.; Fuglestvedt, J.; Huang, J. Anthropogenic and Natural Radiative Forcing. *Clim. Chang.* **2013**, *423*, 658–740.
2. Saunois, M.; Stavert, A.R.; Poulter, B.; Bousquet, P.; Canadell, J.G.; Jackson, R.B.; Raymond, P.A.; Dlugokencky, E.J.; Houweling, S.; Patra, P.K.; et al. The Global Methane Budget: 2000–2017. Under Open Review for Earth System Science Data. *Earth Syst. Sci. Data* **2019**. [CrossRef]
3. *IPCC Climate Change 2014: Impacts, Adaptation, and Vulnerability Working Group II Contribution to the Fifth Assessment Report*; Cambridge University Press: Cambridge, UK, 2014.
4. Aulakh, M.S.; Wassmann, R.; Rennenberg, H. Methane emissions from rice fields—Quantification, mechanisms, role of management, and mitigation options. In *Advances in Agronomy*; Academic Press: Cambridge, MA, USA, 2001; Volume 70, pp. 193–260.
5. Chen, H.; Zhu, Q.; Peng, C.; Wu, N.; Wang, Y.; Fang, X.; Jiang, H.; Xiang, W.; Chang, J.; Deng, X.; et al. Methane Emissions from Rice Paddies Natural Wetlands, Lakes in China: Synthesis New Estimate. *Glob. Chang. Biol.* **2013**, *19*, 19–32. [CrossRef]
6. Baldocchi, D.D. Assessing the Eddy Covariance Technique for Evaluating Carbon Dioxide Exchange Rates of Ecosystems: Past, Present and Future. *Glob. Chang. Biol.* **2003**, *9*, 479–492. [CrossRef]
7. Meijide, A.; Manca, G.; Goded, I.; Magliulo, V.; di Tommasi, P.; Seufert, G.; Cescatti, A. Seasonal Trends and Environmental Controls of Methane Emissions in a Rice Paddy Field in Northern Italy. *Biogeosciences* **2011**, *8*, 3809–3821. [CrossRef]
8. Baldocchi, D.D. How Eddy Covariance Flux Measurements Have Contributed to Our Understanding of Global Change Biology. *Glob. Chang. Biol.* **2020**, *26*, 242–260. [CrossRef] [PubMed]
9. Dai, S.; Ju, W.; Zhang, Y.; He, Q.; Song, L.; Li, J. Variations and Drivers of Methane Fluxes from a Rice-Wheat Rotation Agroecosystem in Eastern China at Seasonal and Diurnal Scales. *Sci. Total Environ.* **2019**, *690*, 973–990. [CrossRef]
10. Ge, H.-X.; Zhang, H.-S.; Zhang, H.; Cai, X.-H.; Song, Y.; Kang, L. The Characteristics of Methane Flux from an Irrigated Rice Farm in East China Measured Using the Eddy Covariance Method. *Agric. For. Meteorol.* **2018**, *249*, 228–238. [CrossRef]
11. Knox, S.H.; Jackson, R.B.; Poulter, B.; McNicol, G.; Fluet-Chouinard, E.; Zhang, Z.; Hugelius, G.; Bousquet, P.; Canadell, J.G.; Saunois, M.; et al. FLUXNET-CH4 Synthesis Activity: Objectives, Observations, and Future Directions. *Bull. Am. Meteor. Soc.* **2019**, *100*, 2607–2632.
12. Hatala, J.A.; Detto, M.; Baldocchi, D.D. Gross Ecosystem Photosynthesis Causes a Diurnal Pattern in Methane Emission from Rice. *Geophys. Res. Lett.* **2012**, *39*, L06409. [CrossRef]
13. McNicol, G.; Knox, S.H.; Guilderson, T.P.; Baldocchi, D.D.; Silver, W.L. Where Old Meets New: An Ecosystem Study of Methanogenesis in a Reflooded Agricultural Peatland. *Glob. Chang. Biol.* **2020**, *26*, 772–785. [PubMed]
14. Chu, H.; Chen, J.; Gottgens, J.F.; Ouyang, Z.; John, R.; Czajkowski, K.; Becker, R. Net Ecosystem Methane and Carbon Dioxide Exchanges in a Lake Erie Coastal Marsh and a Nearby Cropland. *J. Geophys. Res. Biogeosci.* **2014**, *119*, 722–740. [CrossRef]
15. Knox, S.H.; Matthes, J.H.; Sturtevant, C.; Oikawa, P.Y.; Verfaillie, J.; Baldocchi, D. Biophysical Controls on Interannual Variability in Ecosystem-Scale CO_2 and CH4 Exchange in a California Rice Paddy. *J. Geophys. Res. Biogeosci.* **2016**, *121*, 978–1001. [CrossRef]
16. Li, H.; Guo, H.-Q.; Helbig, M.; Dai, S.-Q.; Zhang, M.-S.; Zhao, M.; Peng, C.-H.; Xiao, X.-M.; Zhao, B. Does Direct-Seeded Rice Decrease Ecosystem-Scale Methane Emissions?—A Case Study from a Rice Paddy in Southeast China. *Agric. For. Meteorol.* **2019**, *272–273*, 118–127.
17. Chauhan, B.S.; Jabran, K.; Mahajan, G. (Eds.) *Rice Production Worldwide*; Springer International Publishing: Cham, Switzerland, 2017; ISBN 978-3-319-47514-1.

18. Li, C.; Qiu, J.; Frolking, S.; Xiao, X.; Salas, W.; Moore, B.; Boles, S.; Huang, Y.; Sass, R. Reduced Methane Emissions from Large-Scale Changes in Water Management of China's Rice Paddies during 1980–2000. *Geophys. Res. Lett.* **2002**, *29*, 1972. [CrossRef]
19. Liu, S.; Zhang, Y.; Lin, F.; Zhang, L.; Zou, J. Methane and Nitrous Oxide Emissions from Direct-Seeded and Seedling-Transplanted Rice Paddies in Southeast China. *Plant Soil* **2014**, *374*, 285–297. [CrossRef]
20. Yadav, S.; Gill, G.; Humphreys, E.; Kukal, S.S.; Walia, U.S. Effect of Water Management on Dry Seeded and Puddled Transplanted Rice. Part 1: Crop Performance. *Field Crop. Res.* **2011**, *120*, 112–122. [CrossRef]
21. Caine, R.S.; Yin, X.; Sloan, J.; Harrison, E.L.; Mohammed, U.; Fulton, T.; Biswal, A.K.; Dionora, J.; Chater, C.C.; Coe, R.A.; et al. Rice with Reduced Stomatal Density Conserves Water and Has Improved Drought Tolerance under Future Climate Conditions. *New Phytol.* **2019**, *221*, 371–384. [CrossRef]
22. Damour, G.; Simonneau, T.; Cochard, H.; Urban, L. An Overview of Models of Stomatal Conductance at the Leaf Level. *Plant Cell Environ.* **2010**, *33*, 1419–1438. [CrossRef]
23. Kumar, A.; Nayak, A.K.; Mohanty, S.; Das, B.S. Greenhouse Gas Emission from Direct Seeded Paddy Fields under Different Soil Water Potentials in Eastern India. *Agric. Ecosyst. Environ.* **2016**, *228*, 111–123. [CrossRef]
24. Li, H.; Dai, S.; Ouyang, Z.; Xie, X.; Guo, H.; Gu, C.; Xiao, X.; Ge, Z.; Peng, C.; Zhao, B. Multi-Scale Temporal Variation of Methane Flux and Its Controls in a Subtropical Tidal Salt Marsh in Eastern China. *Biogeochemistry* **2018**, *137*, 163–179. [CrossRef]
25. Vickers, D.; Mahrt, L. Quality Control and Flux Sampling Problems for Tower and Aircraft Data. *J. Atmos. Ocean. Technol.* **1997**, *14*, 512–526. [CrossRef]
26. Wilczak, J.M.; Oncley, S.P.; Stage, S.A. Sonic Anemometer Tilt Correction Algorithms. *Bound.-Layer Meteorol.* **2001**, *99*, 127–150. [CrossRef]
27. Webb, E.K.; Pearman, G.I.; Leuning, R. Correction of Flux Measurements for Density Effects Due to Heat and Water Vapour Transfer. *Q. J. R. Meteorol. Soc.* **1980**, *106*, 85–100. [CrossRef]
28. Finkelstein, P.L.; Sims, P.F. Sampling Error in Eddy Correlation Flux Measurements. *J. Geophys. Res.-Atmos.* **2001**, *106*, 3503–3509. [CrossRef]
29. Reichstein, M.; Falge, E.; Baldocchi, D.; Papale, D.; Aubinet, M.; Berbigier, P.; Bernhofer, C.; Buchmann, N.; Gilmanov, T.; Granier, A.; et al. On the Separation of Net Ecosystem Exchange into Assimilation and Ecosystem Respiration: Review and Improved Algorithm. *Glob. Chang. Biol.* **2005**, *11*, 1424–1439. [CrossRef]
30. Foken, T.; Gockede, M.; Mauder, M.; Mahrt, L.; Amiro, B.; Munger, W. Post-field data quality control. In *Handbook of Micrometeorology: A Guide for Surface Flux Measurement and Aanlysis*; Springer: Berlin/Heidelberg, Germany, 2004; Volume 29, pp. 181–208. ISBN 1383-8601.
31. Kim, Y.; Johnson, M.S.; Knox, S.H.; Black, T.A.; Dalmagro, H.J.; Kang, M.; Kim, J.; Baldocchi, D. Gap-Filling Approaches for Eddy Covariance Methane Fluxes: A Comparison of Three Machine Learning Algorithms and a Traditional Method with Principal Component Analysis. *Glob. Chang. Biol.* **2020**, *26*, 1499–1518. [CrossRef]
32. Aurela, M.; Laurila, T.; Tuovinen, J. Annual CO_2 Balance of a Subarctic Fen in Northern Europe: Importance of the Wintertime Efflux. *J. Geophys. Res. Atmos.* **2002**, *10*, 1–12. [CrossRef]
33. Zhang, A.; Bian, R.; Pan, G.; Cui, L.; Hussain, Q.; Li, L.; Zheng, J.; Zheng, J.; Zhang, X.; Han, X.; et al. Effects of Biochar Amendment on Soil Quality, Crop Yield and Greenhouse Gas Emission in a Chinese Rice Paddy: A Field Study of 2 Consecutive Rice Growing Cycles. *Field Crop. Res.* **2012**, *127*, 153–160. [CrossRef]
34. Chanton, J.P.; Whiting, G.J.; Blair, N.E.; Lindau, C.W.; Bollich, P.K. Methane Emission from Rice: Stable Isotopes, Diurnal Variations, and CO_2 Exchange. *Glob. Biogeochem. Cycles* **1997**, *11*, 15–27. [CrossRef]
35. Huang, Y.; Sass, R.; Fisher, F. Methane Emission from Texas Rice Paddy Soils. 2. Seasonal Contribution of Rice Biomass Production to CH_4 Emission. *Glob. Chang. Biol.* **1997**, *3*, 491–500. [CrossRef]
36. Chanton, J.P. The Effect of Gas Transport on the Isotope Signature of Methane in Wetlands. *Org. Geochem.* **2005**, *36*, 753–768. [CrossRef]
37. Holzapfel-Pschorn, A.; Conrad, R.; Seiler, W. Effects of Vegetation on the Emission of Methane from Submerged Paddy Soil. *Plant Soil* **1986**, *92*, 223–233. [CrossRef]
38. Kim, J.; Verma, S.B.; Billesbach, D.P.; Clement, R.J. Diel Variation in Methane Emission from a Midlatitude Prairie Wetland: Significance of Convective Throughflow in Phragmites Australis. *J. Geophys. Res. Atmos.* **1998**, *103*, 28029–28039. [CrossRef]
39. Alberto, M.C.R.; Wassmann, R.; Buresh, R.J.; Quilty, J.R.; Correa, T.Q., Jr.; Sandro, J.M.; Centeno, C.A.R. Measuring Methane Flux from Irrigated Rice Fields by Eddy Covariance Method Using Open-Path Gas Analyzer. *Field Crop. Res.* **2014**, *160*, 12–21. [CrossRef]
40. Centeno, C.A.R.; Alberto, M.C.R.; Wassmann, R.; Sander, B.O. Assessing Diel Variation of CH4 Flux from Rice Paddies through Temperature Patterns. *Atmos. Environ.* **2017**, *167*, 23–39. [CrossRef]
41. Swain, C.K.; Bhattacharyya, P.; Nayak, A.K.; Singh, N.R.; Neogi, S.; Chatterjee, D.; Pathak, H. Dynamics of Net Ecosystem Methane Exchanges on Temporal Scale in Tropical Lowland Rice. *Atmos. Environ.* **2018**, *191*, 291–301. [CrossRef]
42. Knox, S.H.; Sturtevant, C.; Matthes, J.H.; Koteen, L.; Verfaillie, J.; Baldocchi, D. Agricultural Peatland Restoration: Effects of Land-Use Change on Greenhouse Gas (CO_2 and CH_4) Fluxes in the Sacramento-San Joaquin Delta. *Glob. Chang. Biol.* **2015**, *21*, 750–765. [CrossRef]

43. Hemes, K.S.; Chamberlain, S.D.; Eichelmann, E.; Knox, S.H.; Baldocchi, D.D. A Biogeochemical Compromise: The High Methane Cost of Sequestering Carbon in Restored Wetlands. *Geophys. Res. Lett.* **2018**, *45*, 6081–6091. [CrossRef]
44. van der Gon, H.; Kropff, M.J.; van Breemen, N.; Wassmann, R.; Lantin, R.S.; Aduna, E.; Corton, T.M.; van Laar, H.H. Optimizing Grain Yields Reduces CH4 Emissions from Rice Paddy Fields. *Proc. Natl. Acad. Sci. USA* **2002**, *99*, 12021–12024. [CrossRef]

land

MDPI

Article

Vulnerability Assessment of Maize Yield Affected by Precipitation Fluctuations: A Northeastern United States Case Study

Peng Su [1], Shiqi Li [2], Jing'ai Wang [1,3,*] and Fenggui Liu [1,4]

[1] School of Geographical Science, Qinghai Normal University, Xining 810008, China; 201947331031@stu.qhnu.edu.cn (P.S.); liufenggui@igsnrr.ac.cn (F.L.)
[2] Spatial Science Institute, University of Southern California, Los Angeles, CA 90089, USA; shiqi@usc.edu
[3] Faculty of Geographical Science, Beijing Normal University, Beijing 100875, China
[4] Academy of Plateau Science and Sustainability, Xining 810008, China
* Correspondence: jwang@bnu.edu.cn

Abstract: Crop yields are threatened by global climate change. Maize has high water requirements, and precipitation fluctuations can impact its yield. In this study, we used the Environmental Policy Integrated Climate (EPIC) model to simulate maize yields in eight northeastern U.S. states. We used precipitation fluctuations and the coefficient of variation (CV) of yield as indicators to construct a vulnerability curve for the CV of yield and precipitation fluctuations. We then evaluated the vulnerability of maize yields under precipitation fluctuations in the region. We obtained the following results: (1) the fitted vulnerability curves were classified into three categories (positive slope, negative slope, and insignificant fit), of which the first category accounted for about 92.7%, indicating that the CV of maize yield was positively correlated with precipitation fluctuations in most parts of the study area; and (2) the CV of maize yield under 11 precipitation fluctuation scenarios was mapped to express the CV at the spatial level, and the maize yield in Connecticut and Maryland proved to be the most sensitive to precipitation fluctuations. This study provided a theoretical and experimental basis for the prevention of maize yield risk under fluctuating precipitation conditions.

Keywords: precipitation fluctuation; vulnerability curve; maize yield; EPIC model; risk assessment

Citation: Su, P.; Li, S.; Wang, J.; Liu, F. Vulnerability Assessment of Maize Yield Affected by Precipitation Fluctuations: A Northeastern United States Case Study. *Land* **2021**, *10*, 1190. https://doi.org/10.3390/land10111190

Academic Editors: Baojie He, Ayyoob Sharifi, Chi Feng and Jun Yang

Received: 24 September 2021
Accepted: 1 November 2021
Published: 5 November 2021

1. Introduction

High and stable crop yields are the key to food security and sustainable development. Since the beginning of industrialization, global surface temperatures have increased in the context of climate change, which has led to an increase in terrestrial droughts and greater fluctuations in precipitation, thus adversely affecting food production [1]. Therefore, researchers are increasingly turning their attention to studying the relationships between climate change and crop yield, assessing crop vulnerability under climate change conditions, and preventing and mitigating the effects of hazards caused by climate change on crop yield [2–4]. Vulnerability studies are useful to analyze the impact of precipitation fluctuations on maize yields, so that appropriate planting adjustments can be made to stabilize crop yields.

Disaster risk assessment in a broad sense is a holistic risk assessment of a hazard system based on separate assessments of the hazard-bearing body, the hazard intensity, and the environment [5]. Vulnerability is an important component of crop risk assessment, where vulnerability is defined as the response of the hazard-bearing body to damage by the hazard [6,7]. Vulnerability is used to measure the degree of damage caused to a crop [8]. Vulnerability curves are a way to visually represent losses at each level of hazard causation. The representation of the vulnerability curve consists of two components: the hazard and the hazard-bearing body. Regarding the hazard, Shi et al. [9] divided climate change into

three parts: trends, fluctuations, and extreme events. At present, most studies on vulnerability have focused on extreme events [10–13], and fewer studies have been conducted on trends [14,15] and especially on fluctuations [7]. For example, Zhong et al. [16] assessed the drought risk in the Yun-Gui-Guang region of China by using vulnerability curves, and they calculated agricultural losses under different drought levels; Li et al. [17] studied maize yield loss caused by excessive rainfall in the United States, highlighting the need to study the impact of excessive rainfall on crop yield; Jayanthi et al. [18] obtained drought vulnerability curves for maize by fitting the relative evapotranspiration deficit and relative maize yield loss. It is thus clear that current vulnerability studies focus on direct crop losses, while equally important studies on the yield stability of crops and other responses to climate change are lacking.

Precipitation fluctuations are fluctuations relative to long-term average precipitations [19]. Unlike direct damage to crop yield by extreme precipitation events, precipitation fluctuations can impact on the mean crop yield and its stability at multiple spatial scales [20,21]. Lobell and Burke [22] found that changes in the standard deviation of inter-annual precipitation in the growing season can lead to yield variations of South Asian cereals of up to 8%; Hamilton et al. [23] found that seasonal precipitation variations were positively correlated with changes in forage yield in south-eastern Wyoming, with the yield variation in forage reaching 25.5% under a scenario of a 50% increase in standard deviation of precipitation. All the above studies demonstrated that increased precipitation fluctuations led to increased variability in crop yields and increased crop yield instability; however, these studies did not implement this relationship as a functional relationship and lacked spatialized expressions. Thus, further relationship characterization is still needed.

To construct vulnerability curves using crop yields and climate characteristics, a crop model is required to simulate the relationship between crop growth and yield [24]. Crop models are based on systems science, with temperature, moisture, light, and soil as environmental driving variables, and they use computer technology and mathematical and physical methods to simulate the relationship between crop growth and yield [25,26]. The Environmental Policy Integrated Climate (EPIC) model is one of the models that has been widely used for crop vulnerability studies [27–32]. Jia et al. [33] used the EPIC model to simulate maize yield under different moisture stresses in the Huang-Huai-Hai plain in northern China, resulting in a drought vulnerability curve for the summer maize region, and further mapped the yield loss distribution under different hazard intensities. Wang et al. [34] used the EPIC model to calculate the rate of wheat yield loss of two typical wheat varieties in China under varying water drought stresses, and evaluated the drought vulnerability of wheat in China. Guo et al. [35] used the EPIC model with several irrigation scenarios to construct several global three-dimensional maize drought vulnerability surfaces.

In summary, the use of vulnerability curves to study the vulnerability of crop yield can describe crop losses for different degrees of hazard intensities. In this study, we simulated and plotted maize yield vulnerability curves under different precipitation fluctuation scenarios based on meteorological and crop statistics for eight northeastern U.S. states from 1981 to 2015, to investigate multi-year precipitation fluctuations and maize yield vulnerability. The objectives of this paper were as follows: (1) fit the vulnerability curves between different precipitation fluctuation scenarios and the CV of maize yield, to quantify the functional relationship between maize yield stability and precipitation fluctuation; and (2) spatialize the vulnerability curve characteristics to characterize the degree of vulnerability in different regions. Thus, mitigation measures can be formulated to reduce crop yield instability caused by precipitation fluctuations and to ensure the stability of grain production.

2. Materials and Methods

2.1. Basic Idea and Research Framework

This study focused on the construction of vulnerability curves for maize under precipitation fluctuation scenarios, and analyzed the CV of maize yields under these different scenarios. The framework of this study was as follows: (1) set 11 precipitation fluctuation scenarios and invert 11 precipitation datasets according to the fluctuation scenario; (2) use the EPIC model to calculate maize yield under each fluctuation scenario; and (3) calculate the CV based on simulated maize yields. The results of the EPIC model were also validated using actual maize yield data for the 5-year period from 2000 to 2004, to prove the usability of the EPIC model simulation results.

The overall research framework for the study is shown in Figure 1.

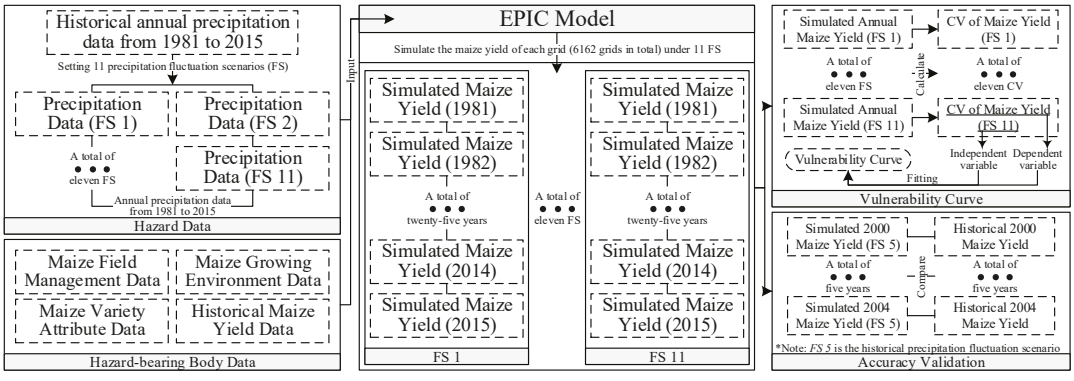

Figure 1. Research framework for the study.

2.2. Case Study

As the world's top exporter of agricultural products, the United States also ranks first in the world in maize production [36]. The northeastern United States region belongs to the mixed agricultural belt, its agriculture being dominated by dairy livestock farming [37]. Silage corn is also grown in large quantities locally as livestock feed [38]. Maize is one of the three major food crops in the world [39], and the yield instability of this crop can have a large economic impact on the world and even threaten world food security [40]. The sensitivity of maize to water scarcity is increasing under a changing climate; thus, it is important to study the vulnerability of maize to precipitation fluctuations.

The study area consisted of eight states in the northeastern United States with a total area of about 399,035 km^2 and a land area of about 362,135 km^2, including New York, Connecticut, Pennsylvania, New Jersey, Delaware, Maryland, West Virginia, and Virginia (Figure 2). The topography of the region has a relative elevation difference of about 1700 m, with many plateaus and mountains, and the Appalachian Mountains running through it. The northern part of the region has a humid continental climate, while the southern part has a humid subtropical climate. The region encompasses the political and economic centers of the United States, and has a large population, accounting for 22% of the total population of the United States.

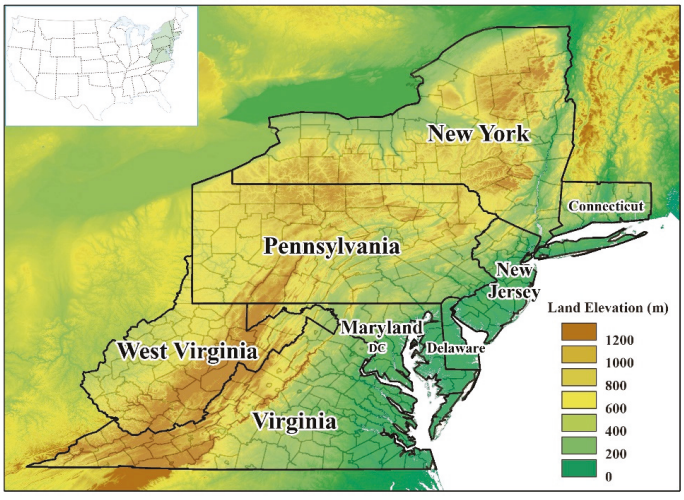

Figure 2. Location map of study area with elevation.

2.3. Data Collection

The data used in this study were divided into three categories (Table 1). The first category was natural environmental data. It included elevation data from the United States Geological Survey (USGS) and slope data calculated from elevation; precipitation, temperature, and wind speed data generated under the GEM2-ES climate model; fertilizer application data from the Socioeconomic Data and Applications Centre (SEDAC); and Soil data from the International Soil Reference and Information Centre (ISRIC). These data were input into the EPIC model. The second category was crop statistics data, including county-by-county maize production and state-by-state growing season information from the United States Department of Agriculture (USDA). The third category was geographic information data. It included state and county boundary vector data and land use data. The boundary data were obtained from the USDA. Land use data used to map farmland came from the Food and Agriculture Organization (FOA).

Table 1. Database.

Data Name	Spatial Resolution	Temporal Resolution	Unit	Source
Elevation	90 m × 90 m	2007	m	USGS-EarthExplorer https://earthexplorer.usgs.gov/ (accessed on 31 October 2021)
Slope	90 m × 90 m	2007	m	Calculated by ArcGIS
Land Use	5′ × 5′	2015	/	EarthStat, FOA http://www.earthstat.org/ (accessed on 31 October 2021) http://www.fao.org/faostat/en/ (accessed on 31 October 2021)
Historical Crop Yield	County unit	2000–2004	t/ha	USDA/NASS QuickStats https://www.nass.usda.gov/Quick_Stats/ (accessed on 31 October 2021)
Fertilization	0.5° × 0.5°	2010	kg/ha	SEDAC https://sedac.ciesin.columbia.edu/ (accessed on 31 October 2021)

Table 1. *Cont.*

Data Name	Spatial Resolution	Temporal Resolution	Unit	Source
Irrigation	County unit	2015	$10^6/m^3$	USGS https://pubs.er.usgs.gov/publication/cir1441 (accessed on 31 October 2021)
Crop Growth Period	State unit	/	/	USDA/NASS QuickStats https://www.nass.usda.gov/Quick_Stats/ (accessed on 31 October 2021)
Soil Type	$5' \times 5'$	2012	/	ISRIC-WISE https://www.isimip.org/gettingstarted/input-data-bias-correction/ (accessed on 31 October 2021)
Precipitation	$0.5° \times 0.5°$	1971–2015	mm	ISIMIP-hadGEM2-ES https://www.isimip.org/gettingstarted/input-data-bias-correction/ (accessed on 31 October 2021)
Temperature	$0.5° \times 0.5°$	1971–2015	°C	ISIMIP-hadGEM2-ES https://www.isimip.org/gettingstarted/input-data-bias-correction/ (accessed on 31 October 2021)
Wind Speed	$0.5° \times 0.5°$	1971–2015	m/s	ISIMIP-hadGEM2-ES https://www.isimip.org/gettingstarted/input-data-bias-correction/ (accessed on 31 October 2021)
Administrative Boundary	County unit	2015	/	USDA/NASS QuickStats https://www.nass.usda.gov/Quick_Stats/ (accessed on 31 October 2021)

2.4. Methods

2.4.1. Calculation of Precipitation Fluctuations

Precipitation fluctuation can be defined as the interannual variation in precipitation after detrend. It can also be understood as the upward and downward variation of precipitation relative to the long-term average condition. Therefore, the standard deviation is generally used to characterize the fluctuation in precipitation. In this study, 11 precipitation fluctuation scenarios were pre-defined. Different scenarios were applied with 11 different precipitation fluctuation multiplicities (FLU): 20%, 40%, 60%, and 80% decreases in standard deviation; 0%, 20%, 40%, 60%, 80%, 100%, and 120% increases in standard deviation. According to a certain precipitation fluctuation scenario, this paper calculated the amount of precipitation corresponding to the scenario, as shown in Equation (1).

$$P(qj) = P + Std(P) \cdot \mathrm{FLU} \quad (1)$$

where $P(qj)$ refers to the annual precipitation under a certain precipitation fluctuation; P refers to the value of annual precipitation from 1981 to 2015; $Std(P)$ refers to the standard deviation of precipitation from 1981 to 2015; and FLU refers to the precipitation fluctuation multiplier with values from −80% to 120% in steps of 20%.

After calculating the annual precipitation for each year from 1981 to 2015 under the 11 precipitation fluctuation scenarios, this paper distributed the annual precipitation in proportion to each day and obtained the daily precipitation data for the 11 fluctuation scenarios. The daily precipitation data were used in the simulation of the EPIC model with daily steps. The detailed daily precipitation distribution process is shown in Equation (2).

$$P_{i,y}(qjd) = P(qj) \cdot \frac{P_{i,y}}{P_y} \quad (2)$$

where i refers to the ith day of the year; y refers to the year (from 1981 to 2015); $P_{i,y}(qjd)$ refers to the daily precipitation under a certain precipitation fluctuation; $P(qj)$ refers to the annual precipitation under a certain precipitation fluctuation; $P_{i,y}$ refers to the value of daily precipitation on the ith day of the y year; P_y refers to the value of annual precipitation of the y year.

2.4.2. Calculation of CV of Crop Yield

In calculating the crop yield variability, the trend of its yield increasing caused by technological progress should be excluded. Thus, the stability of crop yields can be expressed as the coefficient of variation (CV) of the base state multi-year yield. This paper referred to Zhao et al. [41] using the adjusted coefficient of variation to monitor the global trend of grain yield stability. The CV of crop yield is calculated by dividing the standard deviation of crop yield over many years by its arithmetic mean, as shown in Equation (3). A larger CV of crop yield indicates poorer yield stability.

$$\mathrm{CV} = \frac{\sigma}{\mu} \times 100\% \tag{3}$$

where CV refers to the coefficient of variation of maize yield, σ refers to the standard deviation of simulated maize yield in the study area for 35 years (from 1981 to 2015), and μ is the arithmetic mean of simulated maize yield in the study area for 35 years.

In this paper, the vulnerability curve was fitted using the precipitation fluctuation multiplier as the independent variable and the CV value of simulated maize yield as the dependent variable. The fitting equation was as follows (Equation (4)).

$$\mathrm{CV} = \mathrm{k} \times \mathrm{FLU} + \mathrm{b} \tag{4}$$

where the independent and dependent variables refer to the precipitation fluctuation multiplier (FLU) and the coefficient of variation (CV) of maize yield, respectively; k and b are parameters.

2.4.3. Maize Yield Simulation by Using the EPIC Model

The EPIC model is composed of numerous components, including an erosion module, hydrology module, weather generator, crop growth module, and crop management module. A general plant growth model with crop-specific parameters is used to simulate the growth of variety crops, such as rice, wheat, and maize [32]. We used the EPIC0509 version in this paper, which can be downloaded from http://epicapex.tamu.edu/epic/ (accessed on 31 October 2021).

Based on the data input requirements of the EPIC model [42], this paper divided the data in the study area into four categories: (1) maize growing environment data, including the meteorological data (highest temperature, lowest temperature, and precipitation data), terrain data (elevation and slope), and soil property data; (2) maize field management data, including fertilization data and irrigation data; (3) maize variety attribute data, including maize growth period; (4) historical maize yield data. After considering the resolution of the data used, the study area was divided into grids of $5' \times 5'$ (about 10 km). In this paper, the grids with a maize planting percentage greater than 0 were defined as maize planting areas, and 6162 grids were obtained by grid creation and screening by using ArcGIS. Each grid was used as an independent EPIC model run cell, the EPIC model input data for that grid were obtained by spatial overlay calculation in ArcGIS, and the batch EPIC model run on each grid was realized by MATLAB programming. In order to obtain crop yield variation under different precipitation fluctuation scenarios, this study set-up a simulation environment with no temperature stress, aerated stress, and nutrient stress (nitrogen stress, phosphorus stress, and potassium stress), and then simulated the impact of water stress on crop yield.

In the specific application of the EPIC model, the parameters should be adjusted according to the actual local conditions [43]. The model in this paper was adjusted with statistical yield data for five years during 2000–2004, modified the maize variety attribute data to reduce the difference between simulated and statistical yields, and iterated five times to obtain the final maize variety attribute data. These data were used as the final maize variety attributes input data to obtain the simulated yield results. The process is as Figure 3.

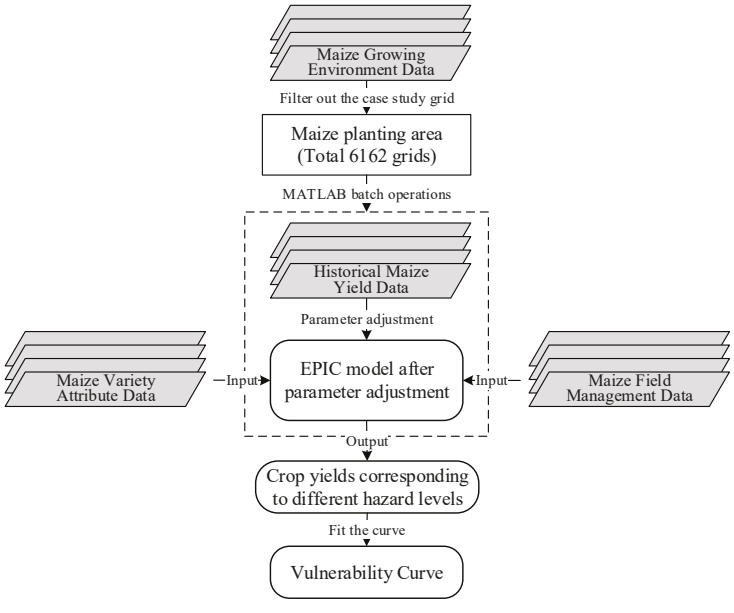

Figure 3. Process of EPIC model.

3. Results

3.1. Accuracy of Epic Model Maize Yield Simulation

In order to verify the accuracy of the simulated results calculated by the EPIC model, the simulated and actual maize yields for each year from 2000 to 2004 were plotted in scatter plots in this paper. The details are shown in Figure 4.

Pearson correlation analysis was conducted for simulated and actual average corn yields for each county from 2000 to 2004. The Pearson correlation coefficients between the average simulated and actual maize yields from 2000 to 2004 were 0.691, 0.195, 0.683, 0.444, and 0.592 (p-value < 0.001), respectively. The simulated yield was 6.81 t/ha and the historical yield was 6.86 t/ha, and the Pearson correlation coefficient was 0.495 ($p < 0.001$), indicating that the overall deviation in the simulated results was not significant. The over-origin fit was completed with the intercept-free model, and the fitted equation was y = 0.998x, with an RMSE of 0.949, indicating a good calibration of the EPIC model in this paper.

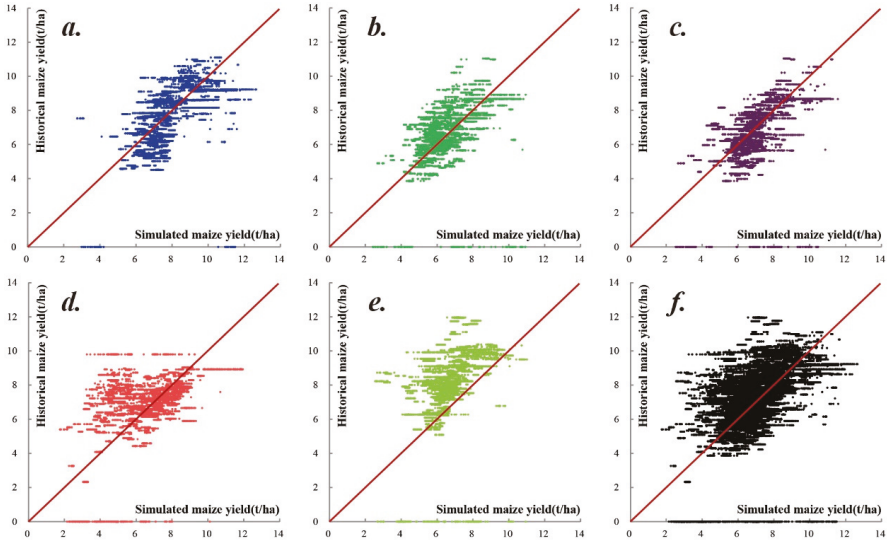

Figure 4. Correspondence between simulated and historical maize yield from years 2000 to 2004. Correspondence in 2000 (**a**); correspondence in 2001 (**b**); correspondence in 2002 (**c**); correspondence in 2003 (**d**); correspondence in 2004 (**e**); correspondence from 2000 to 2004 (**f**).

3.2. "Precipitation Fluctuation and Maize Yield Stability" Vulnerability Curve

Due to the spatial heterogeneity among different grids, it was not possible to plot the overall vulnerability curve for the study area. Therefore, the simulated yield data of 6162 grids in the study area were fitted to plot the "precipitation fluctuation and maize yield stability" vulnerability curve and to generate the corresponding functional equation. Based on the fitted coefficients and slopes, the curves were classified into three categories as follows. The vulnerability curves with a goodness of fit less than 0.6 were defined as Type III "precipitation fluctuation and maize yield stability" vulnerability curves. Type III vulnerability curves had slopes greater than zero or less than zero. These were considered to have an insignificant fit. Their scatter distribution was discrete and irregular. We spatialized Type I vulnerability curves and their slope distribution in Figure 5.

In these grids, the CV of simulated maize yield increased linearly with FLU, indicating that the yield stability deteriorated proportionately with increasing precipitation fluctuations. A total of 5713 grids resulted in Type I vulnerability curves, accounting for about 92.7% of the total maize planting grids. The grids with the lowest CV of maize yield under precipitation fluctuations were mostly located in New York, western Pennsylvania, southern New Jersey, and southern Virginia; the grids with a larger CV of maize yield under precipitation fluctuations were located in eastern Pennsylvania, Delaware, eastern Maryland, West Virginia, and northern Virginia; the grids with the largest CV of maize yield under precipitation fluctuations were located in Connecticut and central Maryland. This showed that maize yield stability in Connecticut and central Maryland was most strongly affected by precipitation fluctuations.

The CV of simulated maize yield decreased linearly with FLU, indicating that the yield stability improved proportionately with increasing precipitation fluctuations. A total of 17 grids were found to be Type II vulnerability curves, accounting for about 0.3% of the total maize planting grids. Type II vulnerability curves were clustered and distributed mainly near the southern state line in Virginia, and in discrete cases in northern New York. This indicated that there were very few cases where the CV decreased because of increasing precipitation fluctuations in the study area. We speculated that the irrigation

water volume of the grids with Type II curves basically meets the needs of maize growth, and precipitation has almost no effect on it.

A total of 433 grids were found as Type III vulnerability curves, accounting for about 7.0% of the total maize planting grids. Type III grids were mainly located in the northern part of New York, Pennsylvania, the southeast corner of Pennsylvania, and the southern part of Virginia. Type III vulnerability curves implied that the yield stability in these grids were less dependent on the precipitation variation. We speculated that field management is the dominant factor affecting maize yield stability in these grids.

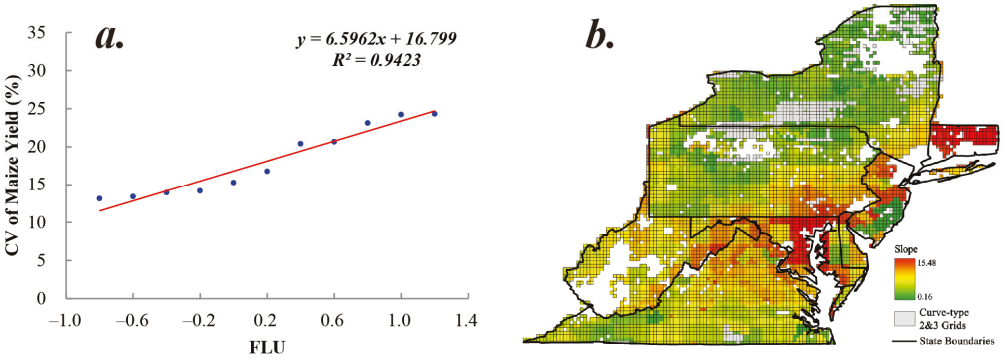

Figure 5. Type I vulnerability curve (**a**) and its slope distribution pattern (**b**).

3.3. Distribution Pattern of CV of Maize Yield under Different Precipitation Fluctuation Scenarios

The model simulation results showed that the CV of maize yield increased with FLU (Figure 6).

As seen in Figure 6, as FLU went from −0.8 to 1.2, the mean values of CV for maize yield in the study area were 0.128, 0.131, 0.137, 0.145, 0.155, 0.169, 0.183, 0.197, 0.208, 0.219, and 0.227. Maize yield instability rose most significantly in Connecticut and Maryland. The CV of maize yield in Connecticut increased from below 0.15 at the FLU = −0.8 level to above 0.33 at the FLU = 1.2 level. The CV of maize yield in Maryland increased from below 0.21 at the FLU = −0.8 level to above 0.39 at the FLU = 1.2 level. The CV of maize yield change was least pronounced in New York, northern Pennsylvania, and central New Jersey, where the CV of maize yield values remained constant at 0.03 to 0.2. The CV of maize yield in northeastern New York was lowest when the FLU was 0 and its CV increased regardless of FLU changes.

To analyze the statistical distribution of the CV of maize yield on each FLU level, the CV of all maize planting grids on each FLU level was plotted scattered in this paper, as in Figure 7.

The results showed that the maximum value of CV of maize yield increased with the FLU, and the maximum value of CV of maize yield increased from 0.28 to 0.43. Besides, the minimum value of CV of maize yield remained around 0.03 and did not change much with the increase in FLU. It can also be seen from Figure 7 that when the FLU is less than 0, the scatter is more uniformly and densely distributed in the longitudinal direction; while, when the FLU is greater than 0, the scatter has obvious vacancies in the segment with CV values from 0.05 to 0.1. This reflects that, excluding the very few CV stability areas (CV stay around 0), the CV of maize yield is positively correlated with FLU levels, and the magnitude of change varies from grid to grid.

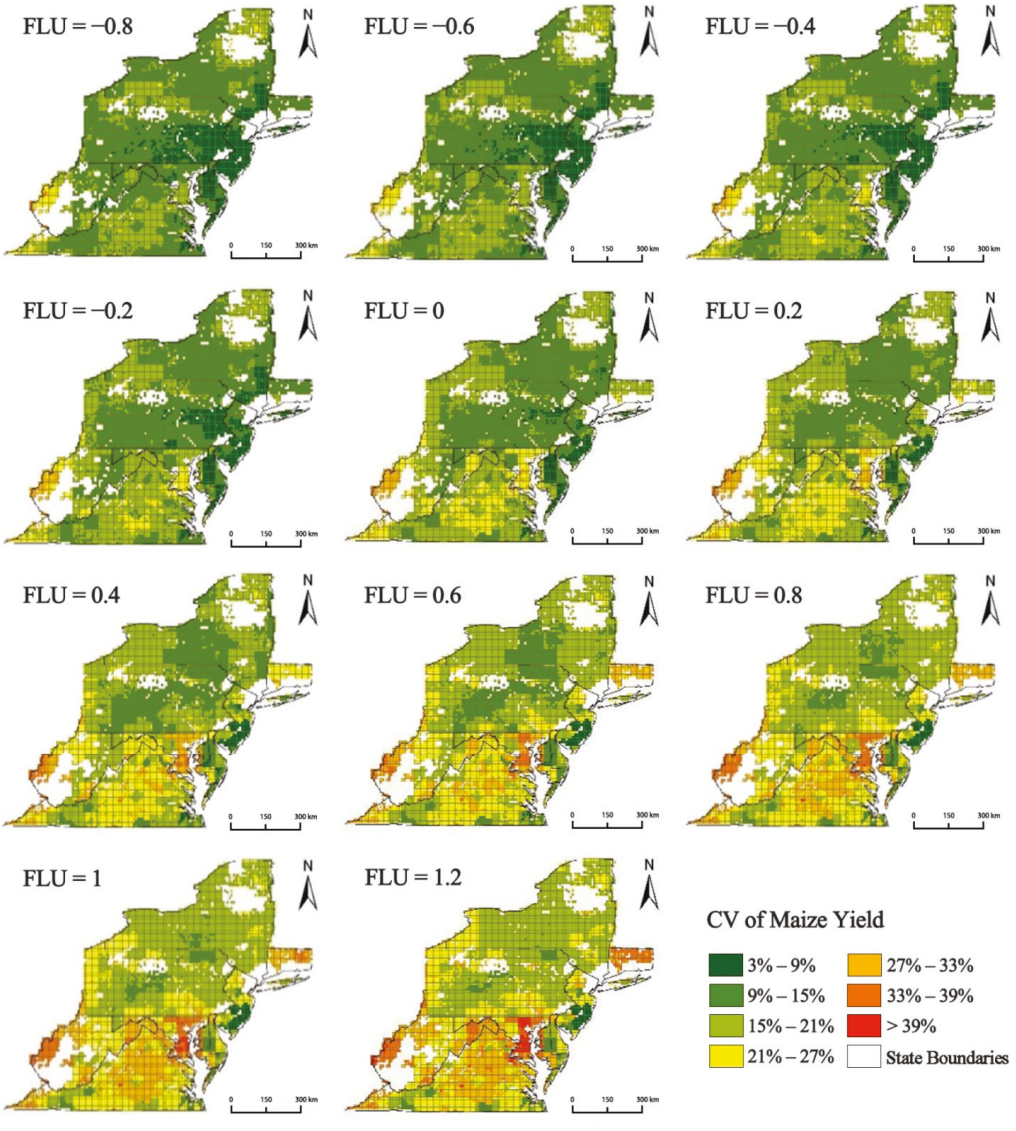

Figure 6. Distribution of CV of maize yield on each FLU level in the study area.

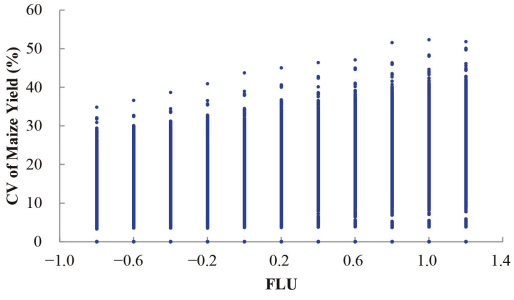

Figure 7. Statistical distribution of the CV of maize yield on each FLU level in the study area.

4. Discussion

4.1. Vulnerability Curve Fitting Method Selection

In this paper, pre-experiments were conducted to choose the vulnerability curve fitting method. The four curve types were exponential, logarithmic, linear, and power functions. The pre-experiment was divided into two steps; first, the scatter points of CV of maize yield under 11 precipitation fluctuation scenarios were fitted to obtain the coefficient of determination (R^2) of the curves on each grid; then, we calculated the mean value of R2 for all grids as the standard for comparing each type of curve. The four types of curve fits for one grid are plotted in Figure 8.

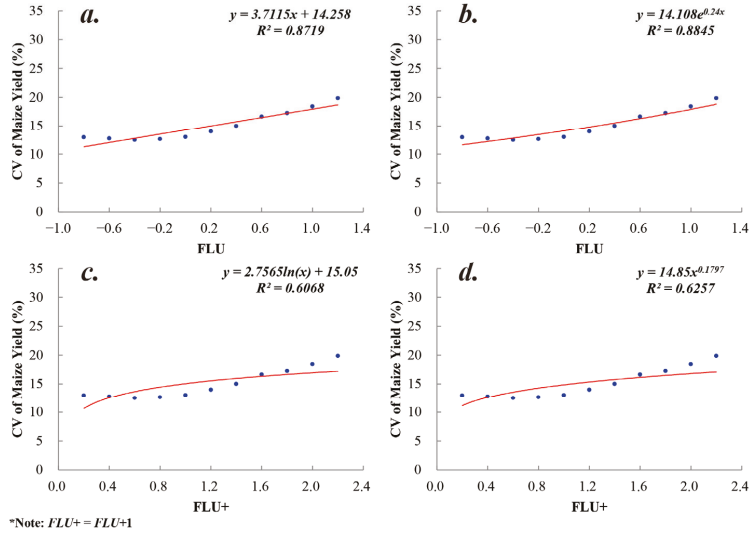

Figure 8. Fitting results of different functions to the vulnerability curve. Linear function (**a**); exponential function (**b**); logarithmic function (**c**); power function (**d**). Because of the value range of the independent variable, the independent variable is 'FLU+' (equal to 'FLU + 1') in (**c**,**d**).

The mean values of R^2 of the four types of curves were calculated as Table 2.

Among the four types of curves, the linear function and exponential function have similar R^2, both above 0.9, with the exponential function having the highest R^2. The R^2 of the logarithmic function with the power function is low, at around 0.6. Given that the linear function is more intuitive in expression and the accuracy of the fitting results is high, the linear function is chosen for fitting in this paper.

Table 2. Average of coefficient of determination (R^2) of the curves.

	Linear Function	Exponential Function	Logarithmic Function	Power Function
R^2	0.9256	0.9287	0.6272	0.6359

4.2. Vulnerability Surface

The disaster vulnerability curve only portrays the relationship between the hazard intensity and the crop yield loss rate [24,44,45]. Vulnerability curves are predicated on the assumption that there is only one input indicator (usually the hazard intensity). It does not fully describe the connotation of disaster vulnerability. If disaster vulnerability is considered as a functional relationship, the output is the crop yield loss, and the input factors include the environment (such as elevation, soil, and slope) and the hazard intensity (such as intensity and duration) [46]. Therefore, the vulnerability of different locations within the region varies, and the greater the spatial extent, the more pronounced the heterogeneity of vulnerability. Vulnerability surfaces are regional disaster vulnerability expressions that combine spatial location differences of the environments with vulnerability curves [5]. In order to compare vulnerability surfaces and vulnerability curves, the vulnerability surfaces of the CV of maize yield to precipitation fluctuations were plotted in this paper using elevation as the environment factor (Figure 9).

By comparing the two expressions, the vulnerability surface adds vulnerability at different elevations, thus reflecting the CV of maize yield under each precipitation fluctuation scenario at different elevations in the region, which makes the information of maize yield variability in the region more abundantly expressed. However, in risk assessment, vulnerability surfaces need to take into account more information about the environment, such as elevation and soil. However, a single vulnerability surface can only express a certain environment, which may require more work in practice. Hence, the study of vulnerability surfaces can be used as a future research direction for future vulnerability studies.

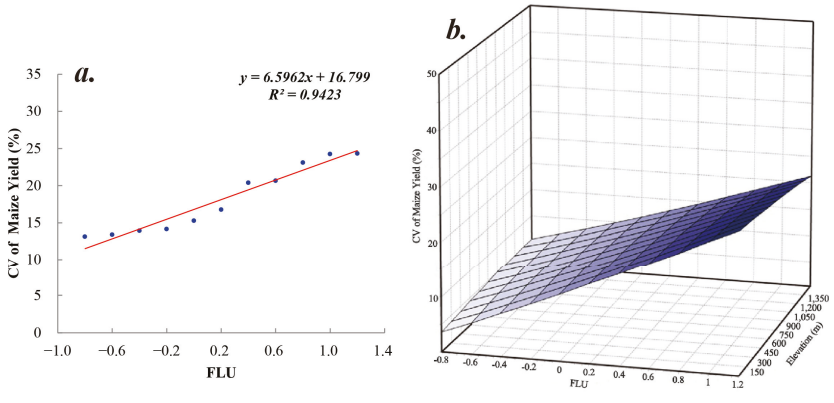

Figure 9. Comparison of vulnerability curve (**a**) and vulnerability surface (**b**).

4.3. Limitations

(1) Due to the availability of data, the climate data used in this paper were all extracted from the HadGEM2-ES climate model, instead of the observed meteorological data. However, the accuracy of the climate data generated by the HadGEM2 climate model has been proven by some studies. Collins et al. [47,48] compared the simulated results of each module of the HadGEM2 model with the observed data (such as aerosol and carbon fluxes), and proved the accuracy of each module of the model. Almagro et al. [49] compared historical climate simulations from the HadGEM2-ES model

with observed precipitation data, and their results also proved that HadGEM2-ES is capable of representing long-term precipitation for the large areas.

(2) For the attribution of Type II and III curves, this paper only gives inferences, but there is no evidence to prove these inferences. Hence, the attribution of unexpected curve types is a direction for further study.

(3) This paper ignores the influence of agro-technological factors, such as sowing date, sowing depth, and variety of maize. Agro-technological factors largely determine the number of crops harvested under the conditions of a deficiency in abiotic factors. Hence, future research needs to take agro-technological factors into consideration.

5. Conclusions

In this study, based on the theory of hazard system risk assessment, the EPIC model was used to simulate maize yields, and its vulnerability curves were applied to study the changes in maize yield stability under 11 precipitation fluctuation scenarios in eight states in the northeastern United States and to analyze their spatial differences. The following conclusions were drawn.

(1) The "precipitation fluctuation and maize yield stability" vulnerability curves were well fitted by a unitary linear function using the FLU and the CV of maize yield of each grid as parameters in the study area (total 6162 grids). These 6162 curves can be classified into three categories (Type I, Type II, and Type III), accounting for 92.7%, 0.3%, and 7.0% of all curves, respectively. Type I has a slope greater than zero and a goodness of fit greater than 0.6, which reflects the positive relationship between maize yield stability and precipitation fluctuations. In the grid of Type I, maize yield stability decreases with precipitation fluctuations. Type II has a slope less than zero and a goodness of fit greater than 0.6, which reflects the inverse relationship between maize yield stability and precipitation fluctuations. Type III has a goodness of fit less than 0.6. In the grid of Type III, the correlation between maize yield stability and precipitation fluctuations is low, indicating that maize yield stability is more susceptible to the influence of other factors in this type.

(2) In the grids of Type I, the high-risk areas for maize cluster in Connecticut and central Maryland when precipitation fluctuations are greater than the historical values; when FLU = 1.2, the CV of maize yield reaches 0.27–0.33 for most of the grids in Connecticut and 0.29–0.45 for the grids in central Maryland. The risk of maize yield stability is also higher in northern Virginia, northern New Jersey, and south-eastern Pennsylvania when precipitation fluctuations are greater than historical values, and the CV of maize yield in these regions is greater than 0.21 when FLU = 1.2. These regions should be priority areas for preventing the effects of precipitation fluctuations on maize.

(3) The study area was divided into eight regions to study the impact of precipitation fluctuation on maize yield. On a state scale, when precipitation fluctuations are greater than historical values, New Jersey and Connecticut have the least stable maize yields and should focus on strengthening maize yield risk prevention under precipitation fluctuations.

The above conclusions can provide a basis for mitigating the effects of maize yield variability under precipitation fluctuations. Besides, they provide a reference for the implementation of supplementary agricultural measures such as field irrigation to ensure high and stable maize yields.

Author Contributions: P.S. conducted the research, analyzed the data, and wrote the paper; S.L. processed the data and did extensive updating of the manuscript; J.W. conceived the research and provided project support; F.L. made suggestions to this paper. All authors have read and agreed to the published version of the manuscript.

Funding: This research was funded by the National Key Research and Development Program of China (Grant No.2016YFA0602402).

Institutional Review Board Statement: Not applicable.

Informed Consent Statement: Not applicable.

Data Availability Statement: Data sharing not applicable.

Conflicts of Interest: The authors declare no conflict of interest.

References

1. Mbow, H.-O.P.; Reisinger, A.; Canadell, J.; O'Brien, P. *Special Report on Climate Change, Desertification, Land Degradation, Sustainable Land Management, Food Security, and Greenhouse Gas Fluxes in Terrestrial Ecosystems (SR2)*; IPCC: Geneva, Switzerland, 2017.
2. Li, Y.; Ye, W.; Wang, M.; Yan, X. Climate change and drought: A risk assessment of crop-yield impacts. *Clim. Res.* **2009**, *39*, 31–46. [CrossRef]
3. Moriondo, M.; Giannakopoulos, C.; Bindi, M. Climate change impact assessment: The role of climate extremes in crop yield simulation. *Clim. Chang.* **2011**, *104*, 679–701. [CrossRef]
4. Challinor, A.J.; Watson, J.; Lobell, D.B.; Howden, S.; Smith, D.; Chhetri, N. A meta-analysis of crop yield under climate change and adaptation. *Nat. Clim. Chang.* **2014**, *4*, 287–291. [CrossRef]
5. Shi, P.-J. Theory on disaster science and disaster dynamics. *J. Nat. Disasters* **2002**, *11*, 1–9.
6. Shi, P.; Xu, W.; Ye, T.; Yang, S.; Liu, L.; Fang, W.; Liu, K.; Li, N.; Wang, M. World atlas of natural disaster risk. In *World Atlas of Natural Disaster Risk*; Springer: Berlin/Heidelberg, Germany, 2015; pp. 309–323.
7. Molua, E.L. Climate variability, vulnerability and effectiveness of farm-level adaptation options: The challenges and implications for food security in Southwestern Cameroon. *Environ. Dev. Econ.* **2002**, *7*, 529–545. [CrossRef]
8. Li, H.; Zhang, P.; Cheng, Y. Concepts and assessment methods of vulnerability. *Prog. Geogr.* **2008**, *27*, 18–25.
9. Shi, P.; Sun, S.; Wang, M.; Li, N.; Jin, Y.; Gu, X.; Yin, W. Climate change regionalization in China (1961–2010). *Sci. China Earth Sci.* **2014**, *57*, 2676–2689. [CrossRef]
10. Wilhelmi, O.V.; Wilhite, D.A. Assessing vulnerability to agricultural drought: A Nebraska case study. *Nat. Hazards* **2002**, *25*, 37–58. [CrossRef]
11. Bewket, W. Rainfall variability and crop production in Ethiopia: Case study in the Amhara region. In Proceedings of the 16th International Conference of Ethiopian Studies, Trondheim, Norway, 2–6 July 2007; pp. 823–836.
12. Simelton, E.; Fraser, E.D.; Termansen, M.; Benton, T.G.; Gosling, S.N.; South, A.; Arnell, N.W.; Challinor, A.J.; Dougill, A.J.; Forster, P.M. The socioeconomics of food crop production and climate change vulnerability: A global scale quantitative analysis of how grain crops are sensitive to drought. *Food Secur.* **2012**, *4*, 163–179. [CrossRef]
13. Farhangfar, S.; Bannayan, M.; Khazaei, H.R.; Baygi, M.M. Vulnerability assessment of wheat and maize production affected by drought and climate change. *Int. J. Disaster Risk Reduct.* **2015**, *13*, 37–51. [CrossRef]
14. Schilling, J.; Freier, K.P.; Hertig, E.; Scheffran, J. Climate change, vulnerability and adaptation in North Africa with focus on Morocco. *Agric. Ecosyst. Environ.* **2012**, *156*, 12–26. [CrossRef]
15. Adnan, S.; Ullah, K.; Gao, S.; Khosa, A.H.; Wang, Z. Shifting of agro-climatic zones, their drought vulnerability, and precipitation and temperature trends in Pakistan. *Int. J. Climatol.* **2017**, *37*, 529–543. [CrossRef]
16. Zhong, S.; Wang, C.; Yang, Y.; Huang, Q. Risk assessment of drought in Yun-Gui-Guang of China jointly using the Standardized Precipitation Index and vulnerability curves. *Geomat. Nat. Hazards Risk* **2018**, *9*, 892–918. [CrossRef]
17. Li, Y.; Guan, K.; Schnitkey, G.D.; DeLucia, E.; Peng, B. Excessive rainfall leads to maize yield loss of a comparable magnitude to extreme drought in the United States. *Glob. Chang. Biol.* **2019**, *25*, 2325–2337. [CrossRef] [PubMed]
18. Jayanthi, H.; Husak, G.J.; Funk, C.; Magadzire, T.; Adoum, A.; Verdin, J.P. A probabilistic approach to assess agricultural drought risk to maize in Southern Africa and millet in Western Sahel using satellite estimated rainfall. *Int. J. Disaster Risk Reduct.* **2014**, *10*, 490–502. [CrossRef]
19. Du, H.; Wu, Z.; Zong, S.; Meng, X.; Wang, L. Assessing the characteristics of extreme precipitation over northeast China using the multifractal detrended fluctuation analysis. *J. Geophys. Res. Atmos.* **2013**, *118*, 6165–6174. [CrossRef]
20. Kang, Y.; Khan, S.; Ma, X. Climate change impacts on crop yield, crop water productivity and food security—A review. *Prog. Nat. Sci.* **2009**, *19*, 1665–1674. [CrossRef]
21. Qiao, J.; Yu, D.; Liu, Y. Quantifying the impacts of climatic trend and fluctuation on crop yields in northern China. *Environ. Monit. Assess.* **2017**, *189*, 532. [CrossRef] [PubMed]
22. Lobell, D.B.; Burke, M.B. Why are agricultural impacts of climate change so uncertain? The importance of temperature relative to precipitation. *Environ. Res. Lett.* **2008**, *3*, 034007. [CrossRef]
23. Hamilton, T.W.; Ritten, J.P.; Bastian, C.T.; Derner, J.D.; Tanaka, J.A. Economic impacts of increasing seasonal precipitation variation on southeast Wyoming cow-calf enterprises. *Rangel. Ecol. Manag.* **2016**, *69*, 465–473. [CrossRef]
24. Zhou, Y.; Wang, J. A Review on Development of Vulnerability Curve of Natural Disaster. *Adv. Earth Sci.* **2012**, *27*, 435–442.
25. Doraiswamy, P.C.; Moulin, S.; Cook, P.W.; Stern, A. Crop yield assessment from remote sensing. *Photogramm. Eng. Remote Sens.* **2003**, *69*, 665–674. [CrossRef]
26. Prasad, A.K.; Chai, L.; Singh, R.P.; Kafatos, M. Crop yield estimation model for Iowa using remote sensing and surface parameters. *Int. J. Appl. Earth Obs. Geoinf.* **2006**, *8*, 26–33. [CrossRef]

27. Rosenzweig, C.; Elliott, J.; Deryng, D.; Ruane, A.C.; Müller, C.; Arneth, A.; Boote, K.J.; Folberth, C.; Glotter, M.; Khabarov, N. Assessing agricultural risks of climate change in the 21st century in a global gridded crop model intercomparison. *Proc. Natl. Acad. Sci. USA* **2014**, *111*, 3268–3273. [CrossRef] [PubMed]
28. Tan, G.; Shibasaki, R. Global estimation of crop productivity and the impacts of global warming by GIS and EPIC integration. *Ecol. Model.* **2003**, *168*, 357–370. [CrossRef]
29. Adejuwon, J. Assessing the suitability of the EPIC crop model for use in the study of impacts of climate variability and climate change in West Africa. *Singap. J. Trop. Geogr.* **2005**, *26*, 44–60. [CrossRef]
30. Yue, Y.; Li, J.; Ye, X.; Wang, Z.; Zhu, A.-X.; Wang, J.-a. An EPIC model-based vulnerability assessment of wheat subject to drought. *Nat. Hazards* **2015**, *78*, 1629–1652. [CrossRef]
31. Mearns, L.; Mavromatis, T.; Tsvetsinskaya, E.; Hays, C.; Easterling, W. Comparative responses of EPIC and CERES crop models to high and low spatial resolution climate change scenarios. *J. Geophys. Res. Atmos.* **1999**, *104*, 6623–6646. [CrossRef]
32. Williams, J.; Jones, C.; Kiniry, J.; Spanel, D.A. The EPIC crop growth model. *Trans. ASAE* **1989**, *32*, 497–0511. [CrossRef]
33. Jia, H.; Wang, J.; Pan, D.; Cao, C. Maize drought disaster risk assessment based on EPIC model: A case study of maize region in northern China. *Acta Geogr. Sin.* **2011**, *66*, 643–652.
34. Wang, Z.; He, F.; Fang, W.; Liao, Y. Assessment of physical vulnerability to agricultural drought in China. *Nat. Hazards* **2013**, *67*, 645–657. [CrossRef]
35. Guo, H.; Zhang, X.; Lian, F.; Gao, Y.; Lin, D.; Wang, J.A. Drought risk assessment based on vulnerability surfaces: A case study of maize. *Sustainability* **2016**, *8*, 813. [CrossRef]
36. Meng, K.; Ekboir, J. *Current and Future Trends in Maize Production and Trade*; CIMMYT (International Maize and Wheat Improvement Center): Veracruz, Mexico, 2001.
37. Brush, S.B. The natural and human environment of the central Andes. *Mt. Res. Dev.* **1982**, *2*, 19–38. [CrossRef]
38. Ray, D.K.; Gerber, J.S.; MacDonald, G.K.; West, P.C. Climate variation explains a third of global crop yield variability. *Nat. Commun.* **2015**, *6*, 5989. [CrossRef] [PubMed]
39. Nuss, E.T.; Tanumihardjo, S.A. Maize: A paramount staple crop in the context of global nutrition. *Compr. Rev. Food Sci. Food Saf.* **2010**, *9*, 417–436. [CrossRef]
40. Meng, Q.; Chen, X.; Lobell, D.B.; Cui, Z.; Zhang, Y.; Yang, H.; Zhang, F. Growing sensitivity of maize to water scarcity under climate change. *Sci. Rep.* **2016**, *6*, 19605. [CrossRef] [PubMed]
41. Zhao, J.; Yang, X.; Sun, S. Constraints on maize yield and yield stability in the main cropping regions in China. *Eur. J. Agron.* **2018**, *99*, 106–115. [CrossRef]
42. Williams, J.R. *The EPIC model. Comput. Models Watershed Hydrol*; Water Resources Publications: Littleton, CO, USA, 1995; pp. 909–1000, ISBN 0918334918.
43. Fan, L.; Lu, C.; Chen, Z. A review of EPIC model and its applications. *Prog. Geogr.* **2012**, *31*, 584–592.
44. Papathoma-Koehle, M.; Keiler, M.; Totschnig, R.; Glade, T. Improvement of vulnerability curves using data from extreme events: Debris flow event in South Tyrol. *Nat. Hazards* **2012**, *64*, 2083–2105. [CrossRef]
45. Wu, S.; Jin, J.; Pan, T. Empirical seismic vulnerability curve for mortality: Case study of China. *Nat. Hazards* **2015**, *77*, 645–662. [CrossRef]
46. Kumpulainen, S. Vulnerability concepts in hazard and risk assessment. *Spec. Pap.-Geol. Surv. Finl.* **2006**, *42*, 65.
47. Collins, W.; Bellouin, N.; Doutriaux-Boucher, M.; Gedney, N.; Hinton, T.; Jones, C.; Liddicoat, S.; Martin, G.; O'Connor, F.; Rae, J. *Evaluation of the HadGEM2 Model*; Met Office Exeter: Devon, UK, 2008.
48. Collins, W.; Bellouin, N.; Doutriaux-Boucher, M.; Gedney, N.; Halloran, P.; Hinton, T.; Hughes, J.; Jones, C.; Joshi, M.; Liddicoat, S. Development and evaluation of an Earth-System model–HadGEM2. *Geosci. Model Dev.* **2011**, *4*, 1051–1075. [CrossRef]
49. Almagro, A.; Oliveira, P.T.S.; Rosolem, R.; Hagemann, S.; Nobre, C.A. Performance evaluation of Eta/HadGEM2-ES and Eta/MIROC5 precipitation simulations over Brazil. *Atmos. Res.* **2020**, *244*, 105053. [CrossRef]

MDPI
St. Alban-Anlage 66
4052 Basel
Switzerland
Tel. +41 61 683 77 34
Fax +41 61 302 89 18
www.mdpi.com

Land Editorial Office
E-mail: land@mdpi.com
www.mdpi.com/journal/land

MDPI
St. Alban-Anlage 66
4052 Basel
Switzerland

Tel: +41 61 683 77 34
Fax: +41 61 302 89 18

www.mdpi.com

ISBN 978-3-0365-3067-3